Resveratrol Nanostructured Lipid Carrier for targeted delivery to breast cancer

by

Chahinez Houacine

A thesis submitted in partial fulfilment for the requirements for the degree of Doctor of Philosophy at the University of Central Lancashire

May 2018

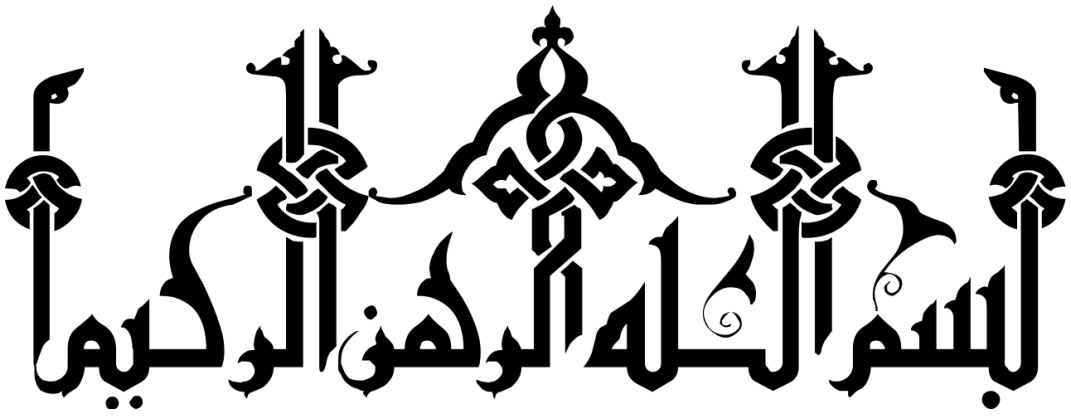

In the Name of Allah, the Most Gracious, the Most Merciful

STUDENT DECLARATION FORM

Concurrent registration for two or more academic awards

I declare that while registered for the research degree, I was with the University's specific permission, a *registered candidate/*enrolled student for the following award:

_____Doctor of Philosophy_____

Material submitted for another award

I declare that no material contained in the thesis has been used in any other submission for an academic award and is solely my own work

Collaboration

Where a candidate's research programme is part of a collaborative project, the thesis must indicate in addition clearly the candidate's individual contribution and the extent of the collaboration. Please state below:

Signature of Candidate _____Chahinez_____

Type of Award _____ Doctor of Philosophy _____

School _____**Pharmacy and Biomedical Sciences**_____

DEDICATION

I would like to dedicate this thesis to my parents;

Arezki Houacine and Yamina Houacine

Acknowledgement

I consider myself exceptionally privileged to have been on this journey and had such lovely people help and support me along the way. I do not think that I will be able wholly express my gratitude or sufficiently acknowledge the support and contribution that each and every person has made to me and my work.

Firstly, I would like to express my sincerest gratitude to my director of studies, Professor Kamalinder Singh. Thank you Professor for everything, for taking me on as a PhD student, for all your continued support, moral boosting and your endless time, patience and expertise. I consider myself extremely lucky to have been under your supervision and I hope that you will be proud of this thesis.

I am indebted to Dr. Jane Alder, Dr. David Adams and Dr. Philip Roberts my second supervisors. Thank you all for your efforts and expertise. It goes without saying that without the knowledge you imparted to me I would not have been able to take this research as far as I have.

I am very fortunate to have come across such wonderful colleagues during this journey. I would like to acknowledge everyone, as I am quite certain that I would miss people and I would not want to be unfair.

PhD can be a very solitary journey; however I was lucky to have come across sincere friends without whom I would certainly not have made it this far. A special word of gratitude is due to the one and only Sakib Yousaf, you have been more than a brother to me, helped me, supported me and cooked for me (channa), and you had to put up with my craziness all the time. I just have to say that PhD would not be easy without your presence; I am aware that how many words I write would not be enough to express how happy I am to have you as a best friend. Thank you.

To my partner in crime Shilpa Pawar-Bhalerao, without you my journey would be incomplete your love and support made it easy for me to carry on in this journey. To my friends Iftikhar Khan thank you for your friendship and support. Special thanks to Dr. Abdullah and Dr. Mohamed for their continuous help and support during this journey.

I would like to acknowledge with gratitude Dr. Julie and Dr. Sarah for their continuous help with tissue culture experiments.

To my family, it goes without saying that you mean everything to me and that everything I am is because of you; Thank you Papa, Mama, Nazim and my wonderful sister Sihem.

ABSTRACT

Background: Breast cancer remains a prominent cause of mortality and morbidity in the female population. Despite advances in terms of novel compounds, exhibiting chemotherapeutic activity successful delivery remains challenging. Particulate-based system such as Nanostructured Lipid Carriers (NLCs) a new generation carrier allow encapsulation of drug and targeting of desired tissue. Resveratrol (RES) is a chemotherapeutic drug limited by its physiochemical properties (i.e. poor solubility and bioavailability), encapsulation into NLCs is potentially viable solution to the aforementioned issues.

Aim: The main aim of the present work is to develop a nanostructured lipid carriers based drug delivery system of RES in order to overcome its physicochemical and pharmacokinetic limitations and impart suitable functionalities for targeting breast cancer cells.

Methods: Box-Behnken experimental design (BBD) was used to understand the effect of three independent factors (amount of liquid lipid, amount of drug and surfactant concentration) and interactions between these factors for each of the six liquid lipids on the selected response variables particle size (PS), polydispersity index (PDI), zeta potential (ZP), drug encapsulation efficiency (%EE), and drug loading (%DL). The formulated resveratrol nanostructured lipid carriers (RES-NLCs) were subjected to a series of physicochemical characterization including particles size, zeta potential measurements, *in-vitro* drug release while the morphology of RES-NLCs was confirmed through various microscopic methods, differential scanning calorimetry, x ray diffraction and Fourier transfer infrared studies was carried out in order to understand the interactions between RES and the components of the formulation. Undertake stability studies for the formulated RES-NLCs, at various storage conditions in order to select the most stable formulation and take it for further functionalization with targeting ligands hyaluronic acid; HA-NLCs, folic acid; FA-NLCs and dual targeting system using both hyaluronic acid and folic acid; HAFANLCs, and optimization of ligand density and quantify the amount of amine groups present on the surface on RES-NLCs.

The efficacy of RES-NLCs was demonstrated through various *in-vitro* cell lines studies carried on three breast cancer cell lines entailed: MCF-7, MCF-10A and MDAMB-231 cells. Finally, the permeability of the formulations was evaluated through Caco-2 monolayer and Caco2/HT29 co-culture cell lines in order to understand the intestinal barrier transport mechanism.

Results: The employed Box Behnken design resulted in the formulation of particles which were <100nm in size, PDI <0.3, a negative surface charge (-24), high entrapment efficiency (91-99%) and drug loading of 3-4%, with tuneable characteristics within the design space. Differential scanning calorimetry and x-ray diffraction indicated amorphous nature of the drug in nanoparticles indicating

its entrapment. Upon exposure to acidic medium (pH 1.2), <20% drug release was observed in 4 hours, with 100% drug release observed upon the increase of pH to 5 over a period of 24 hours.

Upon stability testing of NLCs, nanoparticles formulated with GTO as a liquid lipid showed good stability and therefore was taken forward for further PEGylating and surface modification with three ligands; hyaluronic acid, folic acid and combination of both ligand in order to impart targetability for breast cancer cells. Surface modification drastically reduced drug release to < 2 % at pH 1.2, however at pH 5, drug release time plots indicated slower overall release from the surface modified NLCs.

In-vitro cytotoxicity studies showed that RES-NLCs were effective against both non-TNBC; MCF-7 and TNBC; MDAMB-231 breast cancer cell lines. Dual ligand appended nanoparticles showed 2.7 folds higher toxicity in MCF-7 and 3.6 fold higher toxicity in MDAMB-231 cells as compared to RES-NLC-GTO-PEGS40 demonstrating its potential for treatment in the aggressive triple negative cancer. None of the RES-NLCs formulations containing different liquid lipids or their blanks were cytotoxic to healthy MCF-10A cells demonstrating safety of the formulations. All bare, PEGylated and surface modified RES-NLCs showed time dependent cellular uptake on both MCF-7 and MDAMB-231 cell lines. Surface modification lead to 3 fold increase in the cellular uptake confirming the targetability potential of the ligand appended formulations toward overexpressed receptors on the surface of both cancer MCF-7 and MDAMB-231 cells.

Upon examination of endocytosis mechanisms when cells were treated with the formulations, it was noted that two mechanisms were prominent. Clathrin-mediated endocytosis was identified as the primary method of endocytosis for all formulations. However, specifically for surface modified NLCs receptor mediated endocytosis was also found to be responsible for uptake of nanoparticles. Bidirectional transport study demonstrated that the permeability was sensitive to the type of liquid lipid incorporated with the highest permeability exhibited for PGML based formulation, when studied using a Caco-2 monolayer. On comparison to Caco-2/HT29 co-culture free resveratrol showed higher permeability when compared to the formulated NLCs.

Conclusion: The aforementioned research has demonstrated that resveratrol NLCs are a viable potential product for use in the treatment of breast cancer, exhibiting high versatility and specificity.

Contents

List of Figures

List of Tables

Abbreviations and Acronyms

%DL	Percentage drug loading
%EE	Percentage encapsulation efficiency
µm	micrometre
^{1}HNMR	Proton nuclear magnetic resonance
Ac-DEVD-pNA	acetyl-Asp-Glu-Val-Asp p-nitroanilide
ANOVA	Analysis of Variance
API	Active Pharmaceutical Ingredient
BBD	Box-Behnken experimental design
BCA	Bicinchoninic acid
BCS	Biopharmaceutical Classification System
C6-RES-NLCs	Coumarin-6 loaded RES-NLCs
Caco-2	Colon carcinoma cell lines
CCV	Clathrin coated vesicles
CDI	Carbonyl-di-imidazole
CoA	Coumaroyl-Coenzyme A
–COOH	Carboxylic acids
CQA	Critical quality attributes
CV	Coefficient of variation
CvME	Caveolae mediated endocytosis
DAPI blue	4', 6-diamidino-2-phenylindole
DMEM	Dulbecco's minimal essential medium
DMSO	Dimethyl sulfoxide
DO	Decyl octadec-9-enoate (Decyl Oleate)
DoE	Design of experiments
DSC	Differential Scanning Calorimetry
DT	Doubling time
E80	Egg phospholipid
EDC	1-Ethyl-3-(3-dimethylaminopropyl)-carbodiimide
EDC	1-Ethyl-3-(3-dimethylaminopropyl)-carbodiimide
EMEM	Eagle's minimum essential medium.
EPR	Enhanced permeability and retention
FA	Folic acid
FBS	Foetal Bovine Serum
FDA	Food Drug Administration
FDS	Forced degradation studies
FR	Folate receptors
FTIR	Fourier Transform Infrared Spectroscopy
GIT	Gastrointestinal tract
GTC	Glycerol tricaprylate
GTC	Tricaprylin (Miglyol 808)
GTO	Glyceryl trioleate (Triolien)
h	Hour
HA	Hyaluronic acid
HBSS	Hank's balanced buffer solution
HCL	Hydrochloric acid
HLB	Hydrophilic lipophilic balance

HPH	High-pressure homogenization
HPLC	High Performance Liquid Chromatography
HT29	Colonic cancer cell lines
ICH	International conference of Harmonization
kDa	Kilo Dalton
LOD	Limit of detection
LOF	Lack of fit
LOQ	Limit of quantification
M	Molar
MCF	Breast cancer cell lines
MDAMB-23	Resistant cell lines
MEGM	Mammary Epithelial Cell Growth Medium
min	Minutes
ml	Millilitre
MS	Mean square
MWCO	Molecular weight cut-off
NaOH	Sodium hydroxide
NEAA	Non-Essential Amino Acids
NHS	*N*-hydroxysuccinimide
NLCs	Nanostructured lipid carriers
nm	Nanometre
NMR	Nuclear Magnetic Resonance
NTNBC	Non-triple negative breast cancer cells
O/W	Oil in water
PAH	Polycyclic Aromatic Hydrocarbons
Papp	Apparent permeability
PBS	Phosphate buffer saline
PC	Polygonum cuspidatum
PCG	Propylene glycol-8 caprylic/capric glycer
PCG	Caprylcaproyl macrogol glycerides (Labrasol)
PDA	Photodiode Array detector
PDI	Polydispersity index
PEG	Polyethylene glycol
PEG-40 Stearate	Polyethylene glycol monostearate
PFA	paraformaldehyde
PGMC	Propylene glycol monocaprylate
PGMC	Propylene glycol monocaprylate (type II) NF(Capryol 90)
PGML	Propylene glycol monolaurate (Lauroglycol 90)
P-gp	P-glycoprotein
pNA	Paranitroaniline
PRESS	Predicted residual sum of square
PS	Particle size
PS	Phosphatidylserine
QELS	Quasi-Elastic Light Scattering
R^2	Correlation coefficient
RES	Resveratrol
RES-NLC-PEGS40	PEGylated NLCs
RES-NLCs	Resveratrol Nanostructured Lipid Carriers

RME	Receptor mediated endocytosis
rpm	Revolutions per minute
RSD	Relative standard deviation
RSM	Response surface methodology
S75	Soy phospholipid
SD	Standard deviation
SLNs	Solid lipid nanoparticles
SS	Sum of squares
STS	Stilbene synthase
TB	Trypan blue
TCAA	Trichloroacetic acid
TEER	Transepithelial electrical resistance
TJ	Tight junction
TNBC	Triple negative breast cancer
TNBS	2, 4, 6-trinitrobenzenesulphonic acid
USP	United states Pharmacopeia
V/V	Volume per volume
ZP	Zeta potential

Chapter 1 : General Introduction

This chapter aims to illustrate the prevalence, biodiversity and significance of cancer as a disease state. Specific emphasis is placed upon breast cancer as a cancer subtype, entailing it's; pathophysiology, associated prevalence and impact, as well as current and historic treatment options dating back to its initial identification as a cancer sub-type. Nano-structured lipid carriers (NLC's) are examined in depth as promising drug delivery systems for existing and novel chemotherapeutic agents, such as Resveratrol. The impact of processing parameters and formulation constituents upon formulation characteristics are discussed, as well as the necessitation for more intimate studies of formulation characteristics and interaction in *in vitro* settings.

1.1 Proliferative disease

The term proliferative may be traced back to the French, who derived term from two Latin words; "proles",- meaning offspring/descendants and "fer" meaning bearing, i.e. cells that are proliferating or bearing offspring (Sporn and Harris, 1981). Whilst the term is typically associated with cancer, the term includes many disease states; atherosclerosis, rheumatoid arthritis, psoriasis, idiopathic pulmonary fibrosis, scleroderma and cirrhosis of the liver. The forthcoming sections however focus exclusively upon cancer as a proliferative disease with innumerate sub-disease states, for reasons discussed in the succeeding section.

1.1.2 Cancer

WHO (2017) describes cancer as a generic term for a large group of diseases which are typically characterized by the growth of abnormal cells beyond their natural boundaries, resulting in potential invasion of adjoining parts of the body/organs (WHO, 2017).

Between 2001 and 2014 there has been a steady increase in the number of cancer cases diagnosed per annum with a total increase of 25% in the UK alone. A recent review of cancer statistics, revealed that whilst cancer rates had dropped by 23% over the previous two decades in the USA, it was now identified as the leading cause of mortality in the US population. Inferring that whilst successful diagnoses are increasing and associated mortality is dropping, cancer remains at the forefront of disease states causing mortality (Radtke and Müller, 2001).

The four most common cancers occurring worldwide are breast, lung, prostate and bowel cancer. These four account for about 4 in 10 of all cancers diagnosed worldwide. Moreover, the aforementioned cancers in addition to stomach cancers are amongst the most commonly diagnosed cancers worldwide

since 1975. It is estimated that worldwide there will be 23.6 million new cases of cancer each year by 2030. Gender and geographical differences also are noted to impact incidence rates, with new diagnoses in the UK comparatively lower than the European Union in males, however contrastingly higher in females. Furthermore, specifically the level of area development is proposed to be an influential factor, with more developed regions of the world showing higher incidence for both genders; with rates in the UK are higher than in the less developed regions of the world (Cancer, 2012).

In summary, it is clear that cancer is a diversiform disease state with global variance, which remains at the forefront of diseases causing significant mortality and morbidity. The innumerate subtypes present provide substantial scope for research into treatment, and despite advances in diagnosis and treatment there remains a plethora of unexplored avenues.

1.1.3 Cancer development and metastasis

The development of cancer is multifaceted, however there is a strong association with uncontrolled cell growth and the development of metastatic qualities. The widely agreed upon mechanism behind this process is the activation of oncogenes, and/or the deactivation of tumour suppressor genes. The resultant effect is uncontrolled cell progression and inactivation of apoptotic mechanisms. In contrast to benign tumours, malignant tumours attain metastasis, occurring partly in response to down-regulation of cell adhesion receptors which are necessary for a number of processes, including: tissue-specific cell–cell attachment and up-regulation of receptors that enhance cell motility (Alberts et al., 2002).

Additionally, the activation of metalloproteases provide a route for metastatic cancer cells to spread. There are several agreed upon mechanisms by which these genetic and cellular alterations occur. Widely recognised are; mutation, chromosomal translocation or deletion, and dysregulated expression or activity of signalling pathways. Via these processes genes may be activated which encourage dysregulated cell cycling and/or inactivate apoptotic pathways (Lodish et al., 2000).

The process by which a tumor develops occurs in several stages (Figure 1-1). Four mutations are ultimately responsible for its growth; however, the number of mutations varies significantly depending upon tumor type. The precise number of mutations required for a normal cell to undergo malignancy is unknown, however is theorized to be less than 10. Initially (Figure 1-1 A), a tumor develops when a cell experiences a genetic mutation which results in a greater likelihood of the cell division, than under normal circumstances. The altered cell and its resultant descendant cells grow and divide rapidly, a state referred to as hyperplasia (Figure 1-1. B). Subsequent mutation in descendant cells exponentially

increases this tendency of rapid division. These cells divide excessively and take on an abnormal appearance referred to as dysplasia (Figure 1-1C). The resultant cells are significantly abnormal in terms of growth and appearance (Figure 1-1 D). Once the tumor has formed from these cells, providing that the tumor cells remain within the tissue of origin, the cancer is termed *in situ* cancer. Such cancer may remain constrained within the origin area indeterminately. In the event that individual cells undergo additional subsequent mutations which allow invasion of neighboring tissues or shedding of cells in blood or lymph; the tumor is then term malignant (NIH, 2007).

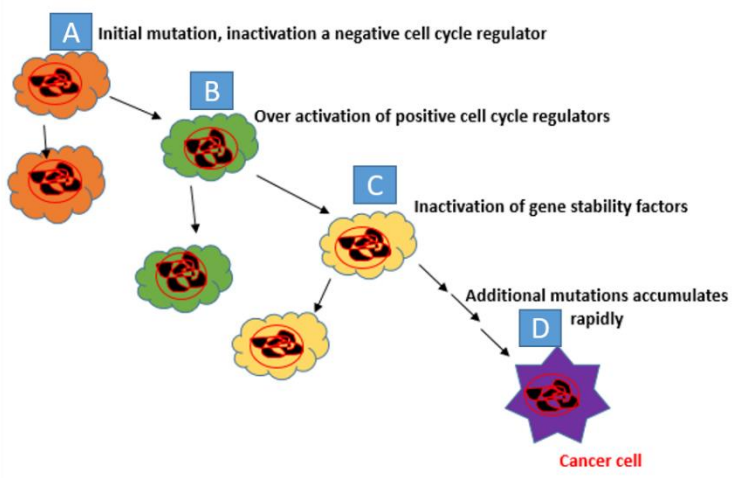

Figure 1-1. Cancer formation process

Metastases is an intricate process with many steps (Figure 1-2). It essentially describes the process by which tumor cells occupy adjacent tissue, enter systemic circulation and reposition via vasculature, forcefully entering surrounding tissue parenchyma and ultimately proliferating from microscopic growths (micrometastasis; the spread of a cancer from its original location to other sites in the body) into macroscopic secondary tumours (Sarkar et al., 2013).

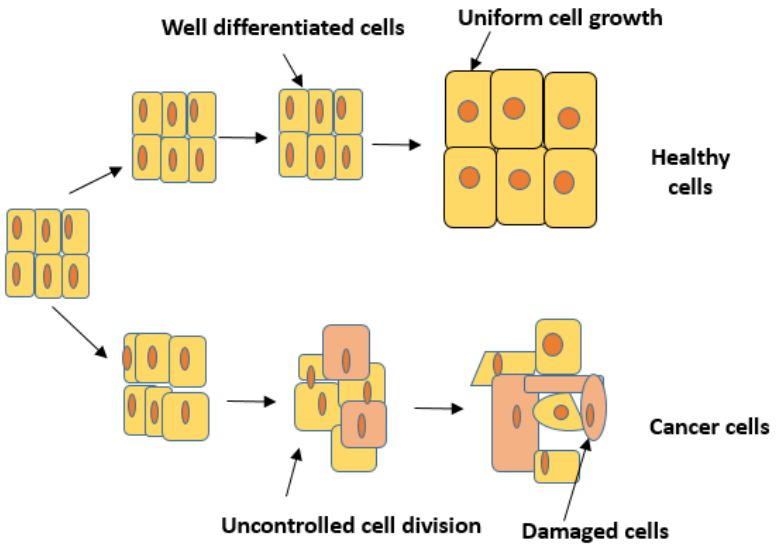

Figure 1-2 .Series of mutations leading to cancer cell formation

1.1.4 Involvement of Cytochrome P-450 in cancer pathology

In the development of active agents against disease states, avenues or pathways, which may be exploited to achieve the desired outcome, are often investigated. Cytochrome P450 (CYP450) enzymes are a collection of enzymes which contain a heme group. The significance of these enzymes lies in their ability to metabolism steroids, drugs and also carcinogens; as a consequence they are frequently incorporated as targets in rational drug design. The group of enzymes however is particularly large with many subtypes including but not limited to; CYP1A1, CYP1A2 and CYP1B1 (Brodie, 1985).

The aforementioned three enzymes are recognised as being responsible for activating pro-carcinogens (i.e. polycyclic aromatic hydrocarbons (PAHs)), with members of this CP450 subgroup of enzymes being found in low concentrations in tissues surrounding the liver (Mikstacka et al., 2012) . Amongst these subtypes CYP1B1 is of particular interest as it found significantly in numerous tumour types when compared directly to non-cancerous tissues, being associated with the formation of tumours as well as being established to activate a number of carcinogens (Shimada et al., 1996, Murray et al., 1997). In addition to CYP1B1's role in cancerous growth formation, alongside CY1P1A1 it is posed that both these enzymes pertain the ability to metabolise chemotherapeutic agents, which may aid in negating the development of chemotherapeutic induced cytotoxicity (McFadyen et al., 2001).

The distinct functions of these enzymes presents an opportunity for the targeting of treatment i.e. chemo-preventative effect may be achieved by the inhibition of CYP1B1. Early studies in mice have demonstrated that chemo-preventative blockade of CYP1B1 may be achieved without detriment to the

animal; providing a basis for further research into possibilities associated with chemo-preventative agents which target CYP1B1(Gonzalez, 2002).

1.1.5 Breast Cancer

There are many subtypes of cancer, breast being a common form, which receives significant media and pharmaceutical attention. Whilst this subtype is largely associated with women, there are documented incidences of men developing breast cancer. Providing that the condition is detected suitably early, prevention of spread to the rest of the body is achievable (NHS, 2014). The incidence for this disease state is high with 1 in 10 women in the United States and Canada at risk of developing this condition; similar rates are observable in European countries. In terms of the female populace, breast cancer is a strongly prevalent cause of malignancy, with incidence rates increase steadily since the 1980's and tailing off during the 1990's through to 2001. Moreover, approximately 70 % of patients diagnosed with this condition go onto develop metastasis resulting mortality; with a further 10 % of patients often presenting with metastasis upon initial diagnosis (Mohan and Ponnusankar, 2013).

Despite many treatment options which aim to conserve the breasts (i.e. hormonal therapy, radiation therapy and chemotherapy), mastectomy (surgical removal of the breasts) remains a common procedure in terms of treatment. The invasive nature of the operation and the plethora of side effects which are associated with treatments geared towards breast conservation form a notable barrier in patient concordance. Chemo-preventative agents are posed as a novel and exciting method of countering breast cancer (Li et al., 2006).

Increase in survival of breast cancer patients may be attributed to the introduction of novel single agents and combinations of chemotherapeutic agents or biologic agents, which are breast cancer specific. Whilst combinations of chemotherapeutic agents provide an overall improvement in survival rate. Novel single agents are being increasingly utilized due reduced toxicity (which is notably higher in combination regimes). In addition to chemotherapy, endocrine therapy is indicated in hormone-responsive breast cancer due to reduced side-effects and also general efficacy (Mohan and Ponnusankar, 2013). Whilst there are benefits and pitfalls to each approach in the treatment of breast cancer; minimization of side-effects without detriment to treatment efficacy is highly desirable, providing the usage of single agents which are novel with an edge in terms of treatment.

1.2 Chemoprevention of carcinogenesis

The term “prevention is better than cure” may be appropriate when taking into account the current scope of research in the treatment or prevention of breast cancer. Mutations in the breast cancer gene (BRCA) in women are essentially identified as a high risk factor for developing the disease state. Chemo-preventative agents may be utilised in two manners; either to negate continued DNA impairment reducing the chances of the formation of cancerous growths, or, to subdue the metastatic phenotype (expressed genotype). Whilst people are widely accepting preventative measures for disease states such as cardiovascular disease, similar enthusiasm is not known exhibited in the prevention of breast cancer (Gabizon and Muggia, 1998). This may be attributed perhaps to the side-effect profile of many chemo-preventative agents.

1.2.1 Novel Chemotherapeutic Agents

Combinations of chemotherapeutic agents whilst achieving the desired effect, come with the disadvantage of an increased side-effect profile unacceptable to many patients. Thus, it is desirable to minimize the number of agents required to achieve therapeutic effect, preferably down to a single drug. This is however difficult to achieve, with many existing drugs utilized as combination therapies. Consequently, the development and testing of novel therapeutic agents is of paramount importance.

1.2.2 Resveratrol

Resveratrol (RES) is an example of one such novel chemotherapeutic agent which has been investigated as potential treatment option for breast cancer.

1.2.2 (I) History and Source of RES

In terms of origins, Resveratrol (RES) is known to have been initially identified in 1940, derived from the roots of the white hellebore (*Veratrum grandiflorum*); as well as in 1963 from the dried roots of Japanese knotweed, *Polygonum cuspidatum* (PC), also known as Ko-jokon in Japan. These were known to be used in traditional Chinese and Japanese herbal medicine in the treatment of a multitude of conditions, including: gonorrhea, vessels inflammation, dermatitis, diabetes, hypertension, cough, cancer, atherosclerosis and hyperlipidemia (Velmurugan and Selvamuthukumar, 2016).

Subsequent research has led to the identification of the compound in approximately 70 plant species (Figure 1-3); with grapes being identified as a crucial source of resveratrol, even in products such as wine; as discovered in 1976 and 1992 (Emami et al., 2012). Interestingly, concentrations of the active compound are found to be highest (50–100 µg per gram) in the skin and seeds of grapes(Freitas and Müller, 1998).

It is however, the definitive lack of severe side effects upon study of the compound in Japanese knotweed, which has led to significant interest in the plant and resveratrol (Mohan and Ponnusankar, 2013, Velmurugan and Selvamuthukumar, 2016).

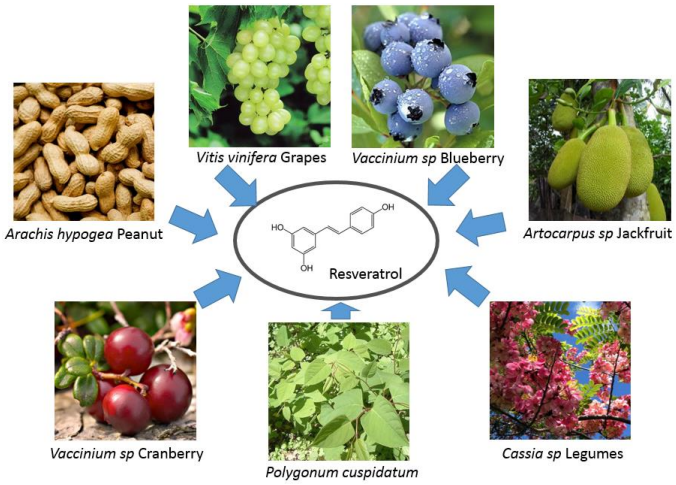

Figure 1-3. Sources of resveratrol from various plants

1.2.2 (II) Biosynthesis of RES

As a drug molecule, Resveratrol (3,5,4'-trihydroxystilbene), belongs to a group of plant compounds referred to as polyphenols. Like many compounds, it occurs as two isomers, *cis* and *trans* (Figure 1-4), with the latter occurring notably more than the former. The isomers are either observed in free form or bound as glucosides; with the *trans*- form possessing the ability to isomerize to *cis*- , upon exposure to light or UV radiation.

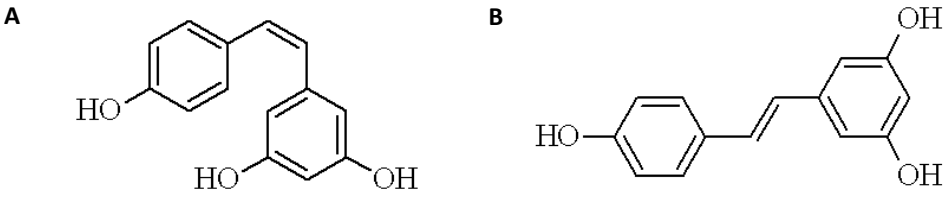

Cis-resveratrol **Trans-resveratrol**

Figure 1-4. Isomers of Resveratrol (a) *cis*- isomer (b) *trans*-isomer

Biosynthesis of resveratrol involves enzyme stilbene synthase (STS), which is stimulated in reaction to environmental stress inducing factors, such as injury, UV radiation and pathogen infestation (Kollipara et al., 2010, Luan et al., 2015). STS is involved in the catalysis of three condensation reactions between coumaroyl-coenzyme A (CoA) and three molecules of malonyl-CoA through cleavage of three carbon dioxide molecules (Figure 1-5). Furthermore, STS also plays a role in the catalysis of the terminal carboxyl group lost, which leads to the production of the C14 molecule resveratrol (Luan et al., 2015, Hu et al., 2005a).

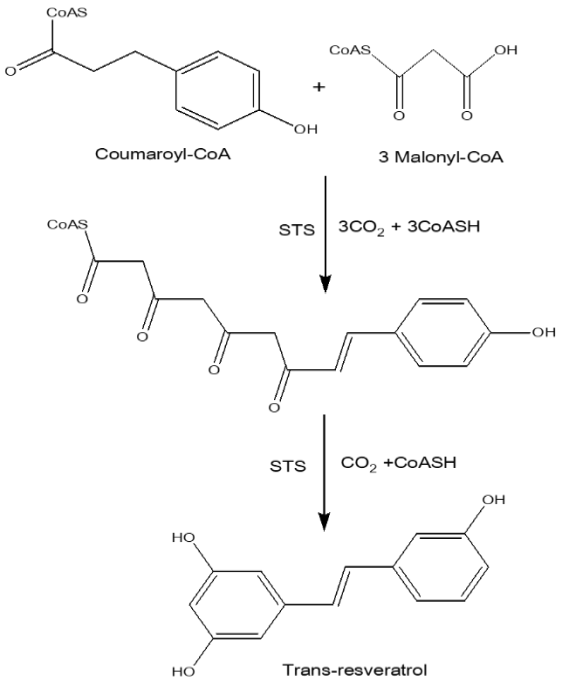

Figure 1-5. Resveratrol biosynthesis

1.2.2 (III) RES mechanism of action and therapeutic potentials

Resveratrol has generated considerable interest in utilizing it as a bioactive agent in foods and pharmaceuticals. It has elicited numerous therapeutic effects, including chemopreventive, antioxidant, cardioprotective (Imamura et al., 2017), anti-obesity (Hou et al., 2003, Gokce et al., 2012, Shabir, 2003), anti-inflammatory (Tadros et al., 2004, ICH, 1995, Tamjidi et al., 2014, ICH, 1999, ICH, 1996, Akhtar et al., 2013, Zhang et al., 2013, Garanti et al., 2016, Lasoń et al., 2013, Elmowafy et al., 2017, Soma et al., 2017), antiaging (Orgován et al., 2017) and neuroprotective effects as evaluated both *in vitro* and *in vivo* (Al Dera, 2017).

1.2.2 (IV) Anticancer effect of RES

Resveratrol has received considerable attention in recent years for its many beneficial effects on health. There is body of evidence, with various research studies demonstrating antioxidant, anti-inflammatory, anti-obesity, and anticancer effects of resveratrol in laboratory animals. With its beneficial effects contributing to improved health and extended life expectancy resveratrol has emerged as promising nutraceutical and functional food (Velmurugan and Selvamuthukumar, 2016).

Chemo-preventive activity of resveratrol was first discovered in 1997 by Jang and colleagues, they illustrated the ability of resveratrol to inhibit the three processes involved in cancer development entailed: initiation, promotion, and progression in different models (Tadros et al., 2004). It has been reported to exhibit anticancer properties against a wide variety of tumour cells, including lymphoid and myeloid cancers; multiple myeloma; cancers of the breast, prostate, stomach, colon, pancreas, and melanoma; thyroid; head and neck squamous cell carcinoma; ovarian carcinoma; and cervical carcinoma. Its potential in colon cancer therapeutics has been shown through anticancer activity in HCT 116 cells, which may be mediated by inactivating PI3K/Akt signalling through up regulating BMP7 (Zheng et al 2017). The anti-tumour potential of resveratrol has been attributed to its ability to bind to Cu2+ and cancer-involved G-quadruplexes in human melanoma cells (Mehnert and Mäder, 2001, Zara et al., 2002).

The exact mechanism of resveratrol's anti-proliferative action remains unknown, however literature is suggestive that resveratrol acts by a number of mechanisms including: proapoptotic, antiproliferative, anti-inflammatory and anti-angiogenesis mechanisms (Park, 2002).

Resveratrol caused apoptosis in a variety of cancer cell lines by inhibiting the cyclooxygenase protein. Breast cancer metastasis was slowed down employing high doses of resveratrol by inhibiting

lamellipodia extension. This property of resveratrol makes it a potential preventive agent of breast cancer. On the other hand, low doses caused an increase in the metastasis and migration (Azios et al., 2007, (Hu et al., 2006).

Bove et al., (2002) conducted an *in-vitro* study establishing that RES inhibited the growth of 4T1 breast cancer cells in a time and dose-dependent manner. In *In-vivo* testing however, RES had no effect upon growth or metastasis rate when administered intraperitoneally daily (1–5 mg/kg) for 23 days starting at the time of tumour inoculation (Bove et al., 2002).

Chen et al., (2004) results showed that RES can act as a potential chemopreventive against dioxin-induced human mammary carcinogenesis by blocking the metabolic formation of the catechol estrogens, thus, inhibiting the both enzymes activity (Chen et al., 2004).

In another study by Miksits et al., (2009); three major human sulfated conjugates of RES were synthesized and their cytotoxic activity evaluated against three breast cancer cell lines (two hormone-dependent: MCF-7 and ZR-75-1; one hormone-independent: MDA-MB-231) and one immortalized breast epithelial cell line (MCF-10A). The results showed that all three sulfated metabolites were less potent against MCF-7, MDA-MB-231 and ZR-75-1 cells, suggesting that any conjugation of the phenolic groups as a sulfate strongly affects the cytotoxicity. Compared to RES, the sulfated metabolites showed poor cytotoxicity in human malignant and nonmalignant breast cancer cell lines. However, the *in-vitro* activity of the metabolites may not necessarily reflect their *in-vivo* activity, as the presence of human sulfatases may convert the metabolites back to RES in humans (Miksits et al., 2009).

Maier-Salamon et al., (2006) studied intestinal absorption of RES using Caco-2 monolayers. The results showed that along with three more metabolites; monosulfate was identified as the dominant metabolite. The total amount of RES transported across the Caco-2 monolayers increased as much as 3.5-fold at 200 µM as biotransformation was either inhibited or saturated. The previous data demonstrated a concentration-dependent biotransformation of RES in Caco-2 cells, which may possibly be applied to human enterocytes affecting oral bioavailability (Maier-Salamon et al., 2006a).

Mikstacka et al., (2007) determined the inhibitory effect of naturally occurring analogues of *trans*-RES on the catalytic activities of human recombinant CYP1A1 and CYP1B1. Pterostilbene (3,5-dimethoxy-4'-hydroxystilbene), desoxyrhapontigenin (3,5-dihydroxy-4'-methoxystilbene and pinostilbene (3,4'-dihydroxy-5-methoxystilbene) demonstrated potent inhibition of CYP1A1 catalytic activity with Ki values of 0.57, 0.16 and 0.13µM, respectively. Results indicated that *trans*-RES analogues in which the hydroxy groups are substituted by methoxy groups exhibiting a remarkably potent inhibitory effect towards CYP1A1 when compared to the parent compound. Conversely, the potency of pterostilbene,

desoxyrhapontigenin and pinostilbene towards CYP1B1 with Ki values of 0.90, 2.06 and 0.91 µM, respectively. Inhibition of CYP1A1 and CYP1B1 catalytic activity by RES analogues can occur regardless of the number and position of hydroxyl groups substitution. The results propose that the RES analogues: pinostilbene, desoxyrhapontigenin and pterostilbene, might be considered as promising chemopreventive agents (Mikstacka et al., 2007).

1.2.2 (V) RES as Nutraceutical

Resveratrol in its free form or its plant sources like Japanese knotweed have been incorporated in a considerable quantities in herbal preparations with varied therapeutic indications including relief from menstrual discomfort and relaxing muscles and joints (Ghaedi et al., 2014). Various brands are commercially available for resveratrol as nutraceutical. Products comprise pure resveratrol capsules or other phytochemicals and multi-ingredient formulations with standardized amounts of resveratrol. Fourteen brands of resveratrol-containing nutraceuticals were assessed in order to validate their actual resveratrol content, and to control if their health-promoting properties are associated to manufacturing quality. Samples were analyzed for total *trans*-resveratrol, flavonoids and the polyphenol content and were compared with the content declared on-label. Out of 14 brands only five met the label values requirements (95–105 % content of active constituent), three were in the 8–64% range and four products were slightly, out of this range (83–111 %). Two of these samples were below the limit of detection (Smith and Hunneyball, 1986).

On the other hand, the solid forms presented very poor water solubility, the liquid forms often made use of excipients well-known to have a predictable action or effect (i.e propylene glycol and ethanol). In recent years, numerous studies have focused on novel formulation in order to improve the stability and protect resveratrol from degradation and breakdown, increase its solubility in water and thereby improving its bioavailability, and achieving Modified Release (Amri et al., 2012).

1.2.2 (VI) Bioavailability, absorption and metabolism of RES

A major limitation of resveratrol is its associated limited bioavailability, which is a major negative impact upon the latent clinical usage of resveratrol in the treatment of cancer. *In vivo,* resveratrol is absorbed via the gastrointestinal tract and is promptly metabolised into its glucuronides, sulfates, and hydroxylates. In humans, resveratrol metabolites include; 3- and 4'-O-sulfate, and 3-O-glucuronide conjugates, which are present less than two hours following ingestion (Park et al., 1997). It is also noted

that intestinal bacteria are involved in the metabolism of resveratrol, acting as varying factor in observed fractional ratio of metabolites amongst individuals. The ability of gut microflora to metabolise resveratrol into the following metabolites; dihydroresveratrol, 3,4'-dihydroxy-transstilbene and 3,4'-dihydroxybibenzyl has also been noted (Park et al., 2001). However, worryingly when examining the pharmacokinetic profiles of resveratrol in healthy volunteers, rapid metabolism of the compound was observed whether single or multiple doses were given. This presents a problem as it leaves an exceptionally narrow window for resveratrol to act upon cancer cells irrespective of dose. Ongoing efforts are hence being focused upon slowing the metabolism of the compound, to allow time for the drug to act. The use of synthetic analogues of resveratrol in order to manage the rapid metabolism of resveratrol (Park, 2002).

As a consequence of the rapid metabolism of resveratrol into its resultant metabolites; researchers pose the possibility that resveratrol metabolites may also possess biological activity, with an indication that specific metabolites such as resveratrol 3-sulphate may also harbour chemo-preventative effects. Research has demonstrated that the body is able to both absorb resveratrol and its resultant metabolites, through various sections of the gastrointestinal tract. Remarkably, once these metabolites are found to reach a tissue level, many of the metabolites are found to possess the ability to regenerate into the original resveratrol molecule. The result, is enhanced penetration of resveratrol and its metabolites into targeted tissues, increasing the chances of an anti-cancer response (Park, 2002).

1.2.2 (VII) Resveratrol Delivery Challenges

Although the anticancer effects of RES have been demonstrated, its clinical application is limited because of a low bioavailability and a rapid clearance from the circulation (Walle et al., 2004). Despite high bioactivity of resveratrol poor water solubility, low oral bioavailability and high chemical instability poses major challenges for its therapeutic delivery. Its poor aqueous solubility is unfavorable for incorporation of high levels of resveratrol in aqueous based pharmaceuticals. In addition, low water solubility reduces the dissolution-rate limited cell absorption (Wenzel and Somoza, 2005), leading to reduced oral bioavailability due to rapid and extensive metabolism. Because of the poor bioavailability of resveratrol, the concentrations of resveratrol at target tissues and cells appear far from sufficient to exhibit efficacy in humans. Studies have shown that the oral absorption of resveratrol appeared to be at least 75 %; however the bioavailability was poor on account of the rapid and extensive metabolism (Walle, 2011). Resveratrol, whose half-life is only 8–14 min, has been found to be quickly metabolized into sulfate and glucuronide metabolites in liver and intestinal epithelial cells in human which appears

to be the rate-limiting step in resveratrol's bioavailability (Lherm et al., 1992).

In addition to the photo-stability issues trans-resveratrol is easily oxidized, and show unfavorable pharmacokinetics (Zhang et al., 2016b). Therefore, successful clinical application, therapeutic or prophylactic of resveratrol is a difficult challenge for the medical and pharmaceutical technology. Researchers have trailed different methods to increase the solubility and bioavailability, including co-administration of inhibitors of *trans*-resveratrol metabolism, searching for analogs and explanation of new *trans*-resveratrol delivery systems (Jenning et al., 2000a).

The therapeutic potential of RES can be realized *in-vivo* only if the limitations tied to its bioavailability are overcome (Amri et al., 2012). Also a study of its formulations for targeting delivery to cancer cells is highly desirable. A number of nano-formulations such as nanoemulsion (Sessa et al., 2014) SEDDS have been studied in order to optimize the bioavailability of encapsulated drug for potential oral administration, however there are no reports on RES for targeted delivery to prostrate or breast cancer. Resveratrol is prone to chemical degradation when exposed to high temperatures, pH changes, light and certain enzymes. The chemical degradation often involves the isomerization of RES to cis form on exposure to UV light and therefore this can lead to loss of bioactivity after isomerization. Another factor limiting the bioavailability and bioactivity of RES is its tendency to undergo first pass metabolism after ingestion, e.g., glucoronide and sulfate conjugates are rapidly formed in the human body (Davidov-Pardo and McClements, 2014).

1.2.2 (VIII) Approaches for Overcoming Delivery Challenges of Resveratrol

Nanotechnology provides avenues for improving the properties of pharmaceuticals and enable their efficient delivery. Encapsulation of resveratrol can be employed to improve its water-solubility, chemical stability, and enhancing its bioavailability (Muller et al., 2000a). Several encapsulation technologies exist that may be able to overcome the challenges associated with employing resveratrol as a bioactive agent in pharmaceuticals**.** In particular, emulsion-based delivery systems has shown as a promising encapsulation technique due to the fact that lipophilic compound can be encapsulated within the hydrophobic core of the lipid droplets where they will be protected from degradation during storage until they are released after ingestion (Uner, 2006). However, it is important that factors for processing it as pharmaceutical should be borne in mind during development. This includes use of safe excipients; Generally recognized as safe (GRAS), robust and commercially viable production process, favorable organoleptic properties in terms of taste and flavor, and reasonable shelf life.

Whilst there are constantly compounds being discovered and tested for therapeutic effect, the importance of a suitable drug delivery system which is able to deliver the active ingredient without detriment to the compound, in adequate, as well as being site specific and biodegradable is extremely high, and also a challenging demand to fulfill. Nevertheless, irrespective of compound efficacy, drug delivery systems play a pivotal role facilitating drugs reaching a desired target

Drug delivery systems that are based upon nanoparticles is an area of research which has received considerable attention. This is demonstrated by 75 % of scientific publications within the field of nanomedicine being dedicated to this topic. The development of a drug delivery system which is able to transport with precision and specificity a drug to a given target is an area of constant interest; as this may open up the possibility of enhancing not only the performance of new novel compounds, but also traditionally used compounds. Whilst many compounds may be efficacious in treating given disease states, solubility of the compound is often a drawback, as this limits gastrointestinal absorption and subsequent bioavailability. Whilst many strategies have been employed to improve solubility i.e. crystal modification, particle size reduction, pH modification and amorphization. In accordance with the Biopharmaceutics Classification System (BCS), drugs may be broadly categorized under four classes (class I, II, III, and IV) based on their solubility and permeability. Particulate lipid based delivery systems are a common solution to this problem based on their solubility and membrane permeability offering a modified and targeted release property , enhanced stability biodegradability and biocompatibility; versatility of excipients and formulations; and low risk profile; these systems are of great interest (Choi et al., 2016)For BCS class II drugs such as resveratrol, dissolution is identified as the rate-limiting process to their gastrointestinal absorption and bioavailability.

1.3 Nanoparticles as drug delivery systems

Essentially, a nanoparticle drug delivery system is comprised of a therapeutic agent encapsulated in nanoparticle platform. Some of the potential issues experienced by novel compounds such as Resveratrol i.e. rapid metabolism may be remedied by encapsulation in such particles. The key purpose behind a nanoparticle drug delivery system is to allow administration of the API via controlled delivery, so that an adequate concentration of drug reaches the target site, in turn leading to increased efficacy of treatment and also boosting patient compliance. Drugs which have been deemed inappropriate (i.e. those associated high toxicity, high dosage requirements, poor solubility and short circulation times *in vivo*) may also benefit from formulation into these drug delivery systems. Several key advantages

associated with nanoparticle drug delivery systems include: targeted delivery, increased bioavailability, protection from degradation and also modify the drug release.

1.3.1 Nano-carriers as potential drug delivery systems in cancer therapy

Without the aid of targeting conventional therapeutic agents may distribute within the body without specificity, impacting upon normal healthy cells in addition to target cells. The overall effect is a reduced therapeutic dose reaching target cells, followed by lack of therapeutic effect, however with excessive toxicity (Hryniuk et al., 1987).

Drug carriers have been able to reduce the toxicity of therapeutic agents, allowing selective targeting of cells without detriment to healthy cells. Drug carriers however are not without their pitfalls, including: instability in blood circulation, undesirable bio-distribution, their own toxicity and lack of oral bioavailability

1.3.2 Types of Nanostructure utilized in cancer therapy

Nano-carriers such as polymeric nanoparticles, solid lipid nanoparticles, magnetic nanoparticles, dendrimers, liposomes, micelles, quantum dots, etc (Figure 1-6) were extensively explored for cancer diagnosis, treatment, imaging, and as ideal vectors to overcome drug resistance by diverting ABC-transporter mediated drug efflux mechanisms (Ayers and Nasti, 2012). Designing drugs with higher cell specificity reduces adverse effects and improves efficacy. Thus, various types of nano-carriers have been developed such as solid lipid nanoparticles, dendrimers, liposomes and radio controlled nanoparticles (Surendiran et al., 2009).

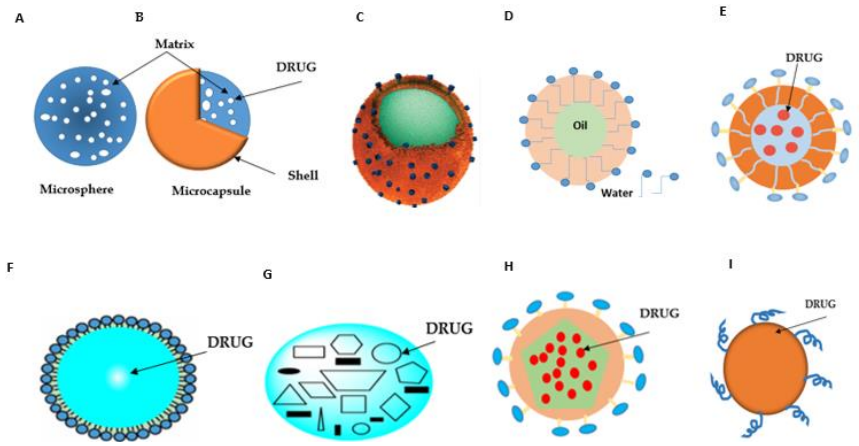

Figure 1-6 Drug delivery systems A) Microspheres B) Microcapsules C) Nanosponges D) Nanoemulsions E) Liposomes F) Solid lipid nanoparticles G) Nanostructured lipid carriers H) Polymeric Nanoparticles I) Nano-suspensions

It is clear that the size of particulate based drug delivery systems is also a contributing factor to formulation properties observed, with small particles (1-30 nm) being cleared rapidly by the kidney. Particles which are in excess of 30 nm are cleared by reticuloendothelial systems. Moreover, particles made from materials which are biocompatible are also highly sought after, as a consequence, amongst the goals of particulate based formulations, lipid nanoparticles have received significant and increasing attention (Muller et al., 2002a).

1.3.3 Solid lipid nanoparticles

The terms lipid nanoparticles is encompassing of subtypes which include solid lipid nanoparticles (SLNs) and nanostructured lipid carries (NLCs). The first solid lipid nanoparticles were formulated from a lipid matric, which was solid at body temperature and stabilized using surfactants (Muller et al., 2000b)

Solid lipid nanoparticles (SLN) were introduced at the beginning of the 1990s as novel nanoparticulate delivery systems produced from solid lipids, as good alternative carrier systems to emulsions, liposomes, and polymeric nanoparticles. The main advantages of the later delivery systems includes physical stability, confer protection to the incorporated sensitive drug from degradation, controlled release, and excellent tolerability (Souto et al., 2004). Interestingly, lipid nanoparticles have been observed to demonstrate successful drug delivery to several forms of cancer (Calixto et al., 2014).

Resveratrol SLNs (RES-SLNs) prepared by the solvent emulsification-evaporation method have resulted in spherical shape particles with an average particle size of 96.7 nm, drug loading of 7.95 +/- 0.21 %, zeta potential -16.3Mv. Crucially the entrapment efficiency has been demonstrated to be approximately 91.34 +/- 0.18%. RES-SLNs with high entrapment efficiency, drug loading and uniform

particle size, exhibited the ability to prolong drug release *in-vitro* and enhance anticancer effect (Zhang et al., 2010a).

In another study solid lipid nanoparticles (SLNs) of resveratrol have been prepared through melt-emulsification process with glyceryl behenate, poloxamer 188 and hydrogenated soybean lecithin, yielding particles with a size and loading capacity of 180 nm and 85%, respectively. Study findings showed that SLNs resveratrol was released in a slow manner. It was also observed that the use of SLNs as resveratrol carriers protected the keratinocytes against the cytotoxic effects induced by resveratrol alone (Wang et al., 2017).

There are many advantages noted for lipid nanoparticles as a whole including ease in scale up of manufacture process to an industrial level, obviation of organic solvents, biodegradability, GRAS status (broadly recognised as safe), prior usage of similar particles in cosmetics products and the ability to produce concentrated suspensions (Mehnert and Mäder, 2001). Equally, there a number of notable disadvantages, including poor loading capacity, drug expulsion as well as a high water content required upon storage (70-99.9%) (Jenning et al., 2000a).

1.3.4 Nanostructured lipid carriers

NLCs may be described as the next generation of lipid-based colloidal carriers, which unlike SLNs are comprised of a mixture of solid and liquid lipid resulting in a lipid matric which is solid at room and body temperature. Unlike SLNs, NLCs possess liquid voids which allow for enhanced accommodation of API i.e. higher entrapment efficiency of the drug inside the nanoparticles(a pitfall of SLNs). The potential problems associated with SLNs are limited drug loading capacity and potential drug expulsion during storage are minimised by new generation nanostructured lipid carriers (NLCs). The introduction of NLCs solved drug expulsion problems together with the drug-loading problem, as NLCs having imperfect crystals allowing more drug incorporation in the lipid matrix (Pardeike et al., 2009, Kamble et al., 2012). However, NLC stability is strongly affected by the type and the amount of liquid oil used. Dispersion stability is enhanced when the oil concentration is increased which leads to a decrease in the crystallization and melting point, an increase in the rate of polymorphic transformation which results in particles having greater sphericity, thus, particles retrain their sphericity over long period of time; accordingly, suspension stability is enhanced.

An attempt to improve the encapsulation efficiency and the drug loading of lipid nanoparticles by mixing the solid lipid with a liquid carrier oil to form NLC upon cooling of the nano-emulsion produced after hot homogenization process (Jenning et al., 2000d). However, some studies suggests that the

modification of the solid lipid matrix by incorporating lipid oil improves loading capacity, physical and chemical stability (Yang et al., 2014).

The higher entrapment efficiency associated with NLCs is attributed to higher drug solubility in liquid lipid as opposed to solid lipid. Moreover, their associated enhanced stability offers a distinct edge when compared to alternative lipid carriers. This is in addition to the ability of incorporating hydrophillic and hydrophobic compounds (Bhaskar et al., 2009, Poonia et al., 2016).

Nanostructured lipid carriers (NLCs) loaded with resveratrol prepared by a modified hot homogenization technique to enhance its oral bioavailability. Morphologic microscopy studies showed spherical and uniform nanoparticles with a smooth surface. Resveratrol entrapment efficiency of ∼70% was obtained. The dynamic light scattering measurements gave a Z-average of 150–250 nm, polydispersity index of ∼0.2, and a highly negative zeta potential of around −30 mV with no statistically significant differences in the presence of RES. These characteristics stayed unchanged for at least two months, demonstrating good stability. Results show that resveratrol remained mostly associated with the lipid nanoparticles after their incubation in digestive fluids. NLCs were found suitable carriers for oral administration, allowing protection to the incorporated resveratrol and conferring a Modified Release (Neves et al., 2013).

1.3.4 (I) Mechanism of NLCs disposition

The journey of NLCs upon delivery is interesting; upon digestion, they undergo lipid digestion with triglycerides in the nanoparticle cleaved into monoglycerides and free fatty acids, through the action of pancreatic enzymes in the duodenum. The carriers may then undergo passive or active transport. Alternatively or additionally, bile salt molecules in intestinal chyme form micelles around the carriers, which allow passing through absorptive layer in the gut (Figure 1-7). The particles size of NLCs is also believed to play a crucial role in intestinal transport i.e. a size below 300nm is desirable in transport across the intestine (Poonia et al., 2016).

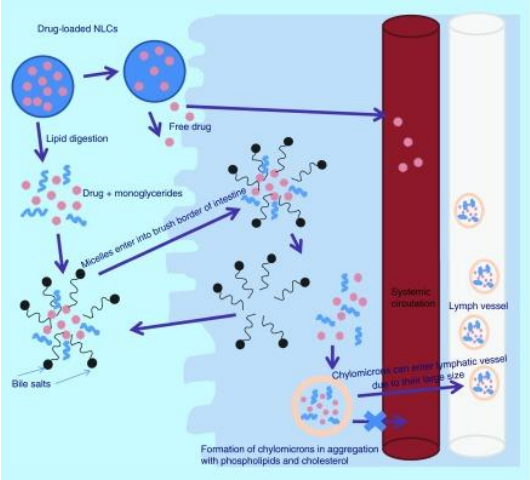

Figure 1-7 Mechanism of nanostructured lipid carriers disposition through the gut membranes. Copied without permission form (Poonia et al., 2016)

1.3.5 Tumor targeting and vasculature permeability

There are many types of drug targeting strategies which aim to increase the therapeutic effect of drugs and minimise the side effect profile, in addition to reduction of cytotoxicity to neighbouring cells.

Passive targeting (Figure 1-8), refers the tendency of therapeutic agents to accumulate in target tissues in accordance with physiochemical/pharmacological aspects of the condition. Due to the higher metabolic demand associated with cancer cells, pores exhibiting enlarged gap junctions between endothelial cells allow for enhanced permeability drug molecules into the tumour tissue. Once tumour cells accumulate to form a tumour of a certain size, normal vasculature remains no longer sufficient to meet the oxygen demand for further proliferation. At this point, cells begin to die, which triggers growth factors which signal the formation of new blood vessels, a process known as angiogenesis. The problem however, is that these blood vessels are also abnormal containing discontinuous epithelium and lacking a basal membrane, typical of normal vascular structures (Freitas and Müller, 1999).

In normal tissues, there is a constant flow of extracellular fluid into the lymphatic vessels; allowing for renewal of interstitial fluid and recycling of extravasated solutes and colloid back into circulation. This mechanism is defective in tumours; only molecules smaller than 4 nm are able to diffuse back in blood circulation and be reabsorbed. Due to this size restriction, it is difficult for nanoparticles to be cleared (Bar-Zeev et al., 2017).

This aspect represents the enhanced retention component of the EPR (enhanced permeability retention) effect. Since the early works of Matsumura and Maeda in the mid-1980s, the EPR effect has been comprehensively documented using various tumour types and animal models; allowing greater

comprehension of the subtleties of the EPR effect and also providing an insight into potential issues in treatment such as nanoparticles accumulation (Bertrand et al., 2014).

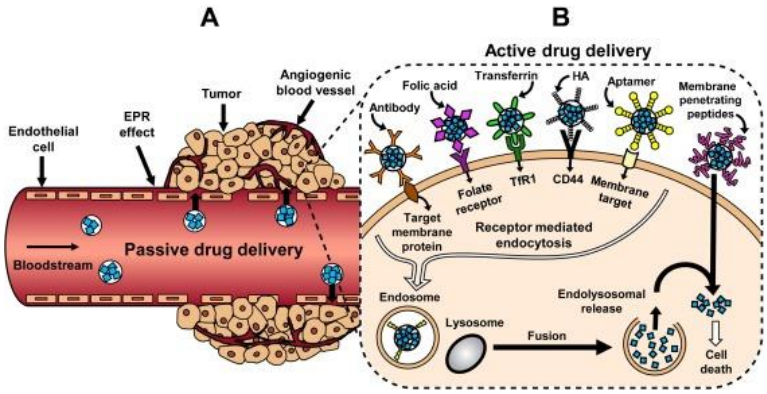

Figure 1-8. Drug targeting strategies: A. Passive drug delivery via EPR effect and B. Active drug delivery mechanisms. Copied without permission from (Bar-Zeev et al., 2017)

Active targeting refers to the usage of targeting of tissues via carriers in order to overcome boundaries such as mucosa. In addition to usage of carriers these may be modified with attachment of ligands or antibodies to enhance targeting of specific disease site tissues and cells (Khodabandehloo et al., 2016). The key goals of NLC formulations are to retain chemical reactivity in addition to targeting. In designing of the NLCs there are several considerations, which are made, these are: that the formulation is able to penetrate membranes to reach the target site, that the carrier is able to avoid the bodies protective mechanism (i.e. opsonization and reticuloendothelial clearance) and that the formulation is able to recognize environmental changes. Modification of NLCs typically involves functionalization of the particle surface with molecules which are responsive to various stimuli (i.e. redox, enzyme, and pH, or exogenous factors such as light, ultra sound, and magnetic fields, or to temperature). Surface functionalization may also inadvertently influence the product half-life, biocompatibility and therapeutic scope, particularly when polymers are used (Lippacher, 2001).

Modification of NLCs including PEGylation may offer enhanced circulation times and also protection enzymatic degradation. Other examples of modification include usage of folic acid. Folic acid binds to folates which are receptors overexpressed on breast cancer cells. As a consequence folate targeted systems i.e. carriers with PEG and folate have been used to improve cell targeting and tumour penetration. Alternatively hyaluronic acid has also be used as a coating layer on nanoparticles due to its histo and cyto-compatability and high binding capacity to the $CD44^{++}$ receptors overexpressed on the breast cancer cells (Siafaka et al., 2016a).

In summary, cancer as a disease state remains at the forefront of conditions resulting in significant morbidity and mortality. In the female populace, breast cancer is prevalent disease state, and despite many treatment options is a notable cause of mortality. Current treatment regimes, which utilize combinations of chemotherapeutic agents, suffer from poor patient concordance to due to an overexpressed side effect profile. However, single novel chemotherapeutic agents alone, such as resveratrol, whilst effective, are limited in terms of delivery to the targeted site due to pertaining physiochemical limitations.

To this end, the introduction of particulate-based drug delivery carrier systems in the nano range, have been fruitful in enhancing the scope of single chemotherapeutic agents. However, pitfalls associated with earlier less sophisticated carrier systems i.e. liposomes and SLNs have prompted the development of NLCs, which do not suffer from the same disadvantages. Thus the potential offered by NLCs in terms of drug delivery and the noted activity of resveratrol as a chemotherapeutic and chemopreventative agent provide sufficient scope for research in the treatment of breast cancer.

1.4 Aim and objectives of the project

1.4.1 Aim

To develop a nanoparticulate drug delivery system of resveratrol to overcome its physicochemical and pharmacokinetic limitations and impart suitable functionalities for targeting breast cancer cells.

1.4.2 Specific objectives

- The preparation of RES nanostructured lipid carriers systems (RES-NLCs) to offer protection, improve oral-bioavailability, modify the release of the drug form the carriers and impart targeting functionalities toward breast cancer cell lines.
- The development and optimization of RES-NLCs employing the quality by design approach, whereby critical quality attribute are determined and studying the effect of various variables on the desired outcome or response variables.
- Carrying out physicochemical characterization of the developed RES-NLCs, to determine the particle size, zeta potential, the morphology and to understand the interactions between RES and the components of the formulation using differential scanning calorimetry, x ray diffraction and Fourier transfer infrared studies.
- Undertake stability studies for the formulated RES-NLCs, at various storage conditions in order to select the most stable formulation and take it for further surface modification.
- Functionalization of the selected RES-NLC with targeting ligands hyaluronic acid; HA-NLCs, folic acid; FA-NLCs and dual targeting system using both hyaluronic acid and folic acid; HAFANLCs, and optimization of ligand density and quantify the amount of amine groups present on the surface on RES-NLCs.
- The efficacy of RES-NLC and functionalized RES-NLC was determined on various breast cancer cell lines entailed: MCF-7, MCF-10A and MDAMB-231 cells.
- To evaluate the cellular uptake, mechanisms of internalization, apoptosis and cell cycle of RES-NLCs on MCF-7, MCF-10A and MDAMB-231 cells.
- To study the cellular uptake, mechanism of internalization and conduct bidirectional permeability study across Caco-2 monolayer and Caco-2/HT29 co-cultures to evaluate the transport of RES-NLCs.

Thesis Outline

Chapter 1: An introduction to cancer, prevalence and some statistics. Also a brief introduction on resveratrol delivery challenges and its potential in cancer treatment, the development of Nanostructured Lipid Carriers (NLCs) as drug delivery systems and finally the employment of concepts of target-ability to cancer cells and various ligands were all included in this chapter.

Chapter 2: Described the analytical method development and validation to allow the accurate quantification of the drug concentration in various substrates throughout all the studies and undertaken assays.

Chapter 3: Outline the optimization and the development of nanoparticles employing design of experiments approach. In addition, Chapter 3 looks through various physicochemical characterizations of optimized formulations. Finishing with a broad overall stability studies to select the best formulation to enable surface modification with various ligands to achieve the target-ability towards breast cancer cells. These surface modified formulations were characterized with different techniques.

Chapter 4: *In vitro* cell lines studies of the developed resveratrol nanostructured lipid carriers along with the surface modified formulations were carrier out to determine the anticancer potential of the formulated nanoparticles. Cytotoxicity studies of six different resveratrol formulations on different cell lines were investigated to determine the efficacy on cancer cells and the safety on healthy cell lines. The ability of formulations to undergo efficient intracellular delivery was studies by uptake studied and various cellular uptake mechanisms were employed to understand the different cellular pathways involved in the cellular uptake of nanoparticles, this was evaluated by both quantitative and qualitative techniques, cell death assays and cell cycle assays were also included in this chapter.

Chapter 5: Describes the cellular permeability across Caco-2 cells monolayer and caco-2/HT29 co-cultures, determining the difference in the permeability of various formulations. Finally heamocompatibly assay for all formulations was undertaken to prove the safety of the formulations.

Chapter 6: Concludes the achieved thesis aims and proposed future work with the previously mentioned nano-carrier systems.

Chapter 2 : Analytical Method Development

2.1. Introduction

The following chapter outlines experiments conducted to develop and validate a High Performance Liquid Chromatography (HPLC) analytical method for identification and quantification of the chemotherapeutic agent Resveratrol in various media. The purpose behind this is to assist in further experiments involving the active agent.

2.1.1 Analytical method validation

A validated High Pressure Liquid Chromatography (HPLC) analytical method is considered a critical factor in the development of pharmaceutical drug substances and alternative drug products, with emphasis placed upon ensuring that the methods employed in the analysis of products generate useful data. Thus, the United States Pharmacopeia (USP) (Rockville, 1999) and US Food and Drug Administration (FDA) (FDA, 1994) has emphasized the importance of this in drug development process, and have raised validation requirements criteria (Renger, 2000). Moreover, the International Conference on Harmonization (ICH) (ICH, 1995), have supplemented to the two aforementioned resource validation method requirements, setting a high precedent for companies to comply with (Shabir, 2003).

During the course of development of resveratrol Nanostructured Lipid Carriers (RES-NLCs), drug content has to be quantified in different Medias and solvents. Therefore, this chapter details the analytical method development used for the estimation of the drug in various substrates during the course of this study.

In order to fully characterize the RES-NLC formulations, an appropriate and validated method is necessary for the critical assessment of pharmaceutical parameters, including: percent entrapment efficiency (% EE) and percent total drug (%TD). A validated HPLC method was developed for the determination of both percent entrapment efficiency (% EE) and percent total drug (%TD), utilising two different standard curves. HPLC methods were also developed and validated in various pH buffers, required for the determination of drug stability in various media. Moreover, an analytical HPLC method for quantifying RES in different dissolution media was developed to determine the concentration of drug released from NLCs. Finally, a HPLC method was developed for the analysis of resveratrol in Hank's Balanced Buffer Solution (HBSS) employed in the bidirectional Caco-2 cell line study.

2.2. Equipment

A UV light cabinet (Uvitec, UK), oven incubator with controlled temperature and humidity (75%) was employed for FDS (Forced Degradation) studies (memmert, Atmosafe, Germany). UV-VIS spectrophotometer (Jenway,UK). Benchtop Spectrafuge 24D was obtained from Jencons-Pls, UK .The High Pressure Liquid Chromatography (HPLC) system (Agilent 1260 Infinity HPLC instrument Agilent Technologies, USA). This system is equipped with a quaternary pump an autosampler, an online degasser, a column compartment with temperature control and photodiode array wavelength detector (PDA). The apparatus was connected to a personal computer with a Data acquisition, analysis and reporting software OpenLAB CDS CS Workstation Agilent Technologies for HPLC data processing.

2.3. Materials

Resveratrol (RES) was purchased from Manchester organics. UK, purity >97 %. HPLC solvents (Acetonitrile, Tetrahydrofuran, Dimethyl sulfoxide and water) all solvents were of HPLC grade, potassium chloride, hydrochloric acid, acetic acid, potassium hydroxide, potassium dihydrogen phosphate, disodium dihydrogen phosphate, monobasic potassium phosphate and sodium hydroxide were purchased from Fisher Scientific. UK, HPLC vials were purchased from Fisher Scientific, filter device 0.22 µm pore size filter (VWR, UK), Hanks balanced buffer solution (HBSS) was obtained from Sigma Aldrich, UK. All other reagents were highest purity commercially available.

2.4. HPLC method development

The objective of any analytical measurement is to obtain consistent, reliable and accurate data. Validated analytical methods play a major role in achieving this goal. The results from method validation can be used to judge the quality, reliability and consistency of analytical results, which is an integral part of any good analytical practice. Validation of analytical methods is also required by most regulations and quality standards that impact laboratories (ICH Harmonized Tripartite Guideline and Methodology Q2 (R1). 2005).

Resveratrol exists as *trans* and *cis* isomers. The *trans* isomer occurs in plants and fruits, low concentrations of the *cis* isomer are present in red wine; it is proposed that the *cis* isomer is a resultant product from the isomerization from the *trans* isomer, during the fermentation process in grapes (Goldberg et al., 1996, Singh et al., 2012). However, few analytical methods have been identified for

the determination of resveratrol (RES) in nanoparticles. HPLC-UV/Vis methods (Gokce et al., 2012) and UV-Vis spectroscopy (Teskač and Kristl, 2010, Neves et al., 2013) have been developed for such purpose; nevertheless, these chromatographic techniques have not been fully validated, with only reports on the mobile phase and other basic chromatographic parameters.

In order to be able to discriminate between the *cis* and *trans* resveratrol, the aim was to develop an accurate, precise and repeatable HPLC method allowing the quantification of both isomers in an analyte sample.

2.4.1 Chromatographic condition

Chromatographic analysis was conducted using a reverse phase Luna C18 column (Phenomenex) with 5 µm particle size, 4.6 mm internal diameter and 250 mm length. The analysis was performed in gradient elution, where two solvents were used in combination as a mobile phase for separation; where solvent A was Acetonitrile and solvent B was Water; with a flow rate of 1 mL/min and injection volume of 20 µL.

The elution profile with a total run time of 15 min was as follows: 0 min, 10% A and 90% B; 13 min 85% A and 15% B; 15 min 10% A and 90% B. Elute was monitored at two different detection wave lengths 286 nm and 306 nm, where the absorbance maxima of *cis* and *trans*-RES isomers are observed, respectively. The column temperature was maintained at 25^{o}C, and the system was equilibrated with mobile phase for 1 h prior to sample injection.

2.4.2 HPLC method development for the determination of % Entrapment Efficiency of RES in NLCs

The free drug was isolated from the formulation by using ultrafiltration units along with centrifugation. Ultracentrifugal filter (Amicon Ultra-0.5, Millipore) with a molecular weight cutoff of 3 kDa (KiloDaltons) was used. A 0.5 mL lipid nanoparticles suspension was transferred into the upper chamber of the centrifuge filter, which was centrifuged at 13000 rpm (revolutions per minute) for 60 min at room temperature. The ultrafiltrate was then analyzed using the developed HPLC method.

2.4.2 (I) Preparation of standard solutions for calibration curve

RES standard stock solution was prepared by accurately weighing 5 mg in 100 mL volumetric flask diluted with acetonitrile: 0.1 % formic acid in water mixture (50:50, v/v) producing concentration of 50 µg/mL, and subsequent dilutions was carried out to obtain eleven working dilutions (0.1, 0.2, 0.4, 0.6, 0.8, 1, 2, 4, 6, 8 and 10 µg/mL). Prior to injection, samples were filtered through a 0.22 µm pore size filter (VWR, UK). 20 µL of sample was injected.

2.4.2 (II) Method validation

The HPLC method was validated in terms of linearity, range, sensitivity (limit of detection and limit of quantification), precision and accuracy (intra-and interday), specificity, robustness and solution stability. Validation of the analytical method was carried out according to the International Conference on Harmonization guidelines [Q2 (R1)] (ICH, 2005).

2.4.2 (III) Linearity and range

The ICH defines linearity of an analytical procedure as its ability (within a given range) to attain results that are directly proportional to the concentration of analyte in the sample. Linearity may be determined by dilution of a standard stock solution or by separately weighing synthetic mixtures of the tested products (ICH, 2005). The linearity can be evaluated graphically, as alternative to mathematical evaluation. The evaluation is done by plotting the peak area as a function of analyte concentration.

The range of an analytical method is the interval between the upper to the lower levels demonstrated to be determined with precision, accuracy and linearity using the HPLC method. The range is usually expressed in percentage or parts per million units that are obtained by the analytical method.
Calibration curves were constructed using eleven standard solutions of RES ranging from 0.1 to 10 µg/mL, by plotting the peak areas against RES concentration. Data collected was processed using Microsoft Excel with linear regression by the least square method employing the following formula (He et al., 2006). Where *Y* is the peak area ratio of drug, m (the slope) and *b* (the *y*-intercept) are constants, and *X* is the *trans*-resveratrol concentration (µg/mL).

$$\boldsymbol{Y = mX + b}$$

Equation 2-1 Linear Regression

2.4.2 (IV) Sensitivity

The limit of quantification (LOQ) is defined as the lowest concentration on the calibration curve which could be detected with a variation of less than 15 % (He et al., 2006).

The limit of detection (LOD) and limit of quantification (LOQ) were determined by measuring the analytical background response i.e. as the LOQ concentration level decreases, the precision increases, (Shimada and Fujii-Kuriyama, 2004). Signal-to-noise ratio was employed to determine the LOD and LOQ. LOD and LOQ were considered to be 3 and 10 times, above the baseline noise, respectively. LOD and LOQ were established using eleven standard solutions from 0.1 to 10 µg/mL. The following equations were used in accordance to the ICH guidelines:

$$\boldsymbol{LOD = 3.3x\sigma/S}$$

Equation 2-2 Limit of Detection

$$\boldsymbol{LOQ = 10x\sigma/S}$$

Equation 2-3 Limit of Quantification

Where σ is the standard deviation of the intercept/response and S is the slope of the calibration curve (Pangeni et al., 2015).

2.4.2 (V) Precision and repeatability

The analytical method is deemed to be precise if it is both repeatable and reproducible, determined by the percent relative standard deviation of the sample (%RSD (Relative Standard Deviation)). The repeatability of the method was determined as per the ICH guidelines; where the intra-day precisions of the analytical method was determined from a minimum of nine determinations of three different standard solutions (0.2, 2, 10 µg/mL, n=9) during the same day under the same experimental conditions. According to the FDA repeatability assessment may be done with a minimum of 10 injections of one sample solution is made with same chromatographic instrument (Shabir, 2003)

The interday precision (intermediate precision) results from within-lab variations such as different day, equipment and analysts variations, was evaluated by testing three different standard samples (0.2, 2, 10 µg/mL, n=3) on three separate days. Results were reported as averages ± standard deviation (SD) and the percent relative standard deviation (% RSD).

2.4.2 (VI) Accuracy

Accuracy of analytical method may be described as the closeness of the data obtained by the analytical method to the actual value. ICH guidelines recommend the collection of data over a minimum of three concentration levels covering the specified range with a minimum of nine determinations (for example, three concentrations and three replicates each). It was calculated by using the recovery method using the following formula:

$$Accuracy = \frac{\text{Calculated results}}{\text{Actual results}} \times 100$$ **Equation 2-4 Recovery Method**

2.4.2 (VII) Specificity and selectivity of HPLC method

The specificity of an analytical method is an indication of how precise the analyte response in the presence of all other sample components such as lipids, surfactants and solvents used is measured.
Specificity of the analytical method was evaluated by comparing the relative chromatograms of samples containing potentially interfering/obscuring substances i.e. the excipients used in NLCs preparations, RES has another isomeric form, the *cis* isomer. For the method to be specific for *trans*-resveratrol the ability to separate both analyte peaks.

2.4.2 (VIII) Robustness

Robustness enables the measurement of the influence of small change in the analytical procedures/parameters on the response (Peak area). A method is deemed to be robust only when the results of HPLC are not affected by small variations/minor adjustments in chromatographic method parameters. This may be evaluated by varying method parameters such as mobile phase compositions, column temperature and flow-rate etc (Shabir, 2003).
Robustness was evaluated by varying the temperature of the analytical column (24^{o}C, 25^{o}C and 26^{o}C), flow rate (0.99, 1 and 1.01 mL/min) and wave length (305,306 and 307 nm). One concentration (10 µg/mL) in triplicate was employed for testing the robustness of the method.

2.4.2 (IX) Stability of analytical solutions

Stability testing is important for estimating the allowed time span between sample collection and sample analysis. It is also important to evaluate an analytical method's ability to measure drug products in the presence of its degradation products

The stability of standard stock and working standard solution, must be determined prior to starting method validation studies in order to produce reliable and reproducible results. Prepared solutions should be sufficiently stable to allow for delays such as overnight analyses or instrument breakdowns, in order to determine the stability of solution. Selected concentration (6 µg/mL) from the calibration curve concentration range was injected in triplicate over the period of one month. The solution stability was used to determine the suitability of the method in the determination of the analyte concentration with time. The solutions were kept at 2-8^{o}C.

2.4.3 (X) HPLC method development and validation for the determination of % Total drug in NLCs

HPLC method was developed for detection of total drug in the NLCs. lipids used are insoluble in the mobile phase, therefore in this method tetrahydrofuran (THF) was used to dissolve the lipids. An alternative new HPLC method was developed using different diluent which could dissolve both the drug and the excipient of the NLCs. However, the mobile phase composition was kept the same.

Drug entrapment efficiency was determined indirectly by measuring the total drug in the formulation and the free drug in the aqueous phase of the nanoparticles dispersion.

A. Preparation of stock and working solutions for calibration curve

RES standard stock solution prepared by accurately weighing 5 mg in 10 mL volumetric flask diluted with acetonitrile: 0.1 % formic acid in water mixture (50:50, v/v) producing concentration of 500 µg/mL, and subsequent dilutions were carried out to obtain six working standard solutions necessary for plotting the calibration curve (1, 2, 4, 6, 8 and 10 µg/mL). Prior to injection, samples were filtered through a 0.22 µm pore size filter (VWR, UK). 20 µL of sample was injected.

The method was validated in a similar manner as discussed previously in section 2.4.2 (I) for linearity, sensitivity, precision, repeatability, accuracy, robustness and analytical solution stability.

2.4.4 Forced Degradation Studies

Forced degradation studies were performed in order to evaluate the specificity of the method. These studies were undertaken to deliberately degrade the sample and provide information on the stability of the sample under stress conditions. The objective of these studies was to develop a method for quantitative analysis of RES which additionally indicated stability. Forced Degradation of RES was

achieved by subjecting the drug to extreme conditions of acid, base, oxidation and heat (Blessy et al., 2014). ICH guidelines propose that forced decomposition studies, should be conducted under varied stress conditions, (ICH, 1999).

A stock solution of resveratrol was prepared in acetonitrile at concentration of 5 µg/mL. For acid degradation study, 2 mL of the stock was transferred to a volumetric flask and 8 mL of 0.1 M hydrochloric acid (HCl) as added and the flasks was then sealed and heated up to 80^{o}C for 30 min. For base degradation study 2 mL of the stock was transferred to a volumetric flask and 8 mL of 0.1 M sodium hydroxide (NaOH) was added, the flasks were then sealed and heated up to 80^{o}C for 30 min. Oxidative stress study was performed by transferring 2 mL of the stock (5 µg/mL) into 10 mL volumetric flask into which 8 mL of hydrogen peroxide was added (20 %, v/v), the flask was then heated at 80^{o}C for 30 min. UV-degradation was carried out following the Q1B in ICH guidelines (ICH, 1996), whereby 10 mL of resveratrol stock was prepared (5 µg/mL) and stored in a transparent volumetric flask in a UV light cabinet an exposed to radiation at wave length of 320–400 nm for 8 h at ambient temperature. Finally, last parameter of degradation study was the effect of dry heat on the stability of resveratrol. Powdered drug (5 mg) was heated at 80^{o}C with 75 ± 5 % RH in an oven chamber for 8 h, the sample was then diluted in the mobile phase to give the final concentration. All degradation samples were diluted with the mobile phase to make up the volume to 10 mL. The samples were filtered through 0.22 µm membrane filter and analyzed using HPLC method with the above chromatographic conditions (Akhtar et al., 2013).

2.4.5 HPLC method for determination of *in vitro* drug release study

Taking into account the poor stability of RES, studies were carried out to select the buffer in which RES exhibits maximum stability. Therefore, four buffers (1.2 hydrochloric acid, 5 acetate buffer, 6.8 phosphate buffer and 7.4 phosphate buffer solutions) were selected for estimation of RES in these buffers calibration curves were constructed. All buffers were prepared according to the European Pharmacopeia 5.0 (Europe, 2004).

2.4.5 (I) Preparation buffer solutions

A. pH 1.2 buffer solution

Potassium chloride (Kcl) (3.727 g) was dissolved in 250 mL distilled water (to make up 0.2 M (Molar) solution).The resultant solution was then mixed with 425 mL pre-prepared 0.2 M Hcl by diluting 9.864

mL Hcl diluted with 500 mL distilled water, with the final volume made up with distilled water up to 1000 mL. pH was adjusted by adding Hcl or NaOH.

B. pH 5 Acetate buffer solution

Acetic acid 1.26 mL was dissolved in 200 mL distilled water and 1.12 g KOH dissolved in 200 mL distilled water. Subsequently, 120 mL from acetic acid solution was mixed with 100 mL of KOH solution and the final volume was made up to 1000 mL; pH was adjusted by adding acetic acid or KOH.

C. pH 6.8 phosphate buffer solution

Potassium dihydrogen phosphate (27.2g) was dissolved in 510 mL distilled water; 71.6 g of disodium dihydrogen phosphate dissolved in 490 mL distilled water, both solutions were mixed pH was adjusted by adding Hcl or NaOH.

D. pH 7.4 phosphate buffer solution

Monobasic potassium phosphate (6.805 g) was dissolved in 250 mL distilled water. Separately, 2 g NaOH was dissolved in 250 mL distilled water. Subsequently 250 mL of monobasic potassium phosphate solution was mixed with 195.5 mL NaOH solution and the volume was made up to 1000 mL with distilled water pH was adjusted using Hcl and NaOH.

A stock solution of RES was prepared by accurately weighing 25 mg of RES diluted in 25 mL with acetonitrile. Four stock solutions in each of the buffers were prepared. Four sets of working standard solutions were prepared in their respective buffers (0.2, 0.4, 0.8, 1, 2, 4, 8 µg/mL)

The method was validated in a similar manner as discussed previously in section 2.4.2 (I) for linearity, sensitivity, precision, repeatability, accuracy, robustness and analytical solution stability.

2.4.6 HPLC method development for the determination of resveratrol in transport media for permeability study

A standard calibration curve of resveratrol was constructed in Hanks' Balanced Salt solution (HBSS) buffer, in order to allow determination of the concentration of drug when studying the permeability of RES in bidirectional permeability studies in Caco-2 cell lines.

RES first stock solution was prepared by accurately weighing 5 mg and diluting it in 10 mL with acetone and subsequent dilutions were carried out with the HBSS transport media to prepare ten standard

working solutions (0.316, 0.729, 1.45, 2.28, 5.71, 11.4, 22.8, 34.2, 45.6 and 182.4 µg/mL). The samples were filtered and 100 µL was injected in HPLC using the same chromatographic conditions described in section 2.4.1. The method was validated for the following parameters: Linearity, sensitivity, accuracy selectivity, precision and repeatability.

2.4.7 Evaluation of coumarin-6 concentration

The most important dye in the green region of the spectrum of coumarin derivatives is 6-amino coumarin and other coumarins which possess an amino group at position 6. In order to calculate the total and the entraped dye in the formulation. The concetration of coumarin-6 as determined by employing UV-VIS spectroscopy. Dye loaded NLCs were emloyed for *in vitro* cell lines studies.

A stock solution of coumarin-6 in ethanol was prepared by accurately weighing 1 mg of coumarin-6 and diluting it with 10 mL ethanol. Serial dilutions were made from the stock solution to prepare the working standard solutions (1, 2, 4, 6, 8 and 10 µg/mL) in order to construct the calibration curve. The absorbance of each solution was measured at a wavelength of 455 nm.

2.5. Results and Discussion

2.5.1 Optimization of chromatographic conditions

Preliminary studies were carried out based on previous reports performed using mixture of water and methanol for the quantification of RES (Chen et al., 2007). Various isocratic modes were investigated with the following ratio of mobile phase viz. 50:50, 70:30, 51:49 and 63:37 (Singh et al., 2012, da Rocha Lindner et al., 2013, Pangeni et al., 2015). All the aforementioned used ratios of mobile phase resulted in peak fronting (Figure 2-1 A), peak broadening (Figure 2-1B) and tailing (Figure 2-1C) causing a drop in peak symmetry. Due to the unsuccessful use of methanol and water based mobile phases, a second method outlined by He et al., 2006 was implemented, which employed a mobile phase consisting of methanol and acetonitrile in a ratio of 75:25. Whilst no peak fronting was observed with this method, multiple peaks were observed to arise at various time points, indicating poor suitability for use (Figure 2-1D). However, none of the methods demonstrated repeatability and accuracy.

The amalgamation of characteristics from both methods resulted in the devising of a new method with a mobile phase comprising of acetonitrile and water in a gradient method as outlined in section 2.4.1.This was deemed to be successful showing no peak fronting, tailing or multiple peaks and

exhibiting a high peak symmetry of 0.89 (Figure 2-1.E), suggesting appropriateness of the chromatographic method for analysis of RES (Omar et al., 2014).

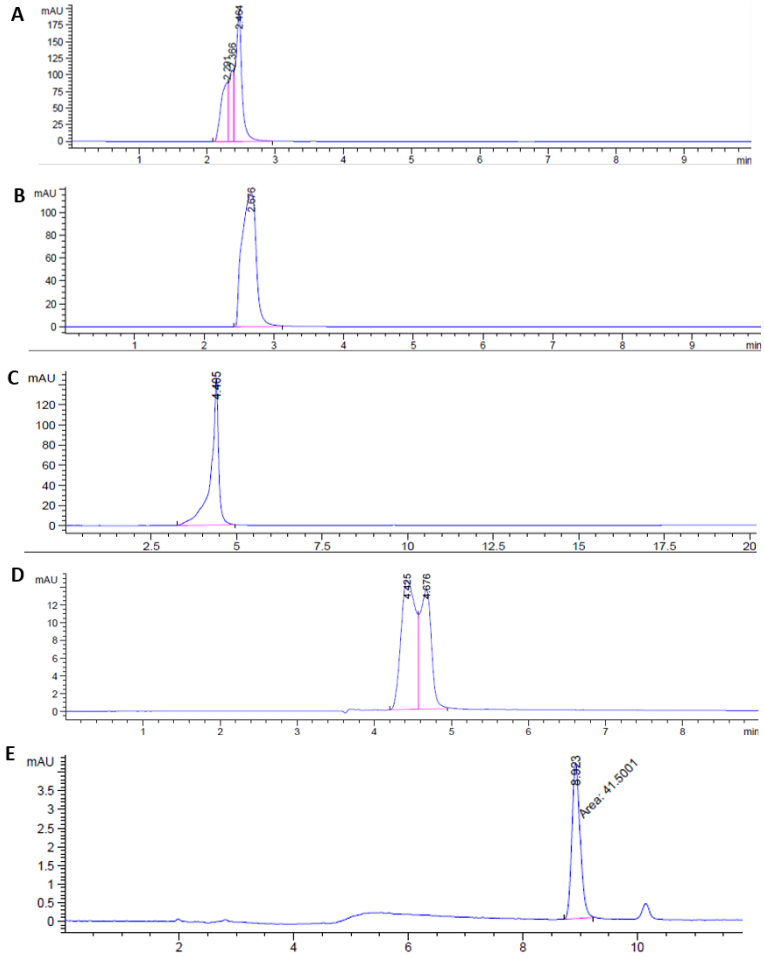

Figure 2-1. Typical HPLC chromatogram of RES in different mobile phases Vis. A, B, C and D represents water: methanol as mobile phase, E represents the Acetonitrile: Water selected mobile phase

2.5.2 HPLC method development and validation for the quantification of % Entrapment efficiency (free drug)

Eleven points concentration calibration curve was constructed (Figure 2-2) and the linearity was evaluated in range of concentrations of 0.1 to 10 µg/mL. The method exhibited a good linearity with correlation coefficient (R^2= 0.9998) calculated using the least squares method and explained via equation of the regression. According to the literature R^2 > 0.999 is considered to fit the data in an acceptable manner (Shabir, 2003). The standard curve was linear in the range of 0.1 to 10 µg/mL.

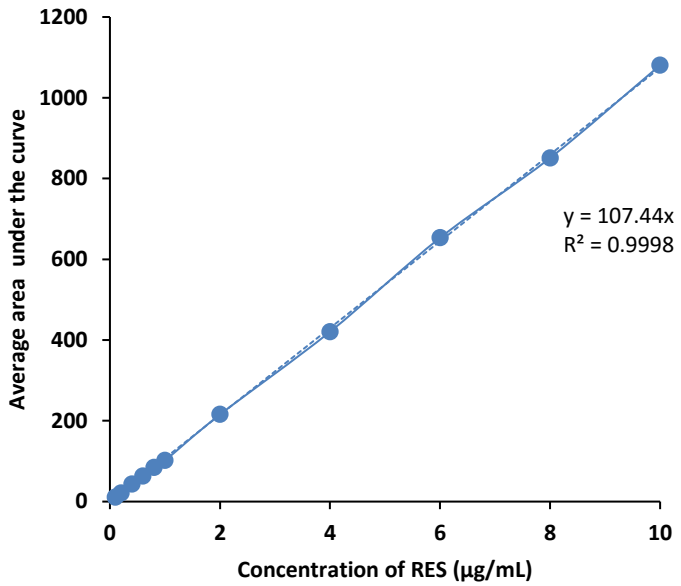

Figure 2-2. Standard calibration curve of RES stock solution in acetonitrile: 0.1% formic acid in water (50:50, v/v) (n=3)

The minimum detectable concentration of *trans*-resveratrol (LOD) was 0.031 µg/mL and the minimum concentration that the HPLC method was able to quantify (LOQ) was 0.093 µg/mL. As indicated by Jangle and Thorat (2013) the established values for LOD and LOQ were deemed to be acceptable as they were under the threshold of ± 15%. Repeatability of the method demonstrated acceptable values with low RSD % (0.323) (Table 2-1). Additionally, the method demonstrated a good accuracy with a relatively high recovery of resveratrol (Table 2-2). On examination of precision values (Table 2-3) , it was noted to be under the threshold deemed to be acceptable (i.e. < 15 %). Pecision criteria for an analytical method is that the instrument precision (RSD) and the intra-assay precision should be ≤ 2%. The data demonstrated good precision and acceptable accuracy for the determined concentrations, thus the method was deemed appropriate to quantify resveratrol in a solution. (FDA, 2001, Jangle and Thorat, 2013).

Table 2-1. Repeatability of HLPC method for the quantification of free drug (6 µg/mL)

RES standard solution concentration (µg/mL)	Measured concentration (µg/mL)
6	6.015
	5.990
	5.995
	5.959
	5.991
	6.002
	5.979
	5.968
	5.966
	5.957
Average	5.982
SD	0.019
RSD (%)	0.323

Table 2-2. Results obtained from accuracy of HPLC method for the quantification of free drug

RES standard solution concentration (µg/mL)	Accuracy (%)	RSD (%)
2	85.683 ± 0.123	0.143
6	85.614 ± 0.391	0.457
10	89.457± 0.491	0.549

Table 2-3. Precision results for the different RES standard solutions for the quantification of free drug

RES standard solution(µg/mL)	Measured concentration ±SD (µg/mL)	RSD (%)
	Intraday precision	
0.2	0.205 ± 0.002	0.032
2	2.023 ± 0.001	0.0341
10	10.213 ± 0.022	0.213
	Interday precision	
Day 1		
0.2	0.2 ± 0.001	0.690
2	2 ± 0.007	0.339
10	10 ± 0.017	0.178
Day 2		
0.2	0.200 ± 0.001	0.521
2	2.008 ± 0.012	0.598
10	10.054 ± 0.026	0.261
Day 3		
0.2	0.204 ± 0.001	0.676
2	2.051 ± 0.011	0.558
10	10.113 ± 0.077	0.765

HPLC analysis as outlined above was established to be selective/specific to the *trans*-isomer of RES. In order to differentiate between two RES isomers (*cis* and *trans*), Figure 2-3 reveals chromatogram of well differentiated two isomers of RES (*cis* and *trans*), sharp symmetrical peak *trans* isomer is visible at 306 nm with retention time of 8.018 min. A well separated second peak at retention time of 9.482 at 286 nm was observed for *cis* isomer (Trela and Waterhouse, 1996). Thus, the method can be successfully used for estimation of the active *trans* isomer and allow the discrimination from interference of *cis* isomer.

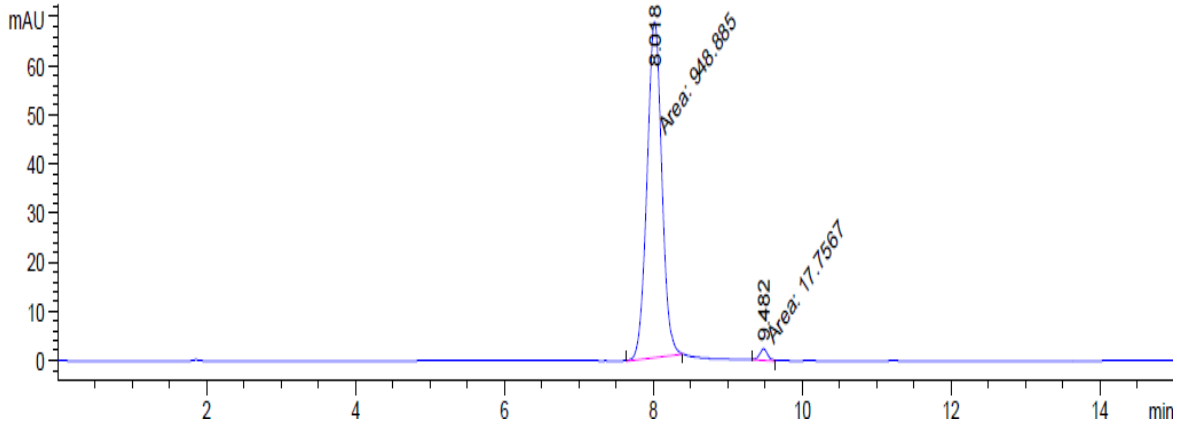

Figure 2-3. HPLC chromatogram of *trans*-RES stock solution in acetonitrile (10 µg/mL) at 306 nm, demonstration of HPLC method selectivity and specificity

Method robustness was established by making incremental changes to flow-rate, temperature and wavelength. These changes in chromatographic conditions did not affect peak symmetry, retention time and the concentration of analyte indicating robustness of the HPLC method (Table 2-4).

Table 2-4. Robustness results for 10 µg/mL RES standard solution

Chromatographic conditions	Measured concentration ±SD (µg/mL)	RSD (%)
Temperature (C)		
24	9.879 ± 0.071	0.717
25	10 ± 0.055	0.549
26	9.972 ± 0.018	0.183
Flow rate (mL/min)		
0.99	10.131 ± 0.382	3.769
1	10 ± 0.069	0.696
1.01	10.191 ± 0.017	0.165
Wavelength (nm)		
305	9.969 ± 0.073	0.729
306	10 ± 0.069	0.696
307	10.004 ± 0.062	0.618

The standard solution of resveratrol (Table 2-5) exhibited a good stability over the period of one month under refrigeration (2-8^{o}C), confirming that the method was appropriate in determining analyte concentration with time.

Table 2-5. HPLC data for Resveratrol standard solution in acetonitrile (6 µg/mL) stability, solutions were all stored at 2-8^{o}C

Time	Measured concentration ±SD (µg/mL)	RSD (%)
Day 0	6 ± 0.013	0.215
Day 2	5.953 ± 0.023	0.394
Day 3	6.042 ± 0.021	0.347
Day 7	5.969 ± 0.007	0.115
Day 10	6.022 ± 0.028	0.467
Day 20	5.929 ± 0.105	1.772
Day 30	6.047 ± 0.017	0.287

2.5.3 HPLC method development and validation for quantification of RES in RES-NLCs (%Total drug)

To determine the total drug in RES-NLCs, 1 mL of RES-NLC was accurately taken and 4 mL tetrahydrofuran was added to it. The solution was mixed to ensure that the lipid and the drug were completely dissolved in tetrahydrofuran. The solution was then filtered using a 0.22 µm filter. The filtrate was diluted with the mobile phase and analyzed by HPLC method.The standard calibration curve (Figure 2-4) between the peak area and RES concentration demonstrated a good linearity (n=3) over the concentration range 1-10 µg/mL. The linear regression of the plot also indicated a good linear relationship between the peak area and RES concentration with R^2 of 0.999.

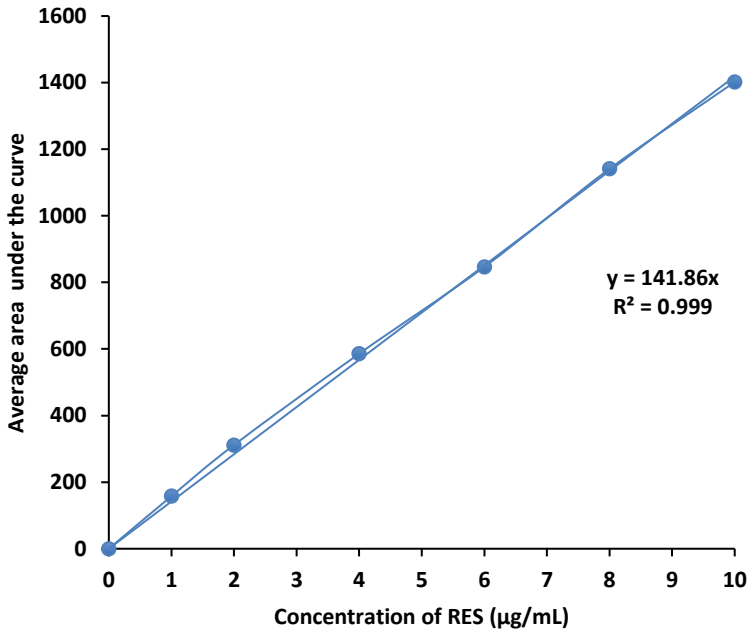

Figure 2-4. Standard calibration curve of trans-RES stock solution in tetrahydrofuran (THF)

LOD and LOQ for *trans*-RES were 0.023 and 0.070 µg/mL, respectively, as determined by the standard deviation method indicating that the method can be employed for the detection and quantification of RES over a wide range of concentrations. The established values for LOD and LOQ were deemed to be acceptable as they were under the threshold of ± 15 % (da Rocha Lindner et al., 2013) The method was noted to be repeatable with low RSD% value of 0.161 (Table 2-6). Little variation in the concentration of the analyte was observed when injected over 10 times. The method demonstrated high accuracy with a mean percent recovery of RES from the samples was 97.911 ± 0.242- 99.818 ± 0.414 (Table 2-7), the data shows agreement between the actual and theoretical values. On examination of precision values (Table 2-8) the results are indicative that precision was achieved because the maximum RSDs of the responses was less than 2 % (Pangeni et al., 2015). Minimal variation was demonstrated by the HPLC data indicating that the method was robust with regard to the small alteration in the chromatographic conditions (Table 2-9). The maximum RSD% obtained was 2.5 % (da Rocha Lindner et al., 2013). The standard solution of resveratrol (Table 2-10) was found to have good stability for the period of one week under refrigeration (2-8^{o}C), however, providing a sufficient window for intended studies to be performed.

Table 2-6. Repeatability of HLPC method for quantification of RES in RES-NLCs (6 µg/mL)

RES standard solution concentration (µg/mL)	Measured concentration (µg/mL)
6	5.999
	6.002
	5.998
	5.994
	5.998
	5.996
	6.009
	6.000
	6.003
	5.972
Average	5.997
SD	0.009
RSD (%)	0.161

Table 2-7. Accuracy of HPLC method for quantification of RES in RES-NLCs

RES standard solution concentration (µg/mL)	Accuracy (%)	RSD (%)
2	99.612 ± 0.274	0.275
6	99.818 ± 0.414	0.415
10	97.911 ± 0.242	0.248

Table 2-8. Precision of the method for quantification of RES in RES-NLCs

RES standard solution(µg/mL)	Measured concentration ±SD (µg/mL)	RSD (%)
	Intraday precision	
2	1.986 ± 0.02	0.097
6	5.999 ± 0.006	0.095
10	9.875 ± 0.055	0.555
	Interday precision	
Day 1		
2	2 ± 0.004	0.223
6	6 ± 0.002	0.033
10	10 ± 0.026	0.256
Day 2		
2	1.941 ± 0.01	0.509
6	6.067 ± 0.019	0.306
10	10.510 ± 0.016	0.153
Day 3		
2	1.899 ± 0.010	0.548
6	5.959 ± 0.017	0.287
10	10.377 ± 0.024	0.231

Table 2-9. Robustness results for quantification of RES in RES-NLCs 10 µg/mL RES standard solution

Chromatographic conditions	Measured concentration ±SD (µg/mL)	RSD (%)
Temperature (C)		
24	10.114 ± 0.223	2.203
25	10 ± 0.026	0.256
26	10 ± 0.284	2.839
Flow rate (mL/min)		
0.99	10.224 ± 0.235	2.298
1	10 ± 0.023	0.234
1.01	9.939 ± 0.214	2.155
Wavelength (nm)		
305	10.032 ± 0.102	1.018
306	10 ± 0.026	0.256
307	10.355 ± 0.259	2.500

In order to determine the method selectivity and specificity of the analyte, chromatograms were examined for interfering peaks from lipids and other formulation components at the retention time of trans-resveratrol. No additional peaks were observed from any of the excipients (Figure 2-5. A,B). This confirmed adequate separation under the described chromatographic conditions, with trans-RES eluted at 8.018 min, and any potentially interfering compounds. Thus, the method was shown to be selective for the intended application for the determination of the drug content in NLCs.

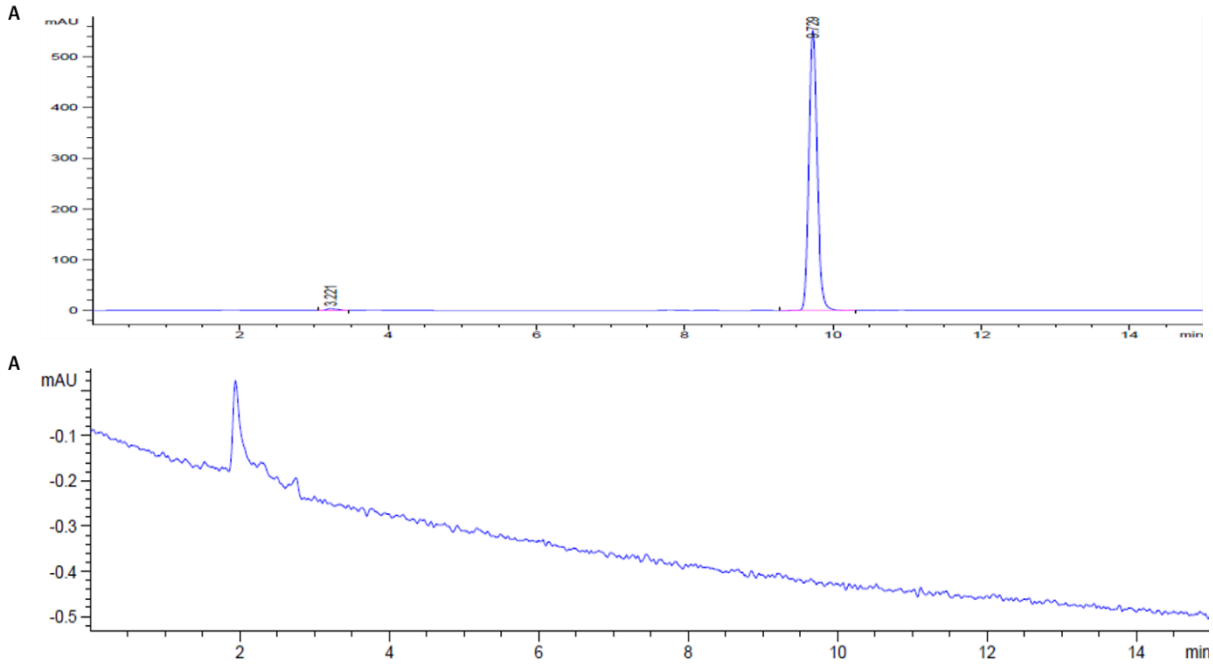

Figure 2-5. HPLC chromatogram of A. RES-NLCs B. Blank NLCs in THF (10 µg /mL) at 306 nm, demonstration of HPLC method selectivity to RES

Table 2-10. Stability of RES standard solution in THF (6 µg/mL), solutions were all stored at 2-8 °C

Time	Measured concentration ±SD (µg/mL)	RSD (%)
Day 0	6.000 ± 0.002	0.033
Day 2	6.067± 0.018	0.302
Day 3	5.959 ± 0.017	0.287
Day 7	5.477 ± 0.350	6.398
Day 10	4.743± 0.107	2.262
Day 20	3.926 ± 0.24	6.124
Day 30	2.879 ± 0.003	0.092

2.5.4 Forced Degradation Studies

Forced degradation studies were carried out under various conditions. A notable reduction in peak area was observed from the HPLC chromatograms under stress conditions (Figure 2-6). This was also accompanied by reduction in the peak area values, as well as the presence of additional peaks; indicating the formation of alternative substances from the degraded drug.

RES was found to be labile to acidic hydrolysis in which almost 82 % of the drug was degraded (Figure 2-6A, B). Whilst resveratrol showed maximum degradation when basic condition was employed were 99 % of the drug was degraded (Figure 2-6. C,D) (Zupančič et al., 2015). Also 95 % of the drug was lost when it was subjected to photo degradation (UV light irradiations) indicating that the drug sample was also susceptible to UV-photolytic stress (Figure 2-6. G) (Muller et al., 2000a). The Photo-stability of RES presents a challenge, when deciding to develop formulations. The photo-stability was carried out employing ^{1}HNMR (Proton Nuclear Magnetic Resonance) technique (Figure 2-7. A,B), which demonstrated that 73% of trans resveratrol was converted into cis isoform after 8 h treatment with UV-irradiation (Bernard et al., 2007). However, RES solution showed a good stability when dry heat was applied with a loss of only 20% of the drug after 8 h incubation at 80^{o}C (Figure 2-6.H). Similarly, with hydrogen peroxide degradation, drug showed reasonable stability with 80 % drug remaining in the solution after the treatment for 30 min.

Thus, it was demonstrated that the drug is unstable in the acid, base and UV light, however drug showed reasonable stability under oxidation (Figure 2-6. E, F) and heat conditions. Summary of the degradation studies of drug is given in Table 12-1.

Table 2-11: Remaining concentration of resveratrol after different conditions were applied resveratrol solution initial starting concentration (5 µg/mL) RDS (%) percent relative standard deviation

Exposure conditions	Remaining concentration of RES (%)	RSD (%)	Fig.no
Acid	16.993 ± 0.010	0.059	Fig 2.5.A,B
Base	0.931 ± 0.063	6.803	Fig 2.5.C,D
H_2O_2 OXIDATION	80.369 ± 0.377	0.469	Fig 2.5.E,F
UV Light	5.267 ± 0.305	5.791	Fig 2.5.G
Dry heat	80.097 ± 0.109	0.137	Fig 2.5.H

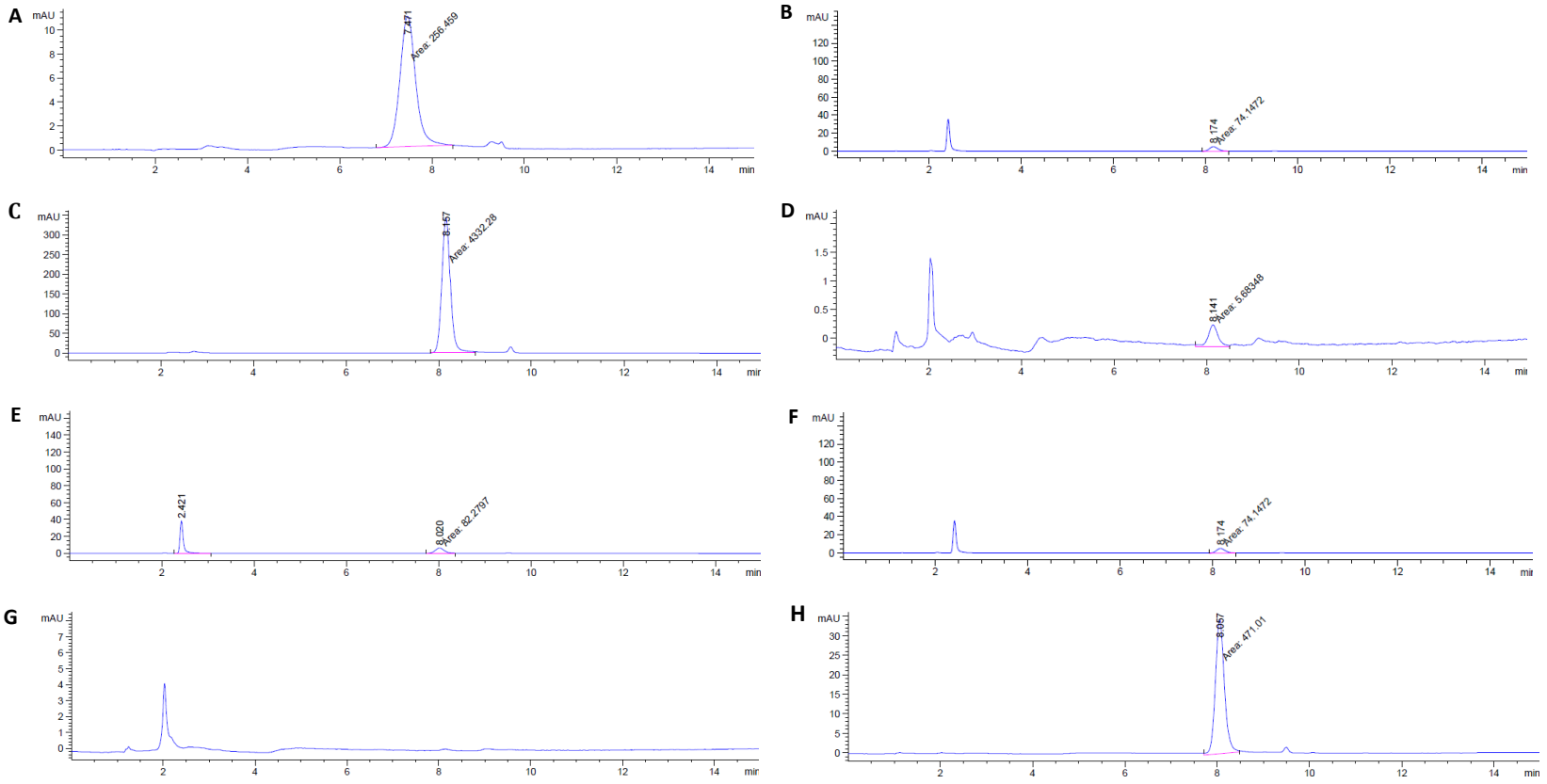

Figure 2-6. Force degradation study of RES at various condition applied: (A) Initial RES solution in HCL (B) Acid, (C) Initial RES solution in NaOH, (D) Base, (E) Initial RES solution in H_2O_2 (F) Oxidation (G) UV light (H) Dry heat

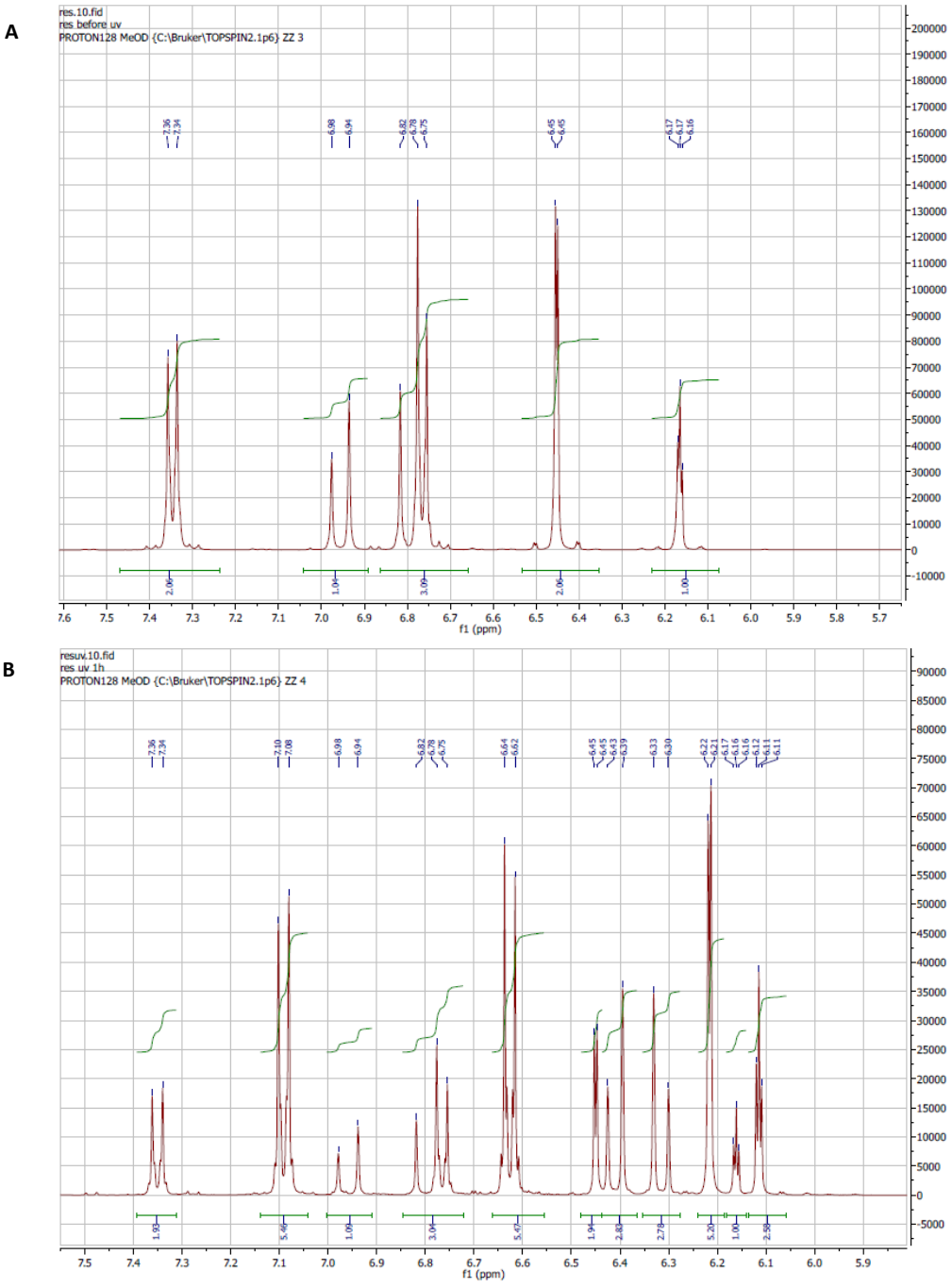

Figure 2-7. ^{1}NMR spectra of RES A. Before and B. After exposure to UV-Irradiation

2.5.5 HPLC method for quantification of RES for *in vitro* drug release studies

Four standard curves in four different sets of media, namely pH 1.2 (Figure 2-8.A), 7.4 (Figure 2-8.B), 6.8 (Table 2-8.C) and 5 (Table 2-8.D) were constructed to allow quantification of the concentration of drug released from the formulation (Table 2-9). HPLC method for all buffers demonstrated a good linearity over the range of concentrations (Table 2-12).

Table 2-12. Linear regression data for the RES standard calibration curve in various buffer solutions

Buffer used	Linearity (R^2)	Range (µg/mL)	LOD (µg/mL)	LOQ (µg/mL)
pH 1.2	0.9993	0.2-8	0.038	0.116
pH 5	0.9999	0.2-10	0.032	0.098
pH 6.8	0.9996	0.2-8	0.046	0.141
pH 7.4	0.9997	0.2-8	0.059	0.180

All buffer solutions in the selected range of concentration exhibited a good linearity with R2 in the range of 0.9993-0.9999. By calculating the correlation coefficient (r) using the least squares method exhibiting good linearity of the analytical method for the selected range of concentrations the regression value.

On examination of precision values for pH 1.2 (Table 2-13) and pH 6.8 (Table 2-16). The accuracy of the method for pH 1.2 (Table 2-18) and pH 6.8 (Table 2-17) showed reasonable RES recovery indicating the fitness of the validated method. Repeatability of the method at pH 1.2 (Table 2-15) and pH 6.8 (Table 2-18) was relatively high indicating a good fit with the data.

At pH 5 also the HPLC method was found to be precise (Table 2-19), accurate with good recovery (Table2-20). The method demonstrated good repeatability with % RDS less than 1 (Table 2-21), and was found to be robust where a small change in the conditions did not affect the concentration of the analyte (Table 2-22). Solutions made at pH 5 were stable for the period of one month, (Table 2-23), exhibiting a steady concentration over the specified period, when stored at 4-8 °C.

Table 2-13. Precision results for the different RES standard solutions at pH 1.2.

RES standard solution(µg/mL)	Measured concentration ±SD (µg/mL)	RSD (%)
	Intraday precision	
0.2	0.205 ± 0.002	0.904
2	2.009 ± 0.012	0.598
8	8.013 ± 0.027	0.334
	Interday precision	
Day 1		
0.2	0.200 ± 0.016	7.769
2	2.000 ± 0.033	1.630
8	8.000 ± 0.059	0.738
Day 2		
0.2	0.169 ± 0.004	2.628
2	2.003 ± 0.039	1.949
8	7.784 ± 0.016	0.206
Day 3		
0.2	0.189 ± 0.004	2.112
2	2.011 ± 0.005	0.243
8	7.819 ± 0.073	0.928

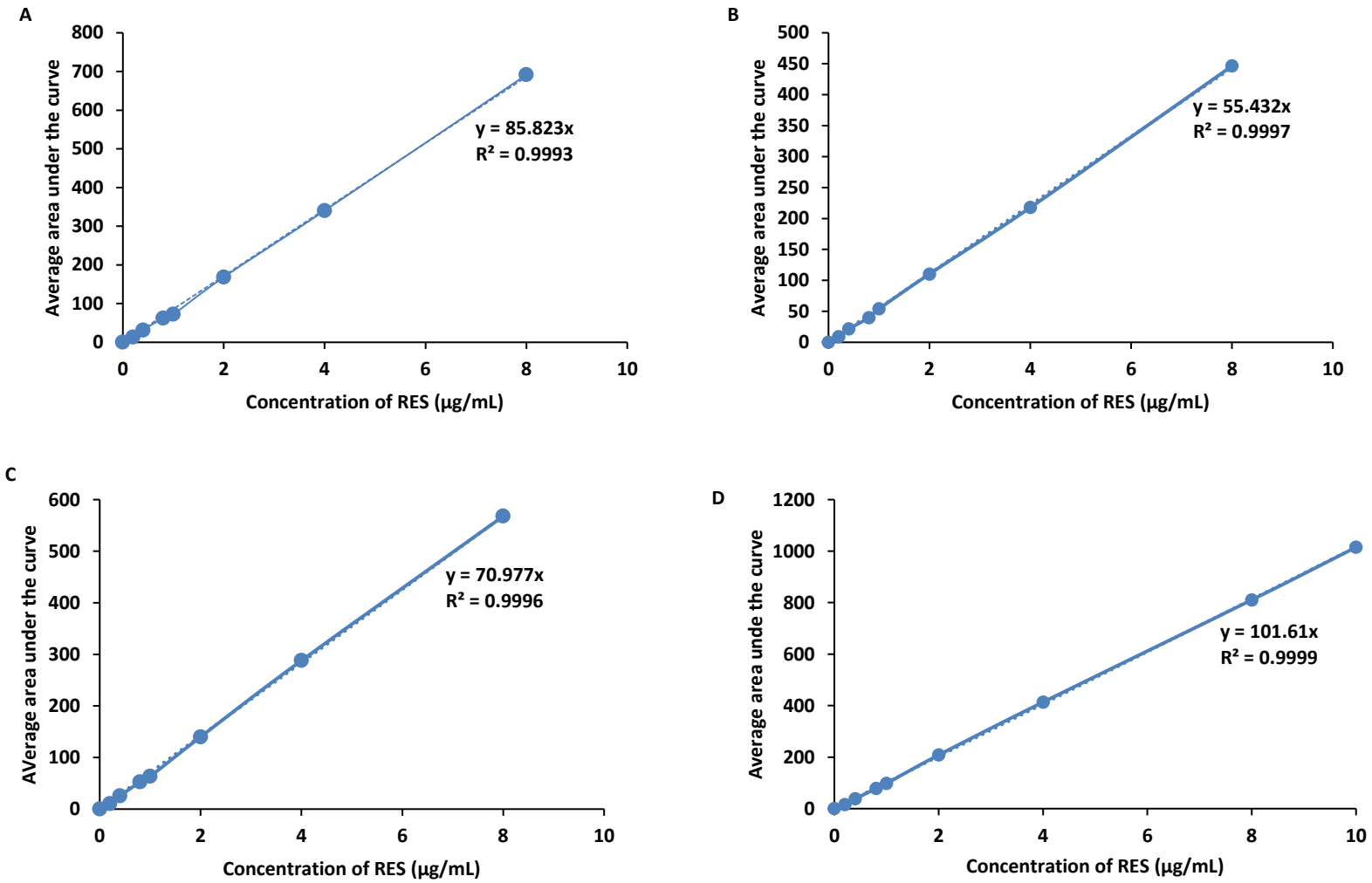

Figure 2-8 Standard calibration curve of trans-RES stock solution in various dissolution medium A) pH 1.2 B) pH 7.4 C) pH 6.8 D) pH 5

Table 2-14 Results obtained from accuracy of HPLC method pH 1.2

RES standard solution concentration (µg/mL)	Accuracy (%)	RSD (%)
0.2	100 ± 7.769	7.769
2	100 ± 1.630	1.630
8	100 ± 0.738	0.738

Table 2-15 Repeatability of HLPC method using the same concentration of RES at pH 1.2 (8 µg/mL)

RES standard solution concentration (µg/mL)	Measured concentration (µg/mL)
8	8.108
	8.100
	8.001
	7.834
	7.855
	7.866
	7.971
	7.831
	7.863
	7.987
Average	7.941
SD	0.107
RSD (%)	1.344

Table 2-16 Precision results for the different RES standard solutions at pH 6.8

RES standard solution(µg/mL)	Measured concentration ±SD (µg/mL)	RSD (%)
Intraday precision		
0.2	0.195 ± 0.004	1.945
2	1.996 ± 0.043	2.132
8	7.947 ± 0.012	0.163
Interday precision		
Day 1		
0.2	0.2 ± 0.005	2.299
2	2 ± 0.019	0.947
8	8 ± 0.019	0.243
Day 2		
0.2	0.198 ± 0.004	2.014
2	1.966 ± 0.018	0.934
8	7.938 ± 0.029	0.366
Day 3		
0.2	0.192 ± 0.007	3.842
2	2.026 ± 0.031	1.522
8	7.954 ± 0.025	0.310

Table 2-17 Results obtained from accuracy of HPLC method pH 6.8

RES standard solution concentration (µg/mL)	Accuracy (%)	RSD (%)
0.2	100 ± 2.299	2.299
2	100 ± 0.947	0.947
8	100 ± 0.243	0.243

Table 2-18 Repeatability of HLPC method using the same concentration of RES at pH 6.8 (8 µg/mL)

RES standard solution concentration (µg/mL)	Measured concentration (µg/mL)
8	7.794
	7.829
	7.798368
	7.774
	7.717
	7.749
	7.735
	7.718
	7.772
	8.237
Average	7.818
SD	0.151
RSD (%)	1.926

Table 2-19 Precision results for the different RES standard solutions at pH 5

RES standard solution(µg/mL)	Measured concentration ±SD (µg/mL)	RSD (%)
	Intraday precision	
0.2	0.195 ± 0.001	0.631
2	1.993 ± 0.003	0.151
8	7.598 ± 0.118	1.55
	Interday precision	
Day 1		
0.2	0.2 ± 0.005	2.264
2	2 ± 0.002	0.098
8	8 ± 0.038	0.476
Day 2		
0.2	0.162 ± 0.004	2.470
2	2.046 ± 0.006	0.281
8	7.080 ± 0.139	1.969
Day 3		
0.2	0.238 ±0.02	0.838
2	1.974 ± 0.009	0.498
8	8.215 ± 0.034	0.420

Table 2-20. Results obtained for the accuracy of HPLC method at pH 5

RES standard solution concentration (µg/mL)	Accuracy (%)	RSD (%)
2	92.548 ± 0.028	0.031
6	99.765 ± 0.152	0.152
10	100 ± 4.425	4.425

Table 2-21 Repeatability of HLPC method using the same concentration of RES at pH 5 (6 µg/mL)

RES standard solution concentration (µg/mL)	Measured concentration (µg/mL)
6	5.996
	5.984
	5.978
	6.097
	5.998
	5.994
	6.027
	6.008
	6.017
	5.996
Average	6.009
SD	0.034
RSD (%)	0.567

Table 2-22. Robustness results for 10 µg/mL RES standard solution at pH 5

Chromatographic conditions	Measured concentration ±SD (µg/mL)	RSD (%)
Temperature (C)		
24	9.701 ± 0.229	2.369
25	10 ± 0.101	1.007
26	9.514 ± 0.031	0.326
Flow rate (mL/min)		
0.99	10.153 ± 0.263	2.593
1	10 ± 0.206	2.062
1.01	10.071 ± 0.060	0.600
Wavelength (nm)		
305	9.972 ± 0.209	2.093
306	10 ± 0.206	2.062
307	10.003 ± 0.206	2.062

Table 2-23 HPLC data for RES standard solution (6 µg/mL) stability at pH 5, solutions were all stored at 2-8 °C

Time	Measured concentration ±SD (µg/mL)	RSD (%)
Day 0	6 ± 0.031	0.521
Day 2	5.921 ± 0.052	0.876
Day 3	5.901 ± 0.041	0.688
Day 7	5.845 ± 0.118	2.016
Day 10	5.901 ± 0.096	1.631
Day 20	5.766 ± 0.039	0.676
Day 30	5.881 ± 0.076	1.296

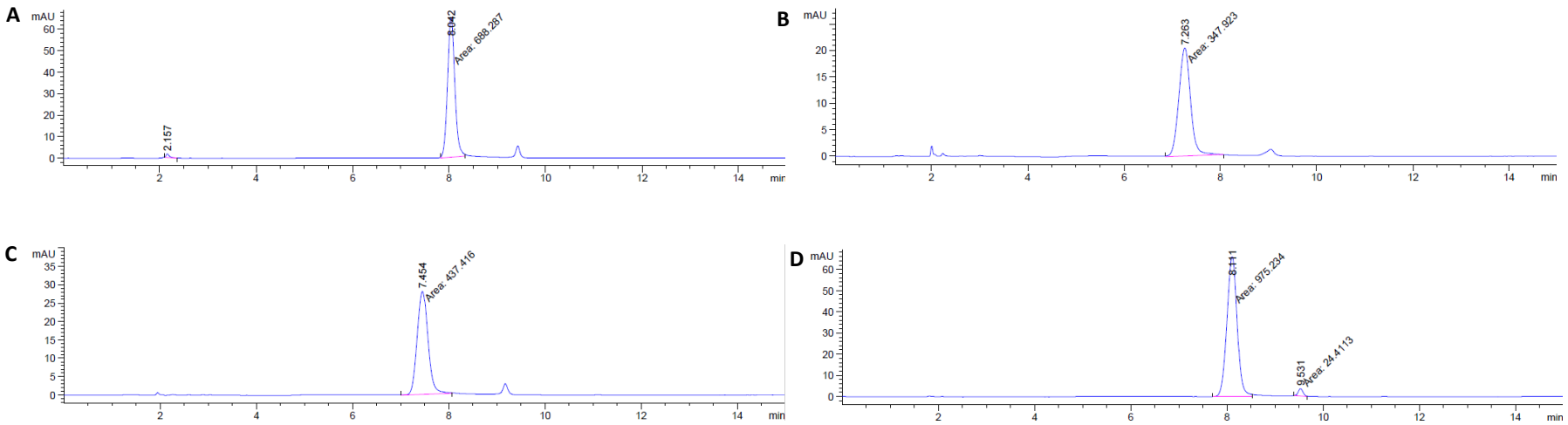

Figure 2-9. HPLC chromatogram showing trans-RES stock solution (8 µg/mL) in various dissolution medium A) pH 1.2 B) pH 7.4 C) pH 6.8 D) pH 5

2.5.6 HPLC method development for the determination of resveratrol in HBSS for Caco2 cell line bidirectional permeability studies

HBSS solution is used as a buffer in the bidirectional Caco-2 cell lines studies. Therefore, an analytical method was developed to quantify the drug and establish linearity in HBSS buffer (Figure 2-10) buffer in range of concentrations from 0.316 to 182.400 µg/mL. Sharp well resolved peak of RES at retention time of 10 min (Figure 2-11) was observed. The method was found to be linear in the selected concentration range regression value of R^2 = 0.9991.

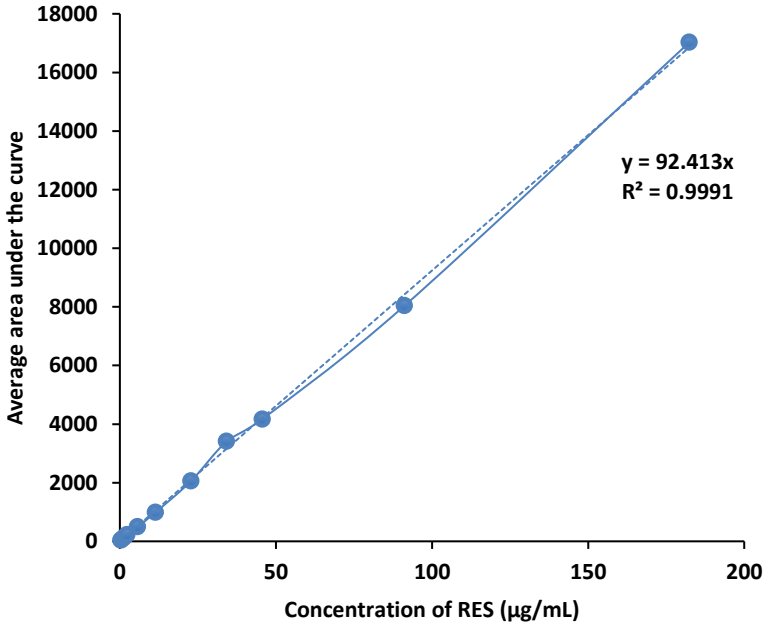

Figure 2-10. Standard calibration curve of trans-RES stock solution in HBSS transport media

The LOD and LOQ for *trans*-RES were 0.035 and 0.108 µg/ml, respectively. The method was found to be accurate (Table 2-24) and precise (Table 2-25) with good recovery of RES from the media (Table 2-25). The established values for LOD and LOQ were deemed to be acceptable within the acceptable limits.

There were no interfering peaks of the transport media or any other components were observed at the retention time of trans-resveratrol (Figure 2-11) indicating the method to be selective and specific. The method also demonstrated a good repeatability, as the concentration of resveratrol remained constant when analysed over the period of time (Table 2-26) and (Figure 2-11).

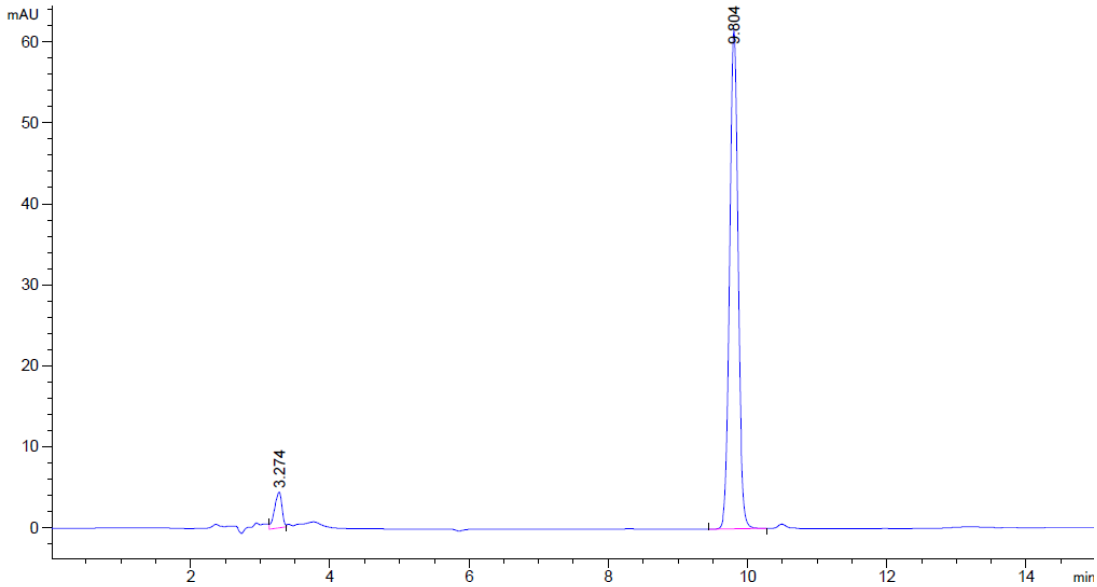

Figure 2-11. HPLC chromatogram of RES in HBSS (5.7µg /mL) at 306 nm, demonstration of HPLC method selectivity to RES

Table 2-24 Results obtained from accuracy of HPLC method

RES standard solution concentration (µg/mL)	Accuracy (%)	RSD (%)
2.28	99.696 ± 0.105	0.106
22.8	99.977 ± 0.202	0.202
182.4	99.916 ± 0.015	0.0149

Table 2-25. Precision results for the different RES standard solutions in HBSS transport media

RES standard solution(µg/mL)	Measured concentration ±SD (µg/mL)	RSD (%)
	Intraday precision	
2.28	2.278 ± 0.011	0.495
22.8	22.913 ± 0.045	0.198
182.4	182.762 ± 0.173	0.095
	Interday precision	
Day 1		
2.28	2.280 ± 0.004	0.179
22.8	22.800 ± 0.009	0.040
182.4	182.400 ± 0.165	0.091
Day 2		
2.28	2.225 ± 0.002	0.106
22.8	22.384 ± 0.045	0.202
182.4	187.866 ± 0.028	0.015
Day 3		
2.28	2.232 ± 0.001	0.046
22.8	22.389 ± 0.007	0.033
182.4	188.024± 0.242	0.129

Table 2-26. Repeatability of HLPC method using the same concentration of resveratrol in HBSS transport media (22.8 µg/mL)

RES standard solution concentration (µg/mL)	Measured concentration (µg/mL)
22.8	22.799
	22.792
	22.810
	22.856
	22.882
	22.905
	22.950
	22.988
	22.898
	22.433
Average	22.831
SD	0.154
RSD (%)	0.675

2.5.7 Evaluation of coumarin-6 concentration in RES-NLCs

The standard curve of coumarin-6 demonstrated good linearity, with R2 value of 0.9996 (Figure 2-12).

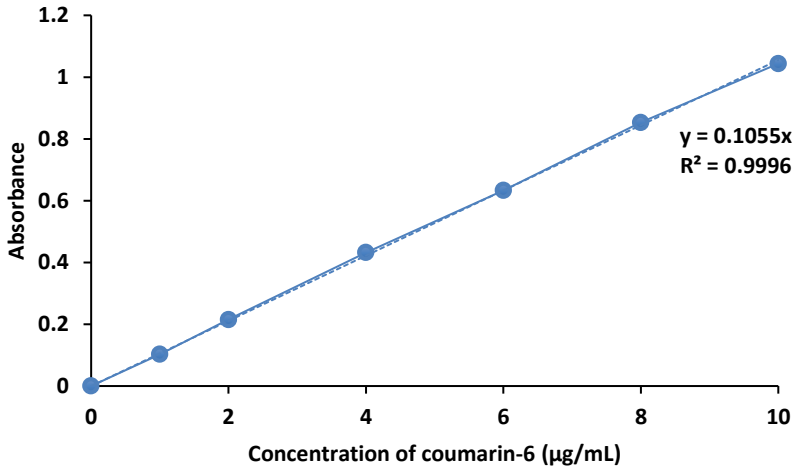

Figure 2-12. Standard calibration curve for coumarin-6 fluorescent dye

For the purpose of undertaking various uptake studies on breast cancer cell lines using flow-cytometry studies RES-NLCs were labled with fluorescent probe coumarin-6. It was important to establish that coumarin did not interfere with RES peak during quantitative analysis of these fluorescently labled NLCs (Figure 2-13) chromatogram showed no interfrence from peaks of coumarin-6 at retention time of RES. Thus coumarin-6 dye could be safely used in labeling RES-NLCs for further studies.

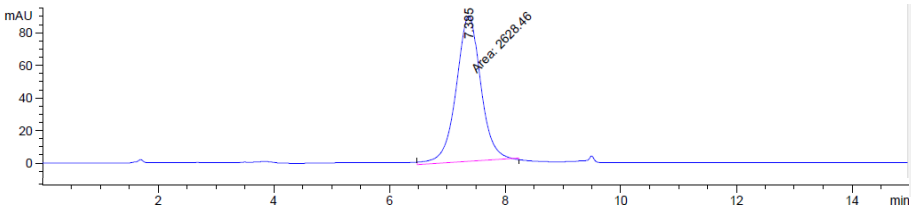

Figure 2-13. HPLC chromatogram of RES-NLCs loaded with coumarin-6 fluorescent dye

2.6. Conclusion

In the development of a pharmaceutical drug a validated method is a crucial component. Throughout the process of development for RES-NLCs, it is necessary to quantify drug content in different substrates. Thus, simple, precise, accurate , sensitive, specific, robust, and reproducible HPLC methods are a stringent requirement. The HPLC analytical methods were successfully developed and validated for the determination of RES content in RES-NLCs, under variant conditions, including: different buffer media, dissolution media and transport media for bidirectional permeability studies.

Sufficient chromatographic separation was attained using a mobile phase which comprised of acetonitrile and water, used at a flow rate of 1.0 mL/min in a gradient elution method for the effective separation of RES in various conditions. The exhibited chromatograms of RES elicited sharp and well separated peaks for the analyte. The developed methods in this chapter were successfully validated for the following parameters: linearity, range, LOD, LOQ, precision, accuracy, reproducibility and robustness as per ICH guidelines.

The method which was developed intended for the quantification of free and total drug entrapped in NLCs exhibited high linearity, with an R^2 ranging from 0.999-0.9998 in the range of 0.1 to 10 µg/mL. The lowest detectable concentration *trans*-resveratrol (LOD) was 0.031 µg/mL and the lowest concentration which the HPLC method was able to quantify (LOQ) was established as 0.093 µg/mL. Both methods were shown to exhibit high precision and accuracy with sample recovery ranging from 85.6-99.8%. Both methods were determined to be repeatable and reproducible following incremental changes in the chromatographic conditions. High specificity and selectivity were demonstrated with respect to RES in the RES-NLCs, this allowed for effective determination of the drug in a mixture of components, whilst maintaining sufficient stability for a time frame of one month. The developed methods may also be applied in the quantification of RES in coumarin-6 tagged RES-NLCs without obscuration from coumarin.

Moreover, the HPLC methods developed were carried out in several pH buffer solutions (1.2, 5, 6.8 and 7.4). The methods revealed high linear regression for all studied buffers and transport media with an R^2 value ranging from 0.9993-0.9999 and were precise and accurate with high RES recovery and stability for the period of one month.

Forced degradation studies revealed degradation of RES in basic, acidic and UV-photolytic stress conditions with maximum degradation in basic conditions (99%) followed light degradation (95%) and then acidic environment (82%). However, a good stability with only 20% degradation under both dry heat and oxidative stress was demonstrated.

Chapter 3 : Formulation Development, Optimization and Physicochemical Characterizations

3.1. Introduction

Resveratrol (RES) is a known anticancer agent with inhibitory activity in all three stages of tumour development i.e. initiation, promotion and progression (Chang et al., 2001, Delmas et al., 2006). Although RES has demonstrated anticancer activity, its clinical application is limited due to its associated low bioavailability and a rapid clearance from circulation (Walle et al., 2004). Moreover, its low water solubility reduces the dissolution-rate limited cell absorption (Wenzel and Somoza, 2005), leading to reduced oral bioavailability due to rapid and extensive metabolism. The therapeutic potential of RES can be realized *in vivo,* only if the limitations bound to its bioavailability are overcome (Amri et al., 2012). This may be achieved through thoughtful formulation as a drug delivery system, which could overcome bioavailability problems and further improve targetability to cancer cells. Recently, nanotechnology platforms were developed in the area of medical biology for both therapy and diagnosis of diseases. Drug delivery that targets specific sites in the body has gained an incredible attention in the research and development of multifunctional nanoparticles as various pharmaceutical drug delivery systems, to support their medical applications (Puri et al., 2009).

Nanotechnology plays a crucial role in the future therapies as “nanomedicine”, raising the therapeutic index by reducing the dose required to produce the desired effect (Koo et al., 2005). These delivery systems in the nano-range size are comprised of encapsulated or conjugated drugs. A number of nanoscale systems consist of liposomes, nanoemulsions, micelles, nanoparticulate systems (polymer-, carbon-, lipid-, albumin, ceramic-based and nanogels), and dendrimers have been investigated for drug delivery (Werengowska-Cie. et al., 2015).

Lipid nanoparticles have been recently developed and are potentially interesting with marketable potentials due to their natural components and the manageable scaled-up processes, which make them attractive options for pharmaceutical industries. Both SLNs and NLCs are well set for large-scale manufacturing, as solvent use can be eliminated utilizing the high-pressure homogenization method (Selvamuthukumar et al., 2012). New generation nanostructured lipid carriers (NLCs) (lipid-based nanoparticles which may entrap therapeutic compounds) were developed in order to overcome the potential problems associated with Solid lipid nanoparticles (SLNs) (i.e. limited drug loading capacity and potential drug expulsion during storage). NLCs were found to successfully resolve drug loading and expulsion issues attributed to their structure holding a greater number of lipid crystal imperfections (due to the presence of liquid lipid) enhancing drug loading and reducing drug expulsion during storage (Puri et al., 2009).

NLCs stability is strongly affected by the type and the amount of liquid oil used, increase of oil concentration is known to lead to a decrease in the crystallization and melting point and an increase

in polymorphic transformation rate which results in particles adapting a more spherical shape, enhancing overall suspension stability upon storage (Yang et al., 2014). There are few studies pertaining to the effect of type of liquid oil on polymorphic transformation and changes in the shape of NLCs (Muller et al., 2002a, Muller et al., 2002b). Alternative studies indicate that the modification of the solid lipid matrix by incorporating lipid oil improves loading capacity, physical and chemical stability (Yang et al., 2014).

Resveratrol-NLCs (RES-NLCs) were prepared using trimyristin as solid lipid. Literature reports the use of different types of liquid lipids for the formulations of NLCs. Selection of liquid lipid is critical to the performance and stability of NLCs. Though researchers have employed a myriad of liquid lipids in order to prepare NLCs, there are no reports of a direct comparison of the effect of liquid lipid on the quality parameters and stability of NLCs (Hu et al., 2006, Villalobos-Hernández and Müller-Goymann, 2006, Tamjidi et al., 2014, Yang et al., 2014, Yu et al., 2016)

This chapter entails a systematic investigation of the impact of liquid lipid on RES-NLC properties. A comparison of six different liquid lipids with different chemical compositions, molecular structures and Hydrophilic lipophilic balance (HLB) on the critical quality parameters and stability of NLCs has been carried out. Two triglycerides, one medium chain triglyceride and one long chain triglyceride, two propylene glycol esters, one fatty acid ester and one PEGylated lipid were employed along with trimyristin as solid lipid for preparation of RES-NLCs.

Statistical design of experiments (DoE), a computer based optimization technique, which identifies the critical factors, their synergistic or antagonistic interactions to find ideal process conditions that achieve the targeted response(s). The DoE approach simplify the screening of both process and product variables, aiming for a robust conditions and testing the suggested settings for ruggedness (Bukhari et al., 2009).The ultimate target of DoE is to build a useful model for all critical response that measures process efficiency and product efficacy (Vaughn and Polnaszek, 2007).

Box-Behnken experimental design (BBD) was used to understand the effect of three independent factors (amount of liquid lipid, amount of drug and surfactant concentration) and interactions between these factors for each of the six liquid lipids on the selected response variable particle size (PS), polydispersity index (PDI), zeta potential (ZP), percent entrapment efficiency (%EE)and drug loading (%DL). The relationship between various factors and responses was established by response surface methodology (RSM) (Candioti et al., 2006, Abul Kalam et al., 2013). The selected six formulations were subjected to detailed characterization.

The stability studies were conducted over the period of six months to identify the stable formulation. Based on the stability studies one best formulation was selected for further surface modification with various ligands, to achieve the targetability towards the breast cancer cells.

The targeted chemotherapeutics consists of ligands linked to the nanoparticles. Therefore, the surface modified nanoparticles will enable the interaction with the proper receptors of the cancer cells (Liu et al., 2007). One of the most beneficial techniques in targeted therapy is the ability to deliver high concentration of anticancer drug to the most resistant cells and ensure the long blood circulation. In order to accomplish that the surface of nanoparticles is functionalized with a suitable ligand which has the affinity for receptors overexpressed on the cancer cells (Werengowska-Cie. et al., 2015).

The selected formulation was first PEGylated to prolong the circulation half-life, then the surface of the nanoparticles was functionalized with different ligands. PEGylation offer a protection for the nanoparticles from being recognized and eventually cleared by the reticuloendothelial cells, in addition to that the PEG forms a hydrophilic shield that mask the antigenic site and reduce the formation of antibodies thus reduce the neutralization and the detection by the immune system (Banerjee et al., 2012, Mishra et al., 2016).

Various candidate ligands have been investigated to target NLCs to tumor cells that are aimed toward overexpressed receptors; these include antibodies and aptamers and small molecules such as vitamins e.g., folic acid (Puri et al., 2009). Two ligands, Hyaluronic acid (HA) and Folic acid (FA) were selected for functionalization of the NLCs to improve their targetability to the breast cancer cells. HA is an anionic, linear polysaccharide comprised of several units of glucuronic acid and N-acetyl-D-glucosamine. Major literature reports the uniform affinity of CD44 receptors for HA, these receptors are associated with tumor progression. CD44 receptors are overexpressed in epithelial cancer cells such as breast cancer, neck cancer etc.The major ligand for CD44 receptors is hyaluronic acid (HA; hyaluronate, hyaluronan) which is used in the design of hyaluronan-based therapeutic agents that target the CD44 receptors, in order to improve the intracellular drug delivery. Thus the modification of the surface of nanoparticles with HA will have an effect on the biological activity and the target ability of the nanoparticles as well as the interaction with CD44 receptors in breast cancer cells (Nascimento et al., 2016).

Folic acid (FA) has been widely studied as a ligand targeting the Folate receptors (FR). Folic acid gets the intracellular access to the cells via FR-mediated endocytosis. Folate receptors are overexpressed in breast cancer cells. Thus it has been utilized as a potentially specific targeting agent for the transport of variety of anticancer agents and carrier systems (nanoparticles) into tumor tissues (Ucar et al., 2017). Apart from functionalization of RES-NLCs with individual ligand, RES-NLCs were also surface modified with a combination of two ligands to achieve dual targeting properties to breast cancer cells.

This chapter will cover the following:

1. Formulation development and optimization of RES-NLCs using BBD.
2. Surface modification of RES-NLCs.
3. Physicochemical characterizations of bare and ligand appended RES-NLCs.
4. Stability studies of optimized RES-NLCs.

3.2 Materials and Methods

3.2.1 Materials employed for the preparation and physicochemical characterization of RES-NLCs

Trimyristin (Dynasan 114) and liquid lipid tricaprylin (Miglyol 808, GTC) were kindly donated as a gift sample from Cremer oleo division. Caprylcaproyl macrogol glycerides (Labrasol, PCG), propylene glycol monolaurate (Lauroglycol 90, PGML), propylene glycol monocaprylate (type II) NF Capryol 90, PGMC) were kindly supplied by Gattefosse was purchased from Sigma-Aldrich.UK. Decyl octadec-9-enoate (Decyl oleate, DO) was provided by BSAF. Sodium cholate, Tween 80, Span 80, hyaluronic acid sodium salt (molecular weight approximately 1.5-1.8X10^6 Da), folic acid, glyceryl trioleate (GTO), 5% (W/V) Trinitrobenzenesulphonic acid (TNBS) solution, trichloracetic acid, L-valine were purchased from Sigma-Aldrich, UK, phosphatidylcholines (Lipoid S75, E80 and Phospholipon 90H) were obtained from Lipoid oleo division, resveratrol was purchased from Manchester Organics, UK. Filter device Amicon 0.5 mL centrifugal tubes (3 KDa molecular weight cut-off, (MWCO)), Incubator used for *in vitro* drug release studies was purchased from Sanyo Incubator, Japan .Spectra/Por® dialysis membrane (3.5 KDa MWCO) was purchased from Spectrum Labs, USA. MYRJ S 52 (polyethylene glycol monostearate PEG-40, molecular weight of 328.537 g/moL) obtained from CRODA, Spain. Sodium bicarbonate, hydrochloric acid, 1-Ethyl-3-(3-dimethylaminopropyl)-carbodiimide (EDC cross-linker) and *N*-hydroxysuccinimide (NHS) were purchased from Thermofisher and Fisher Scientific, UK. All other chemicals were of analytical grade. Purified water was used throughout the study. For ^{1}H-NMR deuterated Dimethyl sulfoxide (DMSO) was purchased from GOSS chemicals, UK.

3.2.2 Instruments used for the preparation of RES-NLCs

Hot plates were purchased from Fisher Scientific, Centrifuge (3-16PK SCIQUIP) was purchased from SIGMA Laborzentrifugen. Germany. T25 basic Ultra- Turrax (IKA, Staufen, Germany), NanoDeBEE 2000 high pressure homogeniser (DeBEE International, USA) fitted with a Z5 nozzle (0.10mm orifice diameter)(BEE-INTERNATIONAL, 2003), Prob sonicator was obtained from Vibra Cell Sonics, USA.

For spray drying of resveratrol nanoparticles Buchi B-290 mini spray dryer was obtained from BUCHI, UK Ltd. Vortex® mixer (Biocote, Stuart) obtained from Cole-Parmer, UK. Ultrasonic Cleaners was purchased from VWR®, UK.

3.2.3 Measurement of resveratrol solubility in liquid lipids

Resveratrol solubility in the six liquid lipids was determined by adding an excess of drug (approximately 200 mg) was added to each individual liquid lipid (5 mL each) in screw-capped bottle (Joshi and Patravale, 2006). After 24h of stirring, the sample was centrifuged (13,000 rpm, 5 min), and the clear supernatant layer was diluted with the mobile phase to achieve the concentration to be detected by HPLC, filtered using Millipore® membrane (0.2 µm) and analysed by validated HPLC method as described in section 2.4.2.

3.2.4 Preparation of RES-NLCs

Various techniques are used for the preparation of NLCs. These techniques include high-pressure homogenization, solvent dispersion, ultrasonic emulsion evaporation, film-ultrasonic method, melt emulsification (Yuan et al., 2007), multiple emulsion water/oil/water methods (Li et al., 2017). The most commonly employed method is the high-pressure homogenization (HPH) method, which uses both high temperature and high pressure (Müller et al., 1998, Sun et al., 2014). Another commonly used method is the high shear homogenization and/or ultrasonication were the melting lipid was dispersed in a solution of surfactant using ultrasonication method. The type of ultrasonic equipment used was probe sonicator (Mei et al., 2003, Rocha et al., 2017). Two methods were investigated for the preparation of RES-NLCs: hot melt HPH and ultrasonication using probe sonicator.

3.2.4 (I) High pressure homogenization method (HPH)

Briefly, a hot aqueous phase containing surfactants : Tween 80 at three different concentration (0.5 %, 0.75 % and 1 %) and Sodium cholate (0.25 %) was preheated to 70^{o}C (5–10°C) above the melting point of the solid lipid (Gaba et al., 2015). Trimyristin was melted and either of the six liquid lipid Propylene glycol-8 caprylic/capric glycerides (PCG), Propylene glycol monocaprylate (type II) NF (PGMC), Propylene glycol monolaurate (PGML), Glyceryl trioleate (GTO), Decyl octadec-9-enoate (DO) or Glycerol tricaprylate (GTC) were subsequently added. All six liquid lipids were taken at three different concentrations (0.25 %, 0.5 % and 0.75 %). Resveratrol (100, 150 and 200 mg) was solubilized in Soy phospholipid (S75), Egg phospholipid (E80) both at a concentration of 0.1% and Phospholipon 90H (0.3 %). The mixture was added to the molten lipid phase. The resultant mix was

left for continued mixing to get a uniform dispersion of lipid phase. The lipid phase was added to the preheated aqueous phase and homogenized for 10 minutes by a T25 basic Ultra- Turrax. The resultant hot oil in water (o/w) nanoemulsion was homogenized using high pressure homogenizer at 10,000, 20,000 and 30,000 bar for 3, 3 and 5 cycles, respectively. The resultant dispersion was left to cool at room temperature for the re-crystallization of the lipid to yield six types of RES-NLCs viz. RES-NLC-GTO, RES-NLC-GTC, RES-NLC-PCG, RES-NLC-PGMC, RES-NLC-PGML and RES-NLC-DO (Figure 3-1).

3.2.4 (II) Ultrasonication method

Melted lipid phase with RES was added to the pre-heated surfactant containing aqueous phase to form the pre-emulsion. The pre-emulsion prepared as described in section 3.2.4.1. was subjected to probe sonication, employing 40 % amplitude with total sonication time of 25 min, the emulsion was kept on ice while processing under probe sonicator, in order to control the temperature of the emulsion not to exceed 60^{o}C. The resultant NLCs were left to cool down at room temperature to allow the solidification and the formation of the nanoparticles. The formed NLCs were then centrifuged at 1000 rpm for 5 min, to remove the titanium produced during the ultrasonication process (Garanti et al., 2016) (Figure 3-1).

3.2.4 (III) Preparation of coumarin-6 loaded RES-NLCs (C6-RES-NLCs)

C6-RES-NLCs were prepared for the purpose of studying the cellular uptake and uptake pathways of RES-NLCs in various cell lines. Coumarin -6 in a concentration of 15 µg/mL was added in the drug phase prior to mixing with the lipid phase. The preparation method was similar to what it was described in section 3.2.4.

3.2.5 Optimization of RES-NLCs by Box and Behnken design

RES-NLCs were prepared using trimyristin as solid lipid and the effect of six liquid lipids was studied on five identified critical quality attributes (CQA) of a NLC formulation. CQA is a physical, chemical, biological, or microbiological property or characteristic that should be within an appropriate limit, range, or distribution to ensure the desired product quality (Sangshetti et al., 2017). According to our prior knowledge and review of the literature, average particle size, polydispersity index, zeta potential, encapsulation efficiency and drug loading are the most influential parameters, which characterize the nanostructured drug delivery system hence were determined as CQAs.

Six liquid lipids that were investigated include: PCG, PGMC, PGML, GTO, DO and GTC along with trimyristin to prepare RES-NLCs (Table 3-1). A 3-factor, 3-level Box–Behnken design was employed

to evaluate the main effects, interaction effects, and quadratic effects of four independent variables at three levels on the five CQAs (Kaur et al., 2016).

Four critical independent variables investigated were namely; concentration of liquid lipid (X_1), surfactant (Tween 80) concentration (X_2), and amount of drug (X_3) and liquid lipid type (D) for the optimization of the dependent variables viz. particle size (Y_1), polydispersity index (Y_2), zeta potential (Y_3), entrapment efficiency percent (Y_4) and Drug loading (Y_5).

For this, thirteen runs for each of six liquid lipids to give a total of 78 formulations, were executed and suitable models for combination of designs comprising of four components include linear, 2Fl, quadratic and cubic models were constructed. Table 3-2 shows the experimental design points with variables coded values (low, medium, and high) used in matrix of experiments. For each liquid lipid, three varied concentrations were utilized i.e. 0.25, 0.5 and 0.75% based upon the total solid content; in order to establish a potential concentration dependent relationship. RES was incorporated at a weight of 100, 150 or 200 mg; in addition to Tween 80, which was also interrogated at three concentrations viz. 0.5, 0.75 or 1%. The aforementioned variables were analysed in parallel to establish the effects of different product variables on the undertaken response.

This cubic design is characterised by a set of points that lie at the midpoint of each edges of the cube. The best fitting mathematical model was selected based upon the comparisons of several statistical parameters comprising the multiple correlation coefficient (R^2), the coefficient of variation (CV), adjusted multiple correlation coefficient (adjusted R^2); and the predicted residual sum of square (PRESS), calculated by Design-Expert® software. Among them, the lowest PRESS indicates how well the model fits the data (Mujtaba et al., 2014).

Two-dimensional contour Plots composed of the relation between two factors while the third factor is kept constant were generated by the Design Expert® software (Trial version 10.0.6).

The linear correlation plots of the actual experimental values were compared to the corresponding predicted values plotted by the design and the R^2 values were obtained for each response for optimum model validation (Figure 3-9 and 3-10)

For Box-Behnken analysis, the regression equation describes the effects of the variables on the responses in terms of Linear, interactive and quadratic models. The non-linear computer-generated quadratic equation is given below:

$$Y = b_0 + b_1X_1 + b_2X_2 + b_3X_3 + b_{12}X_1X_2 + b_{13}X_1X_3 + b_{23}X_2X_3 + b_{11}X_1^2 + b_{22}X_2^2 + b_{33}X_3^2 \quad \text{Equation 5}$$

Where Y is the measured response associated with each factor level combination; b_0 is an intercept; b_{11}–b_{33} are regression coefficients computed from the observed experimental Y values; and X_1, X_2,

and X_3 are the coded levels of independent variables. The terms X_1X_2 and X_i^2 (i = 1, 2, or 3) represent the interaction and quadratic terms, respectively (Abul Kalam et al., 2013).

The optimized formulations were selected on the bases of desirability functions, each response was correlated with its partial desirability function. When the desirability value is at maximum, it's value will be equal to one and if it is totally unacceptable, it's value is zero, hence the desirability can be calculated at a known point in the experiment, where the highest value for desirability is optimal, desirability was explored in the literature instances (Ghaedi et al., 2014, Talebianpoor et al., 2014, Ghaedi et al., 2015). Finally, optimized six formulations with six different liquid lipid compositions was selected for detailed physicochemical characterization.

3.2.5 (I) Statistical analysis

Experimental design, data analysis and desirability function calculations were performed by using the software Stat-Ease Design-Expert trial Version 9.0.4.1.Analysis of Variance (ANOVA) provision available in the software was used to establish the statistical validation of the polynomial equations generated by Design expert®, the design calculate the sum of squares (SS), mean square (MS) Fisher's ratio (F-statistics) and P-value, the F-test was employed to establish the relationship between the dependent and the independent variables at 95 % (*p*-value = 0.05) significance level. The design software perform the response surface methodology (RSM) and give the results in the form of co-efficient of multiple regression analysis (R^2) measure the variation between the two sets of variables (Table 3-3 Table 3-4).

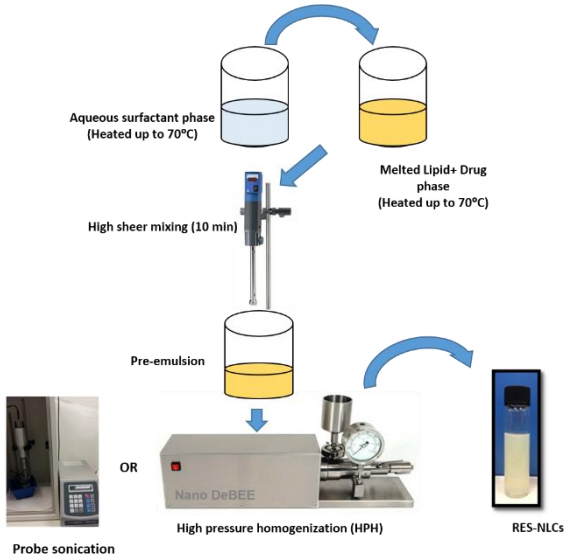

Figure 3-1 Preparation method of RES-NLCs using HPH or ultrasonication method

3.2.6 Preparation of PEGylated RES-NLCs

In order to prolong the circulation time, the RES-NLCs were suitably PEGylated. RES-NLCs with the best stability was selected for PEGylation. Polyethylene glycol monostearate (PEG-40 Stearate) was utilized as PEGylating agent. For the preparation of PEGylated NLCs (RES-NLC-PEGS40), part of (0.166 % w/w) the solid lipid (trimyristin) was replaced by PEG-40 Stearate. The preparation procedure remained unchanged and was same as given in section 3.2.4.2 (Figure 3-2).

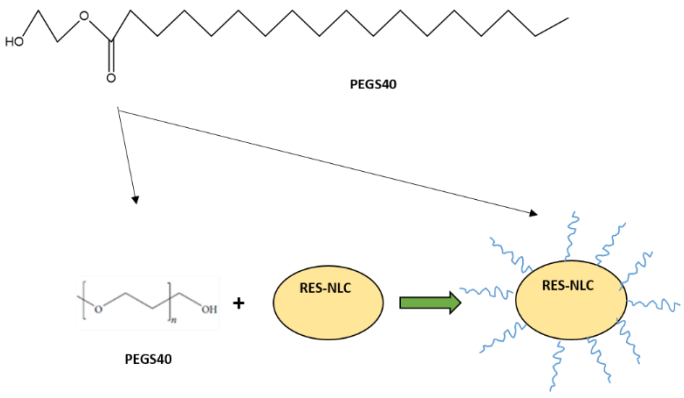

Figure 3-2.Schematic diagram of RES-NLCs-PEGS40

Table 3-1: Physicochemical properties of liquid lipids and RES

Liquid lipid		Chemical formula	Type of liquid lipid	Melting point	HLB Value
Chemical name	**Brand name**				
Propylene glycol-8 caprylic/capric glycerides (PCG)	Labrasol	NA	PEGylated lipid	<20	14
Propylene glycol monocaprylate (type II) NF (PGMC)	Capryol 90	$C_{11}H_{22}O_3$	Propylene glycol ester	<20	6
Propylene Glycol Monolaurate (PGML)	Lauroglycol 90	$C_{15}H_{30}O_3$	PEGylated lipid	<20	5
Glyceryl trioleate(GTO)	Triolein	$C_{57}H_{104}O_6$	C18:1 triglycerides	5	0
Decyl octadec-9-enoate (DO)	Decyl oleate	$C_{28}H_{54}O_2$	Fatty acid ester	<20	NA
Glycerol tricaprylate (GTC)	Miglyol 808	$C_{27}H_{50}O_6$	C8:0 triglycerides	9-10	7

Drug	**Solubility (mg/100mL)**	**Log P**	**Melting point (ºC)**	**pKa**	**Molecular mass (g/mol)**	**Molecular formula**
Resveratrol	0.03	3.1	254	8.99	228.25	$C_{14}H_{12}O_3$

Table 3-2: Experimental factors and levels in the Box-Behnken design for RES-NLCs

Factor	Levels Used, Actual (Coded)		
	Low (-1)	**Medium (0)**	**High (+1)**
A (X_1) = Concentration of Liquid lipid (%)	0.25	0.5	0.75
B (X_2) = Tween 80 concentration (%)	0.5	0.75	1
C (X_3) = Amount of drug (mg)	100	150	200
D= Liquid lipid type	GTO, GTC, PGMC, PGML, PCG, DO		
Dependent Variables	Constraints		
Y_1 = Particle Size (PS)	< 100 nm		
Y_2 = Polydispersity Index (PDI)	< 0.3		
Y_3 = Zeta Potential (ZP)	± 30 mV		
Y_4 = Entrapment Efficiency (EE %)	Maximum		
Y_5 = Drug Loading (%)	Maximum		

3.2.7 Preparation of ligand appended RES-NLCs

3.2.7 (I) Chemical cross linking

RES-NLC-PEGS40 was surface modified to improve both its circulation and targetability to breast cancer cell lines. EDC and NHS were selected as coupling agents to attach HA, FA, and HAFA onto the free amine groups present on the surface of RES-NLCs (Mero and Campisi, 2014). Specific conjugation to carboxylic acids (–COOH) is achieved through Carbonyl-di-imidazole (CDI) which is used to activate carboxylic acids for direct conjugation to primary amines (–NH2) through amide bonds. The most common carbo-di-imide compounds are the water-soluble EDC for aqueous crosslinking. Two reactions are used for cross linking (Conde et al., 2014).

The formation of amide bond proceeds by two stages. The first reaction involves the activation of carboxylic acid groups on the nanoparticles surface by 1-Ethyl-3-(3-dimethylaminopropyl)-carbodiimide (EDC) (EDC carbo-di-imide cross-linker) utilized for coupling the ligands on to the surface of bare RES-NLCs (Hermanson, 2008). The good water solubility of EDC makes it a preferable linking reagent since no organic solvents are required for its dissolution (Figure 3-3.A). The key advantage of this method is that ligand does not require any primary modifications frequently causing the loss of its activity (Nobs et al., 2004, Kocbek et al., 2007).

A.1-Ethyl-3-(3-dimethylaminopropyl)-carbodiimide (EDC) reaction chemistry (EDC carbo-di-imide cross-linker)

EDC reacts with carboxylic acid groups forming an active O-acylisourea intermediate (unstable) which is easily displaced by nucleophilic attack from primary amino groups in the reaction mixture. Amide bond is formed between the primary amine and the original carboxyl group, and an EDC by-product will be released as soluble urea derivative. Carboxyl-to-amine crosslinking with the popular carbodiimide, EDC. Molecules (1) and (2) HA or FA that have respective carboxylate and primary amine groups (Figure 3-3B).

B. N-HYDROXYSUCCINIMIDE (NHS) AMIDE REACTION

N-hydroxysuccinimide (NHS) usually included in EDC coupling protocols in order to improve efficiency or create dry-stable (amine-reactive) intermediates (Figure 3-3 B). EDC couples NHS to carboxyl group forming an NHS ester, that is substantially more stable than the *O*-acylisourea intermediate while permitting the efficient conjugation to primary amines at physiologic pH (7.4).

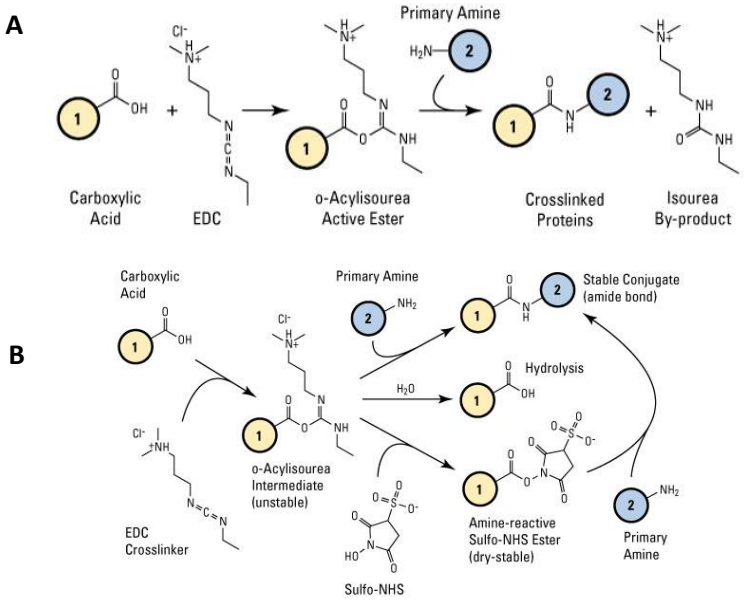

Figure 3-3. Schematic diagram showing the general chemical conjugation reaction A. EDC cross linking, B. NHS amide reaction (copied from Thermofisher site)

3.2.7 (II) Determination of free amine groups

Free amines on the RES-NLC-PEGS40 were determined using the 2, 4, 6-trinitrobenzenesulphonic acid (TNBS) assay via UV-VIS spectroscopy, which is a common reagent for the quantitative determination of primary amine groups in alkaline conditions (Satake et al., 1960). TNBS reacts with amine groups through aromatic nucleophilic substitution reaction (Figure 3-4), resulting in a yellow byproduct with absorption maxima at 340nm (trinitrophenyl amine) and 420nm (Meisenheimer complex) (Gyarmati et al., 2015).

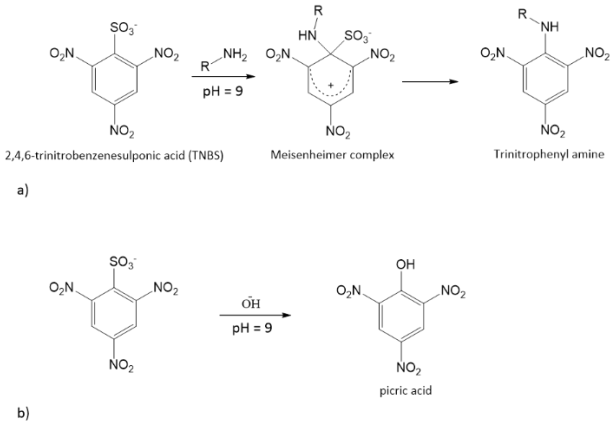

Figure 3-4. Reaction of 2,4,6-trinitrobenzenesulphonic acid (TNBS) with a)primary amines and b)hydroxyl ion. Adapted from (Gyarmati et al., 2015)

A. TNBS calibration curve

TNBS was diluted with sodium bicarbonate solution (4%) adjusted at pH 8 giving concentration of 4 µmol/mL. Two sets of solutions with different volumes were made from the prepared solution and transferred into a 10 ml volumetric flask (65, 135, 205, 270, 340, 480 µL). In one set of flasks, 0.1 mL of L-valine (40 µmol/mL) and 0.1 mL of 1% trichloracetic acid (TCAA) were added. In the other set of flasks, only 0.1 mL of 1% trichloracetic acid was added as the reference (Blank). Both sets of flasks were kept in dark for 1 h at 40^{o}C to react then the reaction was terminated by adding (0.5 µmol/mL) HCl solution to the volume (10 mL). The absorbance (A) was measured at 410 nm. The relationship between TNBS concentration(C) and Absorbance (A) was given by the regression equation **A= mx + c** Equation 6

Where A is the absorbance, m is the slope of the straight line, x is the unknown concentration and C is the intercept.

B. Determination of free amine groups on RES-NLCs

RES-NLCs (0.5 mL) was added into 4 mL (4 µmol/mL) of TNBS solution and incubated in dark for 1 h at 40^{o}C. The mixture was then centrifuged (13300 rpm for 30 min), the supernatant was isolated, and 0.9 mL was transferred into two sets of volumetric flasks in one set 0.1 mL of 0.1% TCAA was added along with 0.1 mL of (40 µmol/mL) L-valine, and in the other set adding only 0.1 mL of TCAA

was added as the reference (Blank). Both sets of flasks were incubated for another hour in dark at 40^{o}C, the reaction was terminated by diluting with (0.5 µmoL/mL) Hcl to the volume. The values obtained absorbance measured at 410 nm were converted into µmoles of free amine group /mL of the formulation, employing the calibration curve (Gao and Zhanga, 2011).

3.2.7 (III) Preparation of hyaluronic acid appended RES-NLCs-GTO-PEGS40 (RES-NLC-GTO-PEGS40-HA)

RES-NLC-GTO-PEGS40 were surface modified by HA (Figure 3-5 A), using three different molar ratios; of amine groups on the surface of NLCs: ligand ratio viz. 12:1, 16:1 and 18:1, corresponding to 2.220, 1.660 and 1.475 mg of HA weight, respectively. EDC and NHS were taken in equimolar ratio to the ligand. EDC was first added to HA and stirred for 1 h. This was followed by the addition of NHS and stirred for another 1 h. Subsequently, 5 mL of RES-NLC-GTO-PEGS40 was added to the mixture and incubated for 24 h; all incubations were done at room temperature. RES-NLC-GTO-PEGS40-HA residual reactants were removed through dialysis using dialysis membrane cutoff 3.5 kDa with distilled water (Figure 3-5 A,C).

3.2.7 (IV) Preparation of folic acid appended RES-NLCs-GTO-PEGS40 (RES-NLC-GTO-PEGS40-FA)

Similarly, RES-NLC-GTO-PEGS40 was surface modified by FA (Figure 3-5 Figure 3-5.B), using three different molar ratios; of amine groups on the surface of NLCs: ligand ratio viz. 2:1, 5:1 and 8:1, corresponding to 3.125, 1.563 and 0.937 mg of FA weight, respectively. EDC and NHS were taken in equimolar ratio to the ligand (Figure 3-5.B,D). Same procedure was followed as given in section 3.2.7 (III).

3.2.7 (V) Optimization of ligands quantity on the RES-NLC s surface

The conjugation of ligands on the surface of nanoparticles will result in changes to the properties of both the surface modified NLCs. Similarly, the size, morphology and surface charge of nanoparticles can also vary. In order to fully understand the properties of functionalized nanoparticles, it is important to determine the effect of the interaction between the nanoparticles and their ligands on the physicochemical properties of the bare nanoparticles. When designing of targeted nanoparticles, the size and shape of the nanoparticles should be taken into consideration. Moreover, the surface charge of nanoparticles have an effect on the efficacy of the targeted nanoparticles. The charge of the bare nanoparticles and that of the ligand will have an effect on the conjugated product and the spatial arrangement of the ligand on the surface. Based on the aforementioned properties, different ligand (HA, FA and HAFA) ratios were employed. In order to select the suitable quantity of ligands to be used on the surface of RES-NLCs, to yield systems. Three ratios of amine groups present on the NLCs surface: the ligand viz. 12:1, 16:1 and 18:1 for HA and 2:1, 5:1 and 8:1 for FA were prepared and their effect was investigated on the particle size, polydispersity index and surface charge of the conjugated molecules. Consequently, one best ratio was chosen to formulate individual ligand appended formulation. While the combination of the two ligands was employed in the formulation of dual ligands appended RES-NLC.

3.2.7 (VI) Preparation of dual targeted RES-NLCs-GTO-PEGS40 (RES-NLC-GTO-PEGS40-HAFA)

As breast cancer cells overexpress both CD44 and folate receptors, an attempt was made to prepare a dual targeted NLC system to target both the receptors to achieve enhanced target ability and improved chemotherapeutic efficacy. RES-NLC-GTO-PEGS40 was surface modified simultaneously by HA and FA (Figure 3-5.E). HA was taken in ration of 12:1, while FA was taken in ratio of 5:1 of amine groups on the surface of NLCs. Accurately weighed quantity of HA (2.22 mg) and FA (1.563 mg) were taken and EDC (0.925 mg) was stirred for 1 h and NHS (0.607 mg) was added and stirred for another hour. 5 mL of RES-NLCs-PEGS40 was added to the mixture and incubated for 24 h. RES-NLC-GTO-PEGS40-HAFA residual reactants were removed through dialysis using dialysis membrane cutoff 3.5 kDa with distilled water.

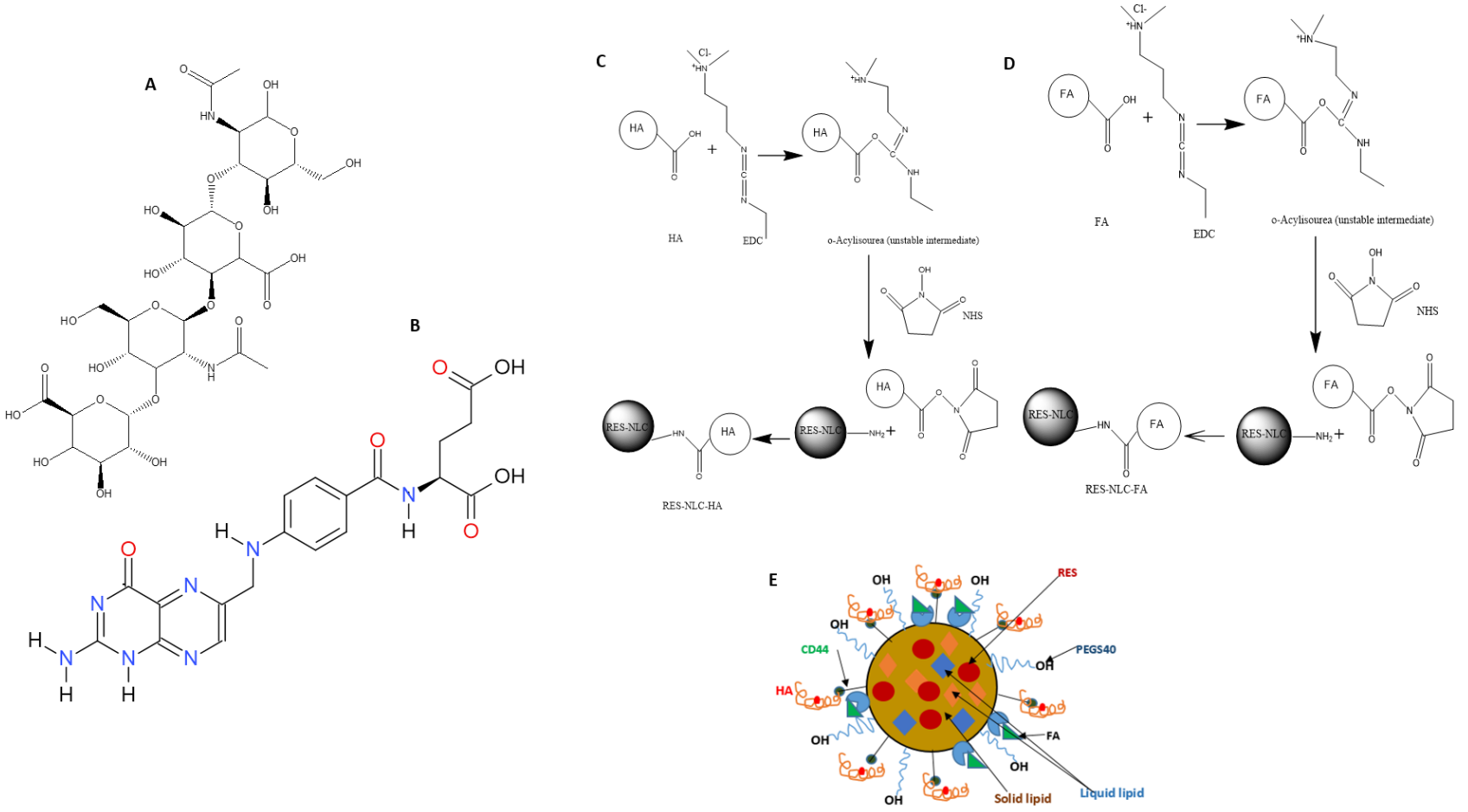

Figure 3-5. Chemical structure of A. Hyaluronic acid (HA), B. Folic acid (FA), Chemical cross linking of RES-NLCs yielding surface modified: C. RES-NLCs-HA, D. RES-NLCs-FA and E. RES-NLC-HAFA

3.2.8 The degree of chemical cross linking

The degree of chemical cross linking of the ligands onto the surface of RES-NLCs was determined by estimating the free amine groups present on the ligand appended formulations. Each of the three ligand appended formulations RES-NLC-PEGS40-HA, RES-NLC-PEGS40-FA and RES-NLC-PEGS40-HAFA, were taken and the free amine group was determined as per the method given in section 3.2.7 (II).

3.2.9 Physicochemical characterization of Optimized RES-NLCs

In order to fully investigate the characteristics of formulated nanoparticles, physicochemical properties of the particles were determined using various techniques as outlined below:

3.2.9 (I) Particle Size and Polydispersity Index

Particle size and polydispersity index (PDI) were measured using a Malvern Zetasizer (Nano ZS, Malvern Ltd., Worcestershire, UK) which utilises photon correlation spectroscopy (PCS) also known as Quasi-Elastic Light Scattering (QELS) technique, It is a size distribution analysis technique, which allows size measurement without detriment to the sample (i.e. the sample can be recovered). Disposable polystyrene cells (10 mm diameter) were employed to measure hydrodynamic diameter (ʒ-average) and PDI of formulated nano-dispersions. Measurements were conducted in triplicate with a scattering angle of 173^{o} at room temperature (Abdelwahab et al., 2013).

3.2.9 (II) Zeta Potential measurements

Zeta potential (ZP) is a measurement which indicates electric charges on particle surfaces; providing an indication to the physical stability of colloidal system (Chinsriwongkul et al., 2012). ZP was determined by the measurement of the electrophoretic mobility using a Malvern Zetasizer Nano ZS (Malvern Instruments, UK). RES-NLCs surface charge was analysed using a special zeta potential cells (DTS1060) obtained from Malvern, UK.

3.2.9 (III) Morphology observation

A. Scanning Electron Microscopy (SEM)

Surface morphology of RES-NLCs was examined using SEM (JEOL, Japan). Prior to imaging, formulations were air dried on SEM stubs and gold coated with a sputter coater using a JFC-1200

Fine Coater (JEOL, Tokyo, Japan) for 2 minutes, followed by examination using an SEM (Quanta-200, FEI) at 20 Kilovolts (kV). The surface morphology of the samples was evaluated.

B. TRANSMISSION ELECTRON MICROSCOPY (TEM)

Morphological studies were performed for RES-NLCs by using TEM Philips CM 120. NLCs were diluted in ultrapure milli-Q® water and approximately 8 µl was placed upon a carbon coated copper grid (400 mesh). After drying at room temperature each grid was observed and photographed utilizing a Bio-Twin TEM (Philips Electron Optics BV, Netherland) operating at 80 Kv.

3.2.9 (IV) Determination of % Entrapment efficiency and %Total drug

The concentration of drug present in the aqueous phase was determined by an ultrafiltration method using centrifugal filter tubes with 3 KDa molecular weight cut-off. Briefly, RES-NLC dispersion was placed into centrifugal filter tube, which was then centrifuged at 13000 rpm for 60 min. Post- centrifugation, the concentration of soluble free drug in the aqueous phase was detected by the developed HPLC method described in section 2.4.2. RES was detected at a wavelength of 306 nm.

To determine the total drug in RES-NLCs, 1 mL of RES-NLC was accurately taken and 4 mL tetrahydrofuran was added to it in order to dissolve the lipids. The solution was mixed to ensure that the lipid and the drug were completely dissolved in tetrahydrofuran. The solution was then filtered using a 0.22 µm filter. The filtrate was diluted with the mobile phase and analyzed in HPLC as described in section 2.4.3. The experiments were performed in triplicate (n = 3).

Encapsulation efficiency EE (%) and Total drug TD(%) was calculated from the equations:

$$EE\ (\%) = \frac{W_{total} - W_{free}}{W_{total}} \times 100\% \qquad \text{Equation 7}$$

$$TD\ (\%) = \frac{W_{total} - W_{free}}{W_{lipids}} \times 100\% \qquad \text{Equation 8}$$

Where W_{free} is the amount of free drug in the supernatant; W_{total} amount of RES added; W_{lipids} is the total amount of lipids.

3.2.9 (V) Differential Scanning Calorimetry

DSC is a thermal analysis which measures the changes in the physical properties of a sample, along with temperature versus time. DSC measures the amount of heat absorbed or released by the sample, based on temperature difference between the sample and the reference material (Gill et

al., 2010). In order to further understand the interaction between RES, solid and liquid lipid, DSC was performed on an array of combinations of the materials used for the preparation of RES-NLCs, using Metller 823^{e} DSC instrument (Switzerland). Initial measurements were conducted upon RES, trimyristin and six liquid lipids individually. DSC of physical mixture of trimyristin with different liquid lipids at three concentrations, as well physical mixture of RES with different liquid lipids concentrations was also investigated.

In order to investigate the impact of liquid lipid upon solid liquid, combinations of various liquid and solid lipid in various concentrations were manually mixed into a homogenous mixture and (3-5 mg) of the mix was transferred to aluminium pans (40 µL). Subsequently, the pans were covered and sealed with an orifice made in the pan lid using a pin provided by Mettler Toledo. An empty sealed pan was employed as a reference material during the scanning process. The sample was heated from 0 to 100^{o}C at a rate of 10^{o}C/min and a nitrogen flow of 0.2 mL/min. The impact of liquid lipid upon drug investigate, by the combinations of various liquid lipids with three different concentrations used in the formulations and drug in various concentrations were manually mixed into a homogenous mixture and transferred to aluminium pans (40 µL) and heated from -10 to 300^{o}C at a rate of 10^{o}C/min and a nitrogen flow of 0.2 mL/min.

DSC studies were also conducted on bare and surface modified RES-NLCs. Accurately weighed formulation samples were placed in 40 µL aluminum pans and heated from 25°C to 300°C at a rate of 10°C/min, with a nitrogen purge of 0.2 mL/min. Subsequently, the sample was cooled down to 0°C with a nitrogen purge of 0.2 mL/min. An isothermal hold was placed on the sample at 0°C for a period of 2 min and then heated once again to 300°C at a rate of 10°C/min. The resulting thermograms were analyzed using Mettler StarE DB V9.10 software. Comparison of the melting enthalpy/g of the individual material with the melting enthalpy/g of the NLCs dispersion provides an estimation of the crystallinity of the drug (Siekmann and Westesen, 1994). The apparatus was calibrated one every two weeks using indium as a reference material.

DSC analysis of physical mixtures corresponding to each RES-NLC was conducted by accurately weighing between 3-7 mg of the homogeneous mix, in a flat bottom 40µL aluminum pan. Samples were heated from 25°C to 70°C, at a heating rate of 10°C/min, with a nitrogen purge of 0.2 mL/min. An isothermal hold was implemented at 70°C for a period of 60 min, and cooled to 0°C at a rate of 10°C/min. A final isothermal hold was maintained at 0°C for 2 min, with the sample heated to 300°C (10°C/min).

3.2.9 (VI) X-Ray Powder Diffraction (XRD)

XRD is a non-destructive analysis technique commonly used for the characterization of micro and nano-crystalline materials such as organic, pharmaceutical compounds and various nanoparticle.

This method has been traditionally applied for quantitative analysis, phase identification and the determination of structure imperfections (Louër, 2017).

The degree of RES crystallinity when formulated as a NLCs was assessed using X-ray diffractometry (X-ray diffractor, D2 PHASER with LYNXEYE, Bruker, Germany). Dried samples were loaded onto inert polymeric discs and smoothed using glass sides, in order to maintain homogenous contact between the sample and equipment. Samples were scanned from 5 to 50^{o} with a set scan type, coupled with two θ (theta) using a scintillation counter and 1-dimensional LYNXEYE detector. Upon sample testing, collation of the generated patterned data was used to ascertain the presence or absence of crystalline RES in the NLCs formulations as well physical mixtures. Several samples were assessed using X-ray diffractometry to allow for data validation, including RES alone (pure drug), RES-NLCs (lyophilized) and their corresponding physical mixtures. Data analysis was performed utilizing the Diffrac. Suite Eva software version 3.0, Germany.

3.2.9 (VII) Fourier Transform Infrared Spectroscopy (FTIR)

FTIR Spectroscopy (Nicolet IR200, ThermoScientific) is a qualitative analytical technique used to identify organic, polymeric, and in some cases, inorganic materials. During FTIR analysis, an absorbance spectra of the sample is created which provides information about the unique chemical bonds (functional groups) and molecular structure of the material.

Samples (individual formulation constituents, RES alone, lyophilized blank NLCs, lyophilized bare RES-NLCs and surface modified RES-NLCs) were employed to obtain FTIR spectrum. The first step was to collect background spectrum to subtract from the test spectra to ensure the actual sample is all that is analysed. The spectra were recorded in the range of 4000-400 cm^{-1}. The sample is analysed by OMNIC 8.0.380 computerized FTIR Spectroscopy software (ThermoScientific) system which generated the absorbance spectra showing the unique chemical bonds and the molecular structure of the sample material. This profile is in the form of an absorption spectrum which shows peaks representing components in higher concentration. Absorbance peaks on the spectrum indicate functional groups. The analytical spectrum was then compared in a reference library program with catalogued spectra to identify components or to find a “best match” for unknown material using the catalogued spectra for known materials.

3.2.9 (VIII) Nuclear Magnetic Resonance (NMR) spectroscopy

NMR is one of the main spectroscopic techniques employed in the characterization of molecular structure of different chemical entities and detailed conformational dynamics at the atomic level. It is a multipurpose, high resolution and non-detrimental analytical technique. It can be used for

both quantitative and qualitative characterization purposes (Emsley and Feeney, 2007, Campagne et al., 2011). RES, Blank NLCs and RES-NLCs were prepared in DMSO and high-resolution proton nuclear magnetic resonance (^{1}H-NMR) spectra were obtained on an NMR Bruker Fourier (Germany), operating at 300 MHz and 20°C. TMS (tetramethyl silane) used as a reference for 0 ppm NMR deuterated DMSO was obtained from GOSS Scientific, UK. NMR spectra were processed employing MestReNova (10.0.2 software, Spain).

3.2.10 *In vitro* drug release studies

In vitro drug release studies is of critical importance in terms of the design, development and testing of formulations (Crane et al., 2004, Siepmann and Peppas, 2001). *In vitro* drug release can be used to extrapolate and determine the *in vivo* release model. In addition, modelling can lead to developing better scientific understanding of the behaviour of a number of studied nano-systems. The solid matrix of NLCs can protect incorporated active ingredients against chemical degradation and highest flexibilities in the modulation of the drug release profiles, can be provided by incorporation of different liquid lipids. *In vitro* drug release studies were undertaken of RES-NLCs prepared with six different liquid lipids to study the effect of liquid lipids on the drug release profile. Also drug release studies were carried out for surface modified NLCs, and the effect of surface functionalization was evaluated on the release of RES.

As the RES stability has been reported to be affected by pH (Zupančič et al., 2015). Chemical stability of RES in four different pH was studied in order to establish the suitable media to carry out the *in-vitro* drug release studies. Solutions with 20 µg/mL of *trans*-RES were prepared in buffers with pH 1.2, 5, 6.8 and 7.4 and stored at 25 and 37°C for 24 h. Samples of 1 mL were withdrawn and immediately analysed via HPLC post filtration.

Drug release study was conducted in two different pH media (1.2 and 5). To determine the release rate of RES from nanoparticles, cellulose dialysis bag diffusion technique was performed. Dialysis bags (Spectra/Por 3 Dialysis Tubing cut off 3.5 kD), were first cut into the appropriate length, washed with distilled water to remove the excess glycerine and then soaked overnight in the release medium prior to the experiment (Elmowafy et al., 2017). 5 mL of NLCs dispersion was added to the dialysis bags, sealed and placed in the glass vessel (ERWEKA® dissolution tester, D-63150 Heusenstamm/Germany) containing 900 mL of dissolution media (pH 1.2 or pH 5) dissolution media maintained at 37 ± 0.5°C using thermostatically controlled water bath. The dissolution media was stirred at 100 rpm ± 2 during the study.

When pH 1.2 buffer was used, 1 mL sample was withdrawn at predetermined time intervals: 30 min, 45 min, 1, 2, 3, 4 h. While when pH 5 was used the samples were withdrawn at time intervals of: 30 min, 45 min, 1,2,3,4,5,6,7,8,9,10,11,12 and 24 h. For both the studies after withdrawal of the

sample the media was replaced with fresh media maintained at the same temperature, in order to maintain the sink condition. Additionally, drug release test on non-encapsulated free resveratrol was performed as a control group. The content of RES released from all formulations, at the each time point was determined by the previously validated HPLC method described in section 2.4.2. The study was conducted in triplicate and the cumulative % of released drug was determined.

The mechanism and kinetics of RES release from NLCs was assessed by plotting graphs of various kinetic models (Soma et al., 2017), R^2 value for each formulation was fitted to the appropriate kinetic model (Guinedi et al., 2005), the release profile for each formulation at the determined pH was fitted into various kinetic models e.g. zero order, first order and higuchi model (Dash et al., 2010). The zero order rate describes the systems where the drug release rate is independent of concentration given by the equation (Hadjiioannou et al., 1993).

$$C = K_0 t \qquad \text{Equation 9}$$

Where, K_0 is zero-order rate constant expressed in units of concentration and t is the time.

The first order describes the release from system where release rate is concentration dependent, equation depicted (Bourne et al., 2002)

$$LogC = LogC_0 - kt / 2.303 \qquad \text{Equation 10}$$

Where, C_0 is the initial concentration of drug and k is first order constant.

Higuchi (1963) described the release of drugs from insoluble matrix as a square root of time dependent process based on Fickian diffusion shown in the below equation (Higuchi, 1963)

$$Q = Kt^{1/2} \qquad \text{Equation 11}$$

Where, K is the constant reflecting the design variables of the system.

3.2.11 Storage stability of RES-NLCs

Stability of the six optimized RES-NLC formulations containing each of the six liquid lipids was evaluated for period of six months. Briefly, samples were stored in sealed amber colour glass bottles at both 4°C and 25°C. Samples were withdrawn at one, three and six month intervals and characterized with respect to particles size, polydispersity index, zeta potential, %EE and %TD(Muppidi et al., 2012). All data obtained was compared to the initial PS, PDI, ZP, %EE and %TD of the formulated NLCs. The stability of surface modified RES-NLCs was assessed over the period of three months, at both 4 and 25°C.

3.2.12 Statistical analysis

All stability study results were expressed as a mean ± SD. The statistical analysis of obtained results was performed by two-way ANOVA followed by Bonferroni post-test to compare replicates (n=3) using the GraphPad Prism 5 for windows version 5.01.August 2007 ® software. Difference at $p < 0.05$ was considered statistically significant, three asterisk indicates $P< 0.001$, two asterisks, $P < 0.01$ and one asterisk $P< 0.05$. The comparison between the Bare RES-NLCs and the surface modified NLCs for various parameters was done through one way ANOVA followed by Dunnett's Multiple Comparison post-test using GraphPad Prism 5 for windows version 5.01.August 2007®software. Difference at $p < 0.05$ was considered statistically significant, *** indicates $P< 0.001$, **, $P < 0.01$ and * $P< 0.05$.

3.3 Results and Discussion

3.3.1 Solubility of RES in different liquid oil

The drug carrying capacity of NLCs is directly dependent upon the solubility of the respective drug in the lipid matrix, and is a crucial factor for the development of NLC formulations. Thus the selection of the suitable lipids and formulation excipients may significantly affect the process of NLC development (Rizwanullah et al., 2016, Barratt, 2000). Oil content in NLCs has been known to considerably affect the size, surface morphology, entrapment efficiency, drug release and stability of NLCs (Emami et al., 2012, Yang et al., 2014). The chosen active pharmaceutical excipients (API) should ideally have high solubility in the liquid lipids in order to achieve maximum entrapment of the drug in the NLCs.

Out of the liquid lipids tested, RES exhibited highest solubility in Labrasol (112.288 ± 4.114 mg/mL) (PCG) which is comprised of 30 % mono-, di- and triglycerides of C8 and C10 fatty acids, 50 % of mono- and di-esters of PEG, and 20% of free PEG 400. It is a clear liquid with high HLB of 14, composed by a mixture of mono-, di- and triglycerides and mono- and di-fatty acid esters of polyethylene glycol as stated in the study done by. Due to the ability of long polyethylene glycol (PEG) chains of PCG, it can incorporate higher concentrations of drug into the lipid matrix. It was reported that lipid matrix comprising of PCG in the lipids mixture increases the solubility and bioavailability of hydrophilic and hydrophobic drug. PEGylation of the Labrasol is deemed to a contributing factor to the high solubility of RES in the liquid lipid (Figure 3-6) (Li et al., 2013a, Thang et al., 2017).

The two propylene glycol esters (PGML and PGMC) also exhibited good solubility for RES though less than PCG. These liquid lipids have been previously used to enhance the solubility of drug (Abhijit et al., 2011, Zhang et al., 2014a).

The two triglycerides GTC and GTO had limited solubility for RES. Between the two short chain C8 triglyceride (GTC) showed higher solubility for drug. The least solubility was shown by DO because of its hydrophilic nature Solubility in different carriers followed the following pattern from high to low solubility order of the drug in the liquid lipid PCG >PGML >PGMC >GTC > GTO> DO (Malzert-Fréon et al., 2010).

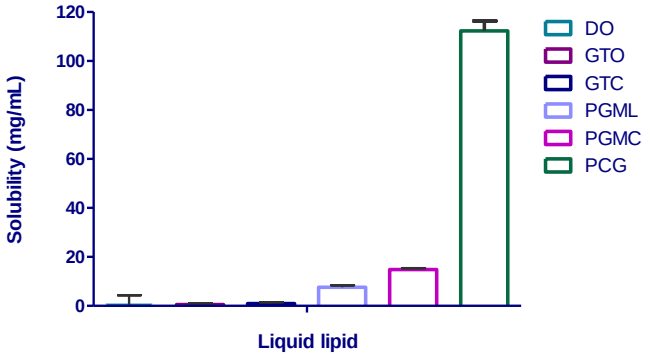

Figure 3-6. Solubility studies of RES in various carriers lipid oils (n = 3), error bars are standard error of the mean

3.3.2 Optimization of RES-NLCs by Box and Behnken design

3.3.2 (I) Response surface analysis

The influence of liquid lipid type employed in each formulation, liquid lipid concentration, surfactant concentration (Tween 80) and drug amount on particle size, PDI, ZP, %EE and %DL are graphically represented in (Figure 3-7Figure 3-8). These contour plots are very useful to establish the interaction effects of the independent variables on the responses of dependent variables. These plots are diagrammatic representation of the response.

They are also used to understand the relationship between independent and dependent variables based on the model polynomial functions, to evaluate change in response surface, the qualitative effect of each factor on the response can be deduced from these plots (Hao et al., 2011). The response surface plots were utilized to assess the interaction effect of two independent factors on the dependent variables or responses, when other factors are kept at constant level (Kim et al., 2007). Figure 3-7 demonstrates the effect of the interaction between the liquid lipid concentration with different amount of drug at medium level of Tween 80 changing the liquid lipid and studying the effect on different responses. While Figure 3-8 shows the interaction between the liquid lipid concentration and the Tween 80 concentration at a low level of drug for each type of liquid lipid with different responses.

3.3.2 (II) Responses fitness to the model

A quadratic model for all the responses (Particle size, PDI,ZP, EE%,DL%) was indicated by the design of experiment software, where high R^2 values (0.743-0.929) were observed by the quadratic model, and was therefore implemented for all responses. It is well established in order for the model to be utilised, the R^2 value should exceed 0.9 and show best model fit to the results generated (Wang et al., 2014a) (Table 3-3). Polynomial equations were generated which explains the individual key effects and interactions effects of independent factors on the dependent variables by Design-Expert software. The appropriateness of the model should be assessed by examining the difference between the observed value of the dependent variable and the predicted values that represents the scatter of the predicted versus actual values (Figure 3-9 and 3-10). The suitability of the model was determined by the R^2 value for each response which ranged from 0.747 to 0.929 indicating a good correlation between the actual and predicted data both the Figure 3-9 and 3-10 show the strong correlation between the variable and the response, where all the values are scattered around the regression line, showing the closeness of the actual and predicted values to each other indicating good fit for the models (Kolaei et al., 2016).

The lack of fit (LOF) is a value that describes the data variation around the fitted model. It also judges the adequacy and accuracy of the model to fit the results. A non-significance value of LOF shows that the model is suitable in fitting the data and predicting the response (Behbahani et al., 2017, Kollipara et al., 2010). Lack of fit is an undesirable characteristic for a model, and generally it should be insignificant. (P> 0.10 is better). Model enhancement is done by the elimination of insignificant terms (Dong et al., 2016). An F-value of LOF for PS, PDI, ZP, %EE and %DL was obtained as 4.91, 2.58, 2.59, 4.59 and 21.80, respectively, that demonstrate the ability model for predicting the response and finding the best formulation conditions. The model p value (LOF) showed significance of the model.

The analysis of the each response was carried out employing the suitable model and the necessary statistical transformation was recommended by the design for each response in order to increase the power of the response that is demonstrated by the Box Cox plot for power transformation for each responses (Figure 3-11).Transformation of the response is an important component of any data analysis. The Box-Cox plot will provide a recommended transformation from the power family. The two non-power law transformations, logit for bounded data and arcsine square root for proportions, must be applied based on the type of response. The Box-Cox plot will often recommend a square root transformation when proportion data is present, and the log

transformation for bounded data. The Box-Cox plot is provided in the Diagnostics plots to help you choose an appropriate power transformation (Miller, 1984).

Design-Expert provides extensive diagnostic capabilities to check if the statistical assumptions underlying the data analysis are met. The ratio of maximum to minimum for all responses Y_1, Y_2, Y_3, Y_4 and Y_5 are 5.260, 4, 1.873, 1.089 and 2.573, respectively. A ratio greater than 10 usually indicate a transformation is required, therefore power transformation has little effect on the resulted values (Zhang et al., 2013).

The desirability function was employed to determine the optimum level of factor to yield the desirable response. The individual and the combined desirability's are shown in Figure 3-12. Each liquid lipid desirability space with the values close to 1 considered was best for the optimized formulation indicating higher desirability of corresponding response properties. The criteria decided for selection of the final optimized formulation was as follows: for the desired particle size range from 50 to 100 nm, polydispersity index of 0.113 to 0.3, zeta potential ranging from -37 to -21 mV, % entrapment efficiency of 94 to 99.546 % and finally a drug loading that range from 3 to 7.55 % (Figure 3-13). Both the individual and the combined desirability shows a value of 1 indicating that in order to obtain an optimized formulation with the criteria we have set above, the independent variables that are the lipid concentration, Tween 80 concentration, drug amount and the liquid lipid type all should be at their maximum level. The formulation with the desirability value close to unity is considered as the optimized formulation. Based on the response surface model and also on the decided criteria, 100 solutions were suggested by the Design-Expert® for each type of liquid lipid.

3.3.2 (III) Influence of investigated parameters on particle size

The particle size was clearly affected by the type of liquid lipid incorporated in the RES-NLCs. Figure 3-7 shows the particle size of NLCs prepared with six different liquid lipids at a fixed concentration of surfactant and drug. The more lipophilic oils GTO, GTC and DO which were more miscible with the solid lipids resulted in lower particle size as compared to the hydrophilic oils (GTC, PGMC and PGML). This is in corroboration with previous study which has demonstrated higher particle size upon the inclusion of labrasol (Malzert-Fréon et al., 2010).

Further the amount of liquid lipid (X_1), surfactant concentration (X_2) and amount of drug (X_3), for each of the liquid lipid type affected the particle size and can be seen by the quadratic equations below generated by the software ($P< 0.05$).

For GTC

Y_1= +103.33462+41.64833× X_1-68.36833× X_2-0.49571× X_3-88.83333× X_1×X_2+0.12487× X_1×X3-0.083767×X_2×X3+23.18667×X_1^2+52.46000×X_2^2+2.32167E-003×$X3^2$ Equation 12

For DO

Y_1=+28.18333×X_1-82.71333×X_2-0.48106×X3-88.83333×X_1×X_2+0.12487×X_1×X3 0.083767×X_2×X3+23.18667×X_1^2+52.46000×X_2^2+2.32167E-003×X^2 Equation 13

For PCG

Y_1= +119.05913+32.47333× X_1-79.84333×X_2-0.51231×X3-88.83333× X_1×X_2+0.12487× X_1× X3-0.083767× X_2 × X3+23.18667× X_1^2+52.46000× X_2^2+2.32167E-003× $X3^2$ Equation 14

For PGMC

Y_1= +108.17029+82.83333× X_1-50.11333× X_2-0.63466× X3-88.83333× X_1×X_2+0.12487× X_1 × X3-0.083767× X_2 × X3+23.18667× X_1^2+52.46000× X_2^2+2.32167E-003× $X3^2$ Equation 15

For GTO

Y_1=+121.03423+39.50833× X_1-72.21333×X_2-0.57738× X3-88.83333× X_1×X_2+0.12487× X_1 × X3-0.083767× X_2 × X3+23.18667× X_1^2+52.46000× X_2^2+2.32167E-003× $X3^2$ Equation 16

For PGML

Y_1=+103.85404+71.22833× X_1-70.10833× X_2-0.52336× X3-88.83333× X_1×X_2+0.12487× X_1× X3-0.083767× X_2 × X3+23.18667× X_1^2+52.46000× X_2^2+2.32167E-003× $X3^2$ Equation 17

Positive sign before a factor in polynomial equations suggest a synergistic effect signifies that the response increases with the factor, whereas a negative sign means the response and factors have reciprocal relation (Rahman et al., 2010). The magnitudes of the coefficients indicate the degree of contribution of the factor to the response (Hao et al., 2012, Behbahani et al., 2017).

The most significant factor contributing to the variation in the particle size was amount of liquid lipid (X_1) as evident from the value of the coefficient shown in equations (8-13). The observation of the increase in particle size with increasing in the amount of liquid lipid was in accordance with the previously reported work (Andalib et al., 2012, Velmurugan and Selvamuthukumar, 2016). This might be attributed to the increase in the coalescence and aggregation, as the amount of the lipid increases the viscosity in turn increase leading to higher surface tension and larger particles are formed. This was also observed by recent reports (Thang et al., 2017).

These observations are also elaborated in the contour plots (Figure 3-8) where it shows the interaction of X_2 (Tween 80 concentration) and X_1 (lipid concentration) with X_3 (drug amount) at its lowest level. The prevalence of the blue region means that the particle size of NLCs is small.

The second factor contributing to the particle size was surfactant concentration (X_2); it had a negative effect on the response of the particle size as the coefficient of X_2 was negative suggesting that the increase in the Tween 80 concentration lead to a reduction in the particle size (Araújo et al., 2010, Chaudhary et al., 2015). Higher concentration of surfactant would results in reduction in the surface tension and production of particles with small sizes whereas lower concentration of surfactant would be insufficient to reduce the interfacial tension yielding larger size particle (Agrawal et al., 2010, Niculae.G. et al., 2013).

The amount of drug (X_3) had negative effect on particle size, suggesting that an increase in amount of drug lead to the reduction in the particle size, The high melting point of resveratrol (267.14°C) compared to that of trimyristin (the solid lipid used; 56–57°C), would probably lead to a more viscous dispersed phase originating in large particle size NLCs. Similar observation that the average diameter of NLCs increased as the amounts of drug increased has been made in previous study (Deli et al., 2009). This effect is also shown in the contour plots (Figure 3-7) where the interaction of both the amount of drug and the liquid lipid concentration keeping the Tween 80 at its middle concentration has been illustrated.

For all types of liquid lipid the interaction between the factors (X_1-X_2 and X_2-X_3) had a negative effect on the particle size suggesting that even though factor X_1 (amount of liquid lipid) had a positive effect on particle size, the interaction with X_2 and X_3 causes a negative effect on particle size. However, the interaction between (X_1-X_3) had a positive effect on particle size even though factor X_3 (amount of drug) had a negative effect on particle size. This interaction can be used favourably for tailoring of particle size in accordance to the values of the different factors.

Further analysis employing Analysis of Variance (ANOVA) indicated the effects of independent variables (p > F, 0.0001) on response particle size (Y_1) (Table 3-3 and Table **3-4**). The Model F-value of 4.91 implies the model is significant. There is only a 0.01% chance that an F-value this large could occur due to noise. Values of "Prob > F" less than 0.050 indicate model terms are significant. A good correlation has been determined between the observed and the predicted value as designated by R^2 value of 0.7477 (Figure 3-9 and 3-10). Adequate Precision measures the signal to noise ratio. A ratio greater than 4 is desirable ratio of 8.983 indicates an adequate signal. This model can be used to navigate the design space to get optimum particle size.

3.3.2 (IV) Influence of investigated parameters on polydispersity index (PDI)

PDI is measure of the heterogeneity of sizes of particles in a mixture and an indicator of aggregation in the particles (Thang et al., 2017). The PDI values obtained around the range of < 0.3 suggest that the nanoparticles exist in monodispersed distribution, with low variability and aggregation (Mitri et al., 2011, Neves et al., 2013, Rizwanullah et al., 2016). Polydisperse system have greater tendency for aggregation than monodisperse system. RES-NLCs prepared using Box-Behnken ranged from fairly monodisperse systems with a PDI 0.113 to PDI 0.452.

Although oil concentration has been reported to not have much effect on PDI of NLC (Jia et al., 2010). However, in this study DO as liquid lipid resulted in more monodisperse formulations (Figure 3-6Figure 3-7 and Figure **3-8**). Of interest was the observation that lower concentration of liquid

lipids resulted in NLCs with lowest PDI. This observation is in accordance to what was previously reported by (Zhang et al., 2013) This might be attributed to the increase in the agglomeration of the particles due to the Van der Waal attraction forces when higher amount of liquid lipid was incorporated (Thang et al., 2017).

The effect on the PDI is shown by the equations below:

For GTC

Y_2=+0.35498-0.25950× X_1-0.22717× X_2+8.26667E-004× X_3+0.18533× X_1 × X_2-1.53333E-004× X_1 × X_3 -5.43333E-004× X_2 × X3+0.039000×X_1^2+0.19033× X_2^2-2.34167E-006X_3^2 Equation 18

For DO

Y_2= +0.26509-0.12600× X_1-0.31917× X_2+1.36917E-003× X_3+0.18533× X_1 × X_2-1.53333E-004× X_1 × X_3-5.43333E-004× X_2 × X_3+0.039000×X_1^2+0.19033× X_2^2-2.34167E-006 X_3^2 Equation 19

For PCG

Y_2= +0.061811-0.061500× X_1+0.010333× X_2+6.74167E-004× X_3+0.18533× X_1 × X_2-1.53333E-004×X_1×X_3-5.43333E-004×X_2×X_3+0.039000×X_1^2+0.19033×X_2^2-2.34167E-006X_3^2 Equation 20

For PGMC

Y_2=+0.25382+1.16573E-015× X_1-0.37767× X_2+1.49167E-003× X_3+0.18533× X_1 × X_2-1.53333E-004× X_1 × X_3-5.43333E-004× X_2×X_3+0.039000×X_1^2+0.19033× X_2^2-2.34167E-006X_3^2 Equation 21

For GTO

Y_2= +0.35697-0.12000× X_1-0.42267× X_2+1.29667E-003× X_3+0.18533× X_1 × X_2-1.53333E-004× X_1 × X_3 -5.43333E-004× X_2 × X_3+0.039000×X_1^2+0.19033× X_2^2-2.34167E-006X_3^2 Equation 22

For PGML

Y_2= +0.27357+0.044000× X_1-0.30917× X_2+1.10417E-003× X_3+0.18533× X_1 × X_2-1.53333E-004×X_1×X_3-5.43333E-004×X_2×X_3+0.039000×X_1^2+0.19033×X_2^2-2.34167E-006X_3^2 Equation 23

The most significant factor affecting the PDI for NLC dispersions was surfactant concentration (X_2) which exhibited a negative effect on this response in equations (14-19). Increasing the amount of Tween 80 concentration will lead to better homogeneity in particle size and reduced aggregation as higher amount of surfactant will cover the nanoparticles thus preventing their coalescence (Hu et al., 2005a, Agrawal et al., 2010). Flocculation is also probably prevented because of steric stabilization of the droplets due to the presence of a surfactant layer at the surface of the NLCs. If the thickness of the surfactant layer is high relative to NLC diameter, an efficient steric protection is assured, and the coalescence is prevented (Joshi and Patravale, 2006). The addition of higher amount of drug led to increased heterogeneity of NLC as demonstrated by the positive coefficient of this factor for all six type of liquid lipids (Tadros et al., 2004). The prevalence of the blue region in the contour plots reveals that the NLCs are homogenous (Figure 3-7Figure 3-8).

The interaction between the factors (X_1-X_2) had a positive effect on the PDI, signify that the increase in both the amount of liquid lipid and the concentration of surfactant will cause increase in the PDI. The presented interactions (X_1- X_3) and (X_2- X_3) displayed significant antagonist effects on the PDI even though factor X_3 had a positive effect on the response. This means that a simultaneous increase in either the amount of liquid lipid or the concentration of surfactant leads to a substantial decrease in the PDI and favoured the forming of more homogeneous distributed nanoparticle. Additional analysis using ANOVA pointed out the effects of independent variables (p > F, 0.0018)

on response Y_2 (Table 3-3 and Table **3-4**). The Model F-value of 2.58 implies the model is significant. There is only a 0.18 % chance that an F-value this large could occur due to noise. Values of "Prob > F" less than 0.050 indicate model terms are significant. Adequate Precision measures the signal to noise ratio. A ratio greater than four is desirable. The ratio of 8.259 indicates an adequate signal. This model can be used to navigate the design space. A nearly good correlation has been illustrated between the observed and the predicted value to obtain RES-NLCs with low PDI as designated by R^2 value of 0.609.

3.3.2 (V) Influence of investigated parameters on zeta potential

Generally high zeta potential (more negative or more positive) is considered as a main contributing factor for the stability of the colloidal dispersions (Luan et al., 2015, Rizwanullah et al., 2016). Generally, ZP of ± 30 mV is considered suitable to get a stable NLC dispersion. This is probably as a result of electrical repulsion between the particles (Salata, 2004, Muller et al., 2001). RES-NLCs were found to have sufficient stability with ZP in the range of -21.3 -39.9 mV. Change in the selected variables did not vary the ZP significantly.

The negative charge can be associated with the presence of hydroxyl ions on the surface of the lipid nanostructures, and is consistent with the observations in the previous studies (Hsu and Nacu, 2003, Klinkesorn et al., 2004, Klinkesorn and Namatsila, 2009, Witayaudom and Klinkesorn, 2017), In addition, another possibility is that the electrical charge of the RES-NLCs arose from the polyphenolic drug or free fatty acids and partial glycerides present in the oils or phospholipids used as stabilizers (Manaf.Y.N.A. et al., 2013, Mehdizadeh et al., 2015).

Additionally Tween 80 being a non-ionic surfactant with an HLB value of 15 being adsorbed on the surface of particles causes reduction in the net charge at the particle surface, resulting in negatively charged NLCs (Pogorzelski et al., 2012, Rizwanullah et al., 2016). Tween 80 also offers a steric hindrance for maintaining the stability of NLCs (Lim and Kim, 2002, Thatipamula et al., 2011).

As observed the liquid lipid played a more prominent role contributing to the increase in the negative surface charge (equations 20-25),due to the adsorption of hydroxyl ions of liquid lipids (Oomaha.B.D. et al., 2000). Some studies suggested (Niculae.G. et al., 2013) that the use of Tween 80 as a surfactant will lead to more negative ZP, furthermore, the use of medium chain liquid lipids produces nanoparticles with larger ZP values.

The amount of drug had a positive effect on the response, thus increasing the drug content will result in a reduction of the zeta potential value. This observation is in accordance to earlier report by Freitas and Muller who have shown that the increased drug amount causes a reduction in the

charge density on NLCs and consequently the absolute values of zeta potential is lowered (Freitas and Müller, 1998).

In conclusion, higher the zeta potential value, higher the repulsion forces between nanoparticles, therefore a low probability for particle aggregation with time and a higher stability of developed formulations will be achieved (Figure 3-7 and Figure **3-8**). Contour plots show the acceptable blue region was due to the reduction of the zeta potential to more negative value.

The quadratic polynomial equations below summarize the effect of six liquid lipids on the ZP

For GTC

Y_3 = -54.56346+11.23333 x X1+35.46667 xX2 +0.062667x X3+3.06667x X1 x X2 -0.041333 x X1 x X3-2.66667E-003x X2 x X3 +0.26667 x $X1^2$ -17.20000x $X2^2$ -1.33333E-004x $X3^2$ Equation 24

For DO

Y_3= -51.13269 +8.93333xX1+37.51667x X2 +0.045417x X3+3.06667x X1 x X2-0.041333x X1 x X3 -2.66667E-003x X2 x X3+0.26667x $X1^2$-17.20000x $X2^2$-1.33333E-004x $X3^2$ Equation 25

For PCG

Y3=-38.50673-0.016667x X1 +28.76667x X2 +0.046417x X3 +3.06667x X1 x X2 -0.041333x X1 x X3 -2.66667E-003x X2 x X3 +0.26667x $X1^2$ -17.20000x $X2^2$ -1.33333E-004x $X3^2$ Equation 26

For PGMC

Y_3= -47.67308 -7.26667x X1 +38.31667x X2 +0.050917x X3 +3.06667x X1 x X2 -0.041333x X1 x X3 -2.66667E-003x X2 xX3 +0.26667x $X1^2$ -17.20000x $X2^2$ -1.33333E-004x$X3^2$ Equation 27

For GTO

Y_3= -53.78462 +2.13333x X1 +38.76667x X2 +0.075667x X3 +3.06667x X1 xX2 -0.041333xX1 xX3-2.66667E-003xX2xX3+0.26667x$X1^2$-17.20000x$X2^2$-1.33333E-004x$X3^2$ Equation 28

For PGML

Y_3= -42.83942 -1.31667x X1+26.66667x X2+0.057417x X3+3.06667x X1 x X2-0.041333x X1 x X3 -2.66667E-003x X2 x X3+0.26667x$X1^2$-17.20000x $X2^2$-1.33333E-004x $X3^2$ Equation 29

The interaction between the factors (X_1-X_2 and X_1- X_3) for all liquid lipid type had positive effect on the ZP. The interaction between X_2- X_3 had a negative effect on the ZP even though both factors individually previously demonstrated a positive effect on the response.

Statistical analysis ANOVA are summarized in (Table 3-3 Table 3-4). The Model F-value of 0.85 implies the quadratic model is not significant relative to the noise. There is a 67.97 % chance that an F-value this large could occur due to noise. Adequate Precision measures the signal to noise ratio. A ratio greater than 4 is desirable. Ratio of 7.283 indicates an adequate signal. This model can be used to navigate the design space for the stabilized NLCs with acceptable ZP.

3.3.2 (VI) Influence of investigated parameters on percent entrapment efficiency (%EE)

Entrapment efficiencies of resveratrol in all the NLC formulations with six liquid lipid were observed to be > 90 % . The effect on entrapment efficiency can be explained by quadratic equations below:

For GTC

Y_4=+90.67318-3.05300×X_1-7.24967×X_2+0.092645×X_3+0.29733×X_1×X_2+0.020640×X_1× X_3+0.018607× X_2 × X_3-1.38400× X_1^2+3.78800× X_2^2-2.81267E-004× X_3^2 Equation 30

For DO

Y_4=+97.14014-5.71900×X_1-9.28967×X_2+0.069875×X_3+0.29733×X_1×X_2+0.020640×X_1× X_3+0.018607× X_2 × X_3-1.38400× X_1^2+3.78800× X_2^2-2.81267E-004× X_3^2 Equation 31

For PCG

Y_4= +88.62314-3.16100× X_1-9.36067×X_2+0.11123×X_3+0.29733×X_1×X_2+0.020640× X_1 × X_3+0.018607× X_2 × X_3-1.38400× X_1^2+3.78800× X_2^2-2.81267E-004× X_3^2 Equation 32

For PGMC

Y_4=+91.63166-2.22400×X_1-7.65667×X_2+0.083855×X_3+0.29733×X_1×X_2+0.020640×X_1× X_3+0.018607× X_2 × X_3-1.38400× X_1^2+3.78800× X_2^2-2.81267E-004× X_3^2 Equation 33

For GTO

Y_4=+89.21141-1.61100×X_1-9.08167×X_2+0.10384×X_3+0.29733×X_1×X_2+0.020640×X_1× X_3+0.018607×X_2×X_3-1.38400×X_1^2+3.78800× X_2^2-2.81267E-004× X_3^2 Equation 34

For PGML

Y_4= +93.11872-1.21300×X_1-9.13767×X_2+0.079765×X_3+0.29733×X_1×X_2+0.020640× X_1 ×X_3+0.018607× X_2 × X_3-1.38400× X_1^2+3.78800× X_2^2-2.81267E-004× X_3^2 Equation 35

As it was expected the increase in the concentration of liquid lipid had a positive effect on the entrapment efficiency (Dai et al., 2010, Khurana.S. et al., 2012, Barratt, 2000), however the most significant factor affecting the response was the X_3 (amount of drug) which showed a positive effect on the %EE (equations 32-37), suggesting an increase in the drug amount will cause an increase in the entrapment efficiency. This is partially attributed to more drug been available for the entrapment in the internal phase. This observation is in accordance to (Thang et al., 2017), as more drug will be available for entrapment in the internal phase. This observation was in accordance with the previous literature (Hao et al., 2011). Liquid lipid type did not show any effect on the entrapment efficiency this might be due to the fact that all NLCs are constructed of many crystal imperfections that provide more space for drug incorporation (Zhang et al., 2013, Jain et al., 2015). Contour plots (Figure 3-7 Figure 3-8) show that the prevalence of blue region was high, indicating higher entrapment efficiency obtained with all NLC formulations.

Tween 80 concentration (X_2) had a negative effect on the %EE in all NLCs with six liquid lipids. This observed effect was in accordance with previously reported studies (Shah et al., 2011, Gaba et al., 2015). This might be due the fact that increasing the concentration of surfactant will lead to more deposition of surfactant on the interface between the water phase and the lipid phase thus reducing interfacial tension. This would lead to the increase in the shear pressure generated during the homogenization process that would result in the formation of small emulsion droplet and thus decreasing the % EE (Subedi et al., 2009, Wang et al., 2014a, Behbahani et al., 2017).

The interaction between (X_1-X_2, X_1 X_3 and X_2 X_3) for all liquid lipids type had a positive effect on the %EE even though $X_1$and X_2 showed a negative effect on the %EE, but the combination with the third factor X_3 made the interaction positive. This can be used to predict the future interactions and effect of each variable on the studied response.

Further statistical analysis employing ANOVA demonstrated that the quadratic Model was followed F-value of 4.79 implies the model is significant. There is only a 0.01 % chance that an F-value this large could occur due to noise. Values of "Prob > F" less than 0.050 indicate model terms are significant. Adequate Precision measures the signal to noise ratio. A ratio greater than 4 is desirable (Table 3-3Table 3-4). The model ratio of 9.584 indicates an adequate signal. Showing that this model can be used to navigate the design space, In this case X3, X3D, X3X2 are significant model terms. Other values greater than 0.100 indicate the model terms are not significant. Therefore, the amount of drug was critical factor in NLC formulations along with type of liquid lipid affecting the maximum entrapment efficiency.

3.3.2 (VII) Influence of investigated parameters on percent drug loading (% DL)

Drug loading is the major challenge in the formulation of nanoparticles, especially for poorly water soluble drugs. Because of the presence of liquid lipid in NLCs higher drug incorporation is expected as compared to SLNs (Muller et al., 2002a, Radtke.M. et al., 2005).

Compared with the reported solubility of resveratrol in water (300 mg/100mL) (Agarwal.A. et al., 2014) the solubility of resveratrol in lipid matrices consisting of trimyristin and different oils was improved by at least 33.3 folds.The percent drug loading ranged between 2.937 to 7.557%, which indicates that the response was extremely sensitive toward the studied factors these results were in accordance to what its was reported by Thang et al, (Thang et al., 2017).

A substantially higher drug loading could be achieved with NLCs as compared to previous reports (Neves et al., 2013).

The physicochemical properties of liquid lipid plays critical role on the drug loading in NLCs. Labrasol (PCG) PEGylated lipid with high HLB and solubility for the drug, resulted in higher drug loading as compared to GTO, DO and GTC which had lower solubility and lower HLB values. The two polyethylene glycol esters PGML and PGMC showed comparable drug loading.

Apart from the nature of liquid lipid, the surfactant concentration and the amount of drug also affect the resveratrol loading in the NLCs which is demonstrated by the following quadratic equations :

For GTC

Y_5= -3.36946+3.31783× X_1+7.79100× X_2+0.039990× X_3-0.12600× X_1 × X_2-3.64000E-003× X_1 × X_3+5.67000E-003× X_2 ×X_3-2.53333× X_1^2-6.11133× X_2^2-4.13667E-005×X_3^2 Equation 36

For DO

Y_5= -5.18163 +2.23283× X_1+10.78100× X_2+0.039805× X_3-0.12600× X_1 × X_2-3.64000E-003× X_1 × X_3+5.67000E-003× X_2 × X_3-2.53333× X_1^2-6.11133× X_2^2-4.13667E-005×X_3^2 Equation 37

For PCG

Y_5= -5.03404+4.31733× X_1+9.04800× X_2+0.042647× X_3-0.12600× X_1 × X_2-3.64000E-003× X_1 × X_3+5.67000E-003× X_2 × X_3-2.53333× X_1^2-6.11133× X_2^2-4.13667E-005×X_3^2 Equation 38

For PGMC

Y_5= -4.81689+4.39033× X_1+8.67450× X_2+0.042885× X_3-0.12600× X_1 × X_2-3.64000E-003× X_1 × X_3+5.67000E-003× X_2 × X_3-2.53333× X_1^2-6.11133× X_2^2-4.13667E-005×X_3^2 Equation 39

For GTO

Y_5= -5.74321+3.74583× X_1+9.04100× X_2+0.049065× X_3-0.12600× X_1 × X_2-3.64000E-003× X_1 × X_3+5.67000E-003× X_2 × X_3-2.53333× X_1^2-6.11133× X_2^2-4.13667E-005×X_3^2 Equation 40

For PGML

Y_5= -4.78191+3.72333× X_1+9.12850× X_2+0.041120× X_3-0.12600× X_1 × X_2-3.64000E-003× X_1 × X_3+5.67000E-003× X_2 × X_3-2.53333× X_1^2-6.11133× X_2^2-4.13667E-005×X_3^2 Equation 41

It is clearly evident that the surfactant concentration (X_2) exerted a strong positive effect on the %DL for all liquid lipid types as is evident from the positive value of the coefficient in equations (26-31). It is clearly evident that the increase in surfactant concentration increased the %DL because of enhanced entrapped drug. The other two factors liquid lipid amount (X_1) and the amount of drug (X_3) also showed a positive effect on the %DL. These factors demonstrated positive coefficients, suggesting that the increase in the amount of liquid lipid will lead to more drug loading. This is attributed to the increase in the auxiliary spaces in the lipid matrix.

Numerous preceding studies have illustrated that incorporation of liquid lipids to solid lipids causes disturbance in solid lipid crystal order, thus allowing more space to accommodate drug molecules (Shah and Pathak, 2010, Sanad et al., 2010).

Liquid lipids act as solubilizing agents for various drugs, which could also be responsible for higher percent drug loading. This effect has been observed in many previous studies (Yang et al., 2010, Zhang et al., 2010b, Jain et al., 2015). The interaction between different variables for each response are shown in the contour plots (Figure 3-7 Figure 3-8). Amount of drug (X_3) had a positive effect on the drug loading with higher drug being entrapped inside the nanoparticles as more drug was added (Emami et al., 2012, Velmurugan and Selvamuthukumar, 2016).

The interaction between factors (X_1-X_2) and (X_1- X_3) for all types of liquid lipids had a negative effect on the %DL, even though all three had a positive effect on the %DL when taken individually. On the other hand, the interaction between (X_2- X_3) demonstrated a positive effect on the %DL, which signifies that the increase in both factors will lead to the increase in the %DL.

The regression coefficient (R2) of this response was found to be 0.747 indicating a good correlation between the response and the factors under study. The Model F-value of 21.80 implies the model is significant. There is only a 0.01 % chance that an F-value this large could occur due to noise. Values of "Prob > F" less than 0.050 indicate model terms are significant. The ANOVA for response R^2 (Table 3-3 and Table **3-4**) in which the "Predicted R-Squared" of 0.816 is in reasonable agreement with the Adjusted R-Squared of 0.8868; i.e. the difference is less than 0.2. Adequate Precision

measures the signal to noise ratio. A ratio greater than 4 is desirable, the ratio of 15.781 indicates an adequate signal, and this model can be used to navigate the design space.

3.3.2 (VIII) Perturbation plots

Perturbation plots (Figure 3-14) were plotted to have a better understanding about the factors that affect the responses the most. Flat curvature shows that the response is insensitive to the changes of a particular factor under study, while a steep curvature indicates high sensitivity of the response to the factor keeping all other factors kept constant at a reference point (Zhang et al., 2013, Velmurugan and Selvamuthukumar, 2016, Myers et al., 2016).

NLCs prepared with different liquid lipids showed different effect on the dependent variables. In case of response Y_1 (particle size), the concentration of liquid lipid (factor A) show a steep curvature for PGML and PGMC as liquid lipid, implying that increasing in these two liquid lipids will cause a reduction in particle size. While this factor showed almost flat curvature for other types of liquid lipids. Major effect was produced by factor B and C (Tween 80 concentration and amount of drug, respectively) on the response, these results are in parallel to what the equations demonstrated. Whereas in case of response Y_2 (polydispersity index) factor A i.e. the concentration of liquid lipid; PCG, PGMC and PGML had steeper curvature. Tween 80 concentration (B) affected the NLC prepared using GTC, PCG, PGMC and GTO, while DO and PGML containing NLCs did not show much effect on PDI. Factor C (amount of drug) only showed prominent perturbation effect with NLC prepared using PCG on Y_2.

As for response Y_3 (zeta potential) factor A and B both showed steep curvature for both liquid lipid GTC and DO containing NLCs, while factor B showed the greatest effect on the response with PCG, PGMC and GTO containing NLCs. However, all factors showed no effect on the response Y_3 in the case PGML when employed as a liquid lipid. The influence of the factors on the last two responses Y_4 and Y_5 for all liquid lipids for preparation of NLCs was deemed to be affected the most by the amount of drug Factor (C) where it showed a steep curvature, illustrating that the increase in amount of drug will lead to both increase in the entrapment efficiency and drug loading, which was previously described by the quadratic equations and the contour plots. Other factors (A and B) showed flat curvatures and did not have significant effect on Y_4 and Y_5 responses.

3.3.2 (IX) Data optimization and model validation

The ICH Q8 defines design space as “the multidimensional combination and interaction of input variables and process parameters that have been demonstrated to provide assurance of quality” (Patel and Sawant, 2017). Graphical optimization was conducted by overlaying the critical response contours with overlay plot. Design space is the space within which the quality of the product can be constructed (Figure 3-15) for each liquid lipid NLC employed in the design. These overlays are composed of two regions yellow coloured region describing the design space with suitable response values and grey region illustrating where response values did not meet the quality product attributes (Shah et al., 2015). Based on the overlay plot and desirability criteria the optimized formulations can be selected from the design space.

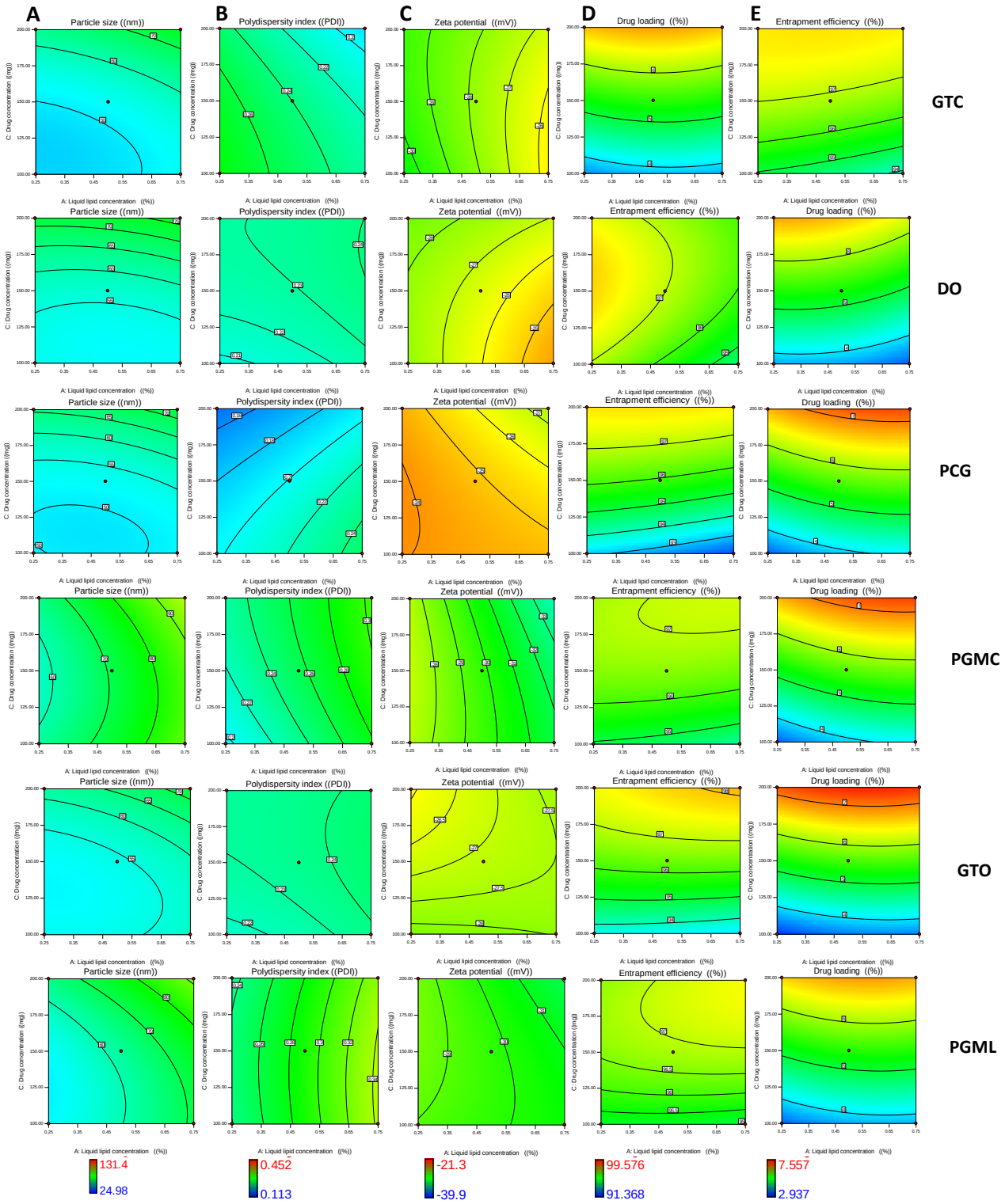

Figure 3-7. Contour plots showing the effect of drug concentration and liquid lipid concentration with medium level of Tween 80 on various response variables:A. PS, B. PDI, C. ZP, D. %EE, E. % DL

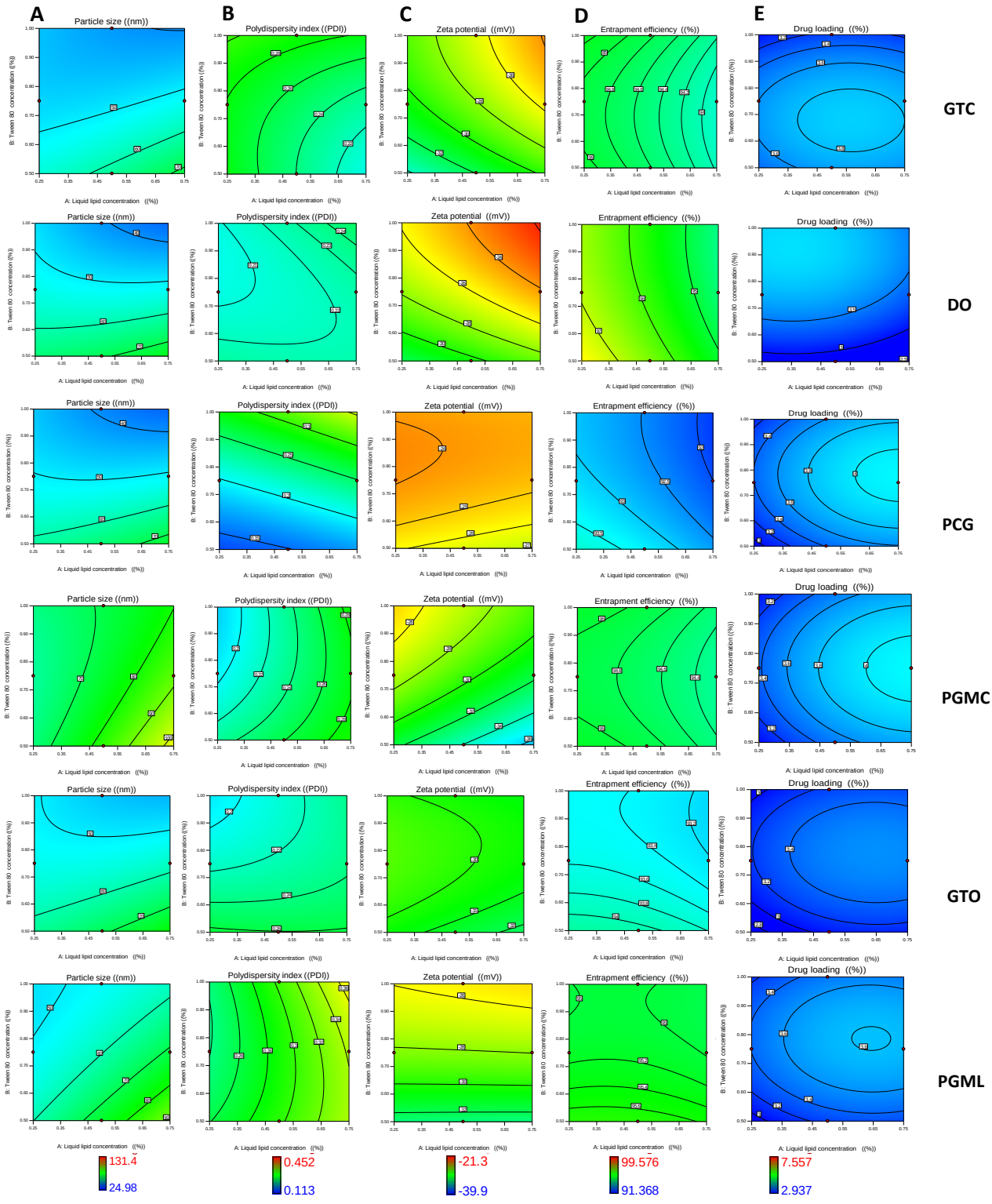

Figure 3-8.Contour plots showing the effect of Tween 80 concentration and liquid lipid concentration with low level of drug on various response variables:A. PS, B. PDI, C. ZP, D. %EE, E. % DL

Table 3-3: Lack-of-fit test for each response (ANOVA) analysis

Response	Source	Sum of squares	D.f	Mean squares	F-value	*p* value (Prob >F)
Y_1 (Particle size)	MODEL	18622.31	29	642.15	4.91	0.0001*
	Residual	6283.71	48	130.91		
	Cumulative Total	24906.02	77			
Y_2 (Polydispersity Index)						
	Model	0.18	29	6.216E-003	2.58	0.0018*
	Residual	0.12	48	2.410E-003		
	Cumulative Total	0.3	77			
Y_3 (Zeta potential)						
	Model	2835.60	29	97.78	0.85	0.6797
	Residual	5545.04	48	115.52		
	Cumulative Total	8380.64	77			
Y_4 (Entrapment Efficiency %)						
	Model	168.41	29	5.81	4.79	<0.0001*
	Residual	58.22	48	1.21		
	Cumulative Total	226.63	77			
Y_5 (Drug Loading %)						
	Model	138.14	29	4.76	21.80	0.0001*
	Residual	10.49	48	0.22		
	Cumulative Total	148.63	77			

*Not significant $\alpha<0.05$ (no lack-of-fit)

Table 3-4: Summary of results of regression analysis for responses. (+ Only the terms with statistical significance are included)

MODEL RESPONSE	R^2	ADJUSTED R^2	PREDICTED R^2	COEFFICIENT OF VARIANCE (C.V. %)	STANDARD DEVIATION (SD)	PRESS	COMMENT
PARTICLE SIZE (PS) (Y_1)							
LINEAR MODEL	0.617	0.573		18.13	11.75	12221.66	suggested
2FL MODEL	0.727	0.588		17.80	11.54	16624.70	-
QUADRATIC MODEL	0.747	0.595	0.307	17.66	11.44	17258.01	-
CUBIC MODEL	0.912	0.549		18.64	12.07	+	aliased
POLYDISPERSITY INDEX (PDI) (Y_2)							
LINEAR MODEL	0.2470	0.159		23.00	0.057	0.290	suggested
2FL MODEL	0.5957	0.389	-0.071	19.61	0.048	0.300	
QUADRATIC MODEL	0.609	0.372		19.87	0.049	0.320	
CUBIC MODEL	0.9386	0.684		14.09	0.035	+	aliased
ZETA POTENTIAL (ZP)(Y_3)							
LINEAR MODEL	0.077	-0.030		39.43	10.59	9947.96	
2FL MODEL	0.314	-0.034		39.52	10.61	14301.64	
QUADRATIC MODEL	0.338	-0.061	-0.065	40.03	10.75	15196.61	
CUBIC MODEL	0.772	-0.169		42.02	11.28	+	aliased
ENTRAPMENT EFFICIENCY (EE%)(Y_4)							
LINEAR MODEL	0.535	0.481		1.28	1.24	135.11	suggested
2FL MODEL	0.691	0.534		1.22	1.17	169.03	
QUADRATIC MODEL	0.743	0.588		1.14	1.10	156.03	suggested
CUBIC MODEL	0.917	0.576	0.312	1.16	1.16	+	aliased
DRUG LOADING (DL%)(Y_5)							
LINEAR MODEL	0.880	0.866		9.960	0.510	22.670	suggested
2FL MODEL	0.915	0.872		9.720	0.500	28.300	
QUADRATIC MODEL	0.929	0.886	0.816	9.160	0.470	27.350	suggested
CUBIC MODEL	0.984	0.921		7.630	0.390	+	aliased

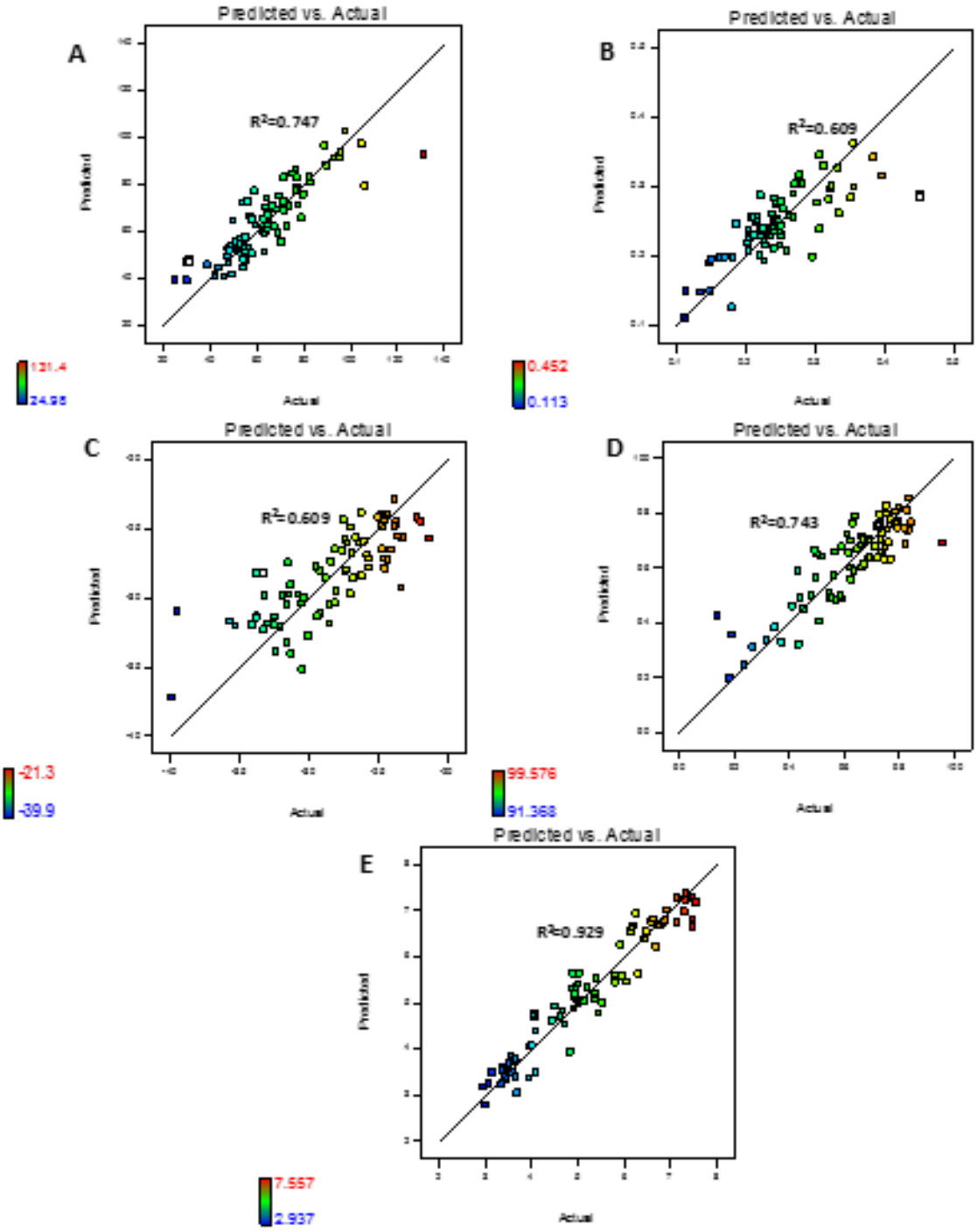

Figure 3-9. Linear correlation plots between the actual and the predicted values of various responses A. PS, B.PDI, C. ZP, D. % EE and E. % DL

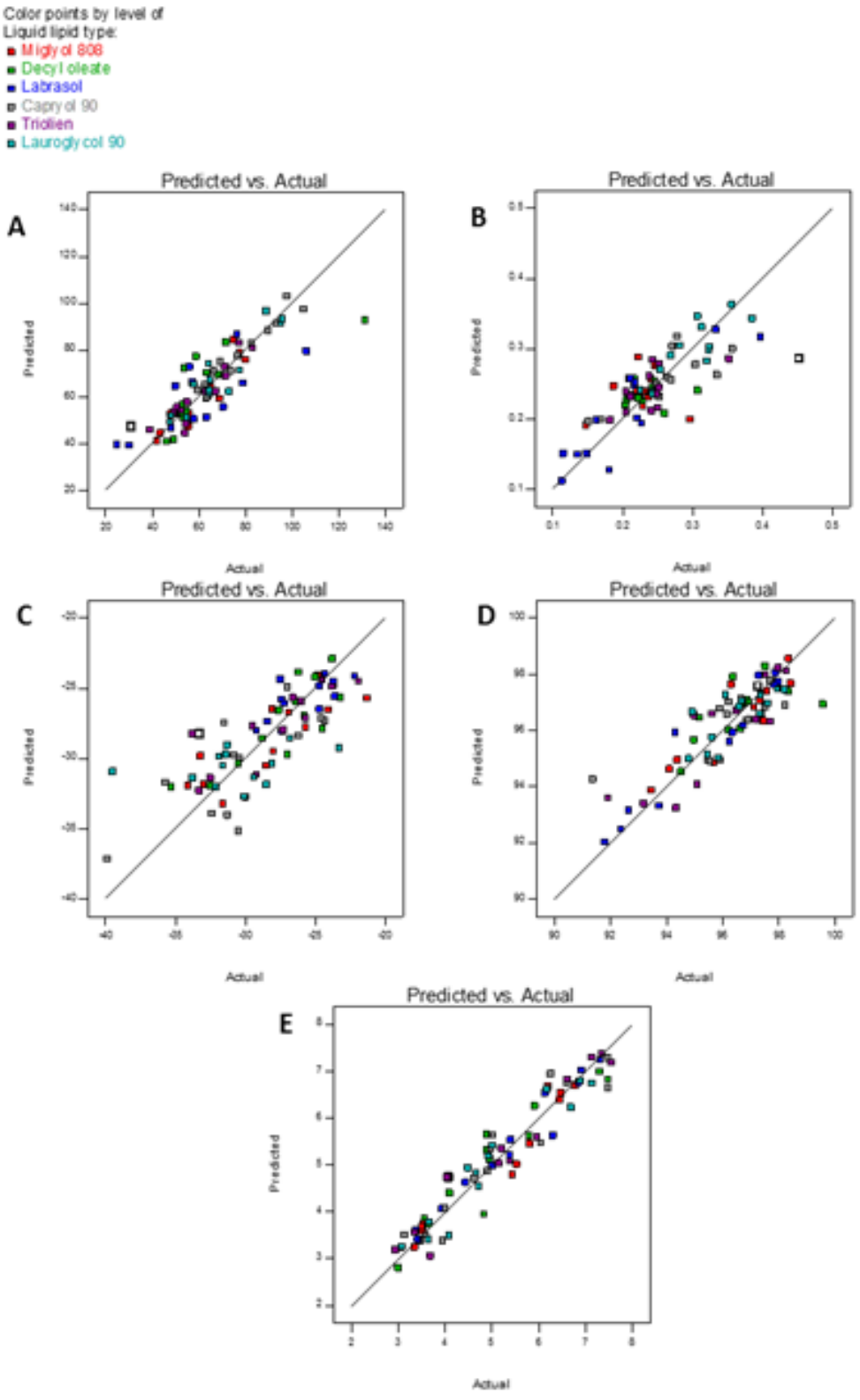

Figure 3-10. Linear correlation plots between the actual and the predicted values of different types of liquid lipids on different responses A. PS, B. PDI, C. ZP, D. %EE and F. %DL. Type of liquid lipid: GTC, DO, PCG, PGMC, GTO and PGML

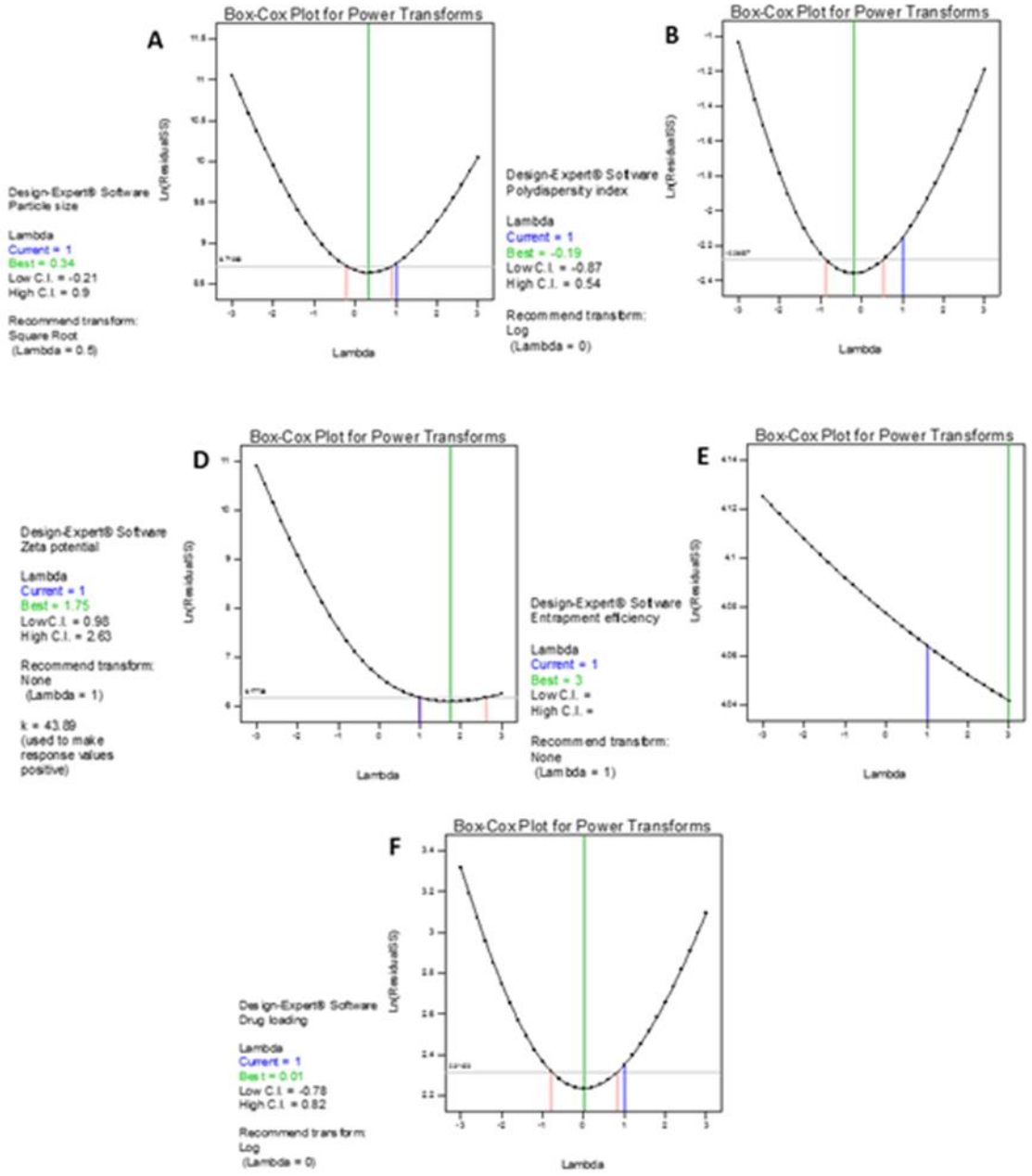

Figure 3-11. Box Cox plot for power transformation for each responses A) PS, B) PDI, C) ZP, D) %EE and F) %DL

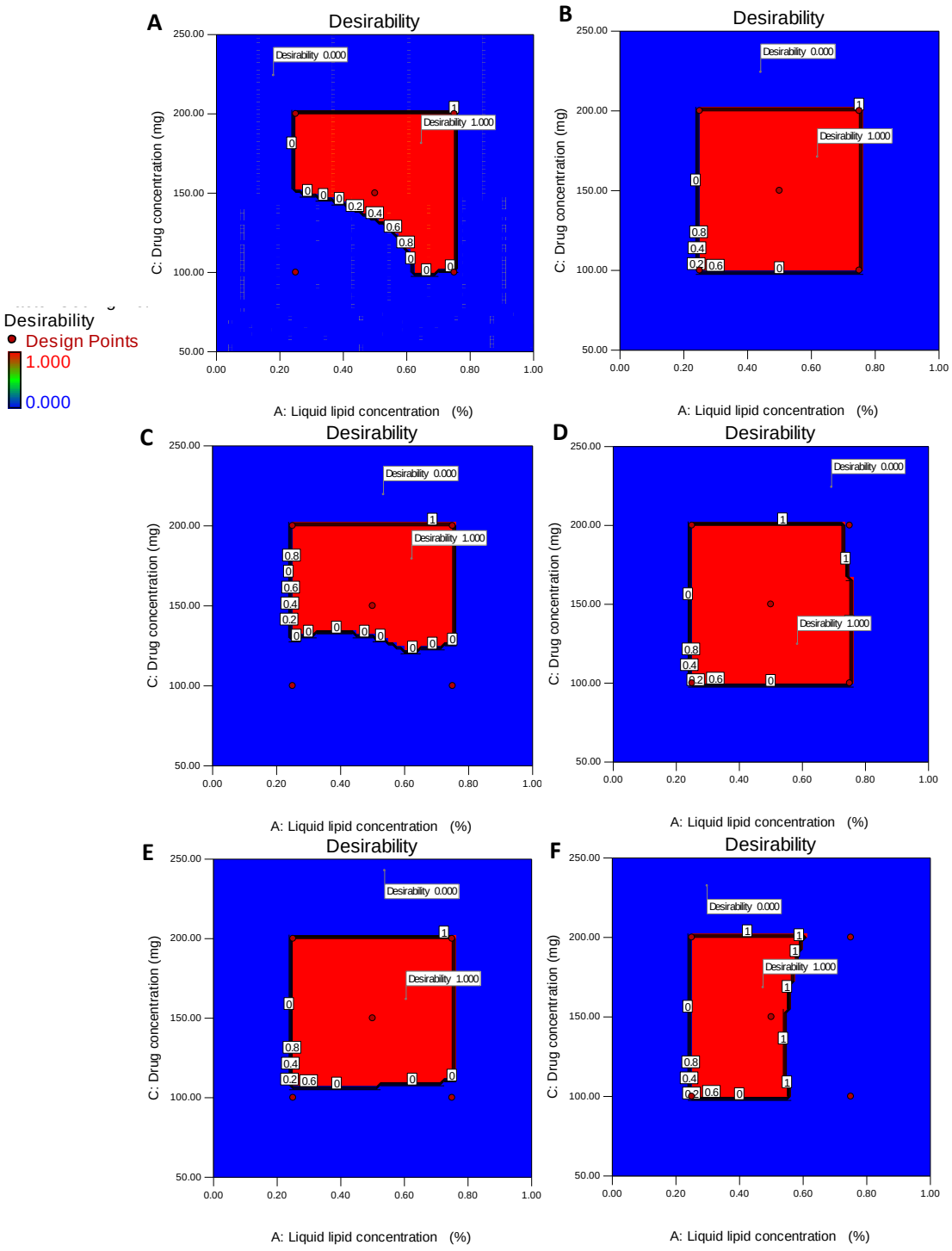

Figure 3-12. Desirability of the design space for different liquid lipid types at medium tween 80 concnetration A: GTC B: DO C: PCG D: PGMC E: GTO F: PGML

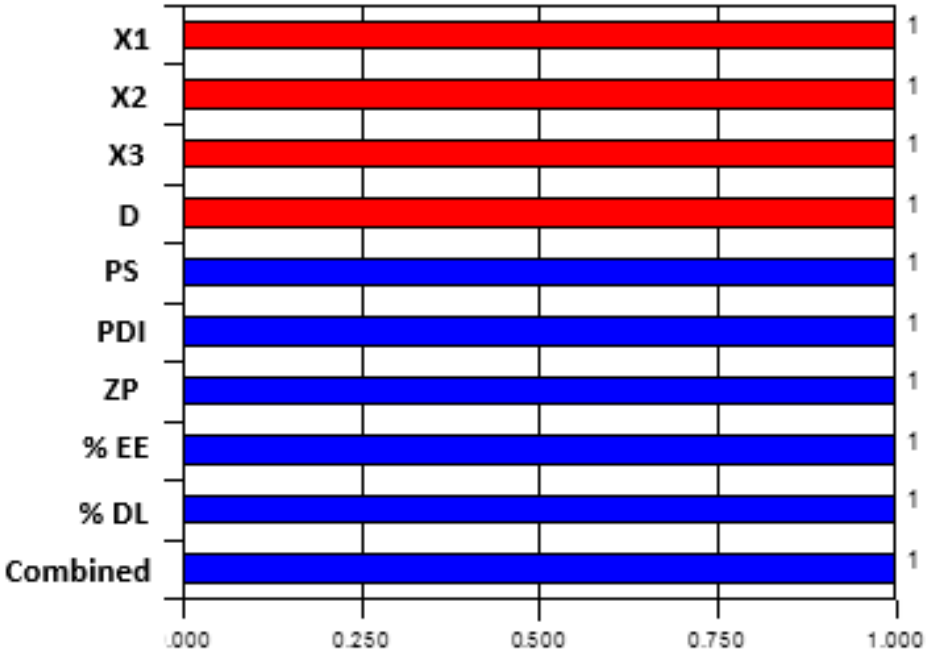

Figure 3-13. The optimal Individual and combined desirability function for the measured responses of both the independent and dependent variables to yield the desired final formulation where: X1. Is liquid lipid concentration, X2. Tween 80 concentration X3. Drug concentration D. Liquid lipid type while PS. Particles size, PDI. Polydispersity index, ZP. Zeta potential, %EE. Entrapment efficiency and %DL. Drug loading.

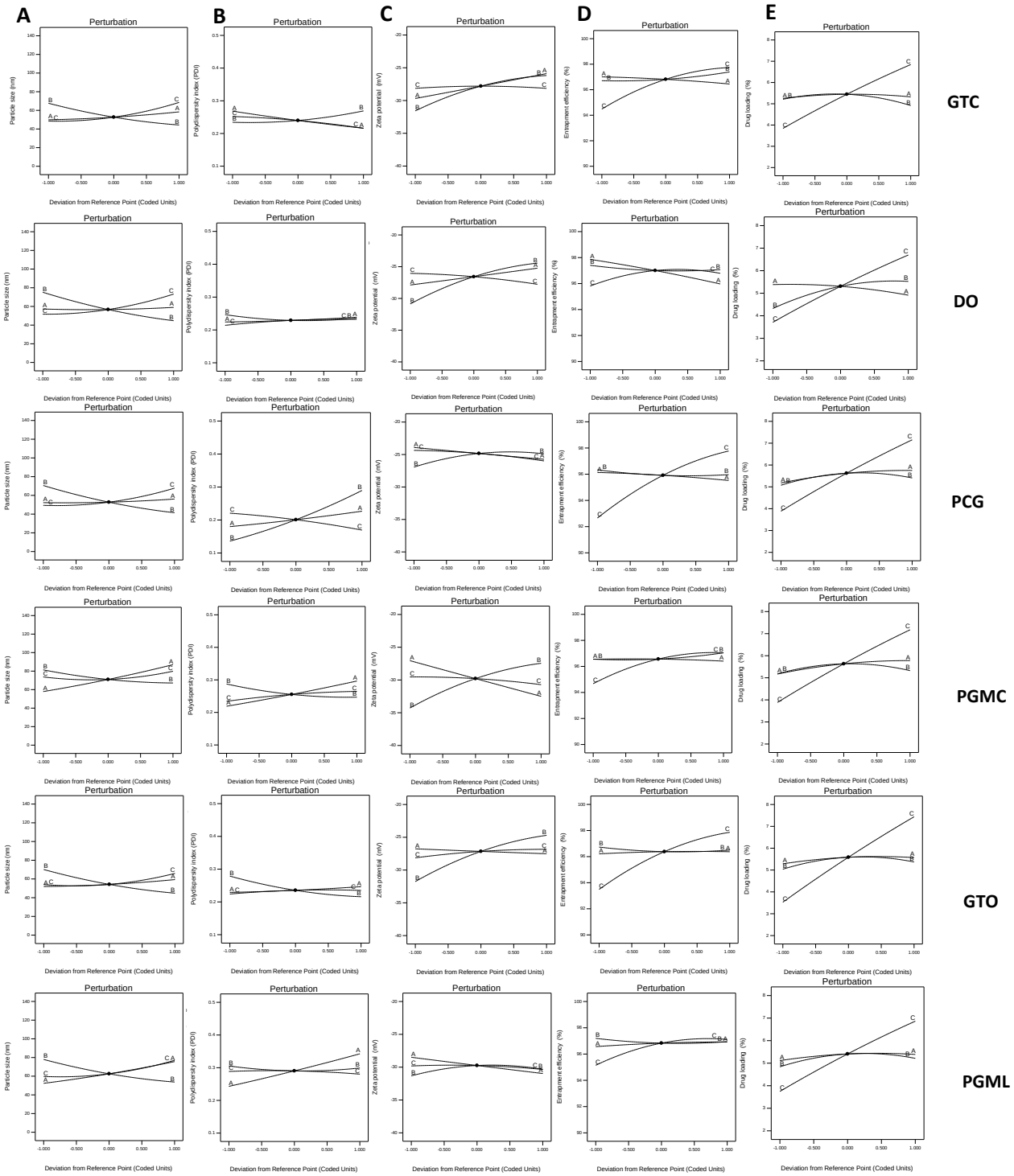

Figure 3-14. Perturbation plots showing the interactions between the drug concentration and liquid lipid concentration and tween 80 concentration all at medium level on variouse response variables A) PS, B)PDI, C)ZP,D)%EE and F)%DL, with different type of liquid lipid

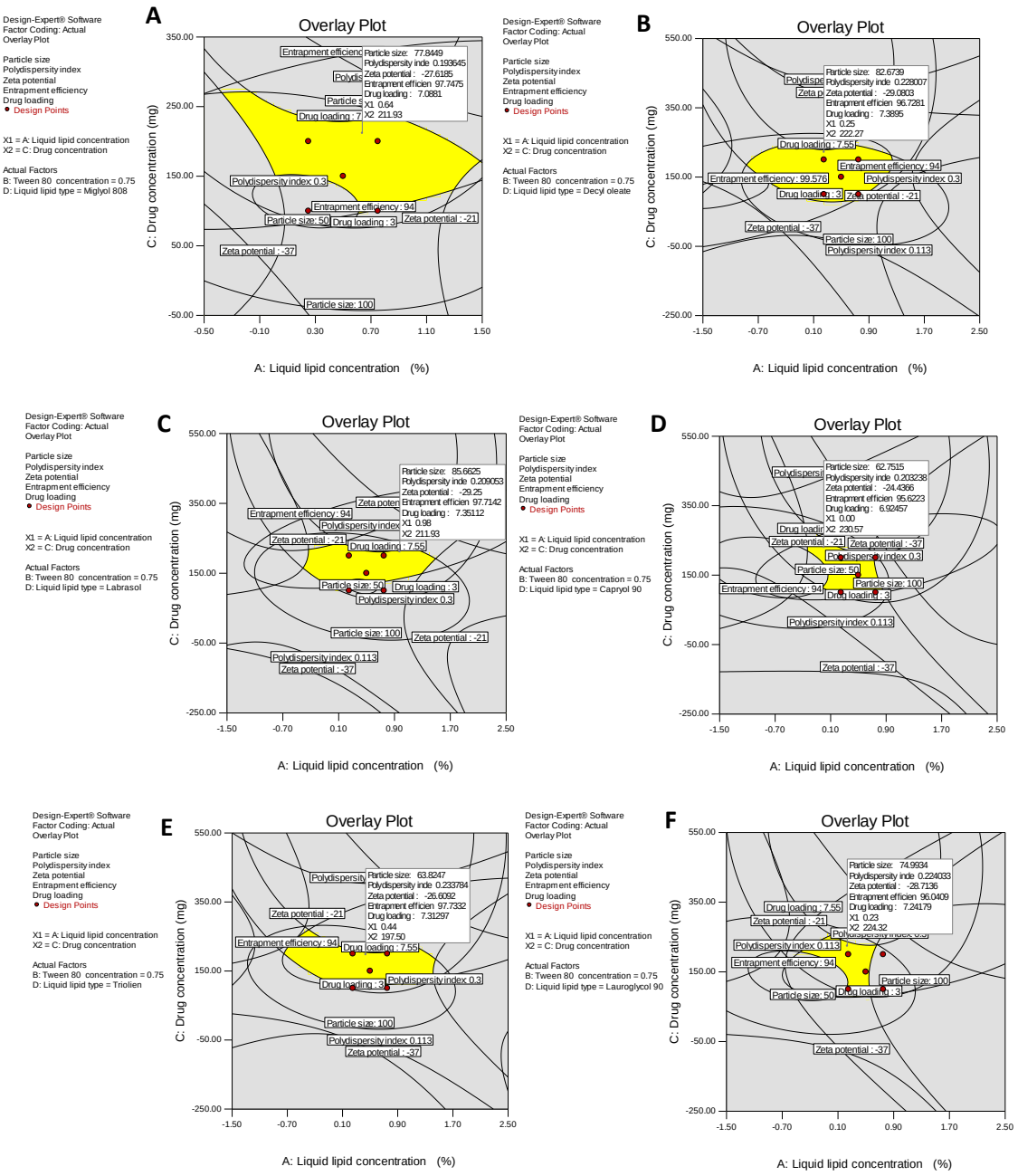

Figure 3-15. Overlay plots showing the location of optimized formulation with respect to the relationship between different responses to the drug and liquid lipid concentration for six different liquid lipids A: RES-NLC-GTC B: RES-NLC-DO C: RES-NLC-PCG D: PGMC E: RES-NLC-GTO F: RES-NLC-PGML

3.3.3 Physicochemical characterization of optimized bare RES-NLCs and surface modified RES-NLCs formulations

A specific characterization of the formulated nanoparticles is a requisite for the control of the quality of the produced nanodispersion. The characterization procedures should be responsive to the key factors of NLCs performance through avoiding artifacts.

3.3.3 (I) Effect of size reduction technique on the particle size, PDI and zeta potential of bare RES-NLCs formulations

HPH has been developed as one of the main reliable technique for the preparation of NLCs as it offers the advantage of scaling up. The homogenization process utilizes high pressure (100–2000 bar) to push the liquid dispersion through a narrow orifice. High shear stress and cavitation forces break the particle into the nanometer range (Lippacher et al., 2000).

Alternatively, ultrasound is widely used technique for the production of lipid nanoparticles, this is attributed to the cheap and the ease of production and processing. However, the main disadvantages is the presence of metal contamination in the final product. In addition longer sonication time is required to obtain particles in the nanorange (Al Khouri Fallouh et al., 1986, Damgé et al., 1990, Mehnert and Mäder, 2001).

The optimized RES-NLCs were produced with different liquid lipids as per the compositions given in Table 3-3 by both the size reduction techniques HPH and ultrasonication technique. Figure 3-16 illustrates the particle size distribution curve and zeta potential of the six optimized batches prepared by both the techniques. The data (Table 3-6) illustrates that there is no significant difference in the particle size of NLCs when PGML and GTC were used as a liquid lipid in their preparations. However, when produced by the two techniques when GTO, PCG, PGMC and DO were used as liquid lipids there was significant ($p < 0.001$) increase in the particle size of the formulations (Figure 3-17.A). Ultrasonication process yielded NLCs with smaller particle size than HPH. Moreover, lower PDI values were observed when using the probe sonication, there was significant difference between all NLCs PDI values when using the two different techniques (Figure 3-17.B). This could be attributed to the fact that when using the lower energy process it yields smaller size and more homogenous NLCs (Lasoń et al., 2013, Ariffin et al., 2015).

The use of different production methods affected the surface charge of the NLCs depending on the choice of liquid lipid, where GTO, PGML and DO as liquid lipids did not affect the zeta potential, while PCG, PGMC and GTC as liquid lipids significantly affected the zeta potential of formulations. (Figure 3-17.C).

Table 3-5: Compositions of the optimized RES-NLCs Formulations contained 100 mg of drug

Formulation	Liquid lipid concentration (%) of the total mixture of lipids (2%)	Tween 80 concentration (%)
RES-NLC-GTO	0.5	1
RES-NLC-PCG	0.25	0.75
RED-NLC-PGMC	0.25	0.75
RED-NLC-PGML	0.5	1
RED-NLC-DO	0.5	1
RED-NLC-GTC	0.5	1

Table 3-6: Optimized RES-NLCs using both high-pressure homogenization and probe sonication

Formulations	Particle size		Polydispersity index		Zeta potential	
	HPH	Ultrasonication	HPH	Ultrasonication	HPH	Ultrasonication
RES-NLC-GTO	52.783 ± 1.226	61.543 ± 0.564	0.279±0.004	0.246±0.001	-21.533± 1.401	-21.833 ± 1.102
RES-NLC-PCG	68.45 ± 1.563	62.343 ± 0.015	0.286±0.004	0.260±0.002	-24.067± 0.611	-21.267 ± 0.252
RED-NLC-PGMC	99.42 ± 1.486	78.563 ± 0.11	0.252± 0.002	0.165±0.021	-21.133± 1.115	-15.833± 0.833
RED-NLC-PGML	71.42 ± 0.805	69.677±2.945	0.284± 0.005	0.217±0.004	-21.9±1.4107	-23.2± 0.5
RED-NLC-DO	64.867 ± 0.548	49.78 ± 0.587	0.253 ± 0.012	0.219±0.007	-22.833± 0.737	-22.133± 2.026
RED-NLC-GTC	61.873 ± 0.887	59.793 ± 0.659	0.24 ± 0.009	0.281±0.004	-20± 0.436	-24.767± 0.950

3.3.3 (II) Surface modified RES-NLCs formulations

As RES-NLC-GTO exhibited good stability in terms of particle size and PDI over the period of six months (section 3.2.11.). It was therefore selected for surface functionalization. PEG is nontoxic, highly soluble in water and FDA-approved compound and insignificantly affecting the drug release from nanoparticles. Modification of drug delivery systems with low molecular weight PEG will form sterically stable particles, thus, avoid the clearance by the reticuloendothelial system and resulting in a longer circulation property for nanoparticles (Owens and Peppas, 2006, Prencipe et al., 2009). Moreover, coating the surface of nanoparticles with PEG increase their hydrophilicity, thus reducing the hydrophobic or electrostatic interactions with the cell surface providing fast mucus penetration through the gastrointestinal mucosa (Jokerst et al., 2011).

PEGS40 stearate was selected to impart surface hydrophilic properties to RES-NLC-GTO to improve its intestinal permeability. Further to achieve the targetability toward breast cancer cells and

ensure higher efficacy as anticancer agents, RES-NLC-GTO-PEGS40 was functionalized with the following ligands: HA, FA and HAFA.

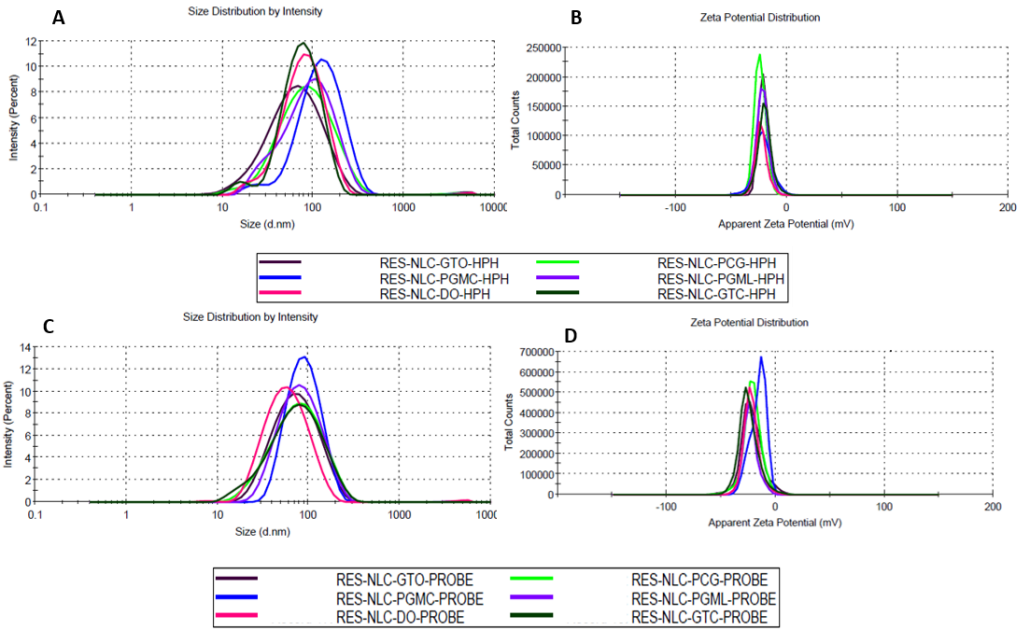

Figure 3-16. Overlays of the optimized RES-NLCs by High Pressure Homogenization method A. Particle size and, B. Surface zeta potential using HPH, C. Particle size and, D. Surface zeta potential using Probe Sonicator of six optimised RES-NLCs

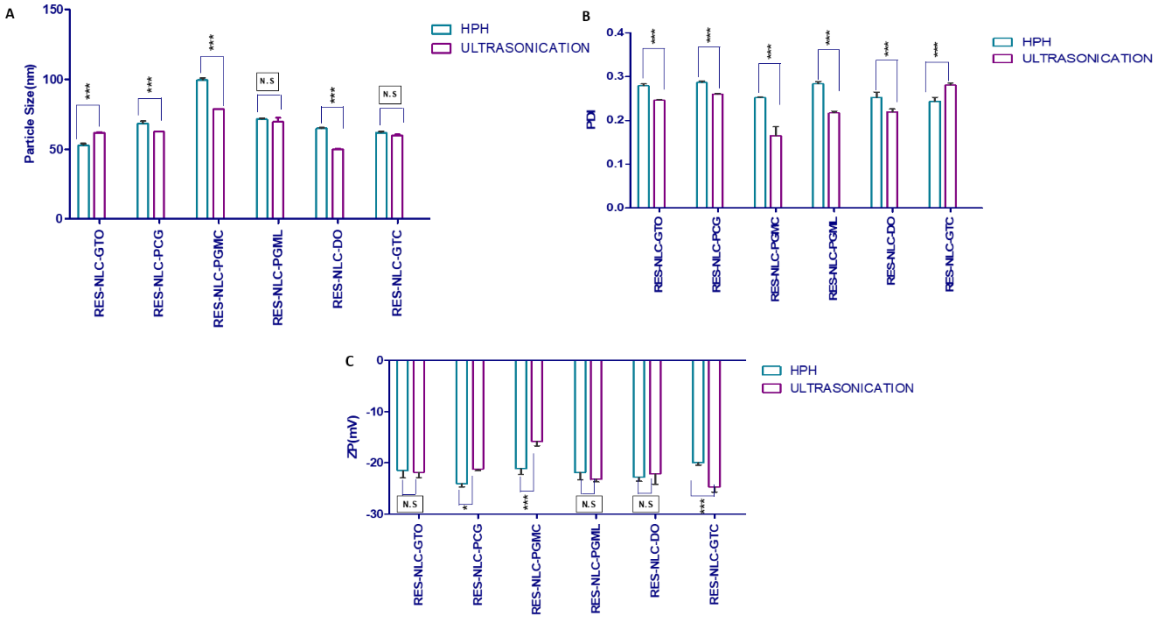

Figure 3-17. Optimized RES-NLCs using both high pressure homogenization HPH and probe sonication, A.PS, B. PDI and C. ZP

A Optimization of surface modified RES-NLC-GTO-PEGS40

Three ratios of amine groups present on the NLCs surface: the ligand viz. 12:1, 16:1 and 18:1 for HA and 2:1, 5:1 and 8:1 for FA were prepared and their effect was investigated on the particle size, polydispersity index and surface charge of the conjugated molecules. Consequently, one best ratio was chosen to formulate the individual ligand appended formulation.

The effect of HA surface modification was observed through the changes in the physicochemical properties including: particle size, polydispersity index and zeta potential, when different ligands ratios were employed (Figure 3-18). Moreover, when 18:1 and 16:1 ratios were used larger particles were observed with particles in the micron range. Whereas, 12:1 ratio showed a good particle size distribution, broader peak was observed when compared to the PEGylated RES-NLC.

Higher amounts of free amine groups: HA resulted in highly polydisperse (0.682) NLC with large particle size, (333.4 nm) (Figure 3-18. A). Amine: ligand ratio 12:1 was found to yield uniform particles with particle size of (64.70 nm), PDI (0.284). Also higher concentration of HA led to highly negative surfaces with zeta potential of -56 mV. The best colloidal stability is achieved with ± 30 mV zeta potential, these NLC systems would lead to aggregation over the long period of time. On the other hand, the ratio 12:1 yield most favourable zeta potential of -27 mV (Figure 3-18.B). Notably this was significantly different from the bare RES-NLC-GTO.

Similar observation were made when NLCs were functionalized with FA as a ligand. The ratio of amine: ligand 5:1 was found to yield small uniform particles with size of (68.51 nm) and PDI (0.213) (Figure 3-19A). However, no difference in particle size, polydispersity index and surface charge when both amine: ligand ratio of 5:1 and 2:1 ratios were used, 5:1 ratio was selected as it had particle size of 68.51 nm, PDI 0.213 and zeta potential of (-22.6 mV) and higher folic acid content (Figure 3-19B).

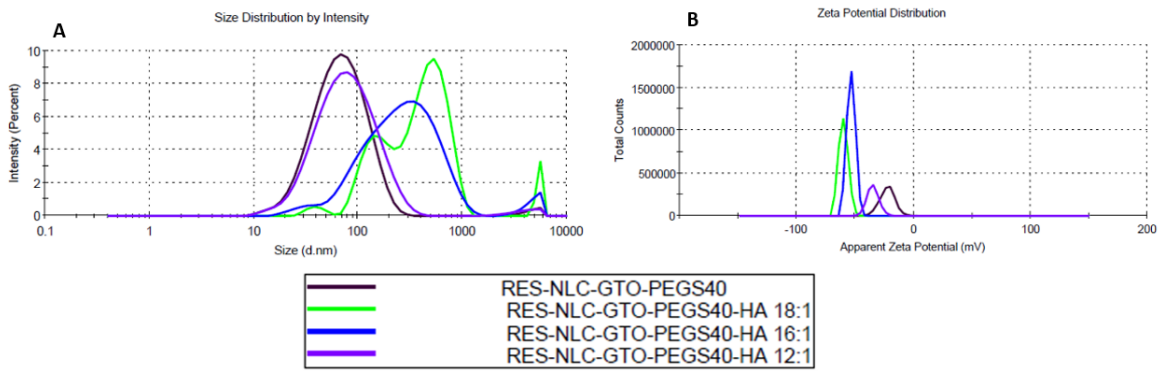

Figure 3-18. Distribution of A. Particle size and B. Zeta potential of RES-NLCs surface modified with HA

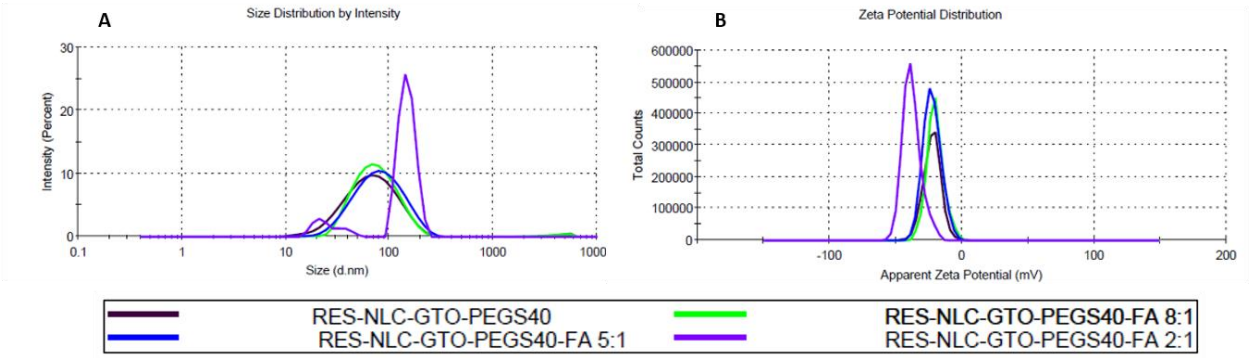

Figure 3-19. Distribution of A. Particle size and B. Zeta potential of RES-NLCs surface modified with FA

For dual targeted system the optimized amine: ligand ratio. Amine: HA ratio of 12:1 and 5: 1 for FA was selected to yield RES-NLC-GTO-HAFA with uniform particle size table (Table 3-8).

A distinct change in the particle size, PDI, ZP, EE and the total drug of the selected surface modified RES-NLCs was observed as compared to the bare NLCs. There was a significant increase in the hydrodynamic diameter of all coated NLCs, when compared to the bare RES-NLCs, indicating a successful binding of ligand to the surface of RES-NLCs. However, the maximum increase was observed when combining both ligands to achieve the dual targeting (Figure 3-20A). The small effect of ligands on the polydispersity index of NLCs, which is still within the agreed range < 0.3, indicating that the surface modified NLCs were homogenously dispersed (Tran et al., 2014, Zhang et al., 2016a)

PEGylated NLCs did not show significant change in the zeta potential value (Garcia-Fuentes et al., 2005). The HA coating of RES-NLCs increased the negative charge on NLCs (Figure 3-20.B). this is attributed to the anionic nature of the HA molecule (Varshosaz et al., 2014). Folic acid positive charge had more affinity to bind to the negative NLCs surface it is demonstrated by an increase in the negative charge of folic acid coated NLCs exhibiting a zeta potential value of -25.933 ± 0.945. The conjugation procedure posed a small difference in the % entrapment efficacy compared to the bare NLCs (Zhou et al., 2015, Zhang et al., 2016b). There was a significant decrease in the total drug of surface modified NLCs compared to the bare NLCs (Table 3-8).

Table 3-7: Optimized surface modified RES-NLCs physicochemical characterizations, in term of particle size (PS), polydispersity index (PDI), zeta potential (ZP), entrapment efficiency (%EE) and total drug (%TD). Difference at p < 0.05 was considered statistically significant, * indicates P< 0.001, **, P < 0.01 and * P< 0.05.**

	Particle Size (nm)	PDI	ZP (mV)	EE (%)	TD (%)
Bare RES-NLC-GTO	61.54 ± 0.564	0.246±0.001	-21.833± 1.102	97.058±0.057	99.799±0.542
RES-NLC-GTO-PEGS40	64.50±0.312*	0.220±0.006*	-22.567±0.208 N.S	97.353±0.001 N.S	89.946±0.226 ***
RES-NLC-GTO-PEGS40-HA	70.27±0.458 ***	0.26±0.003 N.S	-27.133±0.252***	96.189±0.492**	81.432±0.3726 ***
RES-NLC-GTO-PEGS40-FA	68.51±0.529 ***	0.213±0.002*	-25.933±0.945***	96.446±0.246*	76.166±1.351 ***
RES-NLC-GTO-PEGS40-HAFA	73.22±1.405* **	0.255± 0.014 N.S	-22.567±0.231 N.S	96.177± 0.076**	70.263±1.373 ***

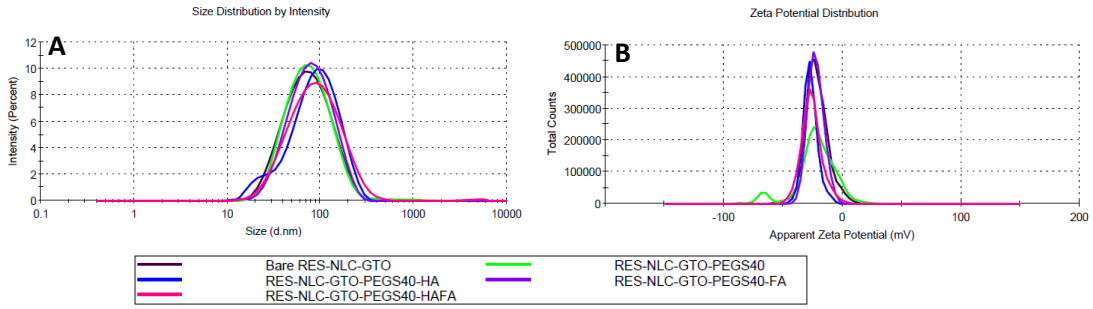

Figure 3-20. Overlays of the Bare RES-NLCs with all surface modified formulations A) particle size and, B) surface zeta potential

B Degree of chemical cross-linking

Free amine groups present on the surface of the nanoparticles was determined by the TNBS method (Gao and Zhanga, 2011, Kouchakzadeh et al., 2014). The concentration of TNBS was determined form the linear calibration curve (Figure 3-21) (R^2 of 0.9971), with the equation A=0.645-0.744), where A is the absorbance and C is the concentration of TNBS. Figure 3-22 A,B shows the blank and sample set with different yellow colour intensities.

The free amine groups on the NLC surface were determined prior and after the surface modification (Figure 3-23). When the RES-NLCs were PEGylated, the number of amine group showed no significant difference from the bare nanoparticles (Figure 3-23). However, on ligand attachment of both HA and FA a significant reduction in the amine groups on the surface on RES-NLCs was noted (Table 3-7), indicating the successful binding of ligand to the surface of RES-NLCs Figure 3-22.C.

Upon folic acid conjugation it gave the highest % of cross linking to the surface of nanoparticles (66%) as compared to HA with (44%), while functionalization with both ligands simultaneously resulted in binding of 55 % (Table 3-7).

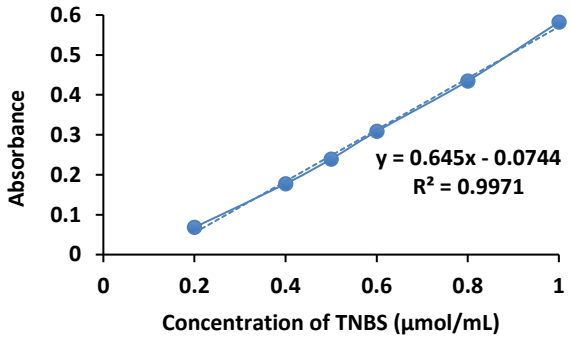

Figure 3-21.Trinitrobenzenesulphonic acid solution (TNBS) calibration curve

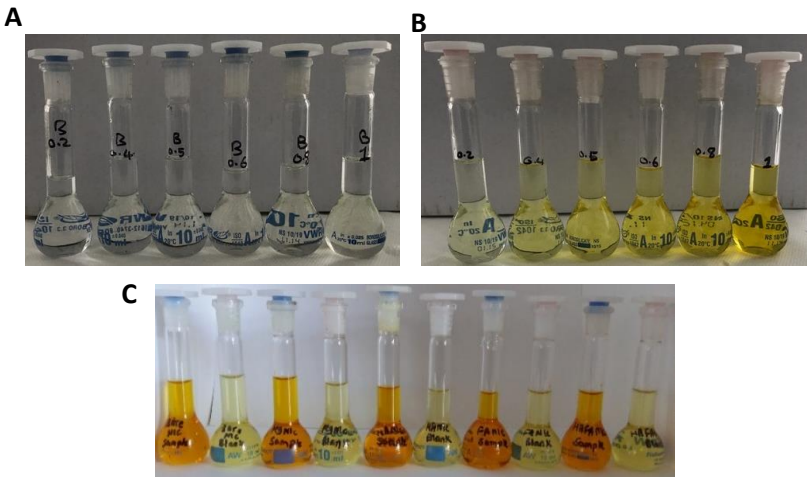

Figure 3-22. Calibration curve for amine group determination A. Blank set, B. Sample set. C. Colour development when RES-NLC reacted mixture with TNBS

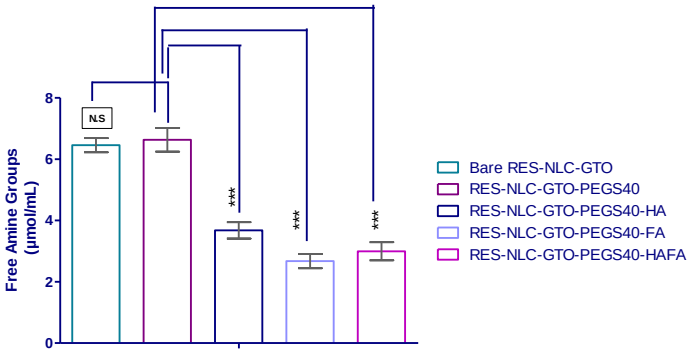

Figure 3-23. Bar graph showing the amount of free amine groups available on the surface of RES-NLCs

Table 3-8: Quantified free amine groups on bare and functionalized RES-NLCs

Formulations	Number of free amine groups (µM)	Degree of chemical cross linking (µM)	% Degree of cross linking
Bare RES-NLC-GTO	6.458±0.233	NA	NA
RES-NLC-GTO-PEGS40	6.634±0.385	NA	NA
RES-NLC-GTO-PEGS40-HA	3.678± 0.269	2.96	44 %
RES-NLC-GTO-PEGS40-FA	2.675± 0.233	3.96	66 %
RES-NLC-GTO-PEGS40-HAFA	2.995±0.296	3.64	55 %

C Differential Scanning Calorimetry (DSC)

DSC analysis was performed to study the effect of the incorporation of different liquid lipids on the crystallinity of solid lipid and its melting behaviour (Figure 3-24). DSC thermogram of trimyristin displayed a sharp endothermic peak at 58.32^{o}C. Incorporation of six liquid lipids at three different concentrations (12.5, 25 and 37.5% of the total solid lipid) into the crystalline lattice of trimyristin (solid lipid) resulted in depression of its melting point indicating distortion in the crystalline lattice of trimyristin (Müller. and Müller, 1986) (Figure 3-27.A).

The degree of melting point of solid lipid depression was affected by the type and concentration of liquid lipid, where the maximum reduction of melting point occurred with the highest concentration of oil (Table 3-2). The order of melting point depression of trimyristin (high to low) observed when 0.75 % of each liquid lipids was employed was PGMC, PGML, DO, GTC, GTO and PGC which correlated to their carbon content. The liquid lipid with smaller molecular structures induced greater distortion in the crystalline lattice of trimyristin than the bulkier liquid lipids. A linear correlation between the concentration of oil and the melting point depression indicated good miscibility, this observation was similar to Jenning et al, study (Jenning et al., 2000b). The difference between the melting and the onset temperatures is the range, at which the melting event of the lipid occurs, and the greater the difference, greater the disorder of the crystals (Severino et al., 2011). This difference increased at higher concentrations of liquid lipids, indicating greater disorder (Table 3-2) this observation was in correlation to Niculae.G. et al, study (Niculae.G. et al., 2013). Data also demonstrated the reduction in the melting enthalpy of lipid mix when the concertation of liquid lipids was at high level (Table 3-2). The lower melting enthalpy values indicate less ordered lattice arrangement of the lipid compared to the bulk material, similar results were obtained by

Abdelbary and fahmy (Abdelbary and Fahmy, 2009). For the less ordered crystal state, the melting of the solid lipid requires less energy to overcome lattice force. In addition, the disruption in the lattice structure would facilitate the encapsulation of drug and increase particle stability during storage (Figure 3-27.B). Moreover, addition of liquid lipid created more amorphous structures. Therefore, the lipid within nanoparticles should exhibit a less ordered arrangement when compared to the bulk crystalline materials (Hou et al., 2003). However the melting temperatures of lipid blends with all six liquid lipids were higher than 40^0C, which ensures the integrity of the particles after formation, these results were comparable to results from Severino study (Severino et al., 2011).

DSC analysis was also performed to study the effect of the incorporation of different liquid lipids on the crystallinity of RES and its melting behaviour (Figure 3-26), Resveratrol demonstrated a sharp endothermic peak at 267.14^{o}C. Resveratrol combination with six liquid lipids at three different concentrations (0.25 %, 0.5% and 0.75 %) showed a depression of melting point and the degree of melting point depression was massively affected by the type and concentration of the liquid lipid where the highest reduction in the melting point and onset temperature was observed at highest concentration of each liquid lipid (Figure 3-28.A) (Müller. and Müller, 1986). At the highest concentration (0.75%) of PGMC the drug was completely dissolved and the thermogram did not therefore reveal any endothermic peak of drug indicating it to be in amorphous form, though at lower concentrations of PGMC the crystallinity of drug was still maintained. Out of the other liquid lipids PCG showed the lowest onset temperature and lowest melting temperature. It also elicited greatest difference between the melting and the onset temperatures indicating greatest distortion of the drug crystal lattice by PCG. This was followed by PGML> DO> GTC > GTO respectively, which also lowered the melting point and onset temperatures of drug in that order. Generally, amorphous materials possess higher saturation solubility than crystalline materials; however, amorphous drugs in metastable state can spontaneously recrystallize and lead to a decreasing bioavailability during the process of storage. To avoid this, the ideally produced nanoparticle system should be crystalline as stated by Kobierski et al (Kobierski et al., 2009). In this context, DO and GTO showed well-defined peak of resveratrol at all oil concentrations indicating maintenance of crystalline structure of the drug even at high concentrations of liquid lipid as shown from the study done by Gove and Hao et al (Gokce et al., 2012, Hao et al., 2012). Data also depicted a significant decrease in the melting enthalpy of resveratrol with a maximum reduction observed when the concentration of liquid lipids was at high level (0.75 %) (Figure 3-28.B), resulting in a less ordered crystalline state where the melting of the drug required less energy to overcome lattice force (Neves et al., 2013).

Thermogram of physical mixture of RES showed an endothermic peak of RES at 267.14 ^{o}C and of trimyristin at 58.32 ^{o}C corresponding to their melting point as depicted in Figure 3-25.The physical

mixture exhibited an endothermic melting peak at 58.5 ^{o}C, 58.86 ^{o}C and 59.6 ^{o}C, when GTO, PGMC and GTC were used. DSC plot of physical mixture of different RES-NLCs (Figure 3-25), showed a depression of melting point and the reduction in peak intensity of the solid lipid to 55.5^{o}C, 55.9^{o}C and 56.83^{o}C when PGC, DO and PGML was utilized, while other liquid lipid didn't not affect the melting point of the solid lipid, it is obvious that the drug peak is absent in all physical mixtures indicating the solubilization of the drug in the presences of different liquid lipids (Isailović et al., 2013, Pandita et al., 2014).

DSC is a potent tool used in the investigation of the crystallization and interaction of drug with different components of NLCs by determining the difference of temperature and enthalpy at phase transition. Figure 3-25 shows DSC thermogram of RES, Trimyristin and six different NLCs. The thermogram of RES showed a main endothermic peak at around 267.49^{o}C representing its melting point and thus indicating crystalline nature. For Trimyristin the melting process took place with maximum peaks at 58.32^{o}C. All RES-NLCs showed main endothermic peak at 103^{o}C-105^{o}C, representing the melting peak of Trimyristin, similar obsevartion was made by Elmowafy et al. (Elmowafy et al., 2017). The shift in melting peak of trimyristin from 58.32^{o}C to 103.71^{o}C was attributed to the small size of NLCs (nanometer range), presence of surfactant and the dispersed state of the lipid.

This phenomenon was also observed in the blank NLCs where formation of NLCs caused the shift of solid lipid peak (Figure 3-25). This is further, substantiated by the fact that physical mixtures of the individual components of the NLCs, showed depression of trimyristin peak from 58.32^{o}C to a range of 55.5-58.85^{o}C. The blank NLCs showed a single peak in the range of 103^{o}C-116^{o}C. The nature of liquid lipid impacted the melting behavior of the solid lipid. While DO and GTO exhibited higher shift to 116 and 111^{o}C respectively, than other liquid lipids (103-104^{o}C).

The shift in endothermic peak along with the absence of characteristic RES endothermic peak at 267.14^{o}C suggested interaction of RES with lipid component and indicated that RES entrapped in lipids was in amorphous state or dispersed molecularly in the NLCs.The use of triglyceride may reduce the mobility of the drug molecules within the lipid core and thus reduce the drug expulsion upon storage (Lee et al., 2007, Li et al., 2011, Ramasamy et al., 2014).

Bare RES-NLCs gave a single sharp endothermic peak at 103.7^{o}C, bulk PEG gave a peak at 46.86^{o}C and the incorporation of PEG into RES-NLCs did not affect the melting endotherm of RES-NLCs (Figure 3-29.A). Bulk HA demonstrate a small peak at 39.74^{o}C which was absent in RES-NLC-GTO-PEGS40-HA confirming that no free HA was present in the surface modified formulation. The RES-NLC-GTO-PEGS40-HA showed a small shift with an endothermic peak at 102.3^{o}C. RES-NLC-GTO-PEGS40-HA also demonstrated a higher width of melting area indicating greater disorder in the crystal structure (Figure 3-29.B).

Similarly, RES-NLC-GTO-PEGS40-FA showed a single endothermic peak at 104.16^{o}C with no free FA present as indicated by the absence of peak of FA (146.38^{o}C) shown in thermogram of bulk FA. The width of melting point was higher as compared to the bare NLC indicating more distorted structure. Similar observations were made with dual targeted systems, when HAFA were appended on NLC giving one sharp peak at 104.16^{o}C. Like bare RES-NLCs, none of the surface modified RES-NLCs showed the shift in the normal endothermic RES peak from 267.14 ^{o}C to the endothermic peak at 267.81^{o}C. The absence of drug peak showed the presence of drug in amorphous form in these formulations (Ramasamy et al., 2014).

3.3.3 (III) X-ray powder diffraction study

The XRD study is carried out to support the data obtained from the DSC analysis (Barratt, 2000). There is a possibility that drug will interact with the lipids and get dissolved because of the lipophilic nature of the drug. If the drug dissolves in the lipid matrix it will convert into molecular dispersion, hence become an amorphous drug. This could have an impact on drug release from the nanoparticle and its solubility. Therefore, the study of drug crystallinity is of importance because it is strongly related to the drug loading capacity and the release rate from the NLCs (de Carvalho et al., 2013).

The diffraction pattern of the resveratrol alone and RES-NLCs revealed the absence of the following peaks of resveratrol at 2Θ value of 6.575°, 13.178°, 16.308°,19.213°, 22.386°, 23.659°, 25.274°, 28.263° in the RES-NLCs. The trimyristin peaks at 7.524°,16.611°, 19.398°, 23.174° and 24.062° (Figure 3-30.A) were also absent in NLC formulations. Absence of drug and lipid peaks in RES-NLCs suggests the incorporation of drug into the lipid matrix, this also confirms the presence of RES in an amorphous form after incorporation into NLCs, results were in correlation to Jose et al studies (Jose et al., 2014).

RES-NLCs diffraction pattern showed peaks at 2Θ value of 8.857^{o}, 12.774^{o}, 13.804^{o}, 14.571^{o}, 15.399^{o}, 16.631^{o}, 16.995^{o}, 17.641^{o}, 18.630^{o}, 21.195^{o}, 22.407^{o} and 23.941^{o} demonstrated the presence of trehalose used as a cryoprotectant in NLCs, as a result the peaks of trimyristin were overshadowed by the high concentration of trehalose.

However, the presence of crystalline trimyristin in RES-NLCs was evident from XRD diffractogram of physical mixtures taken in the absence of trehalose (Figure 3-28 andFigure **3-30**.B). Peaks of trimyristin (7.524°,16.611°, 19.398°, 23.174° and 24.062°) were observed to be shifted and broadened this corroborate with DSC results, which also shows a major shift of the solid lipid peak upon the formulation of NLCs, indicating the crystalline nature of solid lipid being preserved even after the formulation of nanoparticles (Dinda et al., 2013).

The surface modified NLCs also showed absence of RES peaks validating the amorphous nature of the drug in the formulation (Figure 3-30.C). All surface modified RES-NLCs (RES-NLC-GTO-PEGS40, RES-NLC-GTO-PEGS40-HA, RES-NLC-GTO-PEGS40-FA and RES-NLC-GTO-PEGS40-HAFA) showed the distinct peaks of trimyristin with similar shift as observed in the bare NLCs.

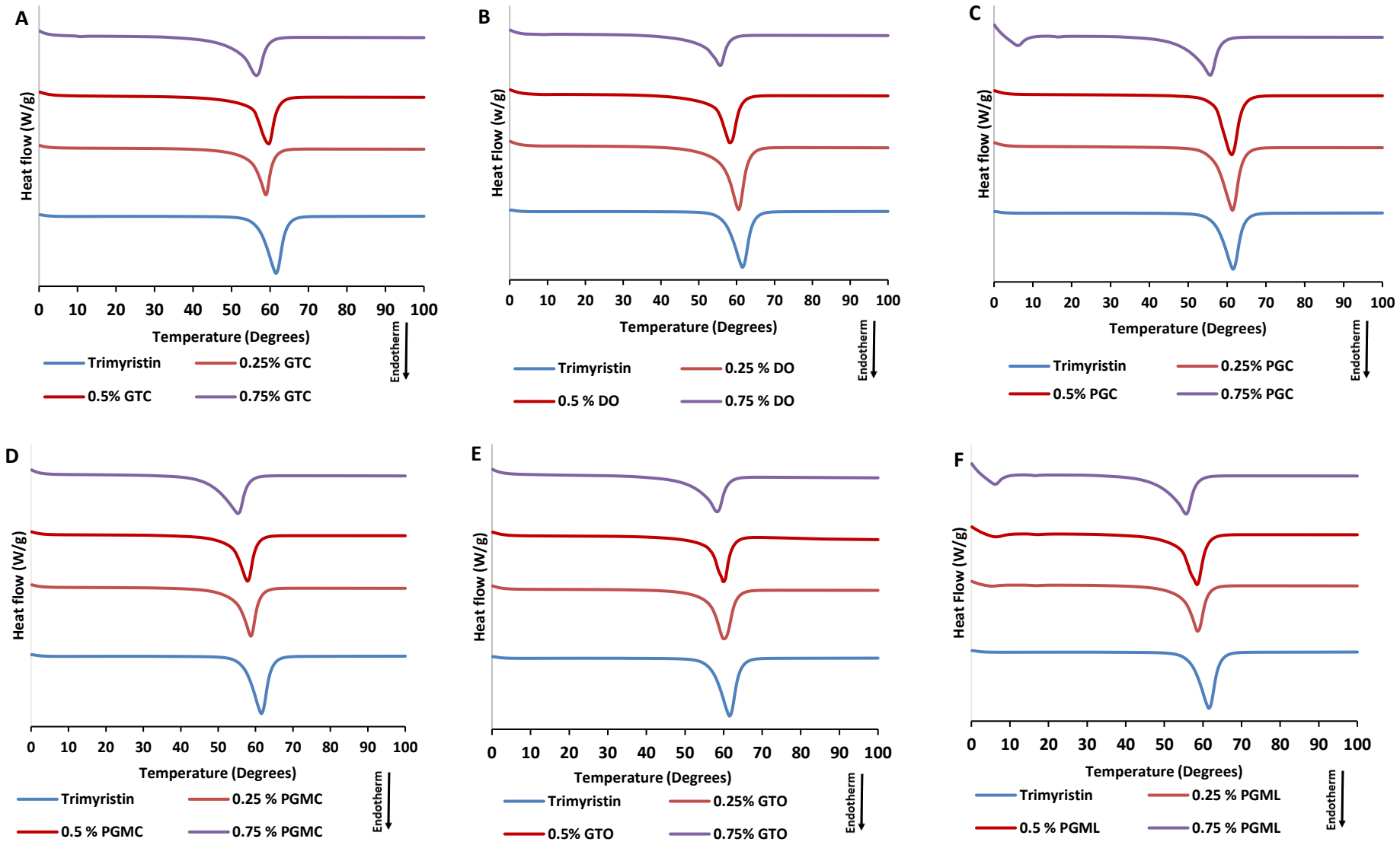

Figure 3-24. DSC Thermograms showing the effect of oil concentration on the solid lipid A. GTC B. DO C. PCG D. PGMC E. GTO F. PGML

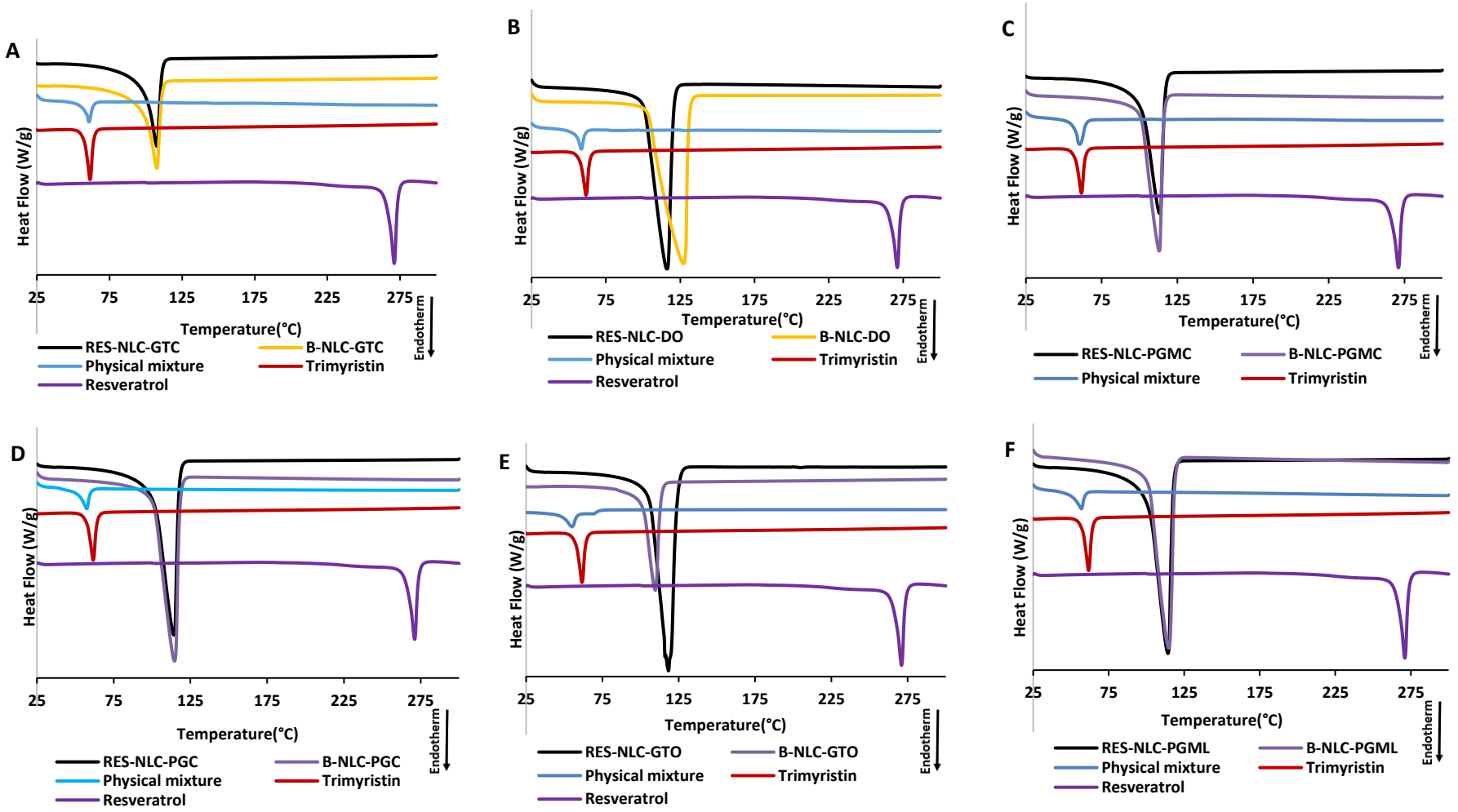

Figure 3-25. DSC heating thermogram of different RES-NLCs, B-NLCs, solid lipid, resveratrol and physical mixtures of A. GTC B. DO C. PCG D. PGMC E. GTO F. PGML.

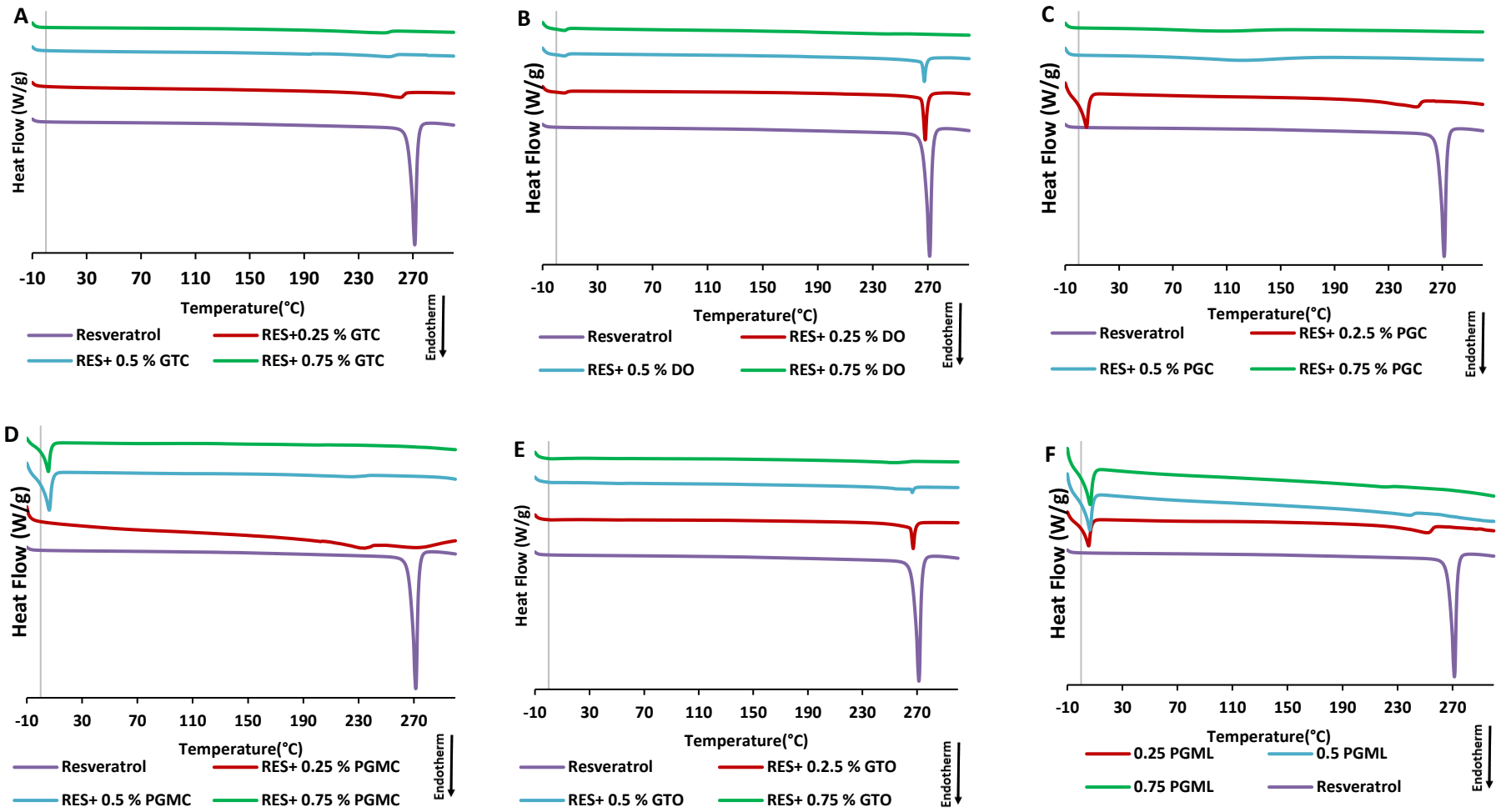

Figure 3-26. DSC Thermograms showing the effect of oil concentration on resveratrol solubility A. GTC B. DO C. PCG D. PGMC E. GTO F. PGML

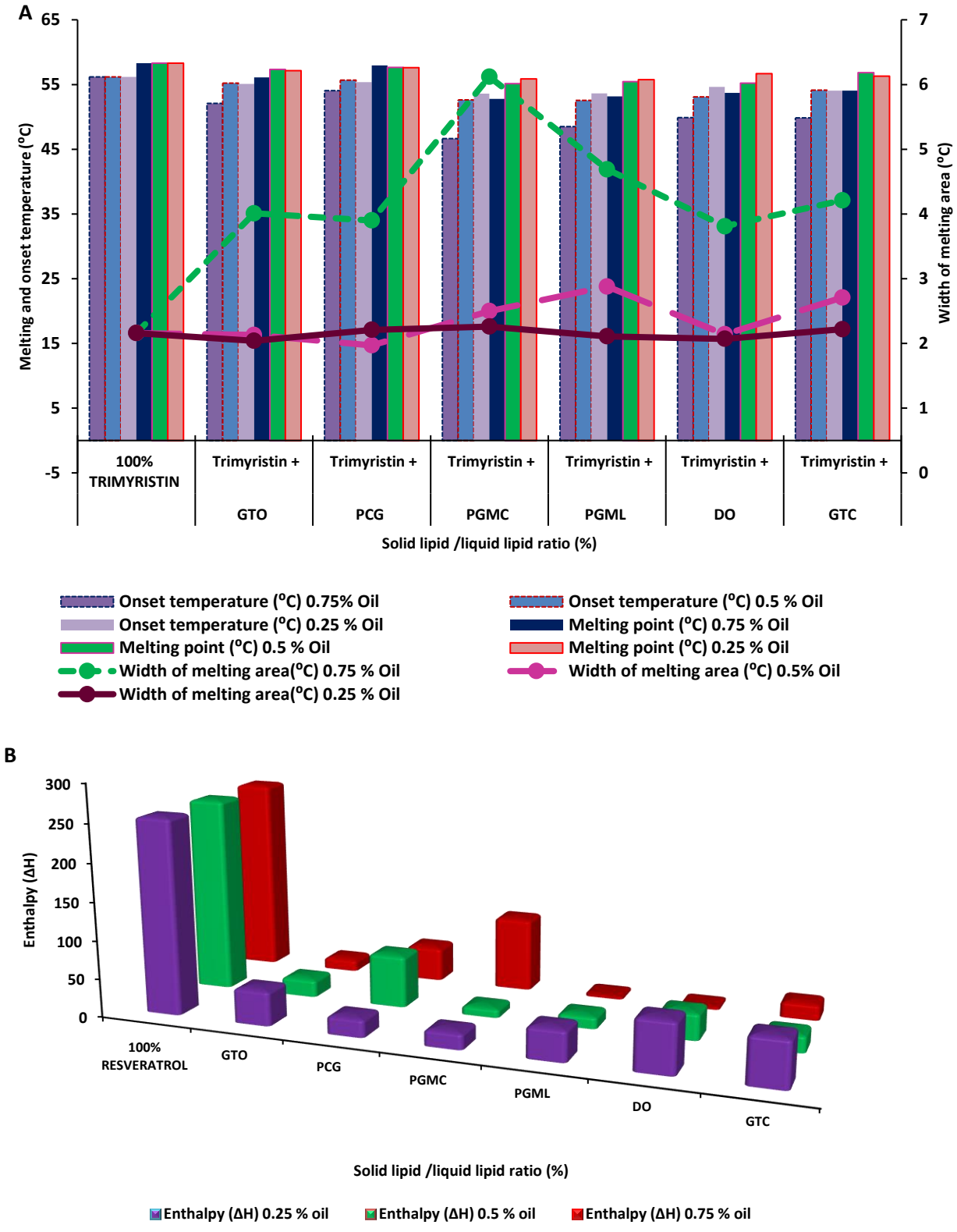

Figure 3-27. Bar graph representing A. Decrease of melting point, onset temperature and increase in the width of melting area of solid lipid with different concentrations of liquid lipids and B. Overlay of the melting enthalpy of solid lipid mixture with all liquid lipid concentration

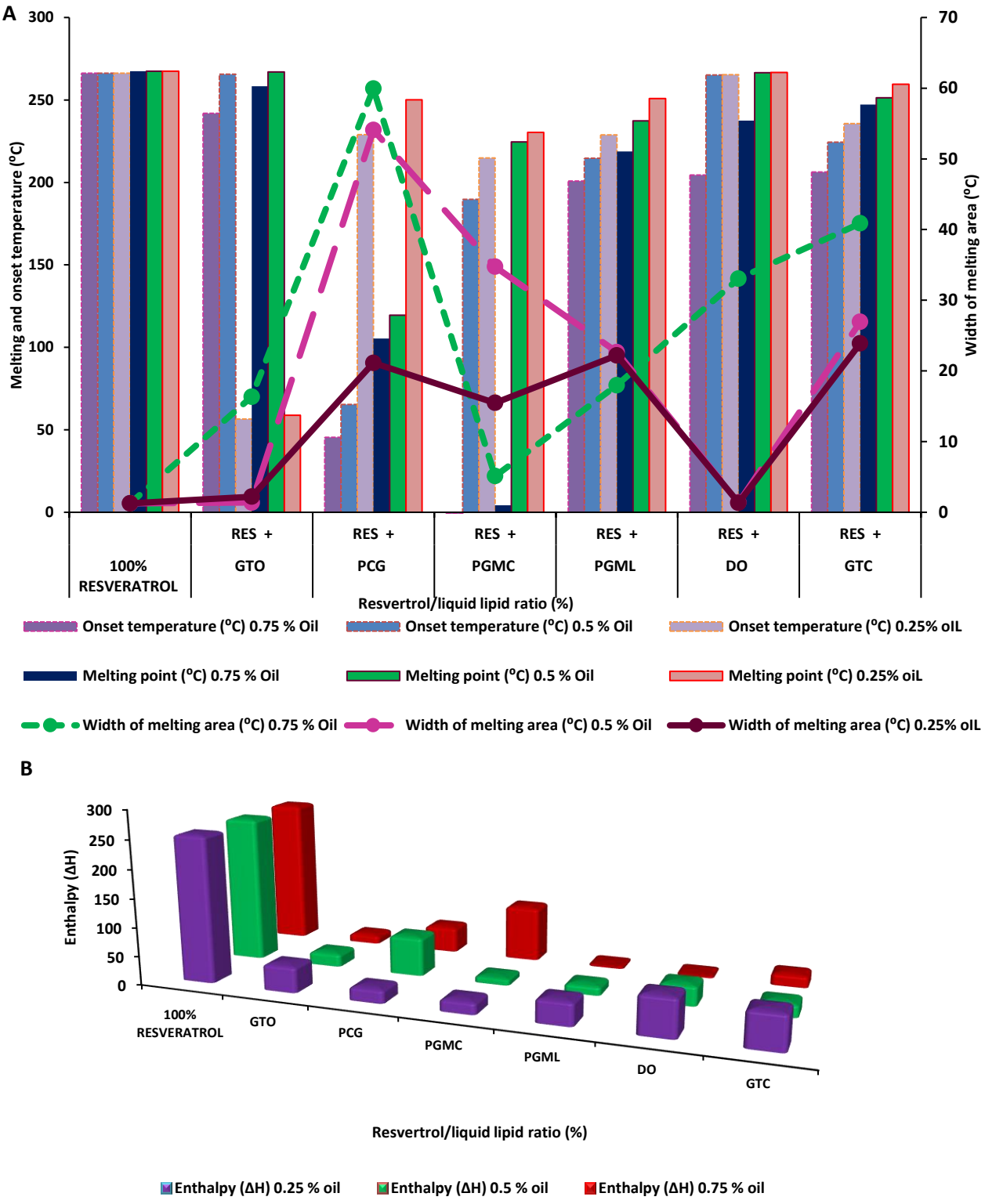

Figure 3-28. Bar graph representing A. Decrease of melting point, onset temperature and increase in the width of melting area of RES with different concentrations of liquid lipids and B. Overlay of the melting enthalpy of RES mixture with all liquid lipid concentration

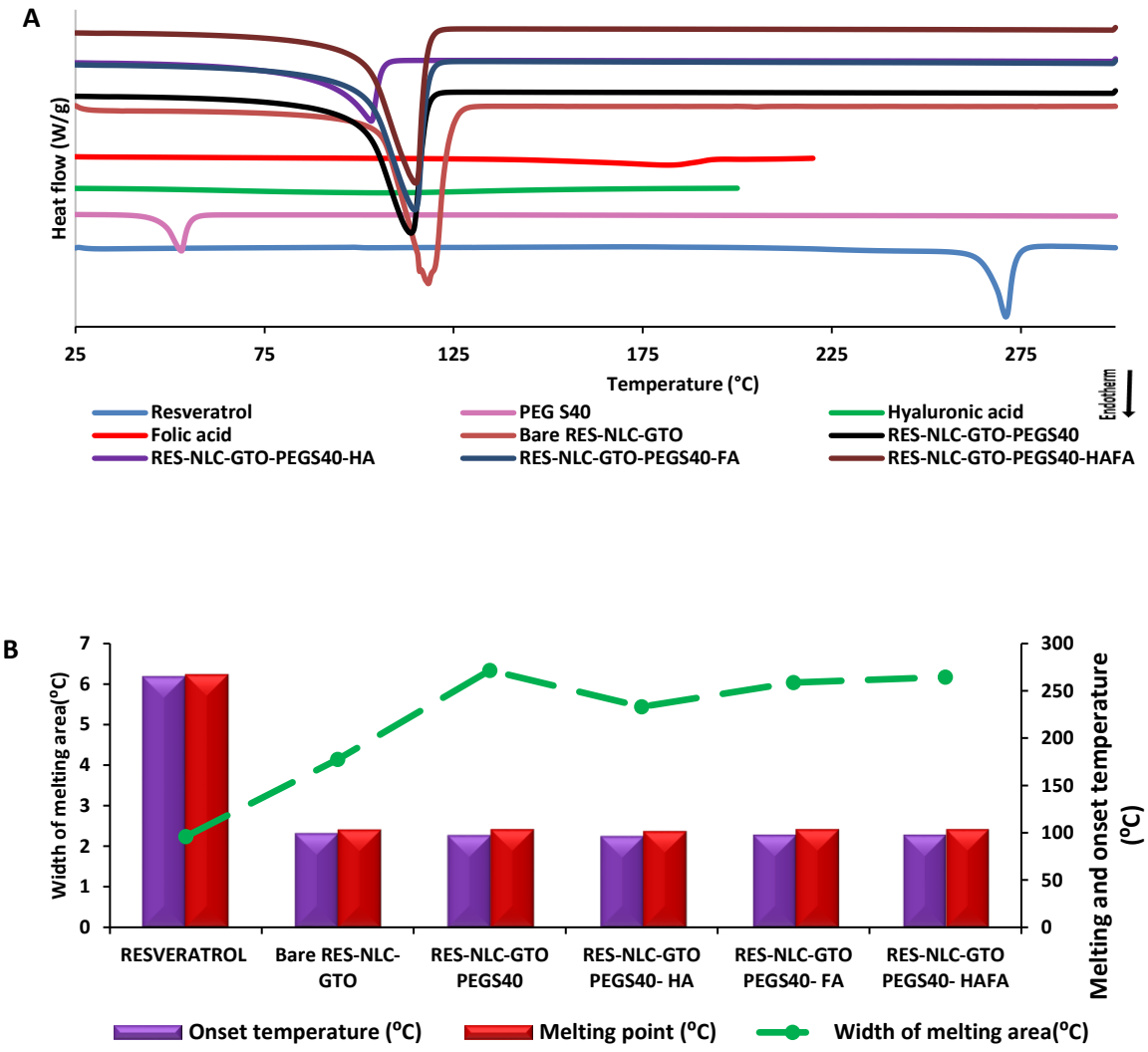

Figure 3-29. A.DSC heating thermogram of different Bare RES-NLCs and different surface modified formulations, B. Graph representation of the decrease of melting point, onset temperature and increase in width of melting area of surface modified RES-NLCs as determined by DSC analysis

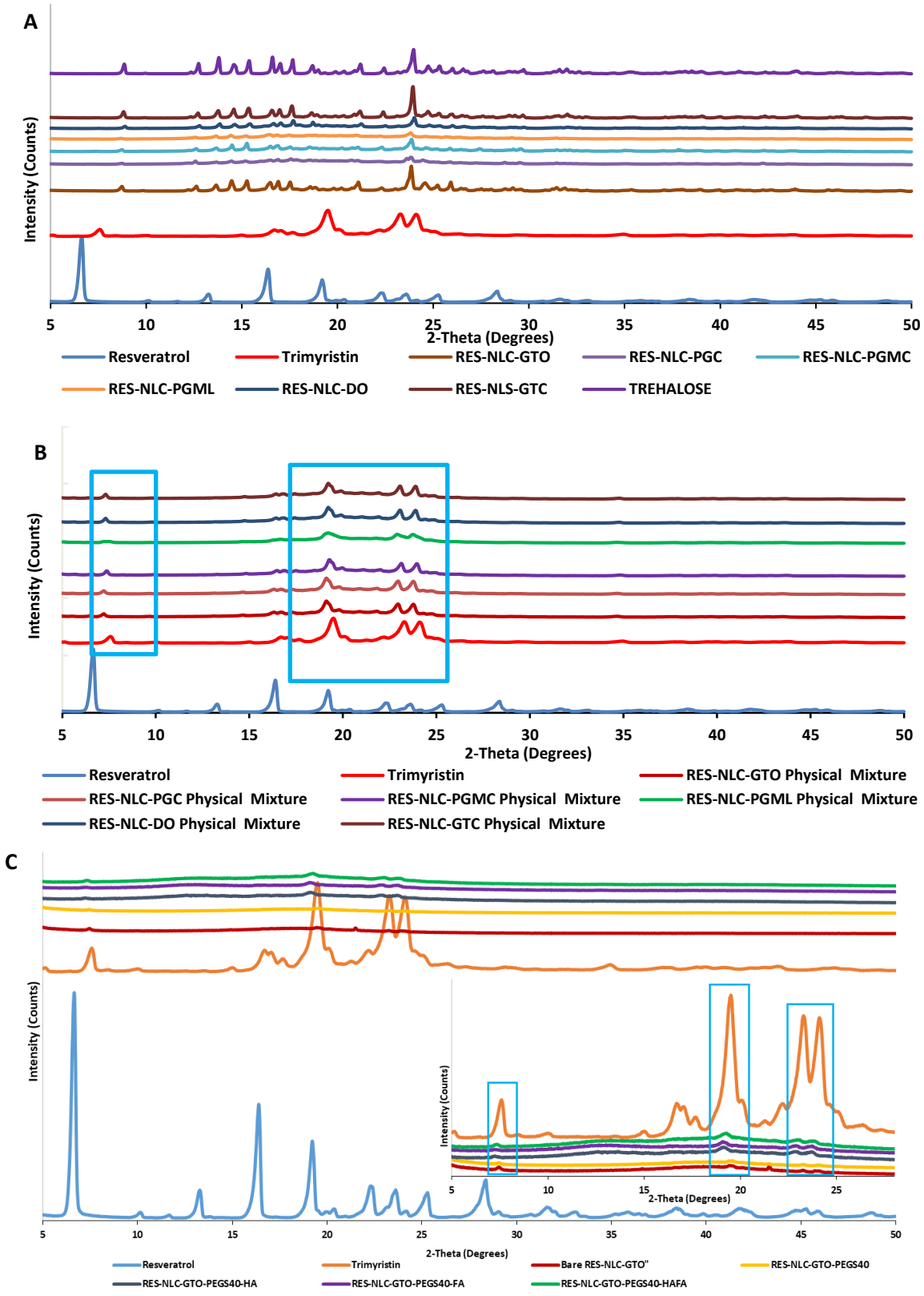

Figure 3-30. A. X-ray diffraction patterns of RES and RES-NLCs with various liquid lipids, B. X-ray diffraction patterns of RES and RES-NLC physical mixtures, C. X-ray diffraction patterns of RES and surface modified RES-NLCs

3.3.3 (IV) Fourier transform infrared

The fingerprints of RES clearly demonstrated four typical prominent absorption bands at 825 cm^{-1}, 1141 cm^{-1} and 1581 cm^{-1} corresponding to =C-H bending, -C-O stretching and C=C olifenic stretch in aromatic ring, respectively (Mont. Kumpugdee-Vollrath et al., 2012). The significant bands of RES disappeared in all bare and surface modified formulations (Figure 3-31 A-F) regardless of employing different liquid lipids (Mont. Kumpugdee-Vollrath et al., 2012), confirming the interaction between drug and individual components of the formulations, allowing for the drug incorporation into the nanoparticles matrix with good chemical stability (Jose et al., 2014).

The FTIR studies were further carried out in order to study the chemical binding of ligands (HA, FA) to the bare RES-NLCs. The presence of HA was characterised by the identifying significant peaks at 625 and 1048 cm^{-1} which corresponds to C-O-C stretching peaks, 1411.64 cm^{-1} for C-O group attached with carbonyl group, 1637 cm^{-1} that indicates the presence of amide II group, at 2685 cm^{-1} for C-H is it stretching or bending peaks, and at 3397 cm^{-1} broad peak corresponds to OH peak of HA. These different peaks obtained in the HA sample are consistent to that of the standard (Figure 3-32A). When compared with RES-NLC-GTO-PEGS40-HA, there was a significant peak shifting observed from 625 to 618 cm^{-1} related to C-O-C stretching, also there was a slight shift from 1411.64 to 1390 cm^{-1} which corresponds to C-O group with C=O peaks, and a peak corresponding to C-H group have shown strong shift from 2685 to 2611 cm^{-1}. The absence of broad OH peak at 3397 cm^{-1} is very distinct confirming that the OH group is replaced (Reddy and Karunakaran, 2013). Significant peak shifts in HA-NLC identified for C-O-C stretching peaks shifted from 625 to 611 cm^{-1}, a distinct peak shift from 1398 to 1388 cm^{-1} corresponding to C-O group with C=O, and absence of peak at 3397 cm^{-1} proves that in RES-NLC the OH group was replaced.

The presence of characteristic peaks of FA in NLC-GTO-PEGS40-FA when compared to the literature values of FA peaks assignment (Hammud et al., 2010) were observed. Peaks at 3350-3660 cm^{-1} were due to the hydroxyl (OH) stretching bands of glutamic acid moiety and NH group of pterin ring. The stretching vibration peak of C=O present at 1740 cm^{-1} and phenyl, 1462 cm^{-1} characteristics of the pterin ring and 3670 cm^{-1} due to OH- stretching. The presence of the later peaks in RES-NLC-GTO-PEGS40-FA indicate the successful binding of the ligand to the surface of the nanoparticle (Figure 3-32.B).

3.3.3 (V) Nuclear magnetic resonance studies

^{1}H-NMR spectra were obtained from RES and RES-NLCs dissolved in Deuterated DMSO (Figure 3-33).

The carbon-bound protons appeared in the region between 6.1 ppm to 7.07 ppm, while the OH protons appeared in the region 9 ppm and 9.5 ppm of the RES-NLCs ^{1}H-NMR spectrum (Orgován et al., 2017), indicates the presence of the drug in all RES-NLC formulations. In addition, the drug peaks were identical to the peaks of the drug in bulk. No chemical shift was observed when the drug was encapsulated in the NLC indicating that the drug was present in the intact form. No degradation of the drug was evident upon the formulation into NLCs (Garcia-Fuentes et al., 2004).

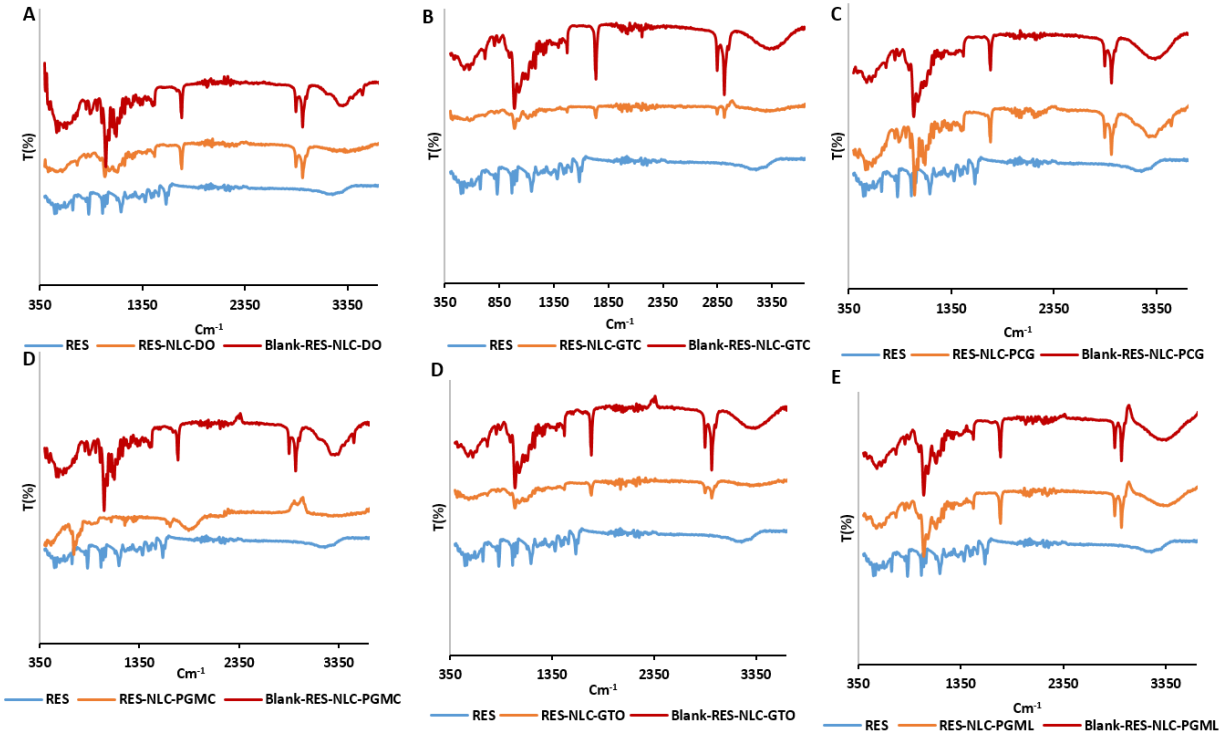

Figure 3-31. FTIR spectra for RES-NLCs A. RES-NLC-GTC and blank, B. RES-NLC-DO and blank, C. RES-NLC-PCG and blank D. RES-NLC-PGMC and blank E. RES-NLC-GTO and blank, F. RES-NLC-PGML and blank

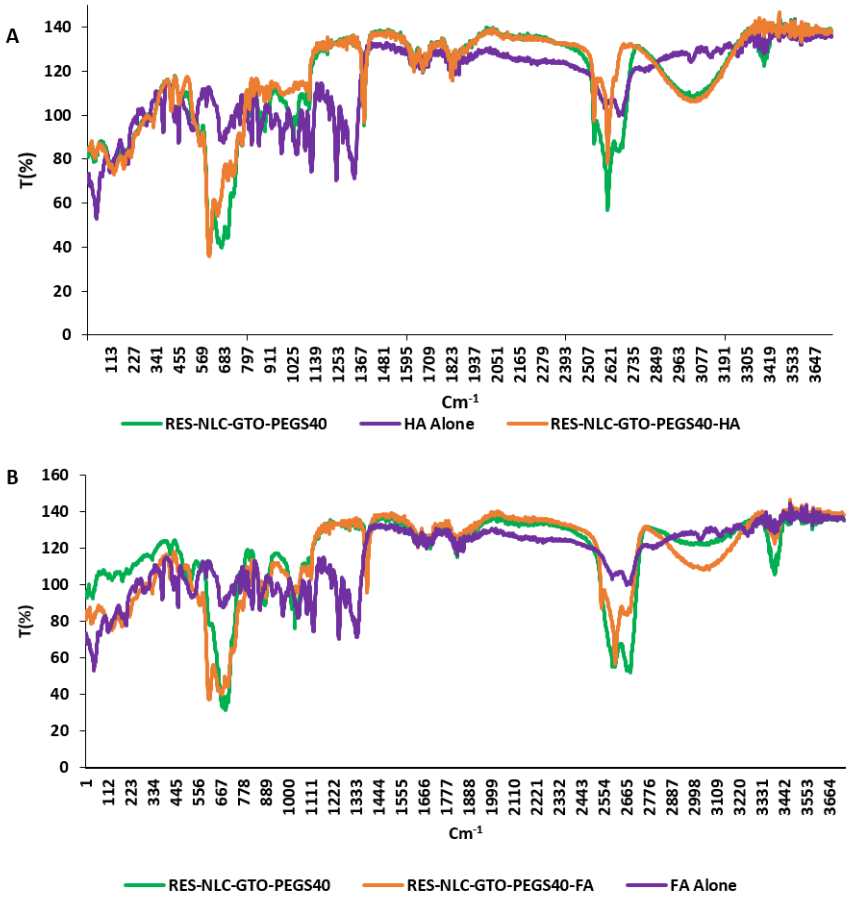

Figure 3-32. FTIR spectra for A. RES-NLC-PEGS40 HA and B. RES-NLC-PEGS40 FA

3.3.3 (VI) Morphology observation

A. SCANNING ELECTRON MICROSCOPY (SEM)

SEM is the technique employed to obtain information about the mean size and the surface morphology of the particles. The images reveal that the NLCs loaded with RES were almost spherical and uniform in shape with smooth surfaces (Figure 3-34). Particles are well separated from each other with no visible aggregation. Furthermore the incorporation of RES did not seem to affect the morphological appearance of the formulation.

B. TRANSMISSION ELECTRON MICROSCOPY (TEM)

NLCs with different liquid lipids were observed under TEM showing distinct NLC particles with high sphericity and smooth surface, confirming the spherical shape as indicated by SEM images. Spherical shape of NLCs was previously reported in many studies (Hu et al., 2005b, García-Fuentes et al., 2003) (Figure 3-35). TEM confirmed the particle size of the formulated RES-NLCs to be less than 200 nm, similar results obtained by Gokce et al (Gokce et al., 2012). NLCs size supports the results obtained from the size measurement by DLS zetasizer. The effect of the various liquid lipid

on the nanoparticle morphology was negligible as shown by TEM and SEM analysis. RES-NLCs showed similarity in shape, but differed in size.

3.3.4 *In vitro* drug release studies

3.3.4 (I) Chemical stability

Literature reports indicate that the pH affect the stability of the drug in the formulations. Therefore, the stability of the RES was studied in different pH buffers at 25^{o}C and 37^{o}C, prior to determining the drug release from formulated NLCs (Zupančič et al., 2015). No degradation of the drug was observed at pH 1.2, 5 and 6.8 over the period of 24 h both at 25^{o}C and 37^{o}C, indicating good stability of RES under these pH conditions. However, at pH 7.4 a sharp reduction in the drug concentration in the first h to 86 % at 25^{o}C (Figure 3-36.A) and 91% at 37^{o}C (Figure 3-36.B) was observed over the period of time with only 58 % remaining at the end of 24 h. the degradation was also evident by the colour change from colourless to a brown opaque colour at pH 7.4.

Figure 3-33. ^{1}HNMR of resveratrol (red pattern), RES-NLCs (green pattern A: GTC B: DO C: PCG D: PGMC E: GTO F: PGML), B-NLCs (blue pattern)

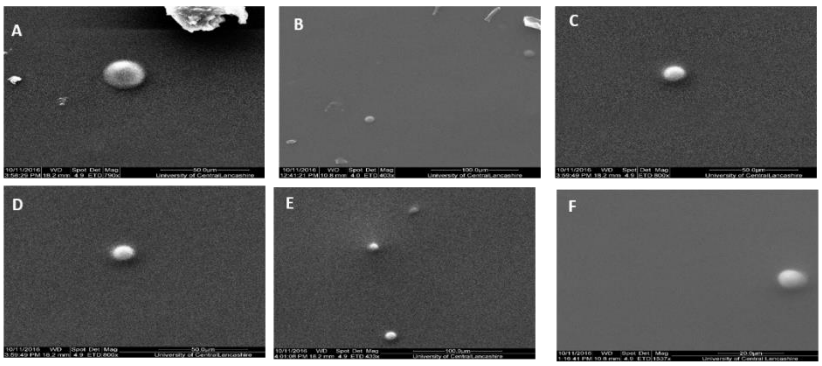

Figure 3-34. Scanning Electron Microscopy of A. RES-NLC-GTC, B. RES-NLC-DO, C. RES-NLC-PCG, D. RES-NLC–PGMC, E. RES-NLC-GTO and F. RES-NLC–PGML

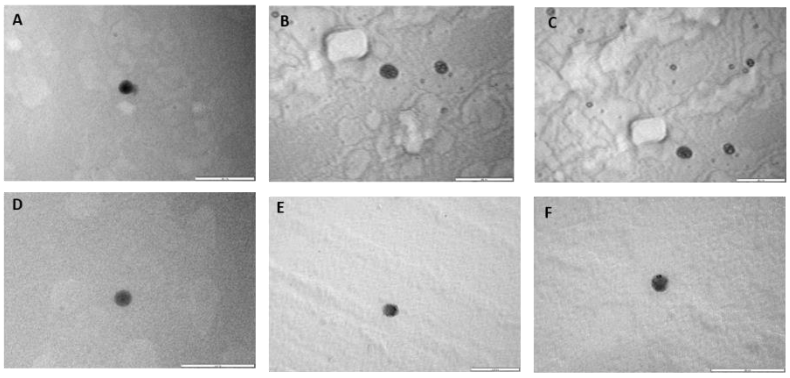

Figure 3-35. Transmission Electron Microscopy of A. RES-NLC-GTC, B. RES-NLC-DO, C. RES-NLC-PCG, D. RES-NLC–PGMC, E. RES-NLC-GTO and F. RES-NLC–PGML

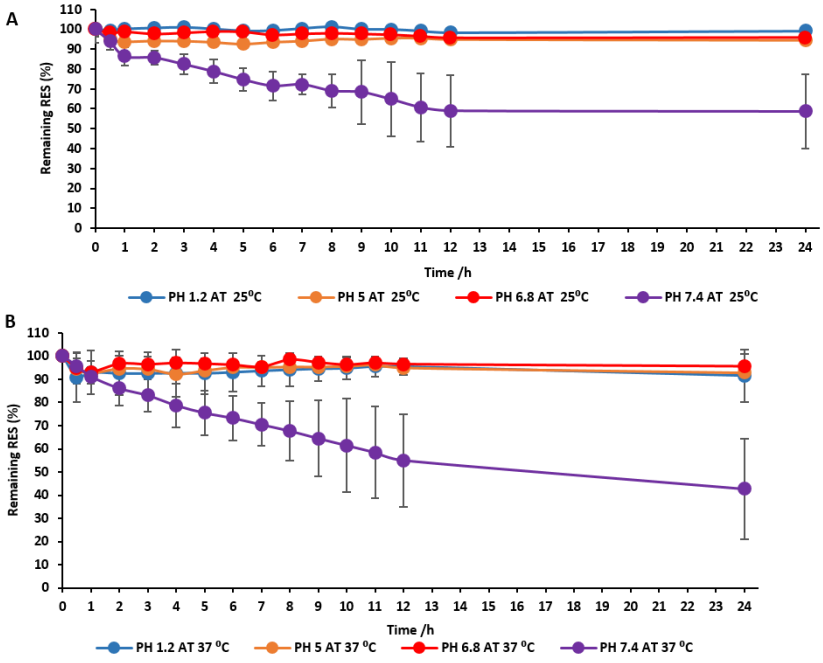

Figure 3-36.Stability of RES in various dissolution media at A. 25°C B. 37°C

3.3.4 (I) *In vitro* drug release from bare RES-NLCs

The main reason for performing the *in vitro* drug release was to study the effect of six different liquid lipids on the release profile of resveratrol from their corresponding NLCs. The release rate of resveratrol from six different NLC formulations varied depending on the carrier liquid lipid employed. *In vitro* release profiles of resveratrol and six different resveratrol loaded NLCs was performed at pH. 1.2 to simulate the acidic environment of the stomach. It was observed that less than 25% of RES was released in all RES-NLCs in the period of 4 h. This was in contrast to 90% release of the free drug. There was significant difference (P value <0.001), between the free drug and the drug released from the NLCs at all-time points. This indicates that the nanoparticles retained the drug and minimized the drug release from NLCs and protected the drug in the gastric environment (Figure 3-37.A).

Since the drug showed degradation in pH 7.4 buffer drug release studies could not be performed at this pH. Though the drug was found to be stable at pH 6.8, however, the formulation did not exhibit stability and showed discoloration at this pH, therefore, further *in vitro* drug release studies were conducted in pH 5 buffer. All RES-NLCs demonstrated slow drug release at pH 5 over the period of 24 h (Figure 3-37.B). A slow release over the period of 24 h from the lipid core of NLCs, defined the slow diffusion of the drug from the lipid matrix (Bhaskar et al., 2009, FDA, 2001, Elmowafy et al., 2017). A difference in release profile of drug was observed with different liquid lipid formulation; this is caused by the difference in nature of the carrier liquid lipids and their properties (Gaba et al., 2015). There was a significant statistical difference in the release profiles between free drug and the different formulations. The release was faster in RES-NLC-GTO with almost 95% of drug being released in 10 h, this was followed by RES-NLC-PCG, RES-NLC-PGML, RES-NLC-PGMC, RES-NLC-GTC and RES-NLC-DO. All RES-NLCs displayed a Modified Release property compared to the free drug release with 100 % being released at the end of 8 h.

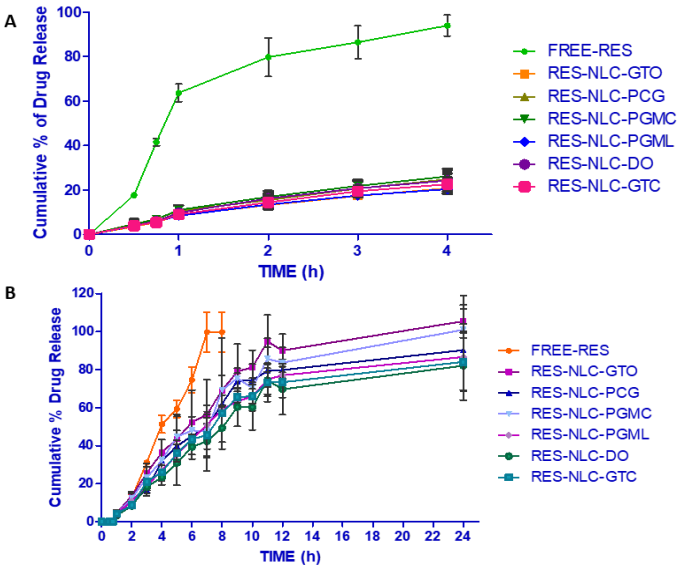

Figure 3-37.*In vitro* drug release profile of RES in NLC dispersions, at A. pH 1.2, B. at pH 5 Mean S.D (n = 3)

Data obtained from the *In vitro* release profiles of resveratrol loaded NLC formulations were fitted using various non-linear regression models such as zero order, first order and Higuchi models (Table 3-9). All bare RES-NLC formulations fitted well with first order model with a high R^2 values indicating that the release behavior of all formulations followed first order kinetics except for RES-NLC-DO and RES-NLC-GTC, which exhibited a high fitness to the Higuchi diffusion model / Fickian diffusion mechanism indicating the lipid matrix erosion was the mechanism employed for the drug release (Soma et al., 2017).

3.3.4 (II) *In vitro* drug release from surface modified RES-NLCs

Upon surface modification of RES-NLCs, the release profile at pH 1.2 of RES was considerably affected, whereby only 2% of the drug was released after 4 hours from the NLCs as compared to almost 100% and 25% release of the free drug and bare RES-NLCs-GTO, respectively. This effect is observed due to the alteration in the surface characteristics of the nanoparticles by PEGylation and appending of the ligands, which offer more protection to the drug and delay the release of the drug in acidic environment (Figure 3-38.A). PEGylation will also offer prolonged circulation time in the blood. It is evident (Figure 3-38.B) that the drug release from the PEGylated and surface modified RES-NLCs at pH 5 was delayed with almost negligible release up to 2 h, following which the drug released slowly observed over the period of next 10 h. The initial slow release could be attributed to the ligand corona on the nanoparticles. This was in contrast to the bare RES-NLCs where 50 % of the drug was released in 4 h. This could be attributed to the long polyethylene glycol chain producing a hydrophilic shield on the surface (Yuan et al., 2013, Chen et al., 2014, Wang et al., 2015, Hu et al., 2015). Further, HA layer forms a barrier holding the drug and restricting its dispersion in

the media, showing slow drug release compared to the bare NLCs, similar observation by Tran et al. (Tran et al., 2014). The modification with FA also hindered the drug release, followed by a continuous release which would help in maintaining a continuous efficiency, these results were in accordance to Zhang study (Zhang et al., 2016a). Surface modified NLCs also demonstrated concentration dependent first order release kinetics as seen from the R^2 values given in Table 3-9.

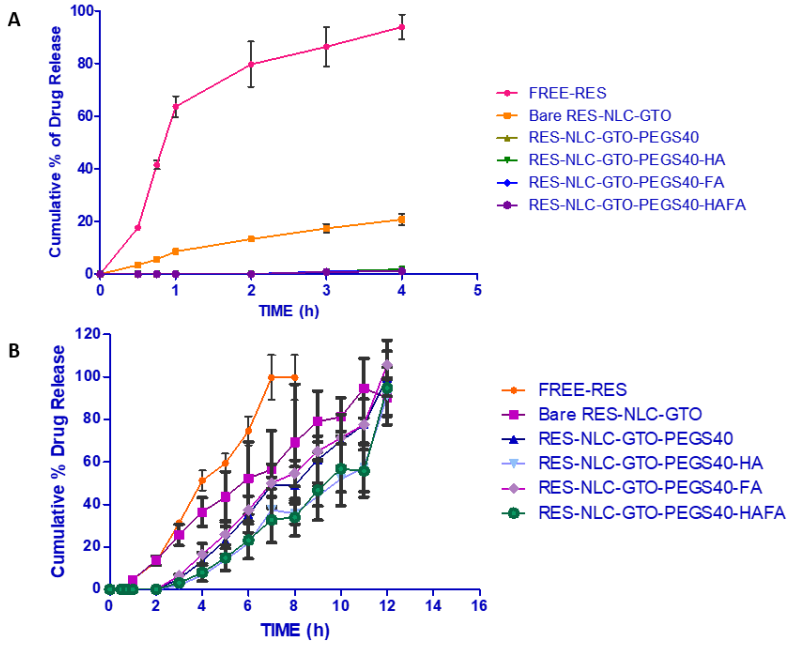

Figure 3-38.*In vitro* drug release profile of resveratrol surface modified NLC dispersions, at A. pH 1.2, B. at pH 5 Mean S.D (n = 3)

Table 3-9: Release kinetic profiles of the optimized RES-NLCs at pH 5

Formulations	Zero order kinetics R^2	First order kinetics R^2	Higuchi model R^2
Free- RES	0.9744	0.958	0.877
RES-NLC-GTO	0.818	0.946	0.934
RES-NLC-PCG	0.797	0.929	0.918
RES-NLC-PGMC	0.830	0.965	0.935
RES-NLC-PGML	0.818	0.937	0.932
RES-NLC-DO	0.831	0.915	0.923
RES-NLC-GTC	0.810	0.922	0.930
RES-NLC-GTO-PEGS40	0.882	0.906	0.869
RES-NLC-GTO-PEGS40-HA	0.806	0.844	0.794
RES-NLC-GTO-PEGS40-FA	0.813	0.928	0.851
RES-NLC-GTO-PEGS40-HAFA	0.763	0.904	0.776

3.3.5 Storage stability of RES-NLCs formulations

3.3.5 (I) Bare RES-NLCs

Particle size and particles distribution of nanoparticles are two important criteria as these factors play a critical role in cellular uptake, drug release rate, bio-distribution to various tissues and finally the stability of the formulated products (Vandervoort and Ludwig, 2002, Leach et al., 2005, Azhar Shekoufeh Bahari and Hamishehkar, 2016). NLCs have been reported to possess improved drug loading, controlled drug release, and minimum drug leakage from the nanoparticles during storage. When oil is incorporated into the solid matrix this observation was reduced because of better emulsification of the lipid matrix. Many reports showed that NLCs demonstrated high stability with minimal increase in particle size (Elnaggar et al., 2011).

Souto et al. have shown good stability with clotrimazole-loaded SLN with Dynasan® 116 as the solid lipid and NLCs with the same lipid accompanied by 30% Miglyol® 812 as the oil. There was no significant difference in size of both formulations the size of both the formulation over the period of 3 months of storage (Souto et al., 2004).

Storage stability of the six optimised RES-NLC formulations containing each of the six liquid lipids was evaluated for the period of six months. Briefly, samples were stored in sealed amber colour glass bottles at both 4°C and 25°C. Samples were withdrawn at one, three and six months and characterized with respect to PS, PDI, ZP, %EE and %DL (Muppidi et al., 2012), all the data obtained was compared to the initial (day zero) PS, PDI, ZP, %EE and %DL of the formulated NLCs. The stability studies clearly demonstrated that the type of liquid lipid had great impact on all the quality parameters of RES-NLCs (Yang et al., 2014).

The mean particle size at 4°C of all RES-NLCs was below 100 nm (Figure 3-39.A) except RES-NLC-PGML which showed increased particle size 209.8 ± 11.607 (Figure 3-42.B). The RES-NLCs containing the PEGylated liquid lipid Labrasol and the two propylene glycol esters, PGML and PGMC showed increase in particle size above 200 nm at the end of 3 months demonstrating peaks at the micron region (Figure 3-42.C). The particles grew in size with time and were quite aggregated at the end of six months with a size of all NLCs above 200 nm for PCG, PGMC and PGML RES-NLCs. While GTO, DO and GTC RES-loaded NLCs showed size below 200 nm at the end of six months (Figure 3-42.D).

On the other hand, all RES-NLC stored at 25°C did not show any significant increase in particles size with the mean particle size well maintained within 100 nm, (Figure 3-42. E, F), except RES-NLC-PGMC and RES-NLC-PGML which showed a significant increase in the particle size (Figure 3-42.G) which increased above 100 nm at the end of six months. This corroborates with previous report where triglycerides GTO and GTC have shown effective retardation of particle aggregation when stored at 25°C, similar results were obtained by Radomska (Radomska-Soukharev, 2007). Between

these two triglycerides, GTC with shorter chain length (C-8:0) exhibited better stability in terms of particle size than GTO containing longer fatty chain length (C18).

The polydispersity index values for all formulations stored at 4°C showed an increase after one month except for GTC loaded RES-NLCs that had a value of 0.279 ±0.030 (Figure 3-39.B). After three months of storage PCG and PGMC showed the highest increase in the polydispersity index showing aggregates and peaks in the micron range (Figure 3-39.B). Six months stability data showed an overall increase of PDI above 0.3 for all NLCs. Additionally, NLCs stored at 25°C revealed no pronounced changes in the measured parameter (PDI). Previous studies have shown better stability of NLCs at 25°C in term of particle size and PDI (Souto et al., 2004, Bhaskar et al., 2009).This could probably be due to better maintenance of lipid structure and drug remaining entrapped with in it at ambient temperature, whereas at lower temperature would lead to crystallization of the drug and eventually increase in the particle size of NLCs.

The increase in particle size for samples stored for stability study can be attributed to a number of mechanisms including coalescence, flocculation and Ostwald ripening. Flocculation and coalescence lead usually to a wide particle size distribution with a high PDI (Tadros et al., 2004, Trujillo and Wright, 2010, Sharma et al., 2011, Witayaudom and Klinkesorn, 2017). Coalescence and Ostwald's ripening are the two main driving forces that have been identified for particle growth (Malzert-Fréon et al., 2010). The mechanism of particles growth is triggered by the change in solubility of nanoparticles depending on their size. Due to the high surface energy and solubility of smaller particles within the dispersion, these re-dissolve and allow the overgrowth of larger particles. The mathematical theory of Ostwald ripening within a close system is described by Lifshitz and Slyozov (Thanh et al., 2014).

Coalescence phenomenon is described by the equation:

$$1/r^2 = /r^2_0 - 8\pi/3\omega t \qquad \text{Equation 42}$$

Where r is the average of radius of NLCs, r_0 is the value at t= 0 and ω is the frequency of rupture per unit of surface of the film. Another mechanism for instability would be Ostwald ripening phenomenon, which describes the redeposit of small crystals onto larger crystals (Forgiarini et al., 2001, Anton et al., 2008, Wu et al., 2011). The Ostwald ripening rate can be evaluated by applying the principal developed by (Lifshitz and Slyozov, 1961), which predicts a linear relationship between the cube of droplet radius, r3, and time t, x being the slope of plots, equation:

$$\omega = dr^3/dt = 8/9\ [C_\infty \gamma (MD / \rho^2 RT)] \qquad \text{Equation 43}$$

The main physicochemical mechanism contributing to particles growth of the NLCs is due Ostwald ripening more than coalescence and flocculation. However if the driving force for the increase in

particle size is Ostwald ripening then a linear relationship between the average droplet radius (r^3) and storage time (t) should be noted according to the Lifshitz–Slesov and Wagner (LSW) theory (Lifshitz and Slyozov, 1961). Therefore, in this study, the r^3 data was plotted as a function of time over the period six months for the NLCs (Figure 3-41. B, D).

The plots of change of particle size with time for RES-NLC-PGMC, DO, PGML and PCG exhibit Oswald ripening as phenomenon for particle growth, similar results were reported from previous studies (Deminiere et al., 1999, Izquierdo et al., 2002, Witayaudom and Klinkesorn, 2017). However, RES-NLC-GTO and GTC (Figure 3-41.A,) shows coalescence to be the mechanism of particle growth. When PGMC used as liquid lipid with larger particle size increase of RES-NLC-PGMC exponentially with time the mechanism for particle grow might be flocculation at the end of storage of six months (Figure 3-41. A.C).

The zeta potential (ZP) is the electrostatic potential reflects the electric charge on the particle surface. It is a key indicator for predicting the long-term physical stability of colloidal dispersion system (KOMATSU et al., 1995, Yuan et al., 2007). From the literature, zeta potential value exceeding ±30 mV is required for excellent physical stability (Riddick, 1968, Müller, 1996).

Many studies reported that the stability of lipid nanoparticles against aggregation is affected by the ionic strength of the continuous phase also on the charge density on the surface of the water and lipid phase (Volkhard Jenning, 2001, Trotta et al., 2003).

Though zeta potential of the fresh RES-NLCs prepared with six different liquid lipids were not significantly different from each other, time dependent change was strongly influenced by the type of liquid carrier (Figure 3-39.C). After storage at 4°C, the zeta potential of the RES-NLCs prepared with the triglycerides GTO and GTC showed no evident reduction in the zeta potential value in the first month (Figure 3-43.B). This validates the particle size and PDI results substantiating that the triglycerides with low melting point can impart stability to the NLC dispersions. Also DO did not show a reduction of ZP value in the first month while Propylene glycol esters PGML and PGMC RES-NLCs revealed sharp decline in zeta potential demonstrating poor colloidal stability. After three month of storage a considerable reduction in the ZP value (Figure 3-43.C) were observed. The stability of RES-NLCs with different liquid lipids showed a deterioration of zeta potential value at the end of six month (Figure 3-43.D). The presence of surfactant in sufficient amounts to cover the nanoparticles providing both the steric and electrostatic stabilization to the formulations (Bunjes et al., 2002).

RES-NLCs at 25°C, GTO, PCG and GTC nanoparticles showed high stability for the first three months (Figure 3-43.E, F). In addition, the triglyceride GTO and GTC showed minimal change of ZP at the end of six months, while all other formulation had a significant reduction in their zeta potential values over the six month (Figure 3-43.G).

When NLCs were stored at 4°C all of them were stable with no change in the total drug, however, only RES-NLC-GTO loaded NLCs showed good stability upon storage at 25°C for the first month (Figure 3-40.D). After 3 months all formulations showed a significant decrease in drug content regardless of their storage conditions, potentially suggesting degradation of the drug with time.

The entrapment efficiency depends on the concentration and the type of lipid mixture utilized in formulating the NLCs (Souto et al., 2004). The percentage of incorporated drug in the lipid matrix (entrapment efficiency) was evaluated over a period of six months (Figure 3-40.E). Incorporation of resveratrol resulted in a high entrapment efficiency, because of the lipophilic nature of the drug. When all NLCs were stored at both 4°C and 25°C showed significant difference in entrapment efficiency from the initial observed values though in some formulations the entrapment efficiency was still above 90%. The high entrapment efficiency despite of low drug content is probably due to minimum drug leakage from the nanoparticles in spite of the degradation of the drug, similar results were obtained by Jenning (Jenning et al., 2000d). NLCs lipid matrix is constituted by a mixture of solid lipids and liquid lipids, where the particle solidifies upon cooling and the recrystallization is prohibited so the loaded drug remain in the amorphous state. Another type of NLC are formed when the lipid composition are chemically different, leading to structure with many imperfections able to accommodate the drug and thus higher drug loading capacity (Souto et al., 2004).These formulations show stability over period of time because of the weak recrystallization process of the loaded drug, the stability is affected by the type of lipid and the emulsifiers amount as well play a role in stabilizing the formulations (Das and Chaudhury, 2011).

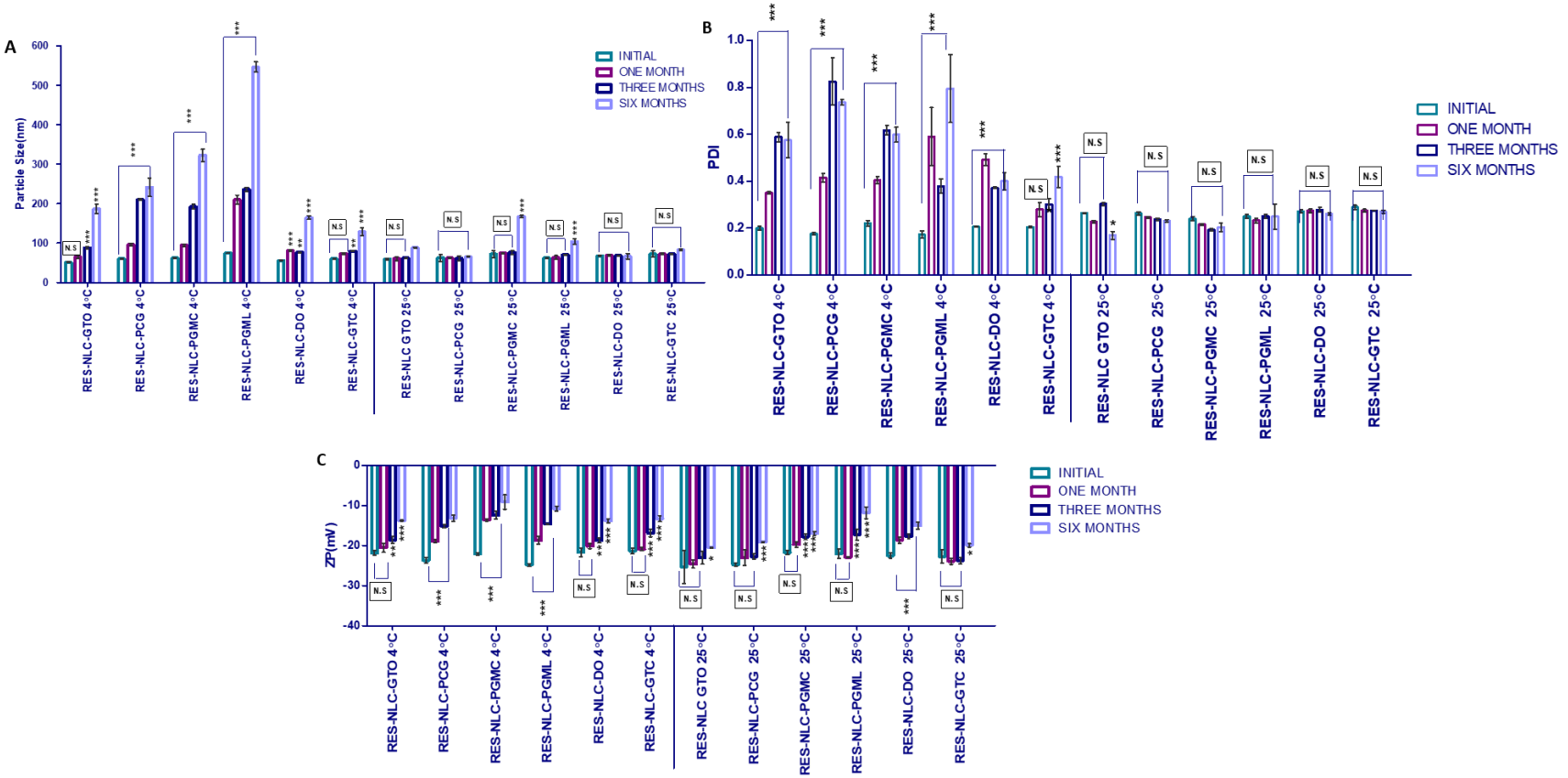

Figure 3-39. Storage stability of RES-NLC at 4 °C and 25 °C Initial (day zero), three months and Six months on A. Particle size, B. Polydispersity index, C. Zeta potential, error bars are standard error of the mean, Difference at p < 0.05 was considered statistically significant, * indicates P< 0.001, **, P < 0.01 and * P< 0.05**

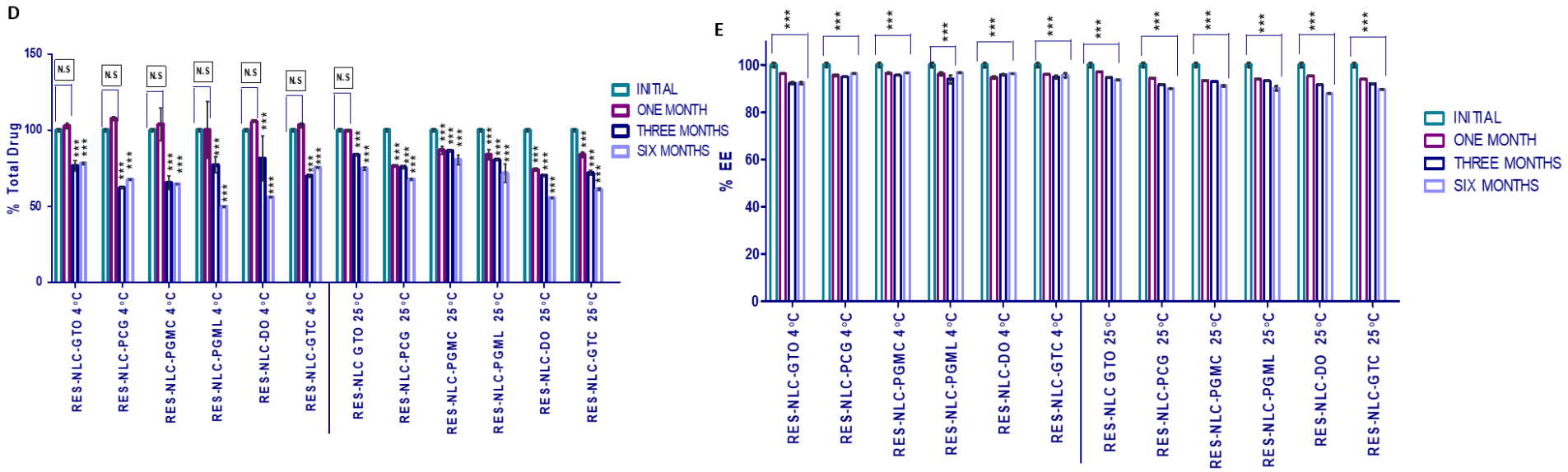

Figure 3-40. Storage stability of RES-NLC at 4 °C and 25 °C Initial (day zero), three months and Six months on D. % Total drug and E. % Entrapment efficiency, error bars are standard error of the mean, Difference at p < 0.05 was considered statistically significant, * indicates P< 0.001, **, P < 0.01 and * P< 0.05**

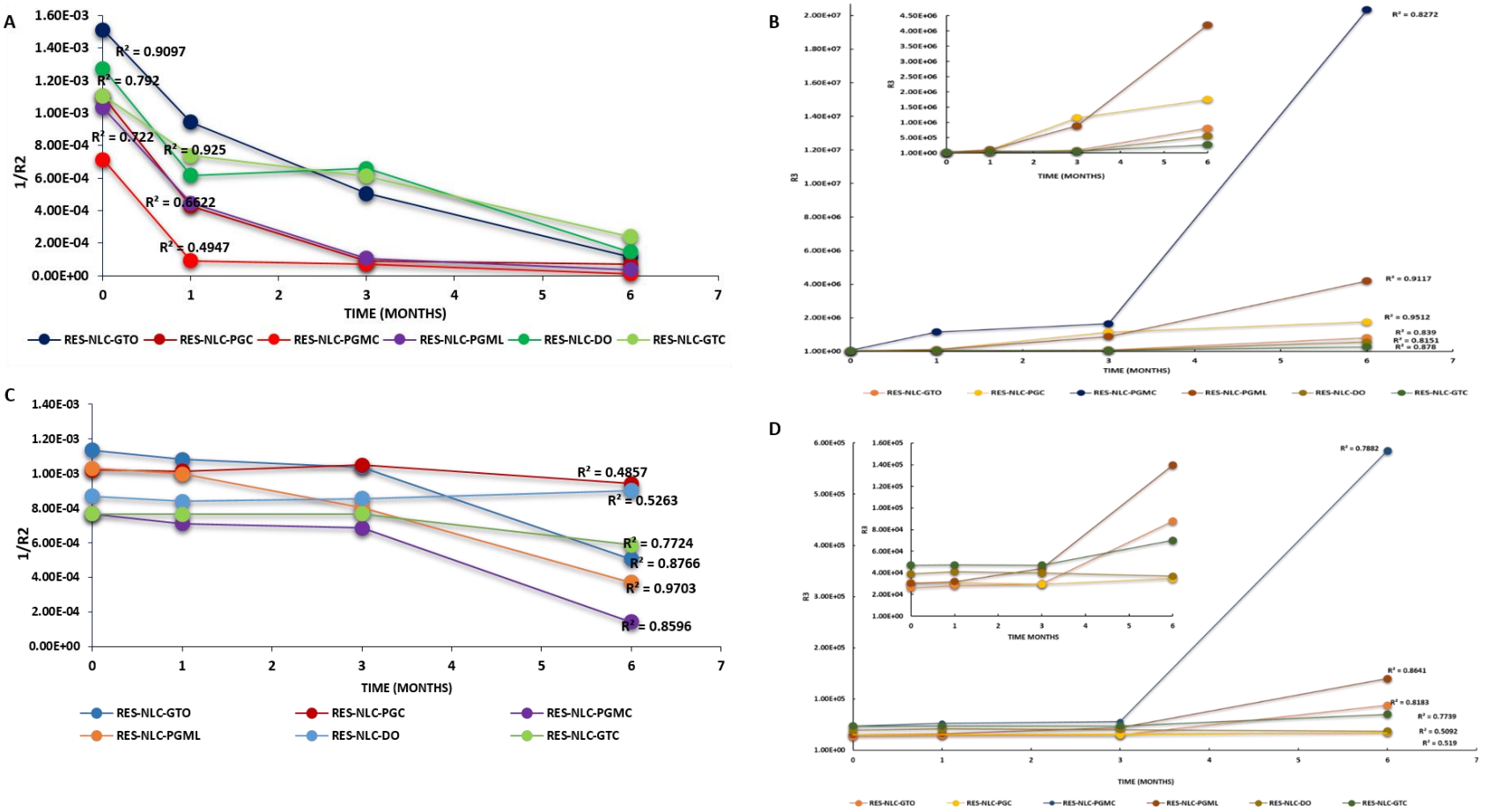

Figure 3-41. A. Coalescence force and B. Ostwald ripening versus time determined for RES-NLC stored at 4°C. C. Coalescence force and D. Ostwald ripening versus time determined for RES-NLC stored at 25°C

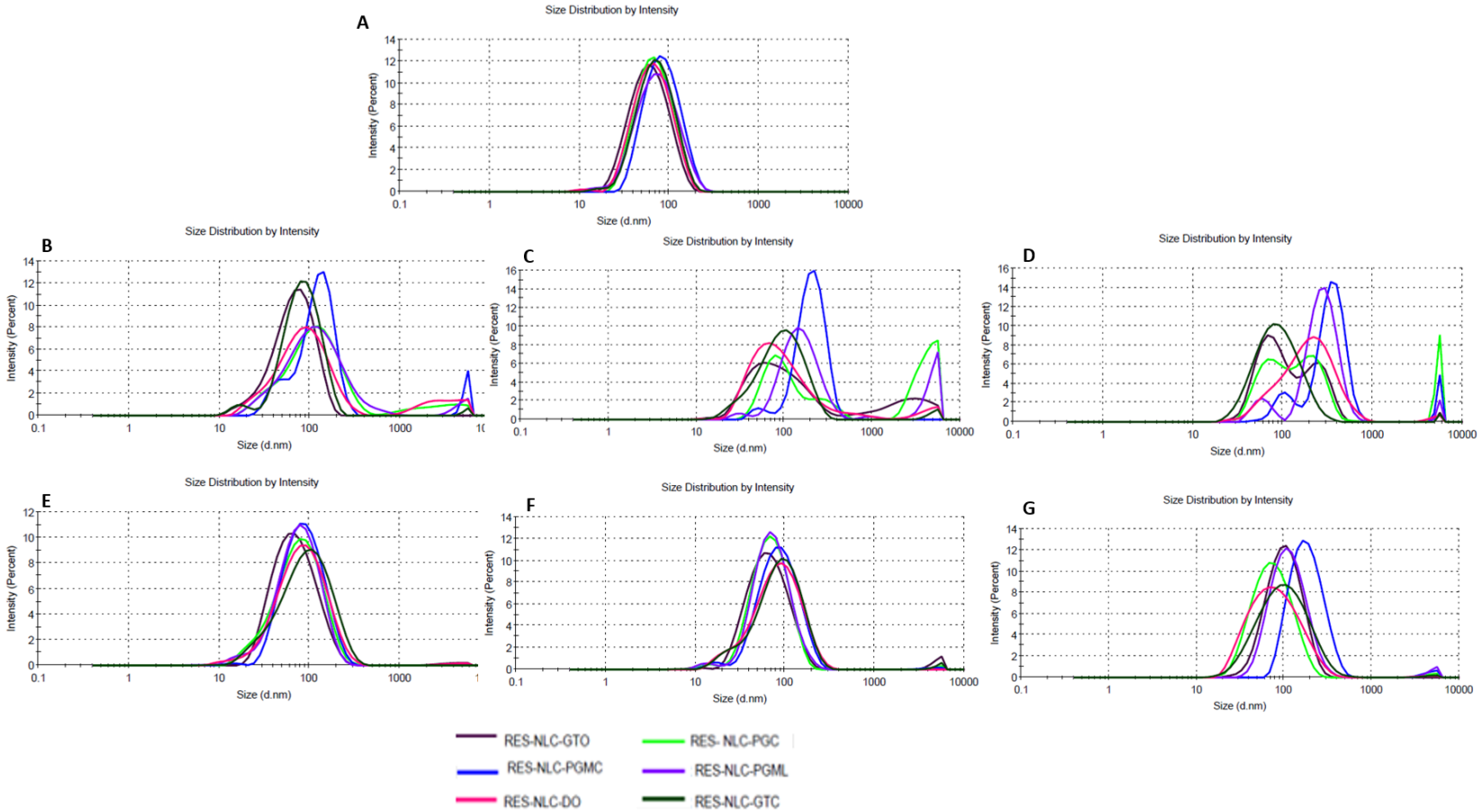

Figure 3-42. Overlay size distribution measured by zetasizer for stability of RES-NLCs after A) Initial (day zero) B. One, C. Three and D. Six months for each liquid lipid type stored at 4^{o}C and E. One, F. Three and G. Six months stored at 25^{o}C, n=3

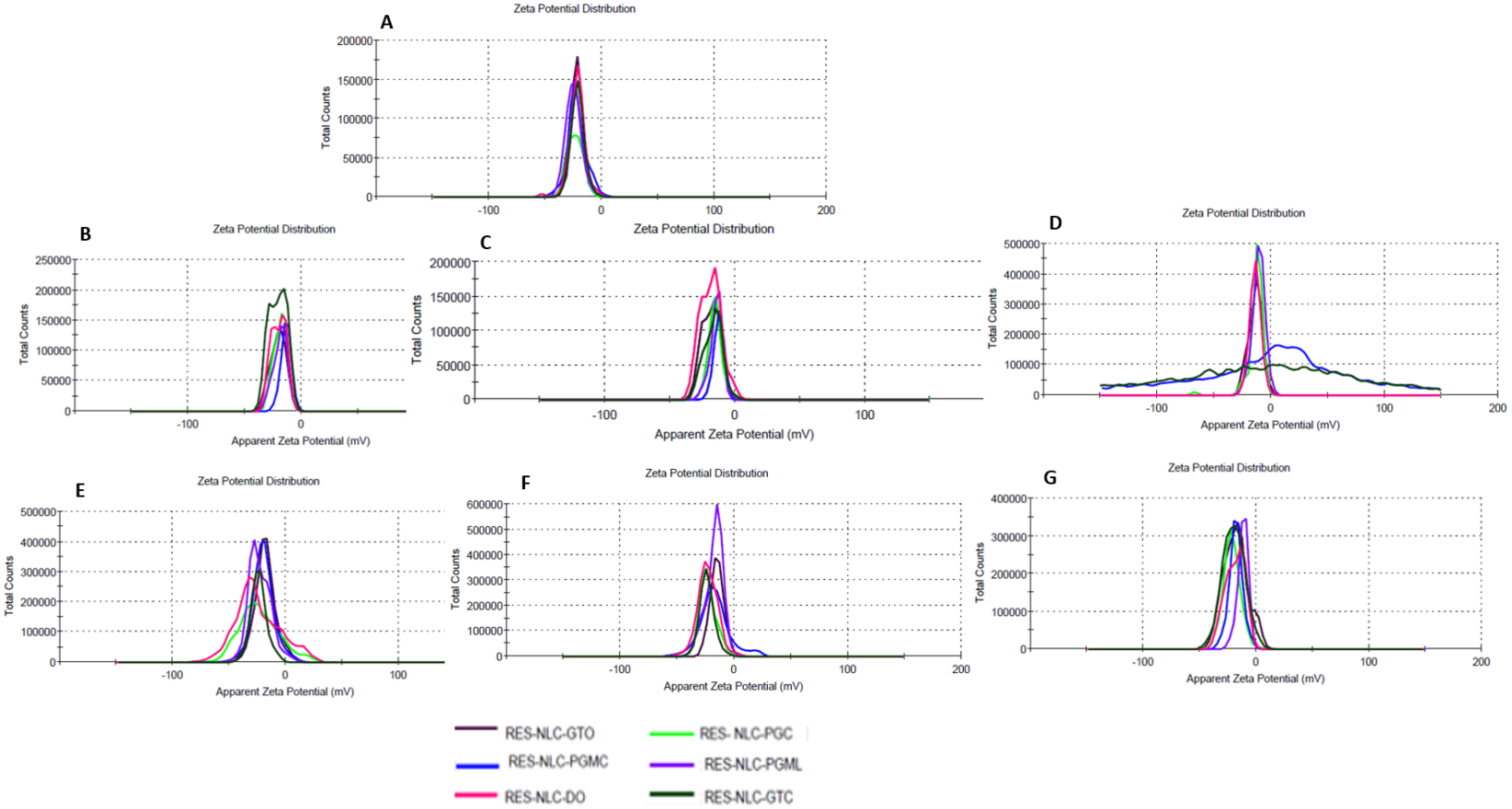

Figure 3-43. Overlay zeta potential measured by zetasizer for stability after A) Initial (day zero) B. One, C. Three and D. Six months for each liquid lipid type stored at 4^{o}C and E. One, F. Three and G. Six months stored at 25^{o}C, n=3

3.3.6 Surface modified RES-NLCs

There are few reports on the stability of surface modified NLCs, most of the reports showed stability investigations for only few days (10 days) after functionalization (Zhang et al., 2014b).

The three surface modified RES-NLCs-GTO were investigated over the period of three months for Stability. Observation for any change in the physicochemical characteristics were noted over this period of time.

There was no significant increase in the particles size and polydispersity index at the end of when stored at $4^{o}C$, except for RES-NLCs-PEGS40-FA which gave the highest increase in the particle size after three months (Figure 3-44.A). A wider particle size distribution was observed (Figure 3-46.B, C) when compared with the initial formulation indicating that the main driving force for the particles to grow and aggregate was the Ostwald ripening (Figure 3-45.B). No particles coalescence was observed during that period (Figure 3-45.A).

The surface modified formulations were stable for 2 months when stored at $25^{o}C$. However, at the end of third month the particle size of all the three functionalized NLCs was found to significantly increase with maximum increase in the particle size with the formulation with the dual ligand (Figure 3-46.D.E), suggesting that the main driving force for particle growth is Ostwald ripening (Figure 3-45. C,D).

Apart from the increase in the particle size, the impact on particle size distribution was also observed. Amongst the formulations stored at $4^{o}C$, both FA and HAFA functionalized RES-NLCs showed wider PDI at the end of three months (Figure 3-44.B). However, for the formulations stored at $25^{o}C$, all the three surface modified RES-NLCs showed an increase in PDI, with the dual ligand formulation being highly polydisperse at the end of three months (Figure 3-44.B). This could be probably due to the dual appended formulations having high ligand density on the surface of the nanoparticles.

These observations were also reflected in the variation zeta potential value of the formulations upon storage (Figure 3-47). Though during the first 2 months the colloidal stability of the formulations was maintained, a significant drop in the ZP was observed at the end of three months for all formulations at both the storage conditions (Figure 3-47. B, C, D, E).

The ligand appending to the nanoparticle surface makes the nanoparticle bulky therefore higher tendency of coalescence and aggregation is observed. Plots of 1/R2 Vs time and R3 vs time were plotted to understand the underlying mechanism of particle growth. As evident from Figure 3-47 A.B the correlation coefficient of both the plots for all the functionalized formulations were within the range of 0.663-0.861. It is apparent that both coalescence and Ostwald ripening contributed to the particle growth with time. This is the first report investigating the mechanistic report behind the particle growth with time.

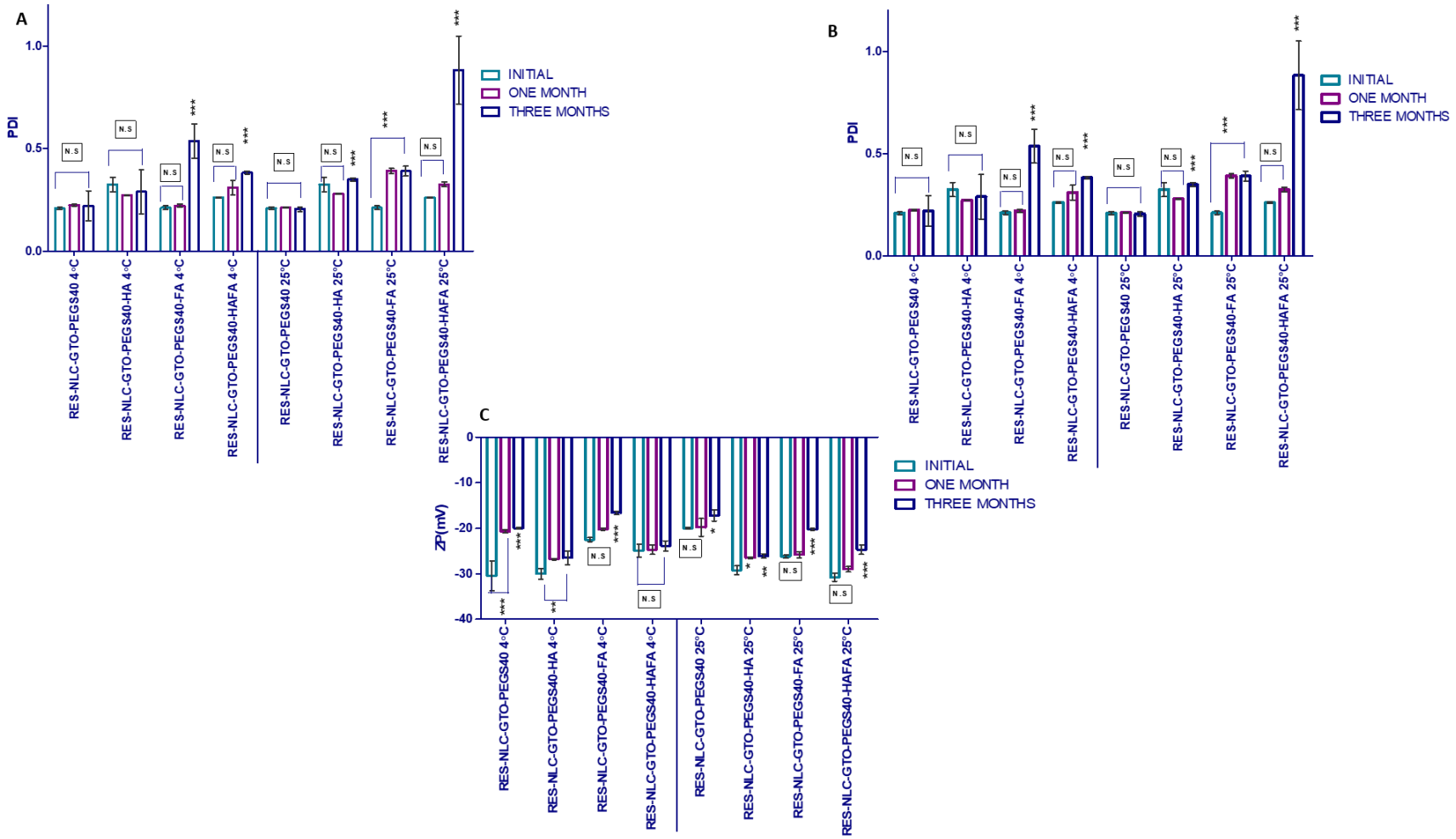

Figure 3-44. Storage stability of RES-NLC measured by zetasizer at 4°C and 25°C Initial (day zero), three months and Six months on A. Particle size, B. Polydispersity index and C. Zeta potential, error bars are standard error of the mean, n=3

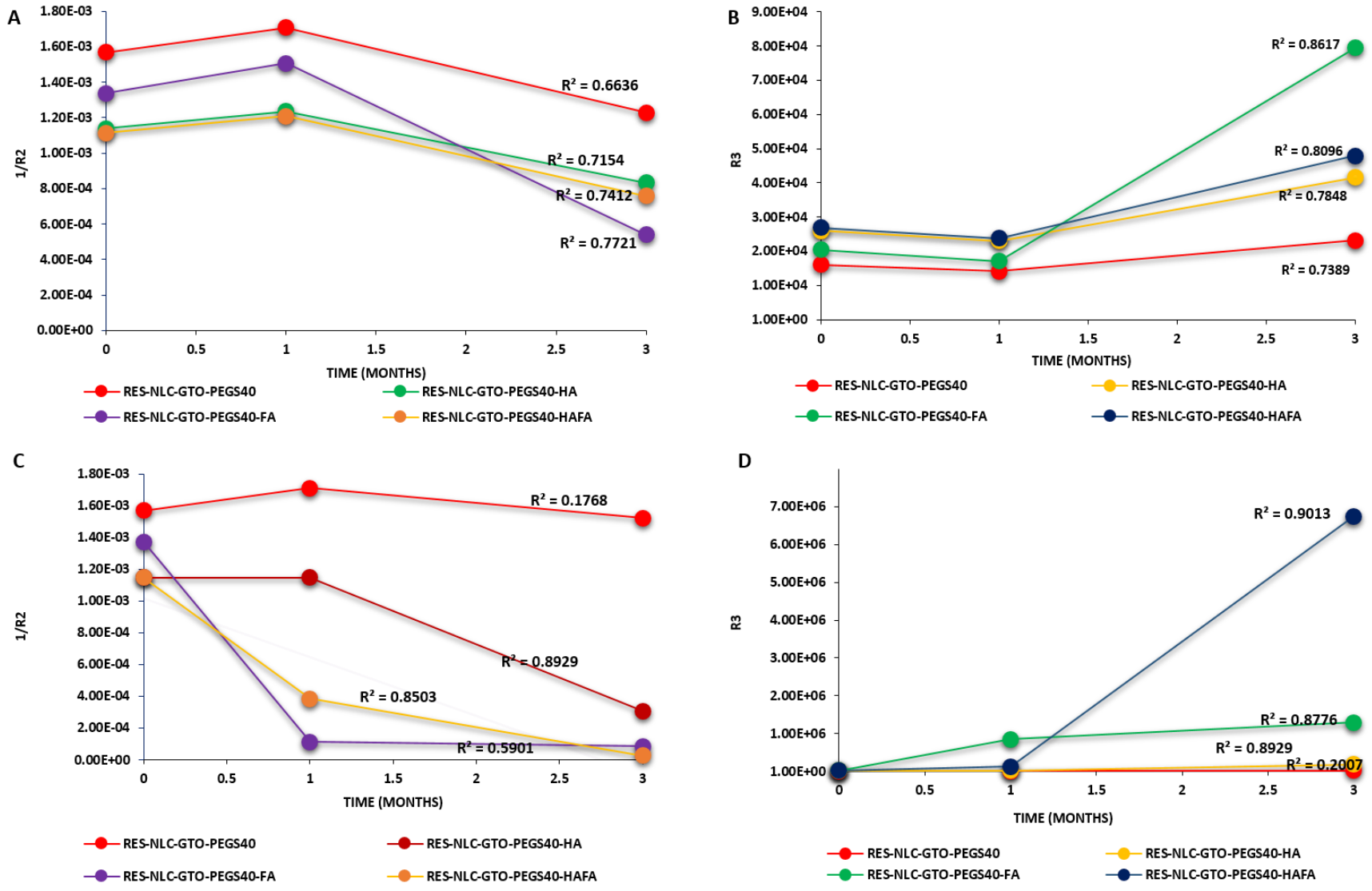

Figure 3-45.A. Coalescence force and B. Ostwald ripening versus time determined for surface modified RES-NLC stored at 4 ^{o}C. C. Coalescence force and D. Ostwald ripening versus time determined for surface modified RES-NLC stored at 25^{o}C

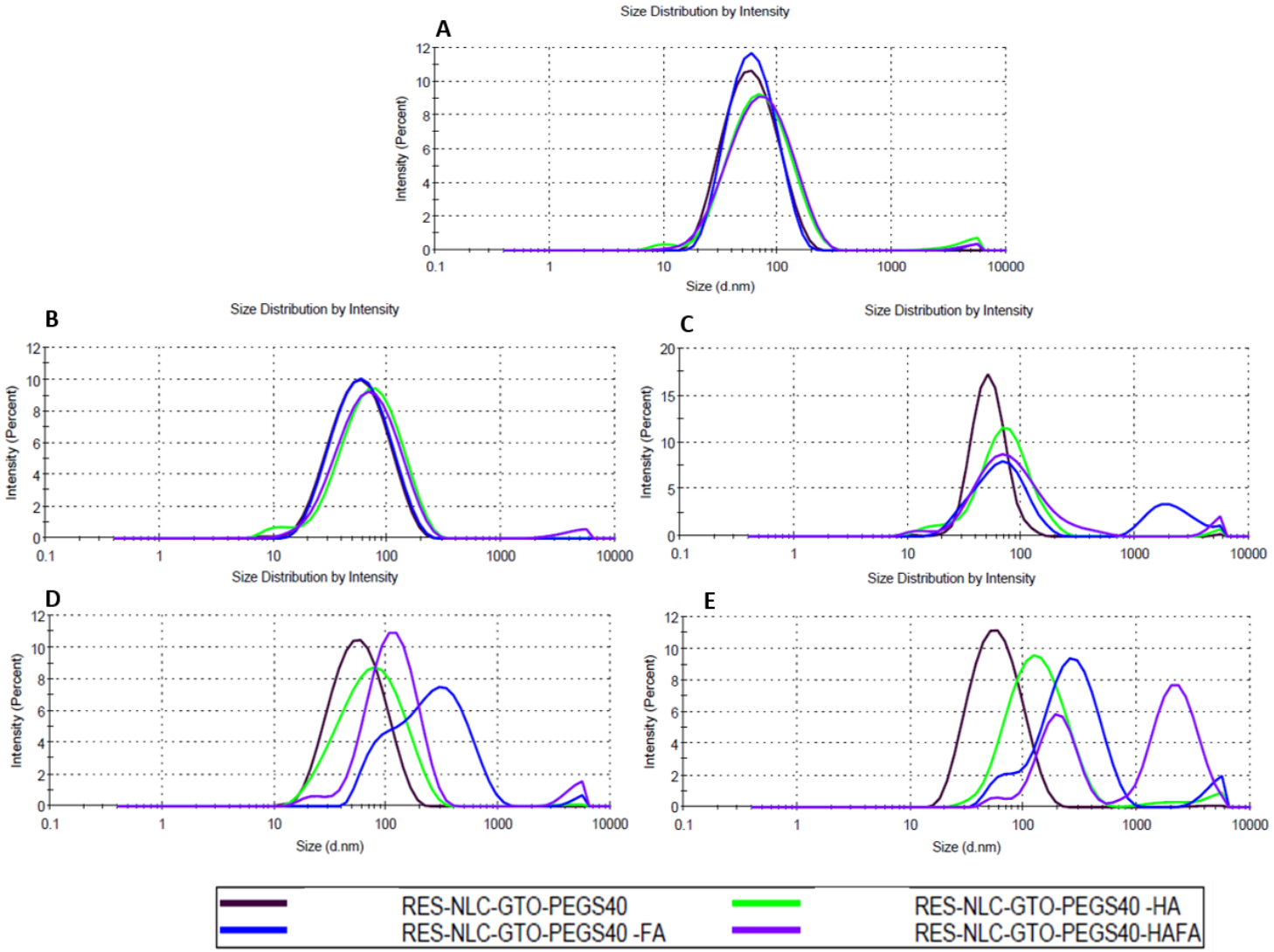

Figure 3-46. Overlay Surface modified RES-NLCs particle size measured by zetasizer after A. Initial (day zero) B. One and C. Three months at 4^{o}C and D. One E. Three months stored at 25^{o}C

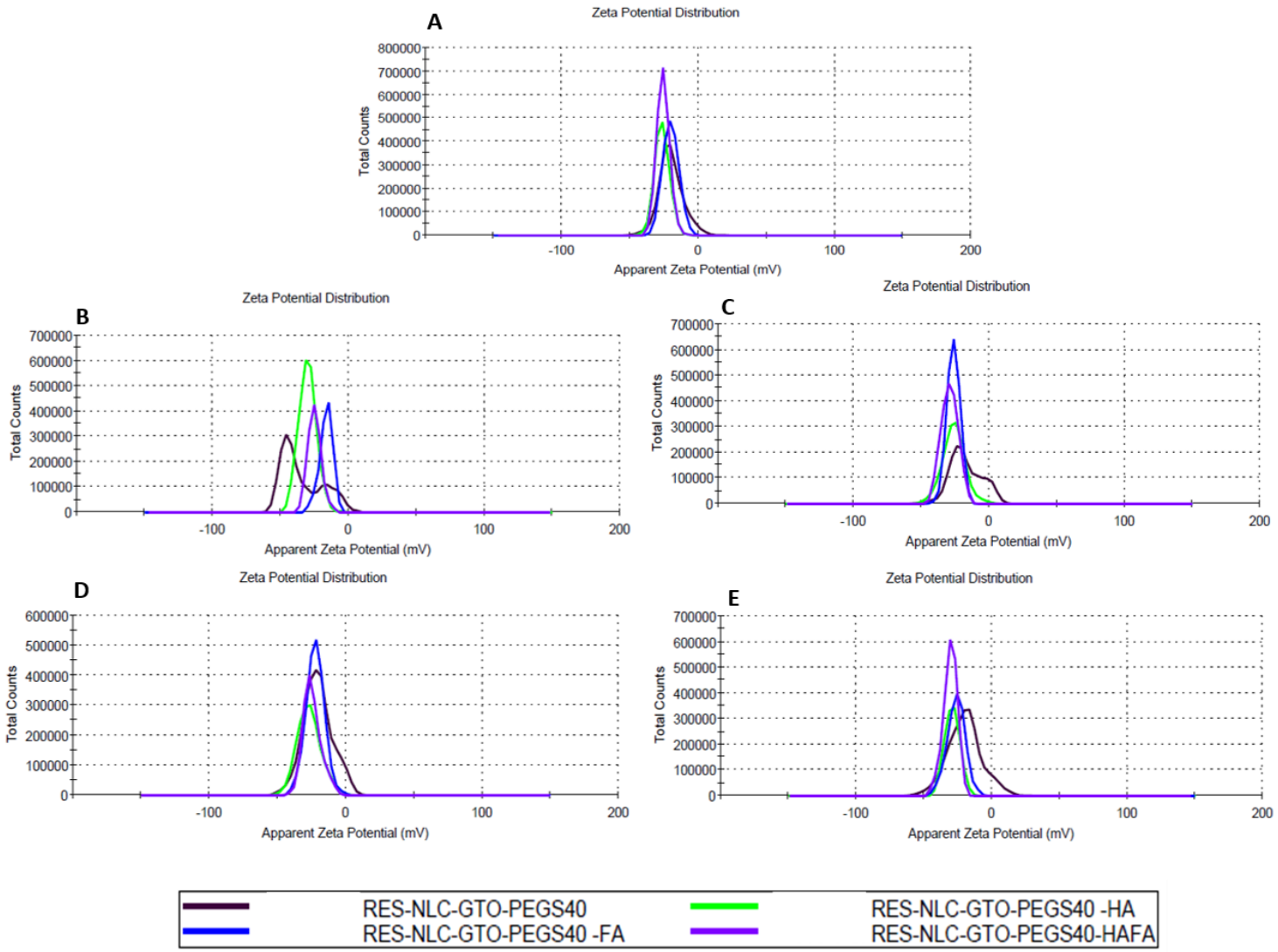

Figure 3-47.Overlays of surface modified RES-NLCs zeta potential measured by zetasizer after A. Initial (day zero) B. One, C. Three months at 4^{o}C and D. One, E. Three months stored at 25^{o}C

3.4. Conclusions

RES-NLCs using trimyristin as solid lipid were successfully optimised using 3-factor, 3-level Box–Behnken design. The effects of four critical independent variables, which included: liquid lipid type, liquid lipid concentration, Tween 80 concentration and drug amount on the response variables viz. particle size, polydispersity index, zeta potential, % entrapment efficiency and % drug loading of RES-NLCs were explored.

The selected six lipids for investigation in the preparation of RES-NLCs were: PCG, PGMC, PGML, GTO, DO and GTC out of which two were triglycerides, one medium chain triglyceride and one long chain triglyceride, two were propylene glycol esters, one was fatty acid ester and one PEGylated lipid. Each liquid lipid desirability space with the values close to 1 were considered the best for the optimized formulation indicating higher desirability of corresponding response properties. Quadratic models were found to be significant for particle size; polydispersity Index, entrapment efficiency and total drug and mathematical equations were derived from these models and design space was created for achieving desired responses.

Particle size of the fabricated RES-NLCs were in the range of 24.98-131.4 nm. The most important factor identified in terms of contributing to the variance in particle size was determine to be liquid lipid concentration; as indicated by the large value of the coefficient in the quadratic equation. RES-NLCs demonstrated monodisperse particles with polydispersity (0.113-0.452). The most prominent contributing factor which influenced PDI was determined to be the surfactant concentration. Increasing the concentration of Tween 80 directly resulted in enhanced homogeneity in terms of particle size and a reduction in terms of aggregation. Negative zeta potential was exhibited by all of the RES-NLCs ranging from -21.3 to -39.9 mV. The most significant factor determined influence zeta potential was the surfactant concentration, which is believed to act as a steric hindrance, and thus contributing to the stability of the formulations for most RES-NLCs. Liquid lipid concentration was also determined to have notable impact upon the % entrapment efficiency of RES- in NLCs as indicated by the positive coefficient from the quadratic equations with entrapment efficiency ranging from 91.368-99.576 %. RES-NLCs displayed a drug loading capacity of of 2.937-7.557%, which was mainly influenced by the surfactant concentration, exhibiting a strong positive effect on the response as evident form the positive value of the coefficient in the quadratic equations. Therefore using the Box-Behnken design, tuneable RES-NLCs could be manufactured with particles sized (< 100 nm), particle size distribution (< 0.3), with negatively charged surface (-24 mV), high entrapment efficiency (91-99%) and drug loading (2-7%) within the established design space.

Modification of the RES-NLCs was achieved by PEGylation as well as surface modification with a number of ligands including: HA and FA targeting ligands using EDC-NHS chemistry. It was established that the amine: HA ratio of 12:1 and amine: FA was 5:1 was the most favorable ratios for conjugation of HA and FA respectively. Surface modification led to increase in size but no change in PDI and total drug.

The RES-NLCs exhibited sphericity and a particle size < 100 nm as observable under scanning electron and transmission electron microscopy. DSC, XRD and FTIR confirmed the presence of entrapped drug in amorphous state in NLCs. FTIR spectral analysis eluded the reduction of free surface amine which allowed for the confirmation of covalent bonding of the ligands to the particle surface.

1HNMR studies demonstrated that the drug is entrapped within particles of the formulation without interaction with other formulation constituents. RES-NLC showed a low drug release at pH 1.2 with less than 20% release rate over the period of 4 h confirming its protection for drug in gastric fluid. Surface modified RES-NLCs showed only 2% release at pH 1.2 over the period of 4 h offering more protection to the drug by delaying the release in acidic environment. Modified Releaseof RES over the period of 24 h at pH 5 would enable prolonged effect in tumour environment from both bare and surface modified formulations. RES-NLC with good stability over the period of six month could be developed with GTO as liquid lipid. However, surface modification reduced the stability of formulations to two months.

Chapter 4 : *In vitro* Anticancer Activity of Developed Resveratrol Nanostructured Lipid Carriers

4.1. Introduction

Cancer is one of the common causes of death worldwide. The primary cause of death from cancer is attributed to its dissemination and metastasis to other organs. The rapid growth and proliferation of cancer cells is one of the main characteristics of cancer. The marketed chemotherapeutics are nonselective as their mechanism of action depends on the cancer cell proliferation kinetics in comparison to targeted delivery systems effectiveness.

Breast cancer includes a group of very heterogeneous diseases (Subik et al., 2010). Triple negative breast cancer (TNBC) are referred to tumours which do not express oestrogen, progesterone and human epidermal growth factor receptors, accounting for almost 20 % of breast cancers. MDAMB-231 is a type of TNBC, and is defined as the clinically aggressive type of cancers because of its very poor responsiveness to chemotherapy (Bauer et al., 2007, Carey et al., 2007). Treating this type of cancer presents a major challenge due to the poor disease prognosis and the need of newer and safer therapies. Recent therapy focused on the use of natural products to treat this cancer (Hoeijmakers, 2001, Rakha et al., 2008). The main drawbacks of chemotherapeutics is their potential toxic effects, this limits the dose to be given that the patient can tolerate (Ruoslahti, 2002). On the other hand, the most preferred route of administration of anticancer agents is the oral route, although it poses problems for some anticancer agents with low water solubility and poor oral absorption, eventually leading to low bioavailability (Stuurman et al., 2013). Therefore, the development of new drug delivery systems based on nanoparticles as a carrier for the active agent, enabling the effective delivery to the cancer cells (Puri et al., 2009).

Tumour cells exhibits a defective lymphatic drainage with the property of leaky vasculature compared to healthy tissues. The leaky vasculature will enhance the infiltration and the retention of nanoparticles in the tumour cells a phenomenon known as enhanced permeation and retention (EPR) effect. This effect allow the nanoparticles to bypass the circulation. The majority of nanoparticles depend on the EPR effect to be able to get access to the cancer cells, that is in turn depending on the particles size of the nanocarriers (Hobbs et al., 1998, Hashizume et al., 2000, Barua and Mitragotri, 2014). The EPR effect enables the passive targeting of cancer cells via the entrapment of different agents in delivery systems such as lipid nanoparticles and liposomes, which selectively target the tumour tissue and deliver the drug in high concentration without causing toxicity to the surrounding normal tissues. However, the tumor targetability of the nanocarriers is still one of the major challenges for drug therapy (Souto, 2011).

The ability of the nanoparticles to stay in the circulation to reach to the tumor site and release the drug is governed by the surface properties of the nanoparticles. PEGylation of the surface by a hydrophilic polymers such as polyethylene glycol (PEG) provide the nanoparticles with longer circulation in the blood streams and their subsequent passive accumulation in the cancer cells, followed by their passive transport to tumor tissue (Koo et al., 2008, Min et al., 2010).

In order to overcome the limitations of passive targeting, new approach has been developed by actively targeting the tumor cells, which involve the interaction of the nanoparticles with cell surface by binding to specific receptors overexpressed on the target cells causing the internalization of nanoparticles (Leamon and Low, 2001, Eliaz and Szoka, 2001).

Surface functionalization of nanoparticles by targeting ligands, i.e., molecules able to recognize and bind to a specific biological target, has been studied for the purpose of promoting the delivery to particular cells and controlling the intracellular uptake of nanocarrier. The internalization pathways of ligand-bearing nanocarriers should be similar to the pathway of individual ligand. Additionally, the concentration of ligands on the nanoparticles surface provides stronger cell interactions when compared to ligand alone (Hillaireau and Couvreur, 2009). Various surface modification techniques with various polymers and ligands were employed in order to enhance the oral bioavailability, transport and eventually the tumour targetability.

Covalent and noncovalent cross linking approaches have been utilized to conjugate ligands moiety onto the surface of nanocarrier. Covalent coupling methods comprise interaction between reactive group(s), such as crosslinking between two primary amines employing coupling agent (e.g., EDC, NHS) or reaction between a primary amine and a carboxylic acid (Siafaka et al., 2016b).

Research reports on hyaluronic acid (HA) coating have demonstrated the ability of functionalized nanoparticles to protect the nanoparticles from degradation by proteolytic enzymes (such as trypsin and pepsin digestion) or the destructive effect of strong-acidic gastric environment (Yang et al., 2013, Gao et al., 2017). The binding affinity of PEGylated HA-nanoparticles to the HA receptors expressed in various tumor cells (SCC7, MDA-MB-231, and HCT116) was evaluated along with their effect on the cellular uptake of nanoparticles (Choi et al., 2011). PEGylated-HA NPs were synthesized in order to prolong the circulation enhancing the tumour targetability by reducing the degradation of nanoparticles by hyaluronidase-1 enzyme (Choi et al., 2011, Gao et al., 2017). Hyaluronic acid (HA), selectively binds to several cancer cells that over-express CD44. It has the ability to accumulate in the cancer tissue through both active and passive targeting mechanisms (Han et al., 2013).

The vitamin folic acid (FA) has been extensively studied as a targeting ligand for nanocarriers, especially for anticancer strategies (Chavanpatil et al., 2006). In particular, folate receptors (FR) are a

glycoproteins with molecular weight 38–44 kDa, often overexpressed on the surface of cancer cells (e.g., ovarian, lung, brain, and colorectal cancer) (Müller and Schibli, 2013), with restriction in normal tissues (Weitman et al., 1992). Furthermore, FR has the capability to transport FA by receptor mediated endocytosis (RME) with successive endosomal entrance through the cytosol (Hilgenbrink and Low, 2005), consequently escaping lysosomal degradation. While, in some cases caveolae mediated endocytosis (CvME) appears to be involved in the uptake of FA (Dauty et al., 2002). FA has been effectively coated onto PEGylated polymeric nanoparticles upon conjugation of the activated N-hydroxysuccinimide FA with the aminated PEG-PHDCA copolymer. This has resulted improved the uptake of the nanoparticles (Stella et al., 2000) and confirmed the versatile targeted delivery of FA and its potential application to various nanocarriers (Hillaireau and Couvreur, 2009, Yameen et al., 2014). The efficacy of folate targeting systems have been widely studied both *in vitro* and *in vivo (*Zhao et al., 2008).

Dual receptors targeting, a new strategy for targeted drug delivery, can efficiently and selectively target nanoparticles to cancer cells. This approach has been applied in the field of drug delivery (Saul et al., 2006, Ying et al., 2010). In order to enhance targeting efficiency, dual-ligand directed nanoparticles have been developed. Double receptor targeting occurs through the simultaneous binding and interaction of two receptors on the surface of cancer cells, leading to greater affinity for nanoparticles. Several reports have demonstrated the advantages of improved therapeutic efficiency with synergistic toxicity to cancer cells utilizing dual-ligand targeted nanoparticles over the individual ligand conjugated nanoparticles (Laginha et al., 2005, Saul et al., 2006, Freitas and Müller, 1999).

In this study, HA polymer was selected as polysaccharide for hydrophilic modification due to its selective targeting to cancer cells via CD44 receptor. Further conjugating with folic acid which will bind to the folate receptors on the cancer cells surface will be helpful to achieve double receptor active targeting (Liu et al., 2011).

RES-NLCs were evaluated in two types of breast cancer cell lines, MCF-7 non-triple negative breast cancer cells (NTNBC) and MDAMB-231 (TNBC) cell lines. MCF-7 is a cancerous cell line known as hormone receptor positive. It expresses estrogen receptor and/or progesterone receptor and human epidermal growth factor receptors on the cell surface; expression of which promotes the cell growth and division. MCF-7 express folate receptors and tumor markers such as CD44 hyaluronate binding sites, making these cells more vulnerable to targeting by various anticancer agents (Seo et al., 2003, Chen et al., 2009, Necela et al., 2015, Thapa and Wilson, 2016). MDAMB-231 is a type of TNBC and is of Human Caucasian breast adenocarcinoma origin. It has high expression of both CD44 and folate receptors (Olsson et al., 2011).

A battery of assays have been used for the measurement of cell viability, *in vitro* cell proliferation, cellular uptake, uptake mechanisms cell cycle, apoptosis study and finally the mechanism of cell death was evaluated through caspase-3 activity assay on both MCF-7 and MDAMB-231 cell lines. The aforementioned studies will allow for the assessment of alterations in membrane permeability, physiological state and morphological changes. Few studies have addressed the *in vitro* cytotoxicity of lipid nanoparticles by comparing different assays, the physiological effect of lipid nanoparticles, toxicity on cells and internalization pathways would allow more knowledge and the extrapolation of the effect for the *in vivo* state. Among the currently available data for the toxicity of nanoparticle, also few studies are done the safety assessment for the selected route of administration and the fate of nanoparticles once they get access in the cells and how the cells will respond to the nanoparticles.

The cytotoxic assessment of resveratrol-loaded and empty NLCs on different breast cancer cell lines MCF-7 and MDAMB-231 was carried out. The cell viability results were compared with that of the healthy MCF-10A (epithelial mammary gland; breast cells) served as a non-tumorigenic control to confirm the level of safety of RES-NLCs on healthy cells. Different RES-NLCs were also assessed for their toxicity on macrophages (RAW 264.7) cell lines to be able to determine the safe concentration for these cells. Cellular uptake of various formulations were assessed on MCF-7, MDAMB-231, MCF-10A and RAW 264.7 cell lines.

The mechanism of endocytosis and internalization pathways of various RES-NLCs were determined on MCF-7 and MDAMB-231 cell lines. Moreover, assays on the cell death and mechanism of cell death and cell cycle assays are also contained within this chapter.

4.2. Materials and methods

Class II microbiological sterile safety cabinet (labcaire system ltd, UK) was used thought out all the cell lines studies, Incubator used for in vitro cell culture studies (Sanyo Incubator, Japan), in which cells were allowed to grow at 37 ^{o}C ± 1 ^{o}C, in a humidified CO_2 environment (5%), to attain a cell growth of above 85% confluency prior to conducting any study.

Sterile tissue culture treated flasks (T25 and T75 cm^3), sterile tissue culture plates (6, 12, 24 and 96 well plates) and sterile centrifuge tubes (15 and 50 mL) were obtained from Fisher Scientific, UK. In order to count the cells before every study, hemocytometer slide was used (Marienfeld, Germany).

4.2.1 Equipment used for visualization of cells

Light microscopy (Leica DML, Microsystems GmbH, Germany), images were taken using MShot camera and the images were analysed using MShot digital imaging system software (China).
Fluorescence imaging of cells was carried out using Carl Zeiss fluorescence microscope obtained from Carl Zeiss Microscopy GmbH, Germany, using using 60X oil objective, fluorescence images were captured using AxioCam MRm Zeiss camera, Germany, the images were processed using Zen lite 2012 software, Germany.

4.2.2 Instruments

Cell viability assays, caspase and protein content studies were carried out using Genios Pro microtiter plate reader (Tecan, Austria), data obtained were processed in Microsoft excel 2016.
Flow cytometry analysis, the cellular uptake and mechanism of nanoparticles endocytosis was carried out using Guava®easyCyte Flow Cytometry Systems (Merck, Millipore, UK), the data was analyzed using Millipore Incyte Guava software version 2.7.0. In order to study the cell death and cell cycle Becton Dickinson FACSAria, USA; with argon laser 488 nm and emission filter 516 nm, results were analyzed by FACSAria software, US and flowing software 2.5.1, Finland

4.2.3 Cell lines types and source

MCF-10A (epithelial mammary gland; breast cells) purchased from the American Type Culture Collection passage 93. MCF-7 (Cell Line human breast adenocarcinoma) Cultures from HPA Culture Collections passage 40. MDA-MB-231 Cell Line human (Triple negative human breast adenocarcinoma) passage 40. Mouse monocyte macrophage (RAW 264.7) passage 4, supplied by European Collection of Authenticated Cell Cultures (ECACC).

4.2.4 Chemicals for cell culture studies

Dulbecco's minimal essential medium (DMEM), non-essential amino acids, 0.25 %trypsin –EDTA, Mammary Epithelial Cell Growth Medium (MEGM BulletKit) were purchased from Lonza, Belgium. Foetal bovine serum (FBS) was obtained from Biosera. Trypsin inhibitor from Glycine max (soybean),

Cholera Toxin from Vibrio cholerae CTX, Cholera enterotoxin (Cholergen), L15 medium without L-glutamine (Leibovitz), Ribonuclease A, caspase 3 Assay Kit Colorimetric, BCA Protein Assay Kit, Cisplatin Trypsin-EDTA Solution 1X, Trypan Blue solution (0.4% w/v), sucrose, propidium iodide solution and Dimethyl sulfoxide (DMSO, sterile cell culture grade) were purchased from Sigma Aldrich,UK. CD44 $^{++}$ FITC MS X Rt antibody conjugate was purchased from Merck Millipore, UK. Alexa Fluor® 488 Annexin V PI double staining Dead Cell Apoptosis Kit was purchased from Invitrogen/Life Technologies, UK. Microscopic slides, cover slips, presto blue cell viability reagent, 16% formaldehyde solution and phosphate buffer saline were purchased from Thermofisher, UK. Cytochalasin B, nystatin were purchased from VWR international, UK. Whereas VECTASHIELD Antifade Mounting Medium with DAPI (4', 6-Diamidino-2-Phenylindole) nuclear stain was purchased from Vector laboratories, USA.

4.3. *In vitro* cell culture studies

4.3.1 Cells growth and culturing conditions

All the experiments in the forthcoming chapter were carried out on MCF-10A normal cell lines (healthy) cells were maintained in Mammary Epithelial Cell Growth Medium with passage 39-100; MCF-7 (breast adenocarcinoma cell lines) passage 40 and mouse monocyte macrophage (RAW-264.7) passage 4-10. Cells were cultured in complete DMEM media supplemented with 15 % Foetal Bovine Serum (FBS) and 1 % L-glutamine (2 Mm); MDAMB-231 (Triple negative resistance breast cancer cell lines) were grown in L-15 supplemented with 2mM Glutamine + 15 % FBS studies conducted with passage range from 40-56.

All cells were kept at 37^{o}C in a humidified CO2 incubator (5 % atmosphere), except MDMB-231 cell lines were grown in a non CO2 incubator.

4.3.1 (I) Thawing of cells from frozen vials

Defrosting of cell suspension (1mL) usually frozen in DMSO, was carried out by keeping the cryogenic vials at 37^{o}C. The thawing process took almost 2-3 min. After obtaining the cell suspension in a liquid form, the cells suspension was immediately transferred into a flask, containing a pre-warmed media (6 mL if T25 cm^3 flasks were used, alternatively 15 mL if T75 cm^3 were utilized) to neutralize the high concentration of DMSO. Cells were maintained in their respective media supplemented with various

nutrients depending on the cell type as mentioned in section 4.3.1. Cells were kept at 37^{o}C in a humidified CO_2 incubator (5 % atmosphere) except for MDAMB-231 cells were kept at 37^{o}C in a non CO_2 incubator. Cells were allowed to attach to the flask wall for 24 h. The media was then aspirated and replaced with a fresh one the next day.

4.3.1 (II) Passaging of cell lines

Passaging of cells is usually performed when the cells reach the desired confluency (~ 80-90%) either to start a study or carry on maintaining the cultures for future use (Figure 4-1). Figure 4-2 details the steps used for cell passaging. After performing the steps (Figure 4-2) cells suspension was diluted suitability to produce the required concentration of cells/mL. A known volume (1 mL) from the cell suspension was transferred into a T75 cm^3 flask and incubated at 37^{o}C, until the cells reach the desired confluency, to use them for further experiments. Passaging of cells was carried out every 5 days.

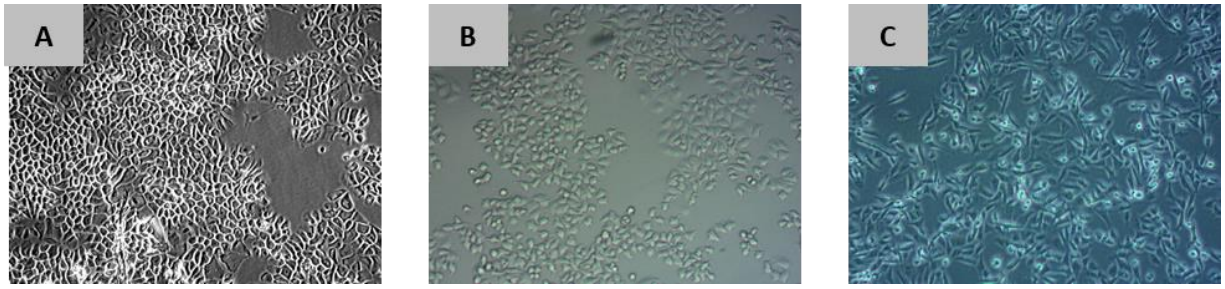

Figure 4-1. Photomicrographs showing the cellular morphology of confluent cells (~ 80-90 %). A. MCF-10A cell lines, B. MCF-7 cell lines, and C. MDAMB-231 cell lines, magnification X10

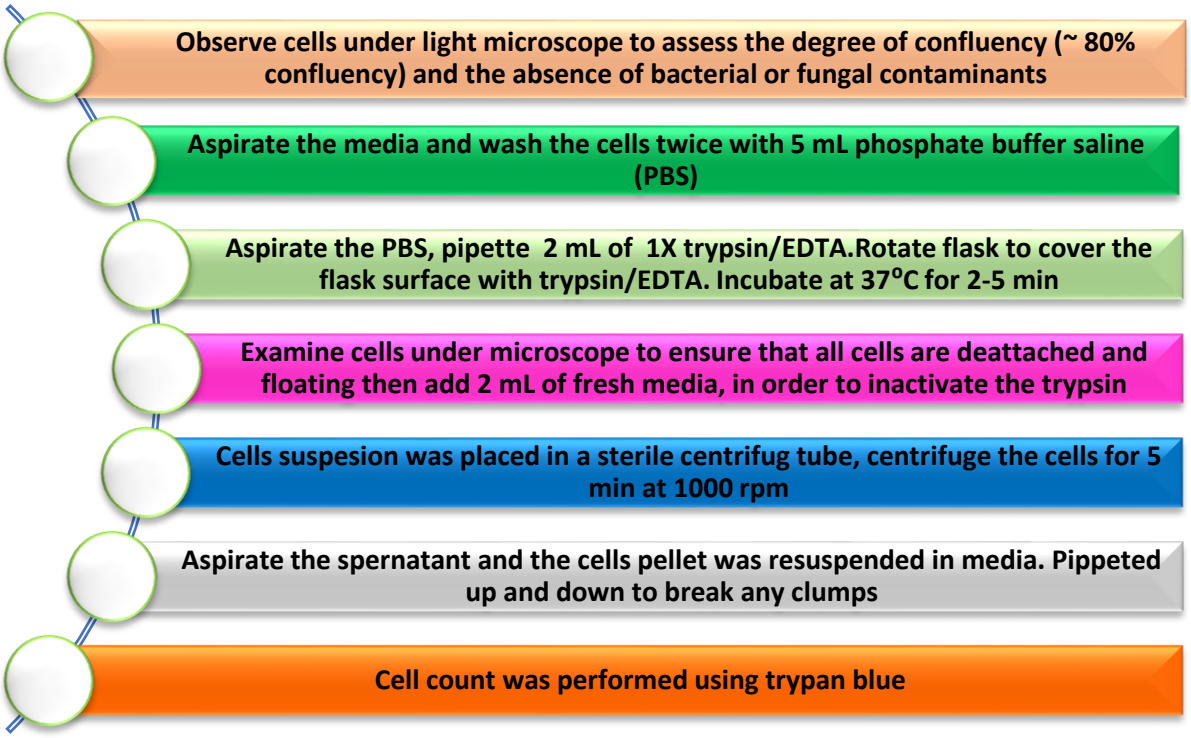

Figure 4-2. Schematic flow diagram of cells passaging technique

4.3.1 (III) Trypan blue exclusion test for cell viability

A viable cell count is crucial to determine the kinetics of cell growth. Hemocytometer was first employed for counting blood cells (Cadena-Herrera et al., 2015). A viable cell count serves various purposes such as the management and maintaining of cell cultures in biological research, in order to be able to carry out different assays etc (Joeris et al., 2002).

Trypan blue is one of many stains recommended for use in dye exclusion procedures for viable cell counting. This method is based on the principle that live (viable) cells will not take up the dye, whereas dead (non-viable) cells will be stained blue due to rupture in their membrane. Staining of cells will facilitates the visualization of cell morphology (Louis and Siegel, 2011).

Among the most common developed viable cell count methods, manual counting with a hemocytometer is known to be the most commonly used method because of its low cost and versatility (Jhonston, 2010). This method is dependent on the analyst's ability to evaluate different cell characteristics irrespective to the cell type; in addition it allows the utilization of different staining techniques depending on the purpose of the analysis (Cadena-Herrera et al., 2015).

Cells were detached as described in section 4.3.1 (II) Cells suspended in media (100 µL) was mixed with 100 µL of 0.4 % trypan blue by gently pipetting up and down to break the cell clumps. Cover slip was placed on the top of the hemocytometer chamber. 20 µL of the homogeneous mix was loaded into the top and the bottom chamber of the hemocytometer. Counts were performed in triplicate under 10× objective according to the standard protocol (Louis et al., 2011). Cells were counted in the 1 mm center square and four 1 mm corner squares. Cells touching the middle line at bottom and right sides were not counted.

Hemocytometer consists of two counting chambers each has 9 large squares with 1 mm length (Figure 4-3). Each square of the hemocytometer, with cover-slip in place, represents a total volume of 0.1 mm^3 or 10^{-4} cm^3. Since 1 cm^3 is equivalent to approximately 1 mL, the subsequent cell concentration per mL (and the total number of cells) can be determined using the following calculations:

Cells per mL = the average count per square × dilution factor × 10^4 (count 10 squares), dilution factor is two in this case.

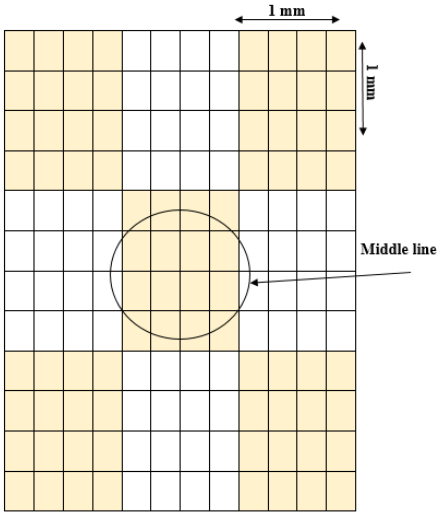

Figure 4-3. Hemocytometer counting technique, the circle indicates the approximate area covered at 10× objective microscope magnification). 4 corners of the square were counted along with the middle square. Include cells on top and left touching middle line. Cells touching middle line outside the middle square were not counted

4.3.1 (IV) Cell lines growth curves

The cell-line growth curves are utilized for the evaluation of the cellular growth characteristics, which directly after seeding shows a "lag-phase", which could take from a few hours up to 48 h. It is defined as the time needed for the recovery of the cell from the trypsinization and rebuild its cytoskeleton. All these requirements enable the cell to enter into a new cell cycle. Afterwards, the cell enter into exponential growth, "log-phase", in which the cell population doubles in number. In this phase, the effects of drugs and nanoparticles that inhibit cell growth can be studied. Finally, the cells enter in a stationary phase, when the cell population metabolize all the substrate, when growth rate drops nearly to zero (Assanga and Lujan, 2013).

In order to study the growth characteristics of both cell lines, trypan blue solution was employed to determine the viability of cells. Once the cell-lines reached confluence of 80 to 90%, they were trypsinized and subsequently diluted (1: 1) with trypan blue exclusion dye. Cells were counted under light microscope using haemocytometer counting method described in section 4.3.1 (III) to determine the cell number parameter. The cells were mixed well and seeded at a density of 30 x 10^4 cells/mL/well in a 6 well plate (38.8 mm of diameter) and 1 mL of media was added to the well to allow the cells to grow and attach for 24 h. Cell count was carried out every day for 7 days and a growth curve for each cells was constructed. The population-doubling time can be established by identifying a cell number

along the exponential phase of the curve, tracing the curve until that number has doubled, and calculating the time between the two drawn lines in the curve. The calculation of doubling time as a measure of cell growth for each cell line has been carried out using either the counting of total viable cells (haemocytometer chambers) or fluoremetric assay as described in presto-blue assay in section 4.3.2.

4.3.2 Cell viability with PrestoBlue assay

The measurement of cell viability plays a main role in the cytotoxicity testing. It is a principal tool for screening new drugs and provides initial knowledge prior to any *in vivo* studies. An extensive range of assays are available for the determination of cell viability. They are based on different cell functions such as cell membrane permeability, mitochondrial enzyme activity and cellular uptake activity.

PrestoBlue (PB) is a membrane permeable solution. It has been developed for determining cell-mediated *in vitro* cytotoxicity. It is a resazurin-based compound. Viable cells mitochondrial enzymes converts it into the reduced form (Boncler et al., 2014). As a result of the reduction the reagent exhibit a shift in its fluorescence and a prominent change in the colour and thus can be quantified employing either fluorometric or spectrophotometric approach. PB is prepared commercially as a water soluble ready-to-use solution and it is a non-toxic reagent. PB assay is rapid live assay for assessing cell viability with an incubation time as short as 10 min. It is also a very sensitive assay, which can detect as few as 12 cells per well (Xu et al., 2015).

By comparing PB to other commercially available reagents viz. MTT (3-[4,5-dimethylthiazol-2-yl]-2,5-diphenyl tetrazoniumbromide), AlamarBlue and XTT (sodium 3’-[1-(phenyl amino-carbonyl)-3,4-tetrazolium]-bis-[4-methoxy-6-nitro] benzene sulfonic acid hydrate), it has been validated as both growth indicator and cell viability reagent (Lall et al., 2013).

In this study, the PB assay was used to serve two purposes:

1. To assess the growth and proliferation parameter of each cell line and to determine the best seeding density for evaluation of cytotoxicity of RES-NLCs formulations.
2. To ensure that PrestoBlue was not toxic to the cell lines under study and that it did not interfere with the measurements.

4.3.2 (I) Determination of cell growth and proliferation using PrestoBlue Assay

Cells were trypsinized and counted by the as per the procedure described in section 4.3.1 (II). Cells suspension was diluted with media to produce three different seeding densities entailed: 5 X 10^4, 5 X 10^5 and 5 X 10^6. Cells were seeded in 96 well plates and 100 µL of diluted cells in media was placed in each well to give 5 X 10^3, 5 X 10^4 and 5 X 10^5 cells/well. Plates were placed at 37^{o}C in a humidified CO_2 environment (5 %) and allowed to attach. The growth of cells was monitored over the period of 10 days. On the day of the experiment, 10 µL of PB was added to each well, the plates were covered by foil paper and incubated for 1 h at 37^{o}C. The fluorescence was determined using Tecan microtiter plate reader at excitation 570 nm and emission 610 nm.

4.3.2 (II) Evaluation of RES-NLCs cytotoxicity using PrestoBlue Assay

The antiproliferation efficiency of all RES-NLNCs was investigated on both breast cancer cell lines MCF-7 and MDAMB-231 and compared with the normal MCF-10A. Also the cell viability test was performed on RAW 264.7 cells. Cell viability assay with PB reagent was performed according to the manufacturer's protocol. The cells in suspension were seeded at a density of 5× 10^4 cells/well in a 96-well plate in 90 µL of growth medium and kept at 37^{o}C in a humidified CO2 environment (5 %).

After 24 h, the media was removed and the cells were treated with different concentrations of resveratrol, six different RES-NLCs, PEGylated (RES-NLC-GTO-PEGS40) and three ligand appended RES-NLCs. Resveratrol working solutions were prepared by diluting the drug stock of 60 µg/mL made in acetone with media to obtain the following working concentrations viz. 1, 5, 10, 25 and 50 µg/mL. All nanoparticle were also suitability diluted with media to obtain same concentration range as that of drug solution. Six wells were kept as free culture medium to serve as a control, and other six wells were filled with only media without cells to serve as a blank. After the treatment of the cells were further incubation in a 5 % CO_2 atmosphere at 37 °C for 24, 48, and 72 h.

Next day 10 µL of PB was added to each well, the plates were covered by foil paper and incubated for 1 h at 37^{o}C. The fluorescence was determined using Tecan microtiter plate reader at excitation 570 nm and emission 610 nm.

Untreated cells were used as a 100% cell viability control and the media served as background reference. The percentage cell viability was calculated compared to the control subtracting the background reference employing the following equation:

$$\% \text{ Cell viability} = \frac{\text{Fluorescence of test compound} - \text{Fluorescence blank media}}{\text{Fluorescence of control} - \text{Blank media fluorescence}} \times 100 \qquad \text{Equation 44}$$

The IC_{50} values for different formulations were calculated using the non-linear regression analysis employing GraphPad Prism 5 program.

4.3.3 Cellular uptake studies and internalization pathways

Endocytosis is a process that cells use to transfer extracellular nanomaterials into the cell interior. It is the major route for nanomedicines transport across the cell membrane. Once internalized, the nanostructures meet different fates by interacting with different compartments: to late endosomes and lysosomes for degradation. The nanostructures are the recycled by endosome to be taken up by plasma membrane then transported to other destinations in the cell.

The process of endocytosis is generally classified into two main pathways including phagocytosis and pinocytosis (Figure 4-4). Phagocytosis, is an actin-dependent process which involves the internalization of large particles such as bacteria. Predominantly occur in the phagocytic cells such as macrophages, neutrophils and monocytes (Aderem and Underhill, 1999).

While, pinocytosis involves internalization of nanoparticles. Pinocytosis can be dependent on two different pathways viz. clathrin dependent coat (clathrin-mediated endocytosis, CME) or independent of clathrin (clathrin-independent endocytosis, CIE), which is based on the proteins involved in the pathways (Wang et al., 2011). Caveolae-dependent endocytosis is also a common cellular entry pathway which could bypass the lysosomal uptake (Benmerah, 2007). Because of this pathway property, it is believed to be a beneficial route for delivery of nanoparticles to enhance the targetability and improve the therapeutic efficacy (Kou et al., 2013). Macropinocytosis it is often defined as transient, clathrin and caveolae independent endocytosis that surround and internalized the nanoparticles into a large vacuoles (Mercer and Helenius, 2009).

CME is the most common pathway of nanoparticle internalization into the inside of the cells. It involves the interaction of the nanomaterials with the receptors in the cell membrane. Clathrin-coated vesicles consists of three-layered structure: the outer layer is formed by clathrin (clathrin lattice), the inside layer is a lipid membrane with protein inclusions, while adaptor proteins are found in the middle. The adaptor protein complexes interact directly with the lipid bilayer, and clathrin binds to the adaptors. It is suggested that endocytosis is initiated by the formation of pits on the inner surface of the cytoplasmic membrane containing the AP-2 adaptor protein complex, clathrin and accessory proteins. The subunits

of the adaptor complex elicit the formation of the clathrin lattice at particular locations of the cytoplasmic membrane and facilitate the interaction between clathrin and the cargo protein. Fusion of the vesicle with the target membrane and delivery of endocytosed “cargo” to the target destination is achieved through the removal of the clathrin coat from the surface of the vesicle (Popova et al., 2013).

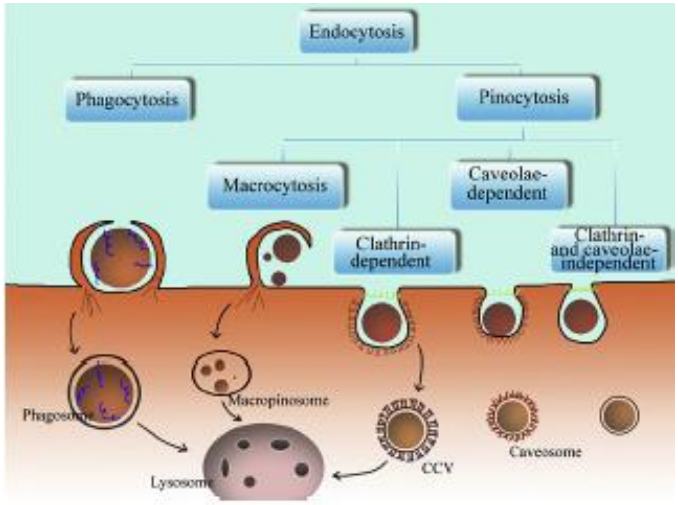

Figure 4-4. Nanoparticles Endocytosis pathways in human cells. CCV: Clathrin coated vesicle. copied without permission from (Kou et al., 2013)

The nanoparticles are wrapped inside a vesicle and pushed into the interior of the cells through the GTPase activity forming clathrin coated vesicles (CCV) (Pucadyil and Schmid, 2009). CME requires energy for the transport of the nanostructures. For a better understanding of the different types of endocytosis, studies involving the inhibition of this process via chemical means made the process clearly understandable.

Many factors can affect the nanoparticles endocytosis pathway. The process is mainly affected by the physicochemical properties of nanoparticles (particle size, surface charge and hydrophobicity, shape of nanoparticles and the cell type).

Nanoparticles with a particles size in the range of 10-500 nm can easy be transported into the cells as compared to large particles being engulfed through macropinocytosis. Particles with size range from 60-80 nm involved in caveolae mediated endocytosis, while particles with a size of about 100 nm will be favored by clathrin mediated transport into the cells (Benmerah, 2007).

A strong electrostatic interaction between the cationic nanoparticles and the negatively charged cell membrane, which will cause a rapid entry into the cell. Conversely, negatively charged nanoparticles

are endocytosed via the interaction with the positive site on protein in the membrane. Cationic nanoparticles enter the cell via the CME pathway, while anionic nanoparticles use majorly the caveolae-dependent endocytosis pathway (Perumal et al., 2008), but there are also some exceptions for the nanoparticles favorability to a certain pathway based on their surface charge (Qaddoumi et al., 2004). The inhibitors studies provide an understanding of the principal mechanism(s) of endocytosis and help to define modes of cellular entry of various materials i.e. nanoparticles. Various inhibitors of endocytosis can be employed to block the specific endocytic pathway to help in confirming whether it is utilized by the nanomedicines to enter cells. It is usually used in combination with different markers to determine the endocytic mechanisms used by the nanomaterials, bearing in mind that inhibitors can block different endocytic mechanisms in different cell type.

Almost all endocytic pathways are energy dependent processes, they can be inhibited by low temperature. Therefore, this can be used to distinguish from the non-endocytic pathways (non-energy dependent). Some widely used inhibitors for specific endocytosis mechanisms, hypertonic sucrose (0.45M) (Iversen et al., 2011), chlorpromazine and potassium depletion can be used to inhibit the clathrin dependent endocytosis. Nystatin, filipin and cholesterol oxidase can be used as the inhibitors for caveolae dependent endocytosis. Amiloride, colchicine and cytochalasin B can block macropinocytosis. The selection of the particular inhibitor is dependent on the concentration that is sufficient to inhibit the pathway and also on the lowest cytotoxicity it causes to the cells being treated. Exposure of cells to different inhibitors was used to explore the possible permeation route of various RES-NLCs formulations (Iversen et al., 2011).

Coumarin-6 was used as fluorescent probe to tag the nanoparticles, prepared by the method mentioned in section 3.2.4.3. Six RES-NLCs (RES-NLC-GTO, RES-NLC-PCG, RES-NLC-PGMC, RES-NLC-PGML, RES-NLC-DO, RES-NLC-GTC), PEGylated RES-NLC-PEGS40 and the ligand appended RES-NLCs (HA, FA and HAFA) were investigated for their cellular uptake *in vitro* on all the four cell lines (MCF-7, MCF-10A, MDAMB-231 and RAW-264.7) using both quantitative and qualitative methods; i.e. flow-cytometry and fluorescence microscopy, respectively. Moreover, the Internalization pathways of all the formulations were elucidated in both the breast cancer cell lines (MCF-7 and MDAMB-231).

4.3.3 (I) Quantitative cellular uptake studies with flow-cytometry

Flow-cytometry is a sophisticated instrument determining multiple physical characteristics of a single cell such as granularity and size instantaneously as the cell flows in suspension via a measuring device. Its functioning depends on the light scattering features of the cells under examination. This approach

makes flow cytometry a potent tool for detailed analysis of complex populations in a short period of time (Adan et al., 2017). Flow-cytometry offers rapid analysis of various characteristics of single cells. The data obtained from flow-cytometry is both qualitative and quantitative. Fluorescent dyes may bind to different cellular components. When labeled cells pass through a light source, the fluorescent molecules are excited to a higher energy state. Upon returning to their resting states, the fluorochromes emit light energy at higher wavelengths. The usage of several fluorochromes, each with comparable excitation wavelengths and different emission wavelengths (or "colors"), permits several cell properties to be measured concurrently. Frequently used dyes include propidium iodide, fluorescein and phycoerythrin (Brown and Wittwer, 2000).

MCF-7 and MDAMB-231 were seeded into 6-well plates at a density of 30x 10^4 cells per well and incubated for 24 h. The medium was aspirated the next day and replaced by 1 mL coumarin (C6) C6-loaded test RES-NLCs (2 µg/mL). The cells were incubated for the following time points: 30 min, 1 and 4 h in order determine the time dependent uptake of nanoparticles. At the end of each time point the media was removed and the cells were washed thrice with PBS, the cells were then trypsinized and centrifuged. The cell pellet was then re-suspended in 0.5 mL PBS along with 5 µL propidium iodide (added to quantify the dead cells upon measurement of cellular uptake) for immediate flow-cytometric measurement. At least ten thousand events per sample were measured by the flow cytometer.

4.3.3 (II) Mechanism of cellular uptake using flow-cytometry

In order to determine the cellular uptake pathways and the mechanisms involved in nanoparticles internalization various treatments were carried out.

The study was conducted in 6 well plates. 30×10^4 cells/mL (MCF-7 or MDAMB-231) were seeded with 1 mL of growth media, to ensure the proper growth of cells. Cells were incubated at 37^{o}C with 5 % CO_2 for 24 h to allow the cells to attach. Next day the media was aspirated in order to study different cellular pathways. To determine the energy dependent pathway the cells were pre-incubating at 4^{o}C for 1 h. To study the effect of different endocytosis inhibitors on the cellular uptake of various RES-NLCs, cells were pre-incubated for 30 min with the following inhibitors at concentration; Sucrose (0.45 M), nystatin (5 µg/mL) and cytochalasin B (5 µg/mL) (Martins et al., 2012). The media was aspirated and replaced with 1 mL of various RES-NLCs formulations prepared in media (2 µg/mL). Cells were incubated with the formulation in the presence of each of the inhibitors for 1 h (Beloqui et al., 2013).. After the incubation time, the media was removed and the cells were washed thrice with PBS in order to ensure the removal of excess C6-RES-NLCs on the outer cell membrane. The cells were trypsinized and

centrifuged; the cell pellet was re-suspended in 0.5 mL PBS and 5 µL of propidium iodide was added to stain the dead cells. The stained cells were placed in round bottom 96 well plates and immediately analyzed by flow-cytometer and read at excitation and emission wave length 460 and 500 nm, respectively.

4.3.3 (III) Qualitative cellular uptake and internalization mechanisms using fluorescence imaging

Qualitative cellular uptake studies was carried out using fluorescence microscopy to visualize the fluorescent coumarin-6 labelled RES-NLCs (C6-RES-NLCs) inside the cells (MCF-7, MCF-10A, MDAMB-231 and RAW-264.7) after incubation of 1 h.

The study was conducted in 6 well plates, in which 30×10^4 cells/mL each type of cells were seeded onto glass cover slips, supplemented with 1 mL media and incubated at 37^{o}C with 5 % CO_2 for 24 h to allow the cells to attach to the glass cover. The media was then removed and replaced with 1ml of various RES-NLCs formulations (2 µg/mL) At the end of the incubation time, the media was aspirated and the cells were washed carefully thrice with PBS in order to ensure the removal of free C6-RES-NLCs. Cells were fixed for 20 min with 4% (V/V) paraformaldehyde (PFA) solution made in PBS then washed thrice with PBS. Cells were washed with glycine (0.3 M) in order to reduce the quenching effect from free aldehyde present on the cover slips (Garanti et al., 2016). Cells were washed for the last time with PBS. One drop of 4', 6-diamidino-2-phenylindole (DAPI blue) mounting medium was placed on a glass slide, cells on cover slips were inverted facing the glass slide and left overnight. DAPI was used to stain the nucleus of the cells. The cover slips were then secured by painting the edges with a colorless nail polish. The slides were allowed to dry prior to imaging. Imaging was done employing Zeiss filter set 49 (DAPI excitation and emission wave length was recorded at 365 and 445/50 nm, respectively. Coumarin 6 imaging was performed with a filter set at 38 GFP excitation and emission wave length was set at 470 and 525/50 nm, respectively using 60X oil objective. Slides were covered and stored in a special slides box at 2-8^{o}C. Zen lite 2012 desk imaging software was used to analyze the images.

In order to back up the data obtained from endocytosis mechanism studies using flow-cytometer internalization mechanism were also investigated using fluorescence microscopy. The cell number was set the same to ensure a cell density similar to the flow cytometry experiments also to keep all parameters affecting the experiment constant sample preparation and cell fixation.

The study was carried out exactly as described above except that the cells were incubated along with pharmacological inhibitors as described in section 4.3.3 (II) Imaging was done using Zeiss filter set 49 DAPI and set at 38 GFP for coumarin 6 fluorescence.

In order to study the internalization pathways using Fluorescence microscopy, the same procedure for seeding cells was carried out as previously mentioned in this section. On the day of the experiment the media was removed and replaced with 1 ml of the following concentration of pharmacologic inhibitors : sucrose (0.45 M), nystatin (5 µg/mL), cytochalasin B (5 µg/mL) and incubated for 30 min. To study the temperature effect the plates were kept at 4^{o}C for 1 h. After the incubation for 1 h with various inhibitors the media was removed and the cells were incubated with various C6 labeled RES-NLCs. After that the cells were treated in the same way as previously mentioned.

4.3.4 Evaluation of targeting potentials of ligand appended nanoparticles

Folate and CD44 receptors competitive inhibition experiments were carried out, in order to determine the receptor mediated internalization process of three ligand appended RES-NLCs. In three separate experiments the cells (MCF-7 and MDAMB-231) were incubated for 1 h with 10X concentration of HA,10X concentration FA and 10X concentration of each HA and FA together (for the dual ligand appended formulation). These treatments were followed by incubation with the ligand appended formulations (RES-NLC-GTO-PEGS40-HA, RES-NLC-GTO-PEGS40-FA and RES-NLC-GTO-PEGS40-HAFA) for another 1 h. After 1 h the media was removed and the cells were washed thrice with PBS, the cells were then trypsinized and centrifuged. The cell pellet was then re-suspended in 0.5 mL PBS along with 5 µL propidium iodide (added to quantify the dead cells upon measurement of cellular uptake) and taken for immediate flow-cytometric measurement. At least ten thousand events per sample were measured by the flow cytometer at excitation and emission wave length 460 and 500 nm respectively. In order to confirm the targeting potential of nanoparticles, fluorescence microscopy was also carried out in both the cancer cell lines (MCF-7 and MDAMB-231) after the incubation with excess of each ligand material followed by treatment with nanoparticles for 1 h and subsequently imaging under fluorescence microscopy. The procedure was similar to what has been detailed in section 4.3.3 (III)

HA is an identified ligand that has the ability to bind to CD44 receptor and when appended on the surface of nanoparticles can impart targetability to the nanoparticles (Negi et al., 2012).Therefore, to evaluate the targetability of fluorescent RES-NLC-GTO-PEGS40-HA towards CD44 receptors overexpressed on both cancer cell lines (MCF-7 and MDAMB-231) the nanoparticles were incubated in

presence of CD44 antibodies which would have competitive binding for CD44 receptors (Surace et al., 2009).

Cells were seeded at a density of 30 x 10^4 cells/mL in 6 well plates and incubated overnight. The media was removed the next day and replaced with 20 µL of FITC conjugated CD44 antibodies for 4h. FITC conjugated CD44 antibodies were also incubated with the cell to serve as a positive control. After 4 h media was removed and replaced with RES-NLC-GTO-PEGS40-HA nanoparticles and incubated for 1 h in the presence of same volume of CD44 antibodies. Same procedure was followed when studying the HA activity on CD44 receptors by fluorescence microscopy.

4.3.5 Apoptosis Assay

Programmed cell death, commonly referred to as apoptosis (Wong, 2011). plays a significant role in both cancer development and cancer treatment (Jensen et al., 2008).

Alterations at the cell surface occur in the early stages of apoptosis. One of these cell membrane changes is the flipping of phosphatidylserine (PS) from the inner side of the cell membrane to the outer layer, leading to the exposure of PS in the surface the cell. Phospholipid-binding protein Annexin V displays a great affinity for PS. Therefore, this protein can be utilized as a sensor for PS exposure on the cell membrane. Translocation of PS outside the cell to the surface is not distinctive to apoptosis, as it occur in cell necrosis. In order to distinguish the two process of apoptosis, in the initial stage of apoptosis the cell membrane retain its integrity. Whereas, after necrosis the cell membrane becomes leaky. Consequently, the measurement of annexin V binding to the cell surface gives indication for apoptosis. It has to be carried out in combination with a dye exclusion test Using FITC-conjugated annexin in conjunction with PI, a fluorescent nuclear stain that detects necrotic cells. Propidium iodide (PI) is used to stain the DNA of dead cells efficiently used to mark the dead cells that have lost their membrane integrity (Vermes et al., 1995, Kepp et al., 2011).

Four distinct regions are distinguishable using this approach: (Q1) necrotic cells annexin V−/PI+ (upper left quadrant), (Q2) late apoptotic cells V+/PI+ (upper right quadrant), (Q3) viable cells annexin V-/PI− (lower left quadrant) and (Q4) early apoptotic cells annexin V+/PI− (lower right quadrant) (Xiao et al., 2015).

The induction of apoptosis was investigated using BD FACSAria flow cytometry using the protocol stated in the Alexa ® Fluor 488-annexin V PI double staining apoptosis kit with few modifications. Both cancer cells (MCF-7and MDAMB-231) were seeded in 24 well plate at a density of 10 x 10^4 cells/well and incubated overnight (Morse et al., 2005). The media was removed and the cells were treated with

free RES and various RES-NLCs at concentration of 15 and 30 µg/mL diluted in media for MCF-7 and MDAMB-231 cells, respectively. Cisplatin was used as a positive control in the concentration of 45 µg/mL (Garanti et al., 2016). Cells were incubated further for 48 and 72 h. After incubation, the media in each well was kept for further analysis and the cells were thoroughly washed with cold PBS to remove excess of nanoparticles on the surface. Subsequently, the cells were trypsinized and the later media was added to the PBS wash and centrifuged at 1000 rpm for 5 min. The cell pellet was rinsed with PBS, 100 µL of the cell suspensions suspended in binding buffer containing 1 µL PI (1:200 v/v dilution) and 5 µL of Annexin V-FITC solution (1:60 v/v dilution). The samples were mixed gently and incubated at room temperature for 15 min in the dark.

Annexin V was detected with FITC channel at 530 nm excitation wave length was set at 488 nm and red fluorescence of PI were collected using 616/23 nm band pass filters. A minimum of 10,000 cells were recorded for each sample and demonstrated as dot plot using Flowing software. Data were processed and analysed using FACSDiva software. A minimum of 10,000 events were acquired for each sample and illustrated as dot plot using Flow-cytometer software.

4.3.6 Cell cycle assay

To determine the whether the anticancer effect of free RES, bare, PEGylated and three surface modified RES-NLCs was associated with the induction of apoptosis, the apoptotic profile was determined by the DNA content after treatment of both cancer cell lines with free RES, bare, PEGylated and three surface modified RES-NLCs (Pozarowski P, 2004).

MCF-7 and MDAMB-231 cells were seeded in 24 well plate at a density of 20 X 10^4 cells/mL, cells were allowed to attach overnight. After incubation the media was removed and the cells were treated with the IC_{50} concentration (13 µg/mL) of the drug and RES-NLCs containing equivalent amount and incubated for 48 and 72 h. The media was aspirated and the cells were washed twice with PBS and trypsinized and collected by centrifugation at 1000 rpm for 5 min, followed by fixing of cells in 70 % ice cold ethanol added in drop wise and stored overnight at -20^{o}C. Cells were centrifuged and the pellet was rinsed twice with PBS and stained with 50 µg/mL of PI in the presence of 100 µg/mL RNAse at 37°C for 30 min protected from light, followed by analysis with BD-FACSAria flow-cytometer (BD Biosciences, USA). The cells distribution in phases of SubG1, G0/G1 and G2/M were measured by FACaria Diva software (Cecchini et al., 2012).

4.3.7 Caspase-3 Assay

The caspases are classified into the ones that are release during the inflammatory response such as caspase-1, -4, -5, -13, and -14) and caspase-2, -3. -6, -7,-8, -9 and -10 which play the main role in apoptosis process (Wong, 2011). The caspases that are involved in the initiation of apoptosis pathways (e.g. caspase-2, -8, -9 and -10), while caspase-3, -6 and -7 are responsible for the breakdown of the cell components during the apoptosis process (Fink and Cookson, 2005).

The Caspase 3 Colorimetric Assay Kit is dependent on the hydrolysis of substrate acetyl-Asp-Glu-Val-Asp p-nitroanilide (Ac-DEVD-pNA) by caspase 3, releasing the p-nitroaniline (pNA) moiety. p-Nitroaniline is detected at 405 nm.

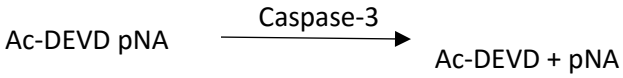

Caspase 3 activity was determined using a Sigma-Aldrich Caspase 3 calorimetric Assay Kit. MCF-7 and MDAMB-231 cells were seeded in 24-well plates at a seeding density of 10 X 10^4 cells /well and incubated overnight. Next day the media was removed and the cells were treated with either free RES or bare, PEGylated and three surface modified RES-NLs for 72 h at a concentration of 13 µg/mL. After the 72 h the media was removed and the cells were washed thrice with PBS and centrifuged at 4^{o}C with 1000 rpm for 5 min. Cells were re-suspended in 100 µL 1X lysis buffer provided in the assay kit and incubated in ice for 15 min. Cells lysate was centrifuged at 16000 rpm for 10 min at 4^{o}C. The supernatant was taken into a new tube and then aliquoted into the 96 well plate. Once the cell lysate was placed in 96 well plate (Table 4-1), caspase inhibitor was added to the appropriate wells. Reaction was started by the addition of 10 µL of caspase substrate. The plates were incubated at 37^{o}C for 90 min. The absorbance was then read at 390 nm. Caspase 3 inhibitor was used to prove that the absorbance was due to caspase 3 activity.

Table 4-1 Reaction scheme for 96 well plate assay method

	Cell lysate	Caspase 3 5 µg/ml	1x Assay buffer	Caspase 3 inhibitor Ac-DEVD-CHO 200 µM	Caspase 3 substrate Ac-DEVD-pNA 2 mM
Reagent blank	----	----	90 µl	----	10 µl
Non-induced cells	5 µl	----	85 µl	----	10 µl
Non-induced cells + inhibitor	5 µl	----	75 µl	10 µl	10 µl
Induced cells	5 µl	----	85 µl	----	10 µl
Induced cells + inhibitor	5 µl	----	75 µl	10 µl	10 µl
Caspase 3 positive control	----	5 µl	85 µl	----	10 µl
Caspase 3 positive control + inhibitor	----	5 µl	75 µl	10 µl	10 µl

4.3.7 (I) Para nitro-aniline standard curve

Working p-nitroaniline solutions with concentration range 1, 2, 5, 10, 20, 50 and 100 µM, were prepared by diluting p-nitroaniline stock solution in 1X Assay Buffer. 100 µL of each dilution was added to the well, 100 µL of assay buffer was used as a blank. The absorbance was then read at 390 nm.

Caspase activity was calculated form the following formula:

$$\text{Activity, µmoL pNA/min/mL} = \frac{\text{µmol pNA x d}}{\text{t x v}}$$

Where: V = represents the volume of sample in mL, d = dilution factor and t =reaction time in minutes

4.3.7 (II) Protein quantitation based on bicinchoninic acid (BCA) Assay

Bicinchoninic acid (BCA) is a commonly used chemical reagent for standard protein analysis (Sapan et al., 1999). In the presence of Cu (II) ions and in combination proteins, BCA yields a colour transformation from green to dark purple. This is due to the reduction of Cu (II) to Cu (I) by the proteins peptide bonds, and the simultaneous formation of Cu (I)–BCA complex. This, enables quantification of protein content in solutions (Biradar et al., 2016).

The determination of the protein concentration in the cell lysate using colorimetric-based detection methods by the preparation of a standard curve in the presence of the protein this was done according to manufacturer's protocol (Sigma-Aldrich).

The BCA working solution was prepared by mixing 50 parts of reagent A with 1 part of reagent B until a green colour is developed. The final solutions were prepared by diluting the protein standard with the prepared BCA working solution to give final concentrations of 200, 400, 600, 800 and 1000 µg/mL. All the preparation were adjusted to a final volume of 200 µL since the experiment was performed in 96 well plates. Plates were covered by a film and incubated at 37^{o}C for 30 min. Plates were removed and the absorbance was read by plate reader at 535 nm.

4.3.8 Statistical analysis

All data are presented as the mean ± standard error of mean (SEM). The significance of difference in controls and the treated cells was determined using two-way ANOVA and Dunnet's post Test using Graph Pad prism version 5.0 (San Diego, CA), where value of $p<0.05$ between the groups was considered as statistically significant difference between the groups. The values obtained represent the average of at least three experiments and the data were expressed as mean ± SD.

4.4 Results and Discussion

4.4.1 Growth curves of cell lines

Various methods are available for the measurement of cell viability and proliferation in cell cultures. In the trypan blue (TB) method TB penetrates dead cell membranes with a distinguishing blue colour; whereas, the living cells are not stained with TB and are counted by hemocytometer under an optical light microscope.

The growth curves for MCF-10A, MCF-7 and MDAMB-231 cell lines were prepared in order to evaluate the characteristics of cellular growth after seeding of the cells. Post seeding MCF-7 and MCF-10A cell lines showed a longer lag period as compared to MDAMB-231 which demonstrated a faster growth pattern. The lag phase is usually the time the cells take to recover from trypsinization and establish linkage between the cells and the substrate followed by cell propagating. The lag phase was followed by the log phase where cells showed exponential growth (Assanga and Lujan, 2013). MCF-10A had the shortest log phase of 4 days, followed by MDAMB-231 (5 days), while MCF-7 showed the longest log phase up to 7 days. Identification of log phase is important as this the phase where drugs and bio-actives show maximum activity on the cells and any drug treatment should be given during this phase. In the log phase the cells double at a characteristic rate called the doubling time. The estimated doubling time (DT) for MCF-10A was 19.2 hours (Figure 4-5. A), while MCF-7 cell lines demonstrated a slow growth rate with an estimated DT of 24 hours post seeding (Figure 4-5. B), MDAMB-231 in contrast showed the fastest growth and doubling only after 14.16 hours (Figure 4-5. C).

Out of the three seeding densities investigated 5×10^4 cells showed the best growth where the cells remained in log phase for sufficient period of time to give suitable treatment during this time. Whereas, 5×10^3 cells seeding density demonstrated a very slow growth which did not reach an evident "log-

phase" after 5 days. On the other hand highest seeding density 5 x 10^5 showed fast growth rate reaching over confluency after 2 days with sudden drop in the cell number and the cells start dying. These results also demonstrate that PB did not have any effect on the growth characteristics of the cells and thus can be safely use as a reagent for cell viability assay (Figure 4-6 A,B) (Harvard et al., 2013).

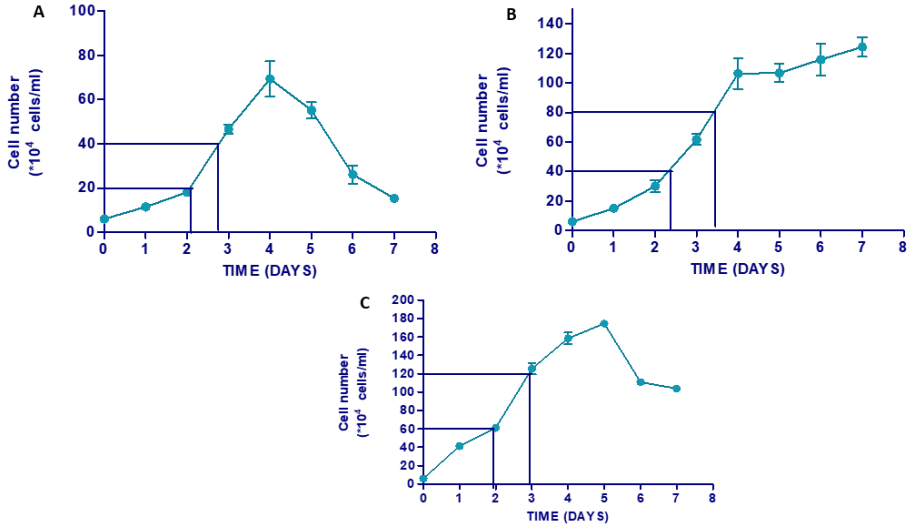

Figure 4-5. Growth curve using Trypan blue solution A. MCF-10A cell lines, B. MCF-7 cell lines, and C. MDAMB-231 cell lines

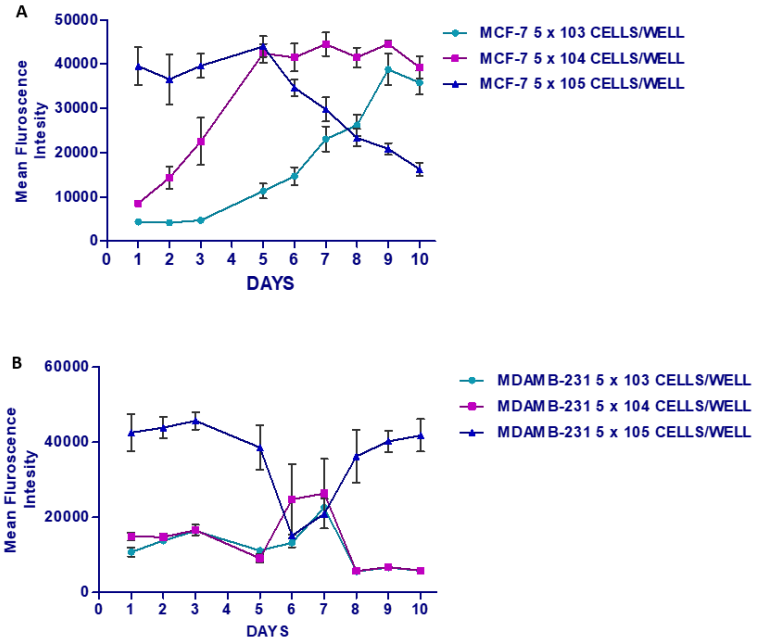

Figure 4-6. Growth curve using PB assay A. MCF-7 cell lines, B. MDAMB-231 cell lines

4.4.2 *In vitro* cytotoxicity assay

4.4.2 (I) Effect of RES-NLCs on the cancer cell viability

As a quantitative marker of cytotoxic effects IC_{50} is defined as the inhibition concentration for a fifty per cent reduction of the cell number per culture (Halle and Göres, 1987, Wang et al., 2012). The anti-proliferative effect of RES and RES-NLCs prepared with six different liquid lipids, in addition to blank NLCs have been evaluated towards MCF-10A, MCF-7, MDAMB-231 and RAW 264.7 cell lines using PrestoBlue cell viability assay (Xu et al., 2015).

Both the concentration and time dependent cytotoxic effect of RES and RES-NLCs on the aforementioned cell lines was observed in the concentration range 1-50 µg/mL. For anticancer drug not only it is important to have efficacy against the tumour cells but the main challenge is to be safe to the normal cells. Therefore, in this study apart from carrying out the cell viability assay in the two breast cancer cell lines, MCF-10A cell line were used as healthy cells to identify the safety of the use of RES-NLCs.

It is noted from the IC_{50} values (Table 4-2) that free RES demonstrated higher toxicity toward MCF-10A normal breast cells at 24 h as compared to all RES-NLC formulations, clearly establishing the superiority of NLC formulation over the free drug.

However, at 48 h RES-NLC-PGML showed lower IC_{50} value as compared to free drug. This could be attributed to the nature of the liquid lipid which is known for its higher penetration properties in the cells (Raymond et al., 2012). While all RES-NLCs-PCG, RES-NLCs-PGMC, RES-NLCs-PGML, RES-NLCs-DO, RES-NLCs-GTC did not show any significant different in IC_{50} as compared the free drug after 72 h incubation except RES-NLC-GTO which showed the least toxicity on MCF-10A cell lines (Figure 4-7)

Amongst all the six RES-NLC investigated RES-NLC-GTO showed the least toxicity toward normal breast cells. The safety of this formulation could be attributed to the chemical nature of the liquid lipid employed, GTO is a long chain triglyceride and its safety has been well established and it is also approved by USFDA for parenteral injections (Souza and Campa, 1999, Raymond et al., 2012).

When MCF-7 cancer cells were treated with different concentrations of RES and RES-NLCs at different time points, all RES-NLCs exhibited concentration dependent increase in the anticancer effects. The cell viability decreased with increasing concentration (Figure 4-8). The IC_{50} values were in the range of 9-12 µg/mL 72 h after the treatment of MCF-7 with RES-NLCs, whereas RES has shown significantly ($p > 0.05$) higher IC_{50} value of 18.71 ± 1.092 µg/mL at 72 h. This was in confirmation with previous studies where lipid nanoparticles have shown cytotoxicity in MCF-7 cells, similar observation was made by

previous studies (Miglietta et al., 2000, Wang et al., 2014b). This could be due to the advantages of nanomedicine, including the high drug transportation efficiency across the cell membrane by the mechanism of endocytosis, after internalization RES-NLCs release the drug over the period of 24 h resulting in a continuous effect of drug (Pucadyil and Schmid, 2009, Wang et al., 2014c).

It is considered as a challenge to develop agents to treat the TNBC (MDAMB-231) which is clinically the most aggressive type of cancer (Tran et al., 2014). The available chemotherapy treatment exhibit serious toxicity issues. Free RES demonstrated higher IC_{50} value (31.31 ± 1.048 µg/mL) as compared to all RES-NLC formulations with an IC_{50} range of 14.88 ± 1.074-31.53 ± 1.040 µg/mL (Figure 4-9). RES-NLCs demonstrated a promising anticancer effect requiring a low drug concentration in order to produce the same *in vitro* therapeutic efficacy, than free RES for MDAMB-231, this observations corroborates with previous report where NLCs have shown better efficacy than the free drug toward MDAMB-231 cell lines (Ng et al., 2015).

The cytotoxic effect was more prominent after 72 h this might be attributed to the fact that the nanoparticles acts as a carrier entrapping the drug within the lipid structure, which will delay the drug release from the nanoparticles and consequently slow effect will be observed on cancer cells. This goes in line with the drug release results from the nanoparticles described in section 3.3.4.

Free RES showed lower efficacy toward MDAMB-231 cells than MCF-7 cells. RES-NLCs also showed differential susceptibilities towards the two different breast cancer cell lines (Figure 4-9). RES-NLCs demonstrated a higher cytotoxic effect on MCF-7 cells as compared to MDAMB-231 with higher concentrations being required to kill the resistant MDAMB-231 cells. The RES-NLCs IC_{50} were 2-3 fold lower toward MCF-7 as compared to MDAMB-231 at 72 h. The MDAMB-231 cell line distinctively higher invasiveness displaying higher expression of malignant parameters which could be the reason for lower efficacy in these cell lines (Thompson et al., 1988).

Cytotoxicity of blank-NLCs were tested on both MCF-7 and MDAMB-231 cells, to understand their effect on the tumour cell lines (Table 4-3). All the six blank-NLCs showed lower toxicity than their respective drug loaded RES-NLC in both the cell lines at all the time points indicating that RES encapsulation is a major contributing factor toward the cytotoxicity of these formulations (Figure 4-10 and 4-11). Macrophage plays a crucial physiological function in eliminating foreign materials, pathogens and cellular debris from circulation (Li et al., 2016b). The effect of RES and RES-NLCs on RAW 264.7 macrophage cell viability was assessed in order to establish the safe concentration to enable to study the uptake of RES-NLCs in cells (Figure 4-12).

RES-NLCs displayed high IC_{50} values ranging from 47.08 ± 1.122 – 176.1 ± 1.143 µg/mL confirming the safety of RES-NLC formulations on macrophages. Various studies have previously demonstrated the safety of lipid nanoparticles in the RAW 246.7 macrophages (Olbrich et al., 2004).

In conclusion, the diminished cytotoxicity of RES-NLC-GTO on non-tumorigenic MCF-10A cells (healthy cells) along with its enhanced efficacy on breast cancer cells with oestrogen and progesterone receptors as well as the triple negative breast cells, suggests that this nanoparticulate formulation would offer promising therapy for both cancer types and was therefore selected further for functionalization to improve its targetability towards breast cancer cells.

Table 4-2. IC50 values for RES and RES-NLCs after treatment of MCF-10A, MCF-7, MDAMB-231 and RAW 264.7 cell lines with different concentrations at different time points (n= 3 ± SD).IC50 values for RES and RES-NLCs after treatment of MCF-10A, MCF-7, MDAMB-231 and RAW 264.7 cell lines with different concentrations at different time points (n= 3 ± SD)

Treatment	Exposure time (h)	IC50 value for MCF-10A	IC50 value for MCF-7	IC50 value for MDAMB-231	IC50 value for RAW 264.7
RES	24	12.61 ± 1.081	140.6 ± 1.388	140.5 ± 1.337	N/A
	48	4.745 ± 1.121	14.95 ± 1.108	79 ± 1.151	N/A
	72	3.712 ± 1.089	18.71 ± 1.092	31.31 ± 1.048	N/A
RES-NLC-GTO	24	102.8 ± 1.224	64.33 ± 1.096	79.53 ±1.121	54.51± 1.123
	48	81.26 ± 1.172	13.6 ± 1.056	29.96 ± 1.014	N/A
	72	61.71 ± 1.386	11.36 ± 1.041	22.06 ± 1.019	N/A
RES-NLC-PCG	24	102.5 ± 1.181	49.57 ±1.036	65.24 ± 1.072	47.08±1.122
	48	17.5 ± 1.062	13.61 ± 1.088	25.58 ± 1.036	N/A
	72	4.258 ± 1.075	11.77 ± 1.057	20.89 ± 1.039	N/A
RES-NLC-PGMC	24	91.17 ± 1.257	57.95 ± 1.027	64.15 ± 1.092	54.66±1.071
	48	9.619 ± 1.030	18.35 ± 1.043	33.03 ± 1.012	N/A
	72	3.249 ± 1.065	9.304 ± 1.058	21.94 ± 1.044	N/A
RES-NLC-PGML	24	94.35 ± 1.079	26.19 ± 1.065	45.98 ± 1.080	65.24 ±1.144
	48	2.648 ± 1.063	9.669 ±1.029	19.49 ± 1.094	N/A
	72	2.706 ±1.087	9.009 ± 1.024	14.88 ± 1.074	N/A
RES-NLC-DO	24	88.47 ± 1.133	42.5 ± 1.052	145.4 ± 1.305	54.04 ± 1.151
	48	6.462 ± 1.079	9.906 ± 1.053	33.38 ± 1.076	N/A
	72	4.26 ± 1.032	11.14 ± 1.040	31.53 ± 1.040	N/A
RES-NLC-GTC	24	78.79 ± 1.140	176.1 ± 1.340	89.44 ± 1.191	176.1 ± 1.143
	48	6.916 ± 1.085	15.93 ± 1.117	44.21 ± 1.059	N/A
	72	3.838 ± 1.062	12.04 ± 1.043	30.91 ± 1.046	N/A

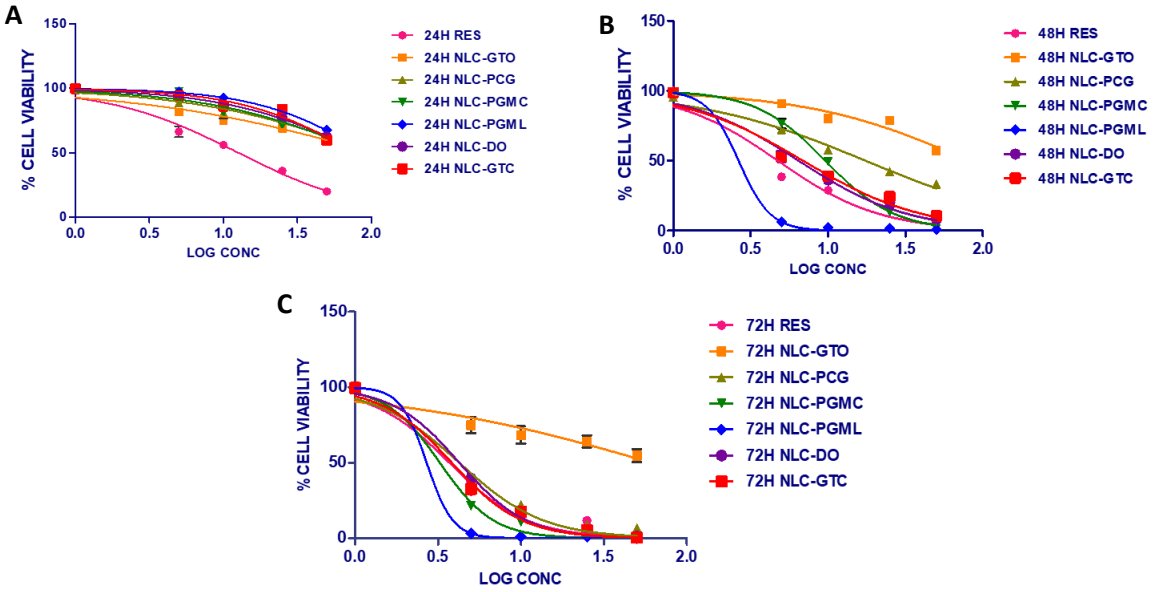

Figure 4-7. Concentration-dependent cytotoxicity of free RES and RES-NLCs in MCF-10A cell lines for A. 24 h, B. 48 h and C. 72 h (n=3 ± SD)

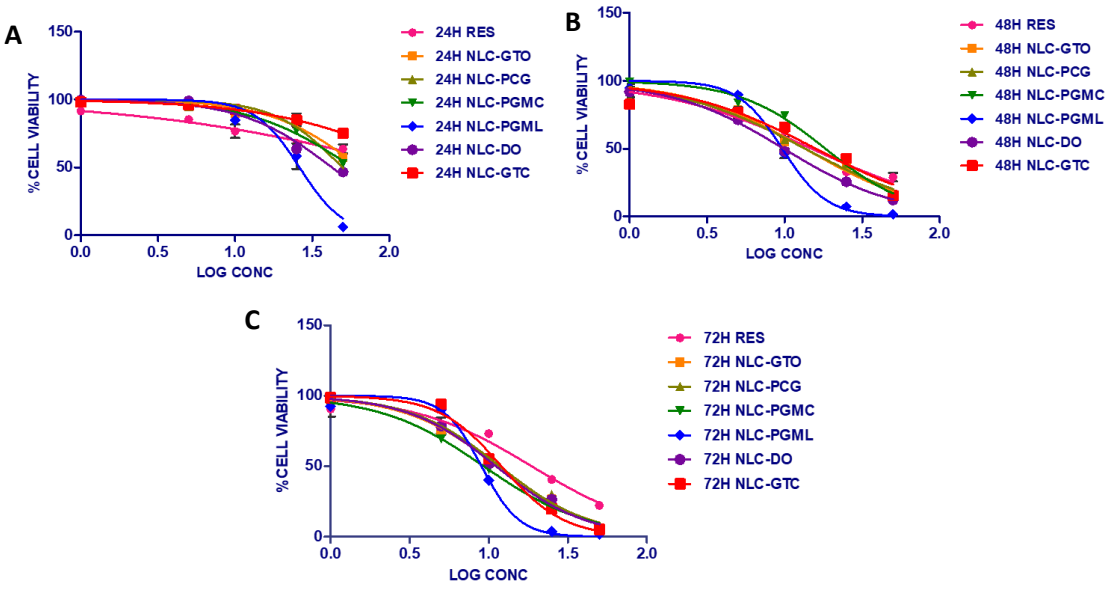

Figure 4-8. Concentration-dependent cytotoxicity of RES NLCs in MCF-7 cell lines for A. 24 h, B. 48 h and C. 72 h (n=3 ± SD)

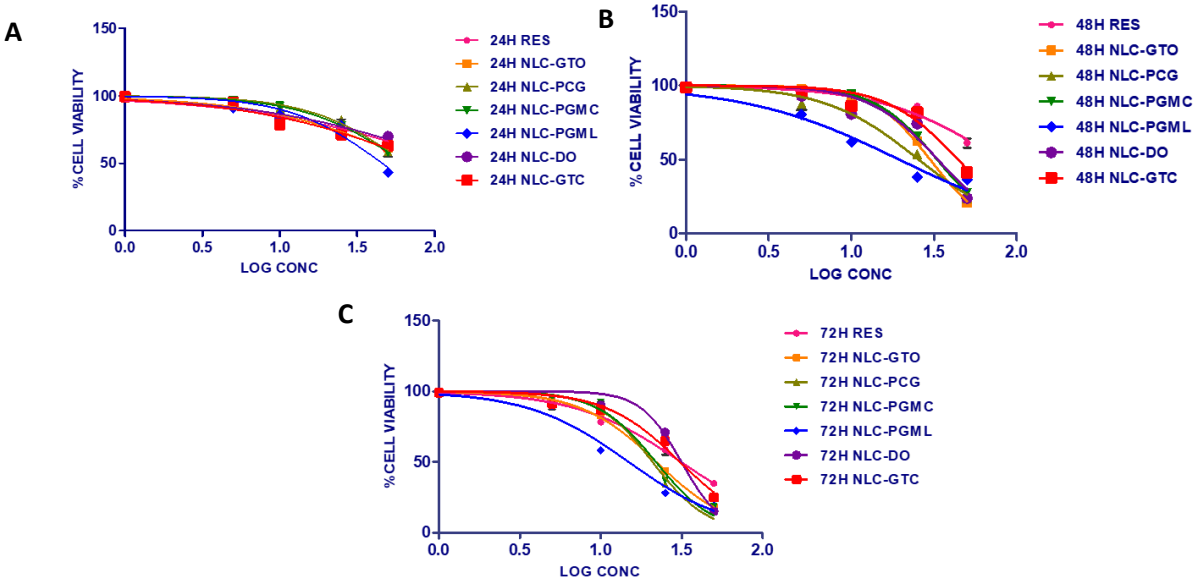

Figure 4-9. Concentration-dependent cytotoxicity of free RES and RES-NLCs in MDAMB-231 cell lines for A. 24 h, B. 48 h and C. 72 h (n=3 ± SD)

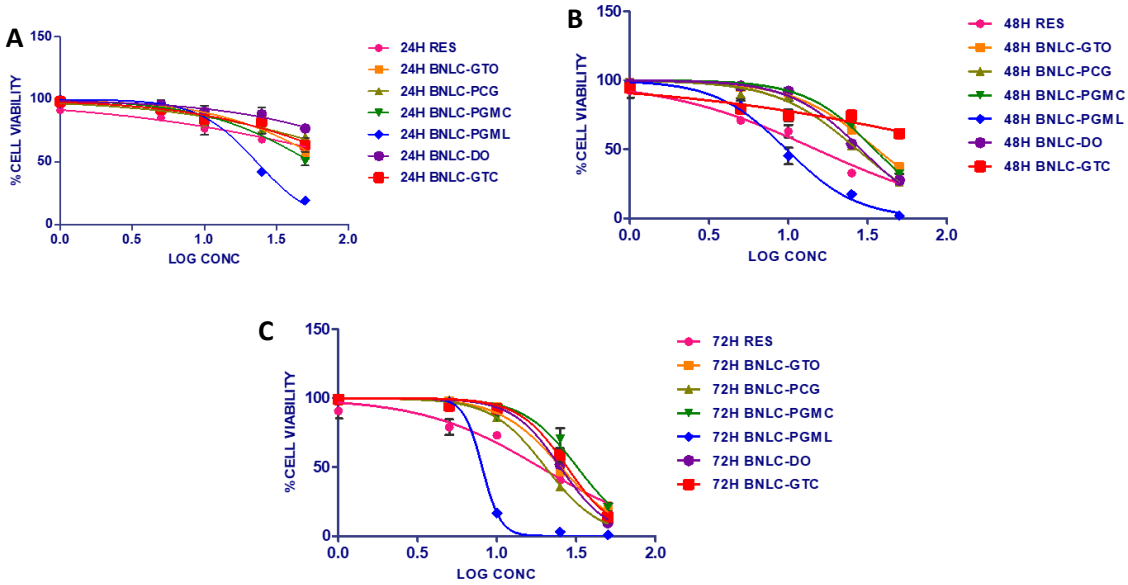

Figure 4-10. Concentration-dependent cytotoxicity of blank NLCs in MCF-7 cell lines for A. 24 h, B. 48 h and C. 72 h (n=3 ± SD)

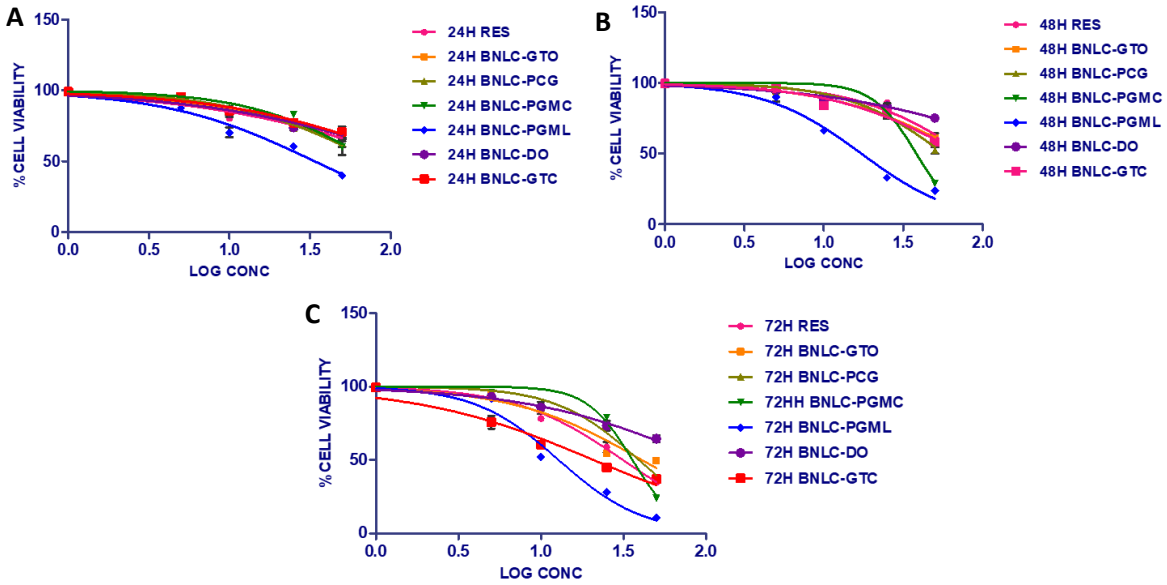

Figure 4-11. Concentration-dependent cytotoxicity of blank NLCs in MDAMB-231 cell lines for A. 24 h, B. 48 h and C. 72 h (n=3 ± SD)

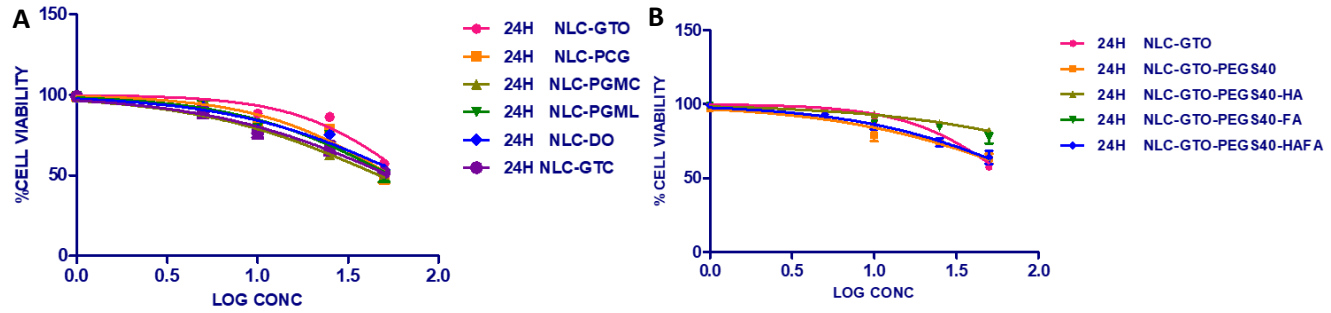

Figure 4-12. Concentration-dependent cytotoxicity of A. RES-NLCs and B. Surface modified RES-NLCs in RAW 264.7 cell lines at 24 h (n=3 ± SD)

Table 4-3. IC50 values for blank-NLCs after treatment of MCF-7 and MDAMB-231 cell lines with different concentrations at different time points (n=3 ± SD)

Treatment	Exposure time (h)	IC50 value for MCF-7	IC50 value for MDAMB-231
BNLC-GTO	24	71.12 ± 1.244	156.2 ± 1.293
	48	36.22 ± 1.027	78.35 ± 1.071
	72	25.33 ± 1.036	40.8 ± 1.106
BNLC-PCG	24	156.4 ± 1.366	80.7 ± 1.090
	48	27.14 ± 1.052	57.06 ± 1.082
	72	20.24 ± 1.022	39.17 ± 1.053
BNLC-PGMC	24	55.57 ± 1.110	77.78 ± 1.165
	48	34.97 ± 1.028	38.25 ± 1.034
	72	32.09 ± 1.065	35.84 ± 1.053
BNLC-PGML	24	23.07 ± 1.037	33.88 ± 1.082
	48	9.708 ± 1.055	17.26 ± 1.055
	72	8.075 ± 1.020	12.8 ± 1.065
BNLC-DO	24	246.2 ± 1.910	166 ± 1.278
	48	28.74 ± 1.029	228.7 ± 1.258
	72	25.1 ± 1.026	96.43 ± 1.149
BNLC-GTC	24	113 ± 1.303	148.3 ± 1.311
	48	162.6 ± 1.535	73.78 ± 1.161
	72	27.69 ± 1.036	20.81 ± 1.093

4.2.4 (II) *In vitro* cytotoxicity of surface modified RES-NLCs

Targeted delivery of anti-cancers to the specific tumour is a major challenge in cancer therapy. Drug delivery systems such as nanoparticles can improve the pharmacologic properties of conventional chemotherapeutics by modifying drug bio-distribution and pharmacokinetics. However, these drug-loaded nanoparticles suffer from shortcomings i.e. the rapid recognition and clearance of nanoparticles from the blood circulation by the reticuloendothelial system limits their usefulness as drug carriers. PEGylation of NLCs is an effective way to increase their circulation time in the blood circulation, to improve their surface hydrophilicity and resist protein adsorption (Luan et al., 2015).

HA is a glycosaminoglycan, it is noted to be a potential targeting agent. It has selective affinity to bind to CD44 receptors on the surface of breast cancer cells (Negi et al., 2012, Zafar et al., 2014).

The cytotoxicity effect of various bare and surface modified RES-NLCs was examined on MCF-10A, MCF-7 and MDAMB-231 cell lines (Table 4-4). The influence on the cell viability was studied over a series of concentration of both RES and RES-NLCs (1- 50 µg/mL) for 24, 48 and 72 h. Both RES and surface modified RE-NLC-GTO formulations appended with different ligands, exhibited concentration and time dependant increase in the anticancer effects and demonstrated significant effect on the cell viability.

RES-NLC-GTO-HA showed higher cytotoxicity (2.4 fold than RES-NLC-GTO-PEGS40) in MDAMB-231 cells (Figure 4-15) as compared to MCF-7 (Figure 4-14) at 72 h (Negi et al., 2012). This could be attributed to the high expression of CD44 receptors on MDAMB-231 (79.6%) and being more aggressive breast cancer tumour cell line as compared to 15.1% occurring in the surface of MCF-7 cell lines, these results were in correlation with other previous reports (Olsson et al., 2011).

RES-NLC-GTO-PEGS40-HAFA showed 2.7 folds higher cytotoxicity in MCF-7 and 3.6 fold higher cytotoxicity in MDAMB-231 as compared to RES-NLC-GTO-PEGS40. The dual targeted formulation was also found to be 1.8 folds higher cytotoxicity in MCF-7 and 2.32 fold higher cytotoxicity as compared to the free drug at 72 h. The increased anti-proliferative effect of the dual ligand appended RES-NLC, could probably be attributed to double receptor targeting of CD44 and folate receptors overexpressed on breast cancer cell lines, similar results were observed by previous studies (Ulbrich et al., 2011).

RES-NLC-GTO-PEGS40, RES-NLC-GTO-PEGS40-HA, RES-NLC-GTO-PEGS40-FA and RES-NLC-GTO-PEGS40-HAFA displayed 10.2, 20, 9.7, 25 fold lower cytotoxicity than the free drug on the healthy MCF-10A, clearly confirming the safety of these formulation the non-tumorigenic cells (Figure 4-13). Appending HA to the surface of RES-NLCs contributed significantly to the improved safety of the formulation, this could be attributed to biodegradability, biocompatibility and non-immunogenic nature of HA which improved the safety profile of the nanoparticles (Zafar et al., 2014).

Table 4-4. IC50 values for surface modified RES-NLCs after treatment of MCF-10A, MCF-7, MDAMB-231 and RAW 264.7 cell lines with different concentrations at different time points (n=3 ± SD)

Treatment	Exposure time (h)	IC_{50} value for MCF-10A	IC_{50} value for MCF-7	IC_{50} value for MDAMB-231	IC_{50} value for RAW 264.7
RES	24	12.61 ± 1.081	140.6 ± 1.388	140.5 ± 1.337	N/A
	48	4.745 ± 1.121	14.95 ± 1.108	79 ± 1.151	N/A
	72	3.712 ± 1.089	18.71 ± 1.092	31.31 ± 1.048	N/A
RES-NLC-GTO	24	81.26 ± 1.172	64.33 ± 1.096	79.53 ± 1.121	54.51 ± 1.123
	48	61.71 ± 1.386	13.6 ± 1.056	29.96 ± 1.014	N/A
	72	102.8 ± 1.224	11.36 ± 1.041	22.06 ± 1.019	N/A
RES-NLC-GTO-PEGS40	24	42.95 ± 1.160	128.9 ±1.264	123 ± 1.254	102.1 ± 1.265
	48	37.96 ± 1.053	22.64 ±1.188	59.41 ± 1.171	N/A
	72	29.22 ± 1.080	27.21 ± 1.036	52.26 ± 1.127	N/A
RES-NLC-GTO-PEGS40-HA	24	65.95 ± 1.114	254.9 ± 1.320	169.5 ± 1.333	489.8 ± 1.341
	48	111.3 ± 1.189	94.26 ±1.165	46.79±1.310	N/A
	72	76.82 ± 1.115	30.47 ± 1.023	21.41 ± 1.046	N/A
RES-NLC-GTO-PEGS40-FA	24	32.28 ± 1.054	229.9 ±1.325	105.7 ± 1.130	N/A
	48	25.27 ± 1.094	64.01 ± 1.338	63.49 ± 1.060	N/A
	72	36.34 ± 1.178	30.75 ± 1.023	27.06 ± 1.072	N/A
RES-NLC-GTO-PEGS40-HAFA	24	81.7 ± 1.377	34.19 ± 1.117	127.9 ± 1.136	97.48 ± 1.193
	48	114.7±1.177	15.46 ± 1.193	46.26 ± 1.059	N/A
	72	95.22±1.162	10.28 ± 1.0817	14.19±1.055	N/A

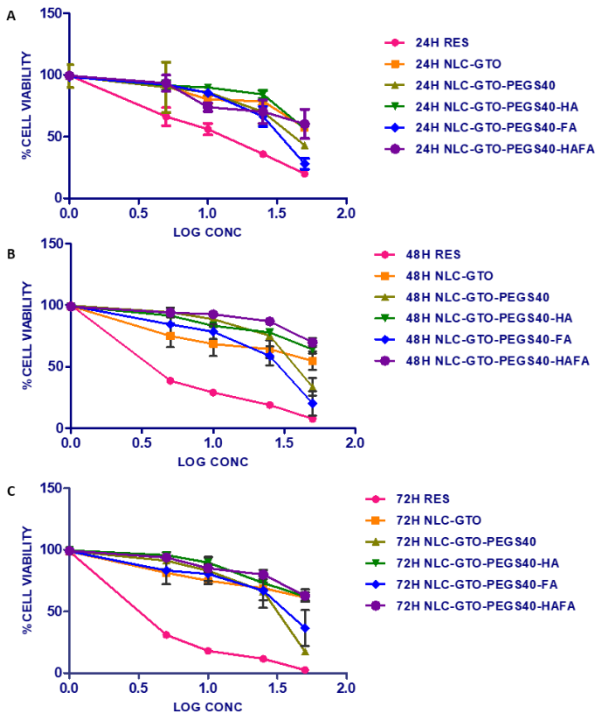

Figure 4-13. Concentration-dependent cytotoxicity of free RES and surface modified RES-NLCs in MCF-10A cell lines for A. 24 h, B. 48 h and C. 72 h (n=3 ± SD)

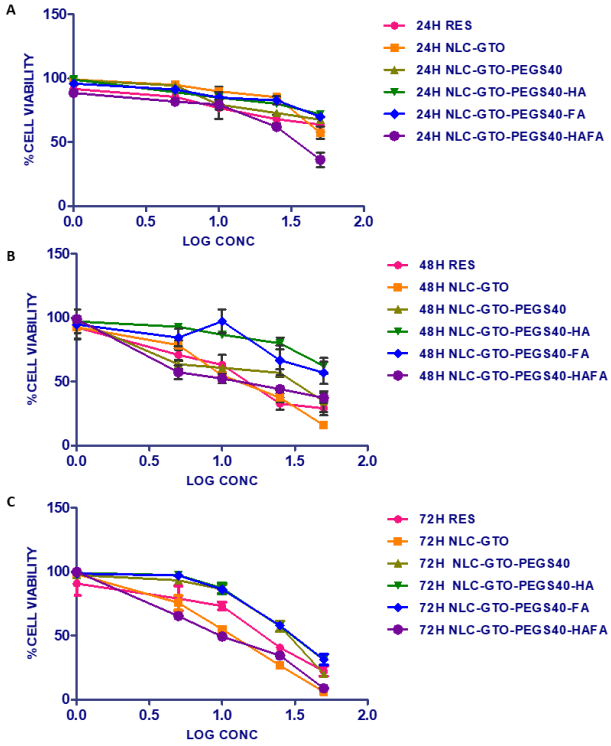

Figure 4-14. Concentration-dependent cytotoxicity of free RES and surface modified RES-NLCs in MCF-7 cell lines for A. 24 h, B. 48 h and C. 72 h (n=3 ± SD)

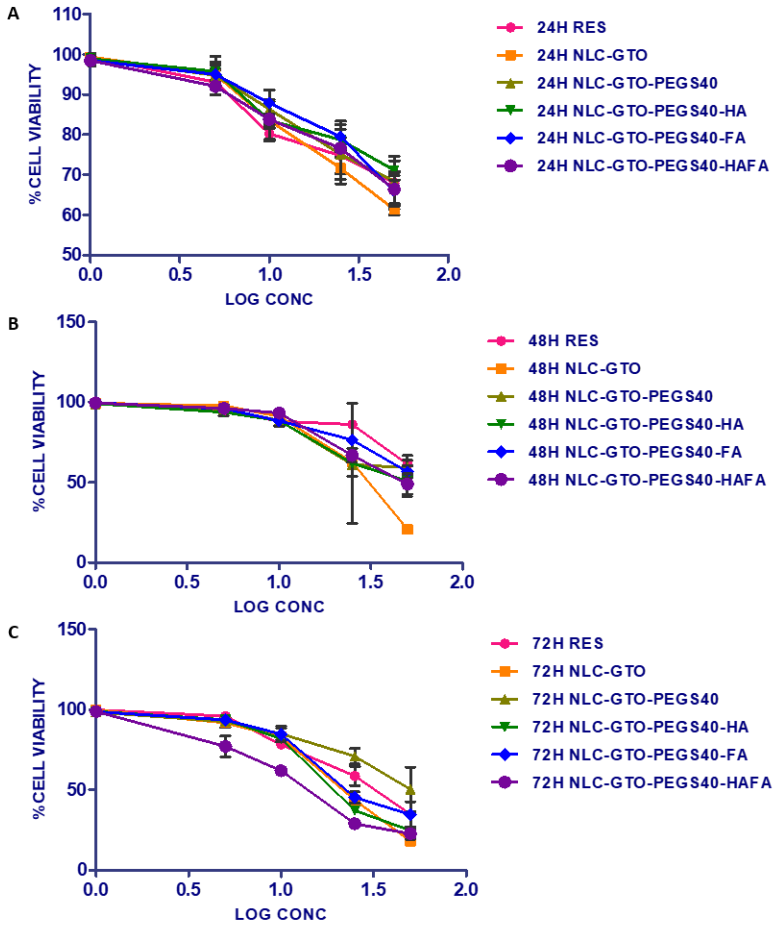

Figure 4-15. Concentration-dependent cytotoxicity of free RES and surface modified RES-NLCs in MDAMB-231 cell lines for A. 24 h, B. 48 h and C. 72 h (n=3 ± SD)

4.4.3 Cellular uptake studies

In order to exert the anticancer effect it is important that the NLCs get internalized by the tumour cells and release RES inside them (Wang et al., 2014c). Endocytosis is crucial for the appropriate signalling, delivery of nutrients into the cell and regulation of surface receptors on the cells. The uptake of nanoparticles occur primarily via the interaction with the plasma membrane. The endocytosis pathway has been classified according to the proteins which play a role in the process (Dutta and Donaldson, 2012). To understand the internalization and the mechanism of uptake of the bare and the surface modified RES-NLC formulations, the cellular uptake was studied by both flow-cytometry and fluorescence microscopy in the four cell lines namely; MCF-7, MDAMB-231, MCF10A and RAW 246.7 cell lines.

4.4.3 (I) Cellular uptake of bare RES-NLCs in MCF-7 and MDAMB-231 cell lines

In order to study the cellular uptake of six selected RES-NLCs, the fluorescently labelled RES-NLCs with fluorescent marker coumarin-6 (C6) were used. Cellular uptake of six selected RES-NLCs was investigated on both cancer cells MCF-7 and MDAMB-231 cell lines at three different time points viz. 30 min, 1, and 4 h, to understand the effect of liquid lipid on the cellular uptake of NLCs.

Cellular uptake of all six RES-NLCs have shown a time dependent trend where the maximum uptake was observed after 1 h incubation which was sufficient for the entry of nanoparticles into MCF-7 cell lines (Figure 4-16). Increased incubation of nanoparticles up to 4 h showed no further increase in the fluorescence intensities. These results are in accordance to previous report that 0.5-2 h incubation with fluorescent nanoparticles is sufficient to achieve the maximal uptake of NLCs (Sun et al., 2013). As higher uptake of nanoparticles was revealed at a lower concentration of nanoparticles (much lower than the IC_{50} of the formulations), indicating that increasing the incubation time and the concentration might lead to the saturation of the receptor-mediated endocytosis process, thus hindering further uptake of nanoparticles (Shao et al., 2009).

Although, RES-NLCs exhibited the highest uptake after 1 h of incubation, the effect of six different liquid lipids was evident in difference in the fluorescence intensities of the six RES-NLC formulations. The highest fluorescence intensity was observed with RES-NLC-GTO followed by RES-NLC-GTC, RES-NLC-PCG, RES-NLC-PGML, RES-NLC-PGMC and RES-NLC-DO. The different in the cellular uptake in MCF-7 cells might be attributed to the type of liquid lipid used in the nanoparticle fabrication, thus, influencing the antitumor effect. This observation is in accordance to a recent report demonstrating the effect of liquid lipids on the cellular uptake of nanoparticles (Safwat et al., 2017). The rapid rate and high amount of uptake of RES-NLCs might be attributed to the particle size of nanoparticles (< 100 nm) (Gratton et al., 2008, Baek et al., 2012).

Further, qualitative determination of cellular uptake of the six RES-NLCs in MC-7 cell lines was carried out using fluorescence microscopy. It is clearly obvious from the images of nanoparticles incubated at 37^{o}C for 1h that C6-RES-NLCs were mostly confined around the cell nucleus in the cytoplasm of the cell. Thus, microscopy data have confirmed the flow-cytometry results for the higher cellular uptake of RES-NLCs.

Upon observation of free coumarin uptake under fluorescence microscopy it has shown very low fluorescence indicating that the coumarin-6 detected in the cells is mainly related with the C6-RES-NLCs. This demonstrates the efficiency of RES-NLCs as carriers to deliver RES into MCF-7 cells, which

could be a contributor to the enhanced antitumor efficacy previously demonstrated in the anti-proliferative studies (Figure 4-16. B).

Cellular uptake of RES-NLCs in MDAMB-231 cell lines also showed maximum uptake was at 1h as observed in MCF-7 (Figure 4-17). However, the order of fluorescence intensity of RES-NLCs was different than that observed in MCF-7 cells. RES-NLC-GTO showed the highest fluorescence followed by RES-NLC-D0, RES-NLC-PGML, RES-NLC-GTC, RES-NLC-PGMC and RES-NLC-PCG. The hydrophobicity of GTO could be a determinant for its higher cellular uptake. Surface hydrophobicity is an important determinant for the nanoparticles interaction with the lipid membrane. Hydrophobic nanoparticles display high affinity to the cell membrane compared to hydrophilic ones. The least cellular uptake of RES-NLC-PCG could be due to the hydrophilic nature of the PEGylated liquid lipid (PGC). Hydrophilic PEG modified nanoparticles, suppress the interaction with the lipid bilayer membrane of cells, thus reducing the cellular uptake (Daou et al., 2009).

MCF-7 cells showed almost two fold higher uptake of RES-NLCs than that observed in MDAMB-231.This might be attributed to the aggressive nature of the tumor and the resistance to the nanoparticle uptake. These results goes in line with the results obtained from the *in vitro* cytotoxicity studies demonstrating better sensitivity of MCF-7 cell lines to the nanoparticles as compared to MDAMB-231 cells. This might be possible due to the rapid and higher uptake in MCF-7 than MDAMB-231 cells. Fluorescence images of free dye uptake by MDAMB-231 cells showed very low green intensity, confirming that the green fluorescence is due to uptake RES-NLCs (Figure 4-17. B).

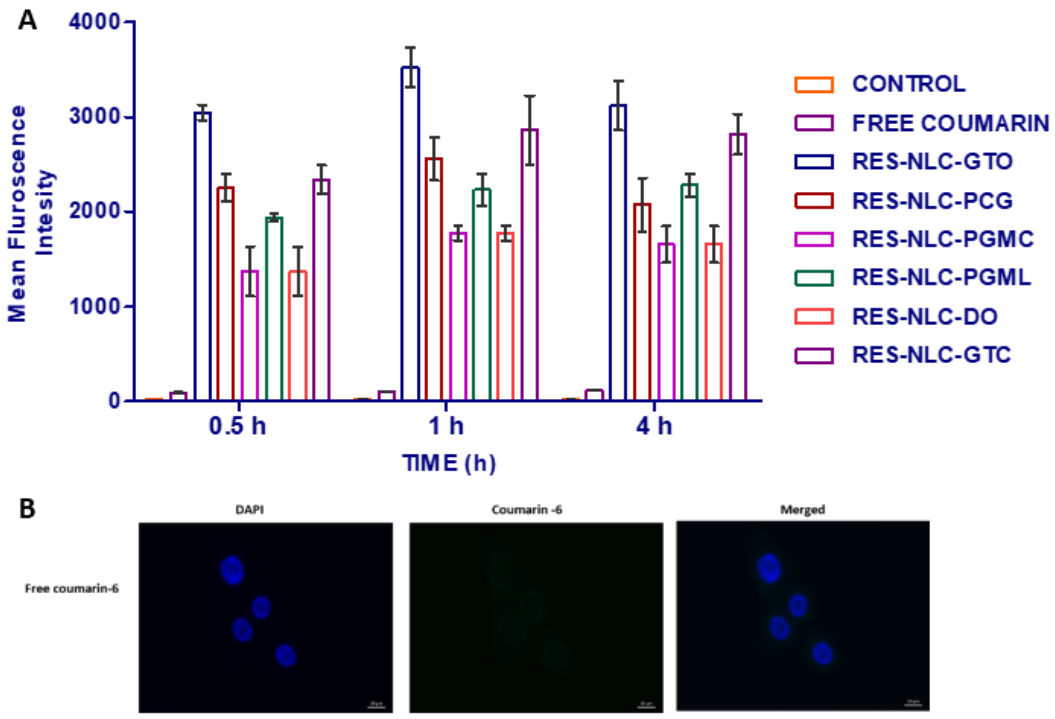

Figure 4-16. A. Cellular uptake of RES-NLCs in MCF-7 after 30 min, 1h and 4 h incubation B. Fluorescence microscopic images of MCF-7 cells incubated with free coumarin-6 at 37^{o}C for 1 h, showing very low green fluorescence. The blue colour represents the DAPI nuclear stain, Green colour of free coumarin-6 dye and the merged image of both DAPI and Coumarin-6. Data shown are mean ± SD (n = 3). Scale bar 10 µm

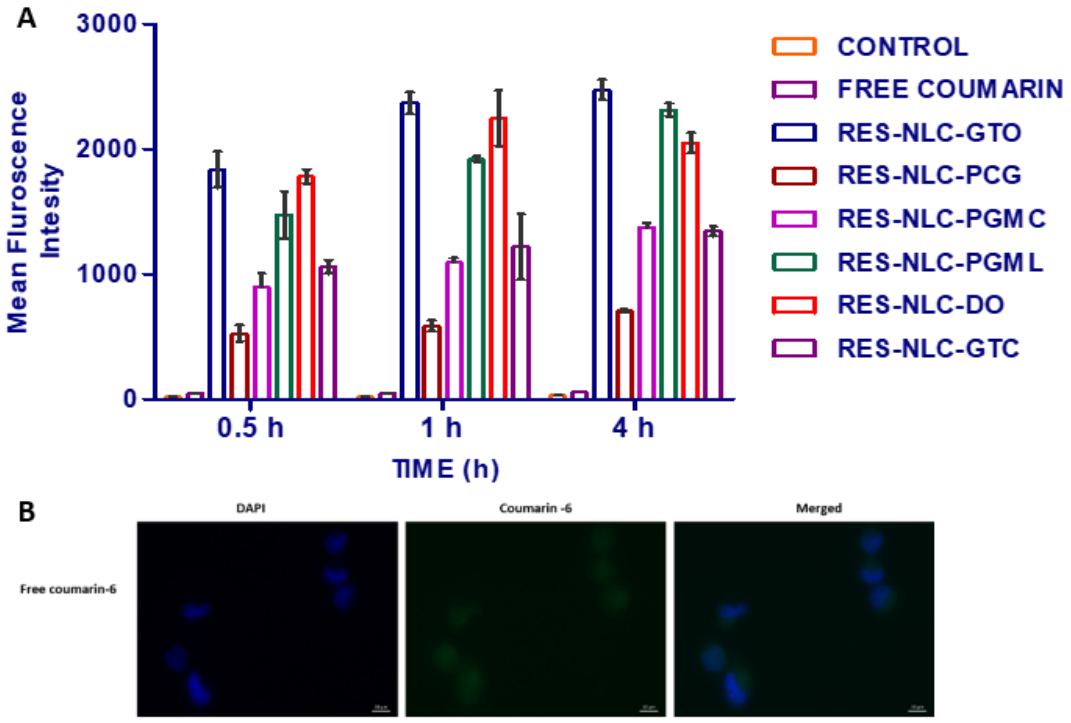

Figure 4-17. A. Cellular uptake of RES-NLCs in MDAMB-231 after 30 min, 1h and 4 h incubation B. Fluorescence microscopic images MDAMB-231 cells incubated with free coumarin-6 at 37^{o}C for 1 h, showing very low green fluorescence. The blue colour represents the DAPI nuclear stain, Green colour of free coumarin-6 dye and the merged image of both DAPI and Coumarin-6. Data shown are mean ± SD (n = 3). Scale bar 10 µm

4.4.3 (II) Cellular uptake of surface modified RES-NLCs in MCF-7 and MDAMB-231 cell lines

One the main advantages of nano-range drug delivery systems is their ability to promote enhanced permeability and retention (EPR) effect into the tumour site. EPR effect is caused by the formation of abnormal blood vessels, which in turn increase the vascular permeability to the tumour site, resulting in the creation of large spaces between the cells and a poor lymphatic drainage. This will limit the clearance of nanoparticles from the cancer site eventually enhancing their retention inside the tumour cells allowing the nanoparticles to release the drug to exert the respective anticancer effect (Fang et al., 2011, Maeda, 2015). However, making use of the passive targeting through the EPR effect is not enough to achieve extensive clinical effect (Nehoff et al., 2014). Thus, the development of new

approaches that allow active targeting to a specific cancer cell are of interest for improved efficacy and targetability (Bertrand et al., 2014).

The active targeting strategy involves the surface modification with specific ligand that binds to tumour cells and enables the effective delivery of the nanocarriers. Various targets are overexpressed at high levels by the cancer cells with lower expression in the neighbouring healthy cells. Ligands promotes the delivery of nanoparticles through a specific interaction with the cell surface (Sakhrani and Padh, 2013, Noble et al., 2014). Active targeting of cancer cells by promoting the interaction between the ligand and the specific cell, overcome the physiological barriers and allow the accumulation, cellular internalization and eventually the delivery of nanoparticle into the tumour cells (Bae and Park, 2011).

Dual receptors targeting, is a novel approach for targeted drug delivery, which can efficiently and selectively target NLCs to tumor cells (Saul et al., 2006, Ying et al., 2010). In this study, HA was selected due to its specific targeting to the tumor cells through the binding to CD44 receptor and further surface modified with FA to target the folate receptors expressed on the surface of both MCF-7 and MDAMB-231 cells thus achieving double receptor targeting (Liu et al., 2011, Maiolino et al., 2015).

Surface modification of RES-NLCs resulted in a maximum cellular uptake after 1 h of incubation in MCF-7 (Figure 4-18. A) and MDAMB-231 cells (Figure 4-18. B). The fluorescence intensity of the functionalized nanoparticles were almost 3 fold higher as compared to the bare RES-NLCs, similar results were observed by the study done by Xia et al (Xia et al., 2017). However, upon the comparison of the fluorescence intensity post functionalization, it has been noted that the PEGylated RES-NLC-GTO-PEGS40 and the three surface modified RES-NLC-GTO-PEGS40-HA, RES-NLC-GTO-PEGS40-FA and RES-NLC-GTO-PEGS40-HAFA didn't show any significant difference in their uptake ($p > 0.05$) (Ulbrich et al., 2011). PEGylation of RES-NLC-GTO with PEGS40 facilitated the cellular uptake of nanoparticles (Yamazaki and Ito T., 1990 , Baek et al., 2015). The cellular uptake of surface modified RES-NLCs (RES-NLC-GTO-HA, RES-NLC-GTO-FA and RES-NLC-GTO-HAFA) targeted toward both the receptors folate and transmembrane glycoprotein CD44 receptors that has strong affinity to bind to FA and HA in both the cell lines (MCF-7 and MDAMB-231), these results were in accordance to results shown by Qhattal (Qhattal and Liu, 2011), thus facilitating improved cellular uptake as compared to the bare RES-NLC-GTO, various reports showed similar outcomes (Youm et al., 2014, Maiolino et al., 2015, Necela et al., 2015, Basakran, 2015, Paulmurugan et al., 2016).

Though, all the surface functionalized nanoparticles showed almost equal cellular uptake, however, the advantage of the dual HAFA appended RES-NLC is distinctly evident by its higher cytotoxicity in both MCF-7 and MDAMB-231 as observed in the anti-proliferative study (Liu et al., 2014b).

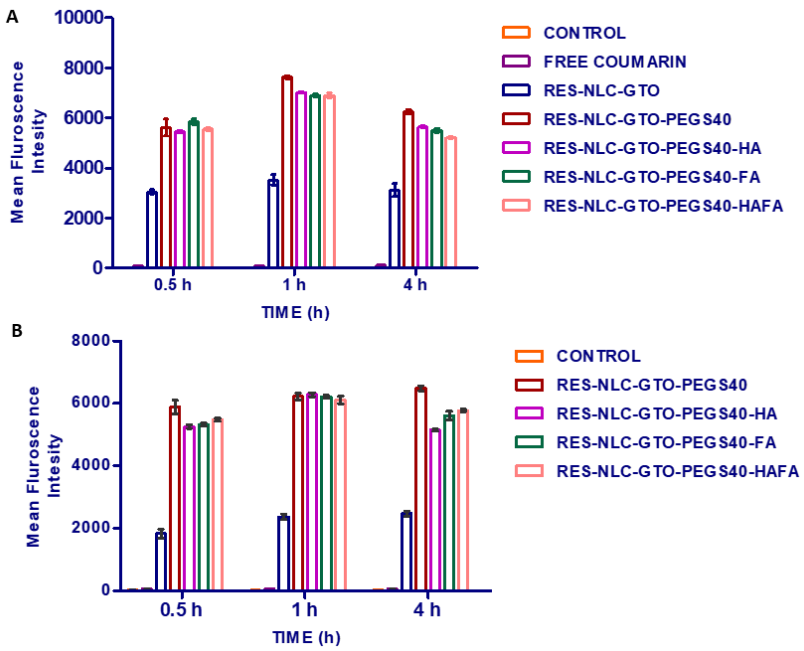

Figure 4-18. Quantitative cellular uptake of Surface modified RES-NLCs in A. MCF-7 and B. MDAMB-231 cell lines with incubation period of 30 min, 1h and 4 h. Data shown are mean ± SD (n = 3)

4.4.3 (III) Cellular uptake of RES-NLCs in MCF-10A and RAW 246.7 cell lines

Cellular uptake of various RES-NLCs in healthy MCF-10A cells was investigated in order to determine the amount of RES-NLCs taken up by MCF-10A cell lines. In this study MCF-10A cells were treated with various C6-RES-NLCs at 37^{o}C for 1 h (maximum uptake of RES-NLCs by MCF-7 and MDAMB-231 cells) and the fluorescence intensity was measured by both flow-cytometry and confirmed by fluorescence microscopy.

RES-NLC-PCG, RES-NLC-DO and RES-NLC-PGML showed the highest uptake by MCF-10A cells (

Figure **4-19**. A). Whereas, RES-NLC-GTO, RES-NLC-PGMC and RES-NLC-GTC demonstrated lowest uptake by MCF-10A cell lines, making them as a good choice to be used as an effective carrier of RES to the breast cancer cells, since their uptake in MCF-10A cells was lower as compared to the uptake in cancer cells.

On the other hand, ligand appended nanoparticles resulted in the lowest uptake by these cells when compared to the bare RES-NL-GTO (figure 4-19.B). The cellular uptake of the surface modified RES-NLCs was almost 3-3.5 folds less than the uptake observed in the cancer cells. This might be attributed to the alteration in the surface properties of the nanoparticles by HA and FA offering better targetability

toward the cancer cells, thus, reducing the toxicity to these cells as similarly demonstrated by other studies (Sakhrani and Padh, 2013, Noble et al., 2014).

Moreover, upon observation of cells under fluorescence microscope (Figure 4-20 andFigure **4-21**), it was noted that the fluorescence intensity s after incubation for 1h with bare and surface modified RES-NLC was much lower in MCF-10A cell than that observed with MCF-7 and MDAMB-231 cells, confirming the results obtained from flow-cytometry. There was a negligible fluorescence intensity when coumarin-6 was incubated with MCF-10A cells, confirming that the fluorescence is due to nanoparticles and not the free dye (Figure 4-20).

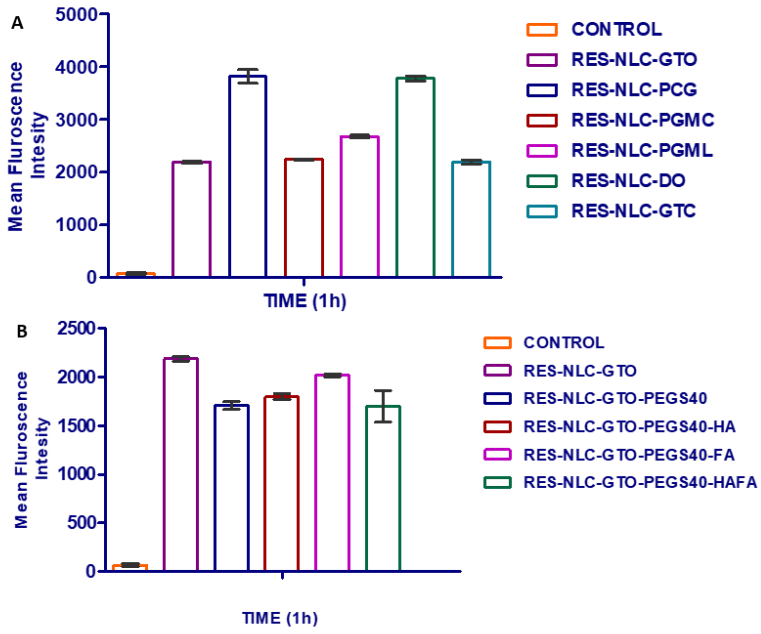

Figure 4-19. Quantitative cellular uptake of A. bare RES-NLCS and B. Surface modified RES-NLCs in MCF-10A cell lines after 1 h incubation period. Data shown are mean ± SD (n = 3)

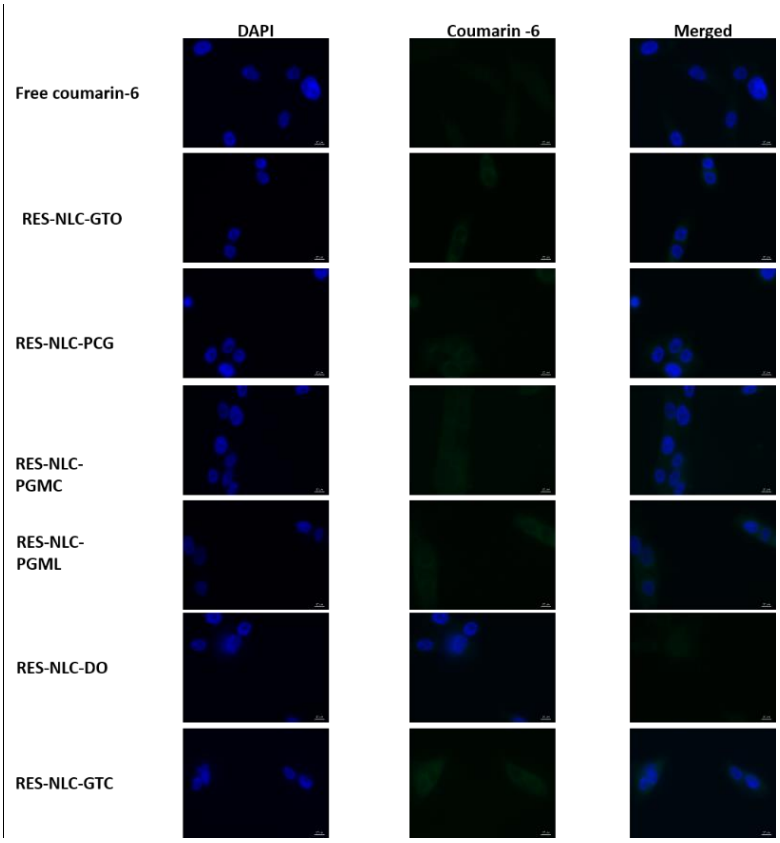

Figure 4-20. Fluorescence microscopy images of RES-NLCs after 1 h incubation with MCF-10A cell lines. The blue colour represents the DAPI nuclear stain, Green colour of coumarin-6 dye in RES-NLCs and the merged image of both DAPI and Coumarin-6. Scale bar 10 µm

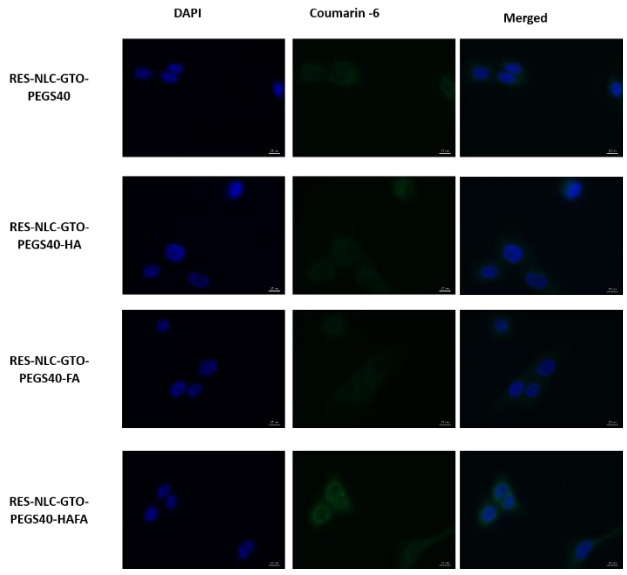

Figure 4-21. Fluorescence microscopy images of surface modified RES-NLCs after 1 h incubation with MCF-10A cell lines. The blue colour represents the DAPI nuclear stain, Green colour of coumarin-6 dye in RES-NLCs and the merged image of both DAPI and Coumarin-6. Scale bar 10 µm

Opsonisation by plasma proteins (opsonin) and clearance by the reticuloendothelial system is the main limitation associated with nanoparticles, leading to poor tumour targeting (Salmaso and Caliceti, 2013). Cellular uptake through macrophages was carried out on RAW 264.7 cell lines, to determine the ability of nanoparticles to be engulfed by macrophages. The uptake by the phagocytic cells is undesired effect as it results in the elimination of nanoparticles from the blood circulation. Six RES-NLCs, PEGylated RES-NLC and three surface modified RES-NLCs were tested for their uptake in macrophages using flow-cytometry.

RES-NLCs were subjected to a very low macrophage uptake after 1 h incubation when compared to their uptake by cancer cells. This was evident from the low fluorescence intensities, with the highest intensity shown by RES-NLC-PCG (Figure 4-22. A), suggesting a high uptake of these NLCs by macrophage once the nanoparticles are available in the blood circulation.

On the other hand, the PEGylated and the functionalized nanoparticles with various ligands avoided the uptake as was seen by the decrease in the fluorescence intensities (Figure 4-22.B) (Siafaka et al., 2016a). Nanoparticles coating with a neutral hydrophilic surface layer called stealth coating using polyethylene glycol (PEG) and the hydrophilic ligand; hyaluronic acid impart hydrophilicity to the NLCs surface, thus having diminutive effect on its cellular uptake by macrophages . PEG shield is the most frequently utilized method to prolong the circulation time and enhance the ability to escape from endosomes this is attributed to the fact that macrophages doesn't express any receptors for PEG covering the nanoparticles, various studies obtained similar results (Jokerst et al., 2011, Yu et al., 2012, Doktorovova et al., 2014). Even though, PEGylation increases the blood circulation of NLCs, by producing a steric barrier preventing the adsorption by opsonin and reducing the recognition of target cells by antibodies on the PEGylated nanoparticles surface (Banerjee et al., 2012).

Hyaluronic acid renders the surface of nanoparticles more hydrophilic, therefore, protect the nanoparticles from elimination and providing nanoparticles with a longer circulation time. RES-NLC-PEGS40-FA did not show any significant difference ($p< 0.05$) in uptake by macrophages when compared to the bare RES-NLCs. While, dual nanoparticles functionalized with both HA and FA demonstrated the lowest cellular uptake by macrophages. The reduced uptake of functionalized nanoparticles might be due to the negative charge on the surface of RES-NLCs causing a repulsion with the negatively charged cell membrane, thus causing a reduction in the adherence to the membrane of the phagocytic cells (Olbrich et al., 2004). Bare (Figure 4-23), PEGylated and three surface modified RES-NLCs (Figure 4-24) showed very low fluorescence upon visualization under fluorescence microscope, indicating the low cellular uptake in macrophages and confirming the results obtained for the flow-cytometry.

There was a negligible fluorescence intensity when coumarin-6 was incubated with RAW 246.7 cells, and observed under florescence microscope confirming that the fluorescence is due to nanoparticles and not the free dye (Figure 4-23).

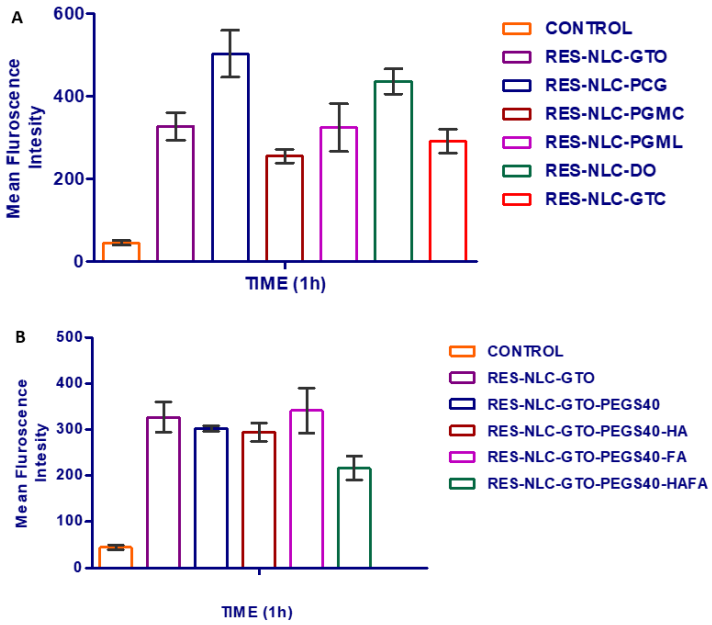

Figure 4-22. Quantitative cellular uptake of A. bare RES-NLCS and B. Surface modified RES-NLCs in RAW 264.7 cell lines after 1 h incubation period. Data shown are mean ± SD (n = 3)

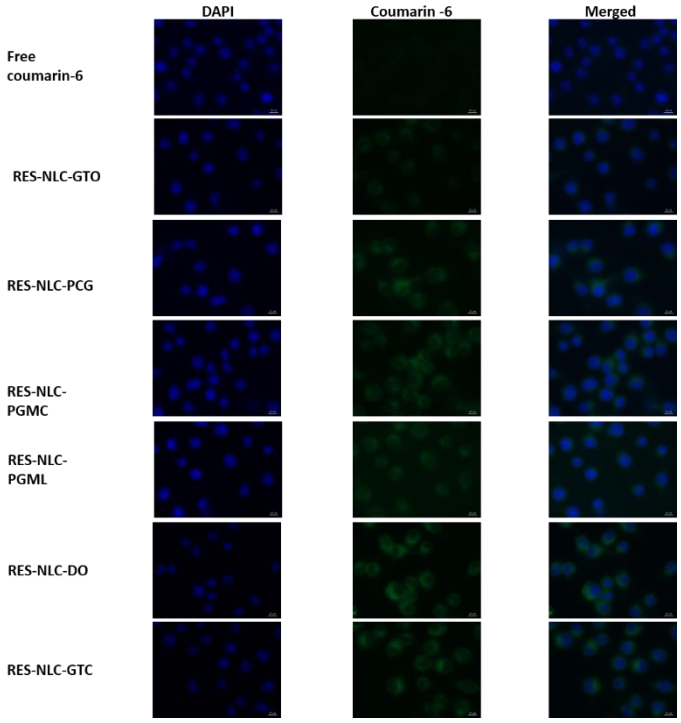

Figure 4-23. Fluorescence microscopy images of RES-NLCs after 1 h incubation with RAW 246.7 cell lines. The blue colour represents the DAPI nuclear stain, Green colour of coumarin-6 dye in RES-NLCs and the merged image of both DAPI and Coumarin-6. Scale bar 10 µm

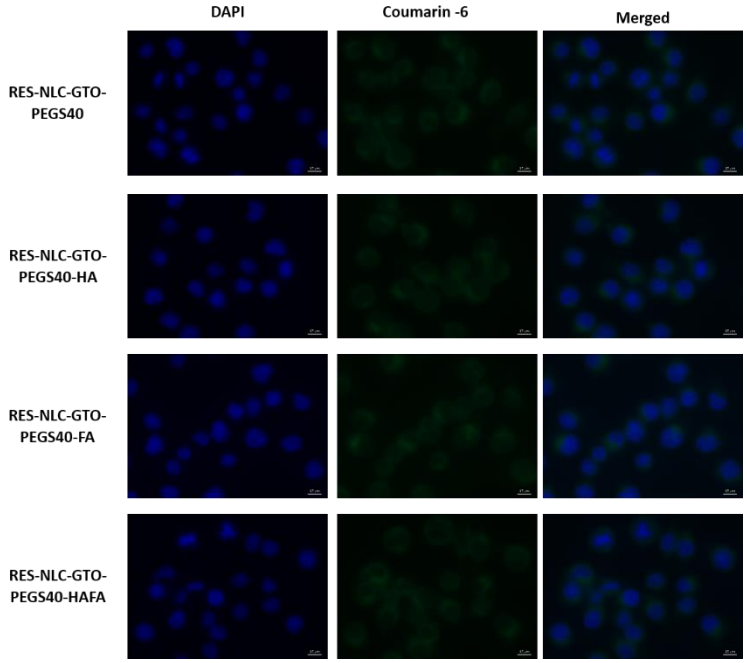

Figure 4-24. Fluorescence microscopy images of surface modified RES-NLCs after 1 h incubation with RAW 246.7 cell lines. The blue colour represents the DAPI nuclear stain, Green colour of coumarin-6 dye in RES-NLCs and the merged image of both DAPI and Coumarin-6. Scale bar 10 µm

4.4.3 (IV) Cellular internalization mechanisms of bare and surface modified RES-NLCs in MCF-7 and MDAMB-231 cell lines

In order to elucidate the endocytosis mechanism and internalisation and trafficking of nanoparticles inside the cells, different pharmacologic inhibitors that block specific endocytotic pathways were employed. Both quantitative and qualitative methods using flow-cytometry and fluorescence microscopy, respectively were utilized to study the effects of different inhibitors on the cellular uptake of bare, PEGylated and three type surface modified RES-NLCs in both MCF-7 and MDAMB-231 cell lines. Endocytosis is an energy dependent uptake mechanism for several extracellular materials. Consequentially, it is blocked after the incubation of cells at low temperature (e.g. 4^{o}C instead of 37^{o}C). Moreover, to assess the role of clathrin in the internalisation of RES-NLCs, incubations with hypertonic sucrose 0.45 M is known to interrupt the formation of clathrin-coated vesicles on the plasma membrane (Kuhn et al., 2014). To further elucidate RES-NLCs cellular uptake via the caveolae or lipid rafts pathway, cells were incubated with nystatin, which is known to disrupt the cholesterol by causing distortion in the structure and function of the cell membrane (Ivanov, 2008, Martins et al., 2012). Endocytosis by phagocytosis (macrophages) or macropinocytosis can be investigated for by treating the cells with cytochalasin B, a strong inhibitor of both phagocytosis/macropinocytosis, by inhibiting the formation of structures that enclose the nanoparticles through depolymerisation of the actin filaments (Dutta and Donaldson, 2012, Oh and Park, 2014).

All bare RES-NLCs cellular uptake studies in MCF-7 (Figure 4-25.A) and MDAMB-231 (Figure 4-26 A) cells showed a good uptake at 37^{o}C. However, the uptake at 4^{o}C was reduced but not completely blocked suggesting the energy dependent process for the uptake of nanoparticles; this was in accordance to various other studies results (Rivolta et al., 2011, Doktorovova et al., 2014). Treatment with nystatin and cytochalasin B did not affect the cellular uptake of nanoparticles indicating that caveolae and macropinocytosis were not involved in the internalization process of nanoparticles.

Upon treatment with hypertonic sucrose all bare RES-NLCs showed a reduction in the fluorescence intensity ($p < 0.05$) suggesting the involvement of clathrin mediated endocytosis in the intracellular trafficking of nanoparticles. A 20-50 % reduction in fluorescence intensities in MCF-7 was observed with different RES-NLCs with the highest reduction demonstrated by RES-NLC-PCG followed by RES-NLC-GTO, RES-NLC-PGMC, RES-NLC-PGML, RES-NLC-GTC and RES-NLC-DO. The difference in the fluorescence intensity might be due to the difference in the liquid lipid nature, which affect the uptake through the cells (Zhang et al., 2013). On the other hand, only 15-30 % reduction in the fluorescence intensity was observed with bare RES-NLC in MDAMB-231 cells and the order of uptake inhibition is as

follow the highest being observed by RES-NLC-PGML followed by RES-NLC-GTC, RES-NLC-DO, RES-NLC-PGMC, RES-NLC-GTO and RES-NLC-PCG. Clathrin mediated uptake of RES-NLCs might be attributed to the small particle size of RES-NLCs that favor their transport via the clathrin pathway, as similarly stated by previous study (Hillaireau and Couvreur, 2009).

Internalisation through clathrin-dependent endocytosis occurs when the clathrin coat on the cell membrane develops invaginations in the membrane resulting in the budding of clathrin coated vesicles and the nanoparticles present on the cell membrane will be trapped inside the vesicles and carried within the cells. Receptor-mediated endocytosis through clathrin-coated pits is the most common pathway of endocytosis. Thus, sucrose inhibit the clathrin resulting in the changes in the structure and function of the formed clathrin pits, where these pits becomes full of small microcages depleting the cytoplasmic clathrin required for the formulation of clathrin pit assembly (Heuser and Anderson, 1989). PEGylated and the three surface modified RES-NLCs in both MCF-7 (Figure 4-25. B) and MDAMB-231 cells (Figure 4-26. B) also demonstrated clathrin dependent endocytosis with almost 20-30 % reduction in the fluorescence intensity when the cells were treated with sucrose.

These results were further supported by the localization of various RES-NLCs in MCF-7 and MDAMB-231 cells employing the qualitative analysis through fluorescence microscopy. Fluorescence images of bare, PEGylated and three surface modified RES-NLCs in both MCF-7 (Figure 4-27,4-28, 4-29, 4-30 and 4-31) and MDAMB-231 (Figure 4-32, 4-33, 4-34, 4-35 and 4-36) cell lines showed a high fluorescence intensity when incubated at 37^{o}C, pretreatment with nystatin and cytochalasin B, while the green fluorescence was very low at 4^{o}C and after hypertonic sucrose treatment suggesting the energy dependent clathrin endocytosis pathway inhibition. Similar results are in conformation with those obtained by flow-cytometric analysis.

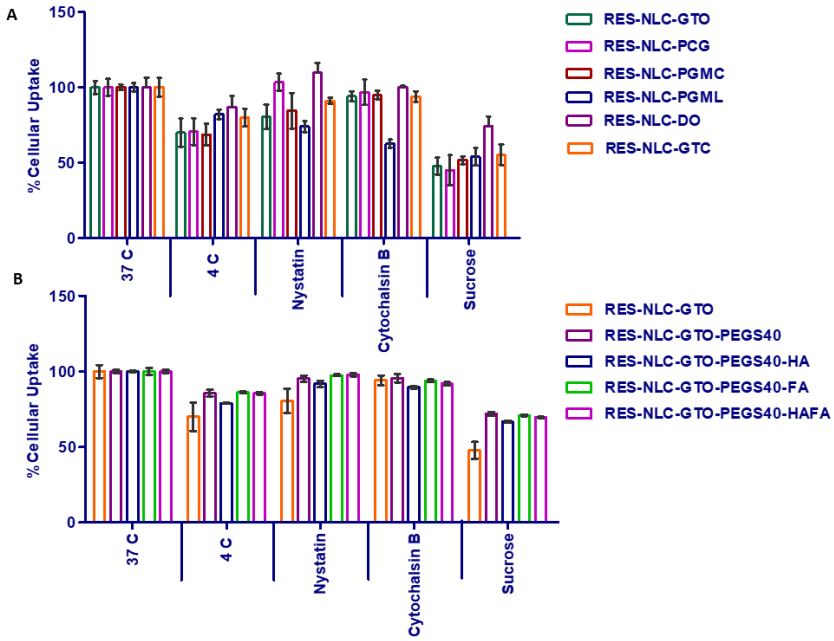

Figure 4-25. Endocytosis mechanisms of A. bare RES-NLCS and B. Surface modified RES-NLCs using various endocytosis pathway inhibitors at 1 h on MCF-7 cells, C. Endocytosis mechanisms of Surface modified RES-NLCs after incubation with excess ligands on MCF-7 cell lines at 1 h. Data shown are mean ± SD (n = 3)

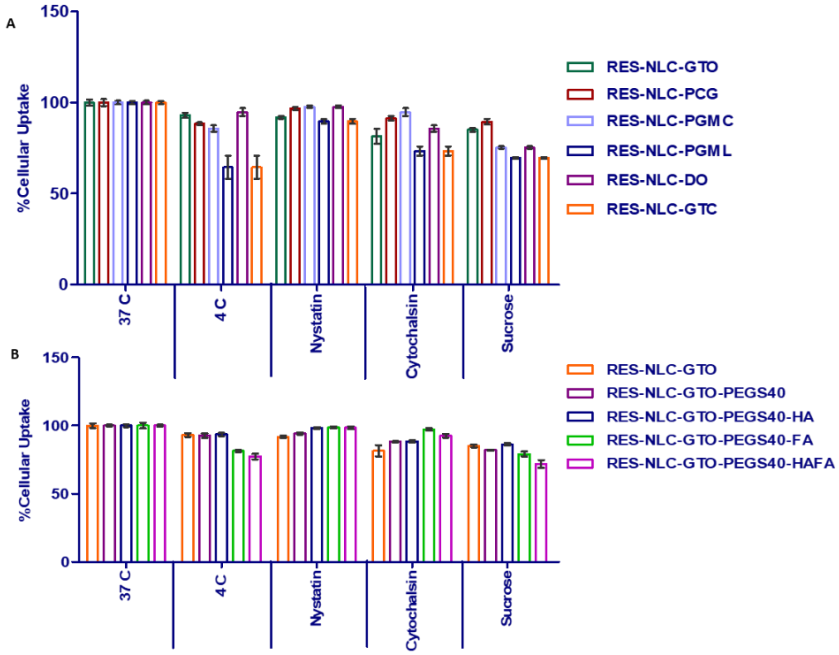

Figure 4-26. Endocytosis mechanisms of A. bare RES-NLCS and B. Surface modified RES-NLCs using various endocytosis pathway inhibitors at 1 h on MDAMB-231 cells, C. Endocytosis mechanisms of Surface modified RES-NLCs after incubation with excess ligands on MDAMB-231 cell lines at 1 h. Data shown are mean ± SD (n = 3)

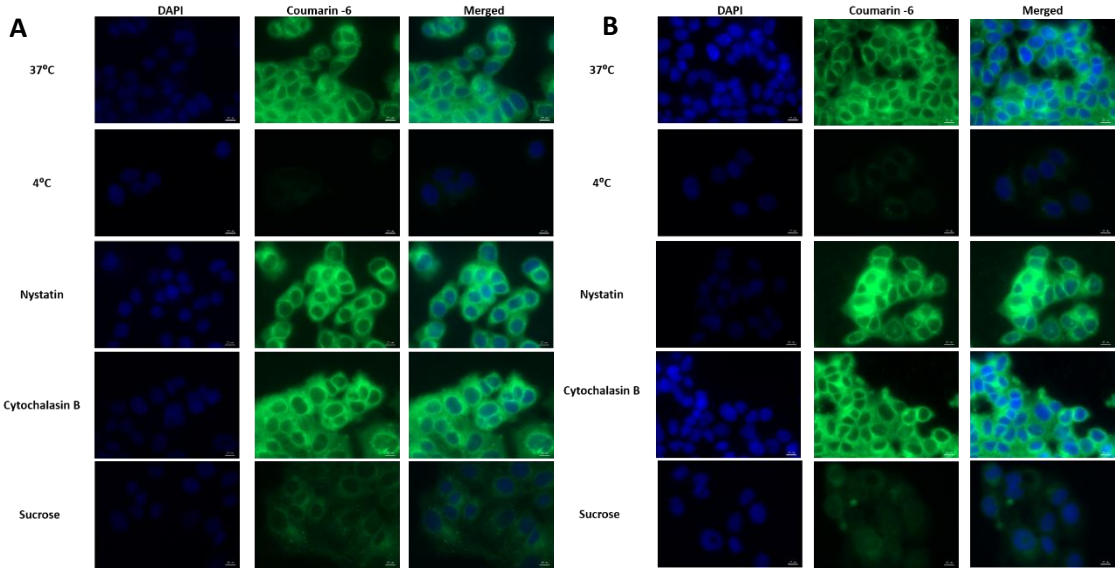

Figure 4-27. Fluorescence microscopy images of MCF-7 cell lines, cells treated with A. C6-RES-NLC-GTO, B. C6-RES-NLC-PCG mechanism of internalization, cells were treated with various endocytosis inhibitors. The blue colour represents the DAPI nuclear stain, Green colour of coumarin-6 dye in RES-NLCs and the merged image of both DAPI and Coumarin-6. Scale bar 10 µm

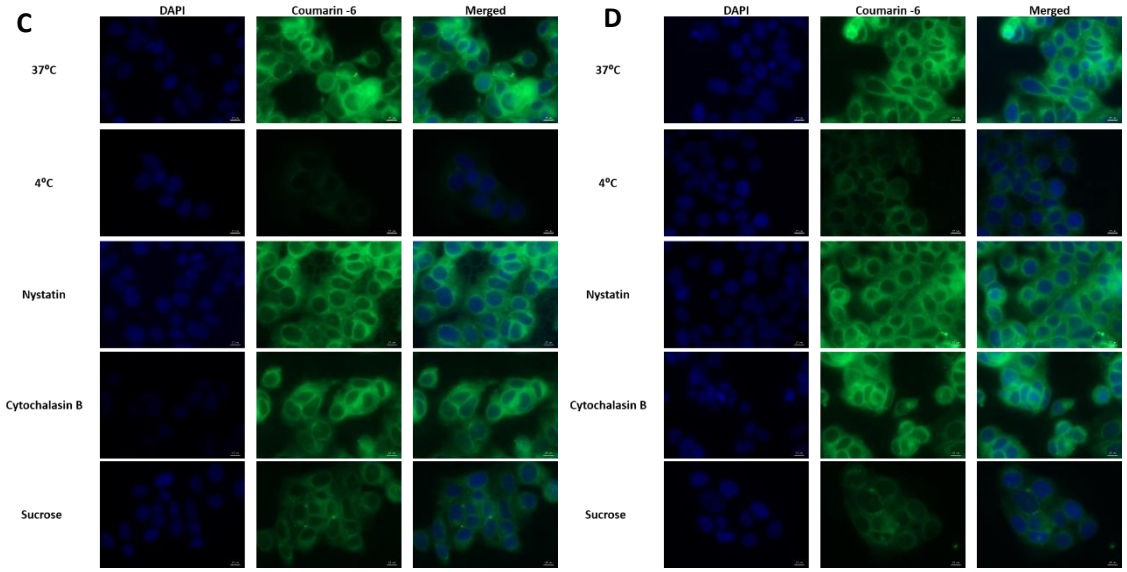

Figure 4-28. Fluorescence microscopy images of MCF-7 cell lines, cells treated with C. C6-RES-NLC-PGMC, D. C6-RES-NLC-PGML mechanism of internalization, cells were treated with various endocytosis inhibitors. The blue colour represents the DAPI nuclear stain, Green colour of coumarin-6 dye in RES-NLCs and the merged image of both DAPI and Coumarin-6. Scale bar 10 µm

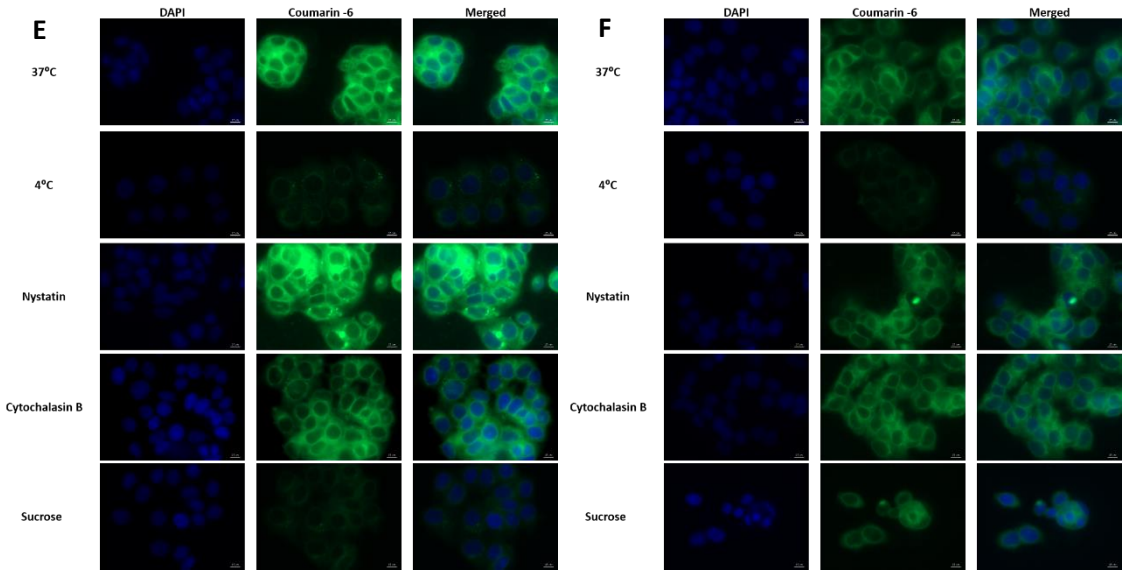

Figure 4-29. Fluorescence microscopy images of MCF-7 cell lines, cells treated with E. C6-RES-NLC-DO, F. C6-RES-NLC-GTC mechanism of internalization, cells were treated with various endocytosis inhibitors. The blue colour represents the DAPI nuclear stain, Green colour of coumarin-6 dye in RES-NLCs and the merged image of both DAPI and Coumarin-6. Scale bar 10 µm

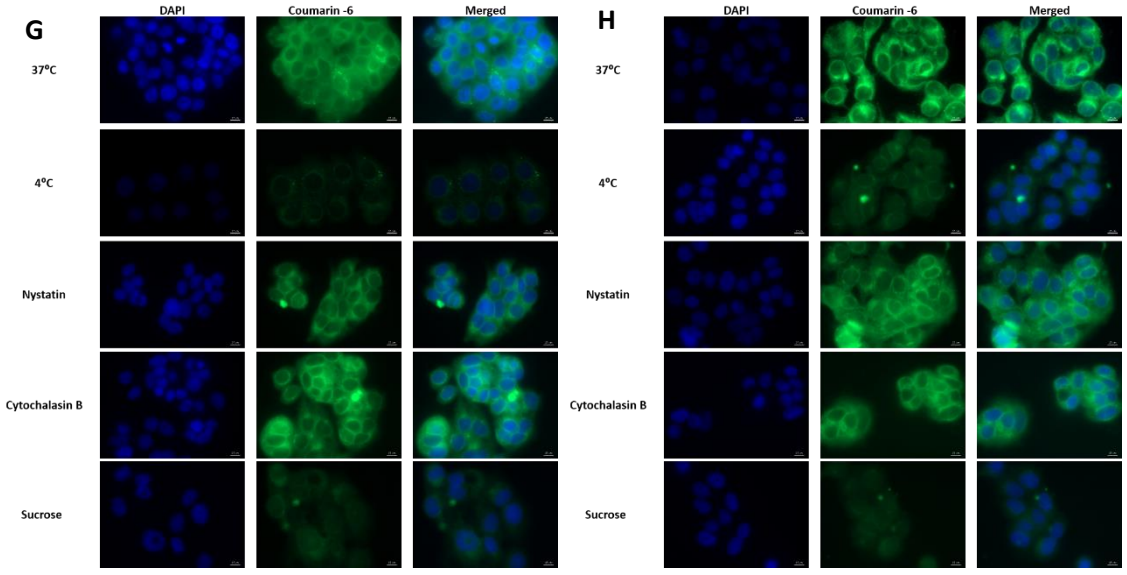

Figure 4-30. Fluorescence microscopy images of MCF-7 cell lines, cells treated with G. C6-RES-NLC- GTO-PEGS40, H. C6-RES-NLC-GTO-PEGS40-HA mechanism of internalization, cells were treated with various endocytosis inhibitors. The blue colour represents the DAPI nuclear stain, Green colour of coumarin-6 dye in RES-NLCs and the merged image of both DAPI and Coumarin-6. Scale bar 10 µm

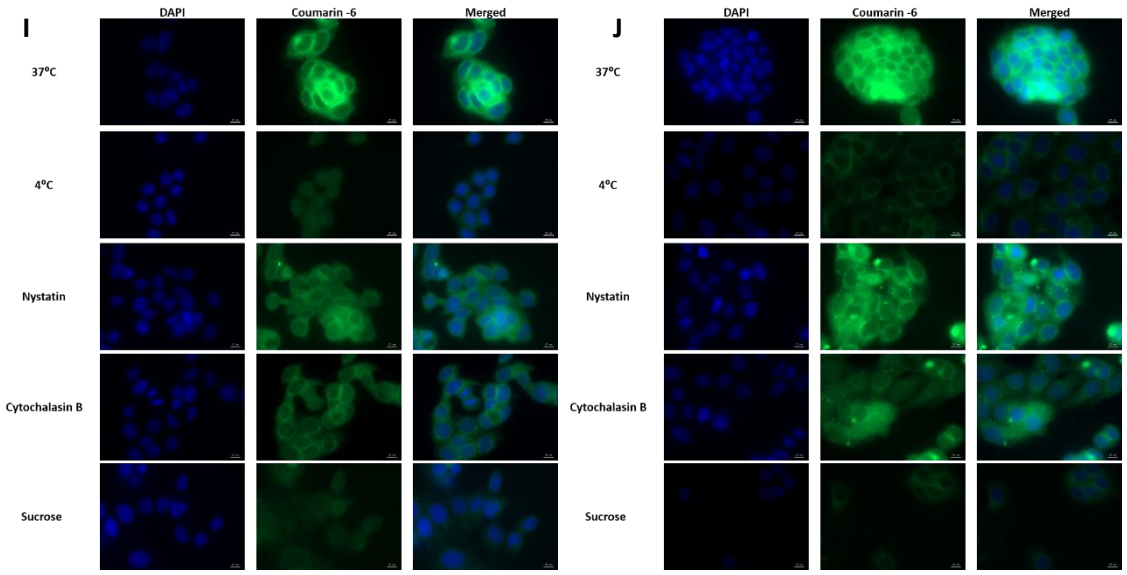

Figure 4-31. Fluorescence microscopy images of MCF-7 cell lines, cells treated with I. C6-RES-NLC-GTO-PEGS40-FA, J. C6-RES-NLC-GTO-PEGS40-HAFA mechanism of internalization, cells were treated with various endocytosis inhibitors. The blue colour represents the DAPI nuclear stain, Green colour of coumarin-6 dye in RES-NLCs and the merged image of both DAPI and Coumarin-6. Scale bar 10 µm

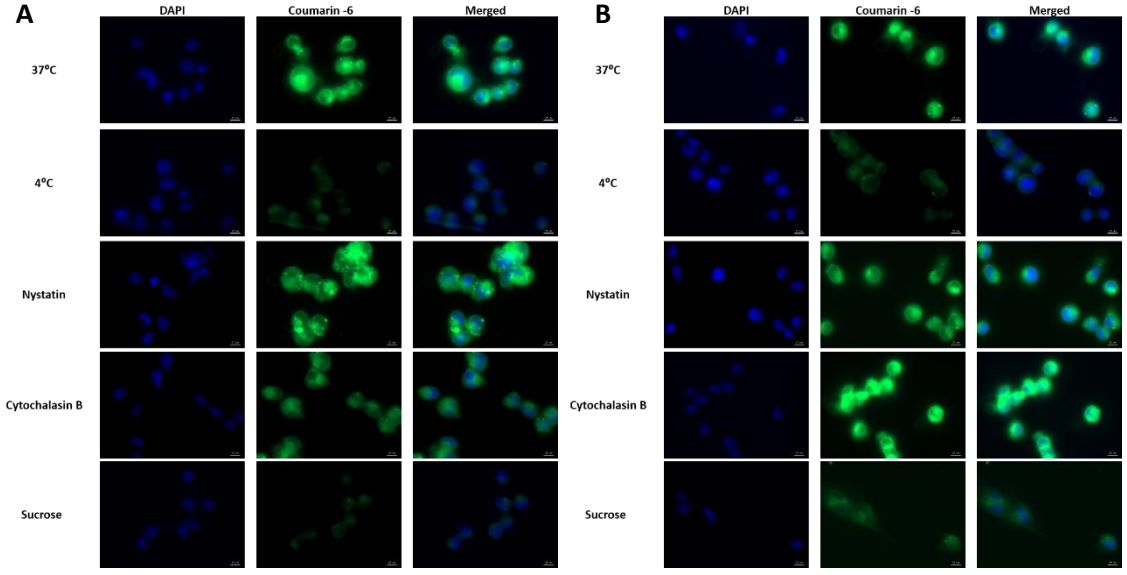

Figure 4-32. Fluorescence microscopy images of MDAMB-231 cell lines, cells treated with A. C6-RES-NLC-GTO, B. C6-RES-NLC-PCG mechanism of internalization, cells were treated with various endocytosis inhibitors. The blue colour represents the DAPI nuclear stain, Green colour of coumarin-6 dye in RES-NLCs and the merged image of both DAPI and Coumarin-6. Scale bar 10 µm

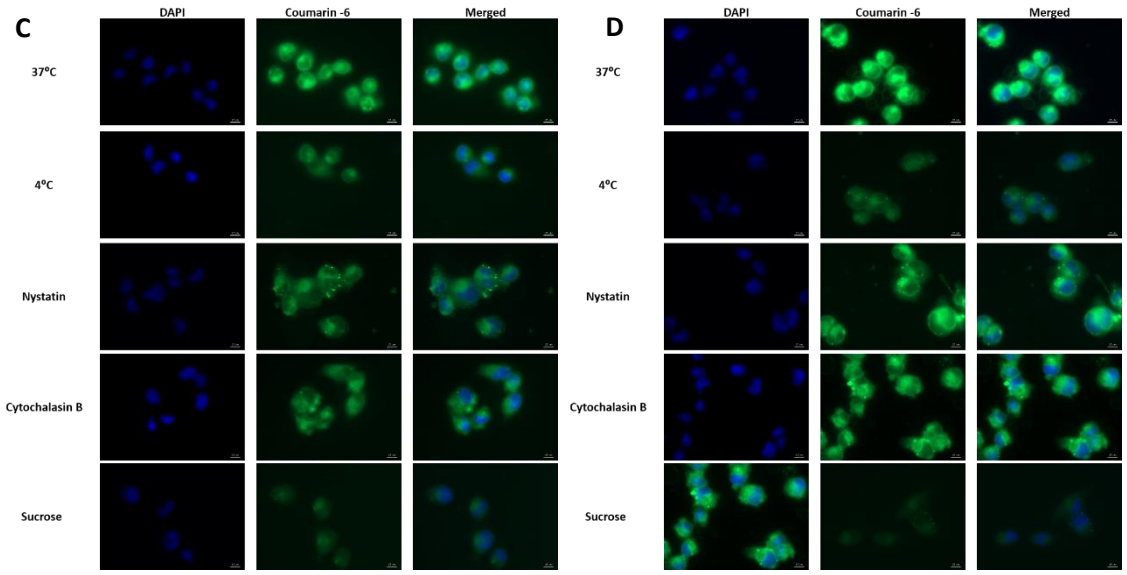

Figure 4-33. Fluorescence microscopy images of MDAMB-231 cell lines, cells treated with C. C6-RES-NLC-PGMC, D. C6-RES-NLC-PGML mechanism of internalization, cells were treated with various endocytosis inhibitors. The blue colour represents the DAPI nuclear stain, Green colour of coumarin-6 dye in RES-NLCs and the merged image of both DAPI and Coumarin-6. Scale bar 10 µm

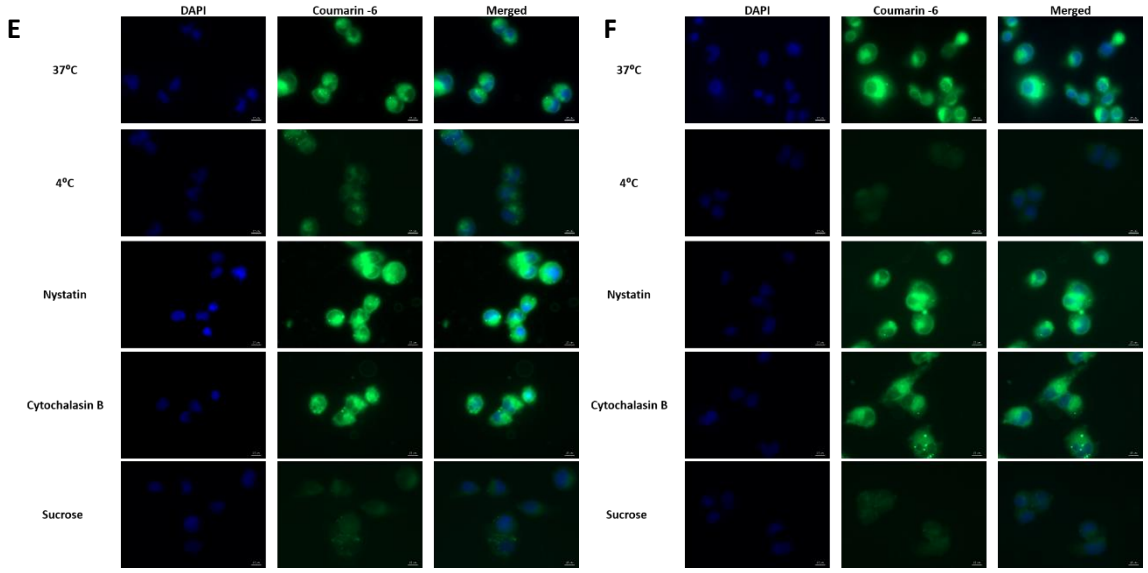

Figure 4-34. Fluorescence microscopy images of MDAMB-231 cell lines, cells treated with E. C6-RES-NLC-DO, F. C6-RES-NLC-GTC mechanism of internalization, cells were treated with various endocytosis inhibitors. The blue colour represents the DAPI nuclear stain, Green colour of coumarin-6 dye in RES-NLCs and the merged image of both DAPI and Coumarin-6. Scale bar 10 µm

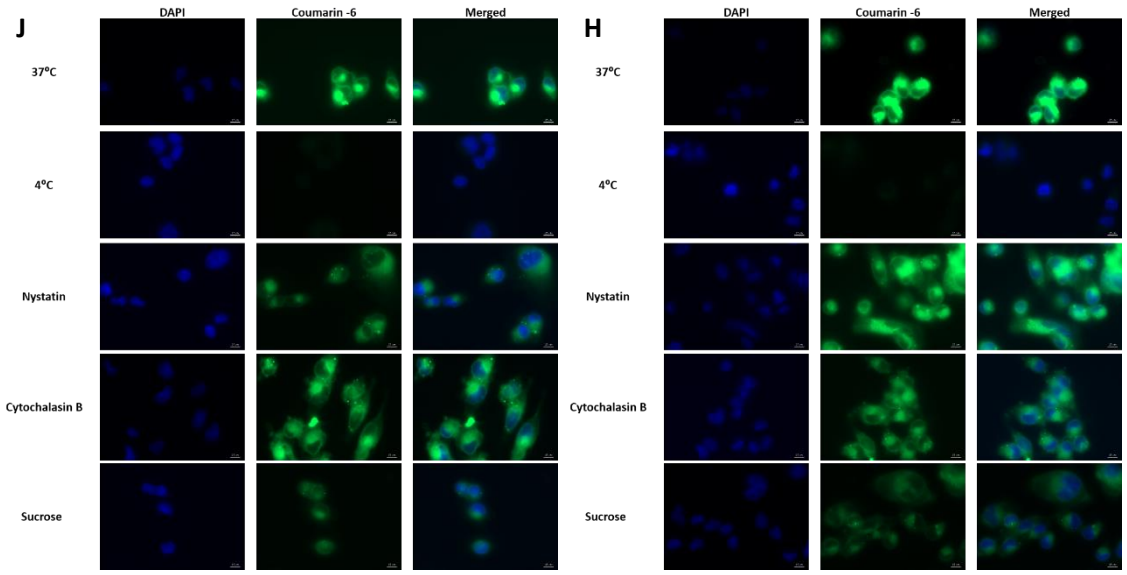

Figure 4-35. Fluorescence microscopy images of MDAMB-231 cell lines, cells treated with G. C6-RES-NLC-GTO-PEGS40, H. C6-RES-NLC-GTO-PEGS40-HA mechanism of internalization, cells were treated with various endocytosis inhibitors. The blue colour represents the DAPI nuclear stain, Green colour of coumarin-6 dye in RES-NLCs and the merged image of both DAPI and Coumarin-6. Scale bar 10 µm

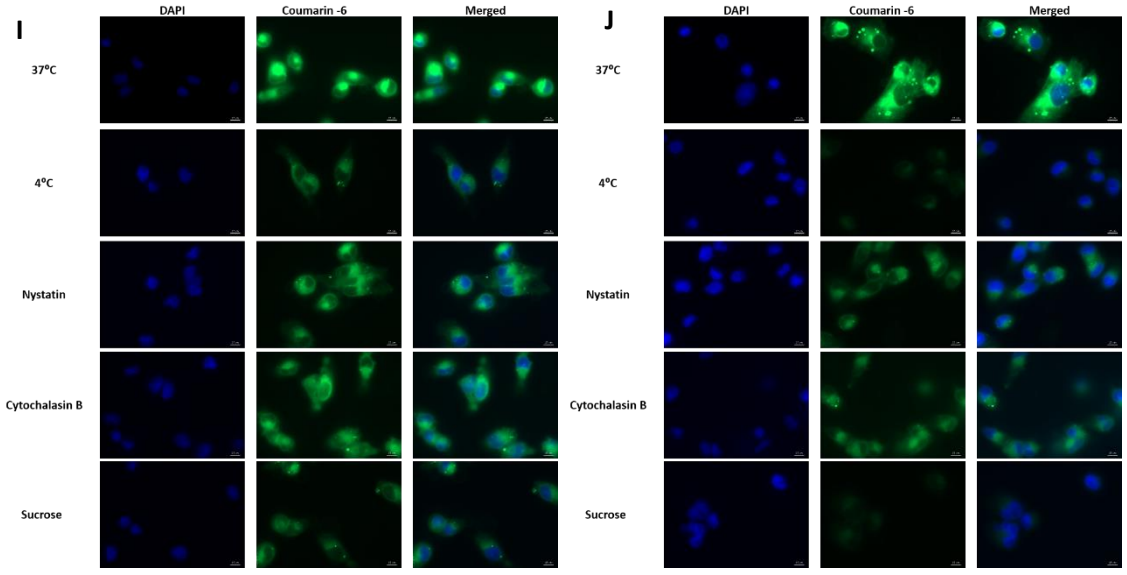

Figure 4-36. Fluorescence microscopy images of MDAMB-231 cell lines, cells treated with I. C6-RES-NLC-GTO-PEGS40-FA, J. C6-RES-NLC-GTO-PEGS40-HAFA mechanism of internalization, cells were treated with various endocytosis inhibitors. The blue colour represents the DAPI nuclear stain, Green colour of coumarin-6 dye in RES-NLCs and the merged image of both DAPI and Coumarin-6. Scale bar 10 µm

4.4.3 (V) Targeting potential of surface modified RES-NLCs

Both cell lines MCF-7 and MDAMB-231 overexpress CD44 receptors that bind to HA and folate receptors that bind FA. In order to test the targeting potential and the selectivity of the individual ligands HA, FA and the dual ligand; HAFA, MCF-7 and MDAMB-231 cells were pre-incubated with excess ligands (HA, FA, HAFA) in order to saturate the receptors on the surface and then treated with their respective surface modified RES-NLCs.

RES-NLC-GTO-PEGS40-HA showed cellular uptake of only 34.2% in MCF-7 cells when pre-treated with excess of HA ligand indicating it selective targeting to CD44 receptors (Figure 4-37. A). Further, to determine the ability of RES-NLC-GTO-PEGS40-HA to target the CD44 receptors on MCF-7 cell lines; cells were incubated with the CD44 antibody, followed by treated with the formulation. For MCF-7 cells it was noted that the cellular uptake was reduced to 67.4 % when compared to the normal uptake of nanoparticles indicating the ability of RES-NLC-GTO-PEGS40-HA nanoparticles to efficiently target the CD44 receptors. This observation was in accordance to previous reports, indicating that the free ligand competed with the ligand appended formulation on the binding to CD44 receptors, various studies demonstrated similar results (Qhattal and Liu, 2011, Zafar et al., 2014).

Similarly after the treatment with excess FA RES-NLC-GTO-PEGS40-FA showed almost 70% reduction in the uptake, indicating folate receptor mediated endocytosis as the main mechanism for cellular uptake (Lee et al., 2016).

RES-NLC-GTO-PEGS40-HAFA targeted the double receptors CD44 and folate as demonstrated by 35.4 % uptake in presence of excess of HAFA in MCF-7 cells. Although, there seemed no distinct differences in the internalization of RES-NLC-GTO-PEGS40-HAFA over RES-NLC-GTO-PEGS40-HA, RES-NLC-GTO-PEGS40-FA as all the three surface modified formulation showed almost similar cellular uptake in the presence of excess ligands. However, RES-NLC-GTO-PEGS40-HAFA has shown improved cytotoxicity as compared to the single ligand appended formulations.

The targetability of RES-NLC-GTO-PEGS40-HA to CD44 receptors expressed on MDAMB-231 (Figure 4-37. B) after excess treatment with HA ligand produced 45.2% reduction in the uptake of the formulation indicating the ability to selectively target CD44 receptors. Moreover, the targeting potential of RES-NLC-GTO-PEGS40-HA towards CD44 receptors was further evaluated by comparing it with the FITC tagged CD44 antibodies. The data demonstrated 43 % reduction in the uptake of RES-NLC-GTO-PEGS40-HA, proving the selective cellular binding and internalization occurring through CD44 receptor interaction, these results were in accordance to various studies (Almalik et al., 2013, Tran et al., 2014, Negi et al., 2015).

On the other hand, pretreatment with excess individual ligand FA showed a lower reduction in the fluorescence intensity (26.3 %). RES-NLC-GTO-PEGS40-HAFA showed higher reduction (51 %) in cellular uptake in presence of excess HAFA ligand, demonstrating the involvement of both the receptors in internalization process.

RES-NLC-GTO-PEGS40-HAFA showed higher concurrent interaction with folate and CD44 receptors on the surface of MDAMB-231 cells as compared to MCF-7 cells.

The internalization of surface modified RES-NLCs was further visualized by fluorescence microscopy. As shown the results agreed with flow-cytometry data. The fluorescence intensity has been reduced when the cells were pretreated with excess free ligand (MCF-7 and MDAMB-231) (Figure 4-38 and Figure **4-39**), which indicate that the surface modification with HA, FA and HAFA enhanced the cellular uptake based on the CD44, FA and CD44 FA receptor mediated internalization, similar results were obtained by Tran et al (Tran et al., 2014).

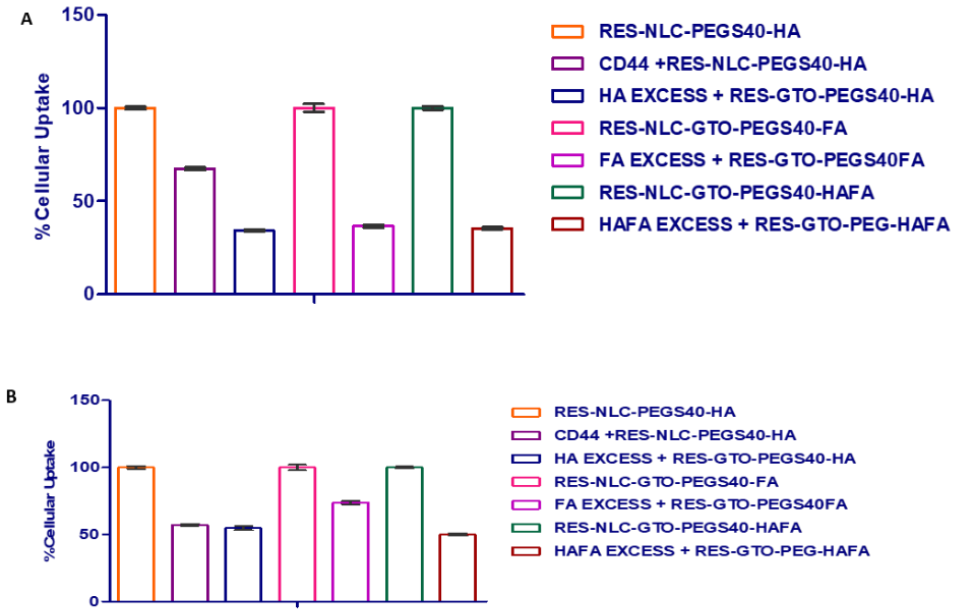

Figure 4-37. Targeting potential of surface modified RES-NLC in A. MCF-7 and B. MDAMB-231 cell lines. Data shown are mean ± SD (n = 3)

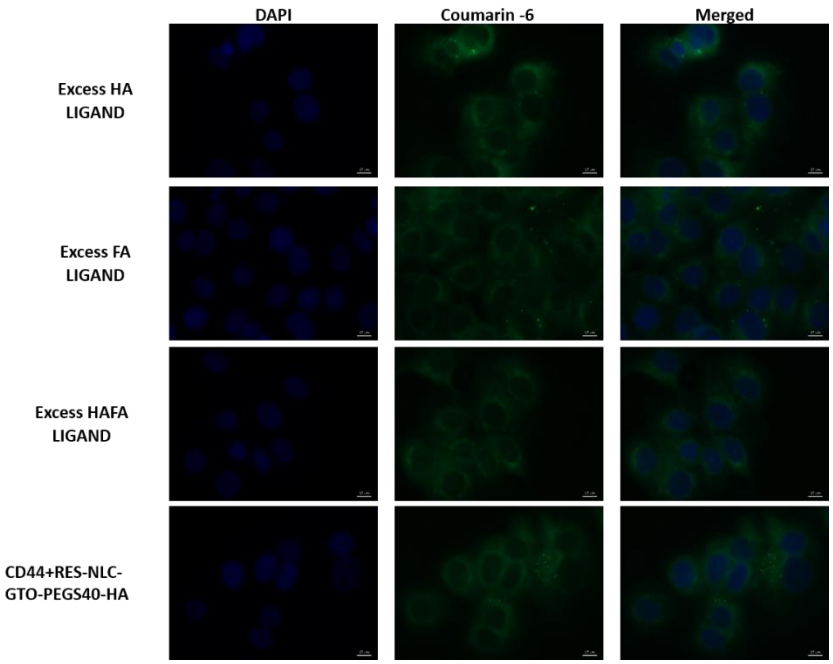

Figure 4-38. Fluorescence microscopy images after treatment of MCF-7 cell lines with excess ligands (HA, FA and HAFA) and CD44 antibody with subsequent addition of RES-NLC-GTO-PEGS40-HA. The blue colour represents the DAPI nuclear stain, Green colour of coumarin-6 dye in RES-NLCs and the merged image of both DAPI and Coumarin-6. Scale bar 10 µm

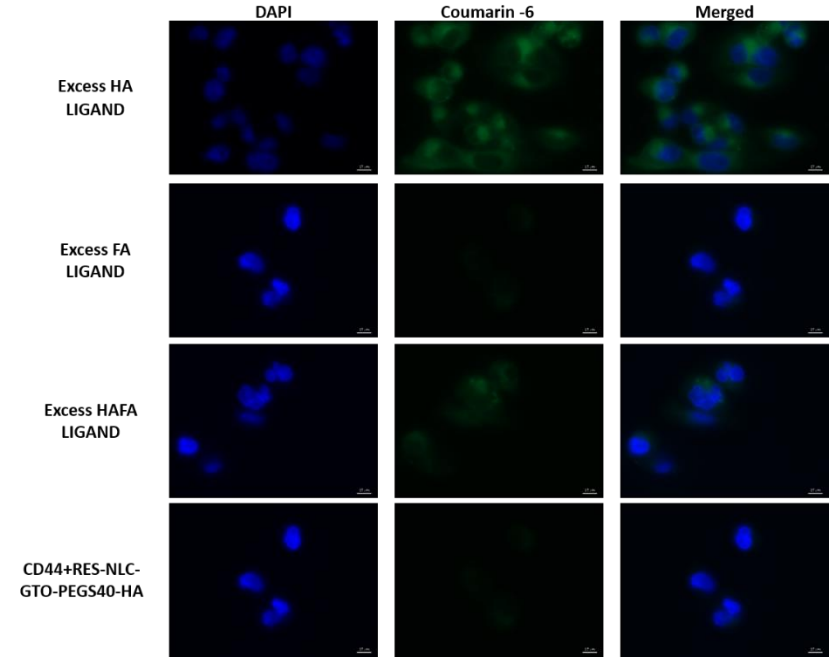

Figure 4-39. Fluorescence microscopy images after treatment of MDAMB-231 cell lines with excess ligands (HA, FA and HAFA) and CD44 antibody with subsequent addition of RES-NLC-GTO-PEGS40-HA. The blue colour represents the DAPI nuclear stain, Green colour of coumarin-6 dye in RES-NLCs and the merged image of both DAPI and Coumarin-6. Scale bar 10 µm

4.4.4 Apoptosis assay

When cells undergo apoptosis this cause a disruption in the integrity of the cell membrane followed by the exposure of phosphatidyl serine. Annexin V conjugated with FITC has a selective affinity toward phosphatidyl serine, based on that early and late apoptotic cells can be identified (Thomas et al., 2016). Therefore, the percentage of cells undergoing apoptosis was investigated using annexin V PI double staining after treatment with RES, bare RES-NLCs, PEGylated and surface modified RES-NLCs for 48 and 72 h. The major role of nanoparticle delivery systems is to cause death of as many cancer cells as possible. The induction of apoptosis was studied on both MCF-7 and MDAMB-231 cell lines.

Treated cells (MCF-7) for 48 h with RES showed 14 % and 47 % in early and late apoptotic stage, respectively, this results were in accordance to Osman study (Osman et al., 2012). On the other hand, when cisplatin was used as a positive control for apoptosis process it has shown only 6 % and 58 % in early and late stages, respectively. However, RES-NLC-GTO, RES-NLC-GTO-PEGS40, RES-NLC-GTO-PEGS40-HA and RES-NLC-GTO-PEGS40-FA showed lower percentage of cells in both early and late apoptosis suggesting the death of cells was induced by necrosis (Figure 4-40. A). RES-NLC-GTO-PEGS40-HAFA showed 69 % of cells in the late apoptosis stage, the presence of high % of apoptosis is indicating that dual ligand appended formulation were successful in targeting both the receptors on MCF-7 cell lines (Bar-Zeev et al., 2017).

Moreover, at 72 h all functionalized RES-NLCs showed movement of cell to the late stage of apoptosis with the highest % produced by RES-NLC-GTO-PEGS40-HAFA showing a better activity than RES (Figure 4-40A). Higher efficacy might be due to the better receptors mediated uptake of the RES-NLC-GTO-PEGS40-HAFA through the cells and thus their greater accumulation in the tumour cells indicating enhanced anticancer effect (Figure 4-41). These results goes in line with the cytotoxicity results which have indicated lower IC_{50} value with the dual appended RES-NLC, this was in correlation to previous studies (Kumar et al., 2014, Sabzichi et al., 2016).

Interestingly, when MDAMB-231 cells were treated with surface modified RES-NLCs it demonstrated highest % of cells in the late stage of apoptosis ranging from 21-55.5 % compared to 19 % produced by RES (Figure 4-40.B). RES-NLCs formulations showed similar trend as observed in MCF-7 cells, with the necrosis as the mechanism of cell death at 48 h of treatment, however, after 72 h incubation almost 50 % of cells were observed in the late apoptosis stage for both the surface modified formulations RES-NLC-GTO-PEGS40-HA and RES-NLC-GTO-PEGS40-FA. While RES-NLC-GTO-PEGS40-HAFA showed 85 %

of cells in late apoptotic stage which was significantly ($P > 0.05$) higher than as observed after treatment with free RES (Figure 4-42).

These findings were consistent with the results observed in the cytotoxicity assay (Ng et al., 2015). The ability of nanoparticles to carry RES and deliver it to the cancer cells, allows RES to exert its apoptosis induction effect through various regulatory mechanisms as stated by Jiang (Jiang et al., 2005).

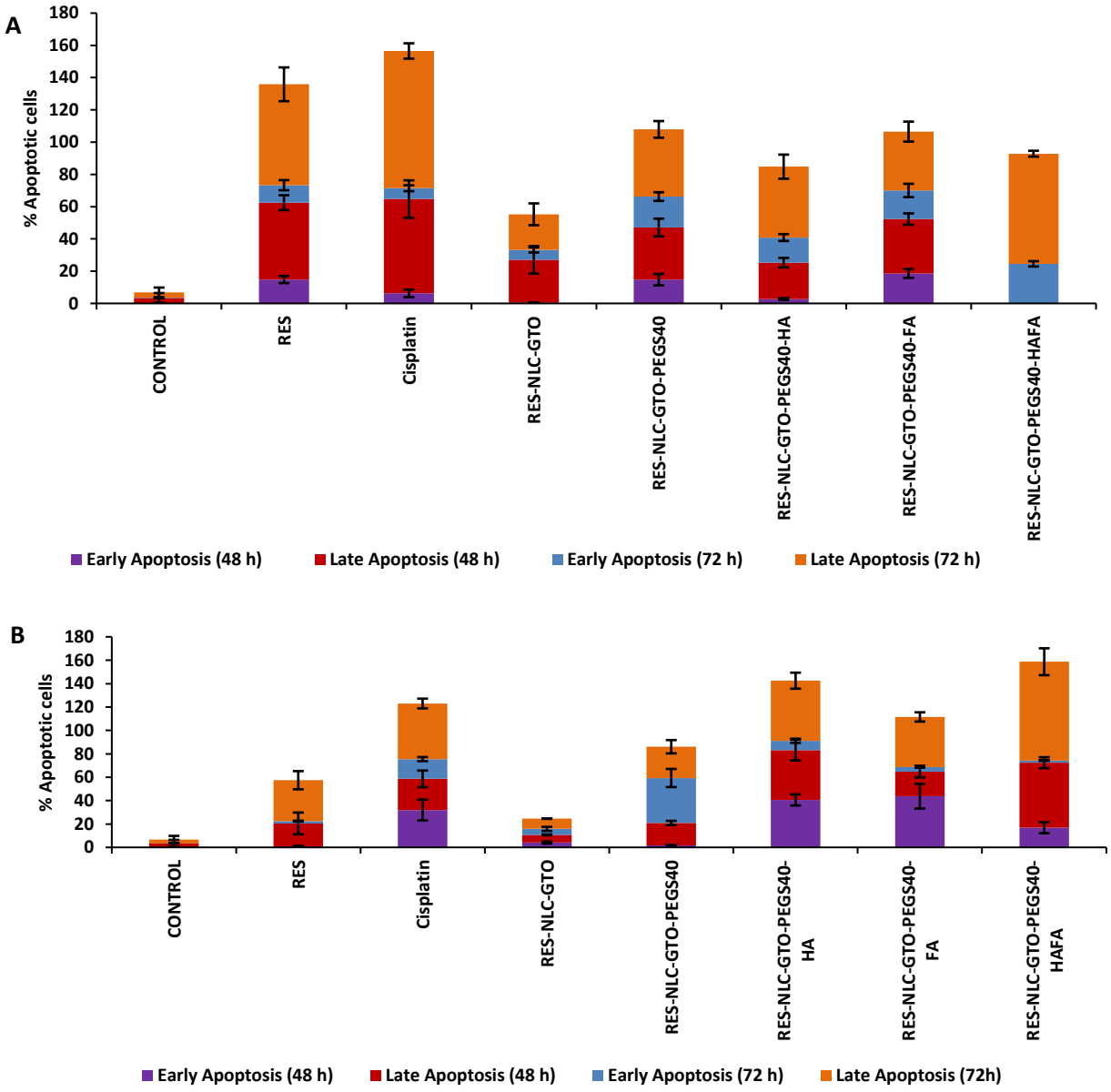

Figure 4-40. Cell apoptosis analysis of A. MCF-7 cells and B. MDAMB-231 by flow-cytometry using Annexin VFITC and PI double stain treated with RES and RES-NLCs for 48 and 72 h. Data shown are mean ± SD (n = 3).

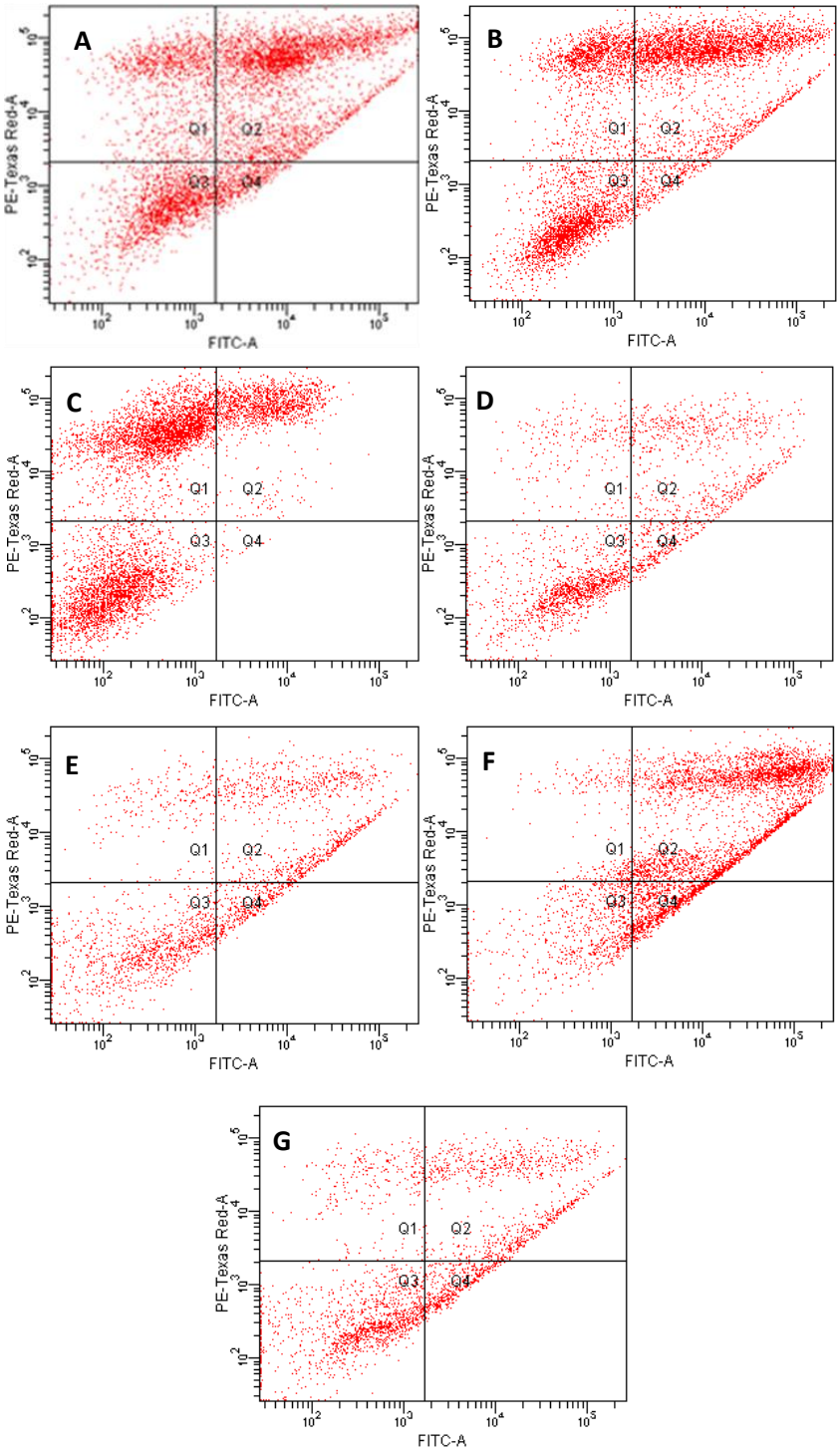

Figure 4-41. Induction of apoptosis by A. RES, B. Cisplatin, C.RES-NLC-GTO, D. RES-NLC-GTO-PEGS40, E. RES-NLC-GTO-PEGS40-HA, F. RES-NLC-GTO-PEGS40-FA and G. RES-NLC-GTO-PEGS40-HAFA on MCF-7 cell lines after 48 h incubation. Four quadrants represent (Q1) necrotic cells annexin (upper left quadrant), (Q2) late apoptotic cells (upper right quadrant), (Q3) viable cells (lower left quadrant) and (Q4) early apoptotic cells (lower right quadrant). Data shown are mean ± SD (n = 3)

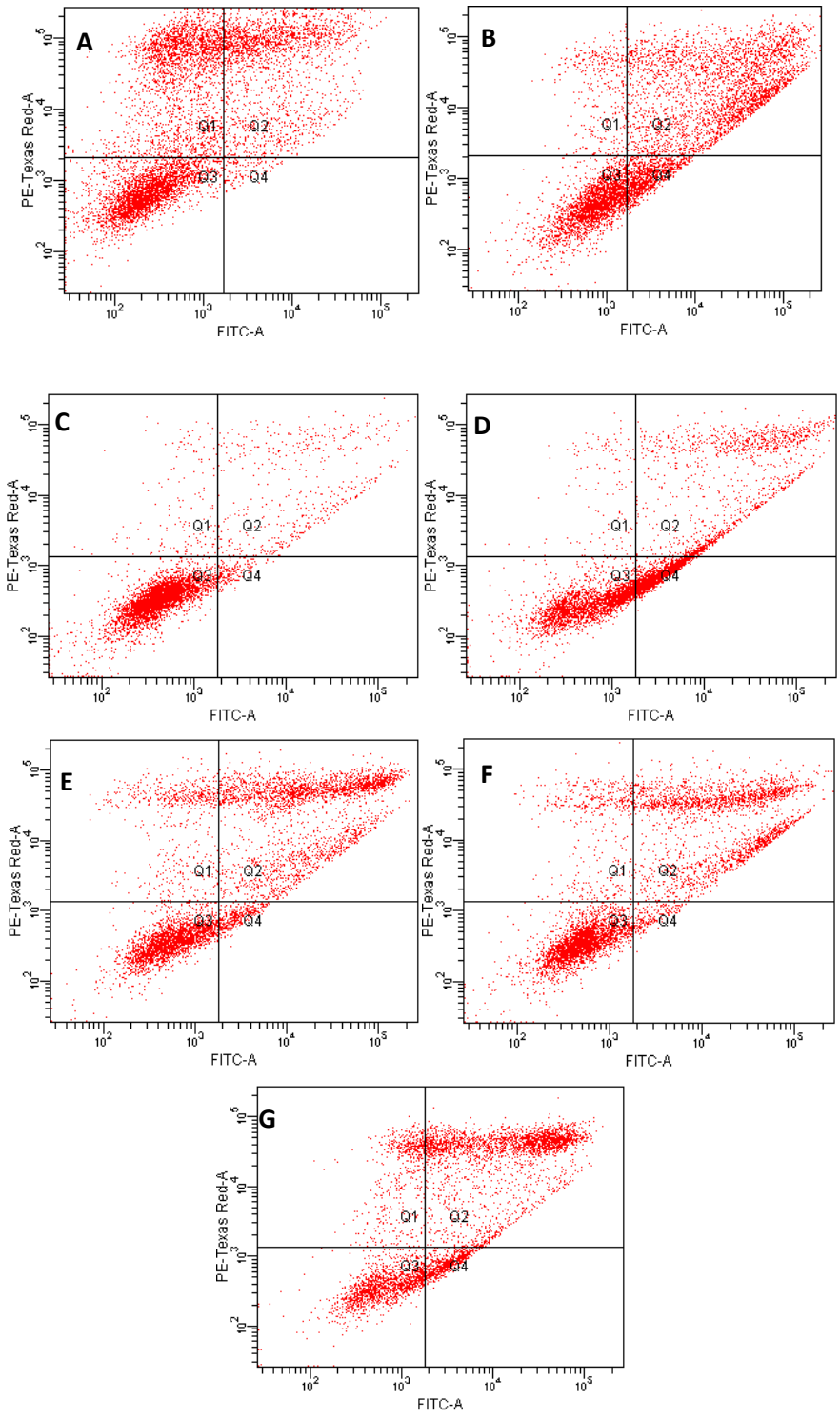

Figure 4-42. Induction of apoptosis by A. RES, B. Cisplatin, C.RES-NLC-GTO, D. RES-NLC-GTO-PEGS40, E. RES-NLC-GTO-PEGS40-HA, F. RES-NLC-GTO-PEGS40-FA and G. RES-NLC-GTO-PEGS40-HAFA on MDAMB-231 cell lines after 48 h incubation. Four quadrants represent (Q1) necrotic cells annexin (upper left quadrant), (Q2) late apoptotic cells (upper right quadrant), (Q3) viable cells (lower left quadrant) and (Q4) early apoptotic cells (lower right quadrant). Data shown are mean ± SD (n = 3)

4.4.5 Cell cycle assay

Cell cycle inhibition and the initiation of apoptosis are the most suggested mechanism(s) for the anticancer effects drugs can exert on a particular cancer cell (Weir et al., 2007). Breakdown of DNA is a critical measure for the determination of apoptosis (Mulik et al., 2012), where the distribution of different phases was assessed by the determination of the DNA content in each phase. The presence of hypo-diploid peak in the subG1 region is an indication of apoptosis (Weir et al., 2007).

The investigation of cell cycle arrest property of RES and RES-NLCs was carried on MCF-7 cell lines employing PI staining and the analysis through flow-cytometry (Figure 4-45). PEGylated and surface modified RES-NLCs showed significantly more percentage of DNA content ranging from 47.3 % ± 1.509 to 52.233 % ± 2.177 in the S-phase compared to only 33.55 % ± 3.464 and 34.7 % ± 1.135 produced by both free RES and RES-NLC-GTO respectively after 48 h incubation (Figure 4-43. A). After 72 h incubation with free RES and RES-NLCs the cells moved to the S phase and a parallel decrease of cells in the G0/G1 and G2/M phases (Figure 4-43. B) (Teskač and Kristl, 2010). This confirmed the induction of apoptosis by RES and surface modified-RES-NLCs in time dependent manner, which is attributed to the arrest of the S-phase which is involved in the DNA synthesis and replication by inhibiting the enzyme responsible for DNA replication such as ribonucleotide reductase, similar results were observed by various studies (Gusman et al., 2001, Joe et al., 2002, Osman et al., 2012).

Furthermore, the cytotoxic effect of free RES, bare and three surface modified RES-NLCs on TNBC (MDAMB-231) cell lines could be elucidated by an increase in the S-phase produced by an inhibition of S or G2-phase transition or a decrease in the progress through the cell cycle. The data shows that MDAMB-231 cells treated with RES and bare and surface modified RES-NLCs results in reduction of S-phase cell cycle with time, in which there was a significant increase in the percent of DNA content in the S-phase (Figure 4-44. A, B), this observation goes in line with Park observation (Park, 2017). This might be attributed the elevated expression of tumor suppressor protein p53 (Huang et al., 1999) and the increase levels of G_1/S positive regulators, such as cyclin D1 facilitating the entrance of the cells to the S-phase (Pozo-Guisado et al., 2002). Resveratrol-induced S phase arrest would eventually lead to apoptotic death as indicated by the increase in S-phase arrest (Figure 4-46).

RES is a known agent that cause arrest of S-phase involved in DNA replication. Thus, the incorporation of RES into nanoparticles did not change the mechanism by which the drug is causing apoptosis of cancer cells, this results were in line to Shimizu results (Shimizu et al., 2006).

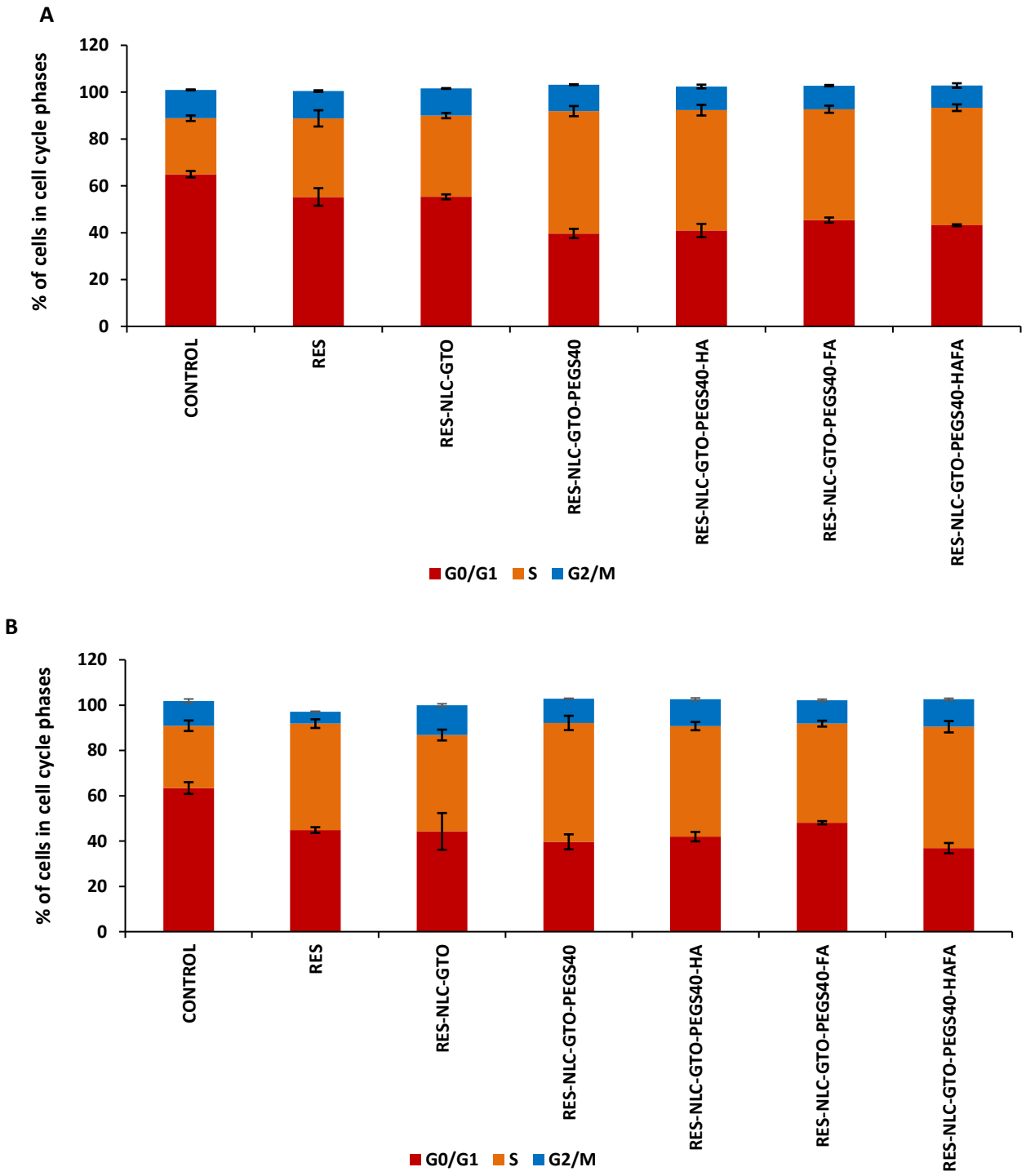

Figure 4-43. MCF-7 cell cycle analysis after A. 48 h, B.72 h exposure to RES and RES-NLCs. The percentage of DNA in cells in each phase of the cell cycle stained with PI solution and analysed using flow-cytometry. Data expressed as mean ± SD (n= 3)

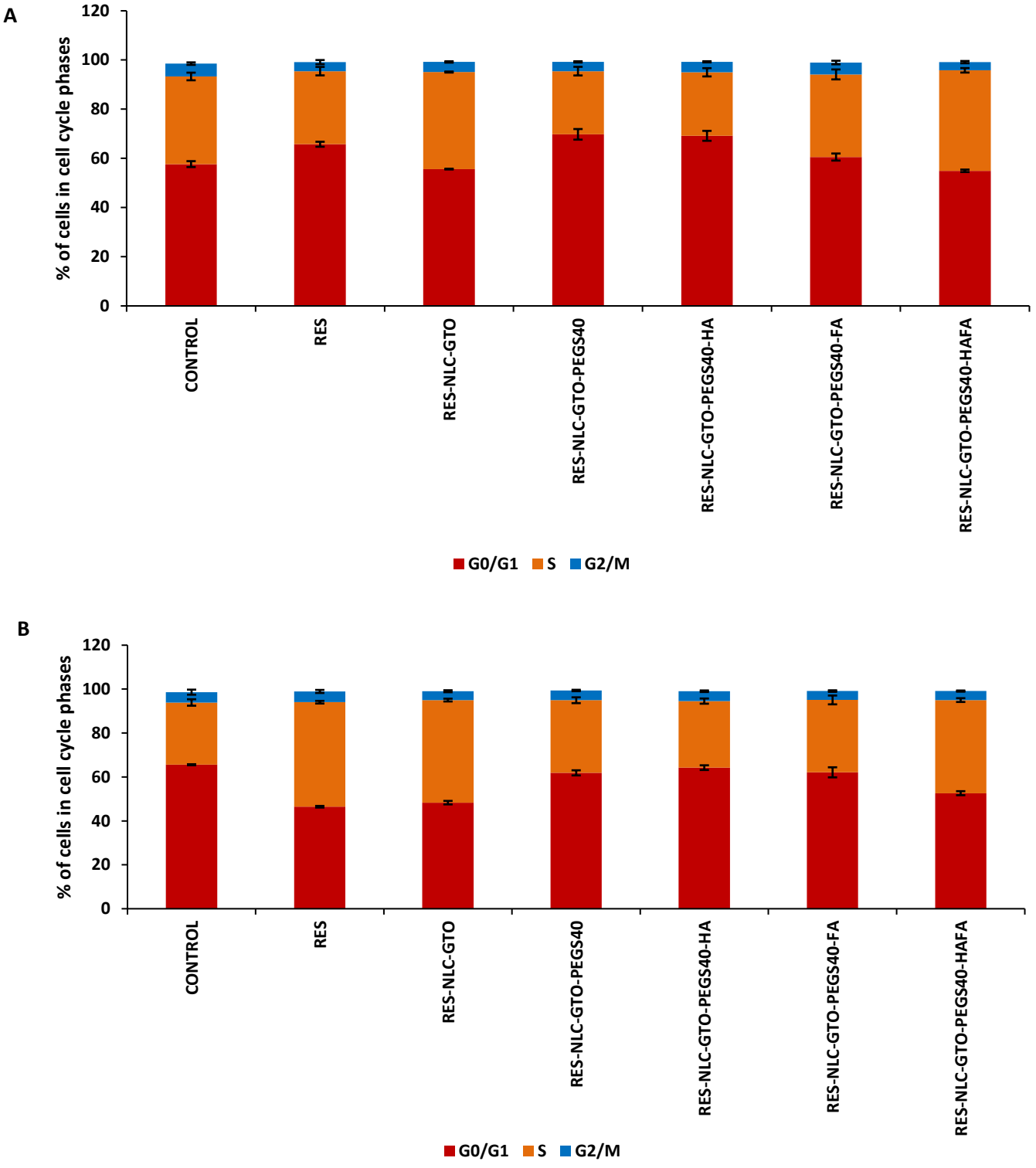

Figure 4-44. MDAMB-231 cell cycle analysis after A. 48 h, B.72 h exposure to RES and RES-NLCs. The percentage of DNA in cells in each phase of the cell cycle stained with PI solution and analysed using flow-cytometry. Data expressed as mean ± SD (n= 3)

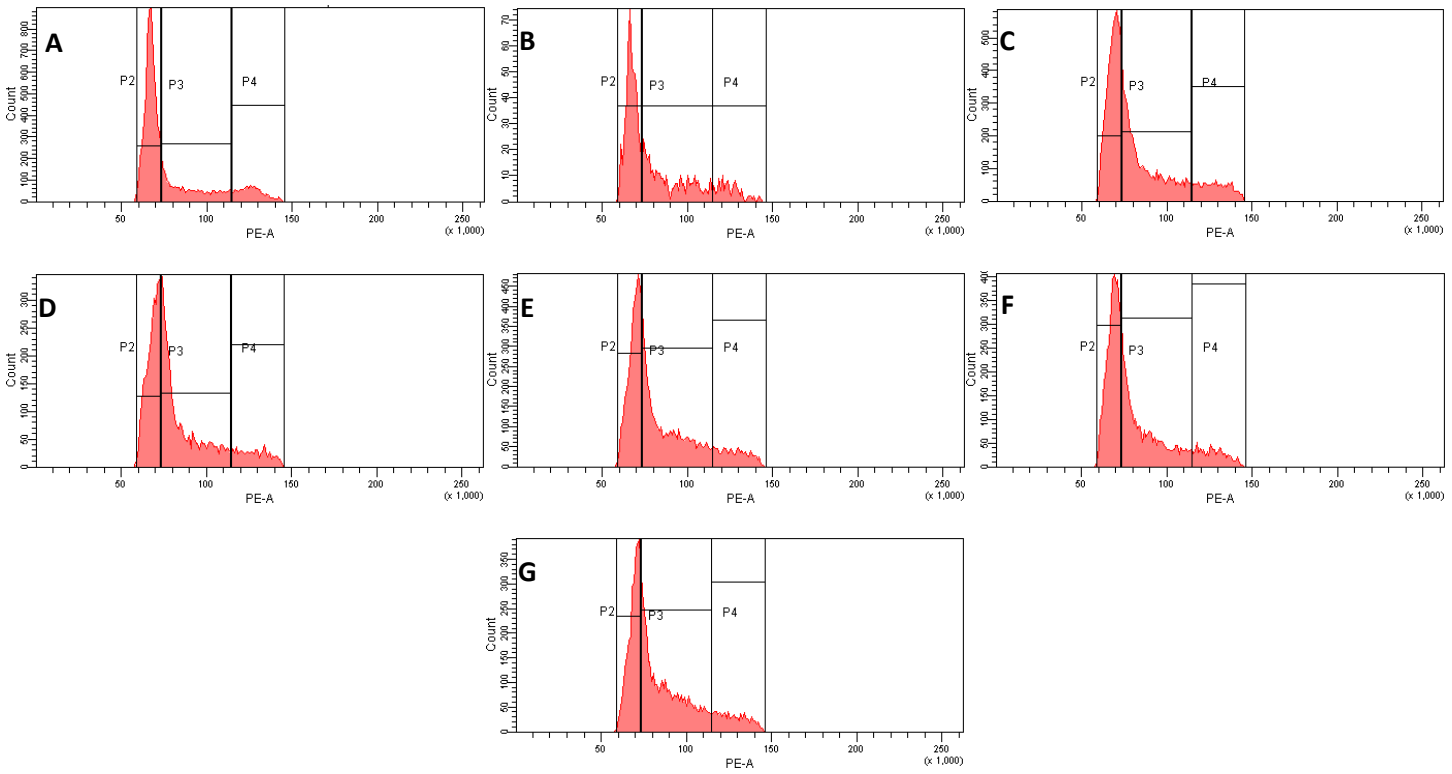

Figure 4-45. Effect of RES and various formulations on the MCF-7-cell cycle distribution profile A. Control, B. Free RES. C. RES-NLC-GTO, D. RES-NLC-GTO-PEGS40, E. RES-NLC-GTO-PEGS40-HA, F. RES-NLC-GTO-PEGS40-FA and G. RES-NLC-GTO-PEGS40-HAFA. Data expressed as mean ± SD (n= 3)

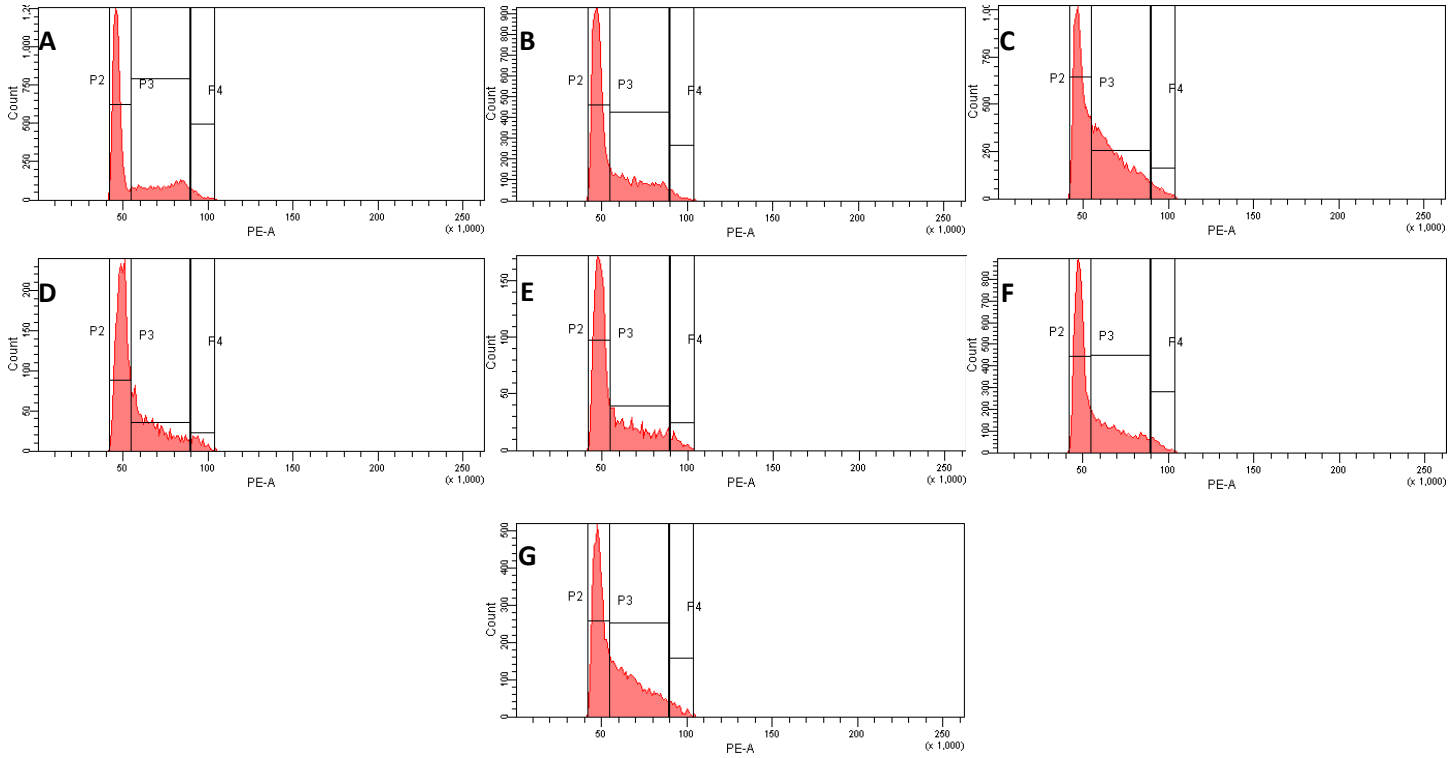

Figure 4-46. Effect of RES and various formulations on the MDAMB-231 cell cycle distribution profile A. Control, B. Free RES. C. RES-NLC-GTO, D. RES-NLC-GTO-PEGS40, E. RES-NLC-GTO-PEGS40-HA, F. RES-NLC-GTO-PEGS40-FA and G. RES-NLC-GTO-PEGS40-HAFA. Data expressed as mean ± SD (n= 3)

4.4.6 Caspase-3 activity

The concentration of the paranitroaniline (pNA) released from the substrate is determined either from the absorbance values at 390 nm or from a calibration curve prepared with pNA standards (Figure 4-47).

The quantification of protein in the cell lysates was determined BCA Assay Kit following the manufacturer's instruction. BCA Protein Assay Kit results were expressed as the amount µg of drug per mg total cell protein (Figure 4-48).

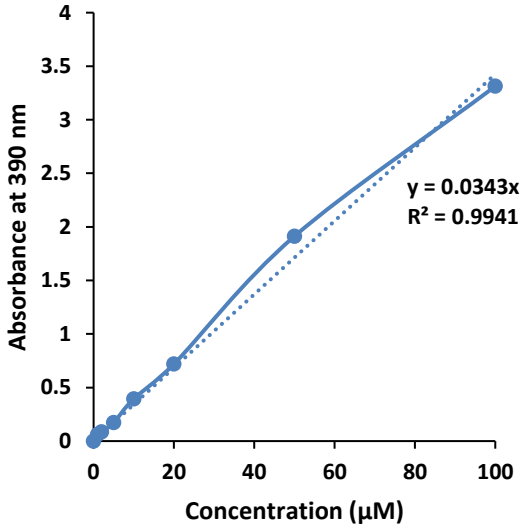

Figure 4-47. Para nitro-aniline calibration curve

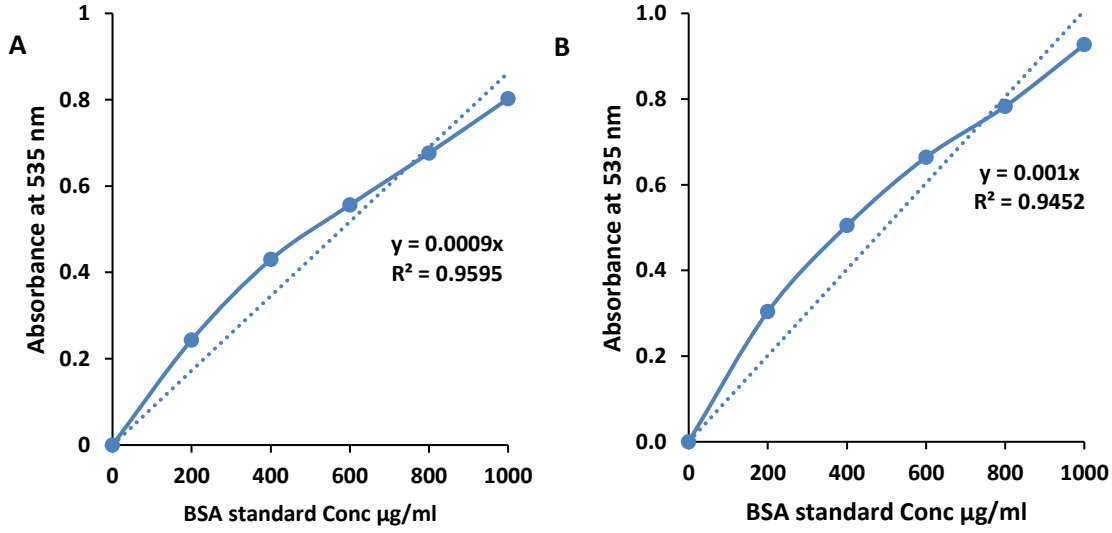

Figure 4-48. BSA calibration curve in A. MCF-7 cell lines, B. MDAMB-231 cell lines

Caspase-3 plays a crucial role in the initiation and accomplishment of apoptosis. Caspase-3 activation is a common marker of apoptosis. The leading cause of the reduction in apoptosis and carcinogenesis is the low level of caspase (Mulik et al., 2012). The elimination of cancer cells by

anticancer drugs involve the stimulation of proteolytic cascade through caspases. The activation of caspases will result in the breakdown of various cytosolic and cellular proteins. Bcl-2 is the protein that regulates the activation of caspase (Nambiar and Hegde, 2016).

The caspase activity of free RES and bare and three surface modified RES-NLCs was investigated on both MCF-7 and MDAMB-231 cell lines using Caspase-3 calorimetric kit reading the absorbance using Tecan plate reader. Caspase activity was observed after treating the cells for 72 h. The amount of protein released during the assay was quantified and used to determine the caspase activity (Table 4-5).

Upon treatment of MCF-7 cell lines with free RES and bare and three surface modified RES-NLCs they triggered apoptosis through the increase in caspase-3 activity when compared to the untreated control (Figure 4-49. A). The increase in caspase-3 activity will in turn cause a reduction in the anti-apoptotic proteins Bcl-2 (Shimizu et al., 2006, Prabhu et al., 2013, Tsai et al., 2017). There was no significant difference ($p< 0.05$) between the activity produced by free RES and bare and three surface modified RES-NLCs. However, all of them increased the caspase-3 activity almost two folds compared to the control.

On the other hand, when MDAMB-231 cell lines were treated with free RES and bare and three surface modified RES-NLCs there was a remarkable increase in caspase-3 activity (almost 75 %), indicating that free RES and bare and three surface modified RES-NLCs have the potential to cause cancer cell death through the activation of caspase-3 pathway. Data showed almost 1.2 to 1.6--fold increase in caspase activity when compared to the untreated control cells (Figure 4-49. B).

It is clear free RES and bare and three surface modified RES-NLCs induced apoptosis in both cell lines by affecting caspase-3 activity with various degrees, showing a progressive effect on MBAMD-231 cell lines giving rise to almost 2 fold increase in the caspase-3 activity compared to MCF-7 cells, this results were in line with Jiang studies(Jiang et al., 2005).

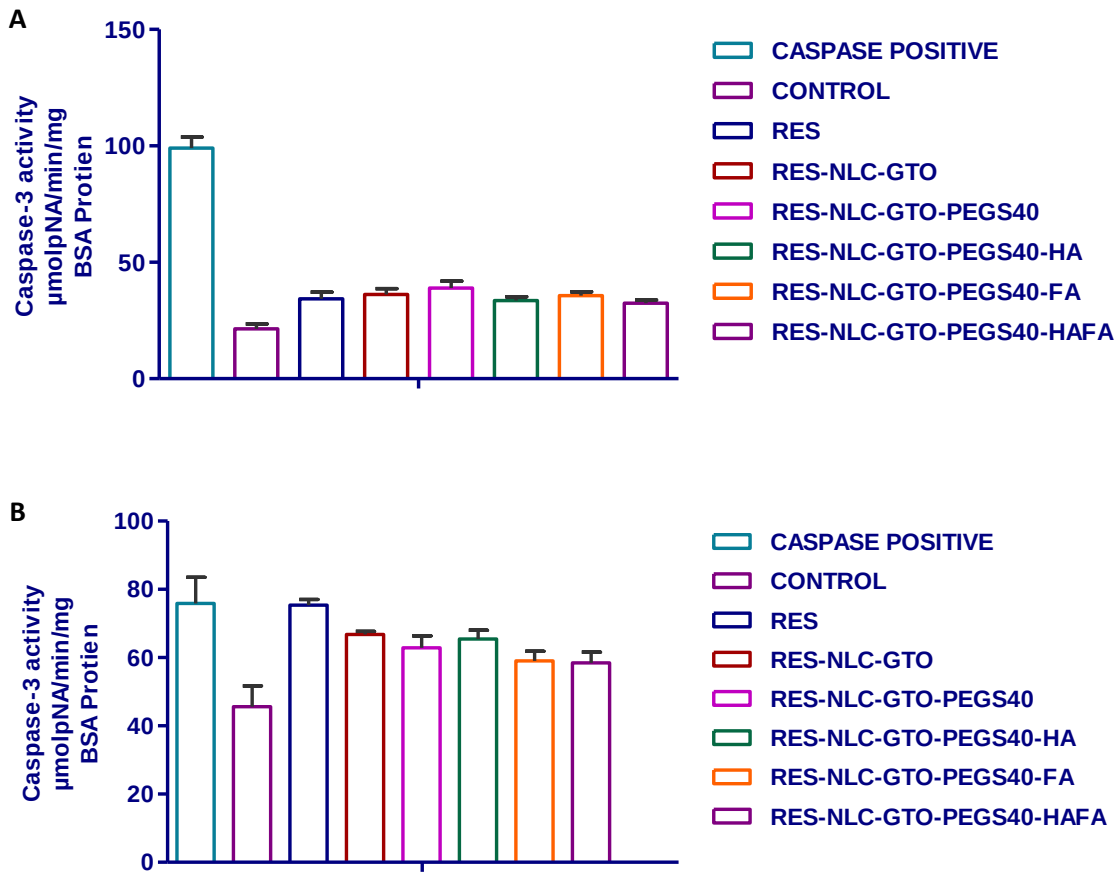

Figure 4-49. Caspase 3 activity (µmol pNA/min/mL/mg BSA protein) in A. MCF-7 cells B. MDAMB-231 following 72 h of incubation with RES and surface modified RES-NLCs. Data shown are mean ± SD (n = 3)

Table 4-5. Caspase-3 activity of RES and RES-NLCs on MCF-7 and MDAMB-231 cell lines after 72 h incubation (n=3 ±SD)

Treatment	Caspase 3 activity in MCF-7 cells (µmol pNA/min/mL/mg BSA protein)	Caspase 3 activity in MDAMB-231 cells (µmol pNA/min/mL/mg BSA protein)
Caspase positive	99.058 ± 4.768	75.902 ± 7.662
Control	21.424 ± 2.196	45.622 ± 6.060
RES	34.348 ± 2.868	75.394 ±1.663
RES-NLC-GTO	36.183 ± 2.454	66.782 ± 0.924
RES-NLC-GTO-PEGS40	38.883 ± 3.091	62.868 ± 3.546
RES-NLC-GTO-PEGS40-HA	33.515 ± 1.611	65.487 ± 2.537
RES-NLC-GTO-PEGS40-FA	35.628 ± 1.623	59.004 ± 2.876
RES-NLC-GTO-PEGS40-HAFA	32.390 ± 1.446	58.419 ± 3.221

4.5 Conclusions

In-vitro cytotoxicity studies using presto blue showed that RES-NLCs were effective against both non-TNBC, MCF-7 and TNBC, MDAMB-231 breast cancer cell lines. HA and FA dual modification of NLCs resulted in specific binding to MCF-7 and MDAMB-231 breast cancer cells as CD44 and folate receptors are overexpressed on both these cells and thus exhibited enhanced targeting. The dual ligand appended RES-NLC-GTO-PEGS40-HAFA showed 2.7 fold higher toxicity in MCF-7 and 3.6 fold higher toxicity in MDAMB-231 cells as compared to RES-NLC-GTO-PEGS40 demonstrating its potential for treatment in the aggressive triple negative cancer.

Out of all the formulations investigated, none of the RES-NLCs formulations containing different liquid lipids or their empty counterparts without drug were cytotoxic to healthy MCF-10A cells demonstrating safety of the formulations and excipients employed. Surface modification further reduced the toxicity on healthy cell lines confirming their safety on the non-tumorigenic cells. All nanoparticles showed a considerable safety on macrophages.

All bare PEGylated and surface modified RES-NLCs showed time dependent cellular uptake on both MCF-7 and MDAMB-231 cell lines. The type of liquid lipid had an impact on cell internalization of the formulations. The highest fluorescence intensity was observed with RES-NLC-GTO in both MCF-7 and MDAMB-231 cells. Surface modification resulted in a 3 fold increase in the cellular uptake confirming the targetability potential of the ligand appended formulations toward overexpressed receptors on the surface of both cancer MCF-7 and MDAMB-231 cells.

The mechanism of cellular uptake was evaluated using various pharmacological inhibitors and ligand appended nanoparticles were internalised by cells by combined mechanisms of clathrin-mediated endocytosis and receptor-mediated endocytosis while internalisation of bare RES-NLCs was governed by clathrin-mediated endocytosis but was independent of receptor mediated endocytosis. All bare and surface modified RES-NLCs showed low uptake by macrophages and MCF-10A cells confirming their safety. Cell cycle analysis showed that nanoparticles arrest MCF-7 and MDAMB-231 cells in S phase of cell cycle.

Chapter 5 : Bidirectional Intestinal Permeability Studies

5.1. Introduction

The gastrointestinal tract (GIT) is an extremely varied organ system. Its primary function is to obtain nutrients, water, electrolytes and vitamins from consumed food, and eliminate waste. Each section of the gut is greatly adapted with regards to its function, though in essence it is a muscular tube lined with mucous (Figure 5-1).

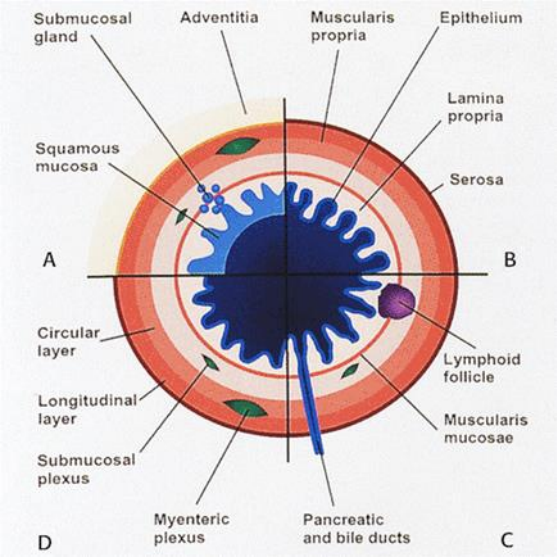

Figure 5-1. Various regions of the gastrointestinal tract A. Oesophagus, B. Stomach, C. Small intestine, and D. Large intestine copied without permission from (Fenoglio-Preiser, 2008)

Despite being a challenging organ (i.e. large variances in pH, fluid volumes, emptying times and susceptibility food and fluids consumed), oral delivery remains the most accepted and economical route for drug administration, with over 80% of the bestselling pharmaceutical products administered via the oral route (Lennernas and Abrahamsson, 2005). Moreover, the oral route offers a critical option in treating life-threatening diseases such as cancer, owing to several advantages, including: high patient compliance, cost-effectiveness and ease of administration. Additionally, due to its non-invasive nature it is preferred for patients suffering from chronic conditions, requiring compounds which may be anti-tumor, antidiabetic or antihypertensive in nature. As a consequence, compounds which exhibit stability in a gastric environment (highly acidic), possess the hydrophillic-lipophillic balance (HLB) required to pass through the intestinal epithelium membrane without detriment to the GI tract (Selvamuthukumar et al., 2012).

However, many compounds do not wholly fulfill these requirements, with in excess of 40% of drugs developed through the drug discovery and development process are unsuitable for oral drug delivery due to their hydrophobicity. This essentially results in poor oral bioavailability as, insufficient drug is offered at the proposed site of action, resulting in significantly reduced

pharmacological action. Poor solubility and poorly permeable drugs presenting poor oral bioavailability, remains a challenge for the pharmaceutical industry.

The Biopharmaceutics Classification System outlines four categories of drugs which are based upon their solubility and permeability. A drug which is administered orally is required to survive transit through GI fluids, mucous layer and epithelium prior to absorption. Whilst most small molecules exhibit resistance to the harsh environment of the GI tract and can be absorbed, intestinal barriers limit the absorption of macromolecules including proteins, vaccines or nucleic acids. Thus in order to prevent destruction of compounds in the GIT and in order to improve oral absorption protective vehicles are needed. Hence, protective vehicles to avoid destruction in the GI tract and potentially enhance oral absorption are needed (Bunjes et al., 1996).

Resveratrol (RES) is known as a bioactive agent with many health potentials viz. anti-inflammatory, anti-aging, neuroprotective, cardio-protective, antioxidant and anticancer activities. RES is a class II biopharmaceutical classification system with low solubility and high permeability properties (Figure 5-2). Therefore, its low oral bioavailability, rapid metabolism is a limitation to its clinical applications (Shi et al., 2008, Walle, 2011, Pandita et al., 2014). Due to the extensive metabolism in the liver, RES exhibit a short plasma half-life of 8–14 min.

The chemical structure of RES leads to low water solubility, resulting in inadequate bioavailability, which finally affect its absorption. Two main metabolites of RES recognized are the glucuronides and the conjugated sulfates. They are both hydrophilic in nature, leading to a high absorption. However, RES efficacy is reduced because of its low bioavailability (Gambini et al., 2015).

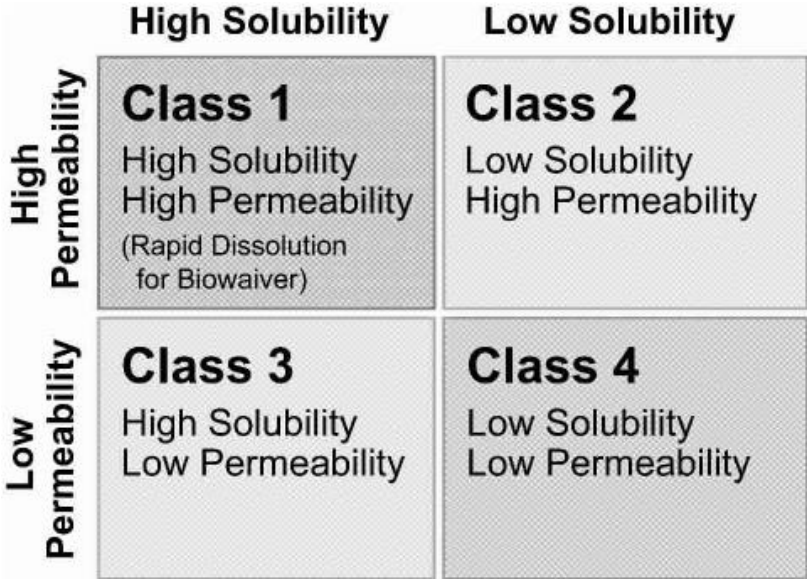

Figure 5-2. Biopharmaceutical classification system copied without permission from (Wu and Benet, 2005)

The primary barrier preventing molecules from the intestinal lumen reaching the blood is the epithelium. Aside from acting as a barrier, it is also the key area of absorption and metabolism in

the human body (Lherm et al., 1992). Consequently, *in vitro* models which study transport across the intestinal epithelium are gradually seeing significant attention in terms of drug. The poor permeability observed across the epithelium is a result of a number of factors, including: first pass metabolism, drug expulsion as a consequence of intestinal drug transporters (i.e. P-glycoprotein (P-gp), in addition to variability due to food (Smith and Hunneyball, 1986, Zur Muhlen et al., 1998). Thus, it is of paramount importance that progress made in oral drug delivery, takes into account the aforementioned factors, in order to achieve desirable therapeutic outcomes.

Epithelium permeability is dependent upon the regulation of the mucosal immune system and intercellular tight junction (TJ). Research conducted in the preceding decade has demonstrated TJ to be comprised of a network of proteins. Permeation studies have demonstrated nanoparticles are able to open the tight junctions of monolayer Caco-2 cells and increase paracellular transportation (Muller, 2000).

The human intestinal epithelium is noted for its absorptive surface with a large surface formed from villi 30-400 m2 (Schenk and Mueller, 2008). Furthermore, one of the major limitations of nanoparticles as oral delivery systems is the requirement that particles need to be absorbed with a sufficient rate and extent from the gastrointestinal tract (GIT) (Jung et al., 2000). Advanced drug delivery systems have been developed with the expectation of overcoming the GI barrier. For example, mucoadhesion drug delivery system has been commonly employed in attempting to improve the residence time of particles in the GI tract (Florey, 1962). Mucus penetrating system has also been engineered with the expectation to penetrate the mucus barrier (Chen et al., 2013; Li et al., 2013; Xie et al., 2014). Nonetheless, most of these efforts have not achieved the intended purposes (Albanese et al., 1994; Gruber et al., 1988; Macadam, 1993; Rieux et al., 2006; Li et al., 2016).

Various strategies have been employed to enhance poor oral bioavailability of active compounds, including but not limited to: nano-sizing of drug molecules, formulation as salts, synthesis as prodrugs, and encapsulation of drugs in nanosized carriers fabricated from various materials i.e. lipids and polymers (Zur Muhlen et al., 1998, Lucks and Müller, 1996, Saupe et al., 2005) and more recently nanostructured lipid carriers (NLCs) (Figure 5-3) were introduced (Mainardes and Silva, 2004).

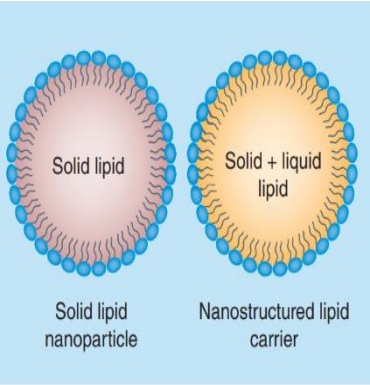

Figure 5-3.Lipid-based systems explored for drug delivery applications. Copied without permission from (Mainardes and Silva, 2004)

Whilst research dedicated to traditional lipid carriers (i.e. micelles, liposomes and nano-emulsions) has produced many notable findings, literature is indicative that these drug delivery systems are vulnerable to degradation under storage as well as when subjected to the harsh environment of the GIT (particularly the low pH of the stomach) (Muller, 2000, Jenning et al., 2000c, Jenning et al., 2000a). To address the issues associated with the aforementioned drug delivery systems, solid lipid nanoparticles (SLNs) were formulated from biocompatible and biodegradable solid lipids in the 1990'S, resolving poor stability and toxicity (Saupe et al., 2005). Despite advances, SLNs are plagued with various pitfalls including poor drug loading and expulsion of active compound when placed under storage (Jenning et al., 2000a, Muller et al., 2000b).

Undoubtedly, the human colon carcinoma cell lines (so-called Caco-2) have been the most widely used *in vitro* cell model in the study of intestinal peptide permeability over the last 20 years (Artursson et al., 2001, Sambuy et al., 2005, Ding et al., 2014, Pan et al., 2015). Generally, Caco-2 monolayer was employed to evaluate nanoparticles permeability and the involved transport mechanisms, for that specific inhibitors of the uptake mechanism can be employed.

Furthermore, co-culture of Caco-2 cells with HT29 cells represent absorptive and mucus secreting goblet cells, respectively, in order to simulate the *in vitro* intestinal epithelium. While HT29 cells function is to provide the mucus protective layer, its presence doesn't affect the transport properties of Caco-2 cells in the co-culture (Artursson et al., 2001, Beloqui et al., 2014).

The active transport of nanoparticles through the enterocytes can be attributed to one or more endocytic processes: clathrin-mediated endocytosis (CME), caveolae-mediated endocytosis (CvME), clathrin- and caveolae-independent endocytosis and macropinocytosis, though, CvME seems to be the most significant mechanism for transcellular transport of nanoparticles. Numerous proteins are involved in CvME viz. glycophosphatidylinositol anchor, folic acid receptor, autocrine motility factor receptor, $\alpha_2\beta_1$-integrin, interleukin-2 receptor, platelet-derived growth factor receptor, CCK receptor, and the epidermal growth factor receptor (Bunjes et al., 1996). Surface modification of nanoparticles with ligands that have the tendency to bind to the corresponding cell

surface proteins facilitate transcytosis of nanoparticles and enhance the oral absorption of encapsulated drug (Roger et al., 2012).

For most cells, CME serves as the major mechanism of internalization for plasma membrane components and macromolecules. CME function through particular receptor-ligand interaction, CME was previously referred to as “receptor-mediated endocytosis” (RME). However, the alternative non-specific endocytosis via clathrin-coated pits also occurs (as well as receptor-mediated but clathrin-independent endocytosis) (Mukherjee et al., 1997).

Macropinocytosis is a type of clathrin-independent endocytosis pathway (Mukherjee et al., 1997), taking place in many cells, including macrophages (Swanson and Watts, 1995), It involves the formation of actin-driven membrane protrusions, similarly to phagocytosis (Hillaireau and Couvreur, 2009).

Polyethylene glycol (PEG) coating of particles is a novel techniques to ensure the effective transport of nanoparticles through the mucus layers. It was used previously for imparting stability by rendering the particle more hydrophilic. Therefore, modifying their bioadhesive characteristics and eventually reducing the interaction between the PEGylated nanoparticles and the mucins permitting their penetration (Lencer et al., 1992, Tanaka et al., 1995).

RES-NLCs were tagged with a fluorescent dye coumarin-6, for quantification using flow-cytometry to determine nanoparticle transport. Also, fluorescent nanoparticles have been visualized under Fluorescence microscope. The fluorescence of nanoparticles was employed for visualization of particles within the cells. In addition, the mechanism of endocytosis was determined by employing various pharmacological inhibitors of uptake specific to a particular pathway. RES and RES-NLCs biocompatibility, and intestinal permeability studies were conducted in a solution or encapsulated in NLCs. Bidirectional intestinal apparent permeability was measured using Caco-2 cell monolayers cultured on permeable filter transwell devices. Caco-2 cell monolayers are the most commonly utilized intestinal models to evaluate the effect of nanoparticles on drug transport and permeation because Caco-2 cells form differentiated monolayers with enzymes, tight junctions, microvilli and transport systems. They are cultured for almost 18-21 days. Furthermore, co-culture of Caco-2 cells with HT29 cells to produce mucus was employed to mimic the intestinal membrane barrier. Finally, the blood compatibility of RES-NLCs was carried out to determine the safety of nanoparticles.

5.2. Materials and methods

5.2.1 Instruments

Millicell® ERS-2 Volt-Ohm Meter for measurement of trans-epithelial electrical resistance (TEER) value was purchased from Millipore, UK.

5.2.2 Cell lines type and source used in cell culture studies

Caco2 derived from caucasian colonic adenocarcinoma passage 43 and HT29 human Caucasian colonic adenocarcinoma cell line passage 141 were purchased from public health, England.
Caco-2 colonic cancer cell lines passage 43-68 and HT29 colonic adenocarcinoma cell lines passage 141-152, were maintained in EMEM supplemented with Glutamine (2 mM), 1 % Non-Essential Amino Acids (NEAA) and 10 % Foetal Bovine Serum (FBS). Cells were kept at 37^{o}C in a humidified CO2 incubator (5 % atmosphere).

5.2.3 Materials employed for the in vitro cell lines studies

Eagle's minimum essential medium (EMEM) with Earle's Balanced Salt Solution without L-glutamine, non-essential amino acids were purchased from Lonza. Hanks' Balanced Salt solution (HBSS) were obtained from Sigma Aldrich, UK. Transwell® permeable supports (12mm diameter insert, 12 well, 0.4 µm polycarbonate membrane) tissue culture treated, polystyrene plates were purchased from Costar, UK. In order to investigate the hemolytic activity of various formulations the porcine blood was kindly gifted from Bamber bridge animal abattoir after ethical approval has been given from UCLan.

5.3. *In vitro* cell culture studies

5.3.1 Cell lines growth curves

Growth curves of both cell lines was established using the methods described in section 4.3.1. Caco-2 and HT29 were seeded at a density of 30 x 10^4 cells/mL/well in a 6 well plate and allowed to grow and attach for 24 h. cells were counted the next day on hemocytometer using trypan blue counting method

5.3.2 *In vitro* cell viability using PrestoBlue assay

Once Caco-2 and HT29 cell lines were confluent (80-90 %) (Figure 5-4), the cells were ready for the experiment. Cytotoxicity assay was performed for the purpose of determining the safe concentration of both RES and RES-NLCs to be used in bidirectional permeability studies.

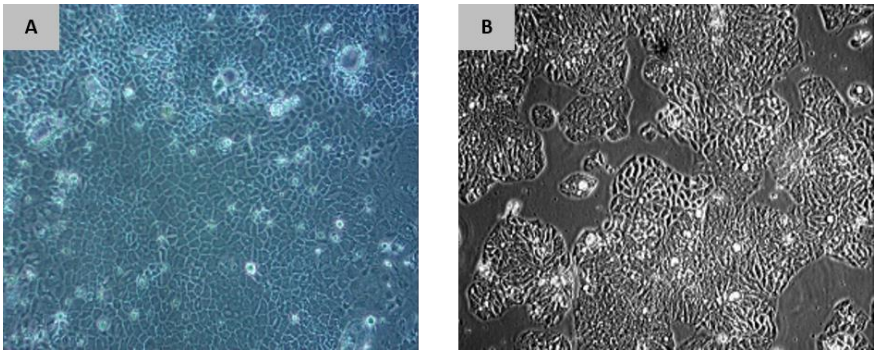

Figure 5-4. Photomicrographs showing the cellular morphology of confluent cells (~ 80-90 %). A. Caco-2 colonic adenocarcinoma cell lines, B. HT29 colonic adenocarcinoma

The cytotoxicity of all RES-NLNCs was investigated on both Caco-2 and HT29 using PB viability assay and was performed according to the manufacturer's protocol. The cells in suspension were seeded at a density of 5× 10^4 cells/well in a 96-well plate and kept at 37^{o}C in a humidified CO2 environment (5 %). After 24 h cells, the media was removed and the cells were treated with different concentrations of free RES, bare RES-NLCs, PEGylated and three surface modifies RES-NLCs. Resveratrol working solutions were prepared by diluting the drug stock of 60 µg/mL made in acetone with media to obtain the following working concentrations viz. 1, 5, 10, 25 and 50 µg/mL. Same concentrations were made for the formulations also. Six wells were kept as free culture medium to serve as a control, and other six wells were filled with only media without cells to serve as a blank.

After the treatment of the cells, they were incubated for another 24 h at 37^{o}C in a humidified CO2 environment (5 %). Next day 10 µL of PB was added to each well, the plates were covered by foil

paper and incubated for 1 h at 37^{o}C. The fluorescence was determined using Tecan microtiter plate reader at excitation 570 nm and emission 610 nm.

The cell viability was expressed as a percentage relative to the untreated cells using the following formula:

$$\% \text{ Cell viability} = \frac{\text{Fluorescence of test compound} - \text{Fluorescence blank media}}{\text{Fluorescence of control} - \text{Blank media fluorescence}} \quad \text{Equation 45}$$

The IC_{50} values for different formulations were calculated using the non-linear regression analysis employing GraphPad Prism 5 program.

5.3.3 Cellular uptake studies

5.3.3 (I) Quantitative cellular uptake studies with flow-cytometry

Caco-2 cells passage between 48 and 50 were seeded into 6-well plates at a density of 30x 10^4 cells/well and incubated for 24 h. The medium was aspirated the next day and replaced by 1 mL C6-loaded RES-NLCs (2 µg/mL). The cells were incubated for the following time points: 30 min, 1 and 2 h in order to quantify the C6-loaded RES-NLCs uptake over the specified time period. At the end of each time point the media was removed and the cells were washed trice with PBS, the cells were then trypsinized and centrifuged. The cells pellet was then re-suspended in 0.5 mL PBS along with 5 µL propidium iodide (added to quantify the dead cells upon measurement of cellular uptake) for immediate flow-cytometric measurement. At least ten thousand events per sample were measured by the flow cytometer. Three time points were investigated in order to determine the maximum uptake time point to carry out the different endocytosis mechanisms.

5.3.3 (II) Quantitative cellular endocytosis uptake mechanisms using flow-cytometry

In order to determine the cellular uptake pathways and the mechanisms involved in nanoparticles internalization various treatments where undertaken.

The study was conducted in 6 well plates, were 30×10^4 Caco-2 cells were seeded. Cells were incubated at 37^{o}C with 5 % CO_2 for 24 h to allow the cells to attach to the plate. The temperature block effect was investigated by pre-incubating the cells at 4^{o}C for 1 h with media alone. To study the effect of different endocytosis inhibitors on the cellular uptake of various RES-NLCs, Caco-2 cell lines were pre-incubated for 30 min with the following inhibitors at a concentration which was

deemed to be safe to the cells. Sucrose (0.45 M), nystatin (5 µg/mL) and cytochalasin B (5 µg/mL) (Martins et al., 2012). The media was aspirated and replaced with 1 mL of various C6-bare RES-NLCs and C6-surface modified RES-NLCs (2 µg/mL) diluted in media. Cells were incubated with C6-RES-NLCs along with the same concentration of each inhibitor for 2 h (time point selected based on the highest cellular uptake determined in section 5.3.3.1) (Beloqui et al., 2013). After this incubation time, the media was removed and the cells were washed thrice with PBS in order to ensure the removal of excess C6-NLC on the outer cell membrane. The cells were trypsinized and centrifuged, the cells pellet was re-suspended in 0.5 mL PBS and 5 µL was added to stain the dead cells.

5.3.3 (III) Qualitative cellular uptake mechanisms using fluorescence imaging

Qualitative cellular uptake studies using fluorescent coumarin-6 loaded RES-NLCs (C6-RES-NLCs) to enable tracking of nanoparticles inside the Caco-2 cells were carried out by fluorescence microscopy to back up the data obtained for the endocytosis uptake studies carried with flow-cytometry. The cell number was set the same to ensure a cell density similar to the flow cytometry experiments and, in order to keep all parameters affecting the experiment constant sample preparation and cell fixation.

The study was conducted in 6 well plates, in which 30×10^4 cells/mL Caco-2 cells were seeded onto glass cover slips, supplemented with 1 mL media and incubated at 37^{o}C with 5 % CO_2 for 24 h to allow the cells to attach to the glass cover. The media was removed the following day and replaced with 1 mL of the following pharmacological inhibitors in various wells: sucrose (0.45 M), nystatin (5 µg/mL), cytochalasin B (5 µg/mL) and incubated for 30 min. To study the temperature effect the plates were kept at 4^{o}C for 1 h. The media was then removed and replaced with 1 mL of C6 loaded bare NLCs (2 µg/mL) and C6-surface modified RES-NLCs (2 µg/mL). The plates were incubated at 37^{o}C, 4^{o}C and also with various inhibitors which were previously mentioned for a period of 2 h. At the end of the incubation time, the media was aspirated and the cells were washed carefully thrice with PBS in order to ensure the removal of free C6-NLCs. Cells were fixed for 20 min with 4 % (V/V) paraformaldehyde (PFA) solution made in PBS then washed trice with PBS. Cells were washed with glycine (0.3 M) in order to reduce the quenching effect from free aldehyde present on the cover slips (Garanti et al., 2016). Cells were washed for the last time with PBS.

One drop of 4', 6-diamidino-2-phenylindole (DAPI blue) mounting medium was placed on a glass slide, cells on cover slips were inverted facing the glass slide and left overnight. DAPI was used to stain the nucleus of the cells. The cover slips were then secured by painting the edges with a colorless nail polish. The slides were allowed to dry prior to imaging.

Imaging was done employing Zeiss filter set 49 (DAPI excitation and emission wave length was recorded at 365 and 445/50 nm, respectively. Coumarin-6 imaging was performed with a filter set at 38 GFP excitation and emission wave length was set at 470 and 525/50 nm, respectively using 64X oil objective Slides were covered and stored in a special slides box at 2-8^{o}C. Zen lite 2012 desk imaging software was used to analyze the images.

5.3.4 Bidirectional transport studies

5.3.4 (I) Cell monolayer integrity via measurement of trans-epithelial electrical resistance (TEER)

Epithelial cells culturing on porous filter supports simulating *in vivo*-like conditions promoting the cell differentiation by permitting nutrient supply from the basolateral compartment and therefore demonstrating similarity to the normal tissues. Transepithelial electrical resistance (TEER) measurement is used to evaluate the barrier function of epithelial cells on these porous supports. When measuring the electrical impedance, a continuous current passing through the cells on both transcellular and paracellular pathways. The transcellular resistance is formed by the apical and basolateral plasma membrane, while the paracellular resistance is produced from cell to cell contacts. The epithelial resistance is largely affected by the specific tight junction proteins (Chen et al., 2015). TEER value reflects the ionic conductance of the paracellular pathway in the epithelial monolayer, whereas the flux of non-electrolyte tracers (expressed as permeability coefficient) shows the paracellular water flow, along with the pore size of the tight junctions. TEER method is non-invasive and can be useful in monitoring the growth of cells and differentiations.The TEER measurement device is known as an Epithelial Millicell ERS-2 Voltohmmeter (EVOM) which uses a pair of electrodes popularly known as a chopstick. Each stick of the electrode pair (4 mm wide and 1 mm thick) contains a silver/silver chloride pellet for quantifying voltage and a silver electrode for passing current (Srinivasan et al., 2015).

TEER measurements were carried out periodically, when the culture media was replaced. Measurements were taken prior to medium replacement in order not to disturb the cells (Figure 5-5).

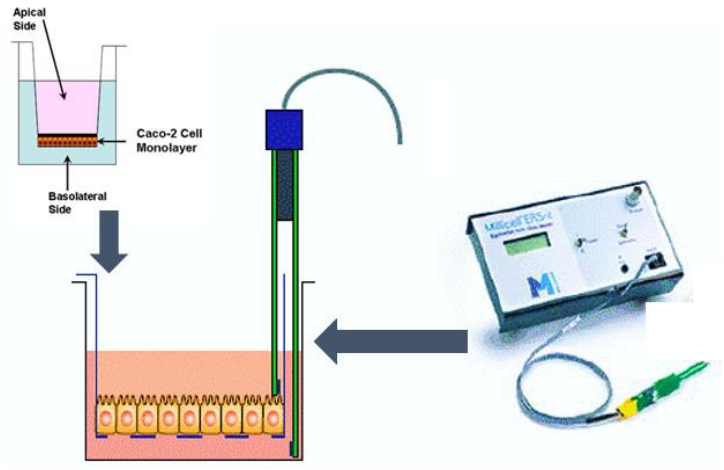

Figure 5-5. The Millicell ERS-2 unit connected to a pair of chopstick electrodes. To the left, a drawing of the electrode placed in a tissue culture insert. The shorter tip of the electrode was not in direct contact with the cell layer, while the long tip just touched the bottom of the outer chamber of Caco-2 cells monolayer

In order to understand the underlying process of transport thought the barrier, the most widely used GI tract *in vitro* human models is the Caco-2 cell line monolayer.

The GIT consists of other type of cells, predominantly goblet cells that doesn't form tight junctions. They are mucus producing cells covering the epithelium with a layer, providing extra diffusion barrier limiting the uptake of various substances (Deitch, 1993). By including these cells the barrier function and physiology will be altered rendering it more permeable and physiological. Immortalized HT29 goblet cell lines when included with Caco-2 cells in the barrier it helps in the development of proper physiological model. Bearing in mind that HT29 cell lines have the potential to overgrow as compared to Caco-2 cells, therefore, optimizing the seeding densities is a must in order to obtain the relevant physiologic transport testing.

5.3.4 (II) Caco-2 monolayer

Caco-2 cells were cultured in Essential Minimum Medium Eagle (EMEM) supplemented with 10 % fetal bovine serum, 1 % L-glutamine, 1 % non-essential amino acids .The cells were incubated at 37^{o}C in a humidified atmosphere of 5 % CO_2. When the cells reached 80-90 % confluency they were sub-cultured by trypsinization and re-suspended in medium. Subsequently, the cells were seeded at a density of 3 x 10^4 cells/mL onto transwell inserts by placing 0.5 mL of the cell suspension giving a final cells concentration of 1.5 x 10^4 (polycarbonate membrane, with 12 mm diameter 0.4 mm pore size,1.12 cm^2 surface growth area) placed in 12 well plate. Cells in transwells were permitted to grow and differentiate to produce a confluent monolayer for 18-21 days and the culture medium was replaced every other day (Hubatsch et al., 2007) for the first two weeks then every day for the last week. The cells employed in this study were between passages 45 to 58.

TEER values from each Transwell was monitored over the period of 18-21 days. Prior to the permeability experiments, the intactness of the monolayer was evaluated by measuring the TEER values. Once the TEER values reached > 1500 Ω.cm^2 cell monolayer was ready for the experiment, wells showing TEER values < 100 Ω.cm^2 were indicative of a leaky barrier and they were therefore excluded from the study. For RES and each RES-NLCs, both "apical to basolateral" (A → B) and "basolateral to apical" (B → A) bidirectional transport routes were investigated in order to determine the mechanism of efflux is carrier-mediated transport or carrier-mediated (Press, 2011). Once the cells have reached to the required TEER values. The cells were pre-incubated in 0.5 mL permeability Hank's balanced buffer solution (HBSS) added to the apical side and 1.5 mL added to the basolateral side of the transwell for 20 min at 37°C (atmospheric CO_2) prior to starting the assay. After that HBSS was removed from all wells except the control well. The HBSS was replaced by the RES solution prepared by accurately weighing 6 mg of RES and dissolving it in acetone, solution was appropriately diluted with HBSS to obtain RES concentration of 4.5 µg/mL. The final working concentration had less than 1 % acetone. RES-NLCs were investigated at a concentration of 9.1 µg/mL which was prepared by diluting it appropriately with HBSS. When A-B transport was investigated 0.5 mL drug or RES-NLCs solutions were placed on the apical side of the transwell. In case of B-A transport 1.5 mL of either RES or RES-NLCs solutions were placed in the basolateral side of the transwell. RES and RES-NLCs transport was investigated in both the directions. Samples aliquots of 0.4 mL were withdrawn at predetermined time points viz. 30 min, 1, 2, 3, 4 and 6 h from apical side when A-B transport was investigated and replaced with fresh warm HBSS to maintain sink conditions, while 0.4 mL was withdrawn from the basolateral side when B-A transport was being investigated. TEER measurements were carried out before taking samples, to minimize the barrier disturbance. TEER values were measured in three different areas in each well and the averages were taken as a final TEER values.

The samples were treated with 1.5 mL DMSO and 1.5 mL THF to promote the disruption of lipids and the release of RES to be quantified. The quantification was performed by HPLC. TEER values were rechecked at the end of the experiment to confirm the integrity of the monolayer after the experiment.

The apparent permeability (Papp) of the compounds was calculated using the following equation (Buyukozturk et al., 2010):

Apparent Permeability (P_{app}) = $$\frac{\mathrm{dQ}}{\mathrm{dt}} \times \frac{1}{AC0}$$ Equation 46

Where Papp is the apparent permeability coefficient (cm/sec), dQ/dt is the linear appearance rate of the compound on the basolateral, A is the surface area of the cell monolayer (1.12 cm^2 for 12 mm diameter transwells), C_0 the initial concentration of compound in the apical chamber (µg/ mL).

5.3.4 (III) Caco-2/HT29 co-culture permeability study

For the following experiments, monocultures of Caco-2 and HT29 cells were seeded on the apical chamber of transwell inserts at a ratio of Caco-2: HT29 (90:10) (Pan et al., 2015). The cells grown in 12-well Transwell (polycarbonate filter membranes with a pore size of 0.4 µm and a surface area of 1.12 cm^2) plates with a seeding density of 1.5 $X10^5$ cells/cm^2 in each insert. 0.5 mL of coculture cell suspension was added to the apical side and 1.5 mL of medium was added to the basolateral side of the transwell chamber. The cells were incubated at 37^oC in a humidified atmosphere of 5 % CO_2 and allowed to grow for 18-21 days with medium changes every other day in the first two weeks and every day in the last week. The seeding densities were selected based on previous literature reports (Yuan et al., 2013). The integrity of the cell monolayer was monitored over the period of 18-21 days by measuring the TEER values. The intrinsic resistance (Ω·cm^2) of the system (insert alone) was subtracted from the total resistance (cell monolayer plus insert, Ω·cm^2) to producing the net monolayer resistance (Ω·cm^2).

Bidirectional experiment was carried out when the TEER exceeded 300 Ω·cm^2. Same procedure was followed, dilutions of both free RES and RES-NLCs were made with the same concentrations as described in section 5.3.4 (II).

5.3.5 Blood compatibility assay

Blood compatibility test is one of the most common tests in studies of nanoparticle interaction with blood components. Most *in vitro* studies of nanoparticle-induced hemolysis evaluate the percent hemolysis using the UV-visible spectrophotometer by detecting free hemoglobin after incubation of particles with blood and then separating intact cells by centrifugation. Further the amount of red-colored hemoglobin released was determined spectrophotometrically, which indicate the extent of the damage of RBCs (Liu et al., 2014a).

Hemolytic activity of bare RES-NLC-GTO, RES-NLC-GTO-PEGS40, RES-NLC-GTO-PEGS40-HA, RES-NLC-GTO-PEGS40-FA and RES-NLC-GTO-PEGS40-HAFA was evaluated by taking 5 mL freshly collected citrated porcine blood. The whole blood was centrifuged at 4500 rpm for 15 min to separate the RBC layer. The supernatant was discarded and the pellet containing erythrocytes was washed three times with normal saline solution (0.9 % NaCl solution) to remove debris and serum protein by centrifugation at 4500 rpm for 15 min. After washing again, an erythrocyte stock dispersion was prepared by addition of saline to obtain 50 % haemocrit.

A 100 µL of aliquot of erythrocytes dispersion was added to 900 µL of RES-NLCs diluted with 0.9 % NaCl solution giving a final concentrations of 0.5, 1, 5, 10, 25 and 50 µg/mL. Samples were incubated at 37^0C for 1 h and 4 h in shaking water bath at low speed. Reaction was interrupted by addition of 50 µL of 25 % glutaraldehyde to abort the hemolysis. The volume of each tube was made up to 3 mL by using 0.9 % NaCl solution. Debris and intact erythrocytes were removed by centrifugation at 45000 rpm for 15 min. Absorbance of the supernatant was measured at 540 nm by UV-visible spectrophotometer using 0.9 % NaCl solution as blank. Complete hemolysis was achieved using 2 % Triton X-100 as a positive control, yielding the 100 % hemolysis value. 100 µL cell suspension in 3 mL 0.9 % NaCl solution served as the negative control causing 0 % lysis. Based on several studies *in vitro* percent hemolysis is graded as "no concern' when it varies from 5 to 25% (Dobrovolskaia et al., 2008). The percent hemolysis was calculated using following equation:

$$\% \text{ Hemolysis} = \frac{\text{Absorbance of sample} - \text{Absorbance of control}}{\text{Absorbance of triton X 100} - \text{Absorbance of control}} \times 100 \qquad \text{Equation 47}$$

5.3.6 Statistical analysis

Statistical analysis was performed for the *in vitro* cytotoxicity studies (PB assay) and the bidirectional studies. Data were expressed as arithmetical means and standard deviations and analyzed by two-way ANOVA with Bonferroni post-tests using Graph Pad Prism® software. A $P < 0.05$ value was considered statistically significant.

5.4. Results and discussion

5.4.1 Growth curves of cell lines

Trypan blue method (TB) was used to construct the growth curves for both the cell lines. This was carried out by calculating the doubling time (DT) of both the cells (Figure 5-6).The estimated DT for Caco-2 cell lines was 16.8 hours (Figure 5-6.A), while that of TH29 cell lines was 12 hours post seeding (Figure 5-6.B). HT29 cells showed faster growth rate than Caco-2 cells. Therefore, the best time to start an assay is treating cells with certain formulation or chemical at these time periods.

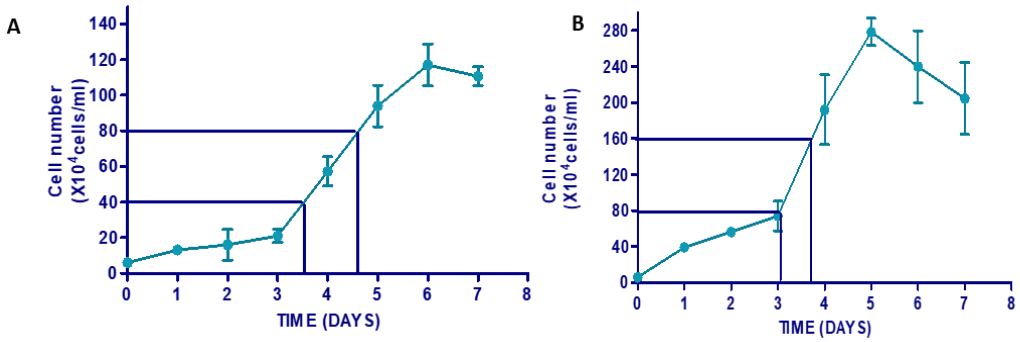

Figure 5-6.Growth curve using trypan blue solution A. Caco2 cell lines, B. HT29 cell lines

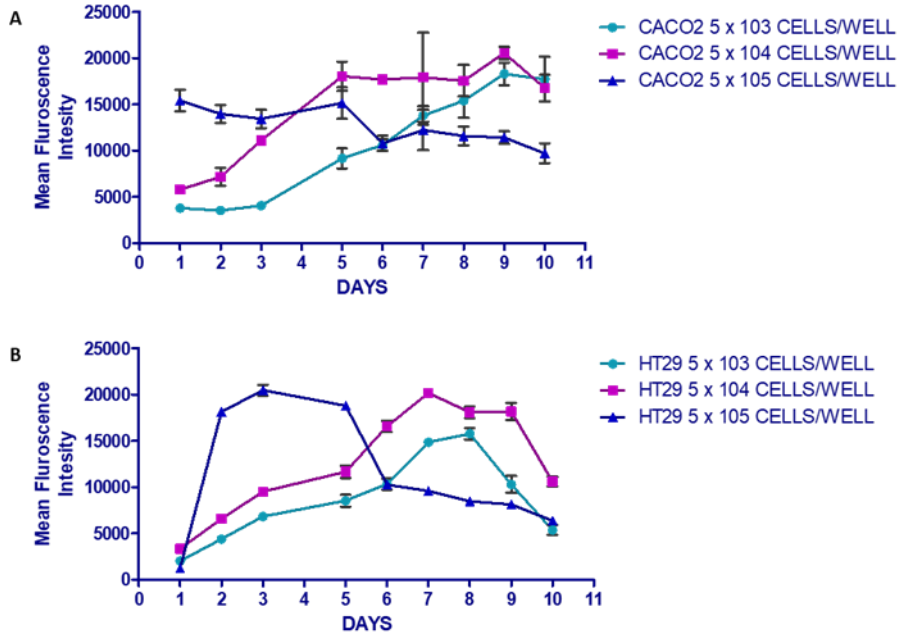

Figure 5-7.Growth curve using PB assay A. Caco2 cell lines, B. HT29 cell lines

Out of the three seeding densities investigated 5 x 10^4 cells showed the best growth for both the cell lines where the cells remained in log phase for sufficient period of time to give suitable treatment during this time. Whereas, 5 x 10^3 cells seeding density demonstrated a very slow growth which did not reach an evident "log-phase" after 5 days (Figure 5-7 A, B). On the other hand highest seeding density 5 x 10^5 cells showed fast growth rate reaching over confluency after 2 days with sudden drop in the cell number and the cells start dying. These results also demonstrate that PB did not have any effect on the growth characteristics of the cells and thus can be safely use as a reagent for cell viability assay (Harvard et al., 2013).

5.4.2 In vitro cytotoxicity assay

5.4.2 (I) Cell viability assay on Caco-2 cell lines

Caco-2 cell viability studies were carried out to assess the cytotoxicity of resveratrol and RES-NLCs in the intestinal barrier. The evaluation of the cytotoxicity of various RES-NLCs was carried out to determine the safest concentration to be used in further studies with Caco-2 cell lines.

As a quantitative marker of cytotoxic effects IC_{50} is defined as the inhibition concentration for a fifty per cent reduction of the cell number per culture (Halle and Göres, 1987). The cytotoxicity of different RES-loaded NLCs on Caco-2 was investigated by measuring cell viability with Presto Blue assay after incubating the cells for 24 h with various concentrations ranging from 1-50 µg/mL. Similar concentrations were employed for the free drug cytotoxicity assay. Among different formulations tested, results indicates that all bare RES-NLCs, PEGylated and surface modified RES-NLCs showed high cell viability at the determined concentrations with an IC_{50} values ranging from 61.200 ± 1.115 to 128.300 ± 1.133 µg/mL did not affect the cell viability (Table 5-1). This suggest that all prepared RES-NLCs are biocompatible and well tolerated by Caco-2 cells and, therefore, will be well tolerated by the gastrointestinal tract (Silva et al., 2011, Chai et al., 2016). This study allowed us to determine the safe concentration of both RES and RES-NLCs for Caco-2 permeability studies, without compromising Caco-2 cell monolayer (Figure 5-8).

Table 5-1.IC50 values of various RES-NLCs in Caco-2 cells lines

Formulation	IC_{50} (µg/mL)
RES	87.080 ± 1.23
RES-NLC-GTO	128.300 ± 1.133
RES-NLC-PCG	114.900 ± 1.650
RES-NLC-PGMC	83.810 ± 1.134
RES-NLC-PGML	72.800 ±1.076
RES-NLC-DO	98.930 ± 1.219
RES-NLC-GTC	110.00± 1.177
RES-NLC-GTO-PEGS40	62.00 ± 1.091
RES-NLC-GTO-PEGS40-HA	80.210 ± 1.138
RES-NLC-GTO-PEGS40-FA	61.200 ± 1.115
RES-NLC-GTO-PEGS40-HAFA	66.960 ± 1.145

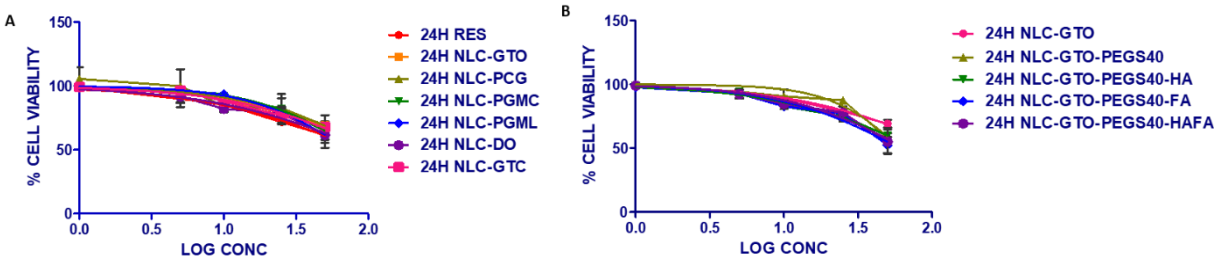

Figure 5-8. Concentration-dependent cytotoxicity of free RES with A. bare RES-NLCs and B. Surface modified RES-NLCs in Caco-2 cell lines for 24 hours (n=3 ± SD)

5.4.2 (II) Cell viability assay on HT29 cell lines

The purpose of evaluation of various RES-NLCs toxicity is to be able to select the safe concentration of the latter, to carry out other different assays which are mainly affected by number of viable cells. The cytotoxicity effect of various bare and surface modified RES-NLCs was examined in HT29 cell lines. The survival rate of HT29 cells incubated with various concentration of RES-NLCs (1- 50 µg/mL) for 24 h, demonstrated significant effect on the cell viability (Figure 5-9). All RES-NLC showed good dose tolerance except for RES-NLC-PGMC (41.160 µg/mL ± 1.062) and RES-NLC-PGML (36.230 µg/mL ± 1.047) which showed lower IC_{50} values when compared to the free RES (47.59 µg/mL ± 1.039) (Table 5-2).

This study also allowed us to choose the non-toxic concentration of RES (4.5 µg/mL) and RES-NLCs (9.1 µg/mL) for the intestinal permeability studies, without compromising Caco-2 cell monolayer and Caco-2/HT29 co-culture monolayer.

Table 5-2. IC50 values of various RES-NLCs on HT29 cells lines

Formulation	IC_{50} (µg/mL)
Resveratrol	47.59 ± 1.039
RES-NLC-GTO	102.0 ± 1.141
RES-NLC-PCG	58.240 ±1.056
RES-NLC-PGMC	41.160 ± 1.062
RES-NLC-PGML	36.230 ± 1.047
RES-NLC-DO	87.690 ± 1.181
RES-NLC-GTC	79.600 ± 1.146
RES-NLC-GTO-PEGS40	90.660 ± 1.151
RES-NLC-GTO-PEGS40-HA	84.210 ± 1.142
RES-NLC-GTO-PEGS40-FA	87.960 ± 1.156
RES-NLC-GTO-PEGS40-HAFA	77.360 ± 1.139

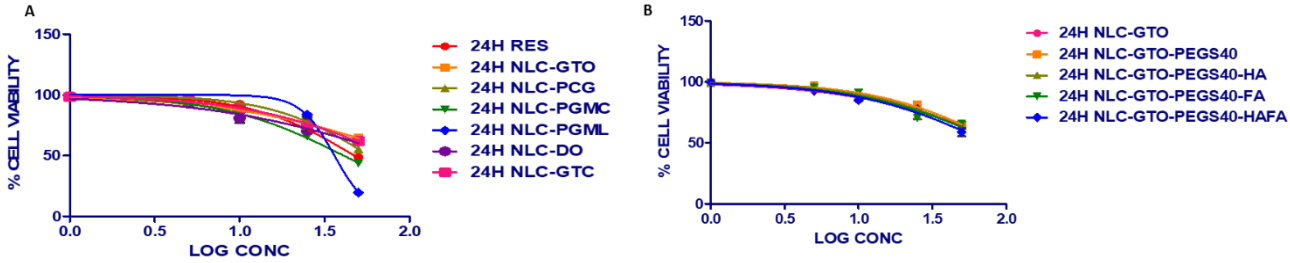

Figure 5-9. Concentration-dependent cytotoxicity of free RES with A. bare RES-NLCs and B. Surface modified RES-NLCs in HT29 cell lines for 24 hours (n=3 ± SD)

5.4.3 Cellular uptake studies

5.4.3 (I) Quantitative cellular uptake of bare, PEGylated and surface modified RES-NLCs in Caco-2 cells using flow-cytometry

Entry of RES-NLCs into Caco-2 cells was determined by flow-cytometry, for which coumarin-6 loaded RES-NLCs were employed. Cellular uptake of six selected bare RES-NLCs were investigated on Caco-2 cell lines at three different time points viz. 30 min, 1, and 2 h, to determine the effect of liquid lipid on the cellular uptake of NLCs.

Similar studies were also carried out for PEGylated and three surface modified RES-NLCs.

The cellular uptake of all RES-NLCs demonstrated a time dependent uptake. The uptake of the RES-NLCs increased significantly when the incubation time was prolonged, reaching a plateau after 2 h of incubation indicating the saturation of the uptake process, these results were in correlation to the same results of the study done by (Chai et al., 2016). However, there was a significant difference in the uptake between the formulations for instance the bare RES-NLC highest uptake was demonstrated by RES-NLC-DO followed by RES-NLC-GTC > RES-NLC-GTO, RES-NLC-PCG, RES-NLC-PGMC and RES-NLC-PGML. This might be attributed to the different nature of liquid lipids employed for fabrication of NLCs (Figure 5-10. A) (Lin et al., 2007, Yin et al., 2009).

On the other hand, RES-NLC-GTO-PEGS40, RES-NLC-GTO-PEGS40-HA, RES-NLC-GTO-PEGS40-FA and RES-NLC-GTO-PEGS40-HAFA demonstrated higher uptake in comparison with the bare RES-NLC-GTO (Figure 5-10. B). PEGylated RES-NLC improved the internalization and cellular uptake by almost 3 folds when compared to the bare RES-NLCs, this might be due to the hydrophilic nature of PEG enhancing the transport of nanoparticles across Caco-2 cell lines, which was also reported by few other studies (Siafaka et al., 2016b, Li et al., 2016a).

Surface modification also improved (3 folds increase in fluorescence intensity) the uptake of nanoparticles in Caco-2 cells, this might be attributed the expression of both CD44 and Folate receptors on the surface of Caco-2 cells, which was previously well studied (Trejdosiewicz et al., 1998, Roger et al., 2012).

All surface modified RES-NLCs demonstrated a greater uptake than the bare RES-NLC indicating that the functionalization of the nanoparticles surface had a distinct effect on the cellular uptake, thus will eventually affect the oral bioavailability of RES.

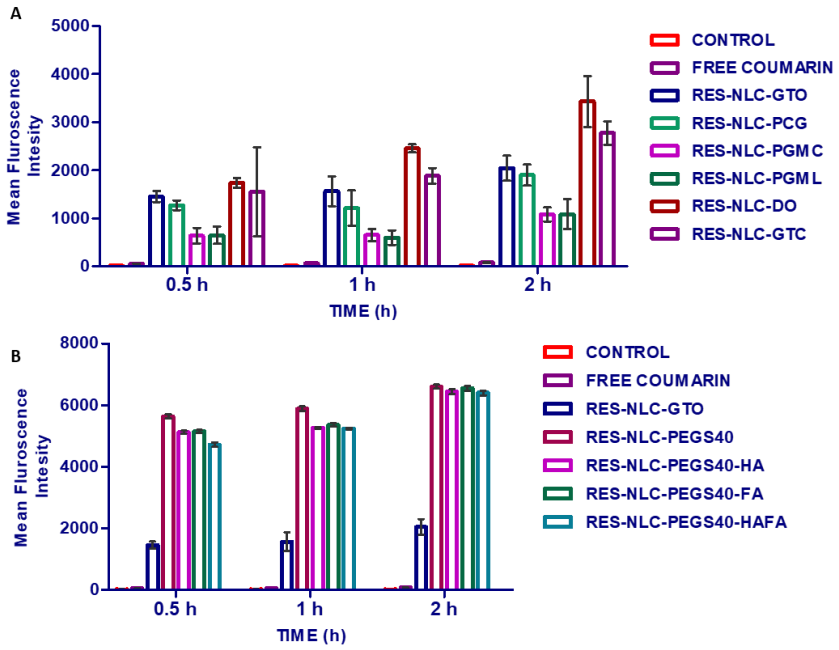

Figure 5-10. Quantitative Caco-2 cellular uptake of A. bare RES-NLCS and B. Surface modified RES-NLCs. Data shown are mean ± SD (*n* = 3)

5.4.3 (II) Endocytosis mechanisms of bare, PEGylated and surface modified RES-NLCs in Caco-2 cells

Nanoparticles enter the cells through endocytosis or energy independent pathways, endocytosis can be divided into clathrin mediated endocytosis, caveolae mediated endocytosis, phagocytosis and macropinocytosis. In order to evaluate the endocytosis mechanisms involved in the uptake of RES-NLCs across Caco-2 cells. Cells were treated with different pharmacologic inhibitors, which block a specific internalization pathway were used to assess the entrance mechanism involved for the uptake of each formulation.

Bare, PEGylated and three surface modified RES-NLCs mechanism of internalization in Caco-2 cells was determined after incubation at 37^{o}C, showing maximum cellular uptake. The cellular uptake was reduced but not completely stopped at 4^{o}C indicating the involvement of energy dependent uptake of RES-NLCs in Caco-2 cells.

Cells treated with hypertonic sucrose a known clathrin inhibitor acts by blocking the clathrin assembly at cell membrane, thus inhibiting the clathrin from forming pits (Heuser and Anderson, 1989). Nystatin was used to block the caveolae mediated endocytosis pathway by causing disturbance in the lipid raft resulting in alteration in the structure and functions of cell membrane. Phagocytosis (macrophages) or macropinocytosis pathways were further investigated by the

treatment of cells with cytochalasin B which acts by blocking the depolymerisation of actin filaments. The non-phagocytic energy dependent pathways comprising caveolae-mediated endocytosis, clathrin-mediated endocytosis and macropinocytosis are the common endocytosis mechanisms of nanocarriers absorption/transcytosis via the oral route (Hillaireau and Couvreur, 2009).

However, the challenge remains when designing nanoparticles that control a specific endocytic pathway. Thus, poorly water soluble drugs absorption can be enhanced through the throughput understanding of the mechanisms involved in the transport of nanoparticles across intestinal barrier and the factors restraining their transport across the GI tract (Rieux et al., 2005, Mathot et al., 2007, Beloqui et al., 2013).

Sucrose, specific inhibitor of clathrin mediated internalization, significantly affected the RES-NLCs uptake, therefore suggesting the clathrin pathway for endocytic cellular uptake of RES-NLCs ($P > 0.05$). The results were expressed as relative percentage assuming that fluorescence in the absence of inhibitor was 100 %. Inhibition of Bare nanoparticles uptake by sucrose showed a reduction in the fluorescence by 39.03-53.9 % ($p < 0.05$). On the other hand, PEGylated and the three surface modified RES-NLCs demonstrated almost 33.3-41.2 % reduction in the cellular uptake in the presence of sucrose.

Physicochemical properties of nanoparticle including the particle size and surface characteristics will have an effect on the endocytosis pathways (Oh and Park, 2014). For instance the clathrin mediated endocytosis involve the internalization of nanoparticles with particle size below 200 nm. As the particle size increased, the pathway shifts to caveolae mediated endocytosis pathway with particle size of 500 nm (Hillaireau and Couvreur, 2009). In this study all nanoparticles exhibited a size less than 100 nm, which favoured the clathrin mediated endocytosis as a pathway for their uptake into Caco-2 cells. In contrast, treatment with nystatin and cytochalasin B had no blocking effect on the cellular uptake of nanoparticles which suggest little or no involvement of the caveolae and macropinocytosis mediated cell entry pathway for RES-NLCs.

The results of flow-cytometry were supported by the qualitative analysis using fluorescence microscopy of Caco-2 cells exposed to C6-RES-NLCs (Figure 5-12Figure 5-13Figure 5-14Figure 5-15Figure 5-16). The images showed high fluorescence intensity at 37^{o}C, upon treatment with nystatin and cytochalasin-B with the nanoparticles being localized around the nucleus in the cytoplasm. While at 4^{o}C and with pre-treatment by hypertonic sucrose demonstrated a reduction in the fluorescence intensity indicating the effective inhibition of the energy dependent pathway.

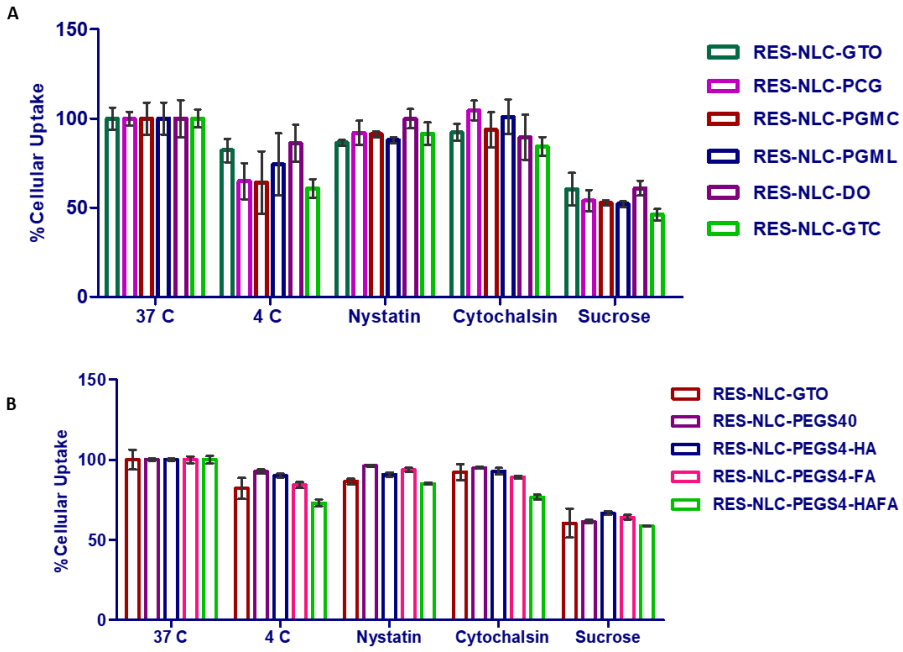

Figure 5-11. Endocytosis mechanisms of A. bare RES-NLCS and B. Surface modified RES-NLCs using various endocytosis pathway inhibitors on Caco-2 cell lines at 2 h. Data shown are mean ± SD (*n* = 3)

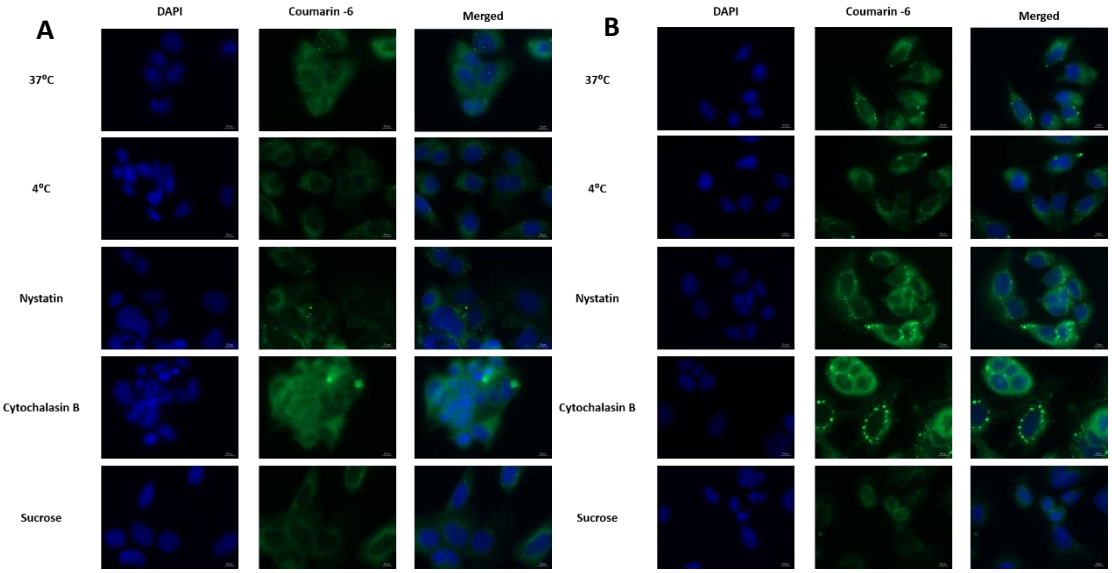

Figure 5-12. Fluorescence microscopy images of MCF-7 cell lines, cells treated with A. C6-RES-NLC-GTO, B. C6-RES-NLC-PCG mechanism of internalization, cells were treated with various endocytosis inhibitors. The blue colour represents the DAPI nuclear stain, Green colour of coumarin-6 dye in RES-NLCs and the merged image of both DAPI and Coumarin-6. Scale bar 10 µm

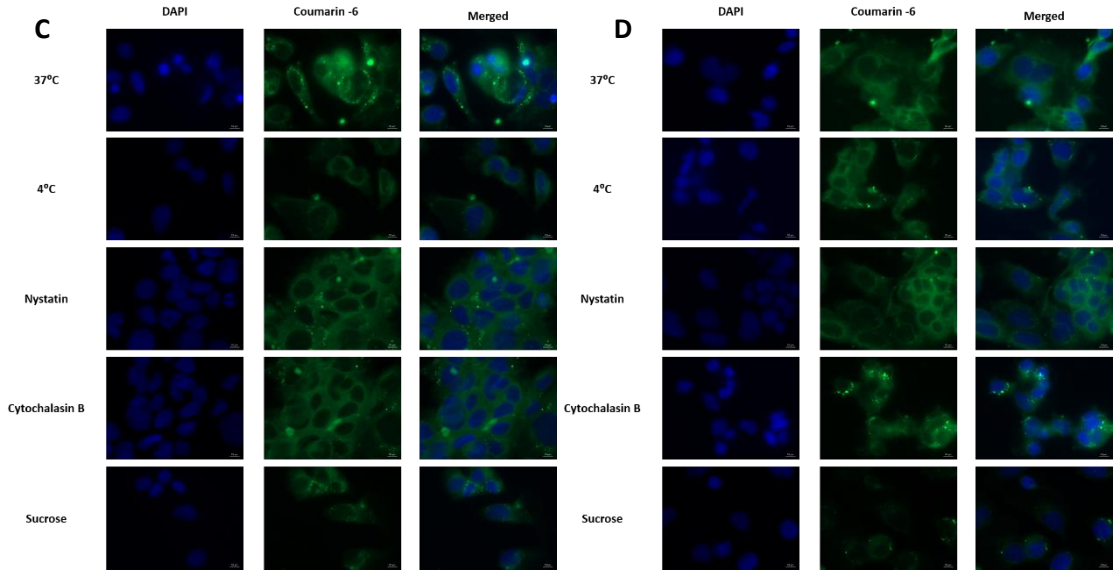

Figure 5-13. Fluorescence microscopy images of MCF-7 cell lines, cells treated with C. C6-RES-NLC-PGMC, D. C6-RES-NLC-PGML mechanism of internalization, cells were treated with various endocytosis inhibitors. The blue colour represents the DAPI nuclear stain, Green colour of coumarin-6 dye in RES-NLCs and the merged image of both DAPI and Coumarin-6. Scale bar 10 µm

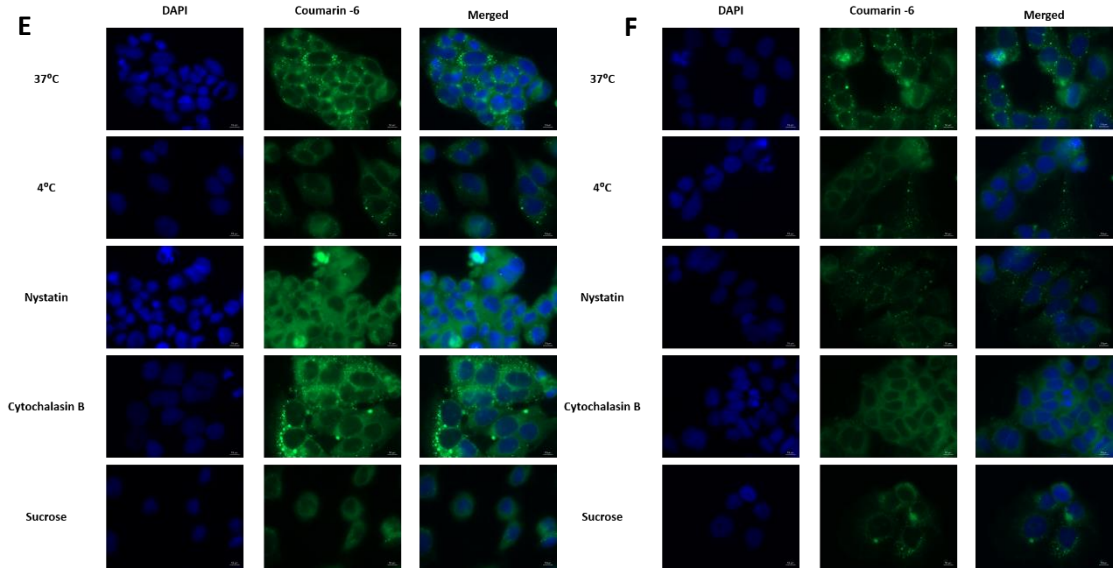

Figure 5-14. Fluorescence microscopy images of MCF-7 cell lines, cells treated with E. C6-RES-NLC-DO, F. C6-RES-NLC-GTC mechanism of internalization, cells were treated with various endocytosis inhibitors. The blue colour represents the DAPI nuclear stain, Green colour of coumarin-6 dye in RES-NLCs and the merged image of both DAPI and Coumarin-6. Scale bar 10 µm

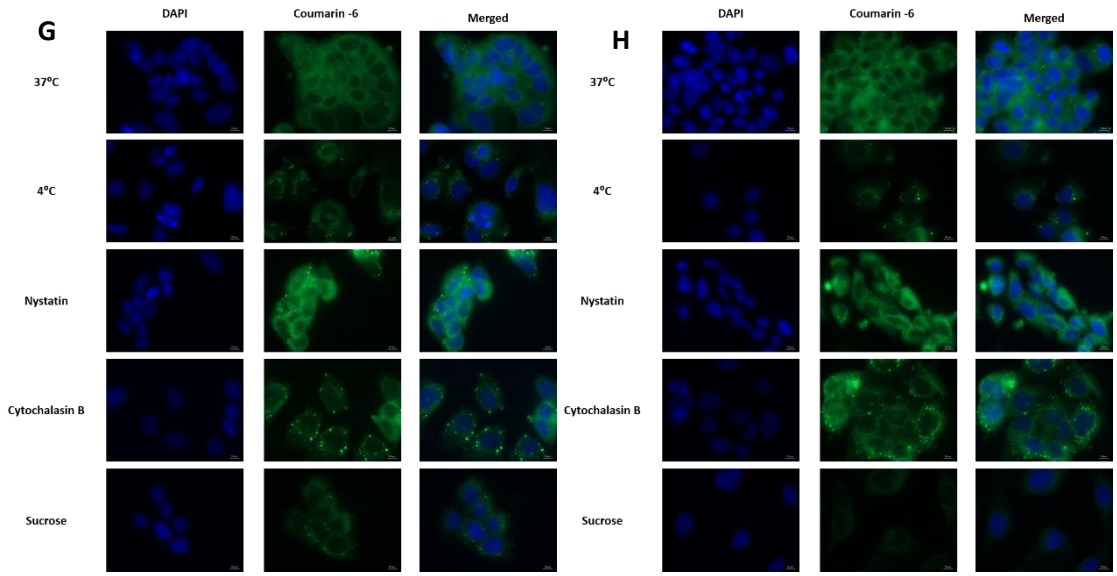

Figure 5-15. Fluorescence microscopy images of MCF-7 cell lines, cells treated with G. C6-RES-NLC-GTO-PEGS40, H. C6-RES-NLC-GTO-PEGS40-HA mechanism of internalization, cells were treated with various endocytosis inhibitors. The blue colour represents the DAPI nuclear stain, Green colour of coumarin-6 dye in RES-NLCs and the merged image of both DAPI and Coumarin-6. Scale bar 10 µm

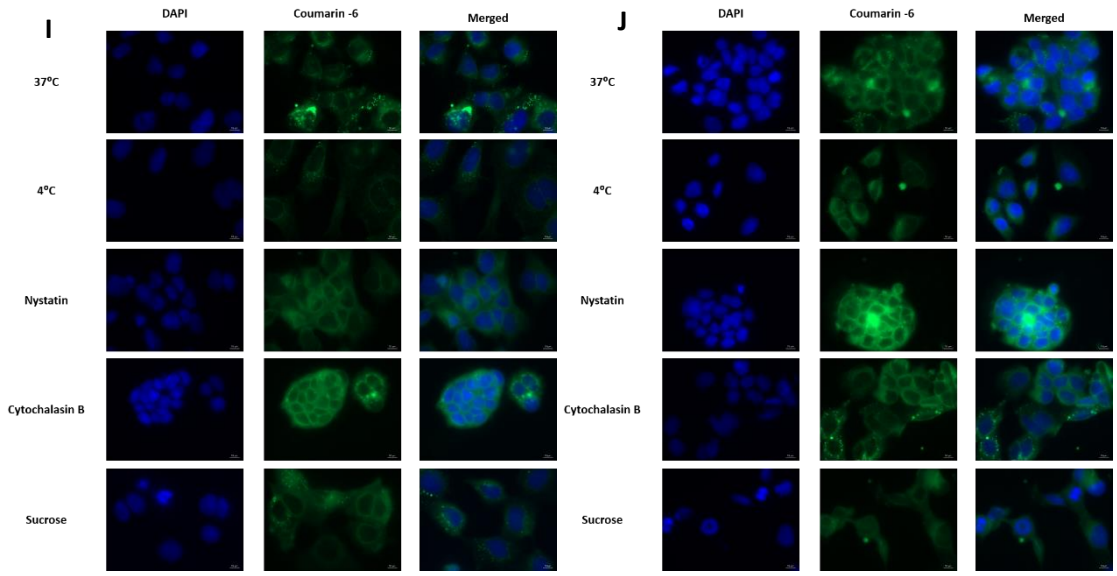

Figure 5-16. Fluorescence microscopy images of MCF-7 cell lines, cells treated with I. C6-RES-NLC-GTO-PEGS40-FA, J. C6-RES-NLC-GTO-PEGS40-HAFA mechanism of internalization, cells were treated with various endocytosis inhibitors. The blue colour represents the DAPI nuclear stain, Green colour of coumarin-6 dye in RES-NLCs and the merged image of both DAPI and Coumarin-6. Scale bar 10 µm

5.4.4 Bi-directional transport across Caco-2 monolayer and Caco-2/HT29 co-cultures studies

Nanoparticles gained the ability to overcome various biological barriers. However, to be effectively delivered to the mucosal sites the nanoparticles has to escape the rapid mucus clearance mechanism and penetrate through the mucus layer to reach to the epithelium (Lai et al., 2009).

Mucus act as a barrier against nanoparticle permeation to epithelial surfaces by two major mechanisms: particles might be retained by interacting with the mucus components or the size of the mucus mesh might obstruct nanoparticle penetration (Sigurdsson et al., 2013).

The aim of this study was not to enhance the permeability of RES, since RES is a highly permeable compound, but the main challenge is the extensive drug metabolism occurring in the GI tract, eventually affecting the oral bioavailability of the drug (Walle et al., 2004, Wenzel and Somoza, 2005, Maier-Salamon et al., 2006b, Cottart et al., 2010, Walle, 2011, Gambini et al., 2015). We hypothesis that RES-NLCs will be able to permeate through the GI tract protecting the drug from any degradation and metabolism and transporting it to the blood circulation to be carried to the tumour cells.

Six NLC formulations differing in the type of liquid lipid, PEGylated and three surface modified RES-NLCs were compared for their transport with free RES across Caco-2 monolayer (enterocyte-like model) and Caco-2/HT29 co-cultures (mucus model). Transport of drugs across Caco-2 monolayer can occur by one of these routes the passive transcellular, paracellular, carrier mediated route and transcytosis.

5.4.4 (I) Optimization of Caco-2 seeding density and monolayer integrity

The small intestinal epithelium, is the primary place for drug absorption and metabolism in the body. This epithelium is a known barrier for materials after the passage through the intestinal lumen prohibiting their access to the blood circulation (Baumgart and Dignass, 2002). Subsequently, established *in vitro* cell models to study the transport across the intestinal epithelium (Pan et al., 2015).

Transepithelial electrical resistance (TEER) is the measurement of electrical resistance through the cellular monolayer, it is a sensitive and consistent method employed in confirming both the permeability and integrity of the monolayer (Srinivasan et al., 2015). The monolayer integrity was determined by observing the TEER values over the period of cell proliferation.

TEER values are described (Reported TEER) in units of $\Omega.cm^2$ and calculated as follow:

$$\text{Reported TEER} = \text{R tissue } (\Omega) \times \text{M area(cm2)}$$

Where R is the resistance, M is the growth area of the semipermeable insert (M_{AREA}) in this case it is 1.12 cm^2.

Optimization and standardization of the timing of Caco-2 differentiation was done by monitoring the TEER values over the period of 27 days. The cells were seeded in five different seeding densities to determine the appropriate seeding density to conduct the transport experiments. Among the five densities only 1.5 $x10^4$ demonstrated better cell growth over the period of 27 days achieving the highest TEER value of 1500 $\Omega.cm^2$ in 17 days, other seeding densities 0.5 $X10^4$, 2.5 $X10^4$ and 5 $X10^4$ showed very low TEER value reached a maximum of 600 $\Omega.cm^2$ after 26 days. While, the highest seeding density 10 $X10^4$ showed an elevation then a drop in the TEER value during the growth period (Figure 5-17).

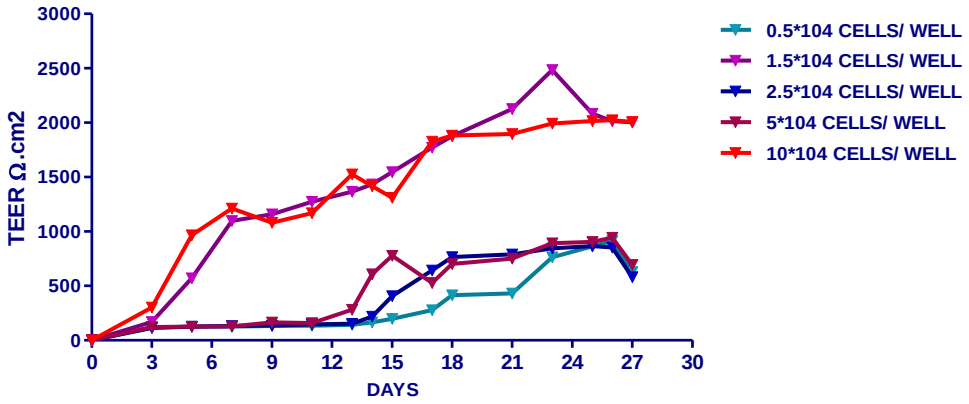

Figure 5-17. Optimization of Caco-2 seeding density for bidirectional permeability study

The TEER value demonstrates the physical structures and properties of filter grown epithelial cultures. TEER measurement has been predominantly applied for evaluating the permeability of tight junctions or the membrane perturbation by toxicants on intestinal epithelial cell lines (Chen et al., 2015).

The GI epithelia are classified based on the TEER values of the model as leaky by values 50-100 $\Omega.cm^2$, as intermediate as the value ranges form 300-400 $\Omega.cm^2$ and tight as the value 2000 $\Omega.cm^2$ (Srinivasan et al., 2015). Cells were seeded at a density of 1.5 x 10^4 cells/ insert (Figure 5-18. A), and allowed to grow and differentiate over the period of 18-21 days, with monitoring the TEER value every other day until they reach confluency (Figure 5-18. B)

In the present study the TEER value was monitored over the period of 18-21 days to give an indication of the time the Caco-2 monolayer is ready for the experiment to be performed. The integrity of monolayer was also verified by TEER measurement before and after the transport studies. After 6 days of culture, the TEER value increased gradually reaching the maximum value of 1700 Ω/cm^2 on day 17 post-seeding (Figure 5-19). Millicell membranes with monolayers TEER

>500 Ω/cm^2 were used for the transport studies. (Chen et al., 2016). Inserts with TEER < 200 Ω.cm^2 were not used for the study, since their integrity of monolayers was not maintained.

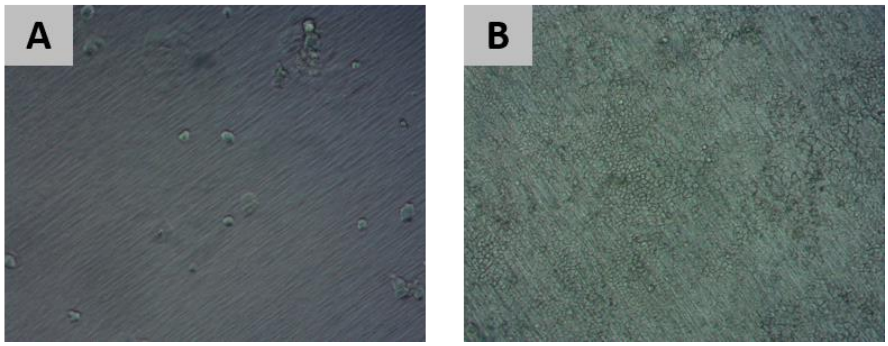

Figure 5-18. Caco-2 cells photographs of inserts A. Immediately after seeding and B. After forming a confluent monolayer 18 days Magnification 100×

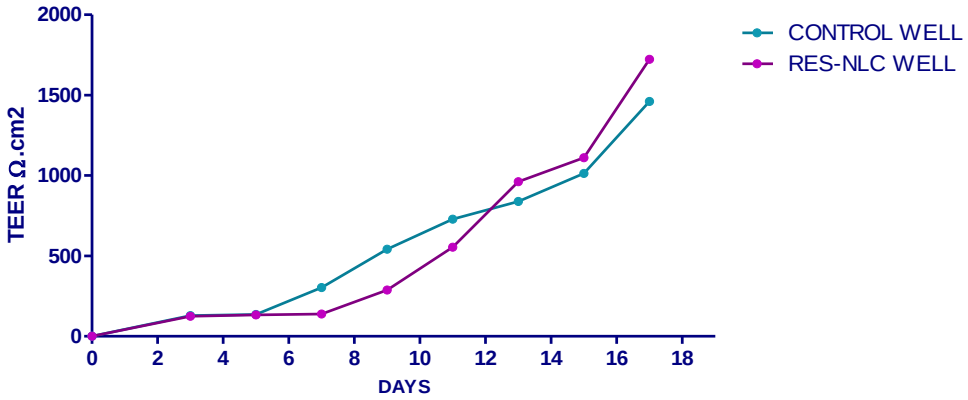

Figure 5-19. Integrity of TEER measurements of Caco-2 monolayer during the cells growth on the insert before the transport experiment.TEER is an indicator of the tight junction integrity of the cell monolayer. Therefore, the effect of RES-NLCs treatment on the ability to modulate the tight junction integrity can be monitored by the changes in the TEER value during the experiment comparing the values before conducting the experiment (Sha et al., 2005).

A study has established the association between TEER values and the monolayer integrity (Duizer et al., 1999). Only monolayers with close-up tight junction (TJ) were utilized for the transport studies. When the transport experiment was carried out from the apical-to-basolateral (A → B) compartment (Figure 5-20), no significant drop in the TEER value was observed as compared to the control at the first hour of RES-NLCs treatment, however, the TEER values showed a time dependent drop from 1 h to 4 h after which it plateaued till 6 h time period.

When basolateral-to-apical (B → A) transport was conducted it showed, pronounced drop in the TEER values at 1 h which further declined up to 4 h and plateauing thereby till 6 h was observed when compared with the control (Yin et al., 2009). A reduction of TEER for A → B compartment was almost 32.323 % and B → A compartment a reduction of 20.833 % (Yuan et al., 2013, Lv et al., 2013).

Both bidirectional transports resulted in a decline of TEER value indicating that NLCs had an effect the integrity of the monolayer. This could probably be due to modulation of the monolayer tight junctions by RES-NLCs, Previous report have that liquid lipids like PCG can affect the tight junctions and open up the tight junctions of the monolayer (Yin et al., 2009).

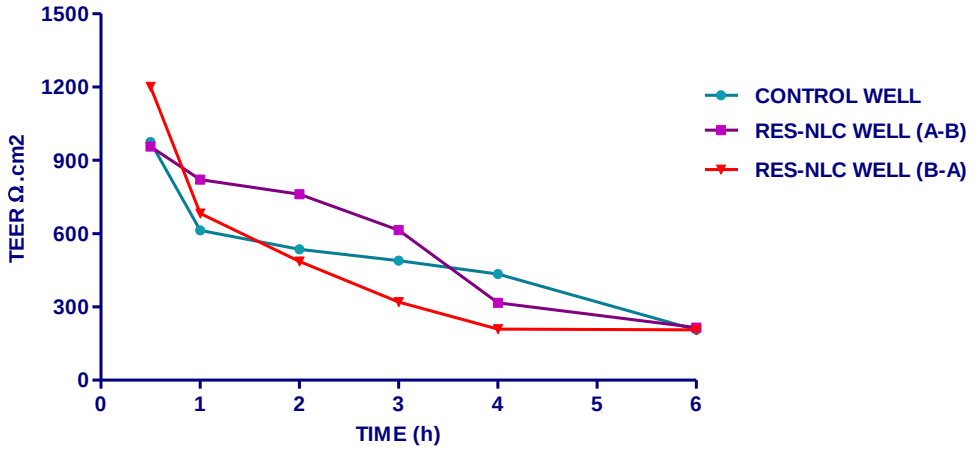

Figure 5-20. Caco-2 cells monolayer TEER values during bidirectional transport study for both control and RES-NLC treated cells transwells

5.4.4 (II) Caco-2 monolayer transport study

In order to investigate the effect of RES-NLCs on the transepithelial transport of RES, the permeability of six bare RES-NLCS, PEGylated and three surface modified RES-NLCs and free RES across Caco-2 cell monolayers were determined (Roger et al., 2012).

The objectives of the bidirectional study on both models were (i) to evaluate the suitability of RES-NLCs to act as a transporter for poorly water soluble drug using RES as biopharmaceutical classification system class II model drug (ii) to study the effect of the mucus layer on RES-loaded nanostructured lipid carriers (RES-NLCs) transport and (ii) to assess the muco-penetrating properties of surface modified RES-NLCs as a permeability enhancement of RES through the GI tract.

Drugs are classified in to three groups based on the previously published permeability of marker molecules (Balimane and Chong, 2005) has been used. Drugs with an apical to basolateral apparent permeability coefficient (A → B P_{app}) lower than 0.5×10^{-6} cm/s were classified as having low permeability, whereas compounds with A → B P_{app} between 0.5 and 10 and above 10 were classified as having moderate and high permeability, respectively (Sevin et al., 2013).

Upon the incubation of Caco-2 monolayer with free RES and various six bare RES-NLCs on basolateral side (A → B) demonstrated highest permeability with RES-NLC-PGML followed by free RES> RES-NLC-PCG> RES-NLC-PGMC> RES-NLC-GTO> RES-NLC-DO and RES-NLC-GTC. As hydrophobic drugs permeates readily through the cell by means of passive transcellular route, RES has Log P value of 3.1, the transport of which is governed by the passive transcellular absorption of

the drug through the intestinal epithelium (Artursson et al., 2001, Toaldo et al., 2015). In addition, the small particle size of RES-NLCs were able to transport across the monolayer into the basolateral compartment through receptor-mediated endocytosis (Chanburee and Tiyaboonchai, 2017).

The difference in the apparent permeability coefficient values (P_{app}) might be attributed to the nature liquid lipid (Sha et al., 2005). PGML being hydrophilic liquid lipid increased the permeability 1.7 folds as compared to RES ($p < 0.05$). PCG had long PEG chains also showed high transport across Caco-2 monolayer due to the increased the hydrophilicity of the compound (Yin et al., 2009). Previous reports have shown increase paracellular transport with polyethylene glycol esters (Uskoković et al., 2012) (Figure 5-21. A).

The higher P_{app} values A → B transport is an indicative for the good oral absorption *in vivo*. Although free RES had high permeability but also all RES-NLCs showed good permeability for free RES. On examination of the P_{app} values A → B transport, data shows that free RES rapidly starts to cross Caco-2 monolayer as early as 30 min showing P_{app} value of 1.7 X 10^{-5} cm/s (Sessa et al., 2014). This initial burst permeability has been previously reported in previous studies where P_{app} of free resveratrol is in agreement with our value of 1.6 × 10^{-5} cm/s in HBSS medium, various studies reported comparable results (Kaldas et al., 2003, Maier-Salamon et al., 2006b, Teng et al., 2012, Willenberg et al., 2015, Muller et al., 2000a). After 30 min the P_{app} values for free RES and all formulations declined, this might be due to the extensive phase II metabolism of free RES by the Caco-2 cells (Willenberg et al., 2015). Upon the examination of the B → A P_{app}, free RES have shown the highest transport from the basolateral side to the apical side with value of 6.7 X 10^{-5} followed by RES-NLC-GTO> RES-NLC-DO> RES-NLC PGMC> RES-NLC-PGML> RES-NLC-PCG and RES-NLC-GTC (Figure 5-21. A).

Although most RES-NLCs did not show high P_{app} values compared to free RES except for RES-NLC-PGML, but they reduced the backward transport of the drug from B → A. This is an important advantage achieved with RES-NLCs as it would lead to higher drug absorption and improve the bioavailability of RES. It is evident that RES-NLCs protected the drug from the degradation at physiologic pH. Another reason might be the due to the limit of single Caco-2 model, the particle size and surface charge of nanoparticles and the underlying cellular trafficking mechanism sharing multiple pathways, as reported by other studies (Kulkarni and Feng, 2013, Shi et al., 2015). It is noteworthy that the order of permeability of RES formulations did not correlate with the data obtained from the intracellular uptake, this might be probably caused by the non-specific mechanisms that lower the transport of RES-NLCs, this was in correlation to other study (Beloqui et al., 2013).

All RES-NLCs showed an efflux ratio (B → A/ A → B) in the range of 0.129 to 0.452 indicating that there is no involvement of active efflux for the drug and the formulations (Figure 5-23.A), since RES

is not a substrate of P-gp efflux transporter, this results were correlated other studies (Wang et al., 2005, Maier-Salamon et al., 2006b).

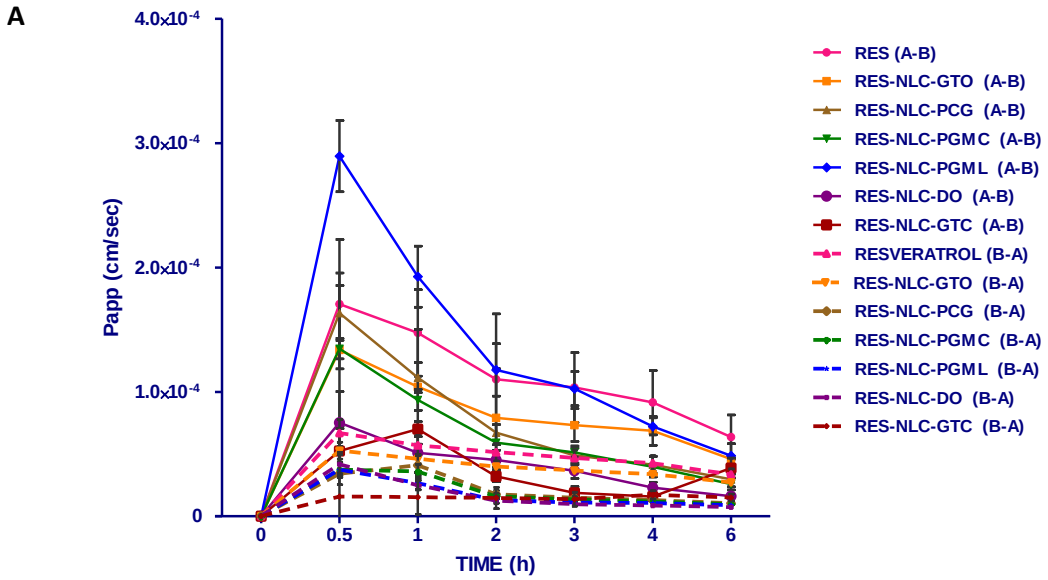

Figure 5-21. Apparent permeability of RES and RES-NLCs from apical-to-basolateral compartment (A-B) / basolateral-to-apical (B-A) across Caco-2 monolayer. Values reported as mean± SD (n =3)

RES-NLC-GTO has shown enhanced cytotoxicity on both MCF-7 and MDAMB-231 cell lines with improved safety on MCF-10A cell lines. Though this formulation showed promising efficacy and safety it revealed low P_{app} value than free RES. Therefore, an attempt was made to improve its permeability by PEGylating and further surface modification with HA and FA ligands.

RES-NLC-GTO-PEGS40 and RES-NLC-GTO-PEGS40-HA shower higher P_{app} values as compared to RES-NLC-GTO indicating that the PEGylation and functionalization with HA offered improvement in permeability. This might be due to the hydrophilic nature of the two polymers (Yuan et al., 2013) (Figure 5-22. B). The transport of RES-NLC-GTO-PEGS40-FA and RES-NLC-GTO-PEGS40-HAFA ($p< 0.05$) was markedly higher than RES-NLC-GTO-PEGS40 and RES-NLC-GTO-PEGS40-HA and Free RES. Thus, these nanoparticles improved the active transport through the enterocytes. This could be because of the CD44 and folate receptors are expressed on the intestinal epithelial cells (Trejdosiewicz et al., 1998, Roger et al., 2012). The functionalized RES-NLCs demonstrated a positive effect on the transcellular transport which eventually improves the drug absorption and the oral bioavailability (Figure 5-22.B).

PEGylated and the three surface modified RES-NLCs showed lower B → A transport when compared to the drug (Figure 5-23. B), also the efflux ratio of PEGylated and the three surface modified RES-NLCs was in range of 0.121 to 0.254 indicating that no active efflux was implicated when compared to the bare RES-NLC-GTO, the threshold for the active efflux was reported to be > 3 (Wang et al., 2005).

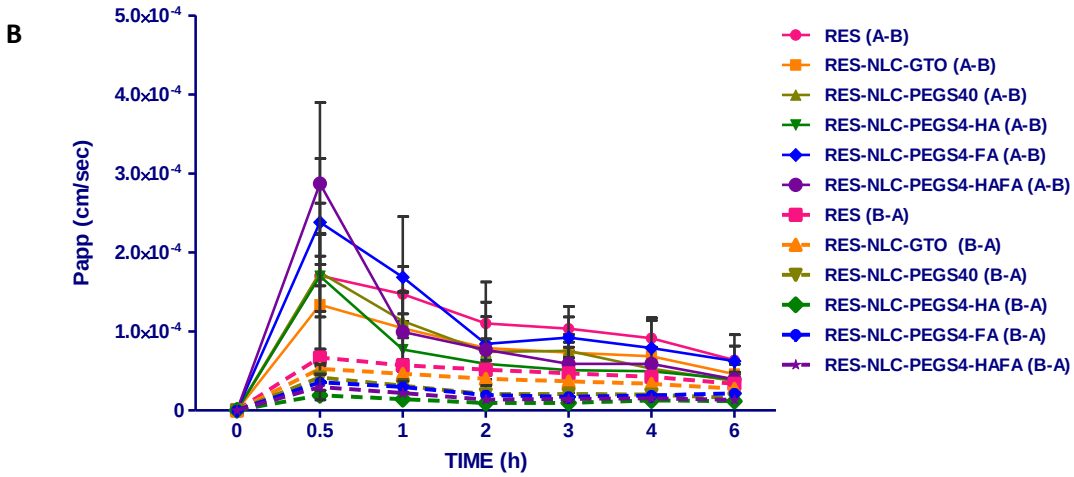

Figure 5-22. Apparent permeability of RES, PEGylated and surface modified RES-NLCs from apical-to-basolateral compartment (A-B) / basolateral-to-apical (B-A) across Caco-2 monolayer. Values reported as mean± SD (n =3)

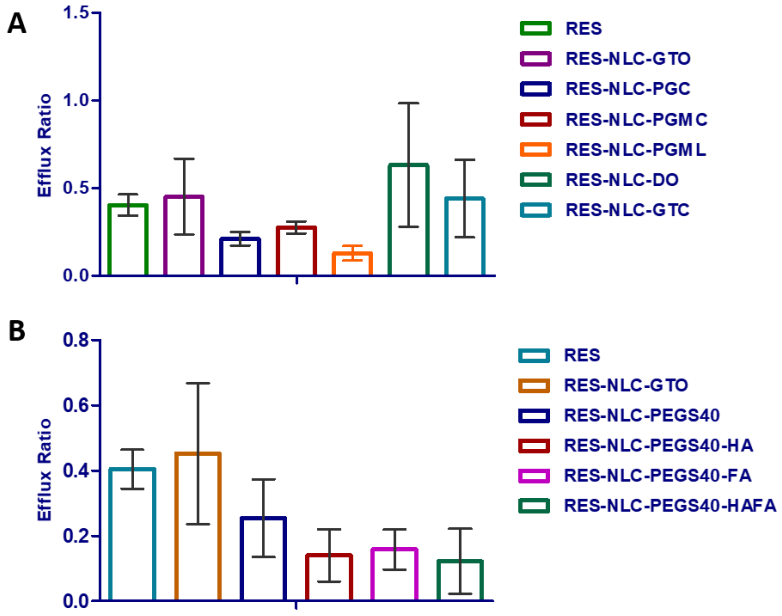

Figure 5-23. Efflux ratios at 30 min after treatment with free RES and A. Bare RES-NLCS, B. PEGylated and surface modified RES-NLCs across Caco-2 monolayer. Values reported as mean± SD (n =3)

5.4.4 (III) Caco-2/HT29 co-cultures transport study

The lack mucous production by Caco-2 cells (enterocytes like cells) results in a low paracellular permeability which limits the usefulness of this model to predict the oral bioavailability (Silva et al., 2006, Lundquist and Artursson, 2016). Moreover, the Caco-2 cells tight junctions are similar to the colon rather than the small intestine, leading to higher TEER values (Le Ferrec et al., 2001). In order to modify and simulate the Caco-2 model, co-cultures with mucous secreting cells HT29 offer better simulations of both the function and morphology of the GI epithelial cells. HT29 are human colorectal carcinoma cells function as goblet cells that secretes various mucins, in addition the tight junctions are not as tight as in Caco-2 monolayer (Li et al., 2013b). The cell monolayer integrity before and during the experiments was determined by TEER measurement using an EVOM epithelial volt-ohm meter equipped with chopstick electrodes to monitor the evolution of confluence and integrity (Yamashita et al., 2000). Three different areas were chosen to detect the TEER values in each well and the results were expressed as averages of the final results. TEER values > 400 $\Omega.cm^2$ were used for the permeability studies (Pan et al., 2015).

Previous studies have established 90:10 (Caco-2:HT29 ratio) as the optimal seeding density for the co-culture model (Béduneau et al., 2014, Martínez-Augustin et al., 2014, Pan et al., 2015). It was observed that including other cells into the model such as goblet cells mucus producing cells will cause a declines in the TEER values producing a more physiological model. The low TEER values is due to the fact that the two cells grow in colonies forming a discontinuous mucous layer (Srinivasan et al., 2015, Lundquist and Artursson, 2016). The data showed (Figure 5-24) that the TEER value increased after 11 days to reach a maximum value of 500 $\Omega.cm^2$ at day 17 post seeding, indicating the formation of the co-culture monolayer (Guri et al., 2013).

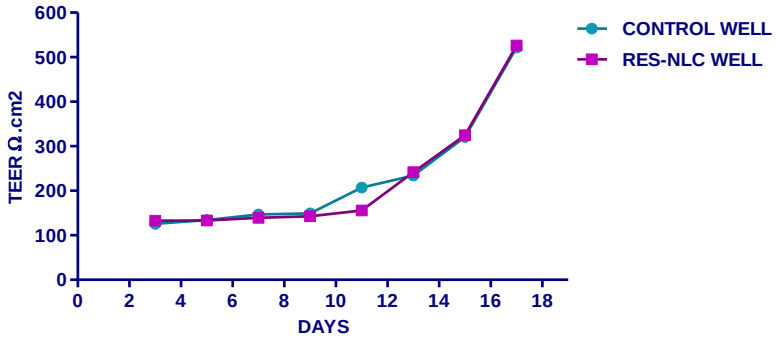

Figure 5-24. Integrity of TEER measurements of Caco-2/ HT29 co-cultures during the cells growth on the insert

The data showed 50 % reduction in the TEER value when A→ B transport was conducted for RES-NLCs over the first 1 h of experiment, while a remarkably lower effect on the TEER value was observed when B → A transport was conducted. This indicates that the RES-NLC affected the

integrity of the co-culture during A→ B transport rather B → A compartment across the cells monolayer.

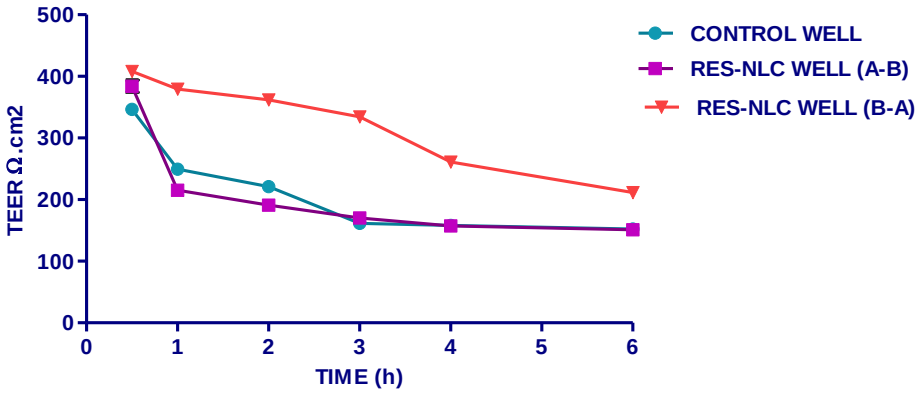

Figure 5-25. Caco-2/HT29 co-cultures TEER values during bidirectional transport study for both control and RES-NLC treated cells transwells

The Transepithelial transport of free RES, six bare RES-NLCS, PEGylated and three surface modified RES-NLCs was investigated on the permeability RES across Caco-2/HT29 co-culture cell. The data for P_{app} values A → B transport demonstrated that free RES was readily present after 30 min in the basolateral side 5 X 10^{-5}, indicating the high transport of the drug. Bare RES-NLCs showed lower permeability when compared to the drug ($p< 0.05$) with RES-NLC-PCG showing high transport (4.39 X10^{-5}) followed by RES-NLC-PGMC> RES-NLC-PGML> RES-NLC-DO> RES-NLC-GTC and RES-NLC-GTO (Figure 5-26.A).

The reduced transport might be attributed to the mucus layer produced by the goblet cells which offer additional barrier against nanoparticles transport. The different permeability pattern exhibited by the nanoparticles could be attributed to the difference in their particle size and surface characteristics (Georgantzopoulou et al., 2016, Lundquist and Artursson, 2016). In this approach the co-culture forms a tighter monolayer than expected under the applied culture conditions (Artursson et al., 2001).

Upon the examination of the B → A P_{app} free RES have shown the highest transport from the basolateral side to the apical side with value of 8.1 X 10^{-5} followed by RES-NLC-PCG> RES-NLC-GTC> RES-NLC PGML> RES-NLC-GTO> RES-NLC-PGMC and RES-NLC-DO (Figure 5-26. A). It is clearly evident that incorporation of the drug in NLCs reduced its transport back into the apical side. This would results in improved bioavailability of RES with RES-NLC formulations.

Bare RES-NLCs showed low efflux ratio (Figure 5-28.A) ranging between 0.105-0.260 indicating the absence of the active efflux process by the model (Wang et al., 2005).

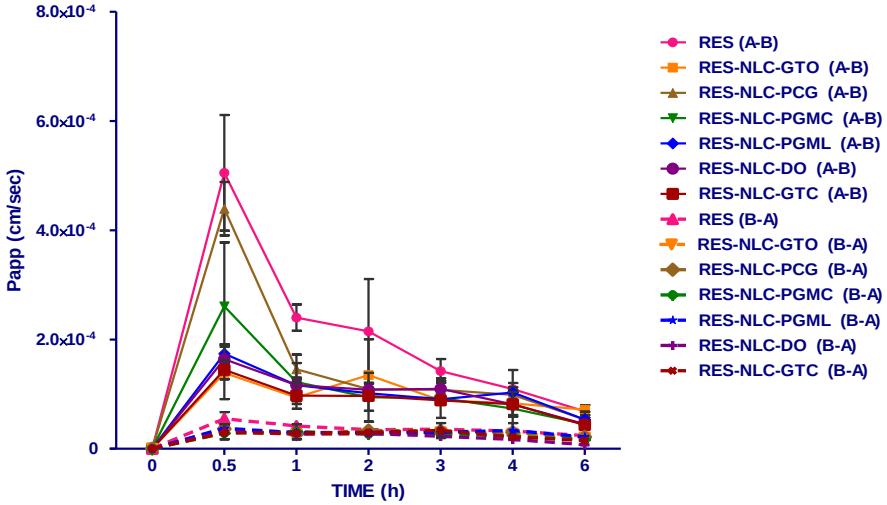

Figure 5-26. Apparent permeability of RES and RES-NLCs from apical-to-basolateral compartment (A-B) / basolateral-to-apical (B-A) across Caco-2/HT29 co-cultures. Values reported as mean± SD (n =3)

Surface modification of nanoparticles with either HA or FA did not improve the transport when compared to the RES-NLC-GTO (Figure 5-27). This might be due to the fact that the nanoparticles were trapped by the mucous produced by HT29 cells in the co-culture (Yuan et al., 2013). However, PEGylation and improved the transport probably due to the hydrophilic nature. Previous report has demonstrated remarkable mucous penetrating ability of PEG lipid nanoparticles (Yuan et al., 2013). Dual ligand HAFA appending of RES-NLCs also showed an improvement in the permeability, this might be attributed to the expression of HA and FA receptors on the enterocytes.

The efflux ratio of the PEGylated and surface modified RES-NLCs showed higher values ranging from 0.105-0.362 but did not exceed the threshold of 3 (Figure 5-28. B) indicating that there is no involvement of active efflux, as demonstrated by wang in their permeability study (Wang et al., 2005).

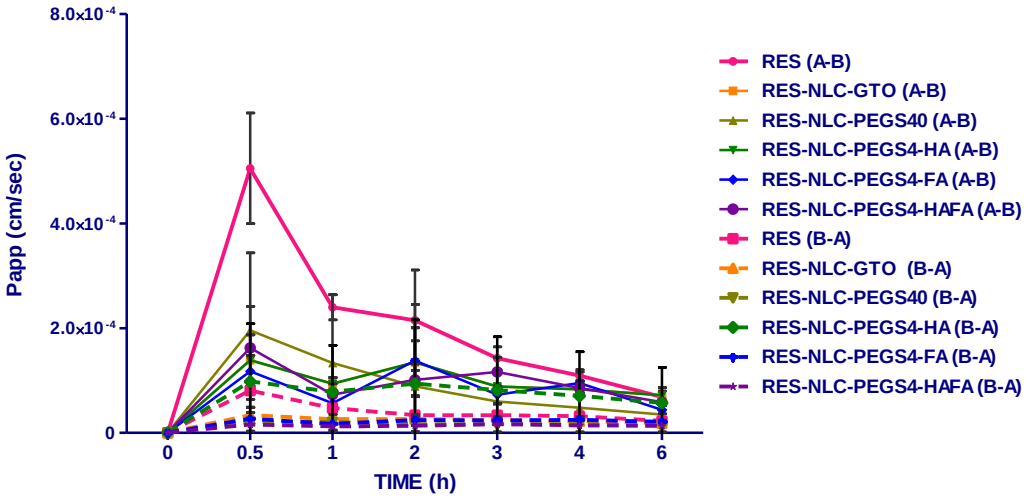

Figure 5-27. Apparent permeability of RES, PEGylated and surface modified RES-NLCs from apical-to-basolateral compartment (A-B) / basolateral-to-apical (B-A) across Caco-2/HT29 co-cultures. Values reported as mean± SD (n =3).

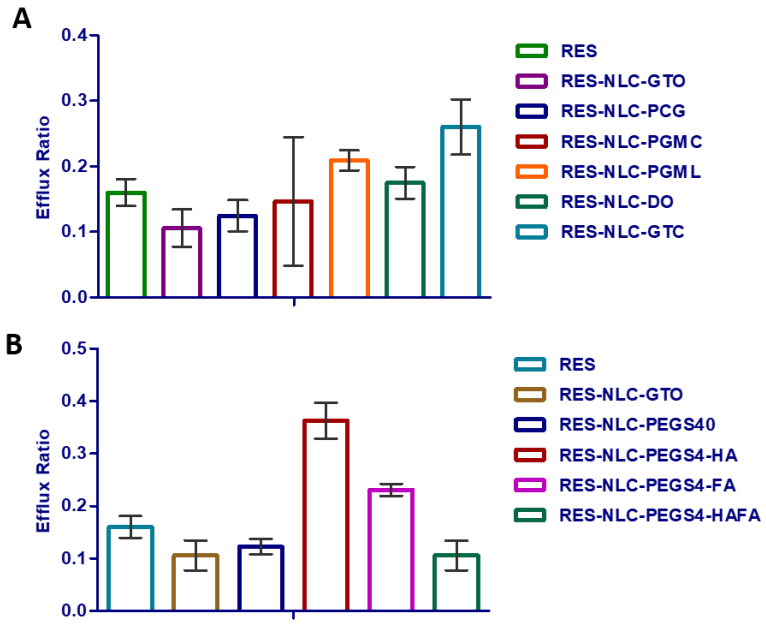

Figure 5-28. Efflux ratios at 30 min after treatment with free RES and A. Bare RES-NLCS, B. PEGylated and surface modified RES-NLCs across Caco-2/ HT29 co-cultures. Values reported as mean± SD (n =3).

Upon comparison RES NLCs made with different liquid lipid showed different permeability in the two models. Though, the co-culture model has an additional mucous secreting barrier still the permeability of nanoparticles were observed to be higher than that revealed by Caco-2 monolayer model.

Free RES showed 2.9 fold increase in the permeability and transport across Caco-2/HT29 layer as compared to the Caco-2 monolayer model. While, the RES-NLCs (PCG, PGMC, DO and GTC) showed 1.6 fold to 2.7 fold increase in the permeability and transport across Caco-2/HT29 layer as compared to the Caco-2 monolayer model. RES-GTO showed comparable permeability in both the models. Surprisingly RES-NLC-PGML unlike other RES-NLCs showed a lower permeability and transport across Caco-2/HT29 layer as compared to the Caco-2 monolayer model. Similar differences in NLCs transport with different models have been observed in a previous study (Beloqui et al., 2013).

5.4.5 Blood compatibility assay

Erythrocytes are amongst the primary cells that come into contact with extraneous materials in the blood system. Hemolysis (destruction of red blood cells) *in vivo* can lead to various disorders such as anaemia, jaundice, and other pathological conditions; therefore the hemolytic potential of various administered pharmaceuticals must be evaluated for early development formulations also during preclinical studies (Amin and Dannenfelser, 2006).

Blood hemolysis assay was conducted to test the hemocompatibility of the optimized RES-NLC-GTO along with the surface modified RES-NLCs by studying their effect on erythrocytes. In order to determine the safety of the formulation once they get into the systemic circulation after administration (Figure 5-29).

Normal saline solution is taken as negative control as it causes no hemolysis and Triton X-100 2 % was taken as positive control and its absorbance was considered as 100 % hemolysis as it showed maximum hemolysis. All RES-NLCs and blank NLC at all concentration level showed less than 5% hemolysis when incubated for 1 and 4 h respectively (Figure 5-30. A, B).

Therefore, it can be concluded that RES nanoparticles were safe and would not cause any hemolysis of RBCs when they come in contact with blood. These results corroborate with previous reports on the safety of lipid nanoparticles upon their interaction with blood (Li et al., 2010, Kumar et al., 2014, Doktorovova et al., 2014).

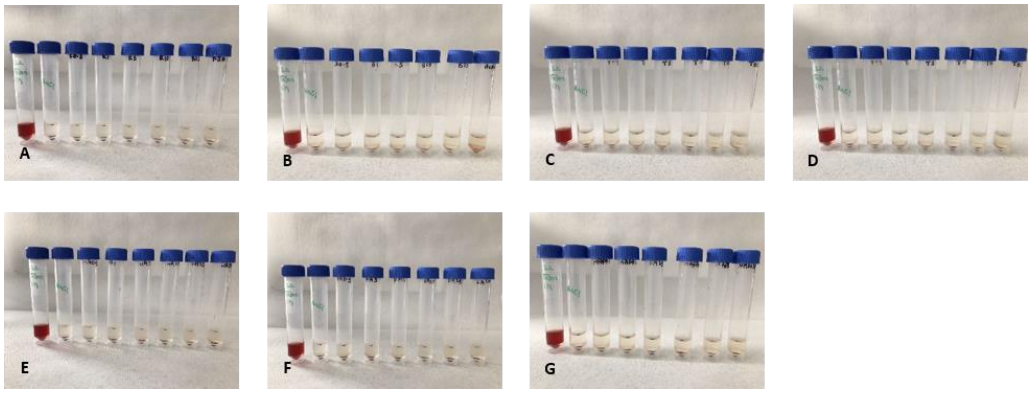

Figure 5-29. Images for the % hemolysis of erythrocyte after incubation for 1h with various NLCs concentrations from left hand side first tube represents the positive control (Triton X100), negative control (0.9 % normal saline solution), 0.5, 1, 5, 10, 25 and 50 µg/mL of A. Free RES, B. Blank NLC-GTO, C. RES-NLC-GTO, D. RES-NLC-GTO-PEGS40, E. RES-NLC-GTO-PEGS40-HA, F. RES-NLC-GTO-PEGS40-FA and G. RES-NLC-GTO-PEGS40-HAFA. Values reported as mean± SD (n =3).

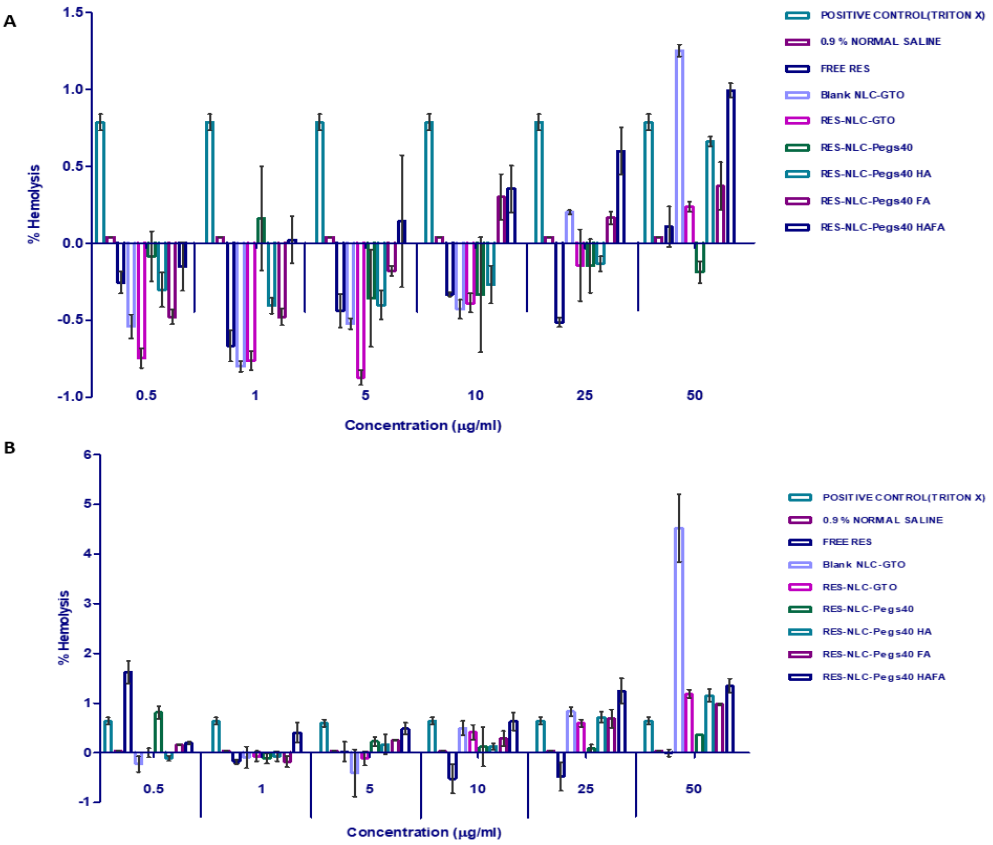

Figure 5-30. % hemolysis of erythrocyte dispersion when incubated for A. 1 h, B. 4 h with various concentrations of free RES, bare, blank , PEGylated and surface modified RES-NLCs. Values reported as mean± SD (n =3)

5.5. Conclusions

Bare, PEGylated and surface modified RES-NLCs were observed exhibit no detrimental effect upon both Caco-2 and HT29 cell lines. All RES-NLCs displayed maximum cellular uptake after 2 h incubation and showed clathrin mediated endocytosis.

The conducted bidirectional transport study showed permeability was impacted by the type of liquid lipid used for fabrication of RES-NLCs with higher permeability obtained with formulation containing PGML as liquid lipid when studied using Caco-2 monolayer. However, free RES exhibited higher permeability when transport studies were conducted using Caco-2/HT29 co-culture potentially due to hindrance provided by mucous production by HT29 cells. This hindrance was overcome by PEGylation and surface modification by HA showing better transport across both Caco-2 monolayers and Caco-2/HT29 co-culture.

Chapter 6 : Conclusions and Future Work

6.1. Overall objectives

The aim of the project was to develop and optimise Nanostructured lipid carrier system of a bioactive phytodrug resveratrol using design of experiments and understanding the effect of liquid lipid on its performance and stability. Moreover, resveratrol NLCs were surface functionalised using dual ligands hyaluronic acid and folic acid to target double receptors, CD44 and folate overexpressed on both non triple negative and triple negative breast cancer cells for improved breast cancer therapeutics.

6.2. Overall Conclusion

6.2.1 Background

Breast cancer includes a group of very heterogeneous diseases. Triple negative breast cancer (TNBC) accounting for almost 20 % of breast cancers is a clinically aggressive type of cancer as it does not express oestrogen, progesterone and human epidermal growth factor receptors. Because of its very poor responsiveness to chemotherapy, treating this type of cancer presents is a major challenge due to the poor disease prognosis and the need of newer and safer therapies. The main drawbacks of chemotherapeutics are their potential toxic effects, which limits the dose to be given that the patient can tolerate. Recent therapy focused on the use of natural products like resveratrol to treat this type of cancer. Despite high bioactivity of resveratrol poor water solubility, low oral bioavailability and high chemical instability poses major challenges for its therapeutic delivery. Its poor aqueous solubility is unfavorable for incorporation of high levels of resveratrol in aqueous based pharmaceuticals. In addition, low water solubility reduces the dissolution-rate limited cell absorption leading to reduced oral bioavailability due to rapid and extensive metabolism. Because of the poor bioavailability of resveratrol, coupled with rapid and extensive metabolism, the concentrations of resveratrol at target tissues and cells appear far from sufficient to exhibit efficacy in humans.

NLCs can provide solution owing to its properties such as nano size, ability to achieve high drug loading and resolve drug expulsion issues during storage and impart stability. In addition, NLCs can improve intestinal permeability, modify biodistribution, pharmacokinetic and metabolism profile of loaded drug and facilitate drug efficacy by surface modification with specific targeting ligands and reduced side effects on normal cells. Additionally PEGylation may offer enhanced circulation times and protection from enzymatic degradation.

A nanostructured carrier system of RES with suitable solid and liquid liquids was envisaged with systematic investigation on the impact of liquid lipid on RES-NLC properties. Considering the overexpression of CD44 and folate receptors on breast cancer cells, HA and FA were conjugated on RES-NLCs to develop a double receptor targeting nanostructured delivery system of resveratrol for improved targeting.

6.2.2 Analytical method development

A validated analytical method is considered a critical factor in the chromatographic development of pharmaceutical drug substances. During the course of development of RES-NLCs, drug content needs to be quantified in different substrates. Therefore, simple, precise, accurate, sensitive, specific, robust, and reproducible HPLC methods were successfully established and validated for the determination of RES in RES-NLCs, different buffer medias, dissolution media and transport media for bidirectional permeability studies.

Optimum chromatographic separation was achieved by a mobile phase consisting of acetonitrile and water, used at a flow rate of 1.0 mL/min in a gradient elution method for the effective separation of RES in various conditions. The chromatograms of RES showed sharp well separated peaks for the analyte. All the developed HPLC methods in chapter 2 were validated for linearity, range, LOD, LOQ, precision, accuracy, reproducibility and robustness as per ICH guidelines.

The HPLC method developed for the quantification of free and total dug in the NLCs demonstrated high linearity with a coefficient of regression ranging from 0.999-0.9998 in the range of 0.1 to 10 µg/mL. The minimum detectable concentration of *trans*-resveratrol (LOD) was 0.031 µg/mL and the minimum concentration that the HPLC method is able to quantify (LOQ) was 0.093 µg/mL. Both methods exhibited high precision and accuracy with sample recovery ranging from 85.6-99.8 %. The methods were also deemed to be repeatable and reproducible after minute alterations in the chromatographic conditions. The methods exhibited high specificity and selectivity to the RES in the RES-NLCs, allowing for the efficient determination of drug in a mixture of components with good stability for the period of one month. The methods could be also applied to quantify RES in coumarin-6 tagged RES-NLCs without any interference from coumarin.

Moreover, the HPLC methods was effectively developed in various pH buffer solutions (1.2, 5, 6.8 and 7.4) enabling the study of drug stability in different buffer solutions and in HBSS transport media for Caco-2 cell line bidirectional studies. The methods revealed high linear regression for all studied buffers and transport media with an R^2 value ranging from 0.9993-0.9999 and were precise and accurate with high RES recovery and stability for the period of one month.

Forced degradation studies revealed degradation of RES in basic, acidic and UV-photolytic stress conditions with maximum degradation in basic conditions (99 %) followed light degradation (95 %) and then acidic environment (82 %). However, a good stability with only 20% degradation under both dry heat and oxidative stress was demonstrated.

6.2.3 Formulation development, optimization and physicochemical characterizations

RES-NLCs using trimyristin as solid lipid were successfully optimized using 3-factor, 3-level Box–Behnken design. The effect of four critical independent variables entailing liquid lipid type, liquid lipid concentration, Tween 80 concentration and drug amount on the response variables viz. particle size, polydispersity index, zeta potential, % entrapment efficiency and % drug loading of RES-NLCs was explored. The six liquid lipids investigated for preparation of RES-NLCs included PCG, PGMC, PGML, GTO, DO and GTC out of which two were triglycerides, one medium chain triglyceride and one long chain triglyceride, two were propylene glycol esters, one was fatty acid ester and one PEGylated lipid. Each liquid lipid desirability space with the values close to 1 was considered best for the optimized formulation indicating higher desirability of corresponding response properties. Quadratic models were found to be significant for particle size; polydispersity Index, entrapment efficiency and total drug and mathematical equations were derived from these models and design space was created for achieving desired responses.

The particle size of the prepared RES-NLCs was in range of 24.98-131.4 nm. The most significant factor contributing to the variation in the particle size was the amount liquid lipid as shown by the large value of the coefficient in the quadratic equation. RES-NLCs demonstrated monodisperse particles with polydispersity (0.113-0.452). The most evident factor affecting the PDI was the surfactant concentration. Increasing the amount of Tween 80 concentration lead to better homogeneity in particle size and reduced aggregation. The RES-NLCs showed negative zeta potential values of -21.3 to -39.9 mV. Zeta potential of RES-NLCs was mostly affected by the amount of surfactant, which has shown to act as steric hindrance, thus contributing to the stability of the formulations. For most RES-NLCs. The liquid lipid concentration demonstrated a prominent effect on the % entrapment efficiency of RES in NLCs as shown by the positive coefficient from the quadratic equations with entrapment efficiency ranging from 91.368-99.576 %. RES-NLCs displayed a loading of 2.937-7.557 %, which was mainly influenced by the surfactant concentration, exhibiting a strong positive effect on the response as evident form the positive value of the coefficient in the quadratic equations. Thus using Box Behnken design, tuneable RES-NLCs can be produced with particles size (< 100 nm), particle size distribution (< 0.3), with negatively charged surface (-24mV), high entrapment efficiency (91-99 %) and drug loading (2-7 %) within the established design space.

RES-NLC were PEGylated for prolonged circulation and further surface modification was performed using HA and FA targeting ligands using EDC-NHS chemistry. It was established that the amine: HA ratio of 12:1 and amine: FA was 5:1 was the most favorable ratios for conjugation of HA and FA respectively. Surface modification led to increase in size but no change in PI and total drug.

RES-NLCs showed spherical shape and particle size < 100 nm as revealed scanning and transmission electron microscopy. DSC, XRD and FTIR confirmed the presence of entrapped drug in amorphous state in NLCs. FTIR spectral analysis and reduction of free surface amines also confirmed the covalent bonding of ligands.[1]NMR studies showed that the drug is incorporated in the formulation without interaction with any other components. RES-NLC showed a low drug release at pH 1.2 with less than 20 % release rate over the period of 4 h confirming its protection for drug in gastric fluid. Surface modified RES-NLCs showed only 2 % release at pH 1.2 over the period of 4 h offering more protection to the drug by delaying the release in acidic environment. Modified Releaseof RES over the period of 24 h at pH 5 would enable prolonged effect in tumour environment from both bare and surface modified formulations. RES-NLC with good stability over the period of six month could be developed with GTO as liquid lipid. However, surface modification reduced the stability of formulations to two months.

6.2.4 In vitro anticancer activity of developed resveratrol Nanostructured lipid carriers

In-vitro cytotoxicity studies using presto blue showed that RES-NLCs were effective against both non-TNBC, MCF-7 and TNBC, MDAMB-231 breast cancer cell lines. HA and FA dual modification of NLCs caused specific binding to MCF-7 and MDAMB-231 breast cancer cells as CD44 and folate receptors are overexpressed on both these cells and thus showing improved targeting. The dual ligand appended RES-NLC-GTO-PEGS40-HAFA showed 2.7 folds higher toxicity in MCF-7 and 3.6 fold higher toxicity in MDAMB-231 cells as compared to RES-NLC-GTO-PEGS40 demonstrating its potential for treatment in the aggressive triple negative cancer.

None of the RES-NLCs formulations containing different liquid lipids or their empty counterparts without drug were cytotoxic to healthy MCF-10A cells demonstrating safety of the formulations and excipients employed. Surface modification further reduced the toxicity on healthy cell lines confirming their safety on the non-tumorigenic cells. All nanoparticles showed a considerable safety on macrophages.

All bare PEGylated and surface modified RES-NLCs showed time dependent cellular uptake on both MCF-7 and MDAMB-231 cell lines. The type of liquid lipid had an impact on cell internalization of the formulations. The highest fluorescence intensity was observed with RES-NLC-GTO in both MCF-

7 and MDAMB-231 cells. Surface modification lead to 3 fold increase in the cellular uptake confirming the targetability potential of the ligand appended formulations toward overexpressed receptors on the surface of both cancer MCF-7 and MDAMB-231 cells.

Mechanism of cellular uptake was evaluated using different pharmacological inhibitors and ligand appended nanoparticles were internalised by cells by combined mechanisms of clathrin-mediated endocytosis and receptor-mediated endocytosis while internalisation of bare RES-NLCs was governed by clathrin-mediated endocytosis but was independent of receptor mediated endocytosis. All bare and surface modified RES-NLCs showed low uptake by macrophages and MCF-10A cells confirming their safety. Cell cycle analysis showed that nanoparticles arrest MCF-7 and MDAMB-231 cells in S phase of cell cycle.

6.2.5 Bidirectional Intestinal Permeability Studies

Bare, PEGylated and surface modified RES-NLCs were found to be safe on both Caco-2 and HT29 cell lines. All RES-NLCs displayed maximum cellular uptake after 2 h incubation and showed clathrin mediated endocytosis.

Bidirectional transport study showed permeability was affected by the type of liquid lipid used for fabrication of RES-NLCs with higher permeability obtained with formulation containing PGML as liquid lipid when studied using Caco-2 monolayer. However, free RES showed higher permeability when transport studies were conducted using Caco-2/HT29 co-culture probably because of hindrance offered by mucous production by HT29 cells. This hindrance was overcome by PEGylation and surface modification by HA showing better transport across both Caco-2 monolayers and Caco-2/HT29 co-culture

Thus, in conclusion robust and rugged optimized RES-NLCs have been successfully developed using design of experiments. Further appending dual ligands HA and FA improved the cytotoxicity and targetability towards both non-TBNC and TBNC cancer cells and improved safety on MCF-10 A normal cells. These dual appended formulations have potential for use in improving breast cancer therapeutics with the use of safer plant derived phytochemical agent resveratrol.

6.3. Future work

Research conducted in present study is by no means exhaustive. Further studies are required to exploit these systems for their potential use in breast cancer therapeutics. Given below is an outline of some of ideas proposed for future work:

- Liquid NLC nano-dispersions have limited stability; therefore, future work encompassing converting the liquid nano-dispersion to spray dried formulations is warranted.
- Whilst the developed NLCs are believed to be suitable and effective for purpose, a long-term stability study of NLCs according to ICH guidelines need to be carried out to explore if they have any potential commercial avenues in future.
- A larger batch is necessary for manufacturing purpose. Scale up of batches many times affect the characteristics of the formulations Thus, future work on how scale-up affects manufacturing of formulation is required.
- *In vitro* investigations demonstrated selective cytotoxicity and specificity for MCF-7 and MDAMB-231 breast cancer cells, however results derived from *in vitro* studies only provide some indications. A detailed pharmacokinetic, biodistribution studies are required to understand the *in vivo* fate of these nanoparticles.
- In addition, efficacy studies in suitable orthotopic TNBC nude mouse models are essential to demonstrate their potential for TNBC treatment.
- The ability of the surface modification to enhance the functionality of the fabricated nanoparticles is an area of continued interest; alternative surface functionalisation using variety of ligands alone or in combination would also be an avenue of future exploration.

References

ABDELBARY, G. & FAHMY, R. H. 2009. Diazepam-Loaded Solid Lipid Nanoparticles: Design and Characterization. *AAPS PharmSciTech,* 10**,** 211-219.

ABDELWAHAB, S. I., SHEIKH, B. Y., TAHA, M. M. E., HOW, C. W., ABDULLAH, R., YAGOUB, U., EL-SUNOUSI, R. & EID, E. E. M. 2013. Thymoquinone-loaded nanostructured lipid carriers: preparation, gastroprotection, in vitro toxicity, and pharmacokinetic properties after extravascular administration. *Int J Nanomedicine,* 8**,** 2163-2172.

ABHIJIT, A. D., NIMISH, V., AARTI, J. & MANGAL, S. N. 2011. Lipid nanocarriers (GeluPearl) containing amphiphilic lipid Gelucire 50/13 as a novel stabilizer: fabrication, characterization and evaluation for oral drug delivery. *Nanotechnology,* 22**,** 275102.

ABUL KALAM, M., SULTANA, Y., ALI, A., AQIL, M., MISHRA, A. K., ALJUFFALI, I. A. & ALSHAMSAN, A. 2013. Part I: Development and optimization of solid-lipid nanoparticles using Box-Behnken statistical design for ocular delivery of gatifloxacin. *J Biomed Mater Res A,* 101**,** 1813-27.

ADAN, A., ALIZADA, G., KIRAZ, Y., BARAN, Y. & NALBANT, A. 2017. Flow cytometry: basic principles and applications. *Critical Reviews in Biotechnology,* 37**,** 163-176.

ADEREM, A. & UNDERHILL, D. M. 1999. MECHANISMS OF PHAGOCYTOSIS IN MACROPHAGES. *Annual Review of Immunology,* 17**,** 593-623.

AGARWAL.A., KHARB.V. & ANAND. S.V. 2014. Process optimisation, characterisation and evaluation of resveratrol-phospholipid complexes using Box-Behnken statistical design. *International current pharmaceutical Journal* 3**,** 301-308.

AGRAWAL, Y., PETKAR, K. C. & SAWANT, K. K. 2010. Development, evaluation and clinical studies of Acitretin loaded nanostructured lipid carriers for topical treatment of psoriasis. *Int J Pharm,* 401**,** 93-102.

AKHTAR, N., TALEGAONKAR, S., KHAR, R. K. & JAGGI, M. 2013. A validated stability-indicating LC method for estimation of etoposide in bulk and optimized self-nano emulsifying formulation: Kinetics and stability effects. *Saudi Pharmaceutical Journal,* 21**,** 103-111.

AL DERA, H. 2017. NEUROPROTECTIVE EFFECT OF RESVERATROL AGAINST LATE CEREBRAL ISCHEMIA REPERFUSION INDUCED OXIDATIVE STRESS DAMAGE INVOLVES UPREGULATION OF OSTEOPONTIN AND INHIBITON OF INTERLEUKIN-1BETA. *Journal of physiology and pharmacology,* 2**,** 5.

AL KHOURI FALLOUH, N., ROBLOT-TREUPEL, L., FESSI, H., DEVISSAGUET, J. P. & PUISIEUX, F. 1986. Development of a new process for the manufacture of polyisobutylcyanoacrylate nanocapsules. *Int J Pharm,* 28**,** 125-132.

ALBERTS, B., JOHNSON, A. & LEWIS, J. 2002. The Molecular Basis of Cancer-Cell Behavior. *Molecular Biology of the Cell. 4th edition.* New York: Garland Science.

ALMALIK, A., KARIMI, S., OUASTI, S., DONNO, R., WANDREY, C., DAY, P. J. & TIRELLI, N. 2013. Hyaluronic acid (HA) presentation as a tool to modulate and control the receptor-mediated uptake of HA-coated nanoparticles. *Biomaterials,* 34**,** 5369-5380.

AMIN, K. & DANNENFELSER, R.-M. 2006. In vitro hemolysis: Guidance for the pharmaceutical scientist. *Journal of Pharmaceutical Sciences,* 95**,** 1173-1176.

AMRI, A., CHAUMEIL, J. C., SFAR, S. & CHARRUEAU, C. 2012. Administration of resveratrol: What formulation solutions to bioavailability limitations? *J Control Release,* 158**,** 182-93.

ANDALIB, S., VARSHOSAZ, J., HASSANZADEH, F. & SADEGHI, H. 2012. Optimization of LDL targeted nanostructured lipid carriers of 5-FU by a full factorial design. *Advanced Biomedical Research,* 1**,** 45-45.

ANTON, N., BENOIT, J.-P. & SAULNIER, P. 2008. Design and production of nanoparticles formulated from nano-emulsion templates—A review. *Journal of Controlled Release,* 128**,** 185-199.

ARAÚJO, J., GONZALEZ-MIRA, E., EGEA, M. A., GARCIA, M. L. & SOUTO, E. B. 2010. Optimization and physicochemical characterization of a triamcinolone acetonide-loaded NLC for ocular antiangiogenic applications. *Int J Pharm,* 393**,** 168-176.

ARIFFIN, F. D., HASHAM, R., ABDULHAMID, M., EID, A. M., MOHAMED, A. T., KELEB, E. I., ELMAHGOUBI, A., ISSA, Y. S. & ELMARZUGI, N. A. 2015. Effect of Techniques in Preparing VCO Nanoparticles *Journal of Biotechnology and Biochemistry* 1**,** 121-124.

ARTURSSON, P., PALM, K. & LUTHMAN, K. 2001. Caco-2 monolayers in experimental and theoretical predictions of drug transport1PII of original article: S0169-409X(96)00415-2. The article was originally published in Advanced Drug Delivery Reviews 22 (1996) 67–84.1. *Advanced Drug Delivery Reviews,* 46**,** 27-43.

ASSANGA, I. & LUJAN, L. 2013. Cell growth curves for different cell lines and their relationship with biological activities. *International Journal of Biotechnology and Molecular Biology Research,* 4**,** 60-70.

AYERS, D. & NASTI, A. 2012. Utilisation of Nanoparticle Technology in Cancer Chemoresistance. *Journal of Drug Delivery,* 2012**,** 12.

AZHAR SHEKOUFEH BAHARI, L. & HAMISHEHKAR, H. 2016. The Impact of Variables on Particle Size of Solid Lipid Nanoparticles and Nanostructured Lipid Carriers; A Comparative Literature Review. *Advanced Pharmaceutical Bulletin,* 6**,** 143-151.

BAE, Y. H. & PARK, K. 2011. Targeted drug delivery to tumors: Myths, reality and possibility. *Journal of Controlled Release,* 153**,** 198-205.

BAEK, J.-S., KIM, J.-H., PARK, J.-S. & CHO, C.-W. 2015. Modification of paclitaxel-loaded solid lipid nanoparticles with 2-hydroxypropyl-β-cyclodextrin enhances absorption and reduces nephrotoxicity associated with intravenous injection. *Int J Nanomedicine,* 10**,** 5397-5405.

BAEK, J., SO, J., SHIN, S. & CHO, C. 2012. Solid lipid nanoparticles of paclitaxel strengthened by hydroxypropyl-β-cyclodextrin as an oral delivery system. *International Journal of Molecular Medicine,* 30**,** 953-959.

BALIMANE, P. V. & CHONG, S. 2005. Cell culture-based models for intestinal permeability: A critique. *Drug Discovery Today,* 10**,** 335-343.

BANERJEE, S. S., AHER, N., PATIL, R. & KHANDARE, J. 2012. Poly(ethylene glycol)-Prodrug Conjugates: Concept, Design, and Applications. *Journal of Drug Delivery,* 2012**,** 17.

BAR-ZEEV, M., LIVNEY, Y. D. & ASSARAF, Y. G. 2017. Targeted nanomedicine for cancer therapeutics: Towards precision medicine overcoming drug resistance. *Drug Resistance Updates,* 31**,** 15-30.

BARRATT, G. M. 2000. Therapeutic applications of colloidal drug carriers. *Pharm Sci Technolo Today,* 3.

BARUA, S. & MITRAGOTRI, S. 2014. Challenges associated with Penetration of Nanoparticles across Cell and Tissue Barriers: A Review of Current Status and Future Prospects. *Nano Today,* 9**,** 223-243.

BASAKRAN, N. S. 2015. CD44 as a potential diagnostic tumor marker. *Saudi Medical Journal,* 36**,** 273-279.

BAUER, K. R., BROWN, M., CRESS, R. D., PARISE, C. A. & CAGGIANO, V. 2007. Descriptive analysis of estrogen receptor (ER)-negative, progesterone receptor (PR)-negative, and HER2-negative invasive breast cancer, the so-called triple-negative phenotype. *Cancer,* 109**,** 1721-1728.

BAUMGART, D. C. & DIGNASS, A. U. 2002. Intestinal barrier function. *Current Opinion in Clinical Nutrition & Metabolic Care,* 5**,** 685-694.

BÉDUNEAU, A., TEMPESTA, C., FIMBEL, S., PELLEQUER, Y., JANNIN, V., DEMARNE, F. & LAMPRECHT, A. 2014. A tunable Caco-2/HT29-MTX co-culture model mimicking variable permeabilities of the human intestine obtained by an original seeding procedure. *European Journal of Pharmaceutics and Biopharmaceutics,* 87**,** 290-298.

BEE-INTERNATIONAL 2003. Nano DeBEE User Manual Version 1.0.

BEHBAHANI, E. S., GHAEDI, M., ABBASPOUR, M. & ROSTAMIZADEH, K. 2017. Optimization and characterization of ultrasound assisted preparation of curcumin-loaded solid lipid nanoparticles: Application of central composite design, thermal analysis and X-ray diffraction techniques. *Ultrasonics Sonochemistry,* 38**,** 271-280.

BELOQUI, A., SOLINÍS, M. Á., GASCÓN, A. R., DEL POZO-RODRÍGUEZ, A., DES RIEUX, A. & PRÉAT, V. 2013. Mechanism of transport of saquinavir-loaded nanostructured lipid carriers across the intestinal barrier. *Journal of Controlled Release,* 166**,** 115-123.

BELOQUI, A., SOLINÍS, M. Á., RIEUX, A. D., PRÉAT, V. & RODRÍGUEZ-GASCÓN, A. 2014. Dextran–protamine coated nanostructured lipid carriers as mucus-penetrating nanoparticles for lipophilic drugs. *Int J Pharm,* 468**,** 105-111.

BENMERAH, A. 2007. Clathrin-Coated Pits: Vive La Différence? . *Traffic,* 8**,** 970-982.

BERNARD, E., BRITZ-MCKIBBIN, P. & GERNIGON, N. 2007. Resveratrol Photoisomerization: An Integrative Guided-Inquiry Experiment. *Journal of Chemical Education,* 84**,** 1159.

BERTRAND, N., WU, J., XU, X., KAMALY, N. & FAROKHZAD, O. C. 2014. Cancer nanotechnology: The impact of passive and active targeting in the era of modern cancer biology. *Advanced Drug Delivery Reviews,* 66**,** 2-25.

BHASKAR, K., ANBU, J., RAVICHANDIRAN, V., VENKATESWARLU, V. & RAO, Y. M. 2009. Lipid nanoparticles for transdermal delivery of flurbiprofen: formulation, in vitro, ex vivo and in vivo studies. *Lipids in Health and Disease,* 8**,** 6-6.

BIRADAR, A. A., BIRADAR, A. V., SUN, T., CHAN, Y., HUANG, X. & ASEFA, T. 2016. Bicinchoninic acid-based colorimetric chemosensor for detection of low concentrations of cyanide. *Sensors and Actuators B: Chemical,* 222**,** 112-119.

BLESSY, M., PATEL, R. D., PRAJAPATI, P. N. & AGRAWAL, Y. K. 2014. Development of forced degradation and stability indicating studies of drugs—A review. *Journal of Pharmaceutical Analysis,* 4**,** 159-165.

BONCLER, M., RÓŻALSKI, M., KRAJEWSKA, U., PODSĘDEK, A. & WATALA, C. 2014. Comparison of PrestoBlue and MTT assays of cellular viability in the assessment of anti-proliferative effects of plant extracts on human endothelial cells. *Journal of Pharmacological and Toxicological Methods,* 69**,** 9-16.

BOURNE, D. W., BANKER, G. S. & RHODES, C. T. 2002. Pharmacokinetics in Modern pharmaceutics. *Eds., Marcel Dekker Inc, New York,,* 4th ed.

BOVE, K., LINCOLN, D. W. & TSAN, M. F. 2002. Effect of resveratrol on growth of 4T1 breast cancer cells in vitro and in vivo. *Biochem Biophys Res Commun,* 291**,** 1001-5.

BRODIE, A. M. 1985. Aromatase inhibition and its pharmacologic implications. *Biochem Pharmacol,* 34**,** 3213-9.

BROWN, M. & WITTWER, C. 2000. Flow Cytometry: Principles and Clinical Applications in Hematology. *Clinical Chemistry,* 46**,** 1221-1229.

BUKHARI, N. I., KAUR, S., BAI, S. H., HAY, Y. K., BAKAR, A., MAJEED, A., KANG, Y. B. & ANDERSON, M. J. 2009. Statistical Design of Experiments on Fabrication of Starch Nanoparticles–A Case Study for Application of Response Surface Methods (RSM).

BUNJES, H., KOCH, M. H. J. & WESTESEN, K. 2002. Effects of surfactants on the crystallization and polymorphism of lipid nanoparticles. *In:* LAGALY, G. (ed.) *Molecular Organisation on Interfaces.* Berlin, Heidelberg: Springer Berlin Heidelberg.

BUNJES, H., WESTESEN, K. & KOCH, M. H. 1996. Crystallization tendency and polymorphic transition in triglyceride nanoparticles. *Int J Pharm,* 129.

BUYUKOZTURK, F., BENNEYAN, J. C. & CARRIER, R. L. 2010. Impact of emulsion-based drug delivery systems on intestinal permeability and drug release kinetics. *Journal of Controlled Release,* 142**,** 22-30.

CADENA-HERRERA, D., ESPARZA-DE LARA, J. E., RAMÍREZ-IBAÑEZ, N. D., LÓPEZ-MORALES, C. A., PÉREZ, N. O., FLORES-ORTIZ, L. F. & MEDINA-RIVERO, E. 2015. Validation of three viable-cell counting methods: Manual, semi-automated, and automated. *Biotechnology Reports,* 7**,** 9-16.

CALIXTO, G., BERNEGOSSI, J., FONSECA-SANTOS, B. & CHORILLI, M. 2014. Nanotechnology-based drug delivery systems for treatment of oral cancer: a review. *Int J Nanomedicine,* 9**,** 3719-35.

CAMPAGNE, S., GERVAIS, V. & MILON, A. 2011. Nuclear magnetic resonance analysis of protein–DNA interactions. *Journal of The Royal Society Interface,* 8**,** 1065-1078.

CANCER, R. 2012. *Worldwide cancer statistics* [Online]. UK. Available: http://www.cancerresearchuk.org/health-professional/cancer-statistics/worldwide-cancer#heading-Zero [Accessed August 2017].

CANDIOTI, L. V., ROBLES, J. C., MANTOVANI, V. E. & GOICOECHEA, H. C. 2006. Multiple response optimization applied to the development of a capillary electrophoretic method for pharmaceutical analysis. *Talanta,* 69**,** 140-7.

CAREY, L. A., DEES, E. C., SAWYER, L., GATTI, L., MOORE, D. T., COLLICHIO, F., OLLILA, D. W., SARTOR, C. I., GRAHAM, M. L. & PEROU, C. M. 2007. The Triple Negative Paradox: Primary Tumor Chemosensitivity of Breast Cancer Subtypes. *Clinical Cancer Research,* 13**,** 2329.

CECCHINI, M. J., AMIRI, M. & DICK, F. A. 2012. Analysis of cell cycle position in mammalian cells. *J Vis Exp***,** 3491.

CHAI, G.-H., XU, Y., CHEN, S.-Q., CHENG, B., HU, F.-Q., YOU, J., DU, Y.-Z. & YUAN, H. 2016. Transport Mechanisms of Solid Lipid Nanoparticles across Caco-2 Cell Monolayers and their Related Cytotoxicology. *ACS Applied Materials & Interfaces,* 8**,** 5929-5940.

CHANBUREE, S. & TIYABOONCHAI, W. 2017. Enhanced intestinal absorption of curcumin in Caco-2 cell monolayer using mucoadhesive nanostructured lipid carriers. *Journal of Biomedical Materials Research Part B: Applied Biomaterials*.

CHANG, T. K., CHEN, J. & LEE, W. B. 2001. Differential inhibition and inactivation of human CYP1 enzymes by trans-resveratrol: evidence for mechanism-based inactivation of CYP1A2. *J Pharmacol Exp Ther,* 299**,** 874-82.

CHAUDHARY, S., GARG, T., MURTHY, R. S. R., RATH, G. & GOYAL, A. K. 2015. Development, optimization and evaluation of long chain nanolipid carrier for hepatic delivery of silymarin through lymphatic transport pathway. *Int J Pharm,* 485**,** 108-121.

CHAVANPATIL, M. D., KHDAIR, A. & PANYAM, J. 2006. Nanoparticles for Cellular Drug Delivery: Mechanisms and Factors Influencing Delivery. *Journal of Nanoscience and Nanotechnology,* 6**,** 2651-2663.

CHEN, H., AHN, R., VAN DEN BOSSCHE, J., THOMPSON, D. H. & O'HALLORAN, T. V. 2009. Folate-mediated intracellular drug delivery increases the anticancer efficacy of nanoparticulate formulation of arsenic trioxide. *Molecular Cancer Therapeutics,* 8**,** 1955-1963.

CHEN, J., HUANG, L., LAI, H., LU, C., FANG, M., ZHANG, Q. & LUO, X. 2014. Methotrexate-Loaded PEGylated Chitosan Nanoparticles: Synthesis, Characterization, and in Vitro and in Vivo Antitumoral Activity. *Molecular Pharmaceutics,* 11**,** 2213-2223.

CHEN, L., LU, X., LIANG, X., HONG, D., GUAN, Z., GUAN, Y. & ZHU, W. 2016. Mechanistic studies of the transport of peimine in the Caco-2 cell model. *Acta Pharmaceutica Sinica. B,* 6**,** 125-131.

CHEN, S., EINSPANIER, R. & SCHOEN, J. 2015. Transepithelial electrical resistance (TEER): a functional parameter to monitor the quality of oviduct epithelial cells cultured on filter supports. *Histochemistry and Cell Biology,* 144**,** 509-515.

CHEN, X., HE, H., WANG, G., YANG, B., REN, W., MA, L. & YU, Q. 2007. Stereospecific determination of cis- and trans-resveratrol in rat plasma by HPLC: application to pharmacokinetic studies. *Biomedical Chromatography,* 21**,** 257-265.

CHEN, Z. H., HURH, Y. J., NA, H. K., KIM, J. H., CHUN, Y. J., KIM, D. H., KANG, K. S., CHO, M. H. & SURH, Y. J. 2004. Resveratrol inhibits TCDD-induced expression of CYP1A1 and CYP1B1 and catechol estrogen-mediated oxidative DNA damage in cultured human mammary epithelial cells. *Carcinogenesis,* 25**,** 2005-13.

CHINSRIWONGKUL, A., CHAREANPUTTAKHUN, P., NGAWHIRUNPAT, T., ROJANARATA, T., SILA-ON, W., RUKTANONCHAI, U. & OPANASOPIT, P. 2012. Nanostructured Lipid Carriers (NLC) for Parenteral Delivery of an Anticancer Drug. *AAPS PharmSciTech,* 13**,** 150-158.

CHOI, K. O., CHOE, J., SUH, S. & KO, S. 2016. Positively Charged Nanostructured Lipid Carriers and Their Effect on the Dissolution of Poorly Soluble Drugs. *Molecules,* 21**,** 672.

CHOI, K. Y., MIN, K. H., YOON, H. Y., KIM, K., PARK, J. H., KWON, I. C., CHOI, K. & JEONG, S. Y. 2011. PEGylation of hyaluronic acid nanoparticles improves tumor targetability in vivo. *Biomaterials,* 32**,** 1880-1889.

CONDE, J., DIAS, J. T., GRAZÚ, V., MOROS, M., BAPTISTA, P. V. & DE LA FUENTE, J. M. 2014. Revisiting 30 years of biofunctionalization and surface chemistry of inorganic nanoparticles for nanomedicine. *Frontiers in Chemistry,* 2**,** 48.

COTTART, C. H., NIVET-ANTOINE, V., LAGUILLIER-MORIZOT, C. & BEAUDEUX, J. L. 2010. Resveratrol bioavailability and toxicity in humans. *Mol Nutr Food Res,* 54**,** 7-16.

CRANE, M., CRANE, L., HEALY, A. M., CORRIGAN, O. I., GALLAGHER, K. M. & MCCARTHY, L. G. 2004. A Pohlhausen solution for the mass flux from a multi-layered compact in the USP drug dissolution apparatus. *Simulation Modelling Practice and Theory,* 12**,** 397-411.

DA ROCHA LINDNER, G., KHALIL, N. M. & MAINARDES, R. M. 2013. Resveratrol-Loaded Polymeric Nanoparticles: Validation of an HPLC-PDA Method to Determine the Drug Entrapment and Evaluation of Its Antioxidant Activity. *The Scientific World Journal,* 2013**,** 9.

DAI, W., ZHANG, D., DUAN, C., JIA, L., WANG, Y., FENG, F. & ZHANG, Q. 2010. Preparation and characteristics of oridonin-loaded nanostructured lipid carriers as a controlled-release delivery system. *Journal of Microencapsulation,* 27**,** 234-241.

DAMGÉ, C., MICHEL, C., APRAHAMIAN, M., COUVREUR, P. & DEVISSAGUET, J. P. 1990. Nanocapsules as carriers for oral peptide delivery. *Journal of Controlled Release,* 13**,** 233-239.

DAOU, T. J., LI, L., REISS, P., JOSSERAND, V. & TEXIER, I. 2009. Effect of Poly(ethylene glycol) Length on the in Vivo Behavior of Coated Quantum Dots. *Langmuir,* 25**,** 3040-3044.

DAS, S. & CHAUDHURY, A. 2011. Recent Advances in Lipid Nanoparticle Formulations with Solid Matrix for Oral Drug Delivery. *AAPS PharmSciTech,* 12**,** 62-76.

DASH, S., MURTHY, P. N., NATH, L. & CHOWDHURY, P. 2010. Kinetic modeling on drug release from controlled drug delivery systems. *Acta Pol Pharm,* 67**,** 217-223.

DAUTY, E., REMY, J.-S., ZUBER, G. & BEHR, J.-P. 2002. Intracellular Delivery of Nanometric DNA Particles via the Folate Receptor. *Bioconjugate Chemistry,* 13**,** 831-839.

DAVIDOV-PARDO, G. & MCCLEMENTS, D. J. 2014. Resveratrol encapsulation: Designing delivery systems to overcome solubility, stability and bioavailability issues. *Trends Food Sci Technol,* 38**,** 88-103.

DE CARVALHO, S. M., NORONHA, C. M., FLORIANI, C. L., LINO, R. C., ROCHA, G., BELLETTINI, I. C. & OGLIARI, P. J., BARRETO, P.L.M., 2013. Optimization of α-tocopherol loaded solid lipid

nanoparticles by central composite design. Industrial crops and products. *Industrial crops and Products* 49**,** 278-285.

DEITCH, E. A. 1993. Nutrition and the gut mucosal barrier. *Current opinion in general surgery***,** 85-91.

DELI, G., HATZIANTONIOU, S., NIKAS, Y. & DEMETZOS, C. 2009. Solid lipid nanoparticles and nanoemulsions containing ceramides: preparation and physicochemical characterization. *J Liposome Res,* 19**,** 180-8.

DELMAS, D., LANCON, A., COLIN, D., JANNIN, B. & LATRUFFE, N. 2006. Resveratrol as a chemopreventive agent: a promising molecule for fighting cancer. *Curr Drug Targets,* 7**,** 423-42.

DEMINIERE, B., COLIN, A., LEAL-CALDERON, F., MUZY, J. F. & BIBETTE, J., . 1999. Cell growth in a 3d cellular system undergoing coalescence. *Physical review letters,* 82**,** 229.

DINDA, A., BISWAL, I., CHOWDHURY, P. & MOHAPATRA, R. 2013. Formulation Development and Evaluation of Paclitaxel Loaded Solid Lipid Nanoparticles Using Glyceryl Monostearate. *Journal of Applied Pharmaceutical Science,* 3**,** 133-138.

DING, L., ZHANG, Y., JIANG, Y., WANG, L., LIU, B. & LIU, J. 2014. Transport of Egg White ACE-Inhibitory Peptide, Gln-Ile-Gly-Leu-Phe, in Human Intestinal Caco-2 Cell Monolayers with Cytoprotective Effect. *Journal of Agricultural and Food Chemistry,* 62**,** 3177-3182.

DOBROVOLSKAIA, M. A., CLOGSTON, J. D., NEUN, B. W., HALL, J. B., PATRI, A. K. & MCNEIL, S. E. 2008. Method for Analysis of Nanoparticle Hemolytic Properties In Vitro. *Nano letters,* 8**,** 2180-2187.

DOKTOROVOVA, S., SOUTO, E. B. & SILVA, A. M. 2014. Nanotoxicology applied to solid lipid nanoparticles and nanostructured lipid carriers – A systematic review of in vitro data. *European Journal of Pharmaceutics and Biopharmaceutics,* 87**,** 1-18.

DONG, S., BORTNER, , M.J. & ROMAN, M. 2016. Analysis of the sulfuric acid hydrolysis of wood pulp for cellulose nanocrystal production: a central composite design study. *Industrial Crops and Products,* 93**,** 76-87.

DUIZER, E., GILDE, A. J., VERSANTVOORT, C. H. M. & GROTEN, J. P. 1999. Effects of Cadmium Chloride on the Paracellular Barrier Function of Intestinal Epithelial Cell Lines. *Toxicol Appl Pharmacol,* 155**,** 117-126.

DUTTA, D. & DONALDSON, J. G. 2012. Search for inhibitors of endocytosis: Intended specificity and unintended consequences. *Cellular Logistics,* 2**,** 203-208.

ELIAZ, R. E. & SZOKA, F. C. 2001. Liposome-encapsulated Doxorubicin Targeted to CD44. *Cancer Res,* 61**,** 2592.

ELMOWAFY, M., IBRAHIM, H. M., AHMED, M. A., SHALABY, K., SALAMA, A. & HEFESHA, H. 2017. Atorvastatin-loaded nanostructured lipid carriers (NLCs): strategy to overcome oral delivery drawbacks. *Drug Delivery,* 24**,** 932-941.

ELNAGGAR, Y. S. R., EL-MASSIK, M. A. & ABDALLAH, O. Y. 2011. Fabrication, appraisal, and transdermal permeation of sildenafil citrate-loaded nanostructured lipid carriers versus solid lipid nanoparticles. *Int J Nanomedicine,* 6**,** 3195-3205.

EMAMI, J., REZAZADEH, M., VARSHOSAZ, J., TABBAKHIAN, M. & ASLANI, A. 2012. Formulation of LDL Targeted Nanostructured Lipid Carriers Loaded with Paclitaxel: A Detailed Study of Preparation, Freeze Drying Condition, and In Vitro Cytotoxicity. *Journal of Nanomaterials,* 2012**,** 10.

EMSLEY, J. W. & FEENEY, J. 2007. Forty years of Progress in Nuclear Magnetic Resonance Spectroscopy. *Progress in Nuclear Magnetic Resonance Spectroscopy,* 50**,** 179-198.

EUROPE, C. 2004. *European Pharmacopoeia 5.0: Vol-2*, Council of Europe.

FANG, J., NAKAMURA, H. & MAEDA, H. 2011. The EPR effect: Unique features of tumor blood vessels for drug delivery, factors involved, and limitations and augmentation of the effect. *Advanced Drug Delivery Reviews,* 63**,** 136-151.

FDA. 2001. *Guidance for industry, bioanalytical method validation* [Online]. US Department of Health and Human Services. Available: http://www. fda. gov/cder/guidance/index. htm. [Accessed 6.9 2017].

FDA, U. 1994. Validation of Chromatographic Methods, Center for Drug Evaluation and Research. *In:* ADMINISTRATION, U. F. A. D. (ed.). Reviewer Guidance

FENOGLIO-PREISER, C. M. 2008. General Features of the Gastrointestinal Tract and Evaluation of Specimens Derived from It. *Gastrointestinal Pathology: An Atlas and Text.* Wolters Kluwer Health/Lippincott Williams & Wilkins.

FINK, S. L. & COOKSON, B. T. 2005. Apoptosis, Pyroptosis, and Necrosis: Mechanistic Description of Dead and Dying Eukaryotic Cells. *Infection and Immunity,* 73**,** 1907-1916.

FORGIARINI, A., ESQUENA, J., GONZÁLEZ, C. & SOLANS, C. 2001. Formation and stability of nano-emulsions in mixed nonionic surfactant systems. *In:* KOUTSOUKOS, P. G. (ed.) *Trends in Colloid and Interface Science XV.* Berlin, Heidelberg: Springer Berlin Heidelberg.

FREITAS, C. & MÜLLER, R. H. 1998. Effect of light and temperature on zeta potential and physical stability in solid lipid nanoparticle (SLN™) dispersions. *Int J Pharm,* 168**,** 221-229.

FREITAS, C. & MÜLLER, R. H. 1999. Correlation between long-term stability of solid lipid nanoparticles (SLN) and crystallinity of the lipid phase. *Eur J Pharm Biopharm,* 47.

GABA, B., FAZIL, M., KHAN, S., ALI, A., BABOOTA, S. & ALI, J. 2015. Nanostructured lipid carrier system for topical delivery of terbinafine hydrochloride. *Bulletin of Faculty of Pharmacy, Cairo University,* 53**,** 147-159.

GABIZON, A. A. & MUGGIA, F. M. 1998. Long Circulating Liposomes: Old Drugs, New Therapeutics. *In:* WOODLE, M. C. & STORM, G. (eds.). Austin, Texas: Springer-Verlag and Landes Bioscience.

GAMBINI, J., INGL, #XE9, S, M., OLASO, G., LOPEZ-GRUESO, R., BONET-COSTA, V., GIMENO-MALLENCH, L., MAS-BARGUES, C., ABDELAZIZ, K. M., GOMEZ-CABRERA, M. C., VINA, J. & BORRAS, C. 2015. Properties of Resveratrol: In Vitro and In Vivo Studies about Metabolism, Bioavailability, and Biological Effects in Animal Models and Humans. *Oxidative Medicine and Cellular Longevity,* 2015**,** 13.

GAO, X., ZHANG, J., XU, Q., HUANG, Z., WANG, Y. & SHEN, Q. 2017. Hyaluronic acid-coated cationic nanostructured lipid carriers for oral vincristine sulfate delivery. *Drug Development and Industrial Pharmacy,* 43**,** 661-667.

GAO, Y., SUN, W., & ZHANGA, J. 2011. Optimization of preparation and property studies on glycosylated albumin as drug carrier for nanoparticles. *Die Pharmazie-An International Journal of Pharmaceutical Sciences,* 66**,** 484-490.

GARANTI, T., STASIK, A., BURROW, A. J., ALHNAN, M. A. & WAN, K.-W. 2016. Anti-glioma activity and the mechanism of cellular uptake of asiatic acid-loaded solid lipid nanoparticles. *Int J Pharm,* 500**,** 305-315.

GARCIA-FUENTES, M., PREGO, C., TORRES, D. & ALONSO, M. J. 2005. A comparative study of the potential of solid triglyceride nanostructures coated with chitosan or poly(ethylene glycol) as carriers for oral calcitonin delivery. *European Journal of Pharmaceutical Sciences,* 25**,** 133-143.

GARCíA-FUENTES, M., TORRES, D. & ALONSO, M. J. 2003. Design of lipid nanoparticles for the oral delivery of hydrophilic macromolecules. *Colloids and Surfaces B: Biointerfaces,* 27**,** 159-168.

GARCIA-FUENTES, M., TORRES, D., MARTÍN-PASTOR, M. & ALONSO, M. J. 2004. Application of NMR Spectroscopy to the Characterization of PEG-Stabilized Lipid Nanoparticles. *Langmuir,* 20**,** 8839-8845.

GEORGANTZOPOULOU, A., SERCHI, T., CAMBIER, S., LECLERCQ, C. C., RENAUT, J., SHAO, J., KRUSZEWSKI, M., LENTZEN, E., GRYSAN, P., ESWARA, S., AUDINOT, J.-N., CONTAL, S., ZIEBEL, J., GUIGNARD, C., HOFFMANN, L., MURK, A. J. & GUTLEB, A. C. 2016. Effects of silver nanoparticles and ions on a co-culture model for the gastrointestinal epithelium. *Particle and Fibre Toxicology,* 13**,** 9.

GHAEDI, M., GHAZANFARKHANI, M. D., KHODADOUST, S., SOHRABI, N. & OFTADE, M. 2014. Acceleration of methylene blue adsorption onto activated carbon prepared from dross licorice by ultrasonic: Equilibrium, kinetic and thermodynamic studies. *Journal of Industrial and Engineering Chemistry,* 20**,** 2548-2560.

GHAEDI, M., MAZAHERI, H., KHODADOUST, S., HAJATI, S. & PURKAIT, M. K. 2015. Application of central composite design for simultaneous removal of methylene blue and Pb2+ ions by walnut wood activated carbon. *Spectrochimica Acta Part A: Molecular and Biomolecular Spectroscopy,* 135**,** 479-490.

GILL, P., MOGHADAM, T. T. & RANJBAR, B. 2010. Differential Scanning Calorimetry Techniques: Applications in Biology and Nanoscience. *Journal of Biomolecular Techniques : JBT,* 21**,** 167-193.

GOKCE, E. H., KORKMAZ, E., DELLERA, E., SANDRI, G., BONFERONI, M. C. & OZER, O. 2012. Resveratrol-loaded solid lipid nanoparticles versus nanostructured lipid carriers: evaluation of antioxidant potential for dermal applications. *Int J Nanomedicine,* 7**,** 1841-1850.

GOLDBERG, D. M., TSANG, E., KARUMANCHIRI, A., DIAMANDIS, E. P., SOLEAS, G. & NG, E. 1996. Method To Assay the Concentrations of Phenolic Constituents of Biological Interest in Wines. *Analytical Chemistry,* 68**,** 1688-1694.

GONZALEZ, F. J. 2002. Transgenic models in xenobiotic metabolism and toxicology. *Toxicology,* 181-182**,** 237-9.

GRATTON, S. E. A., ROPP, P. A., POHLHAUS, P. D., LUFT, J. C., MADDEN, V. J., NAPIER, M. E. & DESIMONE, J. M. 2008. The effect of particle design on cellular internalization pathways. *Proceedings of the National Academy of Sciences of the United States of America,* 105**,** 11613-11618.

GUINEDI, A. S., MORTADA, N. D., MANSOUR, S. & HATHOUT, R. M. 2005. Preparation and evaluation of reverse-phase evaporation and multilamellar niosomes as ophthalmic carriers of acetazolamide. *Int J Pharm,* 306**,** 71-82.

GURI, A., GULSEREN, I. & CORREDIG, M. 2013. Utilization of solid lipid nanoparticles for enhanced delivery of curcumin in cocultures of HT29-MTX and Caco-2 cells. *Food & Function,* 4**,** 1410-1419.

GUSMAN, J., MALONNE, H. & ATASSI, G. 2001. A reappraisal of the potential chemopreventive and chemotherapeutic properties of resveratrol. *Carcinogenesis,* 22.

GYARMATI, B., HEGYESI, N., PUKÁNSZKY, B. & SZILÁGYI, A. 2015. A colourimetric method for the determination of the degree of chemical cross-linking in aspartic acid-based polymer gels. *Express Polymer Letters,* 9**,** 154-164.

HADJIIOANNOU, T. P., CHRISTIAN, G. D., KOUPPARIS, M. A. & MACHERAS, P. E. 1993. Quantitative calculations in pharmaceutical practice and research. *New York: VCH***,** 10210-4606.

HALLE, W. & GÖRES, E. 1987. Prediction of LD50 values by cell culture. *Die Pharmazie,* 42**,** 245-248.

HAMMUD, K. K., AHMED, A. G., LATIF, A. & DIYALA J. 2010. Spectroscopic study of a typical polyaromatic hydrocarbon (naphthalene) and a biological π acceptor (Folic acid) complex. *Pure Science,* 6**,** 71-78.

HAN, H. S., LEE, J., KIM, H. R., CHAE, S. Y., KIM, M., SARAVANAKUMAR, G., YOON, H. Y., YOU, D. G., KO, H., KIM, K., KWON, I. C., PARK, J. C. & PARK, J. H. 2013. Robust PEGylated hyaluronic acid nanoparticles as the carrier of doxorubicin: Mineralization and its effect on tumor targetability in vivo. *Journal of Controlled Release,* 168**,** 105-114.

HAO, J., FANG, X., ZHOU, Y., WANG, J., GUO, F., LI, F. & PENG, X. 2011. Development and optimization of solid lipid nanoparticle formulation for ophthalmic delivery of chloramphenicol using a Box-Behnken design. *Int J Nanomedicine,* 6**,** 683-92.

HAO, J., WANG, F., WANG, X., ZHANG, D., BI, Y., GAO, Y., ZHAO, X. & ZHANG, Q. 2012. Development and optimization of baicalin-loaded solid lipid nanoparticles prepared by coacervation method using central composite design. *European Journal of Pharmaceutical Sciences,* 47**,** 497-505.

HARVARD, ASSANGA, I. & LUJAN, L. 2013. Cell growth curves for different cell lines and their relationship with biological activitie. *International Journal of Biotechnology and Molecular Biology Research,* 4**,** 60-70.

HASHIZUME, H., BALUK, P., MORIKAWA, S., MCLEAN, J. W., THURSTON, G., ROBERGE, S., JAIN, R. K. & MCDONALD, D. M. 2000. Openings between Defective Endothelial Cells Explain Tumor Vessel Leakiness. *The American Journal of Pathology,* 156**,** 1363-1380.

HE, H., CHEN, X., WANG, G., WANG, J. & DAVEY, A. K. 2006. High-performance liquid chromatography spectrometric analysis of trans-resveratrol in rat plasma. *J Chromatogr B Analyt Technol Biomed Life Sci,* 832**,** 177-80.

HERMANSON, G. H. 2008. *Bioconjugate Techniques,* San Diego, Calif, USA.

HEUSER, J. E. & ANDERSON, R. G. 1989. Hypertonic media inhibit receptor-mediated endocytosis by blocking clathrin-coated pit formation. *The Journal of Cell Biology,* 108**,** 389-400.

HIGUCHI, T. 1963. Mechanism of sustained-action medication. Theoretical analysis of rate of release of solid drugs dispersed in solid matrices. *Journal of Pharmaceutical Sciences,* 52**,** 1145-1149.

HILGENBRINK, A. R. & LOW, P. S. 2005. Folate Receptor-Mediated Drug Targeting: From Therapeutics to Diagnostics. *Journal of Pharmaceutical Sciences,* 94**,** 2135-2146.

HILLAIREAU, H. & COUVREUR, P. 2009. Nanocarriers' entry into the cell: relevance to drug delivery. *Cellular and Molecular Life Sciences,* 66**,** 2873-2896.

HOBBS, S. K., MONSKY, W. L., YUAN, F., ROBERTS, W. G., GRIFFITH, L., TORCHILIN, V. P. & JAIN, R. K. 1998. Regulation of transport pathways in tumor vessels: Role of tumor type and microenvironment. *Proceedings of the National Academy of Sciences,* 95**,** 4607-4612.

HOEIJMAKERS, J. H. J. 2001. Genome maintenance mechanisms for preventing cancer. *Nature,* 411**,** 366-374.

HOU, D., XIE, C., HUANG, K. & ZHU, C. 2003. The production and characteristics of solid lipid nanoparticles (SLNs). *Biomaterials,* 24**,** 1781-1785.

HRYNIUK, W. A., FIGUEREDO, A. & GOODYEAR, M. 1987. Applications of dose intensity to problems in chemotherapy of breast and colorectal cancer. *Oncol,* 11.

HSU, J.-P. & NACU, A. 2003. Behavior of soybean oil-in-water emulsion stabilized by nonionic surfactant. *Journal of Colloid and Interface Science,* 259**,** 374-381.

HU, F.-Q., JIANG, S.-P., DU, Y.-Z., YUAN, H., YE, Y.-Q. & ZENG, S. 2005a. Preparation and characterization of stearic acid nanostructured lipid carriers by solvent diffusion method in an aqueous system. *Colloids and Surfaces B: Biointerfaces,* 45**,** 167-173.

HU, F.-Q., JIANG, S.-P., DU, Y.-Z., YUAN, H., YE, Y.-Q. & ZENG, S. 2006. Preparation and characteristics of monostearin nanostructured lipid carriers. *Int J Pharm,* 314**,** 83-89.

HU, F. Q., JIANG, S. P., DU, Y. Z., YUAN, H., YE, Y. Q. & ZENG, S. 2005b. Preparation and characterization of stearic acid nanostructured lipid carriers by solvent diffusion method in an aqueous system. *Colloids Surf B Biointerfaces,* 45**,** 167-73.

HU, X., KANG, X., YING, X., WANG, L. & DU, Y. 2015. Enhanced oral absorption of saquinavir mediated by PEGylated solid lipid nanoparticles. *RSC Advances,* 5**,** 40341-40347.

HUANG, C., MA, W.-Y., GORANSON, A. & DONG, Z. 1999. Resveratrol suppresses cell transformation and induces apoptosis through a p53-dependent pathway. *Carcinogenesis,* 20**,** 237-242.

HUBATSCH, I., RAGNARSSON, E. G. E. & ARTURSSON, P. 2007. Determination of drug permeability and prediction of drug absorption in Caco-2 monolayers. *Nat. Protocols,* 2**,** 2111-2119.

ICH 1995. International Conference on Harmonization,Q2A: Text on Validation of Analytical Procedures. *In:* REGISTER, U. F. F. (ed.).

ICH 2005. VALIDATION OF ANALYTICAL PROCEDURES: TEXT AND METHODOLOGY. *VALIDATION OF ANALYTICAL PROCEDURES.*

ICH HARMONIZED TRIPARTITE GUIDELINE AND METHODOLOGY Q2 (R1). 2005. *ICH Harmonized Tripartite Guideline, Validation of analytical procedures: Text and Methodology Q2 (R1), International Conference on Harmonization. Geneva, Switzerland* [Online]. Available:

http://www.ich.org/fileadmin/Public_Web_Site/ICH_Products/Guidelines/Quality/Q2_R1/Step4/Q2_R1__Guideline.pdf [Accessed 6.9 2017].

ICH, Q. A. 1999. Specifications: test procedures and acceptance criteria for new drug substances and new drug products: chemical substances.

ICH, Q. B. 1996. Photo stability testing of new drug substances and products.

IMAMURA, H., YAMAGUCHI, T., NAGAYAMA, D., SAIKI, A., SHIRAI, K. & TATSUNO, I. 2017. Resveratrol Ameliorates Arterial Stiffness Assessed by Cardio-Ankle Vascular Index in Patients With Type 2 Diabetes Mellitus. *International Heart Journal,* 58**,** 577-583.

ISAILOVIĆ, B. D., KOSTIĆ, I. T., ZVONAR, A., ĐORĐEVIĆ, V. B., GAŠPERLIN, M., NEDOVIĆ, V. A. & BUGARSKI, B. M. 2013. Resveratrol loaded liposomes produced by different techniques. *Innovative Food Science & Emerging Technologies,* 19**,** 181-189.

IVANOV, A. I. 2008. Pharmacological Inhibition of Endocytic Pathways: Is It Specific Enough to Be Useful? *In:* IVANOV, A. I. (ed.) *Exocytosis and Endocytosis.* Totowa, NJ: Humana Press.

IVERSEN, T.-G., SKOTLAND, T. & SANDVIG, K. 2011. Endocytosis and intracellular transport of nanoparticles: Present knowledge and need for future studies. *Nano Today,* 6**,** 176-185.

IZQUIERDO, P., ESQUENA, J., TADROS, T. F., DEDEREN, C., GARCIA, M. J., AZEMAR, N. & SOLANS, C. 2002. Formation and stability of nano-emulsions prepared using the phase inversion temperature method. *Langmuir,* 18**,** 26-30.

JAIN, K., SOOD, S. & GOWTHAMARAJAN, K. 2015. Optimization of artemether-loaded NLC for intranasal delivery using central composite design. *Drug Delivery,* 22**,** 940-954.

JANGLE, R. D. & THORAT, B. N. 2013. Reversed-phase High-performance Liquid Chromatography Method for Analysis of Curcuminoids and Curcuminoid-loaded Liposome Formulation. *Indian J Pharm Sci,* 75**,** 60-6.

JENNING, V., MADER, K. & GOHLA, S. 2000a. Solid lipid nanoparticles (SLN) based on binary mixtures of liquid and solid lipids: a 1H-NMR study. *Int J Pharm,* 205.

JENNING, V., MÄDER, K. & GOHLA, S. H. 2000b. Solid lipid nanoparticles (SLN™) based on binary mixtures of liquid and solid lipids: a 1H-NMR study. *Int J Pharm,* 205**,** 15-21.

JENNING, V., THUNEMANN, A. F. & GOHLA, S. H. 2000c. Characterisation of a novel solid lipid nanoparticle carrier system based on binary mixtures of liquid and solid lipids. *Int J Pharm,* 199.

JENNING, V., THÜNEMANN, A. F. & GOHLA, S. H. 2000d. Characterisation of a novel solid lipid nanoparticle carrier system based on binary mixtures of liquid and solid lipids. *Int J Pharm,* 199**,** 167-177.

JENSEN, M., ENGERT, A., WEISSINGER, F., KNAUF, W., KIMBY, E., POYNTON, C., OLIFF, I. A., RUMMEL, M. J. & ÖSTERBORG, A. 2008. Phase I study of a novel pro-apoptotic drug R-

etodolac in patients with B-cell chronic lymphocytic leukemia. *Investigational New Drugs,* 26**,** 139-149.

JHONSTON, G. 2010. Automated handheld instrument improves counting precision across multiple cell lines. *Cell culture technologies,* 48**,** 325-327.

JIA, L.-J., ZHANG, D.-R., LI, Z.-Y., FENG, F.-F., WANG, Y.-C., DAI, W.-T., DUAN, C.-X. & ZHANG, Q. 2010. Preparation and characterization of silybin-loaded nanostructured lipid carriers. *Drug Delivery,* 17**,** 11-18.

JIANG, H., ZHANG, L., KUO, J., KUO, K., GAUTAM, S. C., GROC, L., RODRIGUEZ, A. I., KOUBI, D., JACKSON HUNTER, T., CORCORAN, G. B., SEIDMAN, M. D. & LEVINE, R. A. 2005. Resveratrol-induced apoptotic death in human U251 glioma cells. *Molecular Cancer Therapeutics,* 4**,** 554.

JOE, A. K., LIU, H., SUZUI, M., VURAL, M. E., XIAO, D. & WEINSTEIN, I. B. 2002. Resveratrol induces growth inhibition, S-phase arrest, apoptosis, and changes in biomarker expression in several human cancer cell lines. *Clinical Cancer Research,* 8**,** 893-903.

JOERIS, K., FRERICHS, J. G., KONSTANTINOV, K. & SCHEPER, T. 2002. In-situ microscopy: online process monitoring of mammalian cell cultures. *Cytotechnology,* 38**,** 129-134.

JOKERST, J. V., LOBOVKINA, T., ZARE, R. N. & GAMBHIR, S. S. 2011. Nanoparticle PEGylation for imaging and therapy. *Nanomedicine (London, England),* 6**,** 715-728.

JOSE, S., ANJU, S. S., CINU, T. A., ALEYKUTTY, N. A., THOMAS, S. & SOUTO, E. B. 2014. In vivo pharmacokinetics and biodistribution of resveratrol-loaded solid lipid nanoparticles for brain delivery. *Int J Pharm,* 474**,** 6-13.

JOSHI, M. & PATRAVALE, V. 2006. Formulation and Evaluation of Nanostructured Lipid Carrier (NLC)–based Gel of Valdecoxib. *Drug Development and Industrial Pharmacy,* 32**,** 911-918.

KALDAS, M. I., WALLE, U. K. & WALLE, T. 2003. Resveratrol transport and metabolism by human intestinal Caco-2 cells. *Journal of Pharmacy and Pharmacology,* 55**,** 307-312.

KAMBLE, M. S., VAIDYA, K. K., BHOSALE, A. V. & CHAUDHARI, P. D. 2012. Solid lipid nanoparticles and nanostructured lipid carriers–an overview. *International Journal of Pharmceutical chemistry Biological Science,* 2**,** 681–91.

KAUR, P., GARG, T., RATH, G., MURTHY, R. S. R. & GOYAL, A. K. 2016. Development, optimization and evaluation of surfactant-based pulmonary nanolipid carrier system of paclitaxel for the management of drug resistance lung cancer using Box-Behnken design. *Drug Delivery,* 23**,** 1912-1925.

KEPP, O., GALLUZZI, L., LIPINSKI, M., YUAN, J. & KROEMER, G. 2011. Cell death assays for drug discovery. *Nat Rev Drug Discov,* 10**,** 221-237.

KHODABANDEHLOO, H., ZAHEDNASAB, H. & ASHRAFI HAFEZ, A. 2016. Nanocarriers Usage for Drug Delivery in Cancer Therapy. *Iranian Journal of Cancer Prevention,* 9**,** e3966.

KHURANA.S., BEDI.P.M.S. & JAIN.N.K. 2012. Development of nanostructured lipid carriers for controlled delivery of mefenamic acid. *International Journal of Biomedical Nanoscience and Nanotechnology,* 2**,** 232-250.

KIM, M.-S., KIM, J.-S., YOU, Y.-H., PARK, H. J., LEE, S., PARK, J.-S., WOO, J.-S. & HWANG, S.-J. 2007. Development and optimization of a novel oral controlled delivery system for tamsulosin hydrochloride using response surface methodology. *Int J Pharm,* 341**,** 97-104.

KLINKESORN, U., H-KITTIKUN, A., CHINACHOTI, P. & SOPHANODORA, P. 2004. Chemical transesterification of tuna oil to enriched omega-3 polyunsaturated fatty acids. *Food Chem,* 87**,** 415-421.

KLINKESORN, U. & NAMATSILA, Y. 2009. Influence of chitosan and NaCl on physicochemical properties of low-acid tuna oil-in-water emulsions stabilized by non-ionic surfactant. *Food Hydrocolloids,* 23**,** 1374-1380.

KOBIERSKI, S., OFORI-KWAKYE, K., MÜLLER, R. H. & KECK, C. M. 2009. Resveratrol nanosuspensions for dermal application–production, characterization, and physical stability. *Die Pharmazie-An International Journal of Pharmaceutical Sciences,* 64**,** 741-747.

KOCBEK, P., OBERMAJER, N., CEGNAR, M., KOS, J. & KRISTL, J. 2007. Targeting cancer cells using PLGA nanoparticles surface modified with monoclonal antibody. *Journal of Controlled Release,* 120**,** 18-26.

KOLAEI, M., DASHTIAN, K., RAFIEE, Z. & GHAEDI, M. 2016. trasonic-assisted magnetic solid phase extraction of morphine in urine samples by new imprinted polymer-supported on MWCNT-Fe 3 O 4-NPs: Central composite design optimization. *Ultrasonics sonochemistry,* 33**,** 240-248.

KOLLIPARA, S., BENDE, G., MOVVA, S. & SAHA, R. 2010. Application of rotatable central composite design in the preparation and optimization of poly(lactic-co-glycolic acid) nanoparticles for controlled delivery of paclitaxel. *Drug Development and Industrial Pharmacy,* 36**,** 1377-1387.

KOMATSU, H., KITAJIMA, A. & OKADA, S. 1995. Pharmaceutical characterization of commercially available intravenous fat emulsions: estimation of average particle size, size distribution and surface potential using photon correlation spectroscopy. *Chemical and pharmaceutical bulletin,* 43**,** 1412-1415.

KOO, A. N., LEE, H. J., KIM, S. E., CHANG, J. H., PARK, C., KIM, C., PARK, J. H. & LEE, S. C. 2008. Disulfide-cross-linked PEG-poly(amino acid)s copolymer micelles for glutathione-mediated intracellular drug delivery. *Chemical Communications***,** 6570-6572.

KOO, O. M., RUBINSTEIN, I. & ONYUKSEL, H. 2005. Role of nanotechnology in targeted drug delivery and imaging: a concise review. *Nanomedicine: Nanotechnology, Biology and Medicine,* 1**,** 193-212.

KOU, L., SUN, J., ZHAI, Y. & HE, Z. 2013. The endocytosis and intracellular fate of nanomedicines: Implication for rational design. *Asian Journal of Pharmaceutical Sciences,* 8**,** 1-10.

KOUCHAKZADEH, H., SHOJAOSADATI, S. A. & SHOKRI, F. 2014. Efficient loading and entrapment of tamoxifen in human serum albumin based nanoparticulate delivery system by a modified desolvation technique. *Chemical Engineering Research and Design,* 92**,** 1681-1692.

KUHN, D. A., VANHECKE, D., MICHEN, B., BLANK, F., GEHR, P., PETRI-FINK, A. & ROTHEN-RUTISHAUSER, B. 2014. Different endocytotic uptake mechanisms for nanoparticles in epithelial cells and macrophages. *Beilstein Journal of Nanotechnology,* 5**,** 1625-1636.

KULKARNI, S. A. & FENG, S.-S. 2013. Effects of Particle Size and Surface Modification on Cellular Uptake and Biodistribution of Polymeric Nanoparticles for Drug Delivery. *Pharm Res,* 30**,** 2512-2522.

KUMAR, S. S. D., MAHESH, A., MAHADEVAN, S. & MANDAL, A. B. 2014. Synthesis and characterization of curcumin loaded polymer/lipid based nanoparticles and evaluation of their antitumor effects on MCF-7 cells. *Biochimica et Biophysica Acta (BBA) - General Subjects,* 1840**,** 1913-1922.

LAGINHA, K., MUMBENGEGWI, D. & ALLEN, T. 2005. Liposomes targeted via two different antibodies: Assay, B-cell binding and cytotoxicity. *Biochimica et Biophysica Acta (BBA) - Biomembranes,* 1711**,** 25-32.

LAI, S. K., WANG, Y.-Y. & HANES, J. 2009. Mucus-penetrating nanoparticles for drug and gene delivery to mucosal tissues. *Advanced Drug Delivery Reviews,* 61**,** 158-171.

LALL, N., HENLEY-SMITH, C. J., DE CANHA, M. N., OOSTHUIZEN, C. B. & BERRINGTON, D. 2013. Viability Reagent, PrestoBlue, in Comparison with Other Available Reagents, Utilized in Cytotoxicity and Antimicrobial Assays. *International Journal of Microbiology,* 2013**,** 5.

LASOŃ, E., SIKORA, E. & OGONOWSKI, J. 2013. Influence of process parameters on properties of Nanostructured Lipid Carriers (NLC) formulation. *Acta Biochim Pol,* 60**,** 773-777.

LE FERREC, E., CHESNE, C., ARTUSSON, P., BRAYDEN, D., FABRE, G., GIRES, P. & GUILLOU, F. 2001. In vitro models of the intestinal barrier *ATLA-Altern Lab Anim,* 29**,** 649–668.

LEACH, W. T., SIMPSON, D. T., VAL, T. N., YU, Z., LIM, K. T., PARK, E. J., WILLIAMS, R. O. & JOHNSTON, K. P. 2005. Encapsulation of protein nanoparticles into uniform-sized microspheres formed in a spinning oil film. *AAPS PharmSciTech,* 6**,** E605-E617.

LEAMON, C. P. & LOW, P. S. 2001. Folate-mediated targeting: from diagnostics to drug and gene delivery. *Drug Discovery Today,* 6**,** 44-51.

LEE, J.-Y., TERMSARASAB, U., PARK, J.-H., LEE, S. Y., KO, S.-H., SHIM, J.-S., CHUNG, S.-J., CHO, H.-J. & KIM, D.-D. 2016. Dual CD44 and folate receptor-targeted nanoparticles for cancer diagnosis and anticancer drug delivery. *Journal of Controlled Release,* 236**,** 38-46.

LEE, M.-K., LIM, S.-J. & KIM, C.-K. 2007. Preparation, characterization and in vitro cytotoxicity of paclitaxel-loaded sterically stabilized solid lipid nanoparticles. *Biomaterials,* 28**,** 2137-2146.

LENCER, W. I., DELP, C., NEUTRA, M. R. & MADARA, J. L. 1992. Mechanism of cholera toxin action on a polarized human intestinal epithelial cell line: role of vesicular traffic. *The Journal of Cell Biology,* 117**,** 1197-1209.

LENNERNAS, H. & ABRAHAMSSON, B. 2005. The use of biopharmaceutic classification of drugs in drug discovery and development: current status and future extension. *J. Pharm. Pharmacol,* 57**,** 273-285.

LHERM, C., MÜLLER, R. H., PUISIEUX, F. & COUVREUR, P. 1992. Alkylcyanoacrylate Drug Carriers II: Cytotoxicity of Cyanoacrylate Nanoparticles with Different Alkyl Chain Length. *Int J Pharm,* 84.

LI, F., WENG, Y., WANG, L., HE, H., YANG, J. & TANG, X. 2010. The efficacy and safety of bufadienolides-loaded nanostructured lipid carriers. *Int J Pharm,* 393**,** 204-212.

LI, H., GUISSI, N. E. I., SU, Z., PING, Q. & SUN, M. 2016a. Effects of surface hydrophilic properties of PEG-based mucus-penetrating nanostructured lipid carriers on oral drug delivery. *RSC Advances,* 6**,** 84164-84176.

LI, L., YI, T. & LAM, C. 2013a. Effects of Spray-Drying and Choice of Solid Carriers on Concentrations of Labrasol® and Transcutol® in Solid Self-Microemulsifying Drug Delivery Systems (SMEDDS). *Molecules,* 18**,** 545.

LI, N., WANG, D. D., SU, I. Z. G., QI, X. Y., JI, L. Y., WANG, X. L. & YANG, L. 2013b. Development of an improved three-dimensional in vitro intestinal mucosa model for drug absorption evaluation. *Tissue Eng C Methods,* 19**,** 708–719.

LI, Q., CAI, T., HUANG, Y., XIA, X., COLE, S. P. C. & CAI, Y. 2017. A Review of the Structure, Preparation, and Application of NLCs, PNPs, and PLNs. *Nanomaterials,* 7**,** 122.

LI, R., EUN, J. S. & LEE, M.-K. 2011. Pharmacokinetics and biodistribution of paclitaxel loaded in pegylated solid lipid nanoparticles after intravenous administration. *Archives of Pharmacal Research,* 34**,** 331-337.

LI, S., FENG, S., DING, L., LIU, Y., ZHU, Q., QIAN, Z. & GU, Y. 2016b. Nanomedicine engulfed by macrophages for targeted tumor therapy. *Int J Nanomedicine,* 11**,** 4107-4124.

LI, Y., LIU, J., LIU, X., XING, K., WANG, Y., LI, F. & YAO, L. 2006. Resveratrol-induced cell inhibition of growth and apoptosis in MCF7 human breast cancer cells are associated with modulation of phosphorylated Akt and caspase-9. *Appl Biochem Biotechnol,* 135**,** 181-92.

LIFSHITZ, I. M. & SLYOZOV, V. V. 1961. The kinetics of precipitation from supersaturated solid solutions. *Journal of Physics and Chemistry of Solids,* 19**,** 35-50.

LIM, S.-J. & KIM, C.-K. 2002. Formulation parameters determining the physicochemical characteristics of solid lipid nanoparticles loaded with all-trans retinoic acid. *Int J Pharm,* 243**,** 135-146.

LIN, Y., SHEN, Q., KATSUMI, H., OKADA, N., FUJITA, T., JIANG, X. & YAMAMOTO, A. 2007. Effects of Labrasol and Other Pharmaceutical Excipients on the Intestinal Transport and Absorption of Rhodamine123, a P-Glycoprotein Substrate, in Rats. *Biological and Pharmaceutical Bulletin,* 30**,** 1301-1307.

LIPPACHER, A. 2001. Pharmaceutical Characterization of Liquid and Semi-Soid SLN Dispersions for Topical Application. *PhD Thesis.* Germany: Free University of Berlin.

LIPPACHER, A., MÜLLER, R. H. & MÄDER, K. 2000. Investigation on the viscoelastic properties of lipid based colloidal drug carriers. *Int J Pharm,* 196**,** 227-230.

LIU, Y., CAI, D., YANG, J., WANG, Y., ZHANG, X. & YIN, S. 2014a. In vitro hemocompatibility evaluation of poly (4-hydroxybutyrate) scaffold. *International Journal of Clinical and Experimental Medicine,* 7**,** 1233-1243.

LIU, Y., MIYOSHI, H. & NAKAMURA, M. 2007. Nanomedicine for drug delivery and imaging: A promising avenue for cancer therapy and diagnosis using targeted functional nanoparticles. *International Journal of Cancer,* 120**,** 2527-2537.

LIU, Y., SUN, J., CAO, W., YANG, J., LIAN, H., LI, X., SUN, Y., WANG, Y., WANG, S. & HE, Z. 2011. Dual targeting folate-conjugated hyaluronic acid polymeric micelles for paclitaxel delivery. *Int J Pharm,* 421**,** 160-169.

LIU, Y., SUN, J., LIAN, H., CAO, W., WANG, Y. & HE, Z. 2014b. Folate and CD44 Receptors Dual-Targeting Hydrophobized Hyaluronic Acid Paclitaxel-Loaded Polymeric Micelles for Overcoming Multidrug Resistance and Improving Tumor Distribution. *Journal of Pharmaceutical Sciences,* 103**,** 1538-1547.

LODISH, H., BERK, A. & ZIPURSKY, S. L. 2000. Proto-Oncogenes and Tumor-Suppressor Genes. *Molecular Cell Biology.* New York: W. H. Freeman.

LOUËR, D. 2017. Powder X-Ray Diffraction, Applications A2 - Lindon, John C. *In:* TRANTER, G. E. & KOPPENAAL, D. W. (eds.) *Encyclopedia of Spectroscopy and Spectrometry (Third Edition).* Oxford: Academic Press.

LOUIS, K. S. & SIEGEL, A. C. 2011. Cell viability analysis using trypan blue: manual and automated methods. *Mammalian cell viability: methods and protocols*, 7-12.

LOUIS, K. S., SIEGEL, A. C., LEVY, G. A. & STODDART, M. J. 2011. Comparison of manual versus automated trypan blue dye exclusion method for cell counting. *Series Methods in Molecular Biology, Springer Protocols, New York*, 7-12.

LUAN, J., ZHENG, F., YANG, X., YU, A. & ZHAI, G. 2015. Nanostructured lipid carriers for oral delivery of baicalin: In vitro and in vivo evaluation. *Colloids and Surfaces A: Physicochemical and Engineering Aspects,* 466, 154-159.

LUCKS, J. S. & MÜLLER, R. H. 1996. *Medication vehicles made of solid lipid particles (solid lipid nanospheres SLN), in EP0000605497*.

LUNDQUIST, P. & ARTURSSON, P. 2016. Oral absorption of peptides and nanoparticles across the human intestine: Opportunities, limitations and studies in human tissues. *Advanced Drug Delivery Reviews,* 106, 256-276.

LV, L.-Z., TONG, C.-Q., YU, J., HAN, M. & GAO, J.-Q. 2013. Mechanism of enhanced oral absorption of hydrophilic drug incorporated in hydrophobic nanoparticles. *Int J Nanomedicine,* 8, 2709-2717.

MAEDA, H. 2015. Toward a full understanding of the EPR effect in primary and metastatic tumors as well as issues related to its heterogeneity. *Advanced Drug Delivery Reviews,* 91, 3-6.

MAIER-SALAMON, A., HAGENAUER, B., WIRTH, M., GABOR, F., SZEKERES, T. & JAGER, W. 2006a. Increased transport of resveratrol across monolayers of the human intestinal Caco-2 cells is mediated by inhibition and saturation of metabolites. *Pharm Res,* 23, 2107-15.

MAIER-SALAMON, A., HAGENAUER, B., WIRTH, M., GABOR, F., SZEKERES, T. & JÄGER, W. 2006b. Increased Transport of Resveratrol Across Monolayers of the Human Intestinal Caco-2 Cells is Mediated by Inhibition and Saturation of Metabolites. *Pharm Res,* 23, 2107-2115.

MAINARDES, R. M. & SILVA, L. P. 2004. Drug delivery systems: past, present, and future. *Curr Drug Targets,* 5.

MAIOLINO, S., MORET, F., CONTE, C., FRAIX, A., TIRINO, P., UNGARO, F., SORTINO, S., REDDI, E. & QUAGLIA, F. 2015. Hyaluronan-decorated polymer nanoparticles targeting the CD44 receptor for the combined photo/chemo-therapy of cancer. *Nanoscale,* 7, 5643-5653.

MALZERT-FRÉON, A., SAINT-LORANT, G., HENNEQUIN, D., GAUDUCHON, P., POULAIN, L. & RAULT, S. 2010. Influence of the introduction of a solubility enhancer on the formulation of lipidic nanoparticles with improved drug loading rates. *European Journal of Pharmaceutics and Biopharmaceutics,* 75, 117-127.

MANAF.Y.N.A., MARIKKAR.J.M.N., LONG.K. & HAZALI.H.M. 2013. Physico-chemical characterisation of the fat from red-skin rambutan (Nephellium lappaceum L.) seed. *Journal of Oleo Science,* 62**,** 335-343.

MARTÍNEZ-AUGUSTIN, O., RIVERO-GUTIÉRREZ, B., MASCARAQUE, C. & SÁNCHEZ DE MEDINA, F. 2014. Food Derived Bioactive Peptides and Intestinal Barrier Function. *International Journal of Molecular Sciences,* 15**,** 22857-22873.

MARTINS, S., COSTA-LIMA, S., CARNEIRO, T., CORDEIRO-DA-SILVA, A., SOUTO, E. B. & FERREIRA, D. C. 2012. Solid lipid nanoparticles as intracellular drug transporters: An investigation of the uptake mechanism and pathway. *International Journal of Pharmaceutics,* 430**,** 216-227.

MATHOT, F., DES RIEUX, A., ARIËN, A., SCHNEIDER, Y. J., BREWSTER, M. & PRÉAT, V. 2007. Transport mechanisms of mmePEG750P(CL-co-TMC) polymeric micelles across the intestinal barrier. *Journal of Controlled Release,* 124**,** 134-143.

MCFADYEN, M. C., MCLEOD, H. L., JACKSON, F. C., MELVIN, W. T., DOEHMER, J. & MURRAY, G. I. 2001. Cytochrome P450 CYP1B1 protein expression: a novel mechanism of anticancer drug resistance. *Biochem Pharmacol,* 62**,** 207-12.

MEHDIZADEH, S., LASEKAN, O., MUHAMMAD, K. & BAHARIN, B. 2015. Variability in the fermentation index, polyphenols and amino acids of seeds of rambutan (Nephelium lappaceum L.) during fermentation. *Journal of Food Composition and Analysis,* 37**,** 128-135.

MEHNERT, W. & MÄDER, K. 2001. Solid lipid nanoparticles: production, characterization and applications. *Advanced drug delivery reviews,* 47**,** 165-196.

MEI, Z., CHEN, H., WENG, T., YANG, Y. & YANG, X. 2003. Solid lipid nanoparticle and microemulsion for topical delivery of triptolide. *European Journal of Pharmaceutics and Biopharmaceutics,* 56**,** 189-196.

MERCER, J. & HELENIUS, A. 2009. Virus entry by macropinocytosis. *Nat Cell Biol,* 11**,** 510-520.

MERO, A. & CAMPISI, M. 2014. Hyaluronic Acid Bioconjugates for the Delivery of Bioactive Molecules. *Polymers,* 6**,** 346.

MIGLIETTA, A., CAVALLI, R., BOCCA, C., GABRIEL, L. & ROSA GASCO, M. 2000. Cellular uptake and cytotoxicity of solid lipid nanospheres (SLN) incorporating doxorubicin or paclitaxel. *Int J Pharm,* 210**,** 61-67.

MIKSITS, M., WLCEK, K., SVOBODA, M., KUNERT, O., HASLINGER, E., THALHAMMER, T., SZEKERES, T. & JAGER, W. 2009. Antitumor activity of resveratrol and its sulfated metabolites against human breast cancer cells. *Planta Med,* 75**,** 1227-30.

MIKSTACKA, R., PRZYBYLSKA, D., RIMANDO, A. M. & BAER-DUBOWSKA, W. 2007. Inhibition of human recombinant cytochromes P450 CYP1A1 and CYP1B1 by trans-resveratrol methyl ethers. *Mol Nutr Food Res,* 51**,** 517-24.

MIKSTACKA, R., RIMANDO, A. M., DUTKIEWICZ, Z., STEFANSKI, T. & SOBIAK, S. 2012. Design, synthesis and evaluation of the inhibitory selectivity of novel trans-resveratrol analogues on human recombinant CYP1A1, CYP1A2 and CYP1B1. *Bioorg Med Chem,* 20**,** 5117-26.

MILLER, D. M. 1984. Reducing Transformation Bias in Curve Fitting. *The American Statistician,* 38**,** 124-126.

MIN, K. H., KIM, J.-H., BAE, S. M., SHIN, H., KIM, M. S., PARK, S., LEE, H., PARK, R.-W., KIM, I.-S., KIM, K., KWON, I. C., JEONG, S. Y. & LEE, D. S. 2010. Tumoral acidic pH-responsive MPEG-poly(β-amino ester) polymeric micelles for cancer targeting therapy. *Journal of Controlled Release,* 144**,** 259-266.

MISHRA, P., NAYAK, B. & DEY, R. K. 2016. PEGylation in anti-cancer therapy: An overview. *Asian Journal of Pharmaceutical Sciences,* 11**,** 337-348.

MITRI, K., SHEGOKAR, R., GOHLA, S., ANSELMI, C. & MÜLLER, R. H. 2011. Lipid nanocarriers for dermal delivery of lutein: Preparation, characterization, stability and performance. *Int J Pharm,* 414**,** 267-275.

MOHAN, A. & PONNUSANKAR, S. 2013. Newer Therapies for the Treatment of Metastatic Breast Cancer: a Clinical Update. *Indian J Pharm Sci,* 75**,** 251-261.

MONT. KUMPUGDEE-VOLLRATH, YVONNE. IBOLD & PORNSAK. SRIAMORNSA 2012. Solid state characterization of trans resveratrol complexes with different cyclodextrins. *The Official Journal of Asian Association of Schools of Pharmacy* 1**,** 125-136.

MORSE, D. L., GRAY, H., PAYNE, C. M. & GILLIES, R. J. 2005. Docetaxel induces cell death through mitotic catastrophe in human breast cancer cells. *Mol Cancer Therapeutics,* 10.

MUJTABA, A., ALI, M. & KOHLI, K. 2014. Formulation of extended release cefpodoxime proxetil chitosan–alginate beads using quality by design approach. *International Journal of Biological Macromolecules,* 69**,** 420-429.

MUKHERJEE, S., GHOSH, R. N. & MAXFIELD, F. R. 1997. Endocytosis. *Physiological Reviews,* 77**,** 759.

MULIK, R. S., MÖNKKÖNEN, J., JUVONEN, R. O., MAHADIK, K. R. & PARADKAR, A. R. 2012. Apoptosis-induced anticancer effect of transferrin-conjugated solid lipid nanoparticles of curcumin. *Cancer Nanotechnology,* 3**,** 65-81.

MÜLLER, C. & SCHIBLI, R. 2013. Prospects in Folate Receptor-Targeted Radionuclide Therapy. *Frontiers in Oncology,* 3**,** 249.

MULLER, R. H. 2000. *Extended patent on the basis of (6), PCT application PCT/EP00/04112*.

MÜLLER, R. H. 1996. Zetapotential und Partikeladung in der Laborpraxis. *Wissenschaftliche Verlagsgeselschaft mbH.Suttgart*.

MULLER, R. H., GOHLA, S., DINGLER, A. & SCHNEPPE, T. 2000a. Large scale production of solid lipid nanoparticles (SLNTM) and nanosuspensions (DissoCubesTM). *In:* WISE, D. L. (ed.) *Handbook of Pharmaceutical Controlled Release Technology.*

MULLER, R. H., JACOBS, C. & KAYSER, O. 2001. Nanosuspensions as particulate drug formulations in therapy. Rationale for development and what we can expect for the future. *Adv Drug Deliv Rev,* 47**,** 3-19.

MULLER, R. H., MADER, K. & GOHLA, S. 2000b. Solid lipid nanoparticles (SLN) for controlled drug delivery- a review of the state of the art. *Eur J Pharm Biopharm,* 50.

MULLER, R. H., RADTKE, M. & WISSING, S. A. 2002a. Nanostructured lipid matrices for improved microencapsulation of drugs. *Int J Pharm,* 242**,** 121-8.

MULLER, R. H., RADTKE, M. & WISSING, S. A. 2002b. Solid lipid nanoparticles (SLN) and nanostructured lipid carriers (NLC) in cosmetic and dermatological preparations. *Adv Drug Deliv Rev,* 54 Suppl 1**,** S131-55.

MÜLLER, R. H., RUNGE, S. H. & BENITA, S. 1998. Solid lipid nanoparticles (SLN1) for controlled drug delivery. *The submicron emulsion in drug targeting and delivery. Harwood Academic Publishers, the Netherlands***,** 219–234.

MÜLLER. & MÜLLER, B. W. 1986. Suppositorien, Wissenschaftliche, Stuttgart *APV Monographie*.

MUPPIDI, K., PUMERANTZ, A. S., WANG, J. & BETAGERI, G. 2012. Development and stability studies of novel liposomal vancomycin formulations. *ISRN Pharm,* 2012**,** 636743.

MURRAY, G. I., TAYLOR, M. C., MCFADYEN, M. C., MCKAY, J. A., GREENLEE, W. F., BURKE, M. D. & MELVIN, W. T. 1997. Tumor-specific expression of cytochrome P450 CYP1B1. *Cancer Res,* 57**,** 3026-31.

MYERS, R. H., MONTGOMERY, D. C. & ANDERSON-COOK, C. M. 2016. Response surface methodology: process and product optimization using designed experiments. *John Wiley & Sons*.

NAMBIAR, S. & HEGDE, V. 2016. Apoptosis in cancer therapy. *Journal of Medicine, Radiology, Pathology & Surgery* 3**,** 10–14.

NASCIMENTO, T. L., HILLAIREAU, H., VERGNAUD, J. & FATTAL, E. 2016. Lipid-based nanosystems for CD44 targeting in cancer treatment: recent significant advances, ongoing challenges and unmet needs. *Nanomedicine,* 11**,** 1865-1887.

NECELA, B. M., CROZIER, J. A., ANDORFER, C. A., LEWIS-TUFFIN, L., KACHERGUS, J. M., GEIGER, X. J., KALARI, K. R., SERIE, D. J., SUN, Z., ASPITA, A. M., O'SHANNESSY, D. J., MALTZMAN, J. D., MCCULLOUGH, A. E., POCKAJ, B. A., CUNLIFFE, H. E., BALLMAN, K. V., THOMPSON, E. A. &

PEREZ, E. A. 2015. Folate Receptor-α (FOLR1) Expression and Function in Triple Negative Tumors. *PLoS One,* 10**,** e0122209.

NEGI, L. M., JAGGI, M., JOSHI, V., RONODIP, K. & TALEGAONKAR, S. 2015. Hyaluronic acid decorated lipid nanocarrier for MDR modulation and CD-44 targeting in colon adenocarcinoma. *International Journal of Biological Macromolecules,* 72**,** 569-574.

NEGI, L. M., TALEGAONKAR, S., JAGGI, M., AHMAD, F. J., IQBAL, Z. & KHAR, R. K. 2012. Role of CD44 in tumour progression and strategies for targeting. *Journal of Drug Targeting,* 20**,** 561-573.

NEHOFF, H., PARAYATH, N. N., DOMANOVITCH, L., TAURIN, S. & GREISH, K. 2014. Nanomedicine for drug targeting: strategies beyond the enhanced permeability and retention effect. *Int J Nanomedicine,* 9**,** 2539-2555.

NEVES, A. R., LUCIO, M., MARTINS, S., LIMA, J. L. & REIS, S. 2013. Novel resveratrol nanodelivery systems based on lipid nanoparticles to enhance its oral bioavailability. *Int J Nanomedicine,* 8**,** 177-87.

NG, W. K., SAIFUL YAZAN, L., YAP, L. H., WAN NOR HAFIZA, W. A. G., HOW, C. W. & ABDULLAH, R. 2015. Thymoquinone-Loaded Nanostructured Lipid Carrier Exhibited Cytotoxicity towards Breast Cancer Cell Lines (MDA-MB-231 and MCF-7) and Cervical Cancer Cell Lines (HeLa and SiHa). *BioMed Research International,* 2015**,** 10.

NHS 2014. Breast cancer (female). NHS Choices information.

NICULAE.G., LACATUSU.L., BADEA.N., OPREA.O. & MEGHEA.A. 2013. OPTIMIZATION OF LIPID NANOPARTICLES COMPOSITION FOR SUNSCREEN ENCAPSULATION *UPB Scientific Bulletin, Series B: Chemistry and Materials Science* 75**,** 79-92.

NIH 2007. *Understanding Cancer*.

NOBLE, G. T., STEFANICK, J. F., ASHLEY, J. D., KIZILTEPE, T. & BILGICER, B. 2014. Ligand-targeted liposome design: challenges and fundamental considerations. *Trends in Biotechnology,* 32**,** 32-45.

NOBS, L., BUCHEGGER, F., GURNY, R. & ALLÉMANN, E. 2004. Current methods for attaching targeting ligands to liposomes and nanoparticles. *Journal of Pharmaceutical Sciences,* 93**,** 1980-1992.

OH, N. & PARK, J.-H. 2014. Endocytosis and exocytosis of nanoparticles in mammalian cells. *Int J Nanomedicine,* 9**,** 51-63.

OLBRICH, C., SCHÖLER, N., TABATT, K., KAYSER, O. & MÜLLER, R. H. 2004. Cytotoxicity studies of Dynasan 114 solid lipid nanoparticles (SLN) on RAW 264.7 macrophages—impact of phagocytosis on viability and cytokine production. *Journal of Pharmacy and Pharmacology,* 56**,** 883-891.

OLSSON, E., HONETH, G., BENDAHL, P.-O., SAAL, L. H., GRUVBERGER-SAAL, S., RINGNÉR, M., VALLON-CHRISTERSSON, J., JÖNSSON, G., HOLM, K., LÖVGREN, K., FERNÖ, M., GRABAU, D., BORG, Å. & HEGARDT, C. 2011. CD44 isoforms are heterogeneously expressed in breast cancer and correlate with tumor subtypes and cancer stem cell markers. *BMC Cancer,* 11**,** 418.

OMAR, J. M., YANG, H., LI, S., MARQUARDT, R. R. & JONES, P. J. H. 2014. Development of an Improved Reverse-Phase High-Performance Liquid Chromatography Method for the Simultaneous Analyses of trans-/cis-Resveratrol, Quercetin, and Emodin in Commercial Resveratrol Supplements. *Journal of Agricultural and Food Chemistry,* 62**,** 5812-5817.

OOMAHA.B.D., LADETB.S., GODFREYA.V.D., LIANGC.J. & GIRARDA.B. 2000. Characteristics of raspberry (Rubus idaeus L.) seed oil. *Food Chemistry,* 69**,** 187-193.

ORGOVÁN, G., GONDA, I. & NOSZÁL, B. 2017. Biorelevant physicochemical profiling of (E)- and (Z)-resveratrol determined from isomeric mixtures. *Journal of Pharmaceutical and Biomedical Analysis,* 138**,** 322-329.

OSMAN, A.-M. M., BAYOUMI, H. M., AL-HARTHI, S. E., DAMANHOURI, Z. A. & ELSHAL, M. F. 2012. Modulation of doxorubicin cytotoxicity by resveratrol in a human breast cancer cell line. *Cancer Cell International,* 12**,** 47.

OWENS, D. E. & PEPPAS, N. A. 2006. Opsonization, biodistribution, and pharmacokinetics of polymeric nanoparticles. *Int J Pharm,* 307**,** 93-102.

PAN, F., HAN, L., ZHANG, Y., YU, Y. & LIU, J. 2015. Optimization of Caco-2 and HT29 co-culture in vitro cell models for permeability studies. *International Journal of Food Sciences and Nutrition,* 66**,** 680-685.

PANDITA, D., KUMAR, S., POONIA, N. & LATHER, V. 2014. Solid lipid nanoparticles enhance oral bioavailability of resveratrol, a natural polyphenol. *Food Research International,* 62**,** 1165-1174.

PANGENI, R., ALI, J., MUSTAFA, G., SHARMA, S. & BABOOTA, S. 2015. Design expert-supported development and validation of stability indicating high-performance liquid chromatography (HPLC) method for determination of resveratrol in bulk drug and pharmaceutical formulation. *International Journal Of Pharmaceutical Sciences And Research,* 6**,** 1000-11.

PARDEIKE, J., HOMMOSS, A. & MÜLLER, R. H. 2009. Lipid nanoparticles (SLN, NLC) in cosmetic and pharmaceutical dermal products. *Int J Pharm,* 366**,** 170-184.

PARK, E. 2017. Data on the effects of anti-cancer drug of resveratrol in breast cancer cells, MDA-MB-231 cells. *Data in Brief,* 12**,** 68-71.

PARK, J. W. 2002. Liposome-based drug delivery in breast cancer treatment. *Breast Cancer Res,* 4.

PARK, J. W., HONG, K., KIRPOTIN, D. B., MEYER, O., PAPAHADJOPOULOS, D. & BENZ, C. C. 1997. Anti-HER2 immunoliposomes for targeted therapy of human tumors. *Cancer Letters,* 118**,** 153-160.

PARK, J. W., KIRPOTIN, D. B., HONG, K., SHALABY, R., SHAO, Y., NIELSEN, U. B., MARKS, J. D., PAPAHADJOPOULOS, D. & BENZ, C. C. 2001. Tumor targeting using anti-her2 immunoliposomes. *Journal of Controlled Release,* 74**,** 95-113.

PATEL, M. & SAWANT, K. 2017. A Quality by Design Concept on Lipid Based Nanoformulation Containing Antipsychotic Drug: Screening Design and Optimization using Response Surface Methodology. *Jornal of Nanomedicine and Nanotechnology,* 8**,** 442.

PAULMURUGAN, R., BHETHANABOTLA, R., MISHRA, K., DEVULAPALLY, R., FOYGEL, K., SEKAR, T. V., ANANTA, J. S., MASSOUD, T. F. & JOY, A. 2016. Folate Receptor Targeted Polymeric Micellar Nanocarriers for Delivery of Orlistat as a Repurposed Drug against Triple Negative Breast Cancer. *Molecular Cancer Therapeutics,* 15**,** 221-231.

PERUMAL, O. P., INAPAGOLLA, R., KANNAN, S. & KANNAN, R. M. 2008. The effect of surface functionality on cellular trafficking of dendrimers. *Biomaterials,* 29**,** 3469-3476.

POGORZELSKI, S., WATROBSKA-SWIETLIKOWSKA. D. & SZNITOWSKA, M. 2012. Surface tensometry studies on formulations of surfactants with preservatives as a tool for antimicrobial drug protection characterization. *Journal of Biophysical Chemistry,* 3**,** 324-333.

POONIA, N., KHARB, R., LATHER, V. & PANDITA, D. 2016. Nanostructured lipid carriers: versatile oral delivery vehicle. *Future Science OA,* 2**,** FSO135.

POPOVA, N. V., DEYEV, I. E. & PETRENKO, A. G. 2013. Clathrin-Mediated Endocytosis and Adaptor Proteins. *Acta Naturae,* 5**,** 62-73.

POZAROWSKI P, D. Z. 2004. Analysis of cell cycle by flow cytometry. *Methods Mol Biol,* 281**,** 301-11.

POZO-GUISADO, E., ALVAREZ-BARRIENTOS, A., MULERO-NAVARRO, S., SANTIAGO-JOSEFAT, B. & FERNANDEZ-SALGUERO, P. M. 2002. The antiproliferative activity of resveratrol results in apoptosis in MCF-7 but not in MDA-MB-231 human breast cancer cells: cell-specific alteration of the cell cycle. *Biochem Pharmacol,* 64**,** 1375-1386.

PRABHU, V., SRIVASTAVA, P., YADAV, N., AMADORI, M., SCHNEIDER, A., SESHADRI, A., PITARESSI, J., SCOTT, R., ZHANG, H., KOOCHEKPOUR, S., GOGADA, R. & CHANDRA, D. 2013. Resveratrol depletes mitochondrial DNA and inhibition of autophagy enhances resveratrol-induced caspase activation. *Mitochondrion,* 13**,** 493-499.

PRENCIPE, G., TABAKMAN, S. M., WELSHER, K., LIU, Z., GOODWIN, A. P., ZHANG, L., HENRY, J. & DAI, H. 2009. PEG Branched Polymer for Functionalization of Nanomaterials with Ultralong Blood Circulation. *Journal of the American Chemical Society,* 131**,** 4783-4787.

PRESS, B. 2011. Optimization of the Caco-2 permeability assay to screen drug compounds for intestinal absorption and efflux. Permeability Barrier: Methods and Protocols. *Methods in Molecular Biology*

PUCADYIL, T. J. & SCHMID, S. L. 2009. Conserved Functions of Membrane Active GTPases in Coated Vesicle Formation. *Science (New York, N.Y.),* 325**,** 1217-1220.

PURI, A., LOOMIS, K., SMITH, B., LEE, J.-H., YAVLOVICH, A., HELDMAN, E. & BLUMENTHAL, R. 2009. Lipid-Based Nanoparticles as Pharmaceutical Drug Carriers: From Concepts to Clinic. *Critical reviews in therapeutic drug carrier systems,* 26**,** 523-580.

QADDOUMI, M. G., UEDA, H., YANG, J., DAVDA, J., LABHASETWAR, V. & LEE, V. H. L. 2004. The Characteristics and Mechanisms of Uptake of PLGA Nanoparticles in Rabbit Conjunctival Epithelial Cell Layers. *Pharm Res,* 21**,** 641-648.

QHATTAL, H. S. S. & LIU, X. 2011. Characterization of CD44-Mediated Cancer Cell Uptake and Intracellular Distribution of Hyaluronan-Grafted Liposomes. *Molecular Pharmaceutics,* 8**,** 1233-1246.

RADOMSKA-SOUKHAREV, A. 2007. Stability of lipid excipients in solid lipid nanoparticles. *Advanced Drug Delivery Reviews,* 59**,** 411-418.

RADTKE, M. & MÜLLER, R. H. 2001. Stability study of creams containing cyclosporine SLN™. *Int Symp Control Rel Bioact Mater,* 28.

RADTKE.M., SOUTO. E.B. & MULLER.R.H. 2005. Nanostructured lipid carriers: a novel generation of solid lipid drug carriers. *Pharmaceutical Technology Europe* 17**,** 45-50.

RAHMAN, Z., ZIDAN, A. S., HABIB, M. J. & KHAN, M. A. 2010. Understanding the quality of protein loaded PLGA nanoparticles variability by Plackett-Burman design. *Int J Pharm,* 389**,** 186-94.

RAKHA, E. A., REIS-FILHO, J. S. & ELLIS, I. O. 2008. Basal-Like Breast Cancer: A Critical Review. *Journal of Clinical Oncology,* 26**,** 2568-2581.

RAMASAMY, T., TRAN, T. H., CHOI, J. Y., CHO, H. J., KIM, J. H., YONG, C. S., CHOI, H.-G. & KIM, J. O. 2014. Layer-by-layer coated lipid–polymer hybrid nanoparticles designed for use in anticancer drug delivery. *Carbohydrate Polymers,* 102**,** 653-661.

RAYMOND, C. R., PAUL, J. S., WALTER, G. C. & MARIAN, E. Q. 2012. *Handbook of Pharmaceutical Excipients – 7th Edition*.

REDDY, K. J. & KARUNAKARAN, K. T. 2013. Purification and characterization of hyaluronic acid produced by Streptococcus zooepidemicus strain 3523-7. *Journal of BioScience & Biotechnology,* 2.

RENGER, B. 2000. System performance and variability of chromatographic techniques used in pharmaceutical quality control. *Journal of Chromatography B: Biomedical Sciences and Applications,* 745**,** 167-176.

RIDDICK, T. M. 1968. Control of Colloid Stability through Zeta Potential. *Zeta-Meter Inc. via Livingston Publishing Company, Wynnewood*.

RIEUX, A. D., RAGNARSSON, E. G. E., GULLBERG, E., PRÉAT, V., SCHNEIDER, Y.-J. & ARTURSSON, P. 2005. Transport of nanoparticles across an in vitro model of the human intestinal follicle associated epithelium. *European Journal of Pharmaceutical Sciences,* 25**,** 455-465.

RIVOLTA, I., PANARITI, A., LETTIERO, B., SESANA, S., GASCO, P., GASCO, M. R., MASSERINI, M. & MISEROCCHI, G. 2011. Cellular uptake of coumarin-6 as a model drug loaded in solid lipid nanoparticles. *Jornal of Physiology and Pharmacology,* 62**,** 45-53.

RIZWANULLAH, M., AHMAD, J. & AMIN, S. 2016. Nanostructured Lipid Carriers: A Novel Platform for Chemotherapeutics. *Current Drug Delivery,* 13**,** 4-26.

ROCHA, K. A. D., KRAWCZYK-SANTOS, A. P., ANDRADE, L. M., SOUZA, L. C. D., MARRETO, R. N., GRATIERI, T. & TAVEIRA, S. F. 2017. Voriconazole-loaded nanostructured lipid carriers (NLC) for drug delivery in deeper regions of the nail plate. *Int J Pharm,* 531**,** 292-298.

ROCKVILLE, M. D. 1999. Validation of Compendial Methods. *In:* CONVENTION, U. S. P. (ed.) *US Pharmacopeia 24, Section 〈1225〉.*

ROGER, E., KALSCHEUER, S., KIRTANE, A., GURU, B. R., GRILL, A. E., WHITTUM-HUDSON, J. & PANYAM, J. 2012. Folic acid-Functionalized Nanoparticles for Enhanced Oral Drug Delivery. *Molecular Pharmaceutics,* 9**,** 2103-2110.

RUOSLAHTI, E. 2002. Drug Discovery Today. 7**,** 1138.

SABZICHI, M., MOHAMMADIAN, J., KHOSROUSHAHI, A. Y., BAZZAZ, R. & HAMISHEHKAR, H. 2016. Folate-Targeted Nanostructured Lipid Carriers (NLCs) Enhance (Letrozol) Efficacy in MCF-7 Breast Cancer Cells. *Asian Pacific Journal of Cancer Prevention : APJCP,* 17**,** 5185-5188.

SAFWAT, S., ISHAK, R. A. H., HATHOUT, R. M. & MORTADA, N. D. 2017. Nanostructured lipid carriers loaded with simvastatin: effect of PEG/glycerides on characterization, stability, cellular uptake efficiency and in vitro cytotoxicity. *Drug Development and Industrial Pharmacy,* 43**,** 1112-1125.

SAKHRANI, N. M. & PADH, H. 2013. Organelle targeting: third level of drug targeting. *Drug Design, Development and Therapy,* 7**,** 585-599.

SALATA, O. V. 2004. Applications of nanoparticles in biology and medicine. *Journal of Nanobiotechnology,* 2**,** 3-3.

SALMASO, S. & CALICETI, P. 2013. Stealth Properties to Improve Therapeutic Efficacy of Drug Nanocarriers. *Journal of Drug Delivery,* 2013**,** 19.

SAMBUY, Y., DE ANGELIS, I., RANALDI, G., SCARINO, M. L., STAMMATI, A. & ZUCCO, F. 2005. The Caco-2 cell line as a model of the intestinal barrier: influence of cell and culture-related factors on Caco-2 cell functional characteristics. *Cell Biology and Toxicology,* 21**,** 1-26.

SANAD, R. A., ABDELMALAK, N. S., ELBAYOOMY, T. S. & BADAWI, A. A. 2010. Formulation of a Novel Oxybenzone-Loaded Nanostructured Lipid Carriers (NLCs). *AAPS PharmSciTech,* 11**,** 1684-1694.

SANGSHETTI, J. N., DESHPANDE, M., ZAHEER, Z., SHINDE, D. B. & AROTE, R. 2017. Quality by design approach: Regulatory need. *Arabian Journal of Chemistry,* 10**,** S3412-S3425.

SAPAN, C. V., LUNDBLAD, R. L. & PRICE, N. C. 1999. Colorimetric protein assay techniques. *Biotechnology and applied Biochemistry,* 29**,** 99-108.

SARKAR, S., HORN, G., MOULTON, K., OZA, A., BYLER, S., KOKOLUS, S. & LONGACRE, M. 2013. Cancer Development, Progression, and Therapy: An Epigenetic Overview. *International Journal of Molecular Sciences,* 14**,** 21087-21113.

SATAKE, K., OKUYAMA, T., OHASHI, M. & SHINODA, T. 1960. THE SPECTROPHOTOMETRIC DETERMINATION OF AMINE, AMINO ACID AND PEPTIDE WITH 2, 4, 6-TRINITROBENZENE 1-SULFONIC ACID. *The Journal of Biochemistry,* 47**,** 654-660.

SAUL, J. M., ANNAPRAGADA, A. V. & BELLAMKONDA, R. V. 2006. A dual-ligand approach for enhancing targeting selectivity of therapeutic nanocarriers. *Journal of Controlled Release,* 114**,** 277-287.

SAUPE, A., WISSING, S. A., LENK, A., SCHMIDT, C. & MÜLLER, R. H. 2005. Solid Lipid Nanoparticles (SLN) and Nanostructured Lipid Carriers (NLC) – Structural investigations on two different carrier systems. *Bio-Med Mater Eng,* 15.

SELVAMUTHUKUMAR, S., ANANDAM, S., KANNAN, K. & MANAVALAN, R. 2012. Nanosponges: A novel class of drug delivery system - Review. *J Pharm Pharmaceut Sci,* 15.

SEO, H.-S., JOURNÉ, F., LARSIMONT, D., SOTIRIOU, C. & LECLERCQ, G. 2003. Decrease of estrogen receptor expression and associated ERE-dependent transcription in MCF-7 breast cancer cells after oligomycin treatment. *Steroids,* 68**,** 257-269.

SESSA, M., BALESTRIERI, M. L., FERRARI, G., SERVILLO, L., CASTALDO, D., D'ONOFRIO, N., DONSI, F. & TSAO, R. 2014. Bioavailability of encapsulated resveratrol into nanoemulsion-based delivery systems. *Food Chem,* 147**,** 42-50.

SEVERINO, P., PINHO, S. C., SOUTO, E. B. & SANTANA, M. H. 2011. Crystallinity of Dynasan® 114 and Dynasan® 118 matrices for the production of stable Miglyol®-loaded nanoparticles. *Journal of thermal analysis and calorimetry,* 108**,** 101-108.

SEVIN, E., DEHOUCK, L., FABULAS-DA COSTA, A., CECCHELLI, R., DEHOUCK, M. P., LUNDQUIST, S. & CULOT, M. 2013. Accelerated Caco-2 cell permeability model for drug discovery. *Journal of Pharmacological and Toxicological Methods,* 68**,** 334-339.

SHA, X., YAN, G., WU, Y., LI, J. & FANG, X. 2005. Effect of self-microemulsifying drug delivery systems containing Labrasol on tight junctions in Caco-2 cells. *European Journal of Pharmaceutical Sciences,* 24**,** 477-486.

SHABIR, G. A. 2003. Validation of high-performance liquid chromatography methods for pharmaceutical analysis. *Journal of Chromatography A,* 987**,** 57-66.

SHAH, B., KHUNT, D., BHATT, H., MISRA, M. & PADH, H. 2015. Application of quality by design approach for intranasal delivery of rivastigmine loaded solid lipid nanoparticles: Effect on formulation and characterization parameters. *European Journal of Pharmaceutical Sciences,* 78**,** 54-66.

SHAH, M., CHUTTANI, K., MISHRA, A. K. & PATHAK, K. 2011. Oral solid compritol 888 ATO nanosuspension of simvastatin: optimization and biodistribution studies. *Drug Dev Ind Pharm,* 37**,** 526-37.

SHAH, M. & PATHAK, K. 2010. Development and statistical optimization of solid lipid nanoparticles of simvastatin by using 2(3) full-factorial design. *AAPS PharmSciTech,* 11**,** 489-96.

SHAO, J., LI, X., LU, X., JIANG, C., HU, Y., LI, Q., YOU, Y. & FU, Z. 2009. Enhanced growth inhibition effect of Resveratrol incorporated into biodegradable nanoparticles against glioma cells is mediated by the induction of intracellular reactive oxygen species levels. *Colloids and Surfaces B: Biointerfaces,* 72**,** 40-47.

SHARMA, V. K., DIWAN, A., SARDANA, S. & DHALL, V. 2011. Solid lipid nanoparticles system: An overview. *International Journal of Research in Pharmaceutical Sciences,* 2**,** 450-461.

SHI, G., RAO, L., YU, H., XIANG, H., YANG, H. & JI, R. 2008. Stabilization and encapsulation of photosensitive resveratrol within yeast cell. *Int J Pharm,* 349**,** 83-93.

SHI, L.-L., CAO, Y., ZHU, X.-Y., CUI, J.-H. & CAO, Q.-R. 2015. Optimization of process variables of zanamivir-loaded solid lipid nanoparticles and the prediction of their cellular transport in Caco-2 cell model. *Int J Pharm,* 478**,** 60-69.

SHIMADA, T. & FUJII-KURIYAMA, Y. 2004. Metabolic activation of polycyclic aromatic hydrocarbons to carcinogens by cytochromes P450 1A1 and 1B1. *Cancer Sci,* 95**,** 1-6.

SHIMADA, T., HAYES, C. L., YAMAZAKI, H., AMIN, S., HECHT, S. S., GUENGERICH, F. P. & SUTTER, T. R. 1996. Activation of chemically diverse procarcinogens by human cytochrome P-450 1B1. *Cancer Res,* 56**,** 2979-84.

SHIMIZU, T., NAKAZATO, T., XIAN, M. J., SAGAWA, M., IKEDA, Y. & KIZAKI, M. 2006. Resveratrol induces apoptosis of human malignant B cells by activation of caspase-3 and p38 MAP kinase pathways. *Biochem Pharmacol,* 71**,** 742-750.

SIAFAKA, P., ÜSTÜNDAĞ OKUR, N., KARAVAS, E. & BIKIARIS, D. 2016a. Surface Modified Multifunctional and Stimuli Responsive Nanoparticles for Drug Targeting: Current Status and Uses. *International Journal of Molecular Sciences,* 17**,** 1440.

SIAFAKA, P. I., ÜSTÜNDAĞ OKUR, N., KARAVAS, E. & BIKIARIS, D. N. 2016b. Surface Modified Multifunctional and Stimuli Responsive Nanoparticles for Drug Targeting: Current Status and Uses. *International Journal of Molecular Sciences,* 17**,** 1440.

SIEKMANN, B. & WESTESEN, K. 1994. Thermoanalysis of the recrystallization process of melt-homogenized glyceride nanoparticles. *Colloids and Surfaces B: Biointerfaces,* 3**,** 159-175.

SIEPMANN, J. & PEPPAS, N. A. 2001. Modeling of drug release from delivery systems based on hydroxypropyl methylcellulose (HPMC). *Advanced Drug Delivery Reviews,* 48**,** 139-157.

SIGURDSSON, H. H., KIRCH, J. & LEHR, C. M. 2013. Mucus as a barrier to lipophilic drugs. *Int J Pharm,* 453.

SILVA, A. C., GONZÁLEZ-MIRA, E., GARCÍA, M. L., EGEA, M. A., FONSECA, J., SILVA, R., SANTOS, D., SOUTO, E. B. & FERREIRA, D. 2011. Preparation, characterization and biocompatibility studies on risperidone-loaded solid lipid nanoparticles (SLN): High pressure homogenization versus ultrasound. *Colloids and Surfaces B: Biointerfaces,* 86**,** 158-165.

SILVA, C. M., VEIGA, F., RIBEIRO, A. J., ZERROUK, N. & ARNAUD, P. 2006. Effect of Chitosan-Coated Alginate Microspheres on the Permeability of Caco-2 Cell Monolayers. *Drug Development and Industrial Pharmacy,* 32**,** 1079-1088.

SINGH, G., PAI, R. S. & PANDIT, V. 2012. Development and validation of a HPLC method for the determination of trans-resveratrol in spiked human plasma. *Journal of Advanced Pharmaceutical Technology & Research,* 3**,** 130-135.

SMITH, A. & HUNNEYBALL, L. M. 1986. Evaluation of poly (lactic acid) as a biodegradable drug delivery system for parenteral administration. *Int J Pharm,* 30.

SOMA, D., ATTARI, Z., REDDY, M. S., DAMODARAM, A. & KOTESHWARA, K. B. G. 2017. Solid lipid nanoparticles of irbesartan: preparation, characterization, optimization and pharmacokinetic studies. *Brazilian Journal of Pharmaceutical Sciences,* 53.

SOUTO, E. 2011. *Lipid nanocarriers in cancer diagnosis and therapy*, Smithers Rapra.

SOUTO, E. B., WISSING, S. A., BARBOSA, C. M. & MÜLLER, R. H. 2004. Development of a controlled release formulation based on SLN and NLC for topical clotrimazole delivery. *Int J Pharm,* 278**,** 71-77.

SOUZA, L. C. & CAMPA, A. 1999. Pharmacological parameters of intravenously administered amphotericin B in rats: comparison of the conventional formulation with amphotericin B associated with a triglyceride-rich emulsion. *Journal of Antimicrobial Chemotherapy,* 44**,** 77-84.

SPORN, M. B. & HARRIS, E. D. 1981. Proliferative diseases. *The American journal of medicine,* 70**,** 1231-1236.

SRINIVASAN, B., KOLLI, A. R., ESCH, M. B., ABACI, H. E., SHULER, M. L. & HICKMAN, J. J. 2015. TEER measurement techniques for in vitro barrier model systems. *Journal of laboratory automation,* 20**,** 107-126.

STELLA, B., ARPICCO, S., PERACCHIA, M. T., DESMAËLE, D., HOEBEKE, J., RENOIR, M., D'ANGELO, J., CATTEL, L. & COUVREUR, P. 2000. Design of Folic Acid-Conjugated Nanoparticles for Drug Targeting. *Journal of Pharmaceutical Sciences,* 89**,** 1452-1464.

STUURMAN, F. E., NUIJEN, B., BEIJNEN, J. H. & SCHELLENS, J. H. M. 2013. Oral Anticancer Drugs: Mechanisms of Low Bioavailability and Strategies for Improvement. *Clinical Pharmacokinetics,* 52**,** 399-414.

SUBEDI, R. K., KANG, K. W. & CHOI, H.-K. 2009. Preparation and characterization of solid lipid nanoparticles loaded with doxorubicin. *European Journal of Pharmaceutical Sciences,* 37**,** 508-513.

SUBIK, K., LEE, J.-F., BAXTER, L., STRZEPEK, T., COSTELLO, D., CROWLEY, P., XING, L., HUNG, M.-C., BONFIGLIO, T., HICKS, D. G. & TANG, P. 2010. The Expression Patterns of ER, PR, HER2, CK5/6, EGFR, Ki-67 and AR by Immunohistochemical Analysis in Breast Cancer Cell Lines. *Breast Cancer : Basic and Clinical Research,* 4**,** 35-41.

SUN, J., BI, C., CHAN, H. M., SUN, S., ZHANG, Q. & ZHENG, Y. 2013. Curcumin-loaded solid lipid nanoparticles have prolonged in vitro antitumour activity, cellular uptake and improved in vivo bioavailability. *Colloids and Surfaces B: Biointerfaces,* 111**,** 367-375.

SUN, R., ZHAO, G., NI, S. & XIA, Q. 2014. Lipid based nanocarriers with different lipid compositions for topical delivery of resveratrol: comparative analysis of characteristics and performance. *Journal of Drug Delivery Science and Technology,* 24**,** 591-600.

SURACE, C., ARPICCO, S., DUFA-WOJCICKI, A., MARSAUD, V., BOUCLIER, C., CLAY, D., CATTEL, L., RENOIR, J.-M. & FATTAL, E. 2009. Lipoplexes Targeting the CD44 Hyaluronic Acid Receptor for Efficient Transfection of Breast Cancer Cells. *Molecular Pharmaceutics,* 6**,** 1062-1073.

SURENDIRAN, A., SANDHIYA, S., PRADHAN, S. C. & ADITHAN, C. 2009. Novel applications of nanotechnology in medicine. *Indian J Med Res,* 130**,** 689-701.

SWANSON, J. A. & WATTS, C. 1995. Macropinocytosis. *Trends in Cell Biology,* 5**,** 424-428.

TADROS, T., IZQUIERDO, P., ESQUENA, J. & SOLANS, C. 2004. Formation and stability of nano-emulsions. *Advances in Colloid and Interface Science,* 108**,** 303-318.

TALEBIANPOOR, M. S., KHODADOUST, S., ROZBEHI, A., AKBARTABAR TOORI, M., ZOLADL, M., GHAEDI, M., MOHAMMADI, R. & HOSSEINZADEH, A. S. 2014. Application of optimized dispersive liquid–liquid microextraction for determination of melatonin by HPLC–UV in plasma samples. *Journal of Chromatography B,* 960**,** 1-7.

TAMJIDI, F., SHAHEDI, M., VARSHOSAZ, J. & NASIRPOUR, A. 2014. Design and characterization of astaxanthin-loaded nanostructured lipid carriers. *Innovative Food Science & Emerging Technologies,* 26**,** 366-374.

TANAKA, Y., TAKI, Y., SAKANE, T., NADAI, T., SEZAKI, H. & YAMASHITA, S. 1995. Characterization of Drug Transport Through Tight-Junctional Pathway in Caco-2 Monolayer: Comparison with Isolated Rat Jejunum and Colon. *Pharm Res,* 12**,** 523-528.

TENG, Z., YUAN, C., ZHANG, F., HUAN, M., CAO, W., LI, K., YANG, J., CAO, D., ZHOU, S. & MEI, Q. 2012. Intestinal Absorption and First-Pass Metabolism of Polyphenol Compounds in Rat and Their Transport Dynamics in Caco-2 Cells. *PLoS One,* 7**,** e29647.

TESKAČ, K. & KRISTL, J. 2010. The evidence for solid lipid nanoparticles mediated cell uptake of resveratrol. *Int J Pharm,* 390**,** 61-69.

THANG, L. Q., HANH, N. D. & DUONG, D. Q. 2017. STUDY ON CAUSE–EFFECT RELATIONS AND OPTIMIZATION OF EXEMESTANE-LOADED NANOSTRUCTURED LIPID CARRIERS. *International Journal of Pharmacy and Pharmaceutical Sciences; Vol 9, Issue 5, 2017DO - 10.22159/ijpps.2017v9i5.17354*.

THANH, N. T. K., MACLEAN, N. & MAHIDDINE, S. 2014. Mechanisms of Nucleation and Growth of Nanoparticles in Solution. *Chemical Reviews,* 114**,** 7610-7630.

THAPA, R. & WILSON, G. D. 2016. The Importance of CD44 as a Stem Cell Biomarker and Therapeutic Target in Cancer. *Stem Cells International,* 2016**,** 15.

THATIPAMULA, R. P., PALEM, C. R., GANNU, R., MUDRAGADA, S. & YAMSANI, M. R. 2011. Formulation and in vitro characterization of domperidone loaded solid lipid nanoparticles and nanostructured lipid carriers. *DARU : Journal of Faculty of Pharmacy, Tehran University of Medical Sciences,* 19**,** 23-32.

THOMAS, E., GOPALAKRISHNAN, V., HEGDE, M., KUMAR, S., KARKI, S. S., RAGHAVAN, S. C. & CHOUDHARY, B. 2016. A Novel Resveratrol Based Tubulin Inhibitor Induces Mitotic Arrest and Activates Apoptosis in Cancer Cells. 6**,** 34653.

THOMPSON, E. W., REICH, R., SHIMA, T. B., ALBINI, A., GRAF, J., MARTIN, G. R., DICKSON, R. B. & LIPPMAN, M. E. 1988. Differential Regulation of Growth and Invasiveness of MCF-7 Breast Cancer Cells by Antiestrogens. *Cancer Res,* 48**,** 6764.

TOALDO, I. M., GROOTAERT, C., BORDIGNON-LUIZ, M. T. & VAN CAMP, J. 2015. Bioavailability and metabolism of grape trans-resveratrol on Caco-2 cells. *COMMUNICATIONS IN AGRICULTURAL AND APPLIED BIOLOGICAL SCIENCES,* 80**,** 165–70.

TRAN, T. H., CHOI, J. Y., RAMASAMY, T., TRUONG, D. H., NGUYEN, C. N., CHOI, H.-G., YONG, C. S. & KIM, J. O. 2014. Hyaluronic acid-coated solid lipid nanoparticles for targeted delivery of vorinostat to CD44 overexpressing cancer cells. *Carbohydrate Polymers,* 114**,** 407-415.

TREJDOSIEWICZ, L. K., MORTON, R., YANG, Y., BANKS, R. E., SELBY, P. J. & SOUTHGATE, J. 1998. INTERLEUKINS 4 AND 13 UPREGULATE EXPRESSION OF CD44 IN HUMAN COLONIC EPITHELIAL CELL LINES. *Cytokine,* 10**,** 756-765.

TRELA, B. C. & WATERHOUSE, A. L. 1996. *J. Agric. Food Chem.,* 44**,** 1253.

TROTTA, M., DEBERNARDI, F. & CAPUTO, O. 2003. Preparation of solid lipid nanoparticles by a solvent emulsification–diffusion technique. *Int J Pharm,* 257**,** 153-160.

TRUJILLO, C. C. & WRIGHT, A. J. 2010. Properties and Stability of Solid Lipid Particle Dispersions Based on Canola Stearin and Poloxamer 188. *Journal of the American Oil Chemists' Society,* 87**,** 715-730.

TSAI, H.-Y., HO, C.-T. & CHEN, Y.-K. 2017. Biological actions and molecular effects of resveratrol, pterostilbene, and 3'-hydroxypterostilbene. *Journal of Food and Drug Analysis,* 25**,** 134-147.

UCAR, E., TEKSOZ, S., ICHEDEF, C., KILCAR, A. Y., MEDINE, E. I., ARI, K., PARLAK, Y., SAYIT BILGIN, B. E. & UNAK, P. 2017. Synthesis, characterization and radiolabeling of folic acid modified nanostructured lipid carriers as a contrast agent and drug delivery system. *Applied Radiation and Isotopes,* 119**,** 72-79.

ULBRICH, K., MICHAELIS, M., ROTHWEILER, F., KNOBLOCH, T., SITHISARN, P., CINATL, J. & KREUTER, J. 2011. Interaction of folate-conjugated human serum albumin (HSA) nanoparticles with tumour cells. *Int J Pharm,* 406**,** 128-134.

UNER, M. 2006. Preparation, characterization and physico-chemical properties of solid lipid nanoparticles (SLN) and nanostructured lipid carriers (NLC): their benefits as colloidal drug carrier systems. *Die Pharmazie,* 61.

USKOKOVIĆ, V., LEE, P. P., WALSH, L. A., FISCHER, K. E. & DESAI, T. A. 2012. *Biomaterials,* 33**,** 1663.

VANDERVOORT, J. & LUDWIG, A. 2002. Biocompatible stabilizers in the preparation of PLGA nanoparticles: a factorial design study. *Int J Pharm,* 238**,** 77-92.

VARSHOSAZ, J., MOHAMMADI GHALAEI, P. & HASSANZADEH, F. 2014. Hyaluronate Targeted Solid Lipid Nanoparticles of Etoposide: Optimization and In Vitro Characterization. *Journal of Nanomaterials,* 2014**,** 12.

VAUGHN, N. A. & POLNASZEK, C. 2007. Design-Expert® software. Stat-Ease, Inc, Minneapolis, MN.

VELMURUGAN, R. & SELVAMUTHUKUMAR, S. 2016. Development and optimization of ifosfamide nanostructured lipid carriers for oral delivery using response surface methodology. *Applied Nanoscience,* 6**,** 159-173.

VERMES, I., HAANEN, C., STEFFENS-NAKKEN, H. & REUTELLINGSPERGER, C. 1995. A novel assay for apoptosis Flow cytometric detection of phosphatidylserine expression on early apoptotic cells using fluorescein labelled Annexin V. *Journal of Immunological Methods,* 184**,** 39-51.

VILLALOBOS-HERNÁNDEZ, J. R. & MÜLLER-GOYMANN, C. C. 2006. Physical stability, centrifugation tests, and entrapment efficiency studies of carnauba wax–decyl oleate nanoparticles used for the dispersion of inorganic sunscreens in aqueous media. *European Journal of Pharmaceutics and Biopharmaceutics,* 63**,** 115-127.

VOLKHARD JENNING, S. H. G. 2001. Encapsulation of retinoids in solid lipid nanoparticles (SLN). *Journal of Microencapsulation,* 18**,** 149-158.

WALLE, T. 2011. Bioavailability of resveratrol. *Ann N Y Acad Sci,* 1215**,** 9-15.

WALLE, T., HSIEH, F., DELEGGE, M. H., OATIS, J. E., JR. & WALLE, U. K. 2004. High absorption but very low bioavailability of oral resveratrol in humans. *Drug Metab Dispos,* 32**,** 1377-82.

WANG, F., CHEN, L., JIANG, S., HE, J., ZHANG, X., PENG, J., XU, Q. & LI, R. 2014a. Optimization of methazolamide-loaded solid lipid nanoparticles for ophthalmic delivery using Box–Behnken design. *Journal of Liposome Research,* 24**,** 171-181.

WANG, H., SUN, G., ZHANG, Z. & OU, Y. 2017. Transcription activator, hyaluronic acid and tocopheryl succinate multi-functionalized novel lipid carriers encapsulating etoposide for lymphoma therapy. *Biomedicine & Pharmacotherapy,* 91**,** 241-250.

WANG, J., BYRNE, J. D., NAPIER, M. E. & DESIMONE, J. M. 2011. More Effective Nanomedicines through Particle Design. *Small (Weinheim an Der Bergstrasse, Germany),* 7**,** 1919-1931.

WANG, L., LI, H., WANG, S., LIU, R., WU, Z., WANG, C., WANG, Y. & CHEN, M. 2014b. Enhancing the Antitumor Activity of Berberine Hydrochloride by Solid Lipid Nanoparticle Encapsulation. *AAPS PharmSciTech,* 15**,** 834-844.

WANG, L., LUO, Q., LIN, T., LI, R., ZHU, T., ZHOU, K., JI, Z., SONG, J., JIA, B., ZHANG, C., CHEN, W. & ZHU, G. 2015. PEGylated nanostructured lipid carriers (PEG–NLC) as a novel drug delivery system for biochanin A. *Drug Development and Industrial Pharmacy,* 41**,** 1204-1212.

WANG, L., WANG, S., CHEN, R., WANG, Y., LI, H., WANG, Y. & CHEN, M. 2014c. Oridonin Loaded Solid Lipid Nanoparticles Enhanced Antitumor Activity in MCF-7 Cells. *Journal of Nanomaterials,* 2014**,** 11.

WANG, Q., RAGER, J. D., WEINSTEIN, K., KARDOS, P. S., DOBSON, G. L., LI, J. & HIDALGO, I. J. 2005. Evaluation of the MDR-MDCK cell line as a permeability screen for the blood–brain barrier. *Int J Pharm,* 288**,** 349-359.

WANG, S., CHEN, T., CHEN, R., HU, Y., CHEN, M. & WANG, Y. 2012. Emodin loaded solid lipid nanoparticles: Preparation, characterization and antitumor activity studies. *Int J Pharm,* 430**,** 238-246.

WEIR, N. M., SELVENDIRAN, K., KUTALA, V. K., TONG, L., VISHWANATH, S., RAJARAM, M., TRIDANDAPANI, S., ANANT, S. & KUPPUSAMY, P. 2007. Curcumin Induces G(2)/M Arrest and Apoptosis in Cisplatin-Resistant Human Ovarian Cancer Cells by Modulating Akt and p38 MAPK. *Cancer biology & therapy,* 6**,** 178-184.

WEITMAN, S. D., LARK, R. H., CONEY, L. R., FORT, D. W., FRASCA, V., ZURAWSKI, V. R. & KAMEN, B. A. 1992. Distribution of the Folate Receptor GP38 in Normal and Malignant Cell Lines and Tissues. *Cancer Res,* 52**,** 3396.

WENZEL, E. & SOMOZA, V. 2005. Metabolism and bioavailability of trans-resveratrol. *Mol Nutr Food Res,* 49**,** 472-81.

WERENGOWSKA-CIE., WIERZ, K. W., NIEWSKI, M., TERZYK, A. P. & FURMANIAK, S. 2015. The Chemistry of Bioconjugation in Nanoparticles-Based Drug Delivery System. *Advances in Condensed Matter Physics,* 2015**,** 27.

WHO. 2017. *Cancer* [Online]. Available: http://www.who.int/cancer/en/ [Accessed 16/9 2017].

WILLENBERG, I., MICHAEL, M., WONIK, J., BARTEL, L. C., EMPL, M. T. & SCHEBB, N. H. 2015. Investigation of the absorption of resveratrol oligomers in the Caco-2 cellular model of intestinal absorption. *Food Chem,* 167**,** 245-250.

WITAYAUDOM, P. & KLINKESORN, U. 2017. Effect of surfactant concentration and solidification temperature on the characteristics and stability of nanostructured lipid carrier (NLC) prepared from rambutan (Nephelium lappaceum L.) kernel fat. *Journal of Colloid and Interface Science,* 505**,** 1082-1092.

WONG, R. S. Y. 2011. Apoptosis in cancer: from pathogenesis to treatment. *Journal of Experimental & Clinical Cancer Research : CR,* 30**,** 87-87.

WU, C.-Y. & BENET, L. Z. 2005. Predicting Drug Disposition via Application of BCS: Transport/Absorption/Elimination Interplay and Development of a Biopharmaceutics DrugDisposition Classification System. *Pharm Res,* 22**,** 11-23.

WU, L., ZHANG, J. & WATANABE, W. 2011. Physical and chemical stability of drug nanoparticles. *Advanced Drug Delivery Reviews,* 63**,** 456-469.

XIA, Q.-S., DING, H.-M. & MA, Y.-Q. 2017. Can dual-ligand targeting enhance cellular uptake of nanoparticles? *Nanoscale,* 9**,** 8982-8989.

XIAO, B., ZHANG, M., VIENNOIS, E., ZHANG, Y., WEI, N., BAKER, M. T., JUNG, Y. & MERLIN, D. 2015. Inhibition of MDR1 gene expression and enhancing cellular uptake for effective colon

cancer treatment using dual-surface–functionalized nanoparticles. *Biomaterials,* 48**,** 147-160.

XU, M., MCCANNA, D. J. & SIVAK, J. G. 2015. Use of the viability reagent PrestoBlue in comparison with alamarBlue and MTT to assess the viability of human corneal epithelial cells. *Journal of Pharmacological and Toxicological Methods,* 71**,** 1-7.

YAMAZAKI, M. & ITO T. 1990 Deformation and instability in membrane structure of phospholipid vesicles caused by osmophobic association: mechanical stress model for the mechanism of poly(ethylene glycol)-induced membrane fusion. *Biochemistry,* 29**,** 1309-1314.

YAMEEN, B., CHOI, W. I., VILOS, C., SWAMI, A., SHI, J. & FAROKHZAD, O. C. 2014. Insight into nanoparticle cellular uptake and intracellular targeting. *Journal of Controlled Release,* 190**,** 485-499.

YANG, C.-R., ZHAO, X.-L., HU, H.-Y., LI, K.-X., SUN, X., LI, L. & CHEN, D.-W. 2010. Preparation, Optimization and Characteristic of Huperzine A Loaded Nanostructured Lipid Carriers. *Chemical and Pharmaceutical Bulletin,* 58**,** 656-661.

YANG, X.-Y., LI, Y.-X., LI, M., ZHANG, L., FENG, L.-X. & ZHANG, N. 2013. Hyaluronic acid-coated nanostructured lipid carriers for targeting paclitaxel to cancer. *Cancer Letters,* 334**,** 338-345.

YANG, Y., CORONA III, A., SCHUBERT, B., REEDER, R. & HENSON, M. A. 2014. The effect of oil type on the aggregation stability of nanostructured lipid carriers. *Journal of Colloid and Interface Science,* 418**,** 261-272.

YIN, Y.-M., CUI, F.-D., MU, C.-F., CHOI, M.-K., KIM, J. S., CHUNG, S.-J., SHIM, C.-K. & KIM, D.-D. 2009. Docetaxel microemulsion for enhanced oral bioavailability: Preparation and in vitro and in vivo evaluation. *Journal of Controlled Release,* 140**,** 86-94.

YING, X., WEN, H., LU, W.-L., DU, J., GUO, J., TIAN, W., MEN, Y., ZHANG, Y., LI, R.-J., YANG, T.-Y., SHANG, D.-W., LOU, J.-N., ZHANG, L.-R. & ZHANG, Q. 2010. Dual-targeting daunorubicin liposomes improve the therapeutic efficacy of brain glioma in animals. *Journal of Controlled Release,* 141**,** 183-192.

YOUM, I., AGRAHARI, V., MUROWCHICK, J. B. & YOUAN, B.-B. C. 2014. Uptake and Cytotoxicity of Docetaxel-Loaded Hyaluronic Acid-Grafted Oily Core Nanocapsules in MDA-MB 231 Cancer Cells. *Pharm Res,* 31**,** 2439-2452.

YU, Q., HU, X., MA, Y., XIE, Y., LU, Y., QI, J., XIANG, L., LI, F. & WU, W. 2016. Lipids-based nanostructured lipid carriers (NLCs) for improved oral bioavailability of sirolimus. *Drug Delivery,* 23**,** 1469-1475.

YU, S. S., LAU, C. M., THOMAS, S. N., JEROME, W. G., MARON, D. J., DICKERSON, J. H., HUBBELL, J. A. & GIORGIO, T. D. 2012. Size- and charge-dependent non-specific uptake of PEGylated nanoparticles by macrophages. *Int J Nanomedicine,* 7**,** 799-813.

YUAN, H., CHEN, C.-Y., CHAI, G.-H., DU, Y.-Z. & HU, F.-Q. 2013. Improved Transport and Absorption through Gastrointestinal Tract by PEGylated Solid Lipid Nanoparticles. *Molecular Pharmaceutics,* 10**,** 1865-1873.

YUAN, H., WANG, L.-L., DU, Y.-Z., YOU, J., HU, F.-Q. & ZENG, S. 2007. Preparation and characteristics of nanostructured lipid carriers for control-releasing progesterone by melt-emulsification. *Colloids and Surfaces B: Biointerfaces,* 60**,** 174-179.

ZAFAR, S., NEGI, L. M., VERMA, A. K., KUMAR, V., TYAGI, A., SINGH, P., IQBAL, Z. & TALEGAONKAR, S. 2014. Sterically stabilized polymeric nanoparticles with a combinatorial approach for multi drug resistant cancer: In vitro and in vivo investigations. *Int J Pharm,* 477**,** 454-468.

ZARA, G. P., CAVALLI, R., BARGONI, A., FUNDARO, A., VIGHETTO, D. & GASCO, M. R. 2002. Intravenous administration to rabbits of non-stealth and stealth doxorubicin-loaded solid lipid nanoparticles at increasing concentrations of stealth agent: pharmacokinetics and distribution of doxorubicin in brain and other tissues. *J Drug Target,* 10.

ZHANG, C., PENG, F., LIU, W., WAN, J., WAN, C., XU, H., LAM, C. W. & YANG, X. 2014a. Nanostructured lipid carriers as a novel oral delivery system for triptolide: induced changes in pharmacokinetics profile associated with reduced toxicity in male rats. *Int J Nanomedicine,* 9**,** 1049-1063.

ZHANG, G., LIU, F., JIA, E., JIA, L. & ZHANG, Y. 2016a. Folate-modified, cisplatin-loaded lipid carriers for cervical cancer chemotherapy. *Drug Delivery,* 23**,** 1393-1397.

ZHANG, Q. H., XIONG, Q. P., SHI, Y. Y. & ZHANG, D. Y. 2010a. [Study on preparation and characterization of resveratrol solid lipid nanoparticles and its anticancer effects in vitro]. *Zhong Yao Cai,* 33**,** 1929-32.

ZHANG, S., LU, C., ZHANG, X., LI, J. & JIANG, H. 2016b. Targeted delivery of etoposide to cancer cells by folate-modified nanostructured lipid drug delivery system. *Drug Delivery,* 23**,** 1838-1845.

ZHANG, W., LI, X., YE, T., CHEN, F., SUN, X., KONG, J., YANG, X., PAN, W. & LI, S. 2013. Design, characterization, and in vitro cellular inhibition and uptake of optimized genistein-loaded NLC for the prevention of posterior capsular opacification using response surface methodology. *Int J Pharm,* 454**,** 354-366.

ZHANG, W., LI, X., YE, T., CHEN, F., YU, S., CHEN, J., YANG, X., YANG, N., ZHANG, J., LIU, J., PAN, W. & KONG, J. 2014b. Nanostructured lipid carrier surface modified with Eudragit RS 100 and its potential ophthalmic functions. *Int J Nanomedicine,* 9**,** 4305-4315.

ZHANG, X., LIU, J., QIAO, H., LIU, H., NI, J., ZHANG, W. & SHI, Y. 2010b. Formulation optimization of dihydroartemisinin nanostructured lipid carrier using response surface methodology. *Powder Technology,* 197**,** 120-128.

ZHAO, X., LI, H. & LEE, R. J. 2008. Targeted drug delivery via folate receptors. *Expert Opinion on Drug Delivery,* 5**,** 309-319.

ZHOU, X., ZHANG, X., YE, Y., ZHANG, T., WANG, H., MA, Z. & WU, B. 2015. Nanostructured lipid carriers used for oral delivery of oridonin: An effect of ligand modification on absorption. *Int J Pharm,* 479**,** 391-398.

ZUPANČIČ, Š., LAVRIČ, Z. & KRISTL, J. 2015. Stability and solubility of trans-resveratrol are strongly influenced by pH and temperature. *European Journal of Pharmaceutics and Biopharmaceutics,* 93**,** 196-204.

ZUR MUHLEN, A., SCHWARZ, C. & MEHNERT, W. 1998. Solid lipid nanoparticles (SLN) for controlled drug delivery — drug release and release mechanism. *Eur J Pharm Biopharm,* 45.